Climate Change – Characterization of Black Carbon and Organic Carbon Air Pollution Emissions and Evaluation of Measurement Methods

Phase I: Method Intercomparison
Volume I: Interim Report

DRI Contract Number: 04-307

Submitted to:

Nehzat Motallebi, Ph.D.

California Air Resources Board
Research Division
1001 I Street
Sacramento, CA 95812

Prepared for:
The California Air Resources Board and the California Environmental Protection Agency

By:

Judith C. Chow, Sc.D.
John G. Watson, Ph.D.
Prakash Doraiswamy, Ph.D.
L.-W. Antony Chen, Ph.D.
David A. Sodeman, Ph.D.
Steven Sai Hang Ho, Ph.D.
Steven D. Kohl, M.S.
Dana L. Trimble, B.S.
Hal Voepel, M.S.

Desert Research Institute
Nevada System of Higher Education
2215 Raggio Parkway
Reno, NV 89512

Kochy K. Fung, Ph.D.

Atmoslytic, Inc.
24801 Alexandra Ct.
Calabasas, CA 91302

7/10/2006

DISCLAIMER

The statements and conclusions in this Report are those of the contractor and not necessarily those of the California Air Resources Board. The mention of commercial products, their source, or their use in connection with material reported herein is not to be construed as actual or implied endorsement of such products.

TABLE OF CONTENTS

TABLE OF CONTENTS

TABLE OF CONTENTS

TABLE OF CONTENTS

LIST OF TABLES

LIST OF TABLES

LIST OF FIGURES

LIST OF FIGURES

LIST OF FIGURES

LIST OF FIGURES

LIST OF FIGURES

ABSTRACT

This interim report covers work completed in *Phase I: Method Intercomparison* of the study, which compared different black carbon (BC)/elemental carbon (EC) and light absorption (b_{abs}) measurements. Carbon aerosols from different sources were generated reproducibly within 15% (diesel, acetylene flame, and electric arc soot) to 50% (wood smoke). EC fractions by the IMPROVE_A, STN and the French two-step protocols were within 5% for the sources tested, except for wood smoke (differed by >45%). The French two-step protocol, which is operated in pure oxygen without charring corrections, was more influenced by the presence of sodium chloride in the aerosol mixture than were the IMPROVE_A and STN protocols for source samples on quartz-fiber filters. The EC absorption efficiency (σ_{abs}) at 1047 nm varied (>50%) between sources, in the range of 2.7 to 5.3 m^2/g. A universal conversion factor between b_{abs} and BC/EC concentration does not exist. The Angstrom absorption exponent (α) differed from unity that is typically used in literature to scale b_{abs} to different wavelengths. These findings indicate the need for a more complex aerosol optical model beyond a fixed BC/b_{abs} conversion factor. Optical properties of the Fresno winter aerosol were similar to that of wood smoke. Optical properties of the Fresno summer aerosol were complex, probably due to the presence of secondary and biogenic organic aerosols.

EXECUTIVE SUMMARY

Background: Black carbon (BC) aerosols contribute to warm forcing (0.2 to 1.0 W/m^2) and enhances evaporation of tropical cumulus. Including the direct and indirect effects of BC into the global- and regional-scale climate models requires accurate BC emission inventories and conversion factors (i.e., mass absorption efficiencies, σ_{abs} [λ]) that translate BC concentration into light absorption coefficients (b_{abs}) for different wavelengths. The overall objective of this study is to improve BC emission inventories by understanding what is currently available, by better characterizing BC and elemental carbon (EC) measurement methods, and by measuring emission rates and profiles from BC-emitting sources. One of the major issues is that there is no single, universally accepted standard for BC or EC measurement, and the available thermal and optical methods vary by more than two to three orders of magnitude. Neither are there widely accepted methods to connect BC or EC to b_{abs}, the relevant observable for radiative transfer. Simplified optical theory for calculating σ_{abs} (λ) and single scattering albedo of BC may not be applied to BC from various sources featuring different size, morphology, and internal mixing.

Methods: Phase I of this study was carried out through four major tasks: 1) For Task 1a, a critical review of literature on 19 different carbon-analysis methods and 80 carbon intercomparison studies published between 1981 and 2005 was conducted; 2) The second task focused on developing carbon analysis quality assurance and quality control (QA/QC) plans (Task 2a); 3) For Task 3a, pure and externally mixed (with sodium chloride, NaCl) aerosols from diesel engine, acetylene flame, electric arc, and wood-combustion aerosols were generated and sampled in the laboratory under controlled conditions. Continuous b_{abs} and BC measurements were made using the photoacoustic analyzer (PA, 1047 nm) and a seven-color aethalometer (7-AE, 370, 470, 520, 590, 660, 880, 950 nm), along with sample collection on Teflon-membrane and quartz-fiber filters. In addition, carbon black and graphite powders were resuspended and collected on quartz-fiber filters for carbon analysis; and 4) The fourth task completed an intensive measurement campaign at the Fresno Supersite between 8/18/05 and 9/17/05, which included six continuous light absorption instruments (two wavelength [2-AE, 370, 880 nm] and 7-AE aethalometers, two PA [532 and 1047 nm], one particle soot absorption photometer [PSAP; 467, 530, 660 nm], and one multi-angle absorption photometer [MAAP; 670 nm]), along with 24-hr sample collection using integrated samplers. This complemented measurements taken during a winter intensive operating period (IOP, 12/1/03 to 12/22/03). Findings from the laboratory intercomparisons were applied in understanding the differences observed at Fresno.

Results: The literature review identified possible biases in thermal and optical methods. For filter-based thermal/optical analyses, the charring correction followed by early EC evolution in an inert atmosphere (due to trace oxidants) represented the most important uncertainty in thermal methods (Chow et al., 2004a), biasing the OC/EC split. For the DRI Model 2001 carbon analyzer, QA/QC procedures were developed including: 1) multi-point temperature calibrations; 2) characterization of analysis atmosphere; 3) carbon analyzer calibration; and 4) calibration of laser intensity using neutral density filters. These procedures have been shown to improve the precision of OC/EC and carbon fraction measurements. For instance, without temperature calibration, the sample temperature is typically biased high by 14 to 22 °C, causing up to 30%

change in carbon fraction concentrations. This does not affect the OC/EC split, however. The review indicated that b_{abs} measurements by the PA compared well (within ±3%) with the difference between light extinction by optical extinction cell (OEC) and scattering by nephelometer for pure soot sample or soot mixed with salts (Sheridan et al., 2005). The studies also pointed out the need for correcting filter-based absorption methods for particle light scattering (b_{scat}), the uncertainty involved in σ_{abs} estimates and its effect on b_{abs} measurements, the influence of organic aerosols on b_{abs}, and its influence on the Angstrom absorption exponent (α).

In terms of total carbon (TC), diesel, acetylene flame, and electric arc samples were generated typically within 15% variability. Wood smoke samples showed as much as 50% variability. EC/TC ratios measured by thermal/optical methods showed consistency within each source type, as well as diversity between source types. The STN and French two-step protocols yielded EC/TC ratio similar to (within ±5%) those of the IMPROVE_A protocol for diesel soot (EC/TC ~60%), acetylene flame soot (~96%), and electric arc soot (~50%). The French two-step and STN protocols were lower for EC (86% and 46%, respectively) in wood smoke compared to the IMPROVE_A protocol. The presence of NaCl caused EC to be released at lower temperatures, and was limited by the presence of oxygen (O_2) and charring correction. While it affected the abundance in the EC fractions, it did not affect the OC/EC split in the IMPROVE_A and STN protocols. The French two-step protocol that operates in pure O_2, without charring corrections, reported >60 to 90% lower EC than IMPROVE_A_TOR for all 19 samples. When comparing the IMPROVE_A EC to PA (1047 nm) b_{abs}, the EC σ_{abs} (1047 nm) varied by ~50% in the range of 2.7 to 5.3 m^2/g among the different source types. There is no universal conversion factor that can be applied to convert b_{abs} to BC/EC concentrations. The ratio of AE b_{abs} to PA b_{abs} was influenced by BC concentrations; lower ratios were found to be associated with higher BC concentrations.

Using the IMPROVE_A protocol, the EC/TC ratios at the Fresno Supersite were 0.22 ± 0.04 and 0.26 ± 0.05 for summer and winter IOPs, respectively. The EC/TC ratio during winter was close to the EC fraction in wood smoke (0.26 ± 0.12). The σ_{abs} (1047 nm) of EC during the winter IOP (2.5 m^2/g) was also similar to that of wood smoke EC (2.7 m^2/g). The value of α in the Angstrom Power Law, determined by 7-AE during the summer IOP (0.95 ± 0.04) was 10% to 20% higher than that observed for diesel and acetylene flame soot (0.79 ± 0.09 to 0.86 ± 0.12), from both pure source aerosol and when mixed with NaCl. This indicates that the summer aerosol at Fresno, while being influenced by diesel emissions, might be mixed with aged or secondary aerosols. The α during the winter period (1.2 ± 0.11) was closer to that observed for emissions from wood combustion (1.2 ± 0.51). Despite the potential bias in the AE, this study confirms a higher α for wood smoke than for diesel soot.

Conclusions: Results suggest that the IMPROVE_A and STN protocols estimate similar EC for the source samples (except wood smoke). The presence of a catalyst such as NaCl changes the abundances in EC fractions, but not the OC/EC split in IMPROVE_A and STN protocols. The French two-step protocol was influenced greatly by the aerosol matrix. A single value of σ_{abs} does not exist. Moreover, $\alpha = 1$ in the Angstrom Power Law that is commonly used to scale b_{abs} to different wavelengths varied from 0.5 to 1.4. These observations may be explained by more complex aerosol optical models that consider particle size distributions, morphology, and internal/external mixing characteristics.

1. INTRODUCTION

1.1 Background

Particulate matter (PM) emissions, which often accompany emissions of greenhouse gases (GHG) such as carbon dioxide (CO_2), affect the Earth's climate, human health, visibility, surface soiling, and crop productivity. Light-absorbing aerosols, mainly black carbon (BC), or "soot," from fossil fuel and biomass combustion, produce a warm forcing of +0.2 to +1 W/m^2 (Lloyd and Cackette, 2001; IPCC, 2001a; 2001b). BC emission inventories rely on different assumptions and on data related to emission activities, PM emission factors, and source profiles, which apportion PM mass to BC and other chemical constituents (Watson et al., 2001). BC and elemental carbon (EC) are defined operationally according to the measurement method applied, though the terms are often used interchangeably. Of the major components of $PM_{2.5}$ (PM with aerodynamic diameter of 2.5 micrometers [μm] or less) and PM_{10} (PM with aerodynamic diameter of 10 μm or less), organic carbon (OC) and EC are the most uncertain with respect to sampling and analysis (Huebert and Charlson, 2000; Jacobson et al., 2000; Chow et al., 2006b). Most characterization of BC and EC involves collecting PM on filters and measuring either the carbon content on the filter or the attenuation of light (b_{abs}) reflected from or transmitted through the filter.

Thermal evolution methods quantify the amount of carbon that leaves the filter at different temperatures (Schmid et al., 2001; Currie et al., 2002; Chow et al., 2006b). Different combinations of temperature and analysis atmospheres are used to evaporate, pyrolyze, and combust the carbon-containing compounds in a filter sample, with subsequent detection of the evolved carbon gases. The separation of OC from EC is ambiguous because some of the OC chars (turns to EC) in an oxygen (O_2)-free atmosphere and EC combusts in an oxidizing atmosphere. Light reflected from (Johnson, 1981; Huntzicker et al., 1982; Chow et al., 1993) or transmitted through the filter during the analysis (Turpin et al., 1990; Birch and Cary, 1996a; 1996b; Chow et al., 2001; Chow et al., 2004a) is used to monitor and correct for this charring. Interlaboratory and inter-method comparisons (Countess, 1990; Schmid et al., 2001; Currie et al., 2002; Chow et al., 2004a; Watson et al., 2005) show EC differences of a factor of two or more among different thermal methods, depending on the protocol and type of sample. Different analysis methods alone can account for the large differences in BC emission rates among inventories. The scattering and absorption properties of particles distributed on top of and throughout a filter are different from those of particles suspended in air, and b_{abs} determined from these filter-based methods are usually biased (Horvath, 1993b). A fundamental measurement of in-situ aerosol b_{abs} can be achieved by the photoacoustic instrument (Moosmüller et al., 1997; Arnott et al., 1999; 2003), which quantifies minute changes in the atmospheric pressure in response to heating and cooling of PM by a modulated laser beam. In this study, thermal, optical, and photoacoustic measurements are collocated with filter samples to relate BC or EC measurements to their absorption properties.

1.2 Objectives

The overall goal of this study is to improve BC emission inventories by understanding what is currently available, by better characterizing BC and EC measurement methods, and by measuring emission rates and profiles from BC-emitting sources. Specific objectives are to:

- Identify, compile, evaluate, and summarize existing information on BC inventories, combustion processes, emission factors, source profiles, and source/ambient measurement methods.
- Develop and apply analysis methods to determine causes of differences among BC or EC measurements in source emission and in ambient monitoring networks.
- Develop relationships between different BC or EC measurement methods and light absorbing properties of emitted particles.
- Measure OC and BC emission factors for selected combustion processes.
- Compile and compare OC and BC emission factors that are relevant to California, the U.S., and global inventories.
- Evaluate and quantify emission inventory uncertainties and describe how the results of this study might reduce them.

The study is conducted in two phases. This report summarizes the work completed in *Phase I—Method Intercomparison*, which intends to gain a better understanding of OC and BC/EC measurement methods. Phase I evaluates previously published literature, develops quality assurance (QA) and quality control (QC) plans, and compares different OC and BC/EC analysis methods and measurements in the laboratory and in the field. It includes the following tasks:

Task 1a: Critically review literature on carbon analysis methods and comparisons

Task 2a: Create carbon analysis QA/QC methods and plans

Task 3a: Conduct a laboratory comparison of OC, EC, BC and b_{abs} measurement methods

Task 4a: Perform a field comparison of different methods at the Fresno Supersite

Task 5a: Prepare Phase I report

Task 1a was completed by identifying and reviewing 19 different carbon analysis methods and 80 carbon intercomparison studies. The review summarizes the precision, lower quantifiable limits (LQL), and potential artifacts affecting the OC/EC split for the 19 thermal/optical carbon analysis methods. In addition to the thermal/optical methods, organic speciation by thermal desorption (TD) is also described, and 25 source and 94 ambient samples were tested by TD in order to identify potential organic markers in combustion sources.

As part of Task 2a, 49 standard operating procedures (SOPs) were identified and assembled. Calibration procedures for analysis temperatures, analysis atmospheres, and optical monitoring were developed. A Quality Assurance Project Plan (QAPP) was completed.

Task 3a was completed by generating test aerosols in a controlled laboratory setting where carbon powders and combustion emissions could be sampled simultaneously from a test chamber by several optical and photoacoustic instruments. PM was also collected onto filters suitable for thermal and optical analyses.

For Task4a, a field evaluation of in-situ and integrated measurements was conducted at the Fresno Supersite (Watson et al., 2000a; 2000b) during summer 2005. These data were compared

with measurements acquired during winter 2003. These field tests help to generalize laboratory test results and provide empirical formulae applicable to other California monitors that do not have collocated measurements. The preparation of this Phase I report (this document) completes Task 5a.

Phase II will compile and evaluate existing emission inventories, determine their similarities and differences, and attempt to ascertain why differences exist. It will also compile and compare available PM and BC emission factors relevant to California combustion sources and determine how these relate to national and global inventories. Limited source testing will be conducted to increase the data base of emission factors from combustion sources.

1.3 Guide to Report

This section states the background and the objectives of this study. Section 2 reviews the different OC/EC analysis protocols and methods, the TD method, and intercomparisons between filter-based EC and continuous BC or b_{abs} measurements (Task 1a). Section 3 summarizes the different sources tested under controlled laboratory conditions (Task 3a). Section 4 reviews the ambient measurements at the Fresno Supersite and describes filter pack and continuous BC, EC, and b_{abs} measurements conducted during summer 2005 and winter 2003 (Task 4a). Section 5 documents the data validation procedures. Section 6 summarizes the method intercomparisons of laboratory and ambient measurements, presents calculated estimates of mass absorption efficiencies (σ_{abs}) that relate b_{abs} to BC and EC, and the Angstrom absorption exponent (α), and draws conclusions as to the generalization of results from laboratory measurements to ambient measurements. Section 7 summarizes the results of the measurement program and evaluates the overall extent to which the objectives were met. The bibliography and references are assembled in Section 8. Published papers (Watson et al., 2005; Park et al., 2006) are assembled in Section 9. A glossary of abbreviations and symbols used in this report is contained in Section 10. Tables and figures referenced in the text are placed at the end of the respective sections. Additional data tables and related information are included in Appendices A through E. The QAPP is included as Volume II of this report.

2. LITERATURE REVIEW

This section reviews carbon analysis methods (including thermal combustion, thermal/optical analysis of OC and EC, and TD of organic components), analysis protocols, and intercomparison studies (Task 1a). Progress has already been made on the compilation of existing source profiles (Task 1b, Phase II).

2.1 Review of Different Carbon Analysis Methods

Nineteen different OC and EC thermal/optical analysis protocols and 42 carbon intercomparison studies were published between 1981 and 2003 (Watson et al., 2005, see Section 9.1). The 19 protocols for quantifying OC and EC (See Table 1 in Watson et al., 2005) include methods commonly used in the United States (e.g., Interagency Monitoring for Protected Visual Environments, IMPROVE [(Chow et al., 1993; 2004a)] and Speciation Trends Network, STN [(Peterson and Richards, 2002)]), as well as in Europe (e.g., French two-step [(Cachier et al., 1989a)] and Germany [(VDI, 1996; 1999)]).

Intercomparisons between different carbon measurements were carried out in several national and international research campaigns (e.g., Countess, 1990; Birch, 1998; Schmid et al., 2001; Currie et al., 2002). Filter EC measurements were compared to BC determined from optical methods, including integrating plate (e.g., Sadler et al., 1981; Bennett, Jr. and Patty, 1982), integrating sphere (e.g., Hitzenberger et al., 1996; 1999), aethalometer (e.g., Hansen and McMurry, 1990; Petzold and Niessner, 1995; Sharma et al., 2002), particle-soot absorption photometer (PSAP) (Reid et al., 1998), multi-angle absorption photometer (MAAP)(Petzold et al., 2003; Petzold and Schönlinner, 2004), and photoacoustic instruments (e.g., Adams et al., 1989; Moosmüller et al., 1998; 2001b). These studies identified possible biases in thermal and optical methods. For filter-based thermal/optical analyses, the charring correction was identified as the most important uncertainty in thermal methods (Chow et al., 2004a). This was followed by the oxidation of EC in an inert atmosphere at high temperatures due to trace oxidants in the sample. In filter-based optical methods, it was found to be difficult to correct for absorption enhancement by the filter matrix.

Detailed procedures, references, studies in which they were applied, pyrolyzed OC (OP) adjustments, and performance for each of the 19 thermal/optical protocols are summarized in Table A-1 of Appendix A, which also documents minimum detection limits (MDLs), LQLs, and precision estimates. Also specified are potential artifacts associated with the OC/EC split, due to variations in analysis atmospheres, temperature protocols, analysis times at each temperature plateau, and pyrolysis corrections.

Since 2003, hundreds of studies have been conducted relating to the quantification of BC and EC. An additional 38 laboratory and field studies that were not included in Watson et al. (2005) are reported in Table B-1 of Appendix B. In selecting these studies, emphasis was given to: 1) method development or validation of BC/EC measurements; 2) inter-method or inter-laboratory comparisons; and 3) investigation of fundamental BC/EC properties including the development of reference materials. These studies reinforced the findings reported by Watson et al. (2005) and pointed out the need for correcting filter-based absorption methods for light scattering, the

uncertainty involved in σ_{abs} estimates and its effect on b_{abs} measurements, the influence of organic aerosol on b_{abs}, and its influence on α.

2.2 Compilation of Existing Source Profiles

Obtaining and documenting reliable PM source profiles (the mass fractions of designated chemical species) are important for: 1) identification of chemical and physical characteristics of primary PM; 2) creation of speciated emission inventories used in air quality models; 3) input to receptor-oriented source attribution models such as Chemical Mass Balance (CMB); and 4) estimation of toxic and hazardous pollutant emissions. Measured source profiles are also used to verify model estimated profiles or results from factor analysis solutions to the CMB equations, Positive Matrix Factorization (PMF), UNMIX, and Principal Component Analysis (PCA).

The U.S. Environmental Protection Agency's SPECIATE database (U.S.EPA, 1999c), which provides an interface for identifying, examining, and formatting source profiles, has not been updated since 1990. Combustion-source profiles documented in 18 aerosol and source characterization studies conducted by the Desert Research Institute (DRI) from 1987 to 2006 have been assembled (Chow et al., 2006a). These include 876 combustion source profiles for: motor-vehicle exhaust (e.g., diesel, gasoline, or mixed), vegetative burning (e.g., agriculture, residential, and wildfire), industrial boilers (e.g., coal, oil, gas, manure), residential meat cooking, and miscellaneous (e.g., residential coal combustion, fluidized catalyst cracker, aircraft exhaust). Laboratory-generated source profiles for diesel exhaust, acetylene flame, electric arc, and wood burning are also included. The number of source profiles within each category is presented in Table 2-1.

Source measurement techniques varied for these profiles. Motor-vehicle exhaust, vegetative burning, industrial boiler, and residential cooking emissions were measured either in a hot-exhaust plume, through a dilution sampler, or by ground-based source sampling of air dominated by a single source (Chow et al., 2004b). Where, when, and how each profile was acquired is described in detail by Chow et al. (2006a), along with the criteria for profile selection.

Each profile contains: 40 elements (See Table 2-2) by X-ray fluorescence (XRF); ions (Cl^-, NO_3^-, $SO_4^=$, NH_4^+, Na^+, K^+) by ion chromatography (IC), automated colorimetry (AC) or atomic absorption spectrophotometry (AAS); and carbon fractions (OC, EC) by thermal/optical reflectance (TOR) method, following the IMPROVE or IMPROVE_A protocol. Additional measurements such as phosphate (PO_4^{3-}), carbonate (CO_3^{2-}), sulfur dioxide (SO_2), and ammonia (NH_3) are available in some of the profiles. Eight carbon fractions (OC1-OC4, EC1-EC3, OP) are included in the more recent profiles. Speciated semi-volatile and volatile organics, including alkanes, hopanes, steranes, polycyclic aromatic hydrocarbons (PAHs), carbohydrates, dicarboxylic acids, fatty acids, alcohols, and amino acids by gas chromatography/mass spectrometry (GC/MS), are contained in measurements from the Northern Front Range Air Quality Study (NFRAQS), General Electric-Energy and Environmental Research Corporation (GEEER), Tahoe Source Apportionment, Southern Nevada Air Quality Study (SNAQS), and gas/diesel split studies. The measured concentrations of these inorganic and organic species were normalized (usually to PM gravimetric or reconstructed mass) to produce source profiles that were then recorded in the database (Chow et al., 2006a).

2.3 Literature Review and Potential Organic Markers by Thermal Desorption

In an effort to identify organic markers in different combustion sources, a review of recent application of thermal desorption (TD) was conducted (Chow et al., 2006c). TD combines efficient sample extraction and rapid transfer of target compounds to the analytical instrument. It offers a cost-saving and high-sensitivity alternative to the conventional solvent extraction methods for the analysis of trace-level organic chemicals. Table 2-3 summarizes the comparisons between TD and solvent extraction methods for organic speciation. Approaches that couple TD with GC/MS to analyzing non-polar alkanes and PAHs (i.e., Helmig et al., 1990; Falkovich and Rudich, 2001; Hays et al., 2003; Ho and Yu, 2004) have been assembled. Different indices, diagnostic ratios, and individual organic markers obtained by the TD-GC/MS method can be used in source apportionment. Table C-1 of Appendix C summarizes the organic species detected with different TD-GC/MS techniques and Table C-2 summarizes the past TD-GC/MS studies.

Twenty-five different source samples, including gasoline, diesel, wood, and 94 ambient samples from the Fresno Supersite taken during 2004 have been analyzed by TD-GC/MS (Ho and Yu, 2004). Table 2-4 summarizes the 127 non-polar organic species that were identified in Fresno samples. MDLs are listed in Table 2-5.

At Fresno, concentrations of total *n*-alkanes, from *n*-C_{15} to *n*-C_{42}, ranged from 29.4 to 107 ng/m^3 during summer and 46.5 to 596 ng/m^3 during winter. The average concentrations were 58 ng/m^3 during summer and 215 ng/m^3 during winter. Figure 2-1 shows examples for *n*-alkane concentrations. Determination of the individual *n*-alkane concentrations allows the calculation of Carbon Performance Index (CPI) and C_{max} (*n*-alkane with the maximum concentration). CPI is the ratio of odd- to even-number carbon *n*-alkanes in a given sample (Bray and Evans, 1961). CPI values could be used to differentiate biogenic sources from petrogenic or anthropogenic sources (Simoneit and Mazurek, 1982; Sicre et al., 1987; Gogou et al., 1994). A CPI value close to unity suggests the influence of petroleum residues (Simoneit, 1985). As CPI exceeds unity (i.e., an odd carbon number is predominant in the *n*-alkane homologue distribution), it suggests the influence of natural plant waxes (Eglinton and Hamilton, 1963). No odd- to even-number carbon predominance was seen in winter, during which the CPI ranged from 0.92 to 1.49 with an average of 1.16. These data suggest that incomplete combustion of fuels was the major *n*-alkane source at Fresno during winter. Dominance of odd-number carbon was observed in summer, during which the CPI values ranged from 1.43 to 2.53, with an average of 1.91. This is indicative of influences from biogenic sources.

The 16 priority PAH concentrations ranged from 0.05 ng/m^3 to 1.37 ng/m^3 with an average concentration of 0.28 ng/m^3 during summer. Higher values were detected during winter, ranging from 0.46 to 27.8 ng/m^3 with an average concentration of 8.1 ng/m^3, 29 times higher than the summer value. Benzo[b+k]fluoranthene was the most abundant PAH with an average concentration of 1.18 ng/m^3. Heavier PAHs, including indeno[1,2,3-cd]pyrene (IcdP) and benzo[g,h,i]perylene (BghiP), were the next most-abundant PAHs in the samples, with an average of 0.47 and 0.51 ng/m^3, respectively. Other than the 16 priority PAHs, retene (a marker for vegetative burning derived from resins in conifer plants) was also detected in Fresno samples. Retene concentrations ranged from 0.06 to 1.71 ng/m^3 with an average of 0.55 ng/m^3 in the winter samples. Relatively lower values were detected in the summer samples, ranging from 0.02

to 0.09 ng/m^3, with an average of 0.04 ng/m^3. The summer samples were less influenced by the residential wood combustion (RWC) emissions.

Similar observations were made in the source samples. The CPI of gasoline and diesel samples ranged from 0.98 to 1.01, whereas much higher ratios from 2.06 to 3.16 were found for the combustion of mesquite wood, Huisache, and grass samples.

C_{max} is the *n*-alkane that has the highest concentration among the *n*-alkane homologues. It also provides information for distinguishing among biogenic and anthropogenic pollution sources. Lower C_{max} values indicate that petroleum residue is a dominant source, whereas higher C_{max} values suggest contribution from biogenic sources (Simoneit, 1984). Wintertime Fresno samples exhibit a C_{max} at C_{23} or C_{24} whereas summertime samples exhibit a C_{max} at C_{31}.

Examples of source profiles in non-polar organic species are shown in Figure 2-2. The extract ion *m/z* 57 gas chromatograms demonstrate the distribution of alkane compounds. No odd- or even-numbered carbon was predominant in diesel-, gasoline-, or coal-combustion samples. However, odd-number alkanes were found to be predominant in the wood-burning sample, especially at higher carbon numbers (> C_{23}), with a C_{max} at C_{29}. The gasoline sample had a C_{max} at C_{24}, whereas the C_{max} was C_{22} for diesel and coal samples. Unresolved carbon matter (UCM; e.g., a hump in the chromatogram) was found in gasoline-, diesel-, and coal-source samples. A larger hump area in the gasoline sample suggests higher UCM emissions than other combustion sources.

The ratios of BghiP/benzo[e]pyrene (BeP) and Coronene (Cor)/BeP have been used to evaluate the extent of vehicle exhaust contributions (Nielsen, 1996), with higher ratios indicating larger contributions. The BghiP/BeP ratios were 2.85 for diesel samples and 3.22 for gasoline, but only 0.56 to 0.88 for vegetative burning sources.

Ratios of IcdP/(IcdP + BghiP) at 0.18, 0.37, 0.56 and 0.62 for gasoline, diesel, coal combustion, and wood burning, respectively, are reported (Grimmer et al., 1983; Gogou et al., 1996). For source samples acquired in Mexico, similar results were found with a ratio of 0.36 and 0.58 for gasoline- and diesel-source samples, respectively. Ratios of Fluoranthene to Fluoranthene and Pyrene (Flu/[Flu + Pyr]) are 0.18 for crude oil and 0.43 for gasoline-powered emissions (Sicre et al., 1987).

Iso- and anteiso-alkanes in Fresno ranged from 0.22 to 0.59 ng/m^3 during winter, indicative of cigarette smoke particles (Rogge et al., 1994). Hopanes and steranes have been identified in exhaust from gasoline-powered motor vehicles, diesel engines, fuel-oil combustion, and coal combustion (Simoneit, 1985; Rogge et al., 1993; Schauer, 1999). High abundances of hopanes and steranes were found in Fresno samples, as well as in the gasoline and diesel source samples, but not in the wood-combustion samples. The abundances of different organic markers in the source and ambient samples demonstrate the feasibility of using TD organic speciation in source apportionment.

Table 2-1. Summary of combustion source profiles acquired and assembled for studies conducted between 1987 and 2006.

Study		SCENIC Denver Brown Cloud Study	ARB California Source Characterization Study	Phoenix PM_{10} &Visibility Study	Imperial Valley/ Mexicali PM_{10} Study	San Francisco Bay Area PM_{10} Study	Mt. Zirkel Visibility Study	LVPS Las Vegas PM_{10} Study	Antarctica (Mc Murdo) PM_{10} Study	NFRAQS (Denver) Visibility Study	South Africa Source Contribution Study	Mexico City PM_{10} Study	Tuscarora Mountain Tunnel Diesel Emission Study	BRAVO (Big Bend National Park) Visibility Study	California Regional PM Air Quality Study (CRPAQS)	GE-EER Combustion Emissions Study	NREL Gas/Diesel Split Study	Lake Tahoe Source Apportionment Study	Southern Nevada Air Quality Study (SNAQS)	ARB BC/OC Study and EPA Carbon StarGrant	Total
Year		***87-88***	***87-88***	***89-90***	***92-93***	***92-93***	***94-95***	***95-96***	***95-97***	***96-97***	***97***	***97-98***	***99***	***99-00***	***01-03***	***98-03***	***01***	***03-04***	***03-04***	***05-06***	***87-06***
Motor Vehicle	Gasoline	16		1f					1e,f	56~,f	2b	8	1~				48~,f				133
	Diesel	3	10^,c	1f		1			2e,f	13~,f		21	1~				53~,f		16~,f	35f	156
	Mixed	7		10f	42	2	18#	27e				20	18~	39^,f				2~,f	11~,f		196
Vegetative Burning	Residential	9f	15^,c				4#	31e		18~,f					6f			18 ~,f			101
	Agriculture		20^,c		9										3f						32
	Forest Fire						5#				2b			29^,f							36
Coal Combustion	Residential						5#				8b										13
Cooking	Commercial				2					5~,f		7		17^,f							31
Industry and Utility	Coal	5					16#							33^,f							54
Emission	Oil		10^,c		1				3e,f					6^,f							20
	Manure				5																5
	Gas	1														26*,~#f					27
Woodsmoke (White Oak)																				23f	23
Acetylene																				10f	10
Electric Arc																				22f	22
Fluidized catalyst Cracker regenerator		1																			1
Incinerator			10																		10
C130 and UH-1 Airplane									2e,f												2
Lime kiln											2										2
Residential paper Waste burning											2										2
Total		42	65	12	59	3	48	58	8	92	16	56	20	124	9	26	101	20	27	90	876

b $PM_{2.5}$, PM_{10}
c PM_1, $PM_{2.5}$, $PM_{10-2.5}$, PM_{10}, TSP
e PM_{10}
i Fluidized catalyst cracker regenerator
j Incinerator
k C130 and UH-1 airplane

^ with carbonate
~ with organics
# with SO_2 and NH_3
n lime kiln
p residential paper waste burning
f with carbon fractions

Table 2-2. Elements analyzed by XRF and their minimum detection limits (MDLs[a]).

Symbol	Element	MDL (µg/m^3)
Na	Sodium	0.0331
Mg	Magnesium	0.0120
Al	Aluminum	0.0048
Si	Silicon	0.0030
P	Phosphorous	0.0027
S	Sulfur	0.0024
Cl	Chlorine	0.0048
K	Potassium	0.0029
Ca	Calcium	0.0022
Ti	Titanium	0.0014
V	Vanadium	0.0012
Cr	Chromium	0.0009
Mn	Manganese	0.0008
Fe	Iron	0.0007
Co	Cobalt	0.0004
Ni	Nickel	0.0004
Cu	Copper	0.0005
Zn	Zinc	0.0005
Ga	Gallium	0.0009
As	Arsenic	0.0008
Se	Selenium	0.0006
Br	Bromine	0.0005
Rb	Rubidium	0.0005
Sr	Strontium	0.0005
Y	Yttrium	0.0006
Zr	Zirconium	0.0008
Mo	Molybdenum	0.0013
Pd	Palladium	0.0053
Ag	Silver	0.0058
Cd	Cadmium	0.0058
In	Indium	0.0062
Sn	Tin	0.0081
Sb	Antimony	0.0086
Ba	Barium	0.0249
La	Lanthanum	0.0297
Au	Gold	0.0015
Hg	Mercury	0.0012
Tl	Thallium	0.0012
Pb	Lead	0.0014
U	Uranium	0.0011

[a] MDL is the concentration at which instrument response equals three times the standard deviation of the response to a known concentration of zero. Typical sample volumes are 28.8 m^3.

Table 2-3. Comparison of thermal desorption and solvent extraction methods in analysis of organic compounds in aerosol filter samples.

	Thermal Desorption	Solvent Extraction
Extraction Theory	- Thermal behavior of analytes (i.e., boiling points).	- Solubility of analytes in extraction solvent.
Sample Size and Loading Required	- Small portion, typically ranging from 0.3 to 5.0 cm^2 subjected to the design of thermal desorption unit and sample loading; - Remnants from any archived filter samples can be used; - As low as a few micrograms of OC per cm^2 can be detected [a]. ≤1 μg OC $\mu g/m^3$ collected on a sampler with a flow rate from 10-30 L/min is an adequate concentration.	- Large portion of sample, depending on the particle loading; - Combined samples may be needed for low loadings; - High collection flow rates (e.g., 100-1,000 L/min) are required to increase the sample loading.
Solvent Consumption	- Low, only few microliters (μL) internal standard containing solvent used per sample.	- High, ranging from 10 to 300 ml per sample; - Common solvents used: dichloromethane (DCM), methanol, 1-butanol, acetone, and *n*-hexane; - Generally more than 90% is lost after volume reductions and cannot be recycled.
Sample Pretreatment	- Simple procedures; - Less labor required, ranging from a few minutes to 30 minutes per sample.	- Complicated steps (i.e., single or multiple volume reductions, extract transfer, and sample filtration); - Labor intensive, usually requires at least 1 to 20 hours per sample.
Total Analysis Time [b]	- Generally 1-2 hours.	- A few to tens of hours.
Analytical Instrument	- Mass spectrometer (MS); - Gas chromatography/flame ionization detector (GC/FID); - Gas chromatography/mass spectrometer (GC/MS).	- Gas chromatographic methods, i.e. GC/MS and GC/FID; - High performance liquid chromatography (HPLC); - Ion chromatography (IC); - Capillary electrophoresis (CE).
Sample Introduction	- 100%.	- Only 0.5 – 25% of the solvent extract.
Sample Contamination	- Low probability; - Potential carryover and transfer loss in thermal desorption unit; - Fragmentation of thermally labile compounds.	- High probability; - Possible contaminants from solvents and complicated extraction procedures; - Loss of volatile compounds during the extraction and pretreatment steps; - Possible carryover from injection port when dirty samples are introduced.
Sensitivity and Limit of Detection (LOD)	- High sensitivity; - *n*-Alkanes: 0.41 to 4.36 ng/sample [c]; - PAHs: 0.08 to 2.40 ng/sample [c];	- Low sensitivity; - *n*-Alkanes: 37.7 to 125 ng/sample [c]; - PAHs: 10.3 to 47.9 ng/sample [c];
Suitability of Filter Matrix	- Any filters can be operated at high desorption temperature, i.e., quartz-fiber, Teflon-impregnated glass fiber (TIGF).	- Any filters can be extracted with solvents, i.e., quartz-fiber, glass-fiber, TIGF.

[a] Calculation was based on the detection limits of the organic compounds reported in the thermal desorption method and typically represents a percentage of their contributions in the organic carbon fraction.
[b] Including sample pre-treatment and analytical separation.
[c] Data obtained from Ho and Yu (2004).

Table 2-4. Non-polar organic compounds derived from thermal desorption using gas chromatography/mass spectrometry.

Compounds	Molecular Weight	Quantification Ion	Compounds	Molecular Weight	Quantification Ion
PAHs			**Alkanes**		
naphthalene	128	128	**n-alkane (n-C14 to n-C44)**		
acenaphthylene	152	152	tetradecane (n-C14)	198	57
acenapthene	154	154	pentadecane (n-C15)	212	57
fluorene	166	166	hexadecane (n-C16)	226	57
phenanthrene	178	178	heptadecane (n-C17)	240	57
anthracene	178	178	octadecane (n-C18)	254	57
fluoranthene	202	202	nonadecane (n-C19)	268	57
pyrene	202	202	icosane (n-C20)	282	57
benzo[a]anthracene	228	228	heneicosane (n-C21)	296	57
chrysene	228	228	docosane (n-C22)	310	57
benzo[b]fluoranthene	252	252	tricosane (n-C23)	324	57
benzo[k]fluoranthene	252	252	tetracosane (n-C24)	338	57
benzo[a]fluoranthene	252	252	pentacosane (n-C25)	352	57
benzo[e]pyrene	252	252	hexacosane (n-C26)	366	57
benzo[a]pyrene	252	252	heptacosane (n-C27)	380	57
perylene	252	252	octacosane (n-C28)	394	57
indeno[1,2,3-cd]pyrene	276	276	nonacosane (n-C29)	408	57
dibenzo[a,h]anthracene	278	278	triacontane (n-C30)	422	57
benzo[ghi]perylene	276	276	hentriacotane (n-C31)	436	57
coronene	300	300	dotriacontane (n-C32)	450	57
dibenzo[a,e]pyrene	302	302	tritriactotane (n-C33)	464	57
			tetratriactoane (n-C34)	492	57
1-methylnaphthalene	142	142	hexatriacontane (n-C36)	506	57
2-methylnaphthalene	142	142	heptatriacontane (n-C37)	521	57
2,6-dimethylnaphthalene	156	156	octatriacontane (n-C38)	535	57
9-fluorenone	180	180	nonatriacontane (n-C39)	549	57
9-methylanthracene	192	192	tetracontane (n-C40)	563	57
anthroquinone	208	208	hentetracontane (n-C41)	577	57
1,8-napthalic anhydride	198	154	dotetracontane (n-C42)	591	57
methylfluoranthene	216	216	tritetracontane (n-C43)	605	57
retene	234	219	tetratetracontane (n-C44)	619	57
cyclopenta[cd]pyrene	226	226	**methyl-alkane**		
benz[a]anthracene-7,12-dione	258	258	2-methylnonadecane	282	57
methylchrysene	242	242	3-methylnonadecane	282	57
picene	278	278			

Table 2-4. Continued.

Compounds	Molecular Weight	Quantification Ion	Compounds	Molecular Weight	Quantification Ion
iso/anteiso alkane[a]			**Hopane**		
iso-C29	408	57	22,29,30-trisnorneophopane (Ts)[a]	370	191
anteiso-C29	408	57	22,29,30-trisnorphopane (Tm)	370	191
iso-C30	422	57	αβ-norhopane (C29αβ-hopane)	398	191
anteiso-C30	422	57	29Ts[a]	398	191
iso-C31	436	57	βα-norhopane (C29βα -hopane)	398	191
anteiso-C31	436	57	αβ-hopane (C30αβ -hopane)	412	191
iso-C32	450	57	30αα[a]	412	191
anteiso-C32	450	57	βα-hopane (C30βα -hopane)	412	191
iso-C33	464	57	αβS-homohopane (C31αβS-hopane)	426	191
anteiso-C33	464	57	αβR-homohopane (C31αβR-hopane)	426	191
iso-C34	478	57	αβS-bishomohopane[a] (C32αβS-hopane)	440	191
anteiso-C34	478	57	αβR-bishomohopane[a] (C32αβR-hopane)	440	191
iso-C35	492	57	22S-trishomohopane (C33)[a]	454	191
anteiso-C35	492	57	22R-trishomohopane (C33)[a]	454	191
branched-alkane			22S-tretrahomohopane (C34)[a]	468	191
pristane	268	57	22R-tetrashomohopane (C34)[a]	468	191
phytane	282	57	22S-pentashomohopane(C35)[a]	482	191
squalane	422	57	22R-pentashomohopane(C35)[a]	482	191
cycloalkane					
octylcyclohexane	196	83	**Sterane**		
decylcyclohexane	224	83	ααα 20S-cholestane	372	217
tridecylcyclohexane	266	82	ααα 20R-cholestane	372	217
n-heptadecylcyclohexane	322	82	αββ 20R-cholestane	372	218
nonadecylcyclohexane	350	82	αββ 20s-cholestane	372	218
			ααα 20S 24S-methylcholestane[a]	386	217
Alkene			13α(H),17α(H)-24-ethyldiacholestane	400	217
squalene	410	69	αββ 20R 24S-methylcholestane	386	218
1-octadecene	252	55	αββ 20S 24S-methylcholestane[a]	386	218
			ααα 20R 24R-methylcholestane[a]	386	217
Phthalate			ααα 20S 24R/S-ethylcholestane	400	217
dimethylphthalate	194	163	αββ 20R 24R-ethylcholestane	400	218
diethyl phthalate	222	177	αββ 20S 24R-ethylcholestane[a]	400	218
di-n-butyl phthalate	278	149	ααα 20R 24R-ethylcholestane	400	217
butyl benzyl phthalate	312	149			
bis(2-ethylhexyl)phthalate	390	149			
di-n-octyl phthalate	390	149			

[a] Due to a lack of authentic standards (for iso-/anteiso-alkanes and a few hopanes and steranes), the organic compound concentrations are estimated by assuming the same response as the respective isomers or the respective *n*-alkanes of the same carbon number.

Table 2-5. Minimum detection limits (MDLs) for PAHs, phthalates, alkanes, alkenes, hopanes, and steranes using the in-injection port thermal desorption method.

Compounds	MDL (ng)	MDL (ng/m^3)[a]	Compounds	MDL (ng)	MDL (ng/m^3)[a]
PAHs			**Alkanes**		
acenaphthylene	2.34	0.083	n-alkane (n-C14 to n-C44)		
acenapthene	1.82	0.065	tetradecane (n-C14)	1.43	0.051
fluorene	0.88	0.031	pentadecane (n-C15)	0.86	0.031
phenanthrene	0.42	0.015	hexadecane (n-C16)	0.89	0.032
anthracene	0.17	0.006	heptadecane (n-C17)	0.76	0.027
fluoranthene	0.25	0.009	octadecane (n-C18)	0.66	0.024
pyrene	0.40	0.014	nonadecane (n-C19)	0.51	0.018
chrysene	0.40	0.014	icosane (n-C20)	0.51	0.018
benzo[b]fluoranthene	0.82	0.029	heneicosane (n-C21)	0.85	0.030
benzo[k]fluoranthene	0.28	0.010	docosane (n-C22)	0.64	0.023
benzo[a]pyrene	0.90	0.032	tricosane (n-C23)	0.74	0.026
perylene	0.97	0.034	tetracosane (n-C24)	0.55	0.020
indeno[1,2,3-cd]pyrene	0.42	0.015	pentacosane (n-C25)	0.59	0.021
dibenzo[a,h]anthracene	0.94	0.033	hexacosane (n-C26)	0.59	0.021
benzo[ghi]perylene	0.62	0.022	heptacosane (n-C27)	0.29	0.010
coronene	0.73	0.026	octacosane (n-C28)	0.73	0.026
dibenzo[a,e]pyrene	0.28	0.010	triacontane (n-C30)	0.96	0.034
			hentriacotane (n-C31)	0.78	0.028
1-methylnaphthalene	0.45	0.016	dotriacontane (n-C32)	0.90	0.032
2-methylnaphthalene	0.15	0.005	tritriactotane (n-C33)	0.57	0.020
2,6-dimethylnaphthalene	0.87	0.031	tetratriactoane (n-C34)	0.67	0.024
9-fluorenone	0.98	0.035	hexatriacontane (n-C36)	0.86	0.031
9-methylanthracene	0.91	0.032	tetracontane (n-C40)	0.84	0.030
anthroquinone	0.48	0.017	*methyl alkane*		
1,8-napthalic anhydride	0.86	0.031	2-methylnonadecane	0.88	0.031
methylfluoranthene	0.28	0.010	3-methylnonadecane	0.94	0.034
retene	1.21	0.043	*other alkane*		
cyclopenta[cd]pyrene	0.28	0.010	pristine	0.99	0.035
benz[a]anthracene-7,12-dione	1.02	0.036	phytane	0.99	0.035
methylchrysene	0.42	0.015	squalane	1.00	0.035
			cycloalkane		
Phthalate			octylcyclohexane	0.94	0.033
dimethylphthalate	0.57	0.020	decylcyclohexane	0.70	0.025
diethyl phthalate	0.87	0.031	tridecylcyclohexane	1.32	0.047
di-n-butyl phthalate	0.46	0.016	n-heptadecylcyclohexane	0.84	0.030
butyl benzyl phthalate	0.86	0.031	nonadecylcyclohexane	0.70	0.025
bis(2-ethylhexyl)phthalate	0.75	0.027			
di-n-octyl phthalate	0.85	0.030	**Alkene**		
			squalene	0.57	0.020
			1-octadecene	0.80	0.028

Table 2-5. Continued.

Compounds	MDL (ng)	MDL (ng/m^3) [a]	Compounds	MDL (ng)	MDL (ng/m^3) [a]
Hopane			**Sterane**		
22,29,30-trisnorphopane (Tm)[b]	0.51	0.018	ααα 20R-Cholestane	0.25	0.009
αβ-norhopane (C29αβ-hopane)	0.32	0.011	αββ 20R-Cholestane	0.66	0.024
βα -norhopane (C29βα -hopane)	1.38	0.049	αββ 20S 24S-Methylcholestane[b]	0.80	0.028
αβ-hopane (C30αβ-hopane)	1.06	0.038	ααα 20R 24R-Methylcholestane[b]	0.58	0.020
βα-hopane (C30βα-hopane)	1.17	0.041	ααα 20S 24R/S-Ethylcholestane	0.78	0.028
αβS-homohopane (C31αβS-hopane)	0.84	0.030	αββ 20R 24R-Ethylcholestane	0.35	0.012
αβR-homohopane (C31αβR-hopane)	0.83	0.030	ααα 20R 24R-Ethylcholestane	0.37	0.013

[a] Assumes a sampled air Volume II8.1 m^3; i.e. 24-hr sampling at 0.113 m^3, and 3 cm^2 used in TD-GC/MS analysis

[b] Due to a lack of authentic standards (for iso-/anteiso-alkanes and a few hopanes and steranes), the organic compound concentrations are estimated by assuming the same response as the respective isomers or the respective *n*-alkanes of the same carbon number.

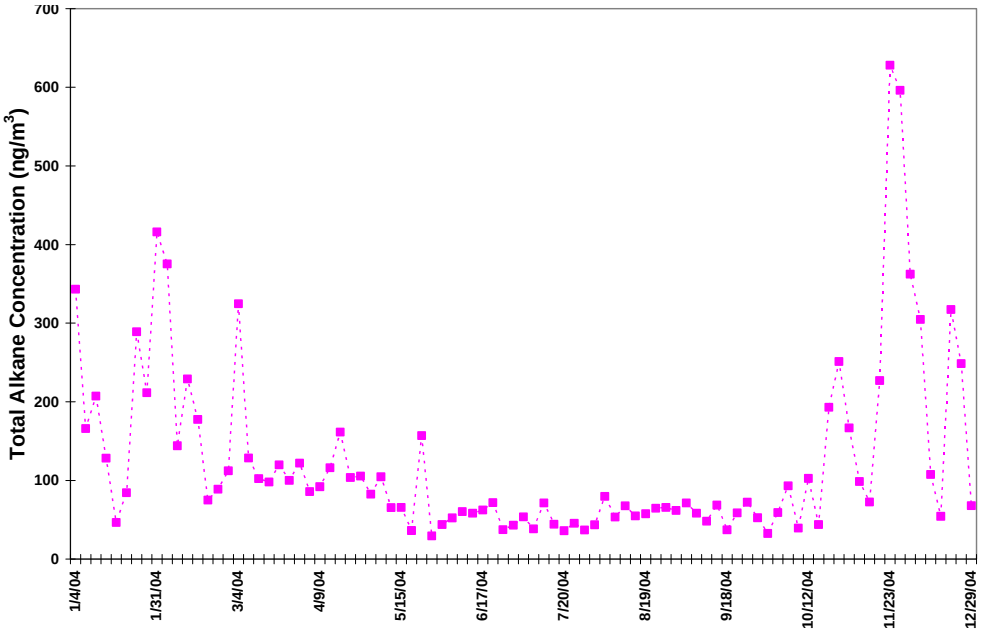

(a)

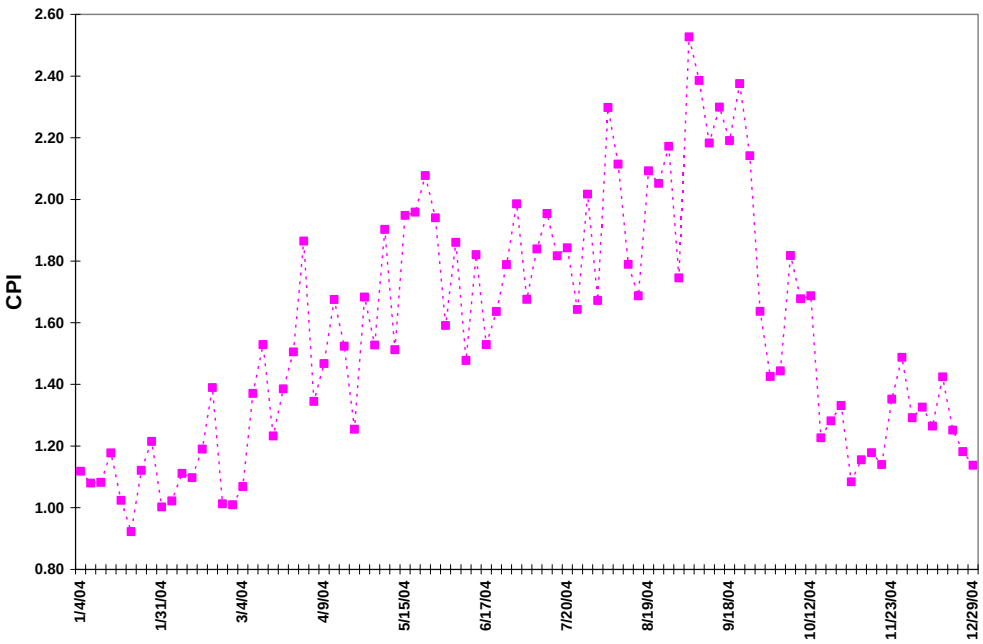

(b)

Figure 2-1. (a) Total n-alkane concentrations and (b) CPI of Fresno samples acquired from 1/4/04 – 12/29/04.

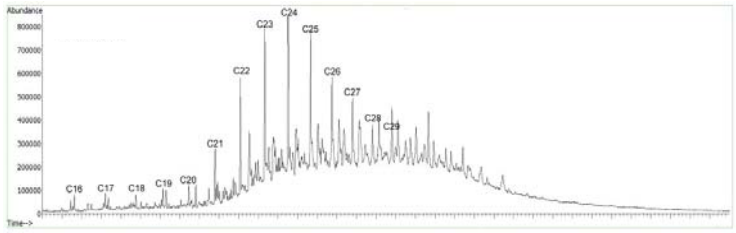

(a) Gasoline-powered vehicle emissions

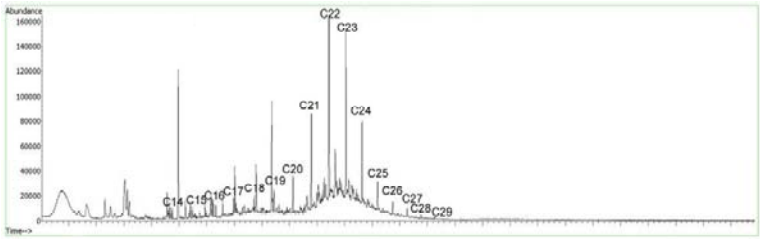

(c) Coal combustion

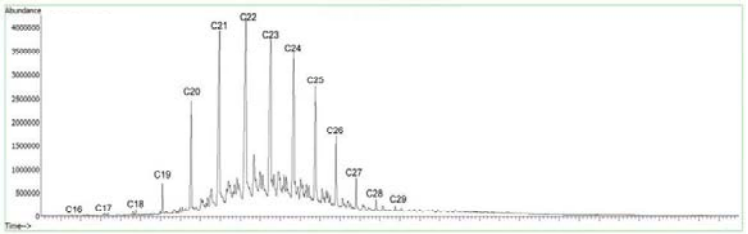

(b) Diesel-fueled vehicle emissions

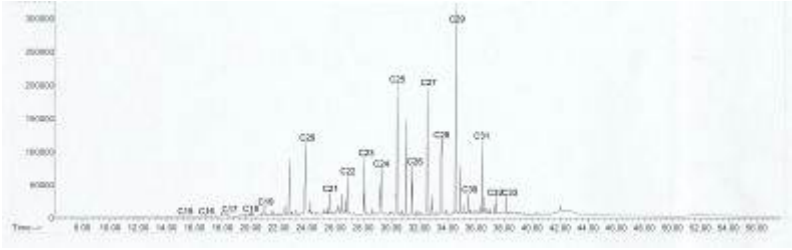

(d) Wood burning

Figure 2-2. Source profiles for: a) gasoline-powered vehicles, b) diesel-fueled vehicles, c) coal-combustion, and d) wood-burning emissions.

3. LABORATORY-GENERATED SOURCE AEROSOL MEASUREMENTS

This section summarizes the methodology employed to generate aerosols from different carbon sources and documents the source characterization experiments. It also describes the different continuous measurements that were utilized during the laboratory tests.

3.1 Establishment of Carbon Source Characterization Laboratory

A carbon source characterization laboratory has been established at DRI to facilitate Phase I method comparisons. Efforts were made to: 1) acquire laboratory space; 2) construct source-emission intakes and ventilation systems; 3) identify, procure, and test new measurement equipment; and 4) modify the dilution sampler to accommodate both real-time and integrated filter measurements. The diesel generator and wood stove were operated in a courtyard outside the laboratory with ventilation (Figure 3-1) through a high-rise stack from which part of the emissions were drawn into the dilution sampler.

The laboratory is equipped with instruments that provide real-time continuous measurement of particle mass, size distribution, b_{abs}, and BC. The setup is configured to produce variable, but reproducible, carbon loadings. It allows for tests of the OC/EC split for the same source aerosol with different optical-density levels. The instruments used in the carbon source characterization laboratory include:

a) Sampling systems:
   - Dilution sampling system (DRI, Reno, NV)
   - Particle resuspension chamber (DRI, Reno, NV)
   - Monomodal aerosol generator (DRI, Reno, NV)

b) Particle size measurements:
   - TSI nano Scanning Mobility Particle Sizer (SMPS; TSI Industries, St. Paul, MN) consisting of:
     - An electrostatic classifier (TSI 3080)
     - A differential mobility analyzer (DMA; TSI 3085)
     - An ultrafine condensation particle counter (UCPC; TSI 3025a)
   - GRIMM SMPS (GRIMM Aerosol Technik GmbH & Co., Ainring, Germany) consisting of:
     - An electrostatic classifier (GRIMM 5.500)
     - A DMA (GRIMM Middle Vienna)

- A CPC (GRIMM 5.403)

- MSP wide range particle spectrometer (WPS; MSP 1000XP; MSP Corporation, Shoreview, MN) consisting of:
  - An SMPS
  - A laser particle spectrometer (LPS)

c) Light scattering and absorption

- A DustTrak photometer for b_{scat} (TSI 8520, TSI Industries, St. Paul, MN)
- Two seven-color aethalometers for b_{abs}(7-AE, model AE31, Magee Scientific, Inc, Berkeley, CA)
- Photoacoustic analyzer for b_{abs} (PA; 1047 nm, DRI, Reno, NV)

d) Particle-bound polycyclic aromatic hydrocarbons

- PAH monitor (EcoChem PAS2000, EcoChem Analytics, League City, TX)

e) Carbon dioxide (CO_2)

- LiCor CO_2 monitor (LI-840, LiCor Environmental, Lincoln, NE)

3.2 Descriptions of Sampling Systems

3.2.1 Dilution Sampling System

The DRI dilution/residence chamber sampling system, shown in Figure 3-2, is similar in design to that of Hildemann et al. (1989). Emissions from a stack or duct are sampled through a flexible copper line (1.3 cm inner diameter [ID], 302 cm long), which is heated to 150 °C to reduce gas-phase condensation on the walls of the tubing. The sample stream passes through a venturi, following which it enters a U-tube (15 cm ID, 265 cm long) mixing chamber where it is mixed with clean dilution air at ambient temperature under turbulent flow conditions. The dilution air consists of ambient air filtered through a high-efficiency particulate air (HEPA) filter to remove particles followed by an activated charcoal bed to remove gas-phase organics. The diluted emissions are then drawn into a cylindrical residence chamber (45 cm outer diameter [OD] and 180 cm high) to simulate atmospheric aging processes and to allow for condensation, coagulation, and any rapid reactions to occur. At the end of the residence chamber, the diluted sample is withdrawn through three Bendix/Sensidyne $PM_{2.5}$ cyclones (each with a 2.5 µm cut-point at 113 liters per minute [L/min]) in parallel with each other, to a multi-port conical sampling manifold which accommodates continuous measurements and sample collection on filter-packs. At a flow rate of 339 L/min through the residence chamber, the residence time in the chamber is approximately 40 sec. The flow through the system is balanced by the total flow rate through the chamber and conical sampling manifold (339 L/min) and the flow pulled by a high-volume sampler pump (Hi-Vol, model TE5070, Tisch Environmental, Inc., Cleves, OH). The Hi-Vol pump is connected to a variable

autotransformer (Model 3PN1210B, STACO Energy Products, Co.) that controls the power delivered to the pump, thus controlling the air flow through the pump. Dilution ratios can be varied by changing the flow rate through the Hi-Vol pump. This setup was used to sample emissions from the diesel generator, acetylene flame, and wood stove.

3.2.2 Particle Resuspension Chamber

The particle resuspension chamber, shown in Figure 3-3, is described by Chow et al. (1994). It consists of eight impactor inlets (each connected to a sampling port) located in a rectangular array within a 0.4 m^3 chamber and mounted on a 76 cm x 64 cm aluminum platform. The impactors may be chosen depending on the size fraction of interest. Particles with aerodynamic diameters larger than the impactor cut-point are removed by a greased impaction plate. The smaller particles flow through a tubular aluminum diffuser (5 cm ID x 32 cm long) and are collected by the filters downstream. The flow rate through each filter is maintained constant by means of a critical orifice. The particle resuspension chamber was used to resuspend carbon black and graphite powders for collection onto Teflon-membrane and quartz-fiber filters.

3.2.3 Monomodal Aerosol Generator

To facilitate the test of powdered carbon, the monomodal aerosol generator shown in Figure 3-4 consists of:

- Nebulizer (HOPE Continuous Medication Nebulizer, P/N 11310, B&B Medical Technologies, Inc.), 200 mL capacity.
- Source of pressurized air or a pump with an in-line HEPA filter and activated charcoal.
- Neutralizer chamber with anti-static devices.

This aerosol generator requires a suitable powder-solvent matrix in which the powder will either dissolve or remain in suspension in order to generate a fine mist. The nebulizer container is filled with the sample matrix. Pressurized air is passed through a nozzle into the nebulizer container and exits immediately at the top of the container, at a right angle to its inlet. This creates a region of low pressure, which results in the suction of the sample matrix. The mixing of the sample matrix with the pressurized air and the subsequent flow through a nozzle results in the fine mist. By controlling the flow rate of pressurized air, the aerosol generation rate can be adjusted. The outlet of the nebulizer is directed through a “T” connection. One outlet of the “T” is directed into the neutralizer chamber, while the other outlet is connected to a drain in order to collect water droplets that separate from the aerosol stream. The neutralizer chamber is a cylindrical container (40.6 cm long × 6.4 cm in diameter) in which five anti-static devices (Staticmaster Ionizers, which are strips of polonium) are placed along the length of the cylinder. The

ionizers neutralize any charge on the aerosols as the air stream passes through the chamber. The complete setup is supported on a wooden base. The outlet of the neutralizer chamber was connected to a silica gel dryer 28.2 cm long × 5.67 cm in diameter (ATI Model 250), before being connected to the sampling system. This generator was used to nebulize sodium chloride (NaCl) and carbon black powders, and was operated at 69.0 kilopascal [kPa] (10 psi), which equals about 4.7 L/min.

3.3 Continuous Instruments

3.3.1 Particle Size Measurements

3.3.1a TSI nano Scanning Mobility Particle Sizer (SMPS)

The TSI nano SMPS system consists of an Electrostatic Classifier (Model 3080), a nano DMA (nDMA: Model 3085) and an UCPC: (Model 3025A). The sampled particles are charged/neutralized to a known charge distribution by the radioactive source. The charged particles enter the nDMA where they are separated by their electrical mobility. This is achieved by having the charged particles enter near the top of two concentric rods—an outer rod which is held at ground, and a center rod that has an applied voltage (which changes with time). At a given voltage, only a narrow size range of charged particles will have the correct electrical mobility to exit the nDMA through a slot in the center rod. The rest of the particles either have too small or too great a mobility, and upon striking the center rod, are neutralized and carried away with the excess flow. The nDMA changes the voltage on the center rod to allow a wide range of charged particles to exit the nDMA (one narrow size range at a time). The charged particles, after exiting the nDMA enter the UCPC. The UCPC has a heated alcohol bath (typically butanol), a condensation chamber and a counting chamber. The alcohol condenses onto the charged particles in the condensation chamber and the particles grow into larger droplets. The droplets are then counted by the detection of laser light scattered by the particle. The nano SMPS is operated at a sheath flow to aerosol flow of 10:1, with a scan-up time of 135 sec and a scan-down time of 15 sec. This yields a size range of 3 to 80 nm.

3.3.1b GRIMM SMPS

The GRIMM SMPS system consists of an Electrostatic Classifier (Model 5.500), a DMA (Model Middle Vienna DMA), and a CPC (Model 5.403). The GRIMM SMPS operates using the same principle as the TSI SMPS, also at a sheath flow to aerosol flow of 10:1. The scan-up time is 220 sec and the scan-down time is 10 sec. This yields a size range of 5 to 350 nm.

3.3.1c MSP WPS

The MSP WPS (Model 1000XP) is a SMPS and a Laser Particle Spectrometer (LPS) housed and operated together as a single unit. The SMPS operates similar to the TSI SMPS. The LPS determines the size of a sampled particle from the amount of light scattered (by the particle) and focused on to a photodetector using a system of mirrors.

Since the amount of light scattered from a particle is a strong function of its size, precise and repeatable sizing of particles is possible. The SMPS has a sheath flow to aerosol flow ratio of 10:1, with a scan-up time of 134 sec and a scan-down time of 10 sec. The SMPS has a size range of 10 to 500 nm, while the LPS has a size range of 500 to 10,000 nm. Together as a single unit, the WPS is able to measure particles from 10 nm to 10,000 nm (i.e., 10 μm). The WPS has the ability to operate the SMPS and LPS separately or together. The LPS has the capability to measure down to 350 nm, but when used in conjunction with the SMPS, the SMPS data is used up to 500 nm and the LPS data is used from 500 nm to 10,000 nm.

3.3.2 b_{scat}, b_{abs}, and PAHs

3.3.2a TSI DustTrak

The TSI DustTrak (Model 8520) uses a light-scattering laser diode to detect forward scattering (b_{scat}) of PM concentrations up to 100 mg/m^3. The laser diode has a wavelength (λ) of 780 nm, which limits the smallest detectable particle to about 0.1 μm. The aerosol sample is drawn into the sensing chamber in a continuous stream. One section of the aerosol stream is illuminated with a small beam of laser light. Particles in the aerosol stream scatter light in all directions. A lens collects a portion of the scattered light and focuses it onto the photodetector. The detection circuitry converts the light into voltage. This voltage is proportional to the amount of scattered light, which in turn, is proportional to the mass concentration of the aerosol. Using an internal calibration factor, the voltage signal is converted to mass concentration, but this varies depending on particle size and composition.

3.3.2b Magee Aethalometer

The seven-color (7-AE; λ=370, 470, 520, 590, 660, 880, and 950 nm) aethalometer (Hansen et al., 1984; Arnott et al., 2005a) samples particle-laden air through a quartz-fiber filter tape. As the particles are collected onto the filter, the change in light transmission through the filter tape is continuously monitored and is used to calculate BC concentration. The filter tape is automatically advanced when its optical density attains 0.75. The light attenuation is converted to a BC mass concentration, using a σ_{abs} (m^2/g) of 14,625/λ, where λ is in nm. For the laboratory experiments, the 7-AE was set to report 2-min average BC concentrations. The aethalometer measurements (and the results reported here) do not include corrections for filter loading, light scattering by filter matrix, or by aerosols, as those in a PSAP (Bond et al., 1999).

3.3.2c DRI Photoacoustic Analyzer

The photoacoustic analyzer (PA) measures in-situ b_{abs} at 1047 nm (Arnott et al., 1999; 2003; 2005b). The PA consists of a modulated laser beam that is at the acoustic resonance frequency of the PA. The particles in the air sample absorb the laser beam resulting in the heating of the surrounding air. The heated air expands, producing a sound

(acoustic) wave at the same frequency as the laser modulation. This acoustic signal is detected by a calibrated microphone, to determine b_{abs} (Mm^{-1}). During these experiments, the PA reported 1-sec data. An empirical σ_{abs} of 5 m^2/g for the 1047 nm was applied to convert PA b_{abs} to BC concentration, based on comparison samples from IMPROVE EC and PA BC measurements of diesel emissions (Arnott et al., 2000; 2005b).

3.3.2d EcoChem PAS 2000

The EcoChem PAS 2000 monitor measures particle-bound PAH concentration. An excimer lamp produces ultraviolet (UV) radiation (λ = 225 nm) that photo-ionizes the sampled particles, while minimizing the ionization of gas molecules. The charged particles are collected on a filter element mounted in a Faraday cage. The electric current, measured with an electrometer, is proportional to the concentration of particle-bound PAHs, weighted according to an average ionization response. The flow rate is maintained at 2.0 L/min by a mass flow meter.

3.3.3 LiCor LI-840

The LI-840 CO_2/H_2O Gas Analyzer is a non-dispersive, infrared (NDIR) gas analyzer based upon a single path, dual wavelength, infrared (IR) detection subsystem. The CO_2 and H_2O measurements are a function of the absorption of IR energy as it travels through the optical path. Concentration measurements are based on the difference ratio in the IR absorption between a reference and sample signal. The CO_2 sample channel uses an optical filter centered at 4.26 μm, corresponding to the absorption band for CO_2. The reference channel for CO_2 has an optical filter centered at 3.95 μm, which has no absorption, due to CO_2. The H_2O sample channel uses an optical filter centered at 2.595 μm, corresponding to the absorption band of H_2O. The reference channel for H_2O has an optical filter centered at 2.35 μm, which is outside the absorption band of H_2O. The LiCor instrument was used only during the wood combustion experiments.

3.4 Sources

The sources tested in this study included: 1) an Onan Cummins diesel generator; 2) acetylene flame; 3) an electric arc generator (PALAS GFG-1000 with graphite rods); 4) wood smoke (white oak) from a wood-burning stove; 5) carbon black (Cabot Corporation), and 6) graphite powders (Fisher Scientific). A summary of the source-sampling matrix for a total of 159 samples (including dynamic blanks), is shown in Table 3-1 and Figure 3-5. A complete list of all source characterization tests is included in Appendix D.

The combustion sources (diesel, acetylene, electric arc and wood smoke) were tested in two different modes: 1) pure combustion aerosol, and 2) combustion aerosol mixed externally with 0.01 to 0.1 molar (M) NaCl (Fisher Scientific). Emissions from the diesel generator, acetylene flame, and wood smoke were sampled through the DRI dilution/residence chamber system (Figure 3-2). Soot from the electric arc generator was sampled through a miniature dilution/residence chamber (53 cm long x 15 cm in

diameter) as shown in Figure 3-6. Figure 3-7 shows the sample flow configuration for continuous monitoring instruments and filter sample collection. For mixed aerosol tests, the combustion aerosol generated by these sources were mixed with a nebulized solution of NaCl, introduced after the source aerosol enters the U-tube mixing chamber of the DRI dilution/residence chamber sampling system. The NaCl solution was nebulized using the DRI aerosol generator and introduced into the U-tube mixing chamber, immediately after the granular activated carbon packing, using a T-connection. Carbon black and graphite powders were sampled using the resuspension chamber following methods described by Chow et al. (1994). Attempts were also made at suspending carbon black powder in methanol and nebulizing it using the DRI monodisperse aerosol generator. However, test reproducibility could not be achieved within ±50%, in terms of aerosol generation rate and the mass loading on the filter. Descriptions of sampling configuration for each source type are given below.

3.4.1 Diesel Generator

The diesel generator used in this study was an Onan Cummins 12.5 kW diesel generator equipped with a Simplex Swifte Plus load bank. The diesel generator was operated at a load of 4 kW (about 32% of the maximum load). The generator oil, fuel, and air filter were replaced before the start of this study, at which point, the generator had an accumulated 2,500 hours of runtime. Figure 3-8 illustrates the setup used for sampling emissions from the diesel generator.

The diesel generator (Figure 3-8a) was allowed to run for at least one hour at the 4 kW load before sampling. A portion of the exhaust (varied between 13 to 25 L/min) was drawn into the dilution tunnel system through a heated sampling line (maintained at 150 °C, Figure 3-8b) and venturi (maintained at 150 °C). The dilution ratio was set to one of the following four values: 18, 40, 80, or 150 to 165, and six, seventeen, nine and three filter sets (Teflon-membrane filter and quartz-fiber filter) were collected, respectively. In addition to the pure diesel source samples, a mixture of the diesel exhaust and a nebulized solution of NaCl (0.1 Molar) were collected at dilution ratios of 18 (three filter sets) and 40 (six filter sets). Sample collection duration was either 20 or 60 min.

3.4.2 Acetylene Flame

Soot from an acetylene flame was generated using a torch with a #1 level tip. Acetylene gas from a cylinder (welding grade) was delivered at 34.5 kPa (5 psi). The torch was lit inside a fume-hood and had no O_2 added other than that present in the surrounding air. The flame length was adjusted to approximately two inches. A small "computer fan" was positioned to blow air at the flame so as to break down the agglomerating soot particles. The generated soot was vented into the fume-exhaust. A portion of the flow was sampled from the exhaust ducting into the DRI dilution/residence chamber system through a 168-cm long black conductive tubing (Figure 3-9).

The dilution ratio was held constant (17) for all acetylene flame tests. Various mass loadings on filters were achieved by varying the sampling duration (20, 40, and 70 min). Ten filter sets were collected with the pure acetylene flame and nine filter sets were collected with a mixture of acetylene flame and a nebulized solution of NaCl (0.05 Molar).

3.4.3 Electric Arc Soot Generator

The PALAS (Model GFG-1000) electric arc soot generator (Figure 3-10) produces ultrafine graphite particles (<100 nm in electrical mobility diameter) by spark discharge between two graphite rods. An argon (Ar) gas stream is used to carry the ultrafine particles out of the spark discharge cell to prevent oxidation. For this study, the electric arc generator used pure graphite rods at current readings of 950 and 300 arbitrary units (a.u.), which corresponded to sparking frequencies of 275 Hz and 75 Hz, respectively. The Ar was delivered at 1.3 bar (130 kPa) pressure. The particles were carried into a miniature dilution/residence chamber (Figures 3-6 and 3-11). Air, passed through a HEPA filter and an activated-charcoal bed, was introduced into this chamber to dilute the aerosol stream. The miniature dilution/residence chamber was connected to a conical sampling manifold for sample collection (Figure 3-11).

Initial experiments were carried out without the use of the conical sampling manifold, i.e., the instruments were connected to the bottom of the cylindrical chamber. Nine sets of filter samples (Teflon and quartz) were collected using in-line Salvellex filter holders (with the impactor removed) connected to the chamber with 0.64 cm (¼ inch) conductive tubing. However, upon carbon analysis by IMPROVE_A, it was found that the center of the filter had more particulate deposit than the edge of the filter (see Section 5.3.1). This configuration with in-line filter holders, at the flow rate of 10 L/min, did not allow enough time for the flow to homogenize, resulting in an inhomogeneous deposit. Thus, these experiments were rerun using the conical sampling manifold (Figures 3-6 and 3-11) to ensure a homogeneous deposit on the filters.

The dilution ratio was held constant (8) for all of the electric arc experiments. Ten and three filter sets were collected using the conical sampling manifold setup for current settings of 950 a.u. and 300 a.u., respectively. A mixture of electric arc-generated graphite particles and a nebulized NaCl (0.01 Molar solution) was also tested. The two aerosols were mixed prior to their entrance to the miniature dilution/residence chamber. Six and three filter sets were collected at the current settings of 950 a.u. and 300 a.u., respectively. Different mass loadings (209 to 755 μg/filter) were achieved by varying the sampling duration (20 and 40 min). No preceding $PM_{2.5}$ inlet was used for the electric arc filter sets. However, the particle size distribution measurements (see Section 5.4.3 and Figure 5-12) indicate that these particles were less than 400 nm in electrical mobility diameter, suggesting that all samples collected were below $PM_{2.5}$ size range.

3.4.4 Wood Smoke

Vegetative burning emissions were simulated by burning white oak wood, the most commonly burnt hardwood in RWC (McDonald et al., 2000). Figure 3-12 illustrates the setup of the wood stove used to burn the wood. Firebricks (each 1.5 inch [3.8 cm] thick) were placed on the bottom and on three sides of the wood stove. The fire was started with black print newspaper. Additional kindling was added using chopped pieces of pine and white oak. Six small pieces of white oak wood, with moisture content ranging between 8 and 22%, and constituting a total weight of four to five pounds (1.8 to 2.3 kilograms [kg]) were added and allowed to burn with the woodstove door open for about 10 min (Figure 3-12b), after which the door was closed. A portion of the exhaust was pulled into the dilution tunnel system through a heated copper line (maintained at 150 °C) and venturi (maintained at 150 °C) (Figures 3-2 and 3-12c). Sample collection on filters was started approximately three min after the wood stove door was closed. Each filter collection lasted 20 to 25 min. After the test was over (typically 20 or 25 min), the woodstove was allowed to cool down until the exhaust temperature was below 170 °C. At this time, the wood stove was opened and the remaining coals (burnt wooden pieces) were broken down. For the next set of filter samples, five to six new pieces of white oak were added and fire was started similar to the previous cycle.

Eight, seven, and eight filter sets were collected at dilution ratios of 18, 40, and 105 to 120, respectively. Also, filter sets were collected with a mixture of wood smoke and a nebulized solution of NaCl (0.05 Molar) at dilution ratios of 18 (seven filter sets) and 40 (seven filter sets).

3.4.5 Carbon Black Powder

The Cabot Carbon Black sample (M-700 grade) was tested in two different ways. The first method consisted of a (dry) resuspension (Figure 3-3) following methods described by Chow et al. (1994). Nine $PM_{2.5}$ filter sets were collected at different mass loadings, ranging from 155 to 1021 μg/filter.

The second approach consisted of suspending the Carbon Black in a solution of 95% deionized-distilled water (DDW) and 5% methanol via sonication for 12 min. The resulting solution was nebulized using the DRI aerosol generator and introduced into the miniature dilution chamber (Figure 3-6). For the nebulized method, three filter sets were collected without preceding inlets. It is expected that samples acquired by the nebulized method are within the $PM_{2.5}$ size range, as indicated by the particle size distribution measurements (electrical mobility diameter less than 400 nm, see Section 5.4.5 and Figure 5-14).

3.4.6 Graphite Powder

The graphite powder (Fisher Scientific) was resuspended (Figure 3-3) using the method developed by Chow et al. (1994). Nine $PM_{2.5}$ filter sets were collected, with mass

loadings ranging from 96 to 1,547 μg/filter. The graphite powder was also tested using the DRI aerosol generator. However, the graphite powder did not suspend well in any methanol-DDW mixture.

3.4.7 Source Blanks

Source blank samples were collected for each experimental configuration. The following terminologies are used to represent the different types of blank samples that were collected:

- Dilution sampling system blank: This blank corresponded to the setup used for diesel, acetylene, and wood smoke experiments (Figure 3-2). It consisted of HEPA-filtered air passed through activated charcoal into the DRI dilution/residence chamber.

- Electric arc blank: This blank corresponded to the setup used for electric arc soot generator tests (Figure 3-6). It consisted of 1.3 bar (130 kPa) of Ar flowing through the electric arc soot generator, with the electric current turned off in the electric arc generator (i.e., no soot generation), which was then passed through the miniature dilution/residence chamber. The rest of the make-up flow used HEPA-filtered air passed through activated charcoal, through the cylindrical chamber and the conical sampling manifold, onto the filters.

- Nebulizer blank: This blank corresponded to the setup used for trial experiments in resuspending carbon black (Figure 3-6) using methanol-DDW matrix. A solution of 10% methanol and 90% DDW, was nebulized using the DRI aerosol generator, using compressed air delivered at 69.0 kPa (10 psi). The nebulized aerosol was passed through the cylindrical chamber, with the rest of the make-up flow consisting of HEPA-filtered air passed through activated charcoal.

Three dilution sampling system blanks were collected with durations of 2 hours, 1 hour, and 45 min. Three electric arc blanks were collected for durations of 20 min each. One nebulizer blank was collected for 45 min. The average dilution sampling system blank was used to correct diesel, acetylene and wood smoke samples. The mean electric arc blank was applied to all electric arc soot generation experiments. The nebulizer blank was applied to the nebulized carbon black experiments. Although the nebulized carbon black experiments used a matrix of 5% methanol/95% DDW, it was assumed that the 10% methanol/90% DDW blank would be valid.

3.5 Source Sample Filter Chemical Analyses

The Teflon-membrane filters were analyzed for mass by gravimetry, for b_{abs} by transmission densitometry (Tobias Associates, Inc., Ivyland, Pennsylvania), and for 40 elements (Na to U; see Table 2-2) by energy dispersive XRF (Dzubay, 1977; Watson et al., 1999). The front quartz-fiber filters were analyzed for water-soluble chloride (Cl^-),

NO_3^-, $SO_4^=$, NH_4^+, Na^+ and K^+ by IC (Mulik et al., 1976; Chow and Watson, 1999) using two to three ~0.5 cm^2 punches. A smaller portion of filter aliquot was used to preserve the samples for future analyses.

The front and back-up quartz-fiber filters were analyzed for OC and EC following the IMPROVE_A (Chow et al., 1993; 2001; 2004a) TOR/TOT protocol. Selected front quartz-fiber filters were analyzed by the STN_TOT (Peterson and Richards, 2002) and the Cachier French two-step (Cachier et al., 1989a; 1989b) protocols. In the IMPROVE_A protocol, a ~0.5 cm^2 punch of the quartz-fiber filter is heated in successive steps to 140 °C (OC1), 280 °C (OC2), 480 °C (OC3) and 580 °C (OC4) in a 100% He environment and 580 °C (EC1), 740 °C (EC2) and 840 °C (EC3) in 98% He/2% O_2. The analysis advances from one temperature step to the next, when a well-defined carbon peak has evolved, with a restriction of a minimum of 150 sec and a maximum of 580 sec at each temperature step. The evolved carbon is oxidized to CO_2 and then reduced to methane (CH_4), which is then detected by a flame ionization detector (FID). The correction for charred or pyrolyzed OC (OP) is done by monitoring the reflectance (TOR) and transmittance (TOT) of the 632.8 nm laser. The portion of EC1 before the laser returns to its initial baseline signal is assigned to OP.

The STN_TOT protocol (Peterson and Richards, 2002) heats the filter punch successively to 310 °C (OC1), 480 °C (OC2), 615 °C (OC3) and 900 °C (OC4) in 100% He environment for OC determination and 600 °C (EC1), 675 °C (EC2), 750 °C (EC3), 825 °C (EC4) and 920 °C (EC5) in 98% He and 2% O_2 environment for EC determination. The residence time of the sample is 60 sec at OC1, OC2 and OC3 temperature steps, and 90 sec at OC4. For the STN EC fractions, the sample residence time is 45 sec at EC1 to EC4 temperature steps and 120 sec at EC5. The portion of EC1 before the laser returns to its initial baseline transmittance signal is assigned to OP.

In the original French two-step protocol (Cachier et al., 1989a; 1989b), the filter punch is heated in 100% O_2 environment at 340 °C for two hours (pre-combustion step). The punch is then analyzed at 1,100 °C in 100% O_2 for ~ 600 sec to determine the refractory carbon content using coulometric titration of CO_2. The pre-combustion step removes OC, while the second step quantifies the amount of EC. The TC content is determined by analyzing a second punch. OC is obtained by the difference between TC and EC. This method was modified to accommodate the DRI Model 2001 carbon analyzer. One analyzer was set-up for the pure O_2 pre-combustion step, with the flow bypassing the reduction oven and the FID. A second analyzer was used to quantify the remaining EC by the IMPROVE_A protocol. Since the DRI Model 2001 analyzers use a reduction oven that is contaminated in a pure O_2 environment, a second analyzer was used for EC analysis. Thus, an ~0.5 cm^2 punch was heated in the first analyzer at 340 °C in 100% O_2 at flow of 10 cm^3/min for two hours at atmospheric pressure, then analyzed immediately by the IMPROVE_A protocol (in a different analyzer) to determine the remaining carbon content. This represents the EC concentration. Another punch is analyzed using the IMPROVE_A protocol to determine TC.

Table 3-1. Source-sampling matrix.

Source	Pure Source # of filter sets	Pure + NaCl # of filter sets	NaCl Conc. (Molarity)	Sampling duration (min)	Filter Flow Rate (L/min) Teflon	Fitler Flow Rate (L/min) Quartz	Dilution Ratio	b_{abs} (Mm^{-1})[a]	Filter Mass Loading (µg/filter)[a]	Samping Conditions
Diesel Generator	3	-	-	60	40	40	150 - 165	340-370	180-230	Diesel Generator @ 4kW, old copper sampling line
	5	-	-	20	40	40	80	760-900	170-200	Diesel Generator @ 4kW
	4	-	-	60	40	40	80	800-960	550-600	Diesel Generator @ 4kW
	3	-	-	20	40	40	40	770-830	160-170	Diesel Generator @ 4kW; old copper sampling line
	6	3	0.1	20	40	40	40	1070-1200	240-270	Diesel Generator @ 4kW
	3	-	-	60	40	40	40	740-840	470-510	Diesel Generator @ 4kW; old copper sampling line
	5	3	0.1	60	40	40	40	1000-1250	700-800	Diesel Generator @ 4kW
	6	3	0.1	60	40	40	18	1280-1500	880-1020	Diesel Generator @ 4kW
Acetylene	4	3	0.05	20	40	40	17	1500-1600	310-370	Acetylene Flame ~2"
	3	3	0.05	40	40	40	17	1440-1630	630-650	Acetylene Flame ~2"
	3	3	0.05	70	40	40	17	1180-1330	960-1010	Acetylene Flame ~2"
Electric Arc	1	-	-	45	10	10	8	3180	1180	Electric Arc @ 950 a.u. current, 1.3 bar Ar, no sampling cone
	5	-	-	20	10	10	8	205, 230, 1730-1900	350-500	Electric Arc @ 950 a.u. current, 1.3 bar Ar, no sampling cone
	3	-	-	40	10	10	8	1740-1800	640-670	Electric Arc @ 950 a.u. current, 1.3 bar Ar, no sampling cone
	5	3	0.01	20	10	10	8	2100-2550	350-380	Electric Arc @ 950 a.u. current, 1.3 bar Ar
	5	3	0.01	40	10	10	8	2080-2300	620-670	Electric Arc @ 950 a.u. current, 1.3 bar Ar
	3	-	-	60	10	10	8	700-770	320-350	Electric Arc @ 300 a.u. current, 1.3 bar Ar
	-	3	0.01	20	10	10	8	-	-	Electric Arc @ 300 a.u. current, 1.3 bar Ar
Wood Smoke	4	-	-	20	10	10	110 - 120	190-380	30-100	White oak, 6 pieces, 4-5 lbs per load, 1 load per filter
	4	-	-	20	25	25	105	20-220	70-125, 630	White oak, 6 pieces, 4-5 lbs per load, 1 load per filter
	7	7	0.05	25	40	40	40	100-320	120-330	White oak, 6 pieces, 4-5 lbs per load, 1 load per filter
	8	7	0.05	25	40	40	18	30-100	10-130	White oak, 6 pieces, 4-5 lbs per load, 1 load per filter
Carbon Black	3	-	-	70, 120, 120	10	10	75	100-170	20-30	Nebulized solution of Carbon Black (0.1g in 200ml (5% Methanol, 95% DDW))
	3	-	-	-	9	10	-	-	150-180	Dry Resuspension
	3	-	-	-	9	10	-	-	450-540	Dry Resuspension
	3	-	-	-	9	10	-	-	980-1020	Dry Resuspension
Graphite	3	-	-	-	9	10	-	-	100-150	Dry Resuspension
	3	-	-	-	9	10	-	-	400-520	Dry Resuspension
	3	-	-	-	9	10	-	-	1160-1550	Dry Resuspension
Blanks	3	-	-	20,60,120	40	40	-	<4	10-20	Dilution Sampling System Blank
Blanks	3	-	-	20	10	10	-	<1	0	Electric Arc Blank, 1.3 bar Ar
Blanks	1	-	-	45	10	10	-	<1	10	Neulizer Blank: 10% Methanol, 90% DDW

[a] b_{abs}, Filter Mass Loading are based on the pure sample filter sets only.

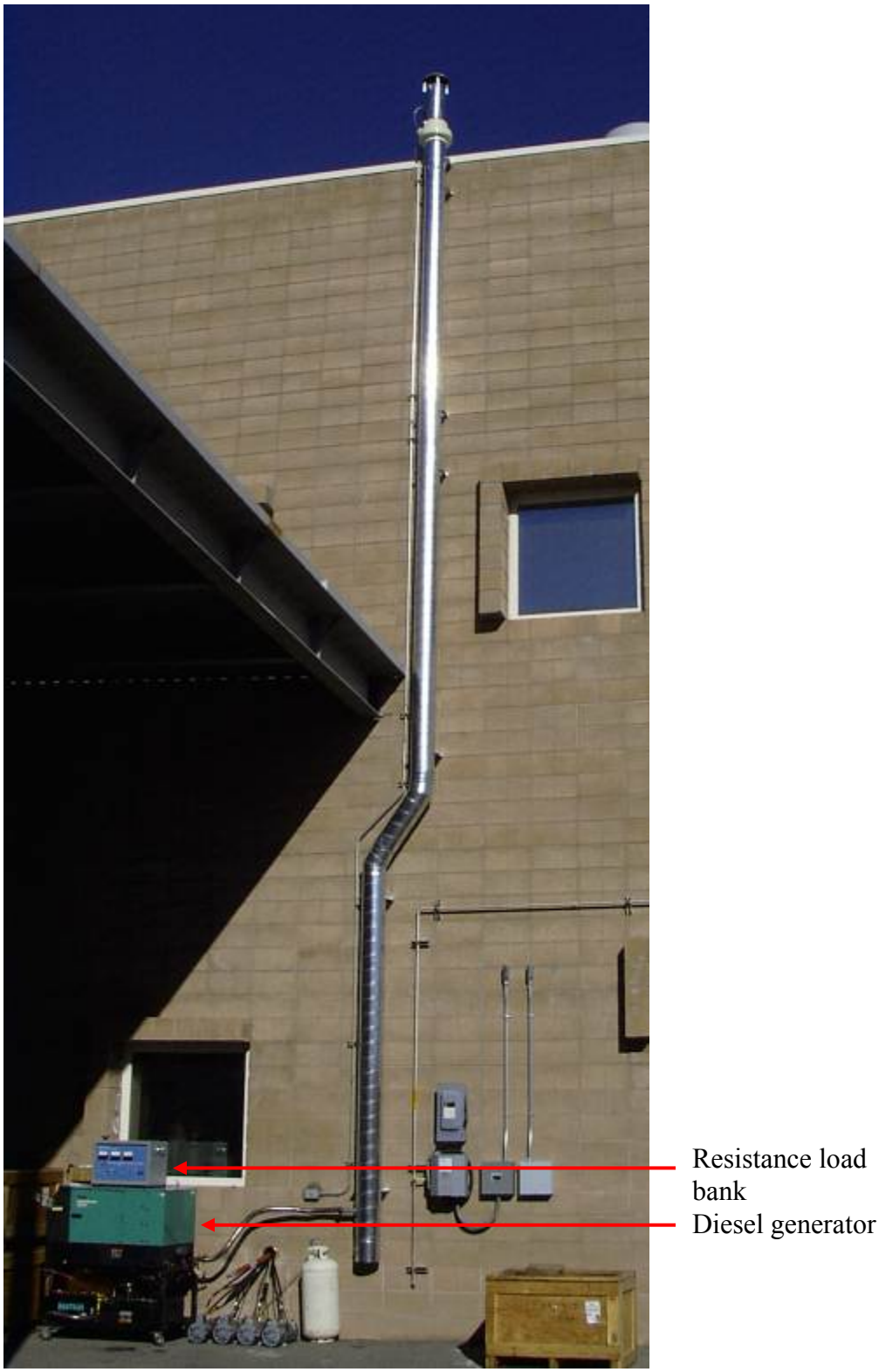

Figure 3-1. Ventilation stack for source emissions. The diesel generator with resistance load bank is shown.

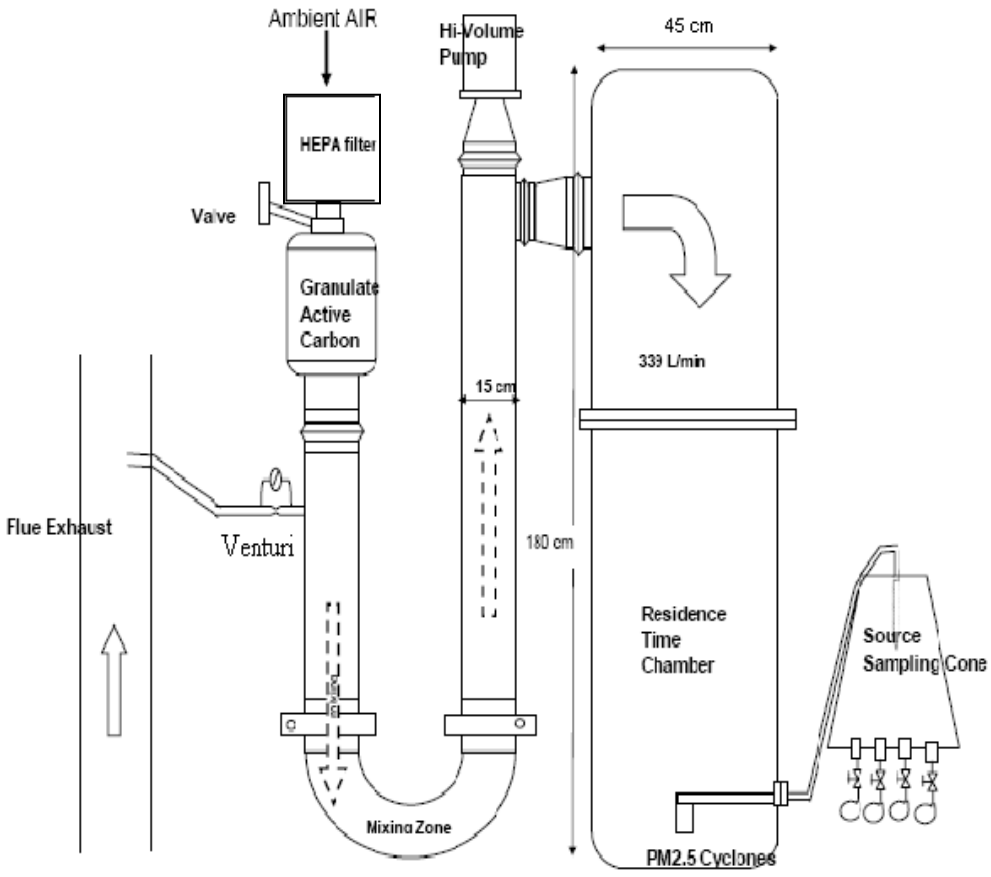

Figure 3-2. Schematic of the DRI dilution/residence chamber sampling system, used for sampling emissions from the diesel generator, acetylene flame, and wood smoke.

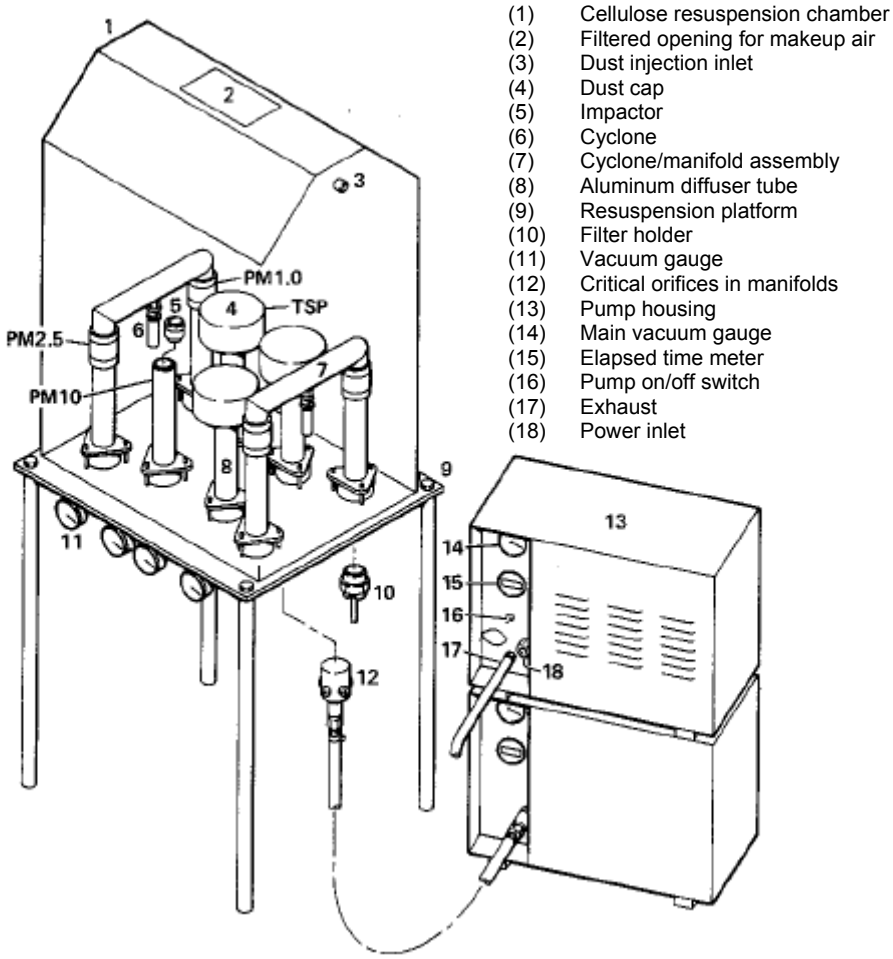

(1) Cellulose resuspension chamber
(2) Filtered opening for makeup air
(3) Dust injection inlet
(4) Dust cap
(5) Impactor
(6) Cyclone
(7) Cyclone/manifold assembly
(8) Aluminum diffuser tube
(9) Resuspension platform
(10) Filter holder
(11) Vacuum gauge
(12) Critical orifices in manifolds
(13) Pump housing
(14) Main vacuum gauge
(15) Elapsed time meter
(16) Pump on/off switch
(17) Exhaust
(18) Power inlet

Figure 3-3. DRI particle resuspension chamber (Chow et al., 1994), used for sampling carbon black and graphite powders.

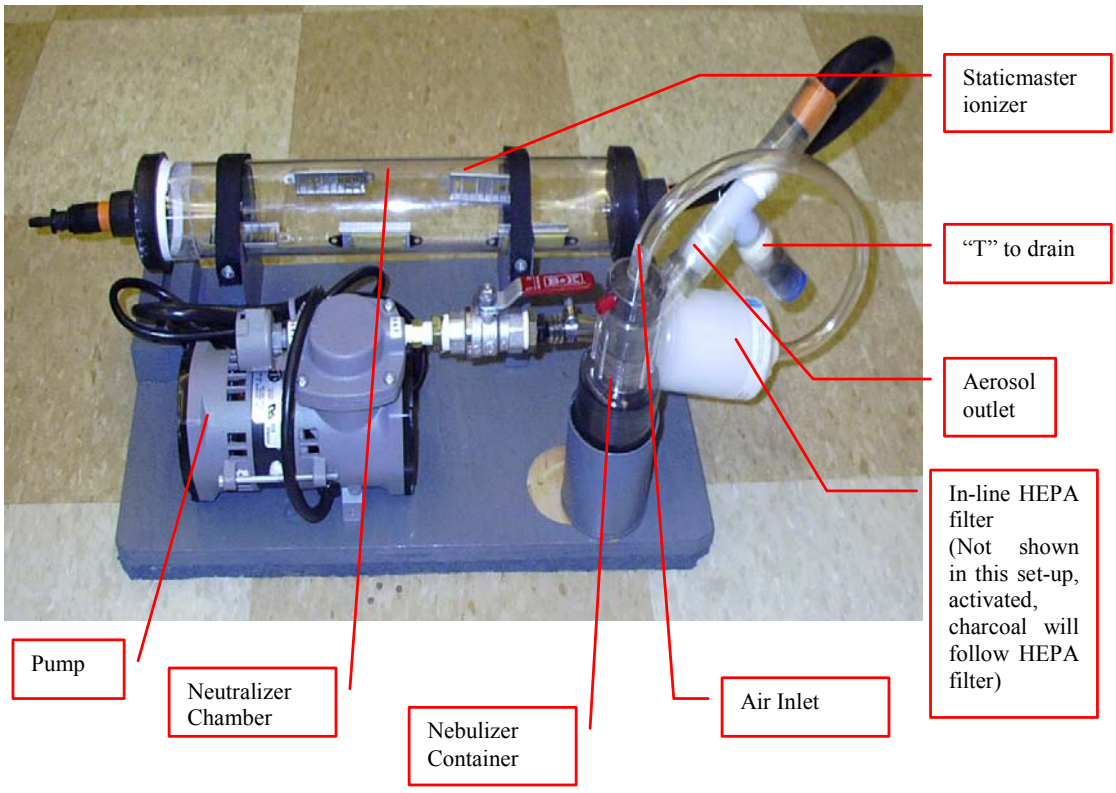

Figure 3-4. DRI Monomodal Aerosol Generator.

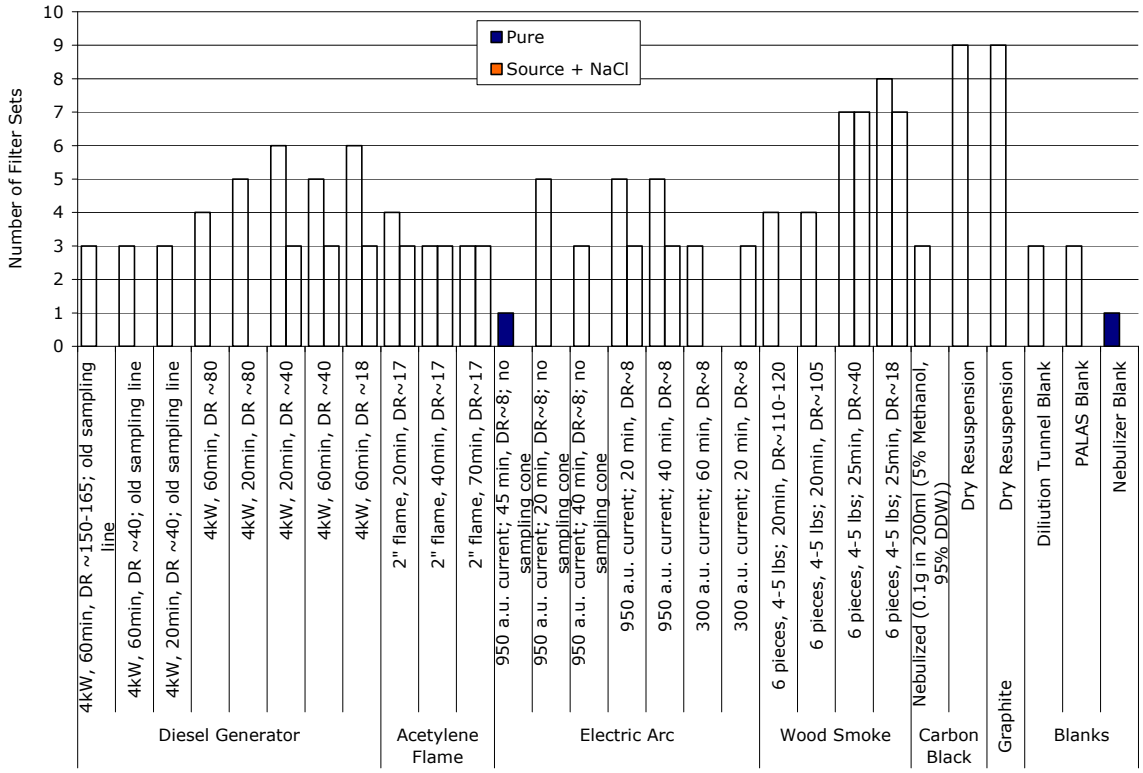

Figure 3-5. Source tests, descriptions, and number of samples.

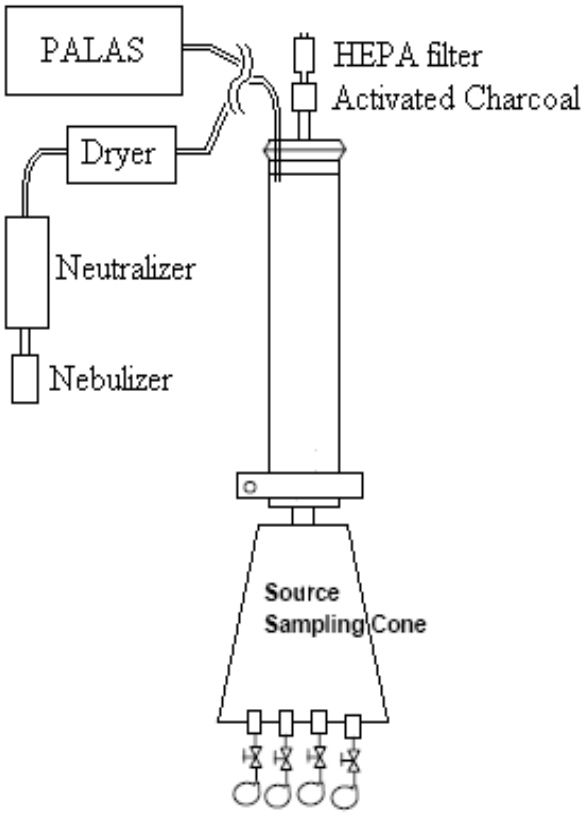

Figure 3-6. Sampling setup for the electric arc and carbon black experiments.

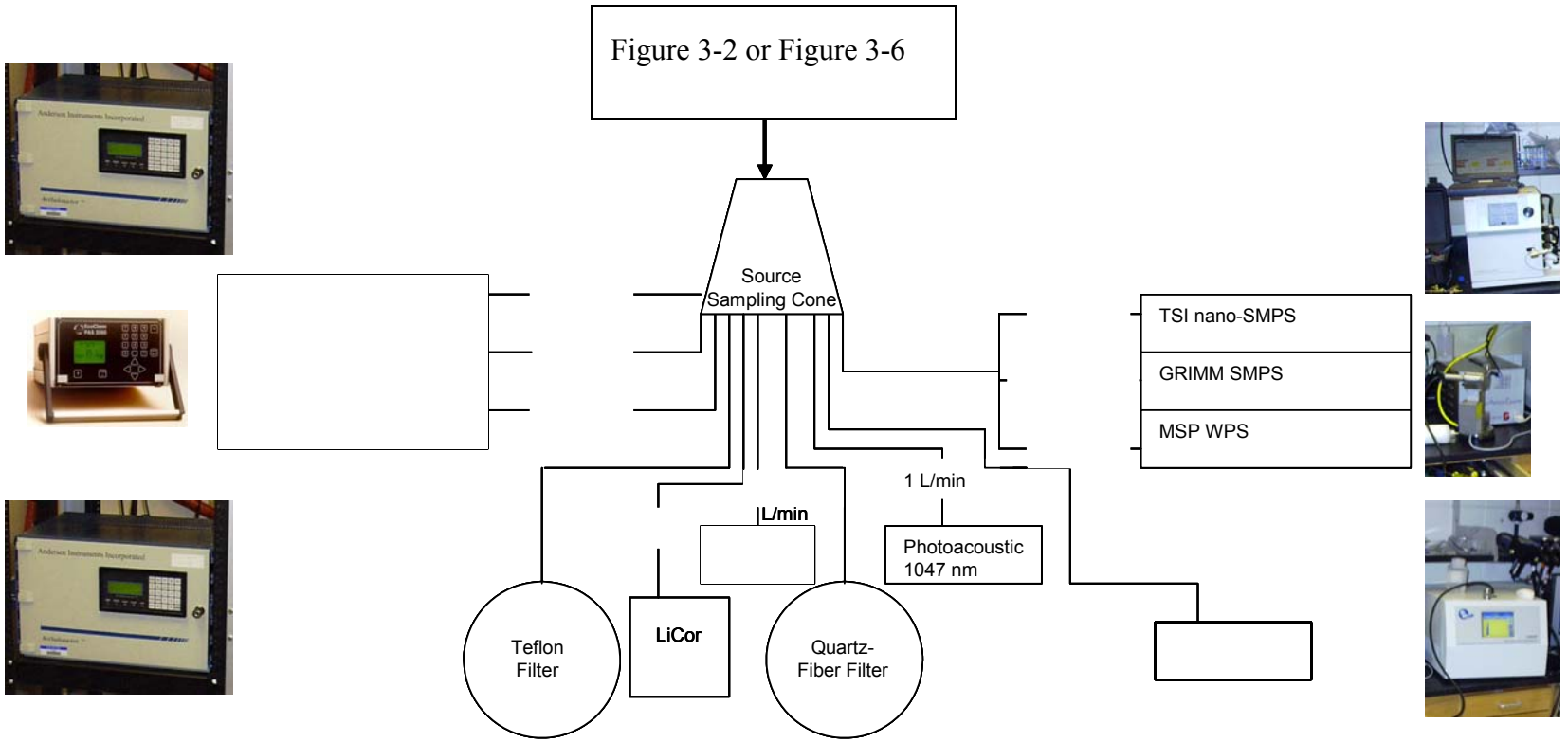

Figure 3-7. Configuration of measurements and filter sample collection.

(a)

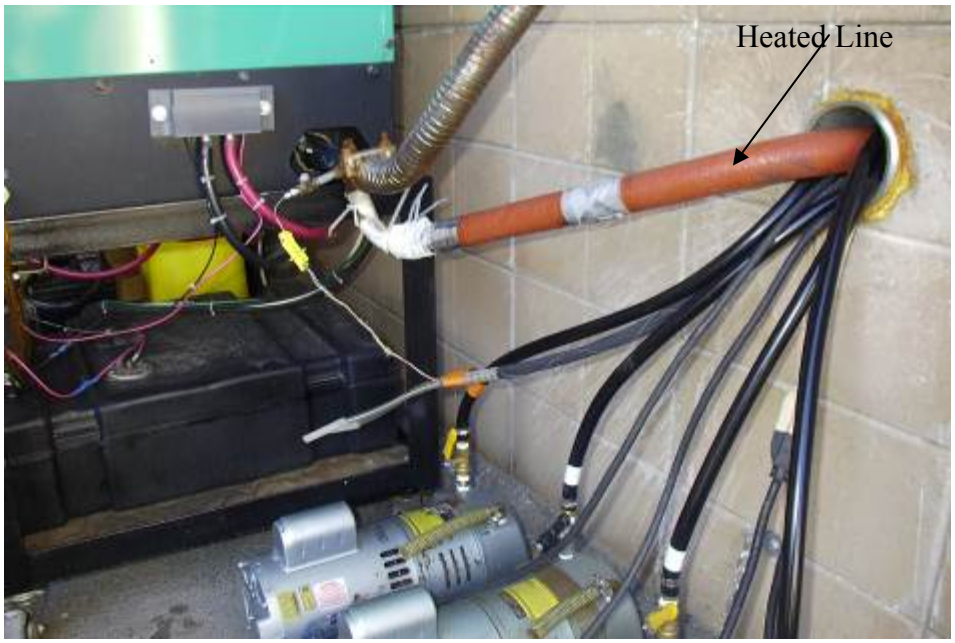

(b)

Figure 3-8. The diesel generator: (a) Diesel generator and engine load controller; (b) exhaust from the diesel generator being sampled through a heated line.

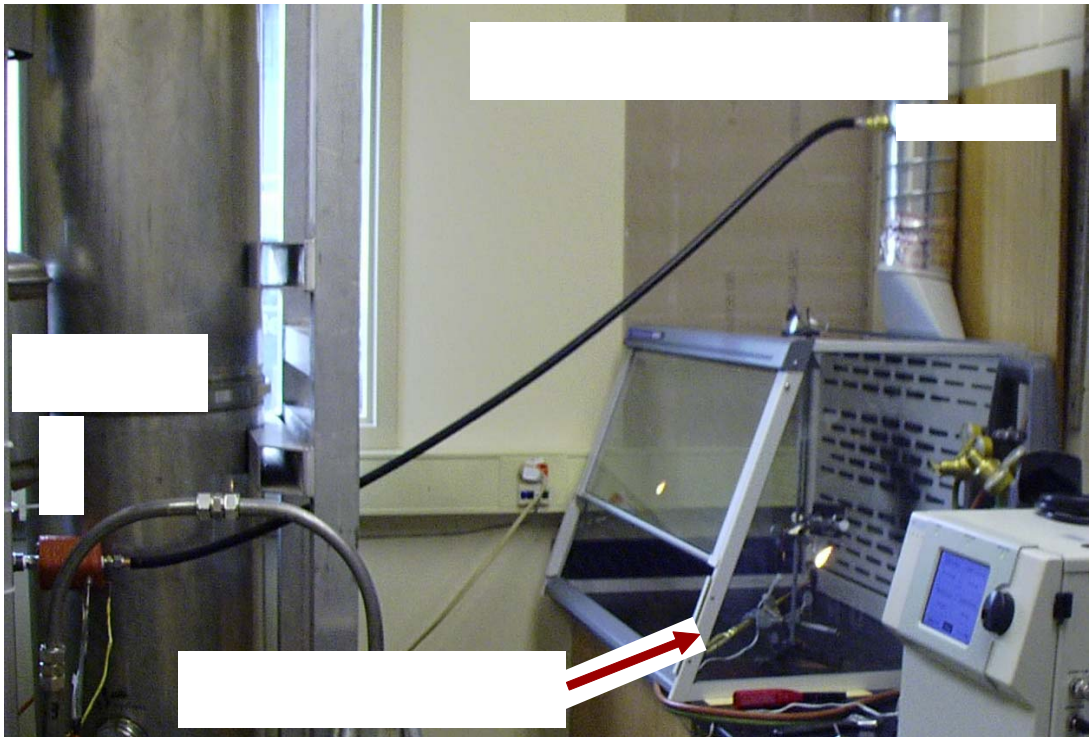

Figure 3-9. Experimental setup for sampling acetylene flame.

Figure 3-10. PALAS electric arc soot generator.

Figure 3-11. PALAS electric arc soot generator experimental setup showing the instrument rack, the miniature dilution/residence chamber with dilution air through an in-line HEPA filter and activated charcoal, and the conical sampling manifold.

(a)

(b)

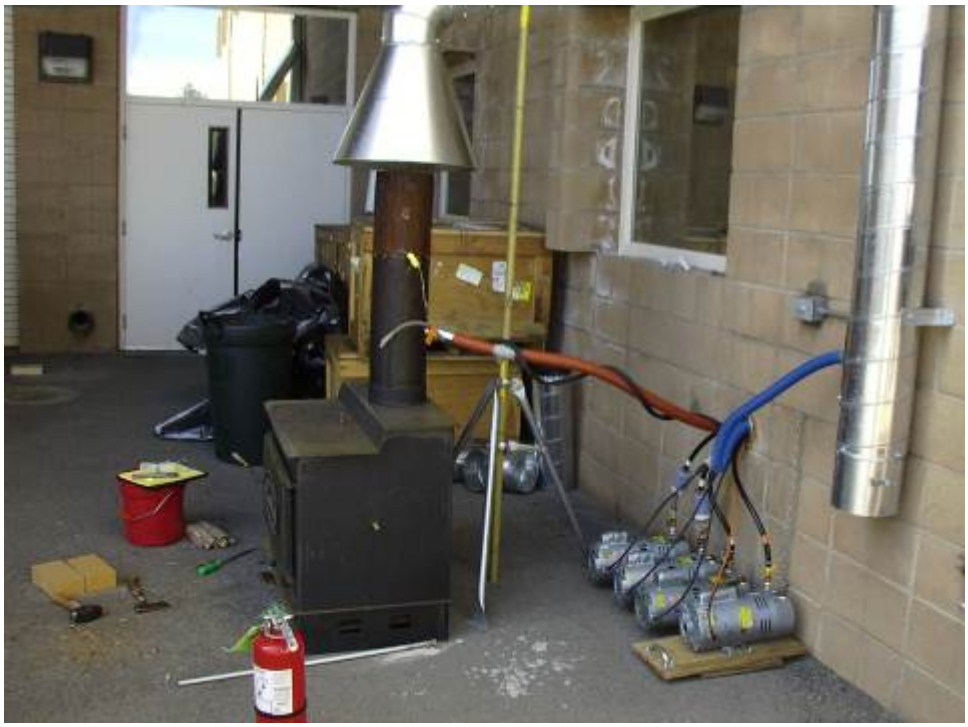

(c)

Figure 3-12. Setup of wood stove: (a) with exhaust vented to stack; (b) showing fire with door open; and (c) with emissions being sampled through a heated copper line connected to the wood stove vent.

4. AMBIENT MEASUREMENTS

This section describes the continuous and integrated measurements conducted during the summer and winter intensive operating period (IOPs) at the Fresno Supersite.

4.1 Site Description

The Fresno Supersite, located at 3425 First Street, Fresno, CA, (coordinates 119.7727725 °W and 36.78184232 °N) is situated in California's San Joaquin Valley (SJV). First Street is a four-lane artery with moderate traffic levels. Fresno is influenced by emissions from different sources, including on-road and non-road mobile sources, RWC, cooking and agricultural sources; and their relative contributions differ among seasons (Watson et al., 2000a). The Fresno Supersite is approximately 5.5 km north-northeast of the downtown commercial district and is surrounded by commercial buildings, churches, restaurants, schools, and residential areas.

Historical data show that $PM_{2.5}$ mass concentrations at Fresno typically exceed the 24-hr average (65 $\mu g/m^3$) and annual average (15 $\mu g/m^3$) national ambient air quality standards (NAAQS) for $PM_{2.5}$ (Watson et al., 2000a). $PM_{2.5}$ concentrations are the highest during winter and fall, and lowest in summer and spring (Watson et al., 2000a). High $PM_{2.5}$ mass concentrations during the winter season are attributed to RWC coupled with surface inversion layers (Schauer and Cass, 2000; Watson et al., 2000a; Watson and Chow, 2002a; Chow et al., 2006e). Diurnal trends of EC during summer typically show peaks during morning (0800-0900 Pacific Standard Time [PST]) and late afternoon (1600-1700 PST) traffic rush hours (Chow et al., 2006e).

Several continuous and integrated measurements are conducted regularly as part of the Fresno Supersite (Watson et al., 2000a), as listed in Table 4-1. A winter 2003 intensive measurement campaign was conducted as part of the Fresno Supersite program. These measurements complement the summer 2005 intensive measurements for carbon comparison.

4.2 Summer and Winter Intensive Measurements

The summer IOP carried out during 8/18/05 to 9/17/05 included: six real-time particle light absorption instruments; five particle light scattering instruments; continuous $PM_{2.5}$ mass, carbon, nitrate, and sulfate monitors; and six particle sizing instruments. The continuous light absorption instruments shown in Table 4-2 included: 1) Magee Scientific (Berkeley, CA) dual wavelength (λ=370 and 880 nm) aethalometer (2-AE); 2) 7-AE (λ=370, 470, 520, 590, 660, 880, and 950 nm); 3) Radiance Research (Seattle, WA) PSAP (λ=467, 530 and 660 nm); 4) Thermo Electron (Franklin, MA) MAAP (λ=670 nm); 5) two DRI (Reno, NV) PA at wavelengths of 532 nm and 1047 nm; and 6) the Sunset Laboratory carbon aerosol analysis field instrument optical BC (Sunset, λ=660 nm) measurements.

The continuous light scattering instruments included: 1) Optec NGN-2 (Lowell, MI) open air nephelometer (λ=550 nm); 2) Radiance Research (Seattle, WA) M903 nephelometer with smart heater, with and without $PM_{2.5}$ inlet (λ=530 nm); 3) Ecotech (East Providence, RI) nephelometer with smart heater (λ=525 nm); and 4) TSI (Shoreview, MN) three-color nephelometer (λ=450, 550, and 700 nm).

Continuous particle chemistry measurements included: 1) Thermo Electron (Franklin, MA) R&P 8400N continuous nitrate (NO_3^-) analyzer; 2) Thermo Electron (Franklin, MA) R&P 8400S continuous sulfate ($SO_4^=$) analyzer; 3) Sunset Laboratory carbon aerosol (OC and EC) analysis field instrument; and 4) EcoChem PAS2000 (League City, TX) particle-bound PAHs (λ=225 nm).

In addition, the TSI nano and standard SMPS acquired data since 8/25/02 and 3/17/00, respectively, at the Fresno Supersite. Two optical particle counters (OPCs), including the Climet Spectro (Redlands, CA) and Lasair (Particle Measuring Systems [PMS], Boulder, CO), have been in operation since 1/6/00. Two additional particle sizing instruments: 1) GRIMM (Ainring, Germany) SMPS; and 2) MSP (St. Paul, MN) WPS were collocated at Fresno during the summer IOP for comparison of particle number measurements and particle size distribution.

Table 4-2 also includes the continuous $PM_{2.5}$ and PM_{10} mass measurements by Met One (Grants Pass, OR) beta-attenuation monitor (BAM), the Kimoto BAM (Tisch Environmental, Cleves, OH) and Thermo Electron tapered element oscillating microbalance (TEOM) at 50 °C, along with continuous gaseous and meteorological measurements.

Twenty-four hour integrated samples (midnight to midnight) were collected every two days from 8/1/05 through 9/18/05, using the following integrated samplers: 1) two single channel (one with Teflon-membrane and the other with quartz-fiber filters) $PM_{2.5}$ Federal Reference Monitors (FRM; Thermo Electron, Franklin, MA); 2) a six-channel $PM_{2.5}$ reference ambient air samplers (RAAS, a speciation sampler; Thermo Electron, Franklin, MA); 3) a $PM_{2.5}$ Hi-Vol sampler (Thermo Electron, Franklin, MA); and 4) an EcoTech (American Ecotech, East Providence, RI) $PM_{2.5}$ Hi-Vol sampler. The Thermo Electron RAAS and Hi-Vol samplers were operated concurrently in pairs, whereas the FRMs and EcoTech Hi-Vol samplers were operated on alternate days, such that filter-based measurements were available every day during the summer IOP.

The winter IOP was conducted from 12/1/03 to 12/22/03, in coordination with Brigham Young University (BYU, Provost, UT), with measurements similar to those of the summer IOP as shown in Table 4-3. The additional winter measurements included: 1) $PM_{2.5}$ mass by 30 °C differential TEOM, and Filter Dynamics Mass Balance System [FDMS] TEOM); 2) Thermo Electron R&P 5400 carbon analyzer; 3) GRIMM Model 1100 monitor for particle light scattering; and 4) Dionex (Sunnyvale, CA) GP-IC continuous ion measurements. BYU also operated the PC-BOSS (Particle concentrator – BYU Organic Sampling System) sampler on three-hour intervals on four days (12/15, 12/17, 12/18, and 12/22/03) that were forecast to be high PM days. In addition, the Thermo Electron RAAS and the Hi-Vol samplers were operated every third day from 12/5/03 to 12/29/03 (except for 12/8/03 when the sample was voided), during this IOP. The FRM sampler was operated every sixth day from 12/5/03 to 12/29/03.

4.3 Real-time Continuous BC/EC Measurements

This section focuses on light absorption measurements that quantify BC (the predominant light absorbing component in the atmosphere), along with thermal EC measurements, which are of direct relevance to this study. Description of measurement principles for the PAH monitor, the

AE, and the PA can be found in Section 3.3.2. The EcoChem PAS 2000 monitor measures particle-bound PAHs. At Fresno, the results were reported in terms of the electrometer output in femptoamps (fA) and are used as an indicator of PAH on a relative basis. The 2-AE and 7-AE reported 5-min BC concentrations at 20 °C and 1 atmosphere (atm) pressure. The DRI PAs, (λ = 532 and 1047 nm) measured in-situ b_{abs} (Arnott et al., 1999; 2003; 2005b). During the summer IOP, the PAs reported 4-sec and 3-sec average data for the 532 nm and the 1047 nm PA, respectively. An empirical σ_{abs} of 10 m^2/g for the 532 nm and 5 m^2/g for the 1047 nm were applied to convert PA b_{abs} to BC concentration (Arnott et al., 2000; 2005b). The PA records the temperature and pressure within the sample chamber and reports b_{abs} measurements at these conditions. Additional light absorption measurements during the summer IOP are described as follows.

The Radiance three-wavelength PSAP monitors the change in transmission of light (at λ = 467, 530 and 600 nm) across a filter (Bond et al., 1999; Virkkula et al., 2005). The instrument reports b_{abs} in Mm^{-1} directly and includes an empirical correction that accounts for scattering by the filter matrix and for the non-linear instrument response as a function of loading. During the summer IOP, the PSAP reported 3-sec average b_{abs} measurements. No default σ_{abs} factors have been recommended by the manufacturer to convert b_{abs} to BC mass concentration. The PSAP reported standard b_{abs} measurements at 0 °C and 1 atm pressure.

The Thermo Electron MAAP samples air through a glass-fiber filter tape (Petzold et al., 2002; Petzold and Schönlinner, 2004; Petzold et al., 2005). The instrument measures the transmittance of 670 nm light at 0^o and reflectance at 130° and 165° from the projected light beam. The b_{abs} of the aerosol sample is then calculated using a two-stream-approximation radiative transfer model, which minimizes biases related to scattering effects caused by the filter and the sampled aerosol. An empirical σ_{abs} (670 nm) of 6.6 m^2/g was applied to convert 1-min b_{abs} to BC mass concentration. At Fresno, the MAAP reported b_{abs} and BC concentrations at actual conditions (ambient temperature and pressure).

The Sunset Laboratory carbon aerosol analysis field instrument (Bae et al., 2004) measures OC and EC based on the thermal/optical transmittance (TOT) method. The sample air is drawn through a parallel plate organic denuder to remove gas-phase organics and then through a quartz-fiber filter for 45 min at 8.5 L/min. The sampling port is then closed for 15 min, and the sample is heated to 250, 500, 650, and 850 °C in 100% Helium (He), then to 650, 750, 850, and 940 °C in 98% He/2% O_2 that backflows through the filter. The evolved carbon is oxidized to CO_2 in a manganese oxide (MnO_2) oven, which is then quantified by a NDIR detector. Charred or pyrolyzed OC (OP) is determined by monitoring the laser transmittance at λ = 660 nm. The carbon that evolves after the transmittance achieves its original value is classified as thermal EC. The filter is presumably free of carbon after the analysis. The sampling inlet is opened, and the cycle begins again for the next hour. The unit also monitors the light attenuation of the transmitted laser signal during the collection phase to obtain a BC measurement by a principle similar to that applied in the aethalometer. The BC measurement quantified by this light attenuation method is denoted as optical BC, to differentiate from the filter EC. The Sunset reports hourly average concentrations at actual conditions (ambient temperature and pressure).

4.4 Filter Pack Measurements

4.4.1 Thermo Electron FRM and RAAS Samplers

Both the Thermo Electron FRM and RAAS samplers were preceded by $PM_{2.5}$ size-selective inlets with an EPA WINS (Well Impactor Ninety-Six) impactor for the FRM and a Teflon-coated modified AIHL (Air Industrial Hygienic Laboratory) cyclone for the RAAS (Watson and Chow, 2001). For FRMs, two single-channel samplers were collocated for complete chemical speciation, one with a Teflon-membrane filter (configured the same as those used in U.S. EPA compliance monitoring network for $PM_{2.5}$) and the other with a quartz-fiber filter.

The RAAS was configured with six channels as shown in Figure 4-1:

1) an undenuded channel with a double-stage front Teflon-membrane/backup quartz-fiber filter pack operated at a flow rate of 16.7 L/min;

2) an undenuded channel with a double-stage front quartz-fiber/backup quartz-fiber filter pack operated at a flow rate of 7.3 L/min;

3) a field blank channel without active flow;

4) a denuded channel with a BYU charcoal-impregnated, glass-fiber filter (CIF) organic gas denuder followed by a double-stage quartz-fiber/backup quartz-fiber filter pack operated at a flow rate of 7.3 L/min;

5) a denuded channel with a sodium carbonate-coated URG (URG corporation, Chapel Hill, NC) glass denuder to remove gaseous nitric acid (HNO_3) followed by a double stage front quartz-fiber/backup nylon filter pack operated at a flow rate of 8.7 L/min; and

6) a denuded channel with a citric-acid-coated URG glass denuder to remove gaseous NH_3, followed by a double-stage front quartz-fiber/backup citric acid impregnated filter pack operated at 8 L/min.

Non-volatilized NO_3^- was collected on 47-mm front quartz-fiber filters in the RAAS and FRM samplers. Volatilized NO_3^- was collected in HNO_3 denuded channels on backup nylon filters in the RAAS sampler. NO_3^- was analyzed on DDW extractions of the filters by IC. Non-volatilized ammonium (NH_4^+) was collected on 47-mm front quartz-fiber filters in the RAAS and FRM samplers. Volatilized NH_4^+ was collected in citric acid denuded channels on backup citric acid impregnated cellulose-fiber filters.

4.4.2 Hi-Vol Samplers

A Thermo-Electron and an Ecotech Hi-Vol sampler, each equipped with a $PM_{2.5}$ size-selective inlet, collected 24-hr samples on a 406 cm^2 and a 500 cm^2, pre-baked quartz-fiber filter,

respectively. Both samplers were operated at 1,130 L/min. These Hi-Vol samples allow for numerous punches that can be used for analysis by different carbon analysis protocols.

4.4.3 Ambient Sample Filter Chemical Analyses

The same procedures applied to chemical analyses of source samples were followed for ambient samples. The Teflon-membrane filters were analyzed for mass by gravimetry, b_{abs} by transmission densitometry, and for 40 elements (Na to U; see Table 2-2) by XRF. For ambient samples, the front quartz-fiber filters were analyzed for water-soluble chloride (Cl^-), NO_3^- and $SO_4^=$ by IC (Mulik et al., 1976; Chow and Watson, 1999); for NH_4^+ by AC (Bolleter et al., 1961); and for Na^+ and K^+ by AAS (Rodes et al., 1989), using half of a 47mm filter.

The front quartz-fiber filters from the FRM and front and back-up quartz-fiber filters from RAAS samplers were analyzed for OC and EC following the IMPROVE_A (Chow et al., 1993; 2001; 2004a) TOR/TOT protocol. Selected front quartz-fiber filters from the RAAS and Hi-Vol samplers were analyzed by the STN TOT (Peterson and Richards, 2002) protocol. Selected filters from the Hi-Vol sampler were also analyzed by the French two-step (Cachier et al., 1989a; 1989b) protocol.

Table 4-1. Summary of air quality and meteorological measurements at the Fresno Supersite.

Observable and Method	Size Range	Avg Time	Frequency	Period
Gases				
Nitrogen oxides (NO/NO_x) (TEI 42 chemiluminescence with internal converter)[a]	Gas	1-hr	daily	1990 onward [b]
NO_2/PAN (UC Riverside Luminol)	Gas	5-min	daily	12/1/00 to 4/25/03
Ozone (API 400 UV absorption) [a]	Gas	1-hr	daily	1990 onward [b]
Carbon monoxide (Dasibi 3008 infrared gas filter correlation)	Gas	1-hr	daily	1990 onward [b]
Non-methane hydrocarbons (TEI 55C flame ionization)	Gas	1-hr	daily	1998 onward [b]
Reactive nitrogen (NOy) (TEI 42C chemiluminescence with external converter) [a]	Gas	1-min	daily	12/15/99 onward
Nitric acid (HNO_3) (TEI 42C chemiluminescence with external converters and denuders) c	Gas	1-min	daily	12/1/00 onward
Filter Mass and Chemistry				
TSP mass (Thermo Electron HiVol w/ quartz filters) and lead	TSP	24-hr	12th day	1990 to 2001 [b]
$PM_{2.5}$ mass and carbon (Thermo Electron HiVol w/ quartz filters)	<2.5 µm	24-hr	Every 3rd to 6th day	8/24/02 onward
PM_{10} mass, sulfate, nitrate, chloride, and ammonium (Thermo Electron HiVol SSI w/ quartz filters)	<10 µm	24-hr	6th day	1990 onward [b]
$PM_{2.5}$ and coarse mass, elements, endotoxins[e], spores[e], molds[e], and fungi[e] (dichotomous samplers with Teflon filters)	<2.5 µm <10 µm	24-hr	6th day	1990 to 2000 [b]
$PM_{2.5}$ and coarse mass, elements, endotoxins[e], spores[e], molds[e], and fungi[e] (two R&P 2025 sequential FRMs w/ Teflon filters)	<2.5 µm <10 µm	24-hr	daily for primary 6th day collocated	3/1/99 to 2007 [b]

Table 4-1. Continued.

Observable and Method	Size Range	Avg Time	Frequency	Period
Filter Mass and Chemistry (continued)				
$PM_{2.5}$ mass, light absorption, elements, ions, and carbon (two Thermo Electron single-channel RAAS 100 FRMs w/ Teflon and quartz filters)	<2.5 µm	24-hr	6th day	7/5/99 onward
$PM_{2.5}$ mass, elements, ions, and carbon (six-channel Thermo Electron RAAS 400 speciation sampler w/ denuders and backup filters)	<2.5 µm	24-hr	6th day	7/5/99 onward
$PM_{2.5}$ mass, ions, and carbon (PC-BOSS [Particle concentration-Brigham Young University organic sampling system] w/ denuders and backup filters)	<2.5 µm	3-hr	daily on 4 episode days	12/15, 12/17, 12/18, 12/22/03
Particle morphology (Airmetrics MiniVol w/ polycarbonate filter for scanning electron microscopy)	< ~30 µm	24-hr	6th day	7/5/99 to 6/29/00 (method evaluation)
$PM_{2.5}$ mass, elements, ions, and carbon (three-channel Met One speciation sampler [SASS])	<2.5 µm	24-hr	3rd day	2001 onward [b]
$PM_{2.5}$ mass, elements, ions, carbon, and ammonia (two-channel DRI sequential filter sampler w/ nitric acid denuders and backup filters; mass on all, chemistry on 100 samples)[a]	<2.5 µm	24-hr	daily	12/1/99 to 2/3/01[d]
$PM_{2.5}$ mass, elements, ions, and carbon (two-channel sequential filter sampler w/ denuders and backup filters) [a]	<2.5 µm	3-, 5-, and 8-hr (5 samples per day)	daily on episode days	15 episode days 12/1/00 to 2/3/01[d]
Toxic species (metals, chromium VI, aldehydes) (Xontec 920)	<~30 µm	24-hr	12th day	1996 onward [b]
R&P 2300 Speciation Sampler	<2.5 µm	24-hr	6th day	7/02 to 1/03
Burkard Pollen and Spore Counter[e]	TSP	168-hr	weekly	8/01 onward
Continuous Particle Mass and Chemistry				
$PM_{2.5}$ mass (50 °C R&P 1400a TEOM)	<2.5 µm	5-min	daily	7/10/99 onward
PM_{10} mass (50 °C R&P 1400a TEOM)	<10 µm	5-min	daily	7/10/99 onward

Table 4-1. Continued.

Observable and Method	Size Range	Avg Time	Frequency	Period
Continuous Particle Mass and Chemistry (continued)				
$PM_{2.5}$ mass (ambient temperature Met One 1020 BAM) [e]	<2.5 µm	1-hr	daily	12/16/99 to 1/2/04
PM_{10} mass (ambient temperature Met One 1020 BAM) [e]	<10 µm	1-hr	daily	12/4/99 onward
PM_{10} mass (ambient temperature Met One 1020 BAM) #2 [e]	<10 µm	1-hr	daily	1/2/04 onward
$PM_{2.5}$ (fine) and PM_{10} (coarse) mass SPM-613 (Kimoto Electric, Tokyo, Japan)	<2.5 µm <10 µm	1-hr	daily	11/30/03 onward (sporadic operation due to frequent instrument problems)
$PM_{2.5}$ mass (30 °C R&P 1400a TEOM)	<2.5 µm	1-hr	daily	12/1/03-12/22/03
$PM_{2.5}$ mass (30 °C R&P Differential TEOM)	<2.5 µm	1-hr	daily	12/1/03-12/22/03
$PM_{2.5}$ mass (30 °C R&P FDMS TEOM)	<2.5 µm	1-hr	daily	12/1/03-12/22/03
$PM_{2.5}$ nitrate Unit 1 (R&P/ADI flash volatilization with NOx detector) [c, e]	<2.5 µm	10-min	daily	08/23/00 onward
$PM_{2.5}$ nitrate Unit 2 (R&P/ADI flash volatilization with NOx detector) [c, e]	<2.5 µm	10-min	daily	10/12/00 onward
$PM_{2.5}$ sulfate (R&P/ADI flash volatilization with SO_2 detector) [e]	<2.5 µm	10-min	daily	1/29/02 onward
$PM_{2.5}$ organic and elemental carbon (R&P Series 5400 thermal evolution, OC at 340 °C, EC at 700 °C) [e]	<2.5 µm	1-hr	daily	1/13/00 to 03/07/05
$PM_{2.5}$ organic and elemental carbon (Sunset Laboratory carbon aerosol analysis field instrument, NDIR detection of carbon) [e]	<2.5 µm	1-hr	daily	7/23/03 onward
Particle-bound polycyclic aromatic hydrocarbons (PAH) (EcoChem Analytics PAS2000 w/ UV radiation and photoelectric aerosol sensors) [e] [PAS-PAH]	<1 µm	5-min	daily	9/30/99 onward
Individual particle size and chemistry (UC Riverside time-of-flight spectrometer)	<10 µm	5-min	daily on episode days	12/1/00 to 2/3/01 [d]

Table 4-1. Continued.

Observable and Method	Size Range	Avg Time	Frequency	Period
Time Integrated Organic Gases and Particles				
Toxic hydrocarbons (C2 to C12) (Xontec 910 canister sampler)	gas	24-hr	12th day	1995 onward
Carbonyls (Xontec 925 2,4-dinitrophenylhydrazine [DNPH] cartridge sampler) [a]	gas	24-hr summer (4 samples per day)	12th day 3rd day	1995 to 2003 [b]
Carbonyls (Xontec 910/912 canister PAMS sampler) [a]	gas	24-hr summer (4 samples per day)	12th day 3rd day	1995 to 2003 [b]
Carbonyls (DRI sequential sampler with DNPH cartridge) [a]	gas	5- to 8-hr, (4 samples per day)	daily for episodes	15 episode days 12/1/00 to 2/3/01 [d]
Light hydrocarbons (C_2 to C_{12}) (canister sampler) [a]	gas	5- to 8-hr, (4 samples per day)	daily for episodes	15 episode days 12/1/00 to 2/3/01 [d]
Heavy hydrocarbons (C_{10} to C_{20}) (TENAX sampler) [a]	gas	5- to 8-hr, (4 samples per day)	daily for episodes	15 episode days 12/1/00 to 2/3/01 [d]
$PM_{2.5}$ organic compounds (DRI sequential sampler with Teflon-coated glass-fiber/PUF/XAD filters) [a]	<2.5 µm	5- to 8-hr, (4 samples per day)	daily for episodes	15 episode days 12/1/00 to 2/3/01 [d]
		24-hr	6th day	6/1/00-9/30/00 [d]
$PM_{2.5}$ organic compounds (Airmetrics Minivol w/ Teflon-coated glass-fiber filters) (aggregate 60 samples for organic compound analysis) [a]	<2.5 µm	24-hr	6th day	2/1/00 to 2/3/01 [d]
Continuous Light Scattering				
Ambient particle light scattering (Optec NGN2 ambient-temperature nephelometer at 550 nm)	<~30 µm	5-min	daily	2/1/00 to 12/21/03
Ambient particle light scattering (Optec NGN2 ambient-temperature nephelometer at 550 nm)	<~30 µm	1-min	daily	12/22/03 onward
Total particle light scattering (Radiance M903 nephelometer with smart heater at 530 nm) [a, e]	<~30 µm	5-min	daily	1/21/00 to 8/5/03
Total particle light scattering (Radiance M903 nephelometer with smart heater at 530 nm) [a, e]	<~30 µm	1-min	daily	8/5/03 onward

Table 4-1. Continued.

Observable and Method	Size Range	Avg Time	Frequency	Period
Continuous Light Scattering (continued)				
$PM_{2.5}$ particle light scattering (Radiance M903 nephelometer with smart heater at 530 nm) [e]	<2.5 µm	5-min	daily	9/8/00 to 8/1/03
$PM_{2.5}$ particle light scattering (Radiance M903 nephelometer with smart heater at 530 nm) [e]	<2.5 µm	1-min	daily	8/1/03 onward
Total particle light scattering (GreenTek GT640A photometer at 780 nm)	<~30 µm	5-min	daily	2/8/00 to 1/22/03
Total particle light scattering (EcoTech M9003 nephelometer at 525 nm)	<~30 µm	5-min	daily	7/31/05 to 9/26/05
$PM_{2.5}$ particle light scattering (TSI 3563 three wavelength nephelometer: 450, 550, 700 nm) [e]	<2.5 µm	5-min	daily	7/30/05 to 9/19/05
Total particle light scattering (TSI DustTrak 8520 photometer at 780 nm)	<2.5 µm	5-min	daily	5/15/99 to 6/28/03
Continuous Light Absorption				
Coefficient of haze (RAC 205019-1 paper tape sampler)	<~30 µm	2-hr	daily	1990 – 2002 [b]
Single-wavelength light absorption (1-AE, Magee AE-16 aethalometer at 880 nm)	<2.5 µm	5-min	daily	12/17/99 to 9/27/02
Dual-wavelength light absorption (2-AE Magee AE-21 aethalometer at 370 and 880 nm) [e]	<2.5 µm	5-min	daily	2/25/03 onward
Seven-wavelength light absorption (7-AE, Magee AE-30 multi-color [370, 470, 520, 590, 660, 880, and 950 nm] aethalometer) [e]	<2.5 µm	5-min	daily	5/12/99 onward
PSAP (Radiance Research light absorption monitor at 467, 530 and 660-nm)	<2.5 µm	3-sec	daily	8/1/05 to 9/17/05
MAAP (Thermo-Electron Black Carbon Monitor at 670 nm)	<2.5 µm	1-min	daily	11/30/03 onward
DRI PA (532 nm)	<2.5 µm	4-sec	daily	8/1/05 to 9/17/05
DRI PA (1047 nm)	<2.5 µm	5-min	daily	12/8/03 to 8/31/04
		3-sec	daily	8/1/05 to 9/17/05

Table 4-1. Continued.

Observable and Method	Size Range	Avg Time	Frequency	Period
Continuous Light Absorption (continued)				
Black carbon SPM-613 (Kimoto Electric, Tokyo, Japan)	<2.5 µm	1-hr	daily	2/9/04 onward (sporadic operation due to frequent instrument problems)
Black Carbon by Sunset Optical	< 2.5 µm	1-hr	daily	7/23/03 onward
Sun Photometer (CIMEL)–operated by JPL	NA	NA	Satellite Uplink	2001 onward
Particle Sizing				
Ultrafine particle number by size (TSI 3936N25A nano-SMPS) [a, e]	3 to 80 nm	5-min	daily	8/25/02 onward
Fine particle number by size (TSI 3936L10 SMPS) [a, e]	10 to 407 nm	5-min	daily	3/17/00 onward
Grimm SMPS	5 to 350 nm	3.5-min	daily	8/18/05 to 9/19/05
WPS (MSP 1000XP)	10 to 10,000 nm	5-min	daily	8/18/05 to 9/18/05
Coarse particle size distribution in 16 size fractions (Climet Spectro .3 optical particle counter) [a]	0.3 to 10 µm (<0.3, <0.4, <0.5, <0.63, <0.8, <1.0, <1.3, <1.6, <2.0, <2.5, <3.2, <4.0, <5.0, <6.3, <8.0, and <10 µm)	5-min	daily	1/6/00 onward
Lasair (Particle Measuring Systems)	0.1 to 2.0 µm	5-min	daily	1/6/00 onward
Mass and ion size distribution in 9 size fractions (MOUDI with Teflon filters for mass and ions)	0.054 to 10 µm (<0.054, <0.105, <0.180, <0.37, <0.54, <1.0, <2.5, <5.6, and <10 µm)	5- to 8-hr	daily for episodes	15 episode days 12/1/00-2/3/01 [d]
Carbon size distribution in 9 size fractions (MOUDI with aluminum filters for organic and elemental carbon)	0.054 to 10 µm (<0.054, <0.105, <0.180, <0.37, <0.54, <1.0, <2.5, <5.6, and <10 µm)	5- to 8-hr	daily for episodes	15 episode days 12/1/00-2/3/01 [d]

Table 4-1. Continued.

Observable and Method	Size Range	Avg Time	Frequency	Period
Meteorology				
Wind speed/direction (Met One 05305L high-sensitivity wind vane and anemometer) [a]	NA [f]	5-min	daily	7/10/99 onward
Ambient Temperature (Met One CS500L platinum resistance sensor) [a]	NA	5-min	daily	7/10/99 onward
Relative humidity (RH) (Met One CS500L capacitance sensor) [a]	NA	5-min	daily	7/10/99 onward
Solar radiation (Li-Cor LI200X-L pyranometer) [a]	NA	5-min	daily	9/30/99 onward
Atmospheric pressure (Met One piezofilm sensor) [a]	NA	5-min	daily	5/24/00 onward
Data Acquisition System				
Campbell Scientific 24-input analog data logger with modem dialup	NA	All times	daily	5/15/99 onward
PC-LABVIEW serial data logger with modem dialup [a]	NA	All times	daily	12/1/99 onward

[a] These ground-level measurements were also taken at the non-urban Angiola site established by the California Regional Particulate Air Quality Study (CRPAQS) from 2/1/00 through 2/3/01 and during pollution episodes. This site is located 100 km south of Fresno in a flat area of the San Joaquin Valley surrounded by agricultural fields dominated by cotton and alfalfa. CRPAQS episodic measurements at Angiola were taken at the same time as those acquired at Fresno.

[b] Part of the California Air Resources Board's (ARB) compliance monitoring network.

[c] Measurements at Angiola are available from 12/1/00 through 2/3/01.

[d] Measurements from CRPAQS. Three to five wintertime episodes of four- to eight-day duration were monitored for a total of 15 days between 12/1/00 and 2/3/01 based on a forecast of high $PM_{2.5}$ concentrations under clear sky stagnation and stagnation with fog conditions.

[e] Part of the Fresno Asthmatic Children's Environment Study (FACES) sponsored by ARB.

[f] Not applicable.

Table 4-2. Measurement specifications for the summer 2005 IOP.

	Instruments[a]	Observable (unit)	Measurement Principle[b]	Wavelength (nm)	Particle Size	Collection Medium	Flow Rate (L/min)	Averaging Time
Continuous Particle Light Absorption	2-AE	b_{abs} (Mm^{-1}) BC ($\mu g/m^3$)	Attenuation of light transmitted through the filter tape is measured and converted to a BC mass concentration using σ_{abs} of 14625/λ (m^2/g).	370, 880	$PM_{2.5}$	Quartz-fiber filter tape	6.6	5 min
	7-AE	b_{abs} (Mm^{-1}) BC ($\mu g/m^3$)		370, 470, 520, 590, 660, 880, 950	$PM_{2.5}$	Quartz-fiber filter tape	6.7	5 min
	MAAP	b_{abs} (Mm^{-1}) BC ($\mu g/m^3$)	Light transmittance at 0° and reflectance from the filter at 130° and 165° from the illumination direction are used in a radiative transfer model to estimate b_{abs} and is converted to BC using σ_{abs} of 6.6 m^2/g.	670	$PM_{2.5}$	Glass-fiber filter tape	16.7	1 min
		b_{abs} (Mm^{-1})	Attenuation of light transmitted through the filter tape is measured.	467, 530, 660	$PM_{2.5}$	Quartz-fiber filter punch	0.5	3 sec
PSAP	PA (532 nm)	b_{abs} (Mm^{-1}) BC ($\mu g/m^3$)	Light absorption by particles in air results in a heating of the surrounding air. The expansion of the heated air produces an acoustic (sound wave) signal which is detected by a microphone to determine b_{abs}, which is confined to BC using σ_{abs}=5 m^2/g for the 1047 nm instrument and σ_{abs}=10 m^2/g for the 532 nm instrument.	532	$PM_{2.5}$	Acoustic resonator	1	4 sec
	PA (1047 nm)			1047				3 sec
	Sunset Optical	BC ($\mu g/m^3$)	Light transmitted through the filter is monitored during the collection phase to quantify BC.	660	$PM_{2.5}$	Quartz-fiber filter tape	8.5	1 hr

Table 4.2. Continued.

	Instruments[a]	Observable (unit)	Measurement Principle[b]	Wavelength (nm)	Particle Size	Collection Medium	Flow Rate (L/min)	Averaging time
Continuous Particle Light Scattering	NGN2	b_{scat} (Mm^{-1})	Measures light scattering coefficient at ambient conditions. The air sample is illuminated and a photodiode detector produces a signal in proportion to the chopped light signal. Zero air calibration is done every 6 to 24 hrs.	550	TSP	none	2	1 min
	Rad903	b_{scat} (Mm^{-1})	The air sample is illuminated and a photodiode detector produces a signal in proportion to the chopped light signal. The nephelometer is calibrated to read zero for particle-free air, which is subtracted to provide a direct estimate of particle light scattering coefficient. A "smart heater" heats the sample when RH increases beyond 70%.	530	$PM_{2.5}$	none	6.9	1 min
				530	TSP	none	6.9	1 min
	Ecotech Neph	b_{scat} (Mm^{-1})	A light source illuminates the sample air, and the light scattered at angles between 10° and 70° is detected. The signal is proportional to the concentration of the particles giving an estimate of the particle light scattering coefficient. Zero air calibrations are performed using particle-free air. It is equipped with a heater that turns on when the RH is > 70%.	525	TSP[d]	none	5	5 min
	TSI 3-color Neph	b_{scat} (m^{-1})	A light source illuminates the sample air and the light scattered at angles between 7° and 170° is detected. The signal is proportional to the concentration of the particles giving an estimate of the particle light scattering coefficient. Zero air calibrations are performed using particle-free air every hour.	450, 550, 700	$PM_{2.5}$	none	20	5 min
Continuous Particle Chemistry	R&P 8400N	Nitrate ($\mu g/m^3$)	Air sample is humidified and impacted on the strip. Flash volatization is followed by transport to a NO_x chemiluminescence sensor.	NA[e]	$PM_{2.5}$	nichrome strip	1.2	10 min
	R&P 8400S	Sulfate ($\mu g/m^3$)	Air sample is humidified and impacted on the strip. Flash volatization is followed by transport to a SO_2 fluorescence sensor.	NA	$PM_{2.5}$	platinum strip	1.2	10 min

Table 4.2. Continued.

	Instruments[a]	Observable (unit)	Measurement Principle[b]	Wavelength (nm)	Particle Size	Collection Medium	Flow Rate (L/min)	Averaging time
Continuous Particle Chemistry (Continued)	Sunset	OC, EC ($\mu g/m^3$)	Particles collected on a quartz-fiber filter are subject to different temperature ramps following the NIOSH 5040_TOT protocol and the resulting CO_2 is analyzed by nondispersive infrared (NDIR). Pyrolysis correction is by laser transmittance.	660	$PM_{2.5}$	Quartz-fiber filter tape	8.5	1 hr
	PAS-PAH	Particle-bound PAH (fA)	The air stream is exposed to UV radiation, which ionizes the particle-bound PAH molecules. The charged particles are collected on a filter element and the piezoelectric current is proportional to the particle-bound PAH.	225	$PM_{2.5}$	Filter element mounted in a Faraday cage	2	5 min
Particle Sizes	TSI nano SMPS	Number ($\#/cm^3$)	The air sample is bipolarly charged to a known distribution. The particles are classified according to their ability to traverse an electric field. The classified particles are coated with alcohol from a heated alcohol bath and grow to a size where they can be counted optically.	NA	3 - 80 nm	none	0.95	5 min
	TSI standard SMPS	Number ($\#/cm^3$)		NA	10 - 407 nm	none	0.95	5 min
	GRIMM SMPS	Number ($\#/cm^3$)		NA	5 - 350 nm	none	0.3	3.5 min
	Climet OPC	Number ($\#/cm^3$)	The air sample is illuminated and the scattered light is focused onto a photodetector. The amount of light scattered is proportional to the particle size.	NA	300 - 10000nm	none	0.95	5 min
	Lasair OPC	Number ($\#/cm^3$)		NA	100 nm - 2000 nm	none	0.03	5 min
	MSP WPS	Number ($\#/cm^3$)	The air sample is split into two flows. The first flow is bipolarly charged to a known distribution; classified according to the charged particle's ability to traverse an electric field; coated with alcohol and counted optically. The second flow is illuminated and the amount of photodetected scattered light is proportional to particle size.	NA	10 - 10000 nm	none	1	5 min
Continuous Mass	MetOne BAM	Mass ($\mu g/m^3$)	Beta rays (electrons) are passed through a filter on which particles are collected. The loss of electrons (beta attenuation) caused by the particle loading on the filter is converted to mass concentration, after subtraction of blank filter attenuation.	NA	PM_{10}	Quartz-fiber filter tape	16.7	1 hr
				NA	$_{2.5}$	Quartz-fiber filter tape	16.7	1 hr

PM

Table 4.2. Continued.

	Instruments[a]	Observable (unit)	Measurement Principle[b]	Wavelength (nm)	Particle Size	Collection Medium	Flow Rate (L/min)	Averaging time
Continuous Mass (Continued)	Kimoto BAM	Mass (μg/m^3)	Beta rays (electrons) are passed through a filter on which particles are collected. The loss of electrons (beta attenuation) caused by the particle loading on the filter is converted to mass concentration, after subtraction of blank filter attenuation.	NA	PM_{10}	Teflon-membrane filter tape	15.4	1 hr
				NA	$_{2.5}$	Teflon-membrane filter tape	1.3	1 hr
	TEOM	Mass (μg/m^3)	Air is drawn through a size selective inlet onto the filter mounted on an oscillating hollow tube. The oscillation frequency changes with mass loading on the filter, which is used to calculate mass concentration by comparing measured frequency to standards.	NAPM	$PM_{2.5}$	Teflon coated borosilicate glass-fiber filter	16.7	5 min
				NA	$_{10}$		16.7	5 min
Integrated Measurements	FRM filter samples analyzed by IMPROVE_A_TOR/TOT	OC, EC, and TC (μg/m^3)	Particles collected on a quartz-fiber filter are subject to different temperature ramps following the IMPROVE_A protocol. The resulting CO_2 is converted to CH_4 and analyzed using FID. Pyrolysis correction is using laser reflectance (TOR) and transmittance (TOT).	PM 632.8	$PM_{2.5}$	Quartz-fiber filter	16.7	24 hr, every 2 days
	RAAS filter samples analyzed by IMPROVE_A_TOR/TOT and STN_TOT	OC, EC, and TC (μg/m^3)	Particles collected on a quartz-fiber filter are subject to thermal carbon analysis following the IMPROVE_A and STN TOT protocols. Pyrolysis correction made by TOR/TOT in IMPROVE_A and laser transmittance in STN_TOT. STN_TOT analysis conducted on selected filters only.	632.8	$PM_{2.5}$	Quartz-fiber filter	16.7 (Channel 1); 7.3 (Channels 2 & 4)	24 hr, every 2 days
	Hi-Vol filter[c] samples analyzed by IMPROVE_A_TOR/TOT, STN_TOT, French two-step	OC, EC, and TC (μg/m^3)	Particles collected on a quartz-fiber filter are subject to thermal carbon analysis following the IMPROVE_A, STN_TOT and French two-step protocols. Pyrolysis correction made by TOR/TOT in IMPROVE_A, by TOT in STN_TOT and none in French two-step protocol. STN and French two-step analysis conducted on selected filters only.	632.8	$PM_{2.5}$	Quartz-fiber filter	1130	24 hr, every 2 days

Table 4.2. Continued.

	Instruments[a]	Observable (unit)	Measurement Principle[b]	Wavelength (nm)	Particle Size	Collection Medium	Flow Rate (L/min)	Averaging time
Continuous Gaseous Measurements	TEI 42	Nitrogen Oxides (NO/NOx)	The sample gas is exposed to O_3 initiating a chemical reaction between NO and O_3 that gives off light (chemiluminescence). A catalytic converter converts any NO_2 in the sample gas to NO, which is then reported as NO_x. NO_2 is calculated as a difference between NO_x and NO.	NA	gas	none	0.6	1 hr
	TEI 42CY	Reactive Nitrogen (NOy) and Nitric Acid (HNO_3)	The air sample is pulled through an external molybdenum converter, reacts with O_3 and the chemiluminescence is measured.	NA	gas	none	1	5 min
	TEI 55C	Non-Methane hydrocarbons (NMHC)	CH_4 is separated using a separation column and detected by FID. NMHC is then flushed out of the column by reversing the carrier gas flow, which is then detected by the FID.	NA	gas	none	0.5	1 hr
	Dasibi 3008	Carbon Monoxide (CO)	Infrared light is absorbed by CO in the air sample. The quantity of light absorbed is proportional to the concentration of CO in the air sample.	NA	gas	none	NA	1 hr
	API 400	Ozone (O_3)	254nm light is absorbed by O_3 in the air sample. The ratio of the scrubbed (O_3 free) air light intensity to that of the sample air is used to calculate the O_3 concentration as per Beer-Lambert law.	NA	gas	none	NA	1 hr
Meteorology	Met One 05305L	Wind Speed/Direction	High-sensitivity wind vane and anemometer.	NA	NA	none	NA	5 min
	Met One CS500L	Temperature	Temperature is measured by the resistance change of a platinum resistance sensor thermistor.	NA	NA	none	NA	5 min
	Met One CS500L	Relative Humidity (RH)	Relative Humidity is measured based upon the capacitance change of a polymer thin film capacitor.	NA	NA	none	NA	5 min

Table 4.2. Continued.

	Instruments[a]	Observable (unit)	Measurement Principle[b]	Wavelength (nm)	Particle Size	Collection Medium	Flow Rate (L/min)	Averaging time
Meteorology (Continued)	Met One	Atmospheric Pressure	Atmospheric pressure is measured by a solid state pressure transducer (Piezofilm sensor) whose voltage response is linear and proportional of pressure.	NA	NA	none	NA	5 min

[a] 2-AE—dual wavelength aethalometer (Magee Scientific, Inc., Berkeley, CA)
7-AE—seven-color aethalometer (Magee Scientific, Inc., Berkeley, CA)
MAAP—Multi-angle absorption photometer (Thermo Electron, Franklin, MA)
PSAP—particle soot absorption photometer (Radiance Research, Seattle, WA)
PA—DRI photoacoustic analyzer (Reno, NV)
Sunset—Semi-continuous Sunset Laboratory aerosol analyzer field instrument carbon analyzer, following the NIOSH thermal/optical transmittance (TOT) 5040 protocol (Sunset Laboratory, Inc., Tigard, OR)
NGN2: Optec—NGN2 Open air integrating nephelometer (Optec, Inc.)
Rad903—Radiance Research M903 integrating nephelometer (Radiance Research, Seattle, WA)
EcoTech Neph—EcoTech M9003 integrating nephelometer (EcoTech, East Providence, RI)
TSI 3-color Neph—TSI 3-color nephelometer (TSI, Shoreview, MN)
R&P 8400N—R&P ambient particulate nitrate monitor (Thermo Electron, Franklin, MA)
R&P 8400S—R&P ambient particulate sulfate monitor (Thermo Electron, Franklin, MA)
PAS-PAH—EcoChem PAS2000 PAH monitor (EcoChem Analytics, Inc., League City, TX)
TSI SMPS—TSI Inc. (Shoreview, MN) scanning mobility particle sizer
GRIMM SMPS: Grimm Aerosol Technik (Germany) SMPS
Climet OPC—Climet instruments (Redlands, CA) Spectro 0.3 optical particle counter
Lasair OPC—Lasair Particle Measuring Systems (PMS, Boulder, CO) optical particle counter
MSP WPS—MSP Corp. (Minneapolis, MN) wide range particle spectrometer
MetOne BAM—MetOne Beta-attenuation monitor (MetOne Instruments, Grants Pass, OR)
Kimoto BAM—Tisch Environmental Kimoto beta-attenuation monitor (Cleves, OH)
TEOM—Tapered element oscillating microbalance series 1400a ambient particulate monitor (Thermo Electron, Franklin, MA)
FRM—Thermo Electron single-channel Federal Reference Monitor (Thermo Electron, Franklin, MA)
RAAS—Thermo Electron reference ambient air speciation sampler (Thermo Electron, Franklin, MA)
Hi-Vol—high volume sampler (collocated Thermo Electron and EcoTech samplers)
TEI 42—Thermo Electron model 42 NO-NO2-NOx analyzer (Thermo Electron, Franklin, MA)
TEI 42CY—Thermo Electron model 42CY NOy analyzer (Thermo Electron, Franklin, MA)
TEI 55C—Thermo Electron direct methane, non-methane analyzer (Thermo Electron, Franklin, MA)
Dasibi 3008—Dasibi model 3008 carbon monoxide analyzer (Dasibi Environmental Corp, Glendale, CA)
API 400—Advanced Pollution Instrumentation, Inc. ozone analyzer (API, San Diego, CA)
All meteorological instruments are from MetOne (MetOne Instruments, Grants Pass, OR)

Table 4-2. Continued.

[b] BC—Black carbon
CO_2—Carbon dioxide
CH_4—Methane
FID—Flame Ionization Detector
IMPROVE_A—Interagency Monitoring of Protected Visual Environments carbon analysis protocol
NDIR—Non-dispersive Infrared
NIOSH_TOT—National Institute for Occupational Safety and Health Thermal/Optical Transmittance
NMHC—Non-methane hydrocarbons
NO—Nitric oxide
NO_2—Nitrogen dioxide
NO_x—Oxides of nitrogen
O_3—Ozone
PAH—Polycyclic-aromatic hydrocarbon
RH—Relative humidity
SO_2—Sulfur dioxide
STN_TOT—Speciation Trends Network thermal/optical transmittance (TOT) protocol
UV—Ultraviolet

[c] Collocated Thermo Electron and EcoTech as High Volume Samplers

[d] TSP—Total suspended particulate matter

[e] NA: Not available, Not applicable

Table 4-3. Summary of measurements made during both summer and winter IOPs.

Measurement	Instrument[a]	Parameter	Winter	Summer
Continuous Mass	MetOne BAM	$PM_{2.5}$ mass	x	x
	MetOne BAM	PM_{10} mass		x
	TEOM @ 50 °C	$PM_{2.5}$ mass	x	x
	TEOM @ 50 °C	PM_{10} mass		x
	TEOM @ 30 °C	$PM_{2.5}$ mass	x	
	Differential TEOM[d] @ 30 °C	$PM_{2.5}$ mass	x	
	FDMS TEOM[d] @ 30 °C	$PM_{2.5}$ mass	x	
Continuous Particle Chemistry	R&P 8400S	$SO_4^=$	x	x
	R&P 8400N	NO_3^-	x	x
	Dionex GP-IC	NO_3^-, $SO_4^=$, NH_4^+	x	
Continuous Carbon	R&P 5400	OC, EC, TC	x	
	Sunset	OC, EC, BC, TC	x	x
	PAS-PAH	Particle bound PAH		x
Continuous Particle Light Absorption	2-AE	b_{abs}/ BC	x	x
	7-AE	b_{abs}/ BC	x	x
	PSAP	b_{abs}		x
	MAAP	b_{abs}/BC	x	x
	PA (532 nm)	b_{abs}		x
	PA (1047 nm)	b_{abs}	x	x
Continuous Particle Light Scattering	NGN2	b_{scat}		x
	Rad903	b_{scat}		x
	EcoTech Neph	b_{scat}		x
	TSI 3-color Neph	b_{scat}		x
	GRIMM Model 1100 monitor[c]	$PM_{2.5}$ mass	x	
Integrated Measurements	FRM by IMPROVE_A_TOR/TOT	OC, EC, TC	x	x
	RAAS by IMPROVE_A_TOR/TOT and STN_TOT	OC, EC, TC	x	x
	Hi-Vol by IMPROVE_A_TOR/TOT, STN_TOT and French two-step	OC, EC, TC	x	x
	PC-BOSS	OC, SVOM[b]	x	

[a] Refer to Table 4-2 for instrument descriptions. Additional instruments are described here.
GRIMM model 1100—GRIMM model 1100 dust monitor (Grimm Aerosol Technik, Germany)
R&P5400—R&P ambient particulate carbon monitor (Thermo Electron, Franklin, MA)
Dionex GP-IC—Dionex continuous ion instrument (Dionex Corporation, Sunnyvale, CA)
FDMS TEOM—R&P Filter Dynamics Mass Balance System TEOM (Thermo Electron, Franklin, MA)
PC-BOSS—Particle Concentrator-Brigham Young University (BYU) Organic Sampling System (BYU, Provost, UT)

[b] SVOM—Semi-volatile organic matter

[c] GRIMM dust monitor measures particle mass based on light scattering. Light scattered by particles culminates in a mirror approximately 90° from the laser source and is detected by a diode. The measured particle size distribution is converted to mass based on protocols developed by GRIMM Technologies, Inc.

[d] Differential and FDMS TEOM measure mass based on TEOM principle. Sample is switched between particle-free (purge) and particle-laden cycles. Measurement during purge cycle quantifies positive and negative artifacts. Particle removal is using an electrostatic precipitator in a differential TEOM and using a filter at 4 °C in FDMS TEOM.

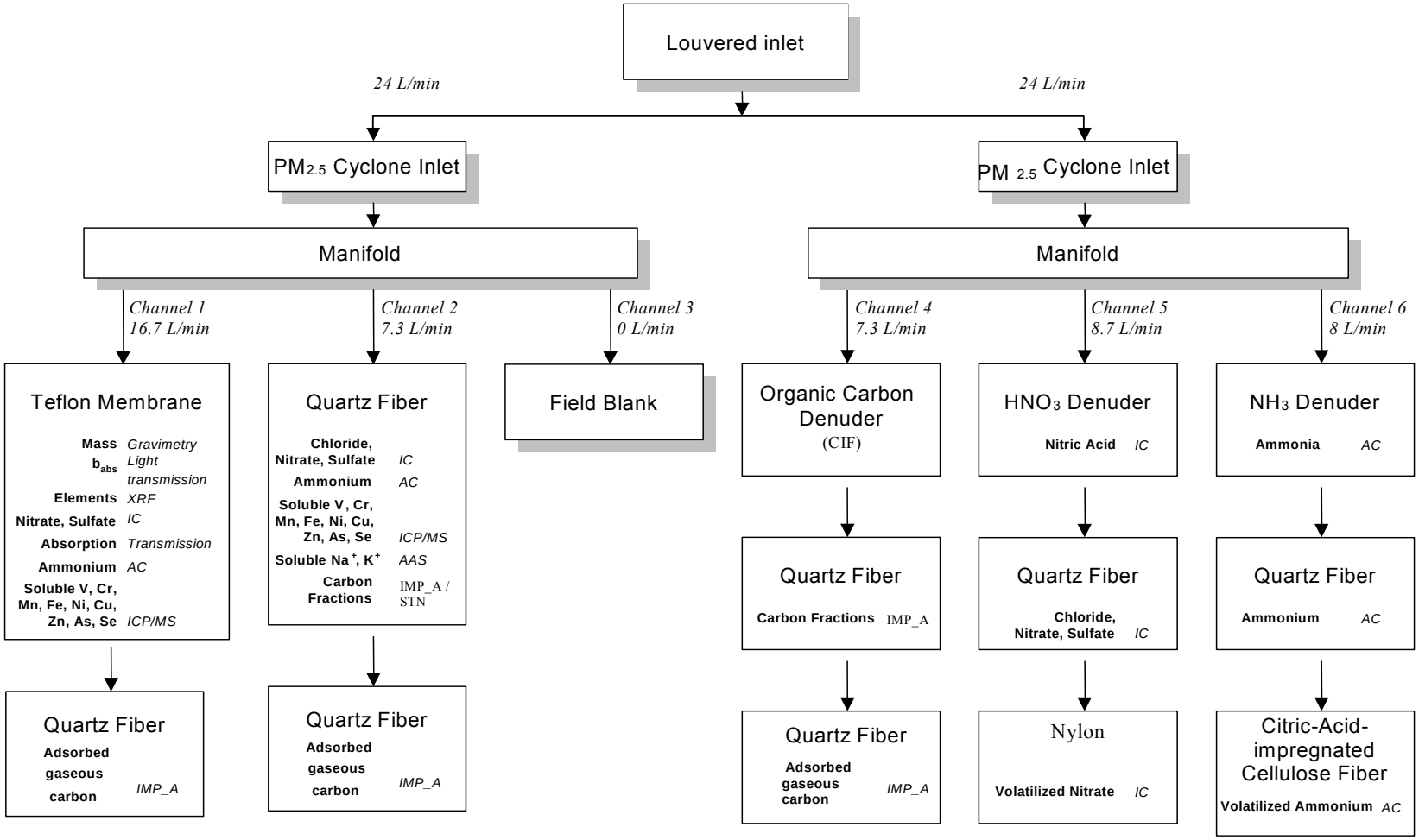

Figure 4-1. Schematic of the six-channel Reference Ambient Speciation Sampler (RAAS).

(AAS—Atomic absorption spectrophotometry; AC—Automated colorimetry; CIF—Charcoal-impregnated glass-fiber filter; IC—Ion chromatography; ICP/MS—Inductively coupled IC/Mass spectrometry; XRF—X-ray fluorescence; IMP_A—IMPROVE_A TOR/TOT protocol; STN—STN_TOT protocol; see text for details).

5. DATA VALIDATION AND QUALITY ASSURANCE

This section defines the precision, accuracy and validity of aerosol measurements. This section also summarizes QA activities conducted as part of the laboratory measurements, including filter deposit homogeneity checks. It evaluates the extent to which the source aerosol generation tests were reproducible.

5.1 Analytical Specifications

Every measurement consists of: 1) a value; 2) a precision; 3) an accuracy; and 4) a validity (Hidy, 1985; Watson et al., 1989; 1995). The measurement methods described in this report were used to obtain the "value". Performance testing via regular submission of standards, blank analysis, and replicate analysis were used to estimate the "precision". These precisions are reported in the data files so that they can be propagated through air-quality models and used to evaluate how well different values compare with one another. Evaluation of independent standards through quality audits estimate "accuracy". "Validity" applies both to the measurement method and to each measurement taken with that method. The validity of the methods was evaluated by tests described in Section 5.2.

5.1.1 Definitions of Measurement Attributes

The precision, accuracy, and validity of the aerosol measurements are defined as follows (Watson et al., 1995):

- A **measurement** is an observation at a specific time and place which possesses: 1) value – the center of the measurement interval; 2) precision – the width of the measurement interval; 3) accuracy – the difference between measured and reference values; and 4) validity – the compliance with assumptions made in the measurement method.

- A **measurement method** is the combination of equipment, reagents and procedures, which provide the value of a measurement. The full description of the measurement method requires substantial documentation. For example, two methods may use the same sampling systems and the same analysis systems; however, these are not identical methods if one performs acceptance testing on the filter media, while the other does not. Seemingly minor differences between measurement methods can result in major differences between measurement values.

- **Measurement method validity** is the identification of the measurement method assumption, the quantification of effects of deviations from those assumptions, the evaluation that deviations are within reasonable tolerances for the specific application, and the creation of procedures to quantify and minimize those deviations during a specific application.

- **Sample validation** is accomplished by procedures that identify deviations from measurement assumptions and the assignment of flags to individual measurements for potential deviations from assumptions.

- **Equivalence:** For $PM_{2.5}$ mass concentration, U.S. EPA (1997) requires Federal Equivalent Methods (FEM) to meet the following requirements when collocated with a FRM: 1) collocated precision of 2 $\mu g/m^3$ or 5% (whichever is larger); 2) linear regression slope of 1 ± 0.05; 3) linear regression intercept of 0 ± 1 $\mu g/m^3$; and 4) linear regression correlation coefficient (r) of ≥ 0.97 (U.S.EPA, 1997). Although these criteria are specific to $PM_{2.5}$ mass equivalence, they are also used for PM carbon and b_{abs} equivalence in the analysis to maintain consistency.

- **Comparability:** A comparable monitor should provide readings in units of mass concentration, be equipped with a standardized size-selective inlet, and yield measurements that are the same as collocated sampler measurements. Within stated precision intervals, the criteria for comparability are met when: 1) the slope (by either ordinary least squares [OLS] or effective variance [EF] weighting) equals unity within three standard errors, or average ratios (Y/X) equal unity within one standard deviation; 2) the intercept does not significantly differ from zero within three standard errors; and 3) the correlation coefficient exceeds 0.9 (Berkson, 1950; Kendall, 1951; Madansky, 1959). This is a less-demanding definition than equivalence because it considers the reported precisions of the two measurements being compared; these may be larger than that required for a FEM used to determine compliance, but still sufficient to discern concentration differences in space and time.

- **Predictability:** Some measurements, such as b_{abs}, may be correlated with BC concentrations even though they measure observables in different units. The criterion for predictability between two measurements is met when the correlation coefficient exceeds 0.9, although the slope may substantially deviate from unity and the intercept from zero. Predictability may be qualified, especially when there is high correlation for all but a few outlier measurements. The regression equation is used to estimate carbon concentrations from the measured observable (Watson and Chow, 2002b).

- **Completeness** measures how many environmental measurements with specified values, precisions, accuracies, and validities were obtained out of the total number attainable. It measures the applicability of the selected measurement processes throughout the measurement period. Databases that have excellent precision, accuracy, and validity may be of little use if they contain many missing values.

These criteria were applied to carbon and b_{abs} measurements obtained in the source aerosol generation tests conducted at the laboratory and for ambient measurements conducted at the Fresno Supersite during the summer and winter IOPs. The intercomparison results are presented in Section 6.

5.1.2 Definition of Measurement Precision

Measurement precisions were propagated from precisions of volumetric measurements, chemical composition measurements, and field blank variability using the methods of Bevington (1969) and Watson et al. (1995). The following equations calculated the precision associated with filter-based measurements:

$$C_i = (M_i - B_i)/V \tag{5-1}$$

$$V = F \times T \tag{5-2}$$

$$B_i = \frac{1}{n}\sum_{j=1}^{n} B_{ij} \quad \text{for } B_i > \sigma_{Bi} \tag{5-3}$$

$$B_i = 0 \quad \text{for } B_i < \sigma_{Bi} \tag{5-4}$$

$$\sigma_{Bi} = STD_{Bi} = \left[\frac{i}{n-1}\sum_{j=1}^{n}\left(B_{ij} - B_i\right)^2\right]^{1/2} \quad \text{for } STD_{Bi} > SIG_{Bi} \tag{5-5}$$

$$\sigma_{Bi} = SIG_{Bi} = \left[\frac{i}{n}\sum_{j=1}^{n}\left(\sigma_{Bij}\right)^2\right]^{1/2} \quad \text{for } STD_{Bi} \le SIG_{Bi} \tag{5-6}$$

$$\sigma_{Ci} = \left[\frac{\sigma_{Mi}^2 + \sigma_{Bi}^2}{V^2} + \frac{\sigma_V^2\left(M_i - B_i\right)^2}{V^4}\right]^{1/2} \tag{5-7}$$

$$\sigma_{RMSi} = \left(\frac{1}{n}\sum_{j=1}^{n}\sigma_{Ci}^2\right)^{1/2} \tag{5-8}$$

$$\sigma_V/V = 0.05 \tag{5-9}$$

where:

B_i = average amount of species *i* on field blanks

B_{ij} = the amount of species *i* found on field blank *j*

C_i = the ambient concentration of species *i*

F = flow rate throughout sampling period

M_i = amount of species *i* on the substrate

M_{ijf} = amount of species *i* on sample *j* from original analysis

M_{ijr} = amount of species *i* on sample *j* from replicate analysis

n = total number of samples in the sum

SIG_{Bi} = the root mean square error (RMSE), the square root of the averaged sum of the squared σ_{Bij}

STD_{Bi} = standard deviation of the blank

σ_{Bi} = blank precision for species *i*

σ_{Bij} = precision of the species *i* found on field blank *j*

σ_{Ci} = propagated precision for the concentration of species *i*

σ_{Mi} = precision of amount of species *i* on the substrate

σ_{RMSi} = root mean square precision for species *i*

σ_V = precision of sample volume

T = sample duration

V = volume of air sampled.

For ambient samples, dynamic field blanks were periodically placed in each sampling system without air being drawn through them to estimate the magnitude of passive deposition for the time period for which the filter packs remained in the sampler (typically 24 hours). Section 3.4.7 specified how dilution sampling system, electric arc, and nebulizer blanks were acquired for the source-testing conducted in the laboratory. After removal of outliers (i.e., concentration exceeding three times the standard deviations of the field blanks), the average field blank concentrations were calculated for each species on each substrate (e.g., Teflon-membrane, quartz-fiber).

5.2 Data Validation

Data acquired from the source testing, the laboratory analysis, and the Fresno Supersite IOPs were subjected to three data validation levels:

- Level 0 sample validation designates data as they come off the instrument. This process ascertains if the field or laboratory instrument is functioning properly.

- Level I sample validation: 1) flags samples when significant deviations from measurement assumptions have occurred; 2) verifies computer file entries against data sheets; 3) eliminates values for measurements that are known to be invalid because of instrument malfunctions; and 4) adjusts the values for quantifiable calibration or interference biases.

- Level II sample validation applies consistency tests to the assembled data based on known physical relationships between variables.

5.2.1 Chemical Analysis of Ambient and Source Samples

Level II data validation of chemical analysis on filters was conducted for physical consistency, cation and anion balances, and mass closure. In addition, specific QA procedures were developed for thermal carbon analysis of filter samples. These are addressed below.

5.2.1a Physical Consistency

The concentrations of various chemical species measured by different chemical analyses were examined. Physical consistency was tested for: 1) water-soluble sulfate versus total sulfur; 2) water-soluble chloride versus chlorine; and 3) water-soluble potassium versus total potassium. This analysis was done for the ambient Fresno samples collected during the winter and summer IOPs and for the laboratory-generated source samples. While the source samples were all analyzed by IC (due to the use of smaller filter punch and extraction in 10 ml of water to conserve the remaining filter aliquot for future analysis), ambient samples were analyzed by IC (chloride, nitrate, and sulfate), AC (ammonium) and AAS (sodium and potassium). Laboratory intercomparisons have demonstrated the equivalence between the different approaches for ion analyses. These samples were normalized to the entire quartz-fiber filter deposit area (11.78 cm^2 for ambient FRM and RAAS samples, and 13.8 cm^2 for source samples) to obtain concentration per filter.

Water-soluble sulfate versus total sulfur

The elemental sulfur mass concentration was measured on Teflon-membrane filters by XRF and water-soluble sulfate was measured on quartz-fiber filters by IC. If all of the sulfur were present as water-soluble sulfate, then the OLS slope would be three (the ratio of the molecular weight of sulfate to sulfur). Figure 5-1 displays the scatter plot of water-soluble sulfate versus total sulfur for the Fresno Supersite ambient measurements (Figure 5-1a) during winter and summer IOPs, and the source samples (Figure 5-1b). The error bars indicate the measurement uncertainty. The uncertainty is two to five times higher in the source compared to the ambient samples at similar mass concentrations. This is due to the fact that the source samples have much smaller sample collection volumes and a smaller punch area was used for source sample IC analysis (1.5 cm^2 for source samples versus 6.9 cm^2 for ambient samples). For the summer ambient samples, the slope was 2.7, with a negligible intercept, indicating that 90% of the sulfur was present as water-soluble sulfate. For the winter ambient samples, the slope was 2.4, with a negligible intercept, indicating that 80% of the sulfur was present was water-soluble sulfate. The source samples showed poor correlation ($r = 0.45$) with an OLS slope of 1.36 and an intercept of 0.79 $\mu g/m^3$. Removing the samples that have sulfate and sulfur concentrations below the limit of detection, and categorizing the source samples into wood smoke or diesel (Figure 5-1c) reveals that the wood smoke samples have an OLS slope of 2.5 and an intercept of 0.87 $\mu g/m^3$. The diesel samples have an OLS slope of 0.55 with an intercept of 0.40 $\mu g/m^3$; however, most of the samples are close to the 1:1 line. This indicates that for the diesel samples, the sulfur is not in the form of water-soluble sulfate. The "non-soluble" sulfur in diesel soot most likely comes from the sulfur in diesel fuel, sulfur dioxide adsorbed onto the diesel soot, organic sulfates, or zinc dialkyldithiophosphate oil additives (Willermet, 1998).

Water-soluble chloride versus total chlorine

The OLS slope of water-soluble chloride by IC to total chlorine by XRF should be less than or equal to unity. Figure 5-2 displays the scatter plot of water-soluble chloride versus total chlorine for the ambient Fresno Supersite (Figure 5-2a) and source (Figure 5-2b) samples. Good correlation ($r > 0.95$) was observed in both cases. The majority of the ambient samples had zero chloride and/or chlorine concentrations. Samples with concentrations greater than the MDL (6 out of 30) showed a slope of 0.92 with an intercept of 0.11 $\mu g/m^3$. For source samples, the slope was 1.01 with an intercept of 1.9 $\mu g/m^3$. The chloride/chlorine concentration was negligible for the sources tested. High concentrations in Figure 5-2b reflect samples where NaCl was mixed externally with pure combustion aerosols. Hence, it is expected that all of chlorine would be chloride and the unit slope indicates the validity of the measurement.

Water-soluble potassium versus total potassium

Figure 5-3 displays the scatter plot of water-soluble potassium by AAS for ambient, and by IC for source samples, versus total potassium by XRF for ambient (Figure 5-3a) and source (Figure 5-3b) samples. Good correlation ($r> 0.95$) was observed in all cases. The slope is 0.90 for the winter samples, and 0.82 for the summer samples, with a negligible intercept for the ambient samples. The OLS slope is 0.99 with an intercept of 0.1 $\mu g/m^3$ for the source samples. All of the non-zero potassium concentrations in source samples originated from wood-burning tests (pure wood smoke and wood smoke mixed with NaCl experiments). None of the other sources contained a large amount of potassium. Soluble potassium is typically used as a marker for vegetative burning emissions.

5.2.1b Anions versus Cations

The anions included in this analysis are the sum of the micro-equivalents of water-soluble chloride, nitrate, and sulfate. The cations consisted of summing the micro-equivalents of water-soluble ammonium, sodium, and potassium. The concentrations of each ion were divided by the molecular weight and charge to convert the concentration from $\mu g/m^3$ to micro equivalents per cubic meter ($\mu eq/m^3$). For the ambient samples, the summer samples had more cations than anions, with an OLS slope of 1.16 and a negligible intercept (Figure 5-4a). The ion concentrations in summer were well below 0.1 $\mu eq/m^3$. Anions not included in the analysis are carbonate and phosphate, which may explain the difference. The winter samples had more anions than cations (slope of 0.92 with a negligible intercept), but were well within the ±10% measurement uncertainty. The two-season linear regression slope is less than unity (slope = 0.88), since the winter samples (although fewer in number) had higher concentrations, which influences the two-season regression slope. For the source samples, the slope was 0.93 with a 0.11 $\mu eq/m^3$ intercept. Excluding the three outliers in Figure 5-4b, the slope was 1.07 with an intercept of 0.04 $\mu eq/m^3$. Source samples with cation and anion levels above 1 $\mu eq/m^3$ were the externally mixed (i.e., combustion aerosol + NaCl) samples. Pure source samples had ion concentrations less than 1 $\mu eq/m^3$. Thus, the cation to anion ratios in source samples were determined by the NaCl concentrations.

5.2.1c Mass Closure

Mass closure was examined by comparing the sum of the blank-subtracted measured species (i.e., sum of all measured elements, ions, and total carbon with the exception of S, Cl^-, and K^+ to avoid double-counting) with the mass concentration (by gravimetric analysis) on the Teflon-membrane filter. It should be noted that the hydrogen, oxygen, nitrogen, and sulfur, associated with OC and mineral elements are not included in the summed mass calculation, and therefore, the summed mass should be less than the gravimetric mass. On the other hand, the positive organic sampling artifact due to adsorption of organic vapor onto quartz-fiber filters may cause the OC level to be higher than that of the particles in the atmosphere. Good correlations (r = 0.93 to 0.99) were found for both ambient (Figure 5-5a) and source (Figure 5-5b) samples. The ambient samples showed a two-season slope of 0.84, while the source samples had a slope of 0.74 with a large intercept (78.45 $\mu g/m^3$). The intercept is caused by the high mass concentration data points that are well below the 1:1 line. The source samples that are noticeably lower than the 1:1 line are the electric arc samples. The source samples that are noticeably higher than the 1:1 line are the wood smoke samples, which contain more than 75% OC and have a larger sampling artifact. Figure 5-5c shows the regression statistics for the electric arc samples only, which indicate a slope of 0.90 and an intercept of -187.27 $\mu g/m^3$. The wood smoke samples have a slope of 0.85 with an intercept of 64.44 $\mu g/m^3$ (Figure 5-5d). Without the electric arc and wood smoke samples, the source samples have a slope of 0.97 with an intercept of 11.10 $\mu g/m^3$ (Figure 5-5e), suggesting reasonable mass closure.

5.2.1d QA/QC of Filter Carbon Analysis

The Quality Assurance Project Plan (QAPP; Volume II) follows U.S. EPA guidance (1998; 1999a; 1999b) and is supported by detailed standard operating procedures (SOPs) describing each measurement process. Table 5-1 lists the 49 SOPs applicable to this study. Each SOP includes: 1) a summary of measurement methods, principles, expected accuracy and precision, and the assumptions for validity; 2) materials, equipment, reagents, and suppliers; 3) individuals responsible for performing each part of the procedure; 4) traceability path, primary standards or reference materials, tolerances for transfer standards, and schedule for transfer standard verification; 5) start-up, routine, and shut-down operating procedures and an abbreviated checklist; 6) data forms; 7) routine maintenance schedules, maintenance procedures, and troubleshooting tips; 8) internal calibration and performance testing procedures and schedules; 9) external performance auditing schedules; and 10) references to relevant literature and related SOPs.

Several new auditing procedures (SOP #2-216.4) have been developed for the DRI Model 2001 Thermal/Optical Carbon Analyzer (Atmoslytic, Inc., Calabasas, CA). Table 5-2 lists the required QA/QC checks for thermal/optical carbon analysis of filter samples. Procedures applied to the various carbon analysis methods, include:

- *Multi-point temperature calibrations*. Temperature calibrations were tested with color-changing sensitive dyes (i.e., Tempilaq° G; Tempil, Inc., South Plainfield, NJ) to match the sample temperature to the sensor temperature reading. Thermocouples used to control the temperature programs deviate from the temperature of the sample owing to variations

of thermal masses and inhomogeneity in the oven. Color changes in Tempilaq° G can be detected optically and compared to the certified decomposition temperatures. A calibration procedure using such temperature-sensitive dyes was developed to match the sample temperature to the sensor temperature reading. Routine temperature calibration is part of the QA/QC in DRI carbon SOP #2-216.4. The temperature calibration factors are entered into the analysis software so that actual sample temperatures can match those specified in the protocol and be recorded in the database. A full temperature calibration with Tempilaqº G is performed every six months, or whenever the thermocouple is replaced. An example of temperature calibration is shown in Figure 5-6, with calibration data summarized in Table 5-3.

- *Characterization of analysis atmosphere*. An acceptance testing procedure has been developed to assure that oxidizing gases in the pure He stream are <100 ppmv for the analysis of OC in thermal/optical carbon analysis. Experiments by Chow et al. (2005a) determined that changes in EC and pyrolysis are negligible below this limit. The test method separates and quantifies trace gases from the ultrapure He carrier gas with precisions of ±1 ppmv using a GC/MS as a detector. This procedure has been integrated as part of the QA/QC activities in the DRI carbon SOP #2-216.4. Characterization of analysis atmosphere is performed quarterly, or whenever a leak in a system is detected.
- *Carbon analyzer calibration*. Each carbon analyzer is calibrated using traceable, calibrated and performance-tested gas standards for CH_4 and CO_2, and solution standards for potassium hydrogen phthalate (KHP) and sucrose. Each analysis instrument is calibrated with multipoint gas concentrations every six months, and methanator efficiencies are verified daily with CH_4 and CO_2 standards. A standard volume of CH_4 is included with each analysis to evaluate calibration and to normalize FID responses to calibration responses.
- *Calibration of laser intensity using neutral density filters*. The absolute reflectance and transmittance of a blank or loaded filter does not affect the optical charring correction during thermal analysis, since the split point is made by comparing the reflectance and transmittance during analysis with those prior to the analysis (initial value). The absolute reflectance and transmittance, however, is useful for more-detailed optical models for studying the increase of absorbance by particles deposited on or within the filter material, or by charred organic material within the filter (e.g., Chen et al., 2004; Petzold et al., 2005). To measure the absolute reflectance and transmittance, the laser intensity is calibrated against a set of neutral density filters with well-characterized attenuation (Wratten Gelatin, Kodak, Rochester, NY) over a broad wavelength region. First, neutral density filters are placed between the laser source and transmittance detector of a carbon analyzer. The relationship between the attenuation rating and transmittance measurement is established by linear regression. The intercept indicates the original laser intensity as detected by the transmittance detector. The reflectance detector is calibrated in the same way, by switching the positions of the two detectors. After calibration, the two detectors are switched back without changing the gain or any other parameter. The absolute reflectance and transmittance of the filter can then be determined by comparing the laser signals measured by the two detectors to the original laser intensity (as measured by each detector). This procedure of calibrating the laser intensity is intended for research

purposes. It is not yet implemented as a routine procedure for carbon analysis, since it affects neither the precision of the OC/EC split nor the carbon fraction measurements.

5.2.2 Data Reduction and QA of Continuous Measurements

5.2.2a Ambient Measurements at Fresno

The continuous measurements from Fresno were initially uploaded in raw format to a database designed specifically for data validation. Data from individual instruments was imported into separate tables identified by instrument name. Level I validation was conducted automatically by using stored procedures within the structured query language (SQL) database. Each instrument has a unique validation program which flags a variety of potential instrument failures and anomalies, including: flow deviation (for example, >5%, 10% or 15%), out-of-range measures, missing data, sampling time deviation, hardware problems, and instrument status codes. Flags, shown in Table 5-4 identify particular problems that occur during time of measure. These data flags were converted to three summary flags: valid (V), suspect (S), and invalid (I) as shown in Table 5-4. Unit conversion and time stamping of individual records is not consistent from instrument to instrument, therefore all time stamps were rolled back to the beginning of the sampling period (e.g., beginning of each five-minute sampling period) for each record as part of the automated procedure. Time corrections are also made during Level I validation. Once data was Level I validated, it was transferred to the main SQL database at DRI for storage and retrieval.

On-site check sheets are kept by ARB staff at the monitoring site at First Street in Fresno, CA, to document maintenance, instrument failure, or other anomalies that may occur. Since nitrate, sulfate, and the nephelometers required a zero and span correction, on-site zeros (typically using filtered air) and span-gas measurements were collected and noted in the instrument check sheets. This information was supplied to the DRI data coordinator, and adjustments were made using a regression algorithm. Data collected during these calibration periods were flagged as invalid along with any other problems noted in the check sheets. Data were given a general suspect level flag "S" if graphical inspection of data indicated potential outliers. A final QC check against the raw data file is performed to make sure that correct data format and proper flags were transferred into the final database.

The continuous instruments provided data on a high time resolution ranging from 3-sec to 1-hr time intervals. Flow rate deviations of 5% or more from the set value were flagged as "suspect" measurements. The PSAP data were adjusted for scattering effects using b_{scat} from a collocated three wavelength integrating nephelometer (Model 3563, TSI Inc., Shoreview, MN), following the procedure outlined by Virkkula et al. (2005). In this report, this adjusted b_{abs} is referred to as PSAP(adj), while the actual b_{abs} reported by the instrument is reported as PSAP(raw).

The PA b_{abs} measurements were compared with the instrument noise. All data points satisfying:

$$b_{abs} > \frac{\text{Noise}}{\sqrt{\text{averaging time}}} \Delta T_{step} \quad (5\text{-}10)$$

were included in the calculation of average absorption. In the above equation, 'b_{abs}' is the raw PA b_{abs} in Mm^{-1}, 'Noise' is the instrument noise corresponding to the reported b_{abs} in Mm^{-1}, 'averaging time' is the time period in seconds, for which the raw data is being averaged into (for 5-min average, it is 300 seconds), and 'ΔT_{step}' is the measurement time step (i.e., the time step over which the actual measurements were taken, which corresponds to the instrument averaging time). The 5-min average b_{abs} calculated using Eq. 5-10 were used to determine 1-hr average values for the purpose of intercomparisons.

Since most real-time instruments do not report measurement uncertainty, they were assumed based on values reported in the literature or in the respective user manuals. Typically, the uncertainties are reported as a percent of the mean measurement value. The actual uncertainty that was used in data processing (except for the PA) was calculated as follows:

$$\text{Resultant instrument uncertainty} = \sqrt{(\text{UNC} \times \text{mean})^2 + \text{MDL}^2} \quad (5\text{-}11)$$

where:

UNC is the reported uncertainty in %; mean is the mean measurement value; and MDL is the minimum detection limit.

Thus, as the mean measurement value (b_{abs} or BC concentration) approaches zero, the resultant uncertainty will approach the MDL of the instrument. Since the PA records instrument noise (Mm^{-1}) along with b_{abs} measurements, the 5-min average noise value was considered to be the resultant instrument uncertainty for PA measurements.

For the aethalometer, the UNC was estimated from collocated BC measurements recorded by the 2-AE and 7-AE using the following equation:

$$\text{AE UNC} = \frac{1}{n} \sum 100 \times \frac{(2\text{AE} - 7\text{AE})}{(2\text{AE} + 7\text{AE})/2} \quad (5\text{-}12)$$

This was estimated to be ~10% for the AE. An uncertainty of 8% was assumed for PSAP, based on results presented by Virkkula et al. (2005). Petzold et al. (2004) reported an uncertainty of 12% in b_{abs} measurements by MAAP. For the Sunset thermal OC, thermal EC, and TC measurements, uncertainties were taken to be 10%, 20%, and 10% respectively (Bae et al., 2004). An uncertainty of 10% was assumed for the Sunset optical BC measurements, since its principle is similar to that of the aethalometer. Table 5-5 summarizes the UNC and MDL used in calculations. Uncertainties for hourly average concentrations (except for the Sunset, which

already reports hourly average) were obtained by calculating the square root of the mean squared (RMS) 5-min instrument uncertainties.

Data were converted to a standard temperature and pressure (STP), defined here as 25 °C and 1 atm pressure, for the intercomparisons. The b_{abs} or carbon (OC, BC, EC, and TC) measurements were converted to 25 °C and 1 atm pressure as follows:

$$CONC_{STP} = CONC_{reported} \times \frac{P_{STP}}{P_{reported}} \times \frac{T_{reported}}{T_{STP}} \quad (5\text{-}13)$$

$$b_{abs(STP)} = b_{abs(reported)} \times \frac{P_{STP}}{P_{reported}} \times \frac{T_{reported}}{T_{STP}} \quad (5\text{-}14)$$

where

$CONC_{STP}$ = Concentration at STP conditions of 25 °C and 1 atm pressure

$CONC_{reported}$ = Concentration at conditions reported by the instrument

$b_{abs(STP)}$ = Light absorption at STP conditions of 25 °C and 1 atm pressure

$b_{abs(reported)}$ = Light absorption at conditions reported by the instrument

P_{STP} = Standard pressure = 1013.25 millibar (mbar)

T_{STP} = Standard temperature = 298.15 degrees Kelvin (°K)

$P_{reported}$ = Pressure at which measurements were reported in mbar

$T_{reported}$ = Temperature at which measurements were reported in degree Kelvin.

For the PA, the temperature and pressure recorded by the instrument was used in the calculations for $T_{reported}$ and $P_{reported}$, respectively. For the MAAP, the Sunset and the filter samplers, hourly (for continuous instruments) or daily averages (for filter samplers) of ambient temperature and pressure were used, for $T_{reported}$ and $P_{reported}$, respectively. The ambient temperature and pressure were obtained from the meteorological measurements made at the Fresno Supersite.

5.2.2b Laboratory Measurements

For measurements conducted in the source characterization laboratory at DRI, data from the continuous instruments were downloaded daily. All data were imported into Microsoft Excel.

The data were compared with laboratory data sheets, and time periods associated with each filter sample collection were highlighted for easy identification and processing. Continuous data collected between filter changes were not considered in any analysis. The data were also manually processed to identify error codes and the identified data were rendered invalid and removed from the processed data set. The measurement uncertainties for the continuous instruments were estimated using the procedure explained in Section 5.2.2a. All laboratory measurements were also converted to STP before conducting intercomparisons.

5.3 QA/QC for Source Testing

5.3.1 Filter Deposit Inhomogeneity

As discussed in Section 3.4.3, inhomogeneity of sample deposit may occur for source samples acquired with the miniature dilution/residence chamber. To test for the homogeneity of particulate deposit on the filters, two or more punches (one from the center and the other from edge of the filter) were analyzed for OC/EC following the IMPROVE_A protocol. This check was performed on at least one sample for each source category and sampling configuration. Initially, all filter samples were subject to this check, but as it became evident that the modified sampling configuration showed a homogeneous deposit, only 10% of the samples were checked. Table 5-6 displays the carbon ratios of center punch to edge punch analyses. It was found that, for the electric arc experiments, the sampling set-up of miniature dilution/residence chamber without the conical sampling manifold (electric arc set-up #1) gave a non-uniform deposit on the filter. The center of the filter showed TC concentrations that were 11 to 60% higher than the edge of the filter. The sampling set-up for the electric arc soot was redesigned by increasing the filter holder inlet diameter from 6.35 mm to 41.28 mm, which was connected to the conical sampling manifold (electric arc set-up #2; see Section 3.4.3, Figures 3-6 and 3-11). This set-up was used for all further electric arc tests. The modified configuration resulted in a center to edge TC ratio ranging from 0.93 to 1.12 (with the exception of one value of 1.25). The set-up that was used for diesel, acetylene, and wood smoke experiments (DRI dilution/residence chamber and conical sampling manifold, see Figure 3-2) showed center to edge TC ratios ranging from 0.94 to 1.15 for diesel (except one value of 1.25), 0.96 to 1.0 for acetylene, and 0.93 to 1.02 for wood smoke experiments. EC/TC and OC/TC ratios were also within 15% between the center and edge punches for diesel, acetylene, and wood smoke samples. Thus, the center and edge punches showed concentrations typically within 10 to 15% for TC, EC/TC and OC/TC. The nine inhomogeneous electric arc samples collected using sampling set-up #1 (Filter IDs STRSQ001 to STRSQ009) were excluded from the intercomparisons.

5.3.2 QA/QC for the Generation of Source Aerosol

As part of QA/QC, several instrument checks were performed before, during, and after source sampling. Upon start up, internal checks were applied to all of the continuous instruments. These instruments were allowed at least 30 minutes of warm-up time before sampling was initiated. The DustTrak was checked with an in-line HEPA filter to determine the instrument response to particle-free air (i.e., zero check). The instrument was re-zeroed, if necessary. Impactors on the sizing instruments and the DustTrak were cleaned daily, or more often, as necessary. During each experiment, the responses of the three sizing instruments were compared

to see if they had similar size profiles and concentrations. If any instrument disagreed from the rest, that instrument was taken offline and the problem was resolved before it was re-connected to the sampling manifold.

The flow rate through each filter was set prior to the start of each sample collection period, and verified at the end of every sample collection, using a rotameter that had been calibrated against a NIST (National Institute of Standards and Technology)-traceable Roots meter. During each run, the flow rates were also monitored using a TSI digital mass flow meter to examine the change in flow rate over the sampling period. If the initial and final flow rates through the filter differed by less than 5%, an arithmetic average of the initial and final flow rate was used to calculate the total volume sampled. If the final flow rate decreased by more than 5% relative to the initial flow rate, the mass flow rate monitored by the TSI digital flow meter was analyzed to examine its temporal variation. In every case, the flow rate decreased linearly during the run. Thus, the arithmetic average of the initial and final flow rate was used to calculate the total sample volume. For the 264 filters, the flow rate varied by 0-5% for 78.8% of the filters; by 5-10% for 19.7% of the filters, and by >10% for 1.5% of the filters. The samples with more than 10% decrease in flow rate corresponded to electric arc samples.

5.4 Reproducibility of Source Aerosol Generation

The reproducibility of aerosol generation was investigated for each source category using replicate runs conducted for each experimental set up. This was evaluated for each of the different source categories by examining the relative standard deviation (RSD, standard deviation divided by the arithmetic mean, expressed in percentage) of carbon (OC, EC, and TC by the IMPROVE_A_TOR protocol), gravimetric mass, and DustTrak b_{scat} expressed as a mass concentration. Table 5-7 summarizes the parameters for the individual filters, as well as the arithmetic average and RSD for each source category, with graphic presentations of RSD displayed in Figures 5-7 through 5-9. With a few exceptions, the overall RSD of TC was ±15% for diesel, acetylene, and electric arc soot. The RSD for wood smoke (e.g., TC and EC/TC) displayed larger variations of 20% to 60%, reflecting the natural variability in wood smoke emissions. In certain cases, OC/TC or EC/TC RSD exceeded 50%. After blank subtraction, the mean OC concentration is low with a larger variability in RSD. Mass, filter b_{abs}, and PA b_{abs} measurements, which are not affected by the OC artifact, generally showed lower RSD. Similar RSDs (±10%) were found for gravimetric and DustTrak mass concentrations with the largest variations (10 to 70%) found in wood smoke and carbon black samples. Reproducibility for b_{abs} was also within ±10%, except for wood smoke and carbon black samples, which showed variations between 10 to 70%.

5.4.1 Diesel Generator

The diesel generator experiments were highly reproducible, with RSDs typically less than 20% for carbon and less than 10% for b_{abs}, and b_{scat} equivalent mass. Diesel samples consisted of 40% OC and 60% EC. The high RSD for OC/TC ratio for Filter IDs STRSQ011 – 013 are due to low OC/TC values, with slight variations in the OC/TC ratio yielding large RSDs. The high RSD (>50%) for Filter IDs STRS014-16 was due to one sample (STRSQ016; Table 5-7) having an abnormally high pyrolysis correction, resulting in a higher OC fraction (87% OC). The majority

(39 out of 44) of the diesel samples had negligible pyrolysis correction. Dilution ratios were within ±6% of the set value.

The particle size distributions for diesel emissions at dilution ratios of 18 and 40 are shown in Figure 5-10. A single mode between 50 and 60 nm was found. The number concentration profile of Filter ID STRQQ097, with a dilution ratio of 18, was similar to those samples with a dilution ratio of 40. This sample was obtained on a different day and with a different batch of fuel. However, carbon fractions, b_{abs}, and gravimetric mass for this sample were similar to other samples with a dilution ratio of 18. It is unclear why this sample had a lower number concentration profile. Figure 5-10 shows that increased dilution ratios result in lower particle number concentrations, but they do not change the modal diameter.

5.4.2 Acetylene Flame

The acetylene flame samples showed less than 10% RSD for TC, PA b_{abs}, and gravimetric filter mass concentration. The filter densitometry b_{abs} (Figure 5-8) and the DustTrak b_{scat} equivalent mass concentrations (Figure 5-9) showed less than 20% RSD. Acetylene soot consisted mostly of EC with less than 7% OC; with half (9 out of 18) of the samples containing less than 1% OC (Table 5-7). These low values yielded large RSDs even with slight variations in OC abundance. Little variability (<5% RSD) was found for dilution ratios, demonstrating that these samples can be generated under controlled environments. Figure 5-11 displays the size distribution of all the acetylene flame samples. The acetylene flame was bimodal, with a sharp peak around 15-18 nm and a broad peak around 250 nm.

5.4.3 Electric Arc

The electric arc soot showed good reproducibility (except for Filter IDs STRQQ081-083 for b_{abs}) with RSDs typically under 15% for OC/TC, EC/TC, and TC and DustTrak b_{scat} equivalent mass, and under 10% for gravimetric mass, filter b_{abs}, and PA b_{abs}. Filter IDs STRQQ088 and STRQQ089 had greater than 30% RSDs for EC/TC and OC/TC. These two samples showed unusually low (18%) EC, as compared to the majority of the electric arc samples at 950 a.u. current, which yielded typically 40 to 50% EC. As shown later in Section 6.2.1c, the electric arc soot showed an unique thermogram (Figure 6-14) that contains a sharp EC1 peak. The peak is so narrow in time (10 – 15 s) and intense in amplitude that the OC/EC split error due to transit time (i.e., the time for the evolved carbon be detected by FID) becomes important. It was found that the transit time in the carbon analyzer analyzing the two outlier samples was off by 2 sec. Due to the very sharp EC1 peak, the slight change in the transit time significantly influenced the amount of carbon assigned to OP and hence the OC/EC split. The electric arc samples at 950 a.u. current have a single mode with a peak between 90 and 110 nm, as shown in Figure 5-12. The electric arc samples at 300 a.u. current has a slightly higher EC (50 to 70%) fraction and has a single mode with a peak between 45 and 60 nm (not shown).

5.4.4 Wood Smoke

The wood smoke samples showed the largest variability among the sources tested, with RSDs typically between 20 and 60% for TC, EC/TC, filter b_{abs}, and PA b_{abs}, and filter and DustTrak b_{scat} equivalent mass concentrations. The OC/TC ratio showed RSDs less than 20% for all wood smoke samples (except for Filter IDs STRQQ171 and STRQQ173), as OC accounted for 65 to 85% of TC. The large RSD was caused by Filter IDs STRQQ171 and STRQQ173, which had unusually low OC/TC values (0 and 25%). The wood smoke number size distribution was highly variable, both in absolute number concentration and location of the modal diameter which varied from 75 to 100 nm (Figure 5-13). It is unclear why a lower dilution ratio of 18 would have lower number concentrations than those with dilution ratio of 40. This is also reflected in TC concentration for both the pure and mixed (wood smoke + NaCl) samples (Table 5-7). The sampling set-up was checked and no problems were noticed. One possible explanation is that the average sample flow rate at the venturi through the heated inlet was lower for the dilution ratio of 18 (19 L/min) compared to the flow rate at the dilution ratio of 40 (22 L/min), which could have influenced the amount of air that reached the fire. The flow rate of air through the sample line would influence the quantity of air entering the wood stove. The ~14% lower venturi flow rate at a dilution ratio of 18, relative to that at a dilution ratio at 40, could have lowered the quantity of air entering the wood stove, resulting in a possibly slower burn rate, which may have led to lower mass emissions. The result of a 14% difference in flow rate leading to more than 50% decrease in emissions demonstrates the sensitivity of wood burning emissions to the combustion conditions.

5.4.5 Nebulized Carbon Black

The nebulized carbon black samples showed high variability, with RSDs between 30 and 70% for b_{abs} and mass, and greater than 100% for carbon. This is probably due to the difficulty in suspending carbon black in solution, resulting in a different aerosol generation rate for each run, as well as the low amount of carbon black deposited on the filter. The average size distributions of three separate nebulized carbon black samples are shown in Figure 5-14. The nebulized carbon black samples were bimodal, with one peak around 15-18 nm, and a second peak between 120 and 140 nm. However, unlike the acetylene flame, the nebulized carbon black samples showed varying peak concentrations for a single condition. The peak around 15-18 nm is due to the solvent matrix (95% DDW, 5% methanol), and is fairly constant during the run (Figure 5-15). However, the carbon black peak between 120 and 140 nm starts off at a low concentration and gradually increases with time. This leads to an increase in mass concentration with time, as seen in Figure 5-16. Increasing the sonication time from 12 to 30 minutes did not change this behavior. However, it is encouraging to note that the modal diameters stayed consistent. This behavior will be investigated further under another research project (U.S. EPA Science to Achieve Results [STAR] Grant No. R831086).

Table 5-1. Summary of Standard Operating Procedures (SOPs) applied to this study.

DRI SOP#	DRI SOP Title
Environmental Analysis Facility	
2-102.5	Gravimetric Analysis Procedure
2-104.3	Impregnating, Drying, and Acceptance Testing of Filters for Sampling Gases in Air
2-106.5	Pre-firing and Acceptance Testing of Quartz-Fiber Filters for Aerosol and Carbonaceous Material Sampling
2-107.2	Light Transmission Analysis Procedure
2-108.3	Sectioning of Teflon and Quartz Filter Samples
2-109.5	Extraction of Ionic Species from Filter Samples
2-110.4	Filter Pack Assembling, Disassembling, and Cleaning Procedure
2-111.5	Sample Shipping, Receiving, and Chain-of-Custody
2-112.2	$PM_{2.5}$ FRM Filter Pack Assembly, Disassembly, and Cleaning
2-113.2	$PM_{2.5}$ FRM Sample Shipping, Receiving, and Chain-of-Custody
2-114.2	$PM_{2.5}$ FRM Gravimetric Analysis
2-203.6	Anion Analysis of Filter Extracts and Precipitation Samples by Ion Chromatography
2-208.1	Cation Analysis of Filter Extracts and Precipitation Samples by Ion Chromatography
2-206.3	Analysis of Filter Extracts and Precipitation Samples by Atomic Absorption Spectroscopy
2-207.5	Analysis of Filter Extracts and Precipitation Samples for Ammonium by Automated Colorimetric Analysis
2-209.1	X-Ray Fluorescence Analysis of Aerosol Filter Samples (Panalytical Epsilon 5)
2-204.6	Thermal/Optical Reflectance Carbon Analysis of Aerosol Filter Samples – IMPROVE Protocol
2-216.4	DRI Model 2001 Thermal/Optical Carbon Analysis (TOR/TOT) of Aerosol Filter Samples – IMPROVE_A Protocol
2-201.2	DRI Model 2001 Thermal/Optical Carbon Analysis (TOR/TOT) of Aerosol Filter Samples – STN Protocol
2-218.1	DRI Model 2001 Thermal/Optical Carbon Analysis of Aerosol Filter Samples – French Two-Step Protocol
2-217.1	In-injection Port Thermal Desorption and Subsequent GC/MS Analysis of Non-Polar Organic Species in Aerosol Filter Samples
Field Instruments	
1-201.1	High Volume (Hi-Vol) Samplers: Operation, Maintenance, and Field Calibration
1-223.1	EcoTech High Volume Sampler (HiVol): Operation and Maintenance
1-226.1	Anderson Single Channel FRM Sampler (FRM): Operation and Maintenance
1-233.1	Andersen Reference Ambient Air Sampler (RAAS) 2.5-400 Chemical Speciation Monitor: Operation and Maintenance
1-221.1	MetOne Beta Attenuation Monitor: Operation and Maintenance
1-215.1	Kimoto SPM-613D Beta Gauge Monitor (BAM): Operation and Maintenance
1-236.1	Rupprecht and Patashnick (R&P) Series 1400a Tapered Element Oscillating Microbalance (TEOM): Operation and Maintenance
1-234.1	Rupprecht and Patashnick 8400N Ambient Particulate Nitrate Monitor: Operation and Maintenance
1-235.1	Rupprecht and Patashnick 8400S Ambient Particulate Sulfate Monitor: Operation and Maintenance
1-224.1	Sunset Laboratory Semi-Continuous OCEC Carbon Aerosol Analyzer: Operation and Maintenance
1-218.1	EchoChem Analytics Realtime Polycyclic Aromatic Hydrocarbon (PAH) Monitor PAS 2000: Operation and Maintenance
1-214.1	TSI DustTrak Photometer: Operation and Maintenance
1-416.1	Optec NGN2 Open-Air Integrating Nephelometer: Operation and Maintenance
1-415.1	Radiance Research Model 903 Nephelometer: Operation and Maintenance
1-413.1	EcoTech Nephelometer: Operation and Maintenance
1-414.1	TSI 3 wavelength Nephelometer: Operation and Maintenance
1-406.1	Magee Aethalometer: Operation and Maintenance
1-417.1	Radiance Research Particle Soot Absorption Photometer (PSAP): Operation and Maintenance
1-225.1	Multi-Angle Absorption Photometer (MAAP): Operation and Maintenance
1-407.1	DRI Photoacoustic Spectrometer (PA): Operation and Maintenance
1-211.1	TSI Scanning Mobility Particle Sizing Instrument (SMPS): Operation and Maintenance
1-212.1	GRIMM Scanning Mobility Particle Sizing + Counter Instrument (SMPS + C): Operation and Maintenance
1-213.1	MSP Wide-Range Particle Spectrometer (WPS): Operation and Maintenance
1-219.1	Climet Instruments SPECTRO 0.3: Operation and Maintenance
1-220.1	Particle Measuring Systems Lasair 1003: Operation and Maintenance
1-250.1	Resuspension of Bulk Samples onto Teflon and Quartz Filters
1-412.1	DRI Dilution Sampling System: Operation and Maintenance
1-216.1	DRI Monomodal Aerosol Generator: Operation and Maintenance

Table 5-2. Summary of QA/QC activities for carbon analysis by DRI Model 2001 Thermal/Optical Carbon Analyzer.

Requirement	Calibration Standard	Calibration Range	Calibration Frequency	Performed By	Acceptance Criteria	Corrective Action
System Blank Check	N/A	N/A	Beginning of analysis day	Carbon Analyst	≤ 0.2 µg C/cm^2	Check instrument and filter lots
Leak Check	N/A	N/A	Beginning of analysis day	Carbon Analyst	Oven pressure drops less than 0.01 per second	Locate leaks and fix
Laser Performance Check	N/A	N/A	Beginning of analysis day	Carbon Analyst	Transmittance >700 mV; Reflectance >1500 mV	Check laser and filter holder position
Calibration Peak Area Check	NIST 5% CH_4/Helium gas standard	20 µg C (Carle valve injection loop, 1000 µl)	Every analysis	Carbon Analyst	Counts >20,000 and 95-105% of average calibration peak area of the day	Discard analysis result and repeat analysis with second filter punch
Auto-Calibration Check	NIST 5% CH_4/Helium gas standard	20 µg C (Carle valve injection loop, 1000 µl)	Beginning of analysis day	Carbon Analyst	95-105% recovery and calibration peak area 90-110% of weekly average	Troubleshoot and correct system before analyzing samples
Manual Injection Calibration	NIST 5% CH_4/Helium or NIST 5% CO_2/Helium gas standards	20 µg C (Certified gas-tight syringe, 1000 µl)	End of analysis day	Carbon Analyst	95-105% recovery and calibration peak area 90-110% of weekly average	Troubleshoot and correct system before analyzing samples
Multiple Point Calibrations	1800 ppm Potassium hydrogen phthalate (KHP) and sucrose; NIST 5% CH_4/Helium and NIST 5% CO_2/Helium gas standards	9-36 µg C for KHP and sucrose; 2-30 µg C for CH_4 and CO_2	Six months	Carbon Analyst	All slopes ±5% of average	Troubleshoot instrument and repeat calibration until results are satisfactory
Sample Replicates	N/A	N/A	Every 10 analyses	Carbon Analyst on same or different analyzer	±10% when OC, EC, TC ≥ 10 µg C/cm^2 or < ±1 µg/cm^2 when OC, EC, TC < 10 µg C/cm^2	Investigate instrument and sample anomalies and rerun replicate if reason for poor result not found
Temperature Calibrations	Tempilaq^o G (Tempil, Inc., South Plainfield, NJ, USA)	Three replicates each of 121, 184, 253, 510, 704, 816 ºC	Six months, or whenever thermocouple is replaced	Carbon Analyst	Reflectance-based method gives a lower liquefying temperature than the transmittance-based method within ±2 °C	Troubleshoot instrument and repeat calibration until results are satisfactory
Oxygen Level in Helium Atmosphere	Certified gas-tight syringe	0-100 ppmv	Quarterly or whenever leak is detected	Carbon Analyst using a GC/MS system	Less than the certified amount in the helium cylinder	Replace the helium cylinder and/or O_2 scrubber

Table 5-3. Examples of temperature calibration for five DRI Model 2001 Thermal/Optical Carbon Analyzers.

Test Date	Tempilaq° G Indicator Temperature (°C)	121 ± 2	184 ± 2	253 ± 3	510 ± 6	704 ± 8	816 ± 9	1. Slope (b) 2. Intercept (a) 3. Number of Tests (n) 4. Correlation (r)
08/17/05	DRI Model 2001 CA#8 $\overline{T}$ [a]	121	184	248	483	671	803	b = 1.0314 ±0.006 a = 1.0211 ±0.905 n = 36 (6×6) r = 0.9995
	ΔT [b]	(-4) to 3	6 to 8	5 to 5	21 to 33	27 to 46	10 to 15	
	$\overline{\Delta T} \pm \sigma_{\Delta T}$ [c]	0 ± 3	7 ± 1	5 ± 0	27 ± 4	33 ± 8	13 ± 2	
07/20/05	DRI Model 2001 CA#9 $\overline{T}$ [a]	117	184	239	489	674	797	b = 1.0249 ±0.005 a = 6.002 ± 2.061 n = 30 (5×6) r = 1.000
	ΔT [b]	2 to 5	7 to 14	10 to 18	20 to 22	27 to 30	11 to 24	
	$\overline{\Delta T} \pm \sigma_{\Delta T}$ [c]	4 ± 1	11 ± 3	15 ± 4	21 ± 1	30 ± 2	19 ± 5	
08/23/05	DRI Model 2001 CA#11 $\overline{T}$ [a]	113	184	234	483	679	811	b = 1.000 ± 0.002 a = 14.909 ± 2.981 n = 36 (6×6) r = 0.9995
	ΔT [b]	8 to 10	12 to 15	15 to 22	23 to 32	24 to 27	4 to 11	
	$\overline{\Delta T} \pm \sigma_{\Delta T}$ [c]	9 ± 1	14 ± 1	19 ± 2	27 ± 5	26 ± 1	6 ± 3	
10/27/05	DRI Model 2001 CA#13 $\overline{T}$ [a]	113	184	235	484	665	796	b = 1.032 ± 0.005 a = 8.008 ± 1.907 n = 36 (6x6) r = 0.9995
	ΔT [b]	7 to 10	11 to 15	15 to 22	18 to 31	34 to 42	19 to 22	
	$\overline{\Delta T} \pm \sigma_{\Delta T}$ [c]	8 ± 1	12 ± 2	18 ± 2	26 ± 6	39 ± 3	20 ± 1	
11/02/05	DRI Model 2001 CA#14 $\overline{T}$ [a]	117	184	248	501	681	804	b = 1.019 ± 0.003 a = 2.089 ± 1.612 n = 36 (6×6) r = 1.000
	ΔT [b]	2 to 5	4 to 9	5 to 5	4 to 14	21 to 25	10 to 14	
	$\overline{\Delta T} \pm \sigma_{\Delta T}$ [c]	4 ± 1	7 ± 2	5 ± 0	10 ± 4	23 ± 1	12 ± 2	

[a] $\overline{T}$ is the average measured temperature.

[b] ΔT is the difference between the measured and rated Tempilaq° G temperatures.

[c] $\overline{\Delta T} \pm \sigma_{\Delta T}$ indicates the average and standard deviation of ΔT.

Table 5-4. List of flags used for continuous data validation of ambient measurements at Fresno.

Data Flag	Final Summary Flag[a]	Description
	V	Null/zero-length string - valid
A	I	Sampler adjustments/maintenance/audits
A4	I	Invalid due to less than 4 one min measurements in average frequency
aQ	S	Suspect analyzer flow
Au	I	Automatic calibration
bL	S	Suspect baseline area
cP	S	Suspect cell pressure
D15	I	Counts in bins 1-5 all zero - physically impossible
D6	I	Counts in bin 6 equal to zero - physically impossible
dP	S	Suspect change in analyzer pressure
dPimp	S	Suspect pressure drop across impactor nozzle
F	I	Instrument failure
fhv	S	Suspect high voltage
fog	S	Fog
fsh	S	Suspect sheath flow stability
I	I	Invalid
I2	I	Invalid meteorological value
I3	I	Particle count out of expected range
I4	I	Measurement out of expected range
I5	I	Invalid high scattering from ambient conditions (high zero and span offsets attributes to reaching instrument max -- wall scattering)
I6	I	Invalid scattering due to power fluctuations, loss, outage, lamp efficiency, brightness, failure. including internal calibration of photomultiplier tube
I7	I	Invalid
Lf	I	Lamp failure
Lh	I	Lamp brightness boundary limits exceeded
lmp	S	Lamp reference below lower limit
lref	I	Laser reference drops below acceptable value of 4.5 volts
O	I	Operational error
P	I	Power failure
Pabs	S	Absolute pressure out of range
Q10	S	Flow deviation > 15%
Q6	S	Flow deviation 5% < q < 10%
Q7	S	Sample flow deviation from nominal by 10% < q < 15%
Q8	I	Flow deviation ± 10% tolerance
Qaer	S	Aerosol flow deviation greater than 5%
Qby	S	Bypass flow out of range
Qimp	S	Impactor flow out of range
Qsh	S	Sheath flow out of range
Qsh2	S	Sheath flow deviation greater than 5%
Qsmp	S	Sample flow out of range
R	V	Replaced serial data with analog data

Table 5-4. Continued.

Data Flag	Final Summary Flag[a]	Description
R2	V	Replaced with ARB data logger
RH	S	Relative humidity out of desired range
S	S	Suspect
S0	S	Suspect due to non-standard sampling conditions
S1	S	Suspect value: Instrumental problems requiring small correction
S2	S	Suspect value: Instrumental problems; data corrections more than 20% from nominal
S3	S	Suspect particle count measurement
S4	S	Suspect measured concentration
S5	S	Suspect scattering measurement
sc	S	Status code output by instrument
SH	S	High b_{scat} reading
SL	S	Low b_{scat} reading
sP	S	Suspect sample pressure
sQ	S	Suspect sample flow
SU	S	Suspect value: uncorrected
T	S	Suspect sample duration
T0	S	Sample time duration variation of less than 10%
T1	I	Sampling interval duration <90% of set (>10% deviation in sampling)
T2	I	Sample time duration variation of greater than 10%
tF	S	Suspect flash duration
Tsh	S	Suspect sheath flow temperature
V	V	Unflagged / valid
Vf	S	Suspect sample volume
VR0	S	Void replace with zero
X	X	Missing data
xQ	S	Suspect cross flow
Y	I	Flow volume error
Y8	S	Flow collection volume variation of ± 10 to 20%
Y12	I	Flow collection volume variation of greater than 20%

[a] V- Valid; S- Suspect; I- Invalid

Table 5-5. Instrument uncertainty and minimum detection limits (MDLs).

Instrument	Uncertainty (UNC), %	MDL[a]	Reference
2-AE, 7-AE	10%, based on collocated measurements	5-min: 0.060 μg/m^3	Aethalometer User manual
PSAP	8%	[b]467 nm:0.48 Mm^{-1} [b]530 nm: 0.13 Mm^{-1} [b]660 nm: 0.09 Mm^{-1}	Virkkula et al. (2005)
MAAP	12%	2-min: 0.1 μg/m^3; 0.66 Mm^{-1} 1-min: 0.141 μg/m^3	Petzold et al. (2002)
PA (532 nm and 1047 nm)	Average instrument noise was taken to be the uncertainty	10 min: 0.4 Mm^{-1} (not used in calculation; listed here for comparison)	Arnott et al. (1999)
Sunset	Thermal OC = 10% Thermal EC = 20% Optical BC = 10% TC = 10%	OC = 0.2 μg/m^3 EC = 0.2 μg/m^3 TC = 0.4 μg/m^3	Bae et al. (2004)

[a] Interpolation from one time basis to another was done as follows:

$$MDL_{t1} = MDL_{t2}\sqrt{\frac{t2}{t1}}$$, where t1 and t2 are the different time basis

[b] Three times standard deviation of 1-min noise (with 60 sec cycle time) reported in Virkkula et al. (2005), converted to 5-min basis

Table 5-6. Carbon analysis of center punch versus edge punch.

Center / Edge Ratios						
Filter ID	**OC**	**EC**	**TC**	**OC/TC**	**EC/TC**	**Set-up Conditions**
STRSQ011	0.90	1.00	0.94	0.96	1.07	Diesel set up: with DRI dilution/residence chamber and conical sampling manifold[b]
STRSQ012	1.16	1.05	1.12	1.04	0.94	
STRSQ014	1.08	1.11	1.09	0.99	1.02	
STRSQ015	0.98	0.97	0.97	1.00	1.00	
STRSQ016	1.04	1.14	1.08	0.97	1.05	
STRSQ018	1.06	1.20	1.11	0.95	1.08	
STRSQ019	0.99	1.05	1.02	0.98	1.03	
STRSQ020	1.04	1.18	1.10	0.95	1.07	
STRSQ042	0.97	1.01	0.98	0.98	1.03	
STRSQ043	0.94	1.01	0.97	0.97	1.05	
STRSQ044	0.93	0.98	0.95	0.98	1.03	
STRSQ045	0.98	1.09	1.02	0.96	1.06	
STRSQ047	0.94	0.96	0.95	0.99	1.01	
STRSQ048	1.13	0.92	1.04	1.09	0.88	
STRSQ049	1.02	0.95	0.99	1.03	0.96	
STRSQ051	1.01	0.86	0.95	1.07	0.90	
STRSQ052	1.02	0.96	1.00	1.02	0.97	
STRSQ053	1.03	1.12	1.07	0.97	1.05	
STRSQ054	1.29	1.20	1.25	1.03	0.96	
STRSQ055	1.09	1.01	1.06	1.03	0.96	
STRSQ056	1.04	0.81	0.94	1.11	0.87	
STRSQ057	1.06	1.05	1.06	1.00	0.99	
STRSQ058	0.99	1.01	1.00	0.99	1.01	
STRSQ060	1.00	1.02	1.01	0.99	1.01	
STRSQ061	0.97	1.00	0.99	0.99	1.02	
STRSQ062	1.25	1.03	1.15	1.08	0.89	
STRSQ063	1.05	0.99	1.02	1.03	0.97	
STRQQF093	1.00	1.12	1.06	0.95	1.06	
STRQQF102	1.02	0.86	1.00	1.03	0.87	Acetylene flame: with DRI dilution/residence chamber and conical sampling manifold[b]
STRQQF114	0.97	0.95	0.96	1.00	0.99	
STRSQ001	1.35	1.20	1.23	1.10	0.98	Electric arc set-up #1: with miniature dilution/residence chamber without conical sampling manifold[a]
STRSQ002	1.19	1.22	1.20	0.99	1.02	
STRSQ003	1.18	1.21	1.20	0.98	1.01	
STRSQ004	1.29	1.02	1.14	1.14	0.90	
STRSQ005	1.36	0.95	1.11	1.22	0.85	
STRSQ006	1.45	1.01	1.20	1.21	0.85	
STRSQ007	1.16	1.10	1.13	1.03	0.98	
STRSQ008	0.94	2.30	1.60	0.59	1.44	
STRSQ009	1.91	0.96	1.55	1.23	0.62	

Table 5-6. Continued.

Center / Edge Ratios						
Filter ID	**OC**	**EC**	**TC**	**OC/TC**	**EC/TC**	**Set-up Conditions**
STRSQ025	0.93	1.17	1.07	0.87	1.10	Electric arc set-up #2: with miniature dilution/residence chamber with conical sampling manifold[b]
STRSQ026	0.97	1.00	0.99	0.98	1.02	
STRSQ027	0.98	0.93	0.95	1.03	0.98	
STRSQ028	0.78	1.23	0.99	0.78	1.24	
STRSQ029	0.90	1.14	1.03	0.88	1.11	
STRSQ030	1.01	0.96	0.99	1.03	0.98	
STRSQ031	1.11	1.13	1.12	0.99	1.01	
STRSQ035	0.77	1.31	1.00	0.76	1.31	
STRSQ036	1.27	0.88	1.06	1.20	0.83	
STRSQ037	0.70	1.25	0.94	0.75	1.33	
STRSQ038	1.01	1.05	1.03	0.98	1.02	
STRSQ039	0.77	1.13	0.96	0.80	1.18	
STRSQ040	0.87	1.26	1.07	0.81	1.18	
STRSQ034	1.07	1.33	1.25	0.86	1.06	
STRQQF133	1.05	1.01	1.01	1.03	0.99	Wood smoke with DRI dilution/residence chamber and conical sampling manifold[b]
STRQQF162	0.90	1.06	1.02	0.88	1.04	
STRQQF171	0.95	0.93	0.93	1.02	1.00	
STRSQ070	0.86	0.95	0.93	0.93	1.02	Carbon Black nebulized, miniature dilution/residence chamber with conical sampling manifold[b]

[a] with filter holder aerosol inlet diameter 6.35 mm
[b] with filter holder aerosol inlet diameter 41.28 mm, see Figure 3-2 and 3-6

Table 5-7. Reproducibility of sources under different experimental set ups for OC, EC, TC, mass concentration, and b_{abs}.

Filter ID	Date	Source	Source Setting	Filter Flow Rate (L/min)	Collection Time (hr:min:sec)	Dilution Ratio	IMPROVE_A TOR OC (μg/m³)	IMPROVE_A TOR EC (μg/m³)	IMPROVE_A TOR TC (μg/m³)	IMPROVE_A TOR OC/TC	IMPROVE_A TOR EC/TC	Filter b_{abs} (Mm^{-1})	PA b_{abs} (Mm^{-1})	PA /Filter	Filter Mass Conc (μg/m³)	DustTrak Mass Conc (μg/m³)	DustTrak/ Filter
STRSQ011	1/7/2006	Diesel Generator	4kW; old sampling line	40	1:00:00	149.3		81.28	97.03	0.17	0.84	694	364	0.52	101	123	1.22
STRSQ012	1/7/2006					162.9	7.14	73.92	80.36	0.09	0.92	618	339	0.55	79	112	1.42
STRSQ013	1/7/2006					165.8	4.85	70.42	74.57	0.07	0.94	577	337	0.58	75	104	1.39
					Average	159.4	9	75	84	0.11	0.90	630	346	0.55	85	113	1.34
					RSD	5.5	64.8	7.4	13.9	50.8	6.2	9.4	4.3	5.5	16.0	8.1	8.0
STRSQ014	1/8/2006	Diesel Generator	4kW; old sampling line	40	1:00:00	41.9	47.96	155.25	202.53	0.24	0.77	1456	816	0.56	230	284	1.24
STRSQ015	1/8/2006					41.1	50.14	166.15	215.60	0.23	0.77	1481	840	0.57	239	299	1.25
STRSQ016	1/8/2006					43.4	179.66	27.75	206.71	0.87	0.13	1396	742	0.53	222	288	1.30
					Average	42.2	93	116	208	0.45	0.56	1444	799	0.55	230	290	1.26
					RSD	2.7	81.4	66.1	3.2	82.1	65.7	3.0	6.4	3.4	3.7	2.6	2.5
STRSQ018	1/8/2006	Diesel Generator	4kW; old sampling line	40	0:20:00	~41	69.14	143.47	211.91	0.33	0.68	1696	767	0.45	223	286	1.28
STRSQ019	1/8/2006					~40	70.43	155.58	225.31	0.31	0.69	1596	826	0.52	238	312	1.31
STRSQ020	1/8/2006					~40	87.45	153.29	240.04	0.36	0.64	1775	792	0.45	232	323	1.39
					Average	N/A	76	151	226	0.33	0.67	1689	795	0.47	231	307	1.33
					RSD	N/A	13.5	4.3	6.2	8.0	4.0	5.3	3.7	8.4	3.2	6.2	4.4
STRSQ042	1/20/2006	Diesel Generator	4kW	40	1:00:00	77.6	69.45	188.16	256.91	0.27	0.73	1421	959	0.68	278	335	1.20
STRSQ043	1/20/2006					78.2	75.78	182.24	257.32	0.29	0.71	1641	882	0.54	280	348	1.24
STRSQ044	1/20/2006					78.5	68.65	169.32	237.27	0.29	0.71	1419	815	0.57	256	297	1.16
STRSQ045	1/20/2006					79.3	79.36	169.26	247.93	0.32	0.68	1664	795	0.48	260	312	1.20
					Average	78.4	73	177	250	0.29	0.71	1536	863	0.57	269	323	1.20
					RSD	0.9	7.0	5.4	3.8	7.0	2.9	8.8	8.6	14.6	4.5	7.1	2.9
STRSQ047	1/23/2006	Diesel Generator	4kW	40	0:20:00	80.6	112.88	166.31	278.50	0.41	0.60	1709	881	0.52	270	321	1.19
STRSQ048	1/23/2006					79.8	125.05	163.68	288.04	0.43	0.57	1635	870	0.53	266	311	1.17
STRSQ049	1/23/2006					79.8	113.48	152.01	264.80	0.43	0.57	1540	793	0.51	244	286	1.17
STRSQ051	1/23/2006					79.4	97.45	164.12	260.88	0.37	0.63	1524	791	0.52	231	291	1.26
STRSQ052	1/23/2006					79.8	80.04	133.59	212.94	0.38	0.63	1503	759	0.50	232	279	1.20
					Average	79.9	106	156	261	0.40	0.60	1582	819	0.52	249	298	1.20
					RSD	0.5	16.5	8.8	11.1	7.0	4.8	5.5	6.6	1.9	7.4	5.9	3.1
STRSQ053	1/23/2006	Diesel Generator	4kW	40	0:20:00	39.6	166.82	218.31	384.45	0.43	0.57	1954	1111	0.57	331	478	1.44
STRSQ054	1/23/2006					41.2	143.46	216.85	359.61	0.40	0.60	2216	1067	0.48	333	465	1.40
STRSQ055	1/23/2006					39.3	132.43	208.39	340.13	0.39	0.61	2059	1082	0.53	333	480	1.44
STRSQ056	1/23/2006					41.7	147.34	215.15	361.79	0.41	0.59	2338	1080	0.46	355	512	1.44
STRSQ057	1/23/2006					40.8	181.54	214.30	395.15	0.46	0.54	1903	1062	0.56	359	536	1.49
STRQQ090	2/8/2006					39.9	153.31	257.43	410.05	0.37	0.63	2314	1197	0.52	380	549	1.45
					Average	40.4	154	222	375	0.41	0.59	2131	1100	0.52	348	503	1.44
					RSD	2.3	11.4	8.0	6.9	7.6	5.3	8.7	4.6	8.0	5.6	6.8	2.0

16.46

Table 5-7. Continued.

Filter ID	Date	Source	Source Setting	Filter Flow Rate (L/min)	Collection Time (hr:min:sec)	Dilution Ratio	IMPROVE_A TOR OC (µg/m³)	IMPROVE_A TOR EC (µg/m³)	IMPROVE_A TOR TC (µg/m³)	IMPROVE_A TOR OC/TC	IMPROVE_A TOR EC/TC	Filter b_{abs} (Mm^{-1})	PA b_{abs} (Mm^{-1})	PA /Filter	Filter Mass Conc (µg/m³)	DustTrak Mass Conc (µg/m³)	DustTrak/ Filter
STRSQ058	1/24/2006	Diesel Generator	4kW	40	1:00:00	38.4	98.63	241.80	339.75	0.29	0.71	1941	1252	0.64	369	519	1.41
STRSQ060	1/24/2006					42.7	87.43	215.31	302.04	0.29	0.71	2086	1100	0.53	330	462	1.40
STRSQ061	1/24/2006					43.0	128.15	198.79	326.24	0.39	0.61	1882	1027	0.55	364	525	1.44
STRSQ062	1/24/2006					40.9	140.61	217.26	357.17	0.39	0.61	2143	1041	0.49	381	544	1.43
STRSQ063	1/24/2006					42.0	117.72	206.92	323.94	0.36	0.64	2044	992	0.49	336	476	1.41
					Average	41.4	115	216	330	0.35	0.66	2019	1082	0.54	356	505	1.42
					RSD	4.5	18.8	7.5	6.2	15.2	8.0	5.3	9.5	12.2	6.1	6.9	1.3
STRSQ064	1/25/2006	Diesel Generator	4kW	40	1:00:00	17.6	201.61	288.48	489.39	0.41	0.59	2380	1500	0.63	503	726	1.44
STRSQ065	1/25/2006					18.1	262.93	211.81	474.05	0.55	0.45	2817	1375	0.49	497	707	1.42
STRSQ066	1/25/2006					16.1	191.19	254.28	444.76	0.43	0.57	2253	1282	0.57	495	708	1.43
STRSQ067	1/25/2006					17.9	197.56	240.31	437.16	0.45	0.55	2620	1297	0.50	478	683	1.43
STRSQ068	1/25/2006					17.8	247.46	202.91	449.66	0.55	0.45	2596	1276	0.49	481	659	1.37
STRQQ097	2/9/2006					18.3	261.21	137.89	398.40	0.66	0.35	2215	1329	0.60	428	600	1.40
					Average	17.6	227	223	449	0.51	0.49	2480	1343	0.55	480	681	1.42
					RSD	4.5	14.8	23.2	7.0	18.5	19.1	9.5	6.3	11.4	5.7	6.7	1.9
STRQQ091	2/8/2006	Diesel Generator + NaCl	4kW; 0.1M NaCl @ 10psi	40	0:20:00	37.1	137.14	209.79	346.24	0.40	0.61	2687	1120	0.42	629	1121	1.78
STRQQ092	2/8/2006					40.5	161.49	216.34	377.14	0.43	0.57	2490	1123	0.45	652	1139	1.75
STRQQ093	2/8/2006					41.8	147.69	203.58	350.57	0.42	0.58	2621	1088	0.42	653	1168	1.79
					Average	39.8	149	210	358	0.42	0.59	2599	1110	0.43	645	1143	1.77
					RSD	6.1	8.2	3.0	4.7	4.1	2.9	3.9	1.8	4.8	2.1	2.1	1.3
STRQQ094	2/8/2006	Diesel Generator + NaCl	4kW; 0.1M NaCl @ 10psi	40	1:00:00	41.7	116.73	192.12	308.16	0.38	0.62	2299	1013	0.44	611	1155	1.89
STRQQ095	2/8/2006					41.1	107.14	177.95	284.40	0.38	0.63	1987	944	0.48	700	1261	1.80
STRQQ096	2/9/2006					40.7	228.22	212.91	440.44	0.52	0.48	2295	1248	0.54	613	921	1.50
					Average	41.2	151	194	344	0.42	0.58	2193	1068	0.49	642	1112	1.73
					RSD	1.3	44.7	9.0	24.4	19.1	14.1	8.2	14.9	10.8	7.9	15.6	11.7

Table 5-7. Continued.

Filter ID	Date	Source	Source Setting	Filter Flow Rate (L/min)	Collection Time (hr:min:sec)	Dilution Ratio	IMPROVE_A TOR OC (µg/m^3)	IMPROVE_A TOR EC (µg/m^3)	IMPROVE_A TOR TC (µg/m^3)	IMPROVE_A TOR OC/TC	IMPROVE_A TOR EC/TC	Filter b_{abs} (Mm^{-1})	PA b_{abs} (Mm^{-1})	PA /Filter	Filter Mass Conc (µg/m^3)	DustTrak Mass Conc (µg/m^3)	DustTrak/ Filter
STRQQ098	2/9/2006	Diesel Generator + NaCl	4kW; 0.1M NaCl @ 10psi	40	1:00:00	18.1	140.87	253.75	393.92	0.36	0.64	2682	1257	0.47	665	1079	1.62
STRQQ099	2/9/2006					17.9	124.55	264.76	388.62	0.32	0.68	2699	1275	0.47	679	1092	1.61
STRQQ101	2/9/2006					17.7	144.58	247.30	391.18	0.37	0.63	2621	1299	0.50	689	1120	1.62
					Average	17.9	137	255	391	0.35	0.65	2667	1277	0.48	678	1097	1.62
					RSD	1.3	7.8	3.5	0.7	7.3	3.9	1.5	1.6	3.0	1.8	1.9	0.6
STRQQ103	2/17/2006	Acetylene Flame	# 1 level tip, 2" flame	40	0:20:00	16.8	36.89	479.21	515.39	0.07	0.93	2459	1570	0.64	457	400	0.87
STRQQ104	2/17/2006					16.7	19.54	469.08	487.49	0.04	0.96	2146	1567	0.73	516	383	0.74
STRQQ106	2/17/2006					16.9	43.86	472.95	516.11	0.08	0.92	2057	1513	0.74	454	360	0.79
					Average	16.8	33	474	506	0.07	0.94	2221	1550	0.70	476	381	0.80
					RSD	0.7	37.5	1.1	3.2	35.2	2.5	9.5	2.1	7.8	7.4	5.3	8.3
STRQQ107	2/17/2006	Acetylene Flame	# 1 level tip, 2" flame	40	0:40:00	16.7	9.54	454.59	463.43	0.02	0.98	2591	1631	0.63	474	470	0.99
STRQQ108	2/17/2006					16.8	0.00	425.79	417.49	0.00	1.02	2038	1499	0.74	462	377	0.82
STRQQ109	2/17/2006					16.7	0.00	431.87	428.10	0.00	1.01	2211	1438	0.65	468	338	0.72
					Average		3	437	436	0.01	1.00	2280	1523	0.67	468	395	0.84
					RSD	0.4	173.2	3.5	5.5	173.2	2.0	12.4	6.5	8.4	1.2	17.1	16.2
						16.7											
STRQQ110	2/17/2006	Acetylene Flame	# 1 level tip, 2" flame	40	1:10:00	16.7	0.00	397.00	386.01	0.00	1.03	2175	1333	0.61	431	290	0.67
STRQQ111	2/17/2006					16.5	0.00	389.80	376.24	0.00	1.04	1867	1179	0.63	402	239	0.59
STRQQ112	2/17/2006					16.5	0.00	381.47	371.15	0.00	1.03	2002	1281	0.64	405	284	0.70
					Average	16.5	0	389	378	0.00	1.03	2015	1264	0.63	413	271	0.66
					RSD	0.7	ND	2.0	2.0	ND	0.4	7.7	6.2	2.2	3.8	10.5	8.7
STRQQ113	2/21/2006	Acetylene Flame + NaCl	# 1 level tip, 2" flame; 0.05M NaCl @ 10 psi	40	0:20:00	16.9	26.57	499.72	525.59	0.05	0.95	2780	1705	0.61	716	764	1.07
STRQQ114	2/21/2006					16.8	43.33	551.93	594.56	0.07	0.93	2743	1562	0.57	768	725	0.94
STRQQ115	2/21/2006					17.0	38.12	439.95	477.37	0.08	0.92	2746	1434	0.52	666	734	1.10
					Average	16.9	36	497	533	0.07	0.93	2756	1567	0.57	717	741	1.04
					RSD	0.7	23.8	11.3	11.1	22.6	1.6	0.7	8.7	8.0	7.1	2.8	8.0

Table 5-7. Continued.

Filter ID	Date	Source	Source Setting	Filter Flow Rate (L/min)	Collection Time (hr:min:sec)	Dilution Ratio	IMPROVE_A TOR OC (µg/m^3)	IMPROVE_A TOR EC (µg/m^3)	IMPROVE_A TOR TC (µg/m^3)	IMPROVE_A TOR OC/TC	IMPROVE_A TOR EC/TC	Filter b_{abs} (Mm^{-1})	PA b_{abs} (Mm^{-1})	PA /Filter	Filter Mass Conc (µg/m^3)	DustTrak Mass Conc (µg/m^3)	DustTrak/ Filter
STRQQ116	2/21/2006	Acetylene Flame + NaCl	# 1 level tip, 2" flame; 0.05M NaCl @ 10 psi	40	0:40:00	16.7	0.00	437.62	435.31	0.00	1.01	2223	1508	0.68	664	768	1.16
STRQQ117	2/21/2006					16.7	0.62	436.15	436.07	0.00	1.00	2525	1463	0.58	649	777	1.20
STRQQ118	2/21/2006					17.4	2.61	429.01	430.93	0.01	1.00	2405	1367	0.57	665	751	1.13
					Average	16.9	1	434	434	0.00	1.00	2384	1446	0.61	659	765	1.16
					RSD	2.3	126.7		0.6	127.1		6.4	5.0	9.9	1.3	1.8	2.9
STRQQ119	2/22/2006	Acetylene Flame + NaCl	# 1 level tip, 2" flame; 0.05M NaCl @ 10 psi	40	1:10:00	17.0	66.75[1.1]	297.27	363.32	0.18[0.5]	0.82	1593	1219	0.77	572	629	1.10
STRQQ120	2/22/2006					16.9	0.00	397.42	393.45	0.00	1.01	1958	1194	0.61	579	615	1.06
STRQQ121	2/22/2006					16.8	0.00	381.08	374.40	0.00	1.02	1421	1124	0.79	579	619	1.07
					Average	16.9	22	359	377	0.06	0.95	1657	1179	0.72	577	621	1.08
					RSD	0.6	173.2		4.0	173.2		16.5	4.2	13.6	0.6	1.2	1.8
STRSQ038	1/19/2006	Electric Arc	300 a.u. strom current, 1.3 bar Ar	10	1:00:00	8.3	97.64[15.0]	216.03	310.89	0.31[11.9]	0.69	1584	708	0.45	639	136	0.21
STRSQ039	1/19/2006					8.4	88.11	190.12	275.46	0.32	0.69	1746	730	0.42	634	145	0.23
STRSQ040	1/19/2006					8.3	133.68	239.74	370.64	0.36	0.65	1801	765	0.42	688	156	0.23
					Average	8.4	106	215	319	0.33	0.68	1710	735	0.43	653	146	0.22
					RSD	0.8	22.6	11.5	15.1	7.7	3.9	6.6	3.9	3.5	4.6	7.1	4.1
STRSQ025	1/17/2006	Electric Arc	950 a.u. strom current, 1.3 bar Ar	10	0:20:00	8.0	842.13	664.94	1504.36	0.56	0.44	5724	2543	0.44	2164	868	0.40
STRSQ026	1/17/2006					7.5	1163.22	807.31	1967.82	0.59	0.41	5375	2489	0.46	2136	697	0.33
STRSQ027	1/17/2006					7.7	1205.67	560.12	1763.06	0.68	0.32	5885	2320	0.39	2168	629	0.29
STRSQ028	1/17/2006					8.0	861.38	677.75	1536.39	0.56	0.44	5587	2094	0.37	2131	632	0.30
STRSQ029	1/17/2006					7.7	916.41	694.77	1608.40	0.57	0.43	5324	2269	0.43	2079	512	0.25
					Average	7.8	998	681	1676	0.59	0.41	5579	2343	0.42	2136	668	0.31
					RSD	2.8	17.4	12.9	11.4	8.8	12.8	4.2	7.7	8.6	1.7	19.6	18.4

Table 5-7. Continued.

Filter ID	Date	Source	Source Setting	Filter Flow Rate (L/min)	Collection Time (hr:min:sec)	Dilution Ratio	IMPROVE_A TOR OC (µg/m^3)	IMPROVE_A TOR EC (µg/m^3)	IMPROVE_A TOR TC (µg/m^3)	IMPROVE_A TOR OC/TC	IMPROVE_A TOR EC/TC	Filter b_{abs} (Mm^{-1})	PA b_{abs} (Mm^{-1})	PA /Filter	Filter Mass Conc (µg/m^3)	DustTrak Mass Conc (µg/m^3)	DustTrak/ Filter
STRSQ030	1/17/2006	Electric Arc	950 a.u. strom current, 1.3 bar Ar	10	0:40:00	7.4	696.01	667.62	1360.85	0.51	0.49	4964	2247	0.45	1933	545	0.28
STRSQ031	1/17/2006					7.4	788.78	629.66	1415.65	0.56	0.44	5006	2140	0.43	1942	602	0.31
STRSQ035	1/19/2006					8.2	611.95	723.08	1332.27	0.46	0.54	5458	2308	0.42	2015	622	0.31
STRSQ036	1/19/2006					7.8	843.49	703.68	1544.41	0.55	0.46	5085	2077	0.41	1920	520	0.27
STRSQ037	1/19/2006					7.9	676.81	642.39	1316.43	0.51	0.49	4978	2082	0.42	1862	466	0.25
					Average	7.7	723	673	1394	0.52	0.48	5098	2171	0.43	1934	551	0.28
					RSD	4.3	12.8	5.9	6.6	7.4	7.9	4.0	4.7	3.9	2.8	11.5	9.0
STRQQ081	2/7/2006	Electric Arc + NaCl	300 a.u. strom current, 1.3 bar Ar; 0.01M NaCl @ 10psi	10	0:20:00	8.0	312.75	283.63	593.67	0.53	0.48	2918	1148	0.39	1417	861	0.61
STRQQ082	2/7/2006					7.4	149.10	254.98	401.35	0.37	0.64	1794	862	0.48	1236	736	0.60
STRQQ083	2/7/2006					7.6	159.49	236.30	393.07	0.41	0.60	2176	753	0.35	1206	781	0.65
					Average	7.7	207	258	463	0.43	0.57	2296	921	0.41	1286	793	0.62
					RSD	3.5	44.2	9.2	24.5	18.8	14.5	24.9	22.2	16.8	8.9	8.0	4.4
STRQQ084	2/7/2006	Electric Arc + NaCl	950 a.u. strom current, 1.3 bar Ar; 0.01M NaCl @ 10psi	10	0:20:00	7.0	898.41	568.02	1463.69	0.61	0.39	5229	2096	0.40	2083	1298	0.62
STRQQ085	2/7/2006					6.9	733.13	649.41	1379.82	0.53	0.47	5878	1979	0.34	2492	1192	0.48
STRQQ086	2/7/2006					7.1	738.22	698.94	1434.43	0.51	0.49	5389	2110	0.39	2409	1177	0.49
					Average	7.0	790	639	1426	0.55	0.45	5499	2062	0.38	2328	1222	0.53
					RSD	1.7	11.9	10.3	3.0	9.6	11.8	6.2	3.5	9.2	9.3	5.4	15.2
STRQQ087	2/7/2006	Electric Arc + NaCl	950 a.u. strom current, 1.3 bar Ar; 0.01M NaCl @ 10psi	10	0:40:00	7.0	401.49	819.13	1217.89	0.33	0.67	5368	2104	0.39	2319	1160	0.50
STRQQ088	2/7/2006					7.0	961.85	188.41	1147.53	0.84	0.16	5201	1959	0.38	2264	1120	0.49
STRQQ089	2/7/2006					7.2	872.91	248.43	1118.61	0.78	0.22	5117	2017	0.39	2252	1063	0.47
					Average	7.1	745	419	1161	0.65	0.35	5229	2027	0.39	2279	1114	0.49
					RSD	1.4	40.4	83.2	4.4	42.9	78.9	2.4	3.6	2.5	1.6	4.4	3.0

Table 5-7. Continued.

Filter ID	Date	Source	Source Setting	Filter Flow Rate (L/min)	Collection Time (hr:min:sec)	Dilution Ratio	IMPROVE_A TOR OC (µg/m^3)	IMPROVE_A TOR EC (µg/m^3)	IMPROVE_A TOR TC (µg/m^3)	IMPROVE_A TOR OC/TC	IMPROVE_A TOR EC/TC	Filter b_{abs} (Mm^{-1})	PA b_{abs} (Mm^{-1})	PA /Filter	Filter Mass Conc (µg/m^3)	DustTrak Mass Conc (µg/m^3)	DustTrak/ Filter
STRQQ122	3/8/2006	Wood smoke	6 piceces of wood, 4-5lbs per load, 1 load per filter	10	0:20:00	117.1	351.34	27.14	377.79	0.93	0.07	708	187	0.26	261	445	1.70
STRQQ123	3/8/2006					117.7	752.63	144.85	896.79	0.84	0.16	1471	320	0.22	589	1498	2.54
STRQQ124	3/8/2006					110.8	337.27	80.19	416.76	0.81	0.19	823	373	0.45	174	277	1.59
STRQQ125	3/8/2006					110.2	588.81	103.21	691.31	0.85	0.15	989	277	0.28	408	1025	2.51
					Average	113.9	508	89	596	0.86	0.14	998	289	0.30	358	811	2.09
					RSD	3.5	39.4	55.2	41.0	6.0	35.7	33.7	27.2	33.9	50.8	68.9	24.4
STRQQ126	3/8/2006	Wood smoke	6 piceces of wood, 4-5lbs per load, 1 load per filter	25	0:20:00	107.8	333.47	68.49	401.26	0.83	0.17	809	141	0.17	292	676	2.31
STRQQ127	3/8/2006					106.0	327.57	92.52	419.39	0.78	0.22	993	223	0.22	258	804	3.12
STRQQ128[a]	3/8/2006					*105.0*	*1040.33*	*121.15*	*1160.77*	*0.90*	*0.10*	*1127*	*37*	*0.03*	*1522*	*6440*	*4.23*
STRQQ129[b]	3/8/2006					*104.5*	*262.92*	*26.54*	*288.75*	*0.91*	*0.09*	*133*	*21*	*0.16*	*162*	*228*	*1.41*
					Average	106.9	331	81	410	0.81	0.20	901	182	0.20	275	740	2.72
					RSD	1.2	1.3	21.1	3.1	4.4	18.0	14.4	32.1	18.2	8.9	12.2	21.0
STRQQ130	3/9/2006	Wood smoke	6 piceces of wood, 4-5lbs per load, 1 load per filter	40	0:25:00	41.1	198.23	46.75	244.27	0.81	0.19	573	109	0.19	209	343	1.64
STRQQ131	3/9/2006					42.8	235.49	104.52	339.30	0.69	0.31	1015	312	0.31	387	1131	2.92
STRQQ132	3/9/2006					41.0	198.48	97.09	294.86	0.67	0.33	982	315	0.32	379	1210	3.20
STRQQ133	3/13/2006					39.2	253.21	64.12	316.63	0.80	0.20	792	141	0.18	321	799	2.49
STRQQ134	3/13/2006					40.0	209.95	46.49	255.75	0.82	0.18	729	140	0.19	255	537	2.11
STRQQ135	3/13/2006					40.5	132.13	53.61	185.05	0.71	0.29	559	170	0.30	205	561	2.74
STRQQ136	3/13/2006					38.6	73.80	43.83	116.93	0.63	0.37	399	144	0.36	131	284	2.17
					Average	40.5	186	65	250	0.73	0.27	721	190	0.26	269	695	2.47
					RSD	3.4	33.5	38.8	31.1	10.3	28.4	31.6	45.3	28.4	35.8	52.6	21.6

Table 5-7. Continued.

Filter ID	Date	Source	Source Setting	Filter Flow Rate (L/min)	Collection Time (hr:min:sec)	Dilution Ratio	IMPROVE_A TOR OC (µg/m^3)	IMPROVE_A TOR EC (µg/m^3)	IMPROVE_A TOR TC (µg/m^3)	IMPROVE_A TOR OC/TC	IMPROVE_A TOR EC/TC	Filter b_{abs} (Mm^{-1})	PA b_{abs} (Mm^{-1})	PA /Filter	Filter Mass Conc (µg/m^3)	DustTrak Mass Conc (µg/m^3)	DustTrak/ Filter
STRQQ137	3/15/2006					18.5	71.08	27.81	98.20	0.72	0.28	357	82	0.23	71	227	3.20
STRQQ138[c]	3/15/2006					*17.3*	*116.68*	*43.05*	*159.04*	*0.73*	*0.27*	*518*	*83*	*0.16*	*142*	*617*	*4.33*
STRQQ139	3/15/2006					17.5	61.41		100.06		0.39	387	99	0.25	69	190	2.75
STRQQ140	3/15/2006	Wood smoke	6 piceces of wood, 4-5lbs per load, 1 load per filter	40	0:25:00	18.1	45.15	20.58	65.04	0.69	0.32	195	48	0.25	52	119	2.30
STRQQ141	3/15/2006					17.9	39.31 39.34	25.67	64.28 0.61	0.61	0.40	293	49	0.17	69	288	4.19
STRQQ142	3/15/2006					17.7	30.35	12.00	41.66	0.73	0.29	164	36	0.22	44	149	3.40
STRQQ143[c]	3/15/2006					*17.7*	*20.94*	*12.00*	*32.24*	*0.65*	*0.37*	*131*	*36*	*0.28*	*0*	*86*	*ND*
STRQQ144	3/15/2006					17.9	12.71	18.16	30.16	0.42	0.60	165	49	0.30	27	90	3.28
					Average	17.9	43	24	67	0.63	0.38	260	61	0.24	55	177	3.19
					RSD	1.7	48.7	39.3	42.9	18.3	31.5	38.1	40.0	17.9	31.6	41.2	20.1
STRQQ160	4/5/2006					40.5	88.83		116.37		0.24	371	75	0.20	204	583	2.86
STRQQ161	4/5/2006					40.5	88.25		96.23		0.09	368	27	0.07	191	416	2.18
STRQQ162	4/5/2006					41.5	29.87 28.25	21.13	50.29 0.76	0.59	0.42	335	93	0.28	150	314	2.10
STRQQ163	4/5/2006	Wood smoke + NaCl	6 piceces of wood, 4-5lbs per load, 1 load per filter; 0.05M NaCl @ 10psi	40	0:25:00	42.2	33.31		40.51		0.20	268	64	0.24	125	268	2.14
STRQQ164	4/5/2006					42.4	27.16 8.69	11.19	37.64 0.92	0.72	0.30	201	39	0.19	121	252	2.09
STRQQ165	4/5/2006					42.3	67.61	13.19	80.09	0.84	0.16	431	62	0.14	200	624	3.12
STRQQ166	4/5/2006					42.5	43.45 7.91		52.63 0.82		0.19	268	45	0.17	158	432	2.73
					Average	41.7	54	14	68	0.78	0.23	320	58	0.19	164	413	2.46
					RSD	2.1	50.2 9.89	52.9	44.8 0.83	13.3	46.5	24.5	38.6	35.3	21.1	35.7	17.6
STRQQ167	4/6/2006					19.0	28.23		36.38		0.24	295	49	0.17	179	438	2.45
STRQQ168	4/6/2006					19.1	27.49	16.19	42.98	0.64	0.38	296	72	0.24	181	395	2.18
STRQQ169	4/6/2006					19.1	12.82		19.60		0.38	231	39	0.17	169	369	2.18
STRQQ170	4/6/2006	Wood smoke + NaCl	6 piceces of wood, 4-5lbs per load, 1 load per filter; 0.05M NaCl @ 10psi	40	0:25:00	19.5	14.03 8.84		21.50 0.78		0.38	165	27	0.17	145	334	2.29
STRQQ171	4/6/2006					19.3	0.00	11.49	9.98	0.00	1.15	265	67	0.25	173	392	2.26
STRQQ172	4/6/2006					19.4	9.30 7.48	8.17	16.76 0.65	0.55	0.49	199	22	0.11	154	315	2.04
STRQQ173	4/6/2006					19.5	4.28 8.18	12.77	16.34 0.65	0.26	0.78	232	56	0.24	162	382	2.36
					Average	19.3	14	10	23	0.51	0.54	240	48	0.19	166	375	2.25
					RSD	1.1	78.5	30.6	50.8	54.3	58.2	20.2	39.7	27.3	7.9	11.0	6.0

Table 5-7. Continued.

Filter ID	Date	Source	Source Setting	Filter Flow Rate (L/min)	Collection Time (hr:min:sec)	Dilution Ratio	IMPROVE_A TOR OC (µg/m^3)	IMPROVE_A TOR EC (µg/m^3)	IMPROVE_A TOR TC (µg/m^3)	IMPROVE_A TOR OC/TC	IMPROVE_A TOR EC/TC	Filter b_{abs} (Mm^{-1})	PA b_{abs} (Mm^{-1})	PA /Filter	Filter Mass Conc (µg/m^3)	DustTrak Mass Conc (µg/m^3)	DustTrak/ Filter
STRSQ069	4/4/2006	Carbon Black powder	0.1g in 200ml (95%H2O, 5% Methanol)	10	1:10:00 or 2:00:00	9.0	60.14	19.59	79.72	0.75	0.25	69	96	1.39	2	40	26.11
STRSQ070	4/4/2006					9.0	0.00	21.47	2.40	0.00	8.96	65	98	1.51	0	37	ND
STRSQ071	4/4/2006					9.0	0.00	31.18	25.58	0.00	1.22	208	170	0.82	0	81	ND
					Average	9.0	20	24	36	0.25	3.48	114	121	1.24	1	53	26.11
					RSD	0.2	173.2	25.8	110.5	173.2	137.4	71.4	34.8	29.8	173.2	46.3	ND

NA: Not available due to missing data; dilution ratios shown are approximate.
ND: Mathematically not defined; division by zero.
[a] Filter STRQQ128 was not included in the average due to excessive smoke from the wood.
[b] Filter STRQQ129 was not included in the average due to different sampling conditions.
[c] Filters STRQQ138 and STRQQ 143 were not included in the average due to mass concentration outliers.

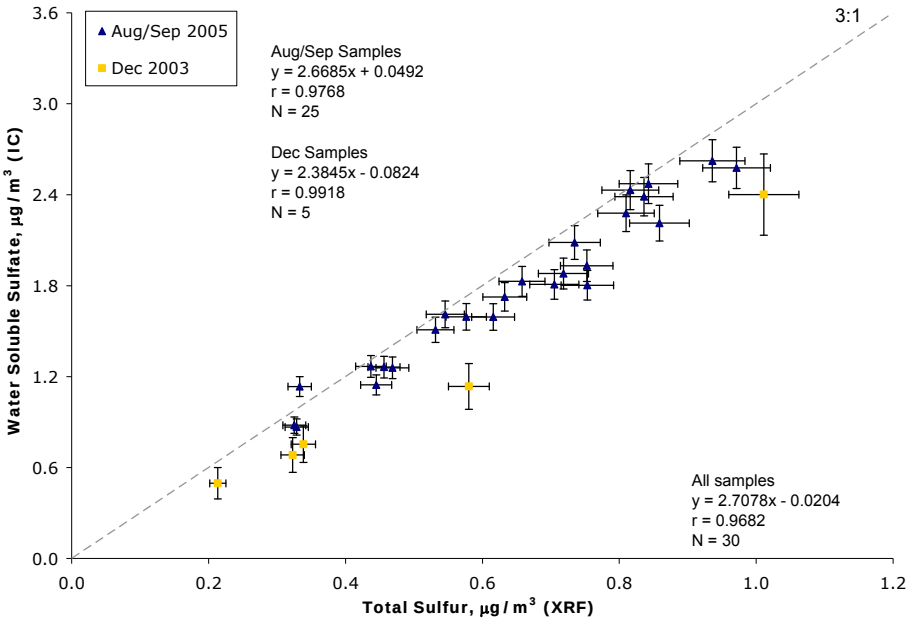

(a)

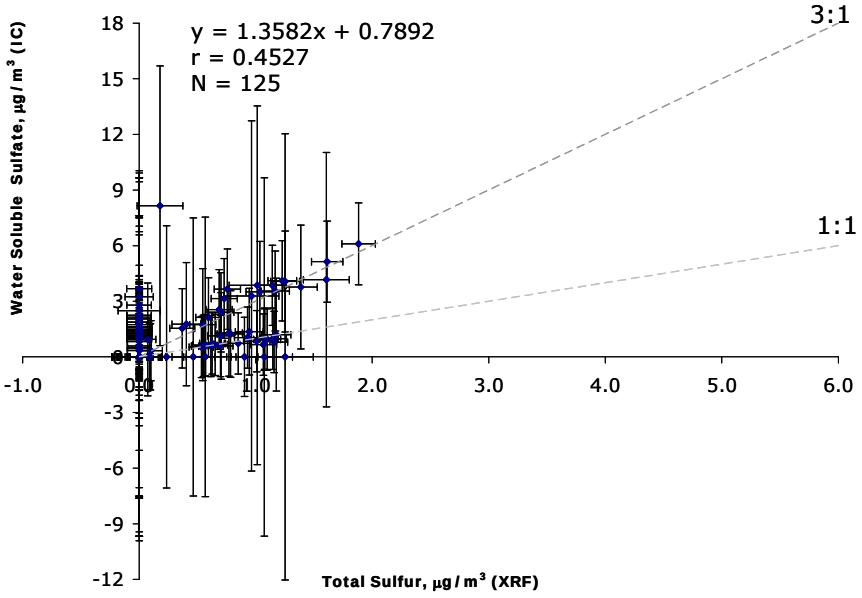

(b)

Figure 5-1. Water-soluble sulfate on quartz-fiber filters by ion chromatographic (IC) analysis versus total sulfur on Teflon-membrane filters by x-ray fluorescence (XRF) analysis for: (a) ambient samples during the summer and winter IOPs; (b) laboratory-generated diesel, acetylene, electric arc, wood smoke, and nebulized carbon black source samples; and (c) laboratory-generated diesel and wood smoke source samples.

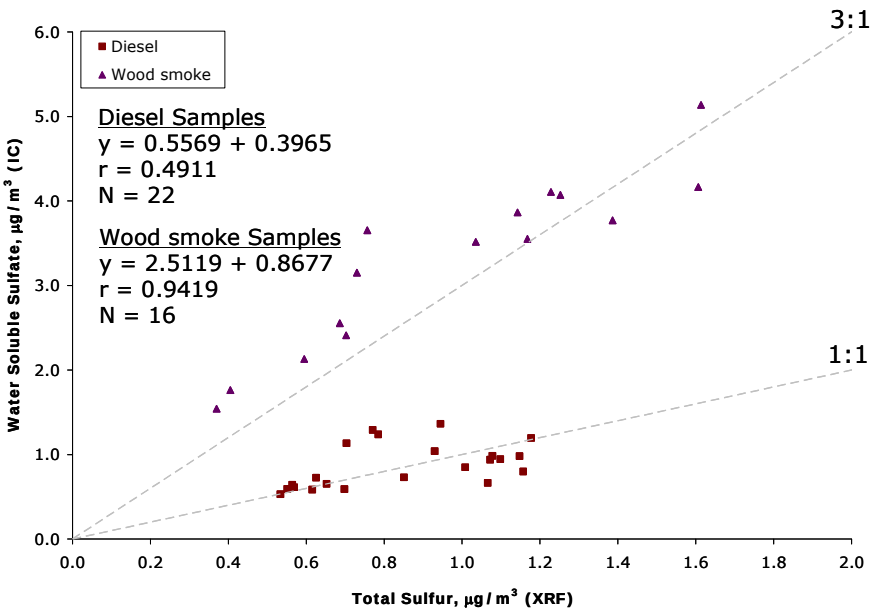

(c)

Figure 5-1. Continued.

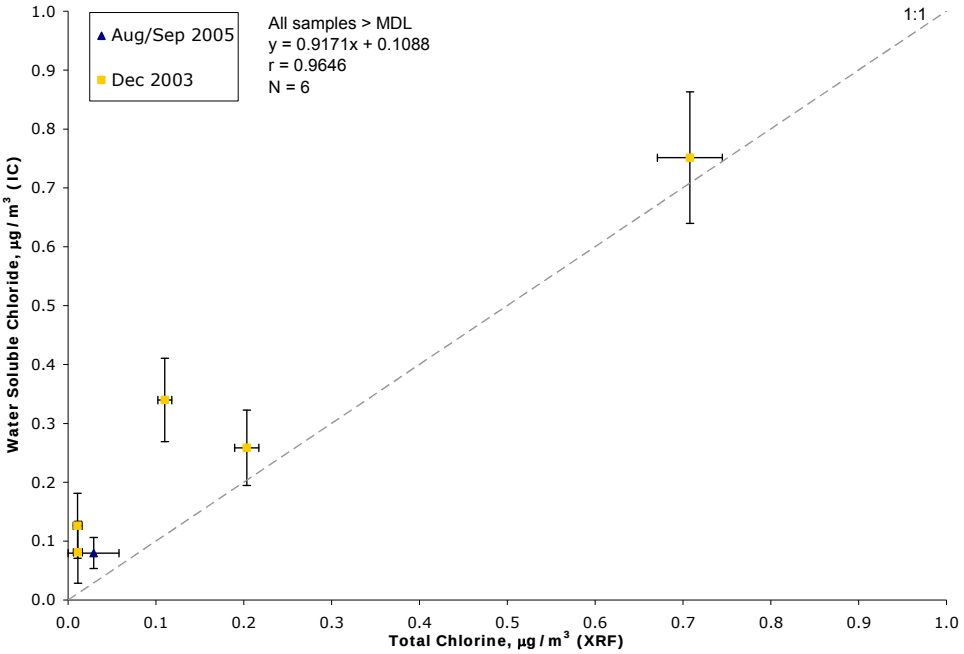

(a)

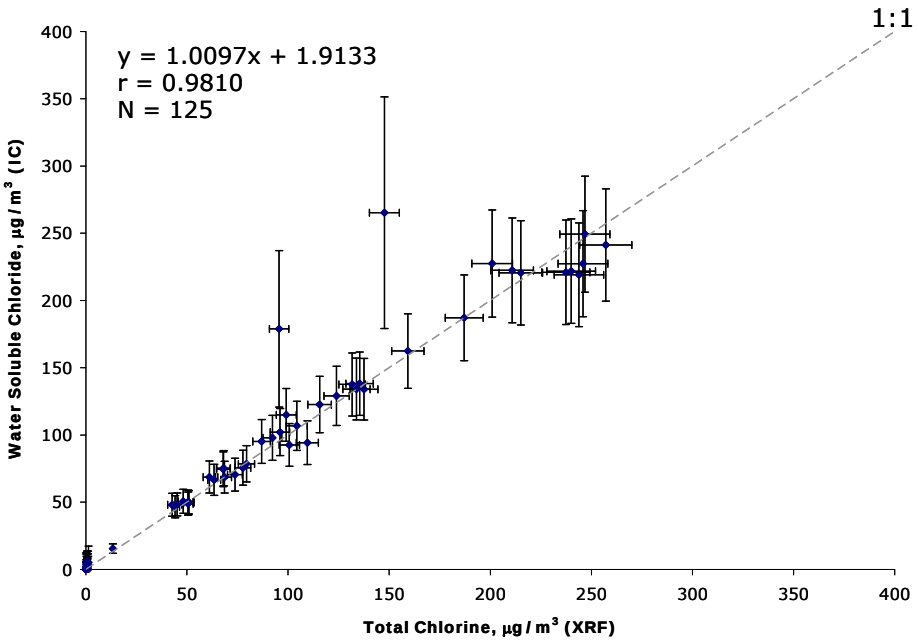

(b)

Figure 5-2. Water-soluble chloride on quartz-fiber filters by ion chromatographic (IC) analysis versus total chlorine on Teflon-membrane filters by x-ray fluorescence (XRF) analysis for: (a) ambient samples during the summer and winter IOPs; and (b) laboratory-generated diesel, acetylene, electric arc, wood smoke, and nebulized carbon black source samples.

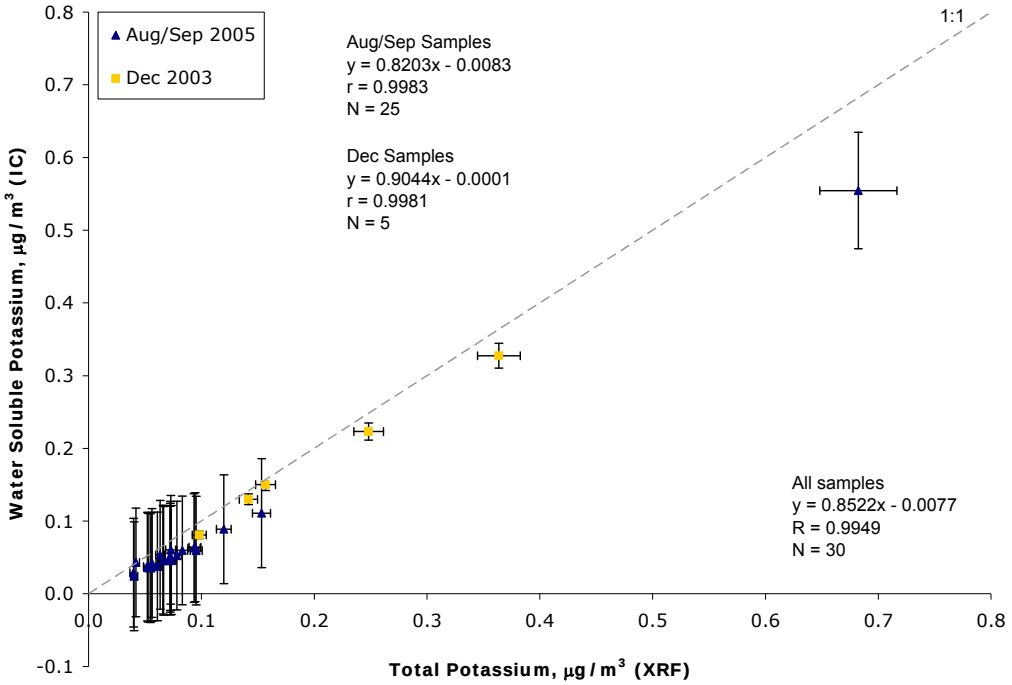

(a)

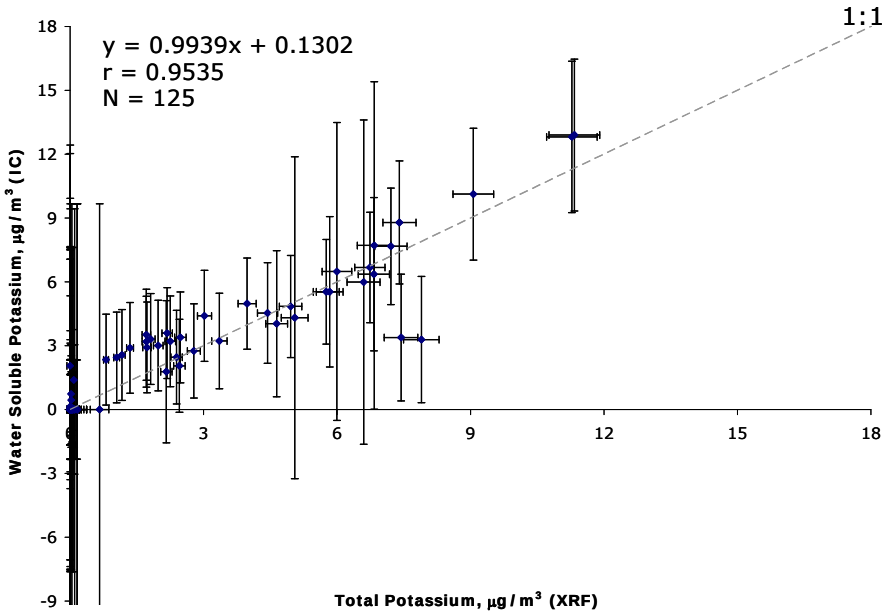

(b)

Figure 5-3. Water-soluble potassium on quartz-fiber filters by ion chromatographic (IC) analysis versus total potassium on Teflon-membrane filters by x-ray fluorescence (XRF) analysis for: (a) ambient samples during the summer and winter IOPs; and (b) laboratory-generated diesel generator, acetylene flame, electric arc, wood smoke, and nebulized carbon black source samples.

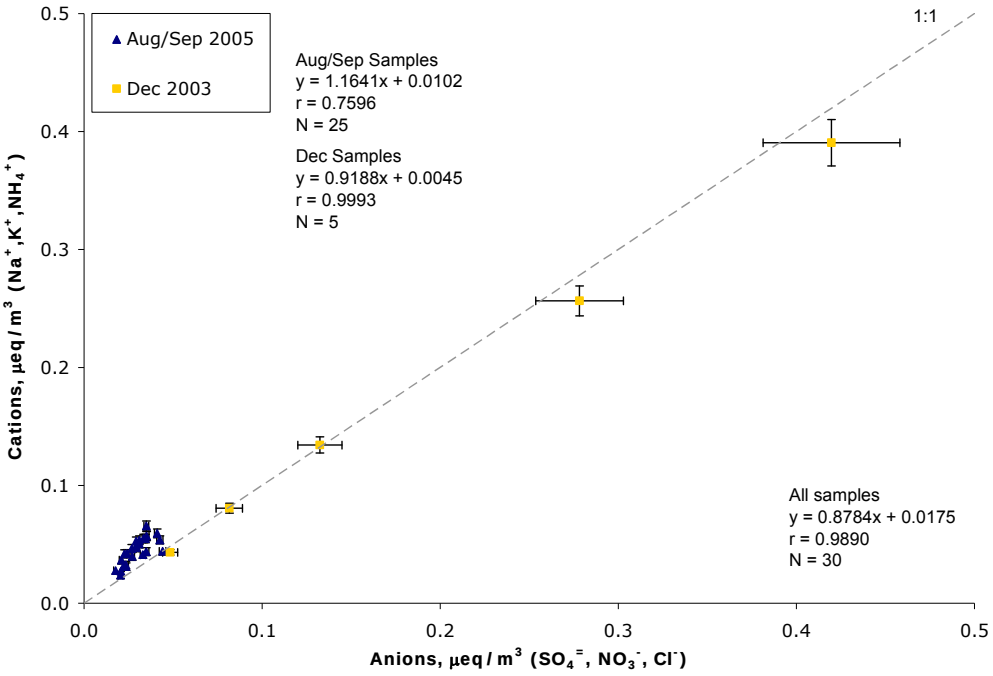

(a)

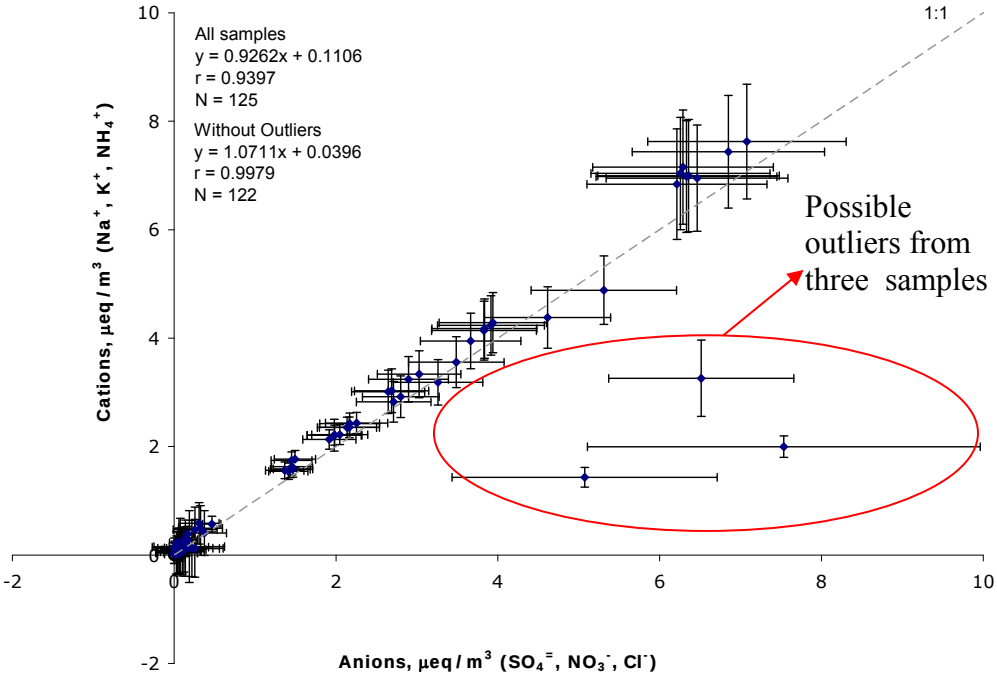

(b)

Figure 5-4. Anions versus cations for: (a) ambient samples during the summer and winter IOPs; and (b) laboratory-generated diesel generator, acetylene flame, electric arc, wood smoke, and nebulized carbon black source samples.

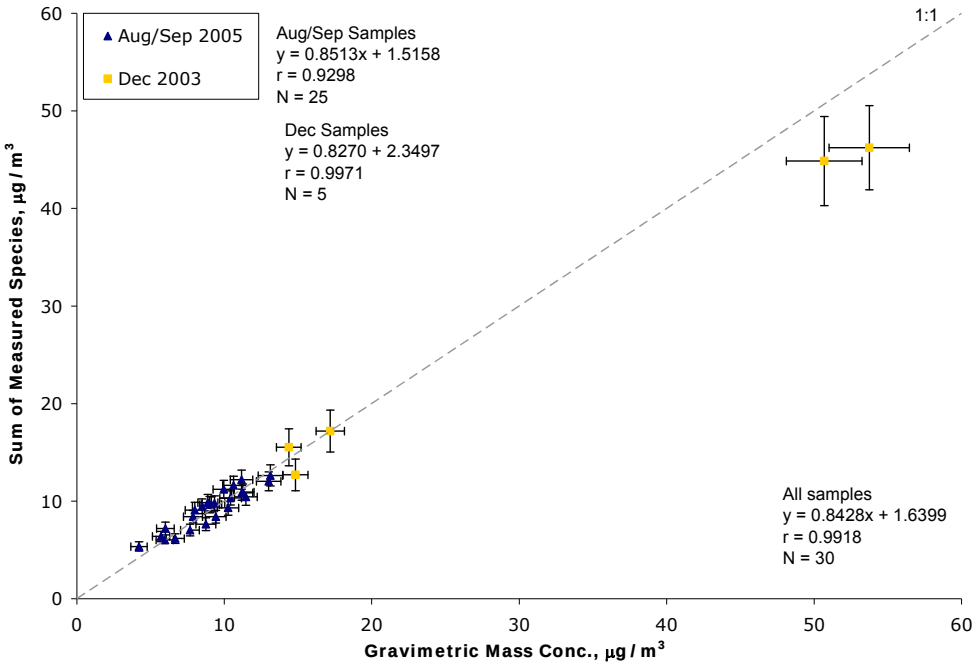

(a)

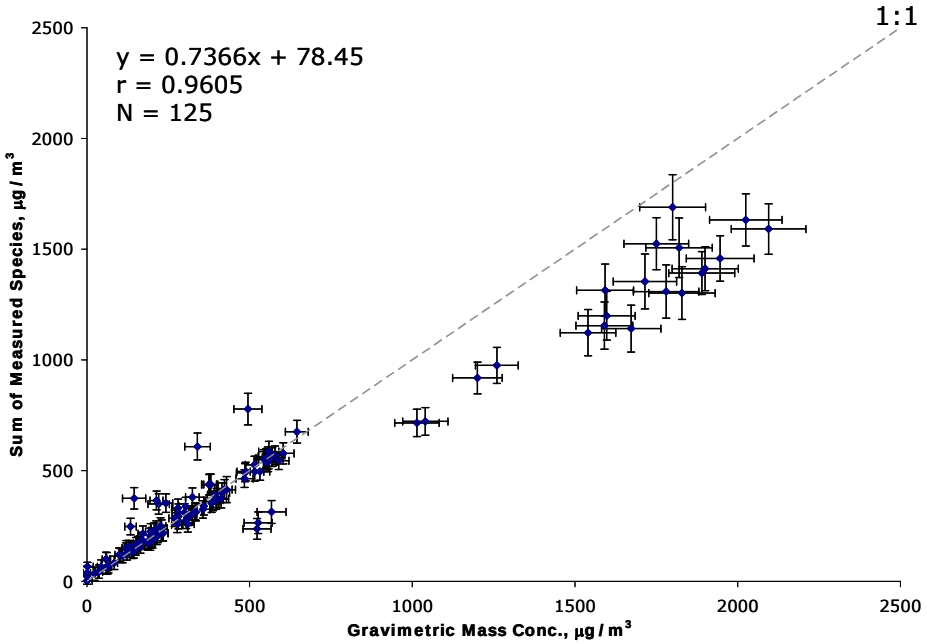

(b)

Figure 5-5. Total mass concentration versus sum of measured species mass concentration for: a) ambient samples during the summer and winter IOPs; b) laboratory-generated diesel generator, acetylene, electric arc, wood smoke, and nebulized carbon black source samples; c) electric arc source samples only; d) wood smoke samples only; and e) all source samples without electric arc and wood smoke samples.

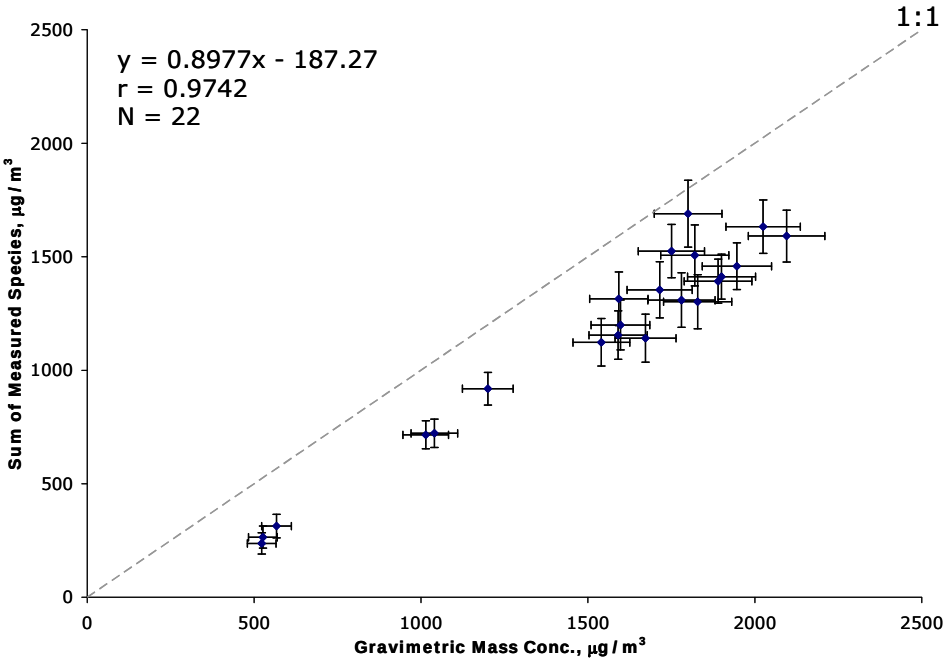

(c)

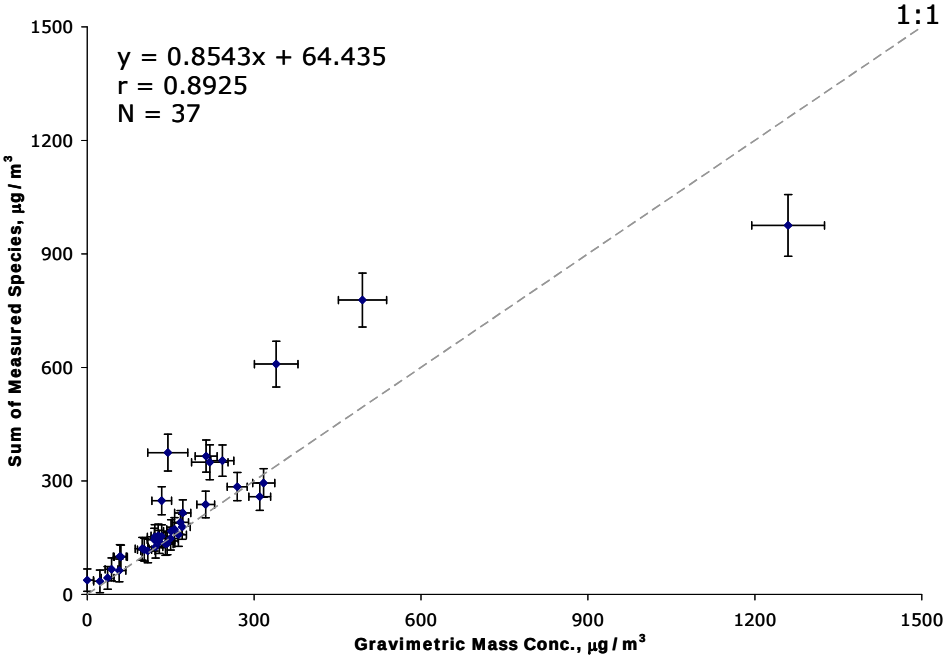

(d)

Figure 5-5. Continued.

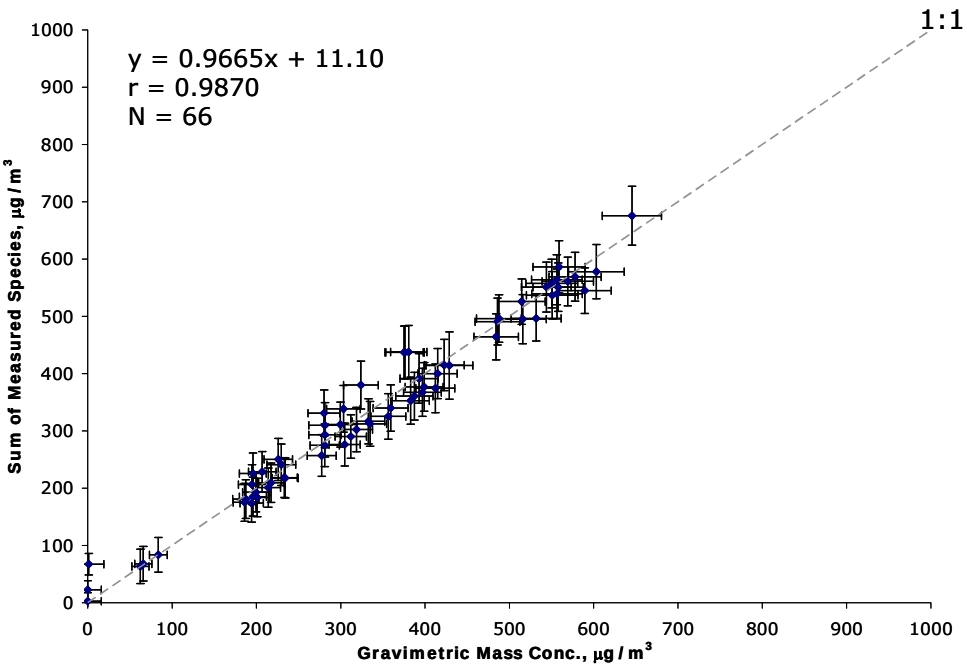

(e)

Figure 5-5. Continued.

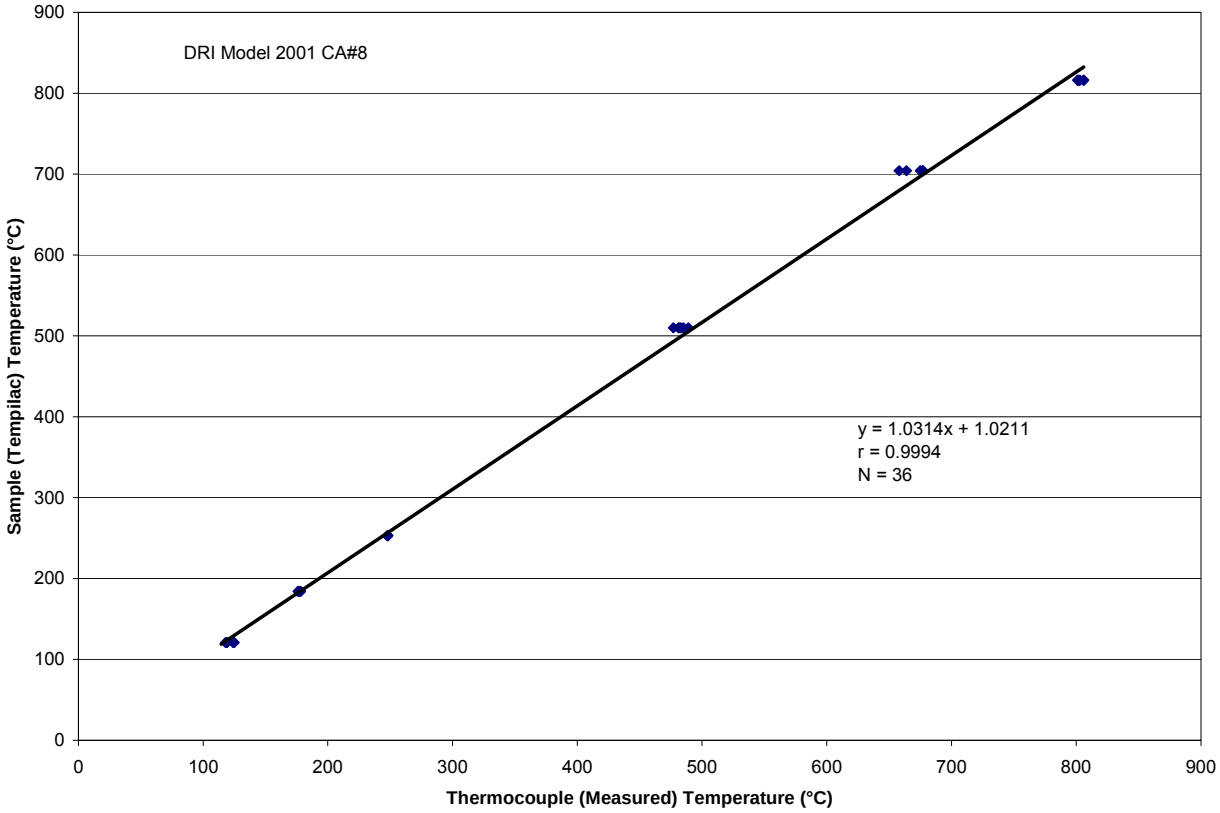

Figure 5-6. Example of temperature calibration for the DRI Model 2001 Thermal/Optical Carbon Analyzer.

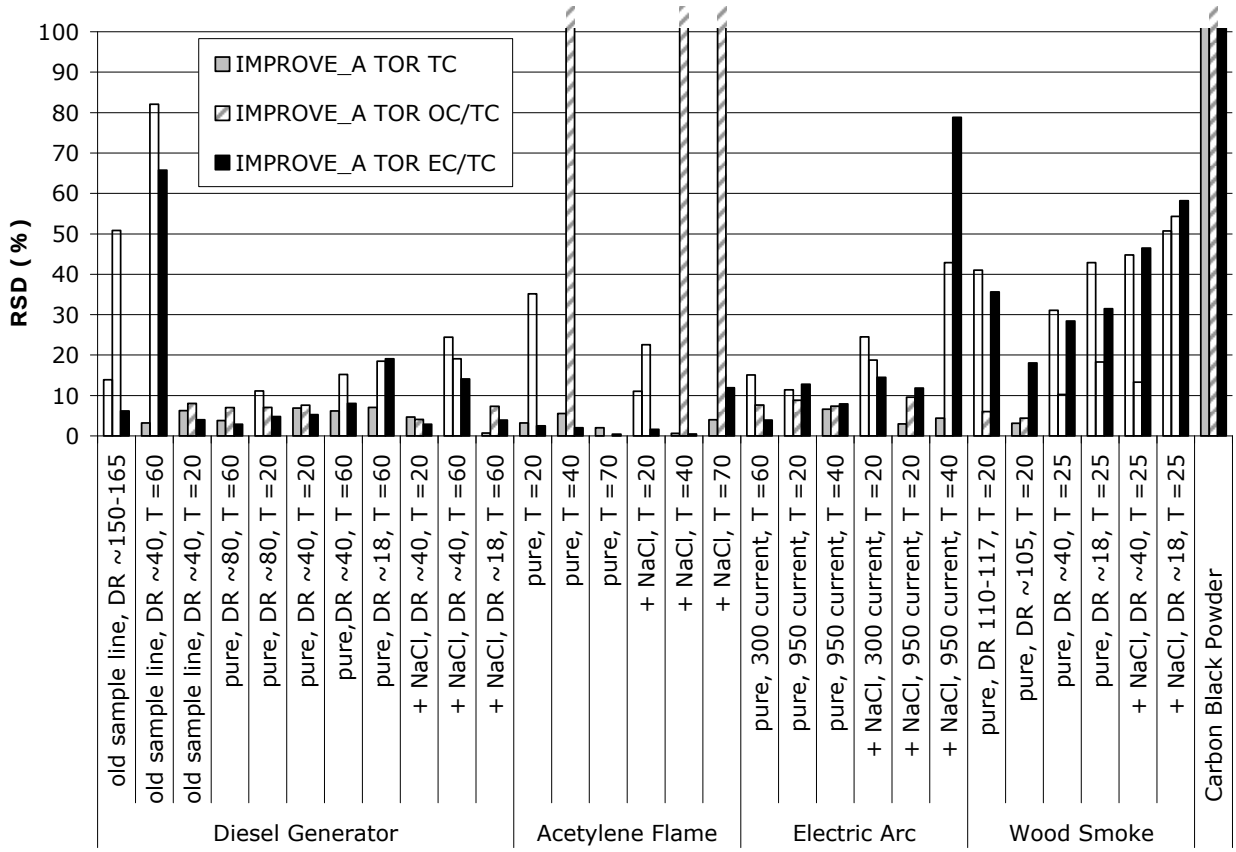

Figure 5-7. Relative standard deviation (RSD) for TC, OC/TC, and EC/TC following the IMPROVE_A protocol on quartz-fiber filters. (DR is dilution ratio and T is sampling time in minutes; old sample line refers to the kinked heated sample line that was initially used for the diesel experimental set up.)

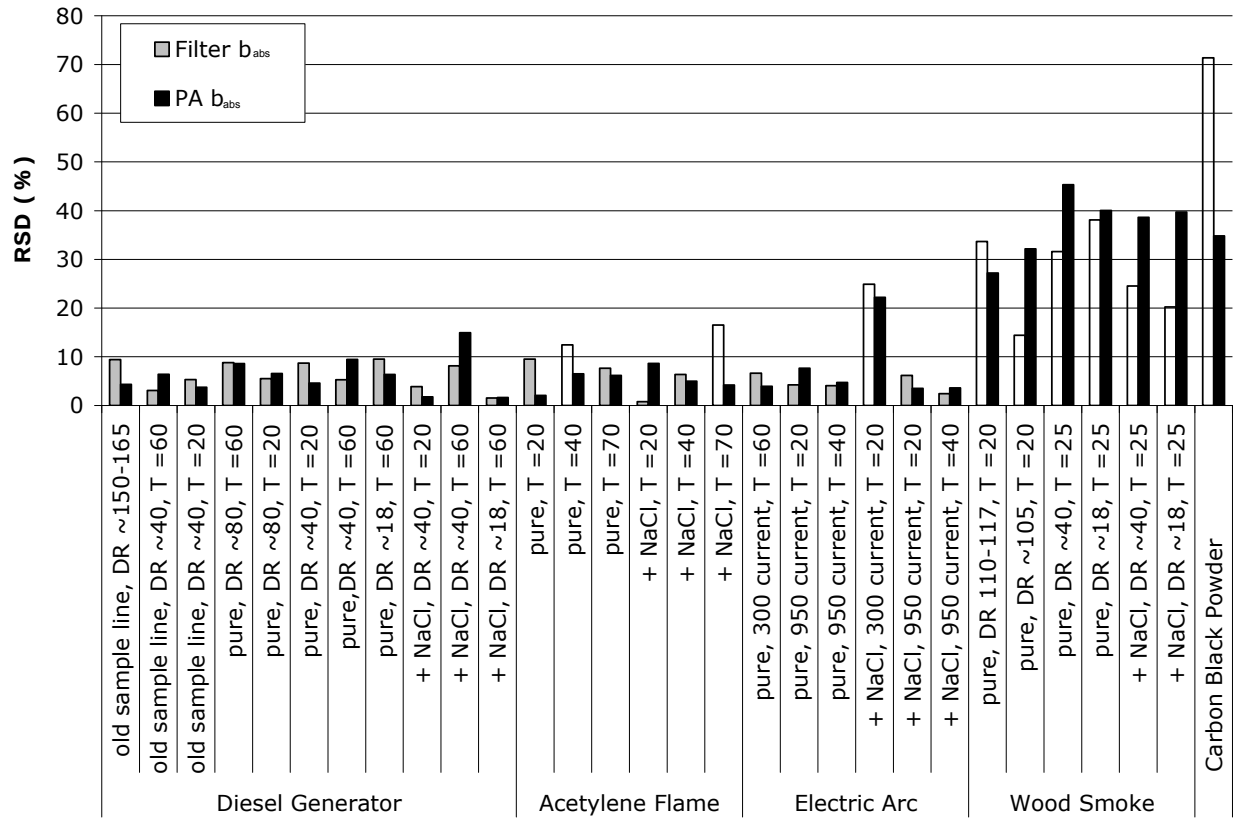

Figure 5-8. Relative standard deviation (RSD) for b_{abs} by densitometry on Teflon-membrane filters and by direct photoacoustic measurements. (DR is dilution ratio and T is sampling time in minutes; old sample line refers to the kinked heated sample line that was initially used for the diesel experimental set up.)

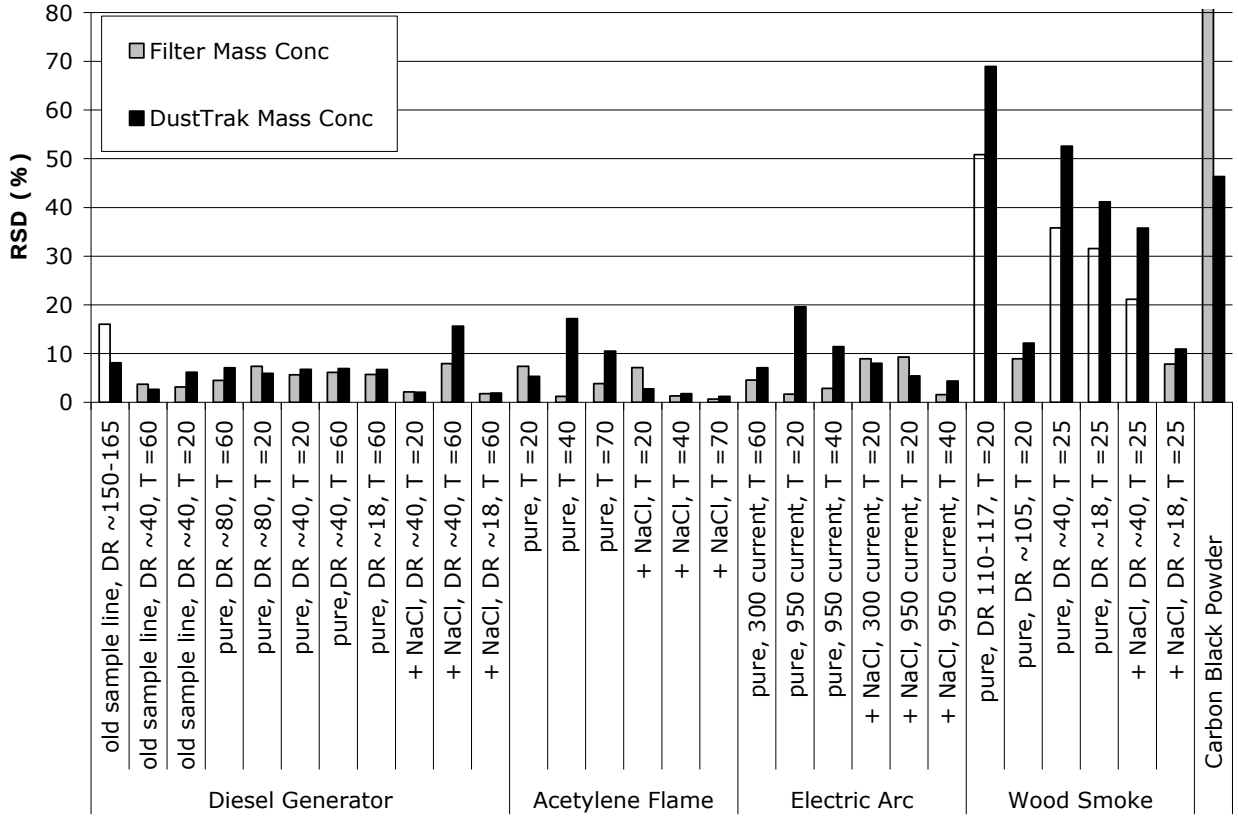

Figure 5-9. Relative standard deviation (RSD) for gravimetric filter mass and DustTrak mass concentrations. (DR is dilution ratio and T is sampling time in minutes; old sample line refers to the kinked heated sample line that was initially used for the diesel experimental set up.)

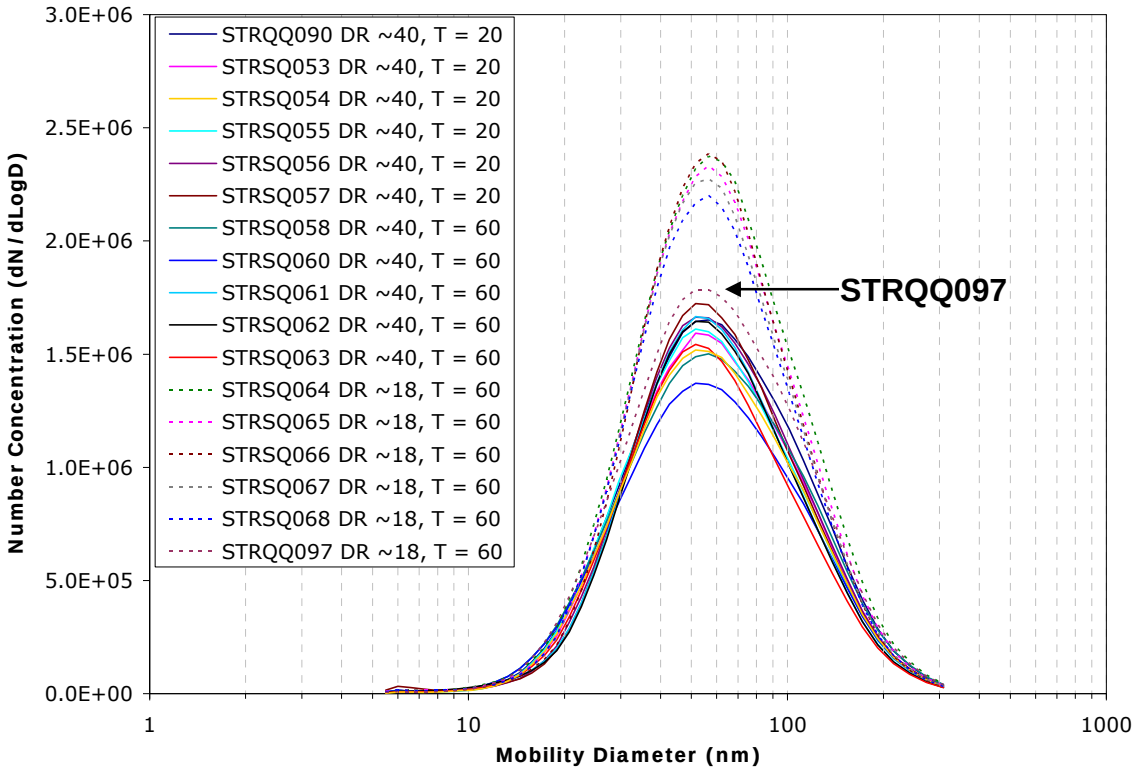

Figure 5-10. Size distributions of 17 diesel generator samples with dilution ratios (DR) of 18 and 40. (T is sample time in minutes.)

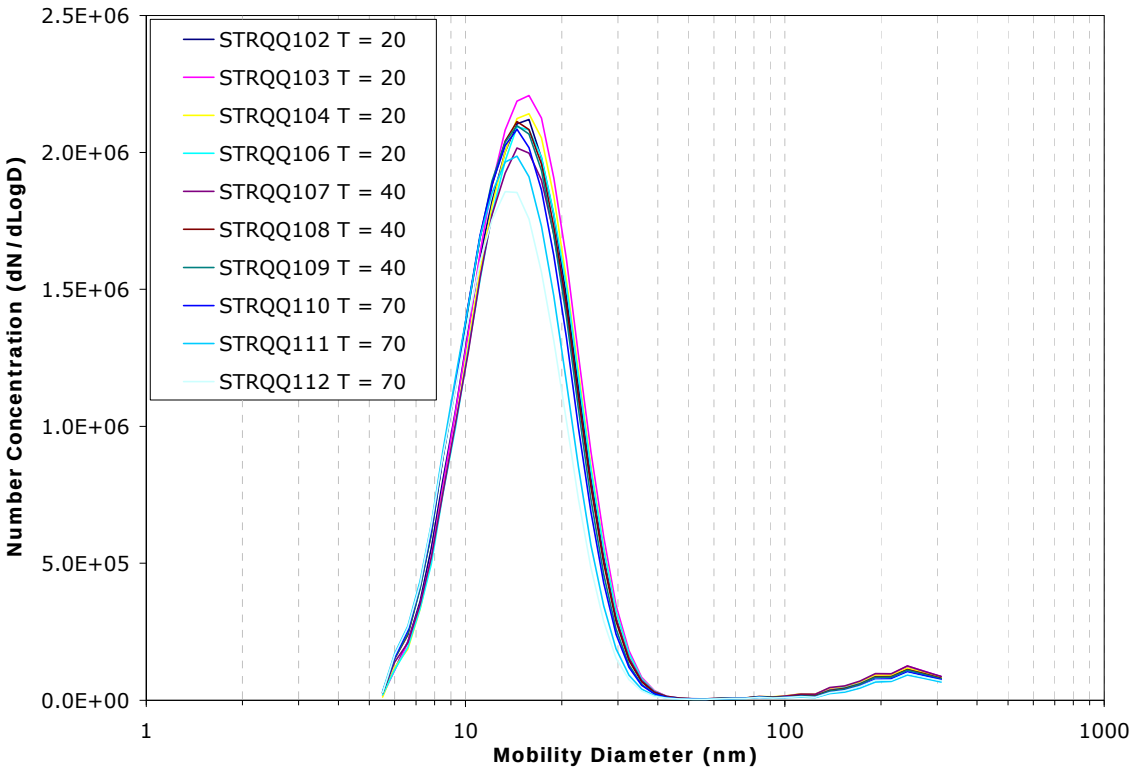

Figure 5-11. Size distributions of 10 acetylene flame samples with dilution ratios of ~17. (T is sample time in minutes.)

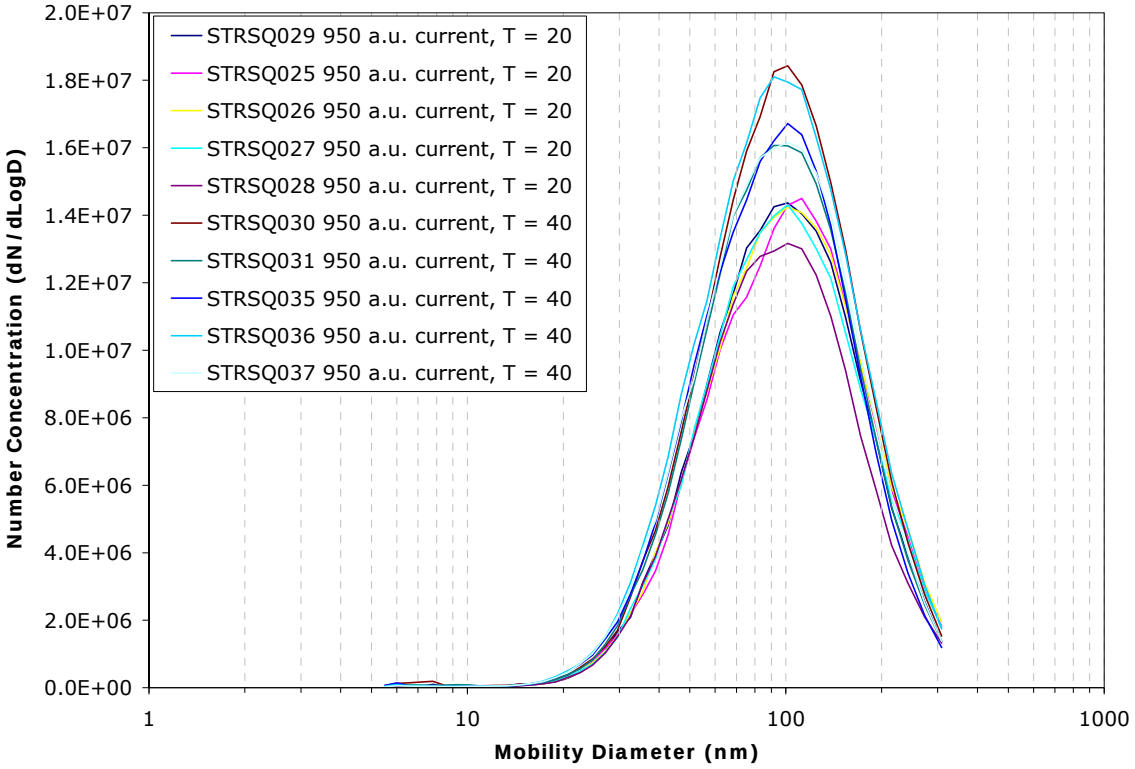

Figure 5-12. Size distributions of 10 electric arc samples with dilution ratios of eight at 950 a.u. current. (T is sample time in minutes.)

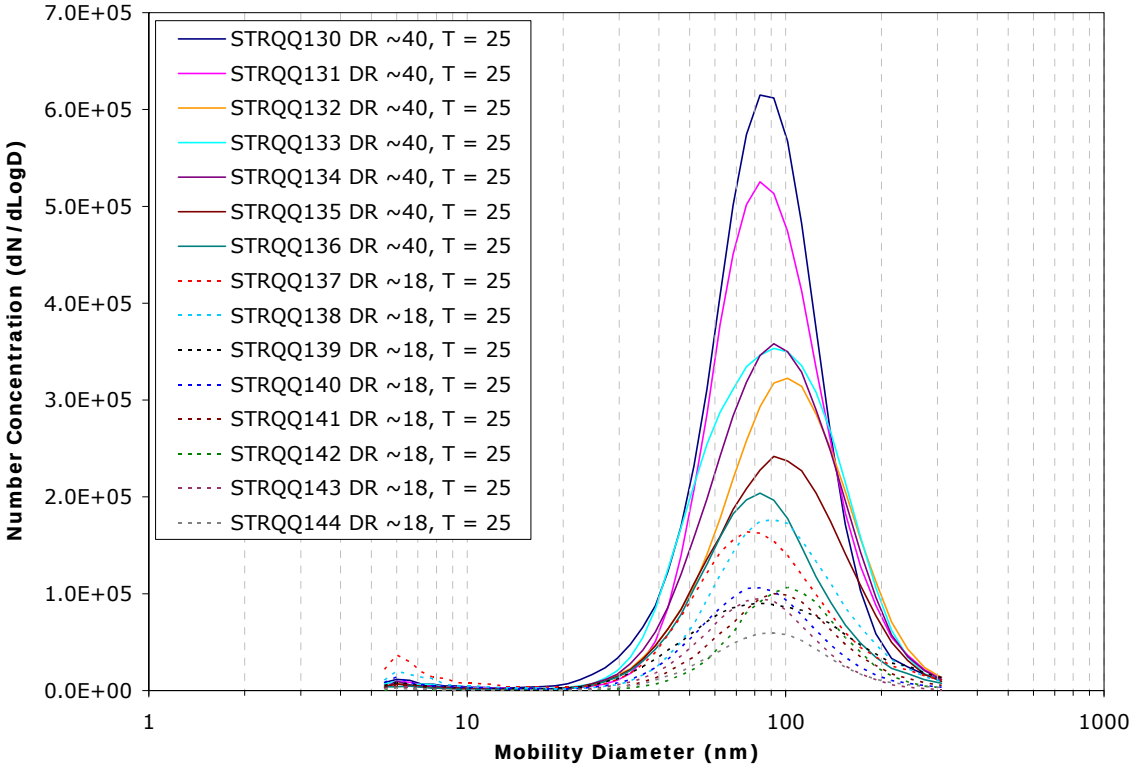

Figure 5-13. Size distributions of 15 wood smoke samples with dilution ratios (DR) of 18 and 40. (T is sample time in minutes.)

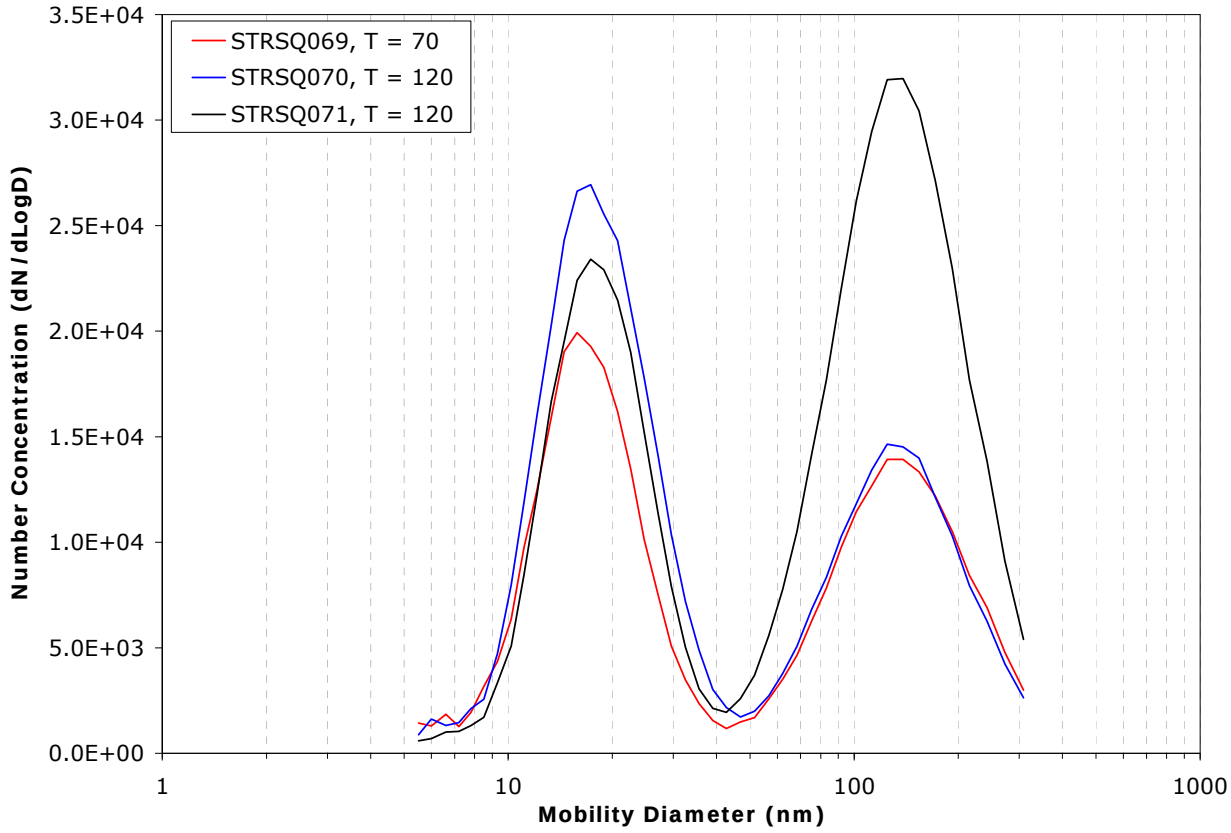

Figure 5-14. Size distributions of three nebulized carbon black samples. (T is sample time in minutes.)

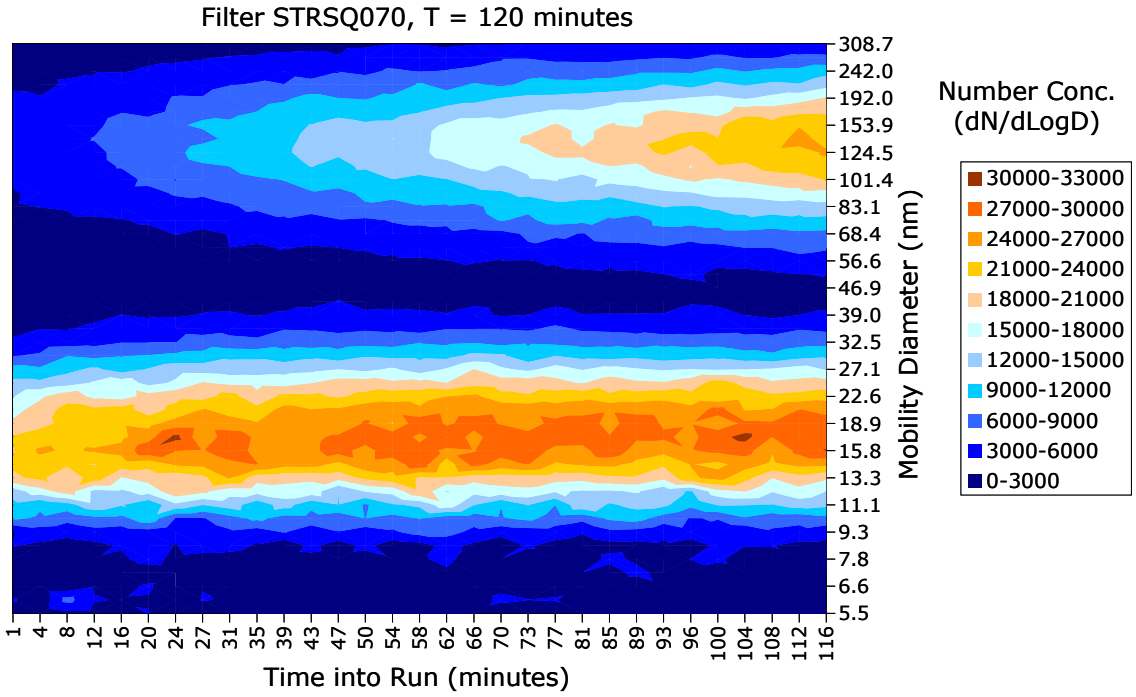

Figure 5-15. Temporal size distribution of one nebulized carbon black sample.

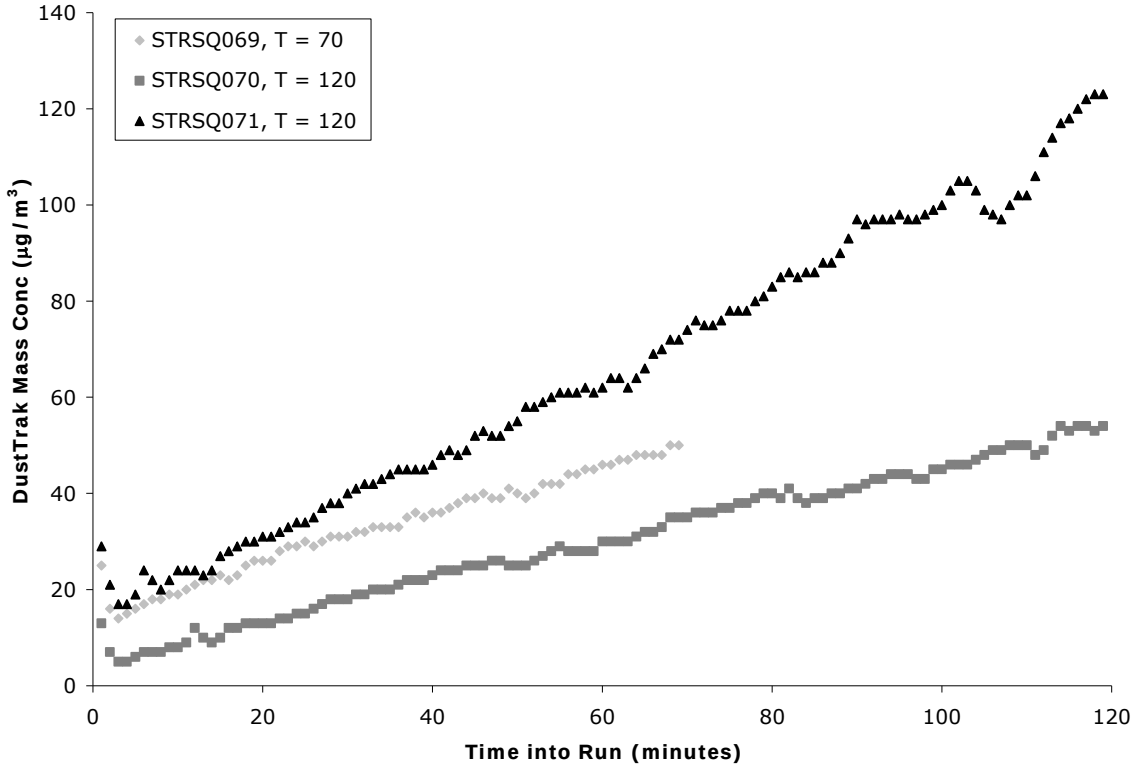

Figure 5-16. Temporal mass concentration profiles of three nebulized carbon black samples using the DustTrak. (T is sample time in minutes.) Note that DustTrak b_{scat} is expressed in equivalent µg/m^3 using the manufacturer's calibration constant.

6. METHOD INTERCOMPARISONS

This section reviews previous field studies that include PA measurements. Following this, the OC/EC fractions for source samples collected in the laboratory, and for ambient samples collected at the Fresno Supersite, are presented and discussed. Comparisons of continuous and integrated measurements for source and ambient samples are discussed next. The applicability of radiative transfer models to understand the effects of filter loading, pyrolysis within and on the surface of the filter, and multiple scattering within the filter and within the aerosol deposit is then evaluated. Finally, these results are synthesized to develop an overall understanding of how the methods compare for different sources, and how the laboratory measurements could be used to understand the differences seen in the ambient BC and EC measurements at Fresno and other locations.

6.1 Review of Previous Studies

Several previous studies have compared PA with other BC or EC measurement techniques. These studies cover both ambient (urban and rural) and source environments (motor vehicle and vegetative burning emissions), including: 1) Fresno Supersite; 2) Reno Aerosol Optics Study (RAOS); 3) Big Bend Regional Aerosol and Visibility Study (BRAVO); 4) Northern Front Range Air Quality Study (NFRAQS); 5) Southern Nevada Air Quality Study (SNAQS); 6) Gas/Diesel Split source sampling; and 7) Missoula Forest Fire Characterization Study. To use the photoacoustic technique as a benchmark for b_{abs} measurements and establish the BC emission inventory, it is important to determine, if possible, conversion factors under various conditions.

6.1.1 Fresno Supersite Study

As explained in Section 4.1, multiple continuous and integrated instruments have been in operation at the Fresno Supersite (Table 4-1). Park et al. (2006) compared measurements of eight optical, thermal, and photoacoustic methods acquired over 12 months (12/1/03 to 11/30/04; see Section 9.2). The results showed good correlations ($r > 0.90$) with slopes ranging from 0.2 to 2.0 among all BC or EC measures, except for the R&P 5400 EC. Site-specific σ_{abs} estimated by comparing b_{abs} with IMPROVE_TOR EC concentrations were 5.5 m^2/g for the MAAP at 670 nm, 10.0 m^2/g for the 7-AE at 880 nm, and 2.3 m^2/g for the PA at 1047 nm. These differ from the previously assigned efficiencies of 6.5, 16.6, and 5.0 m^2/g, respectively. Scaling absorption by inverse wavelength (i.e., Angstrom Power Law, $\lambda^{-\alpha}$, where $\alpha = 1$) did not provide equivalent b_{abs} among the instruments. Park et al. (2006) also showed that an α between one and two might be more appropriate for mixed and aged aerosol, such as that found at the Fresno Supersite. In order to reconcile BC and EC measurements from different methods, a better understanding is needed of the wavelength dependence of b_{abs} and σ_{abs}, and how they vary with different aerosol composition. The λ dependence of σ_{abs} during winter and summer and its relationship with α were explored further using the data acquired during the winter and summer IOPs (Sections 6.4 and 6.5).

6.1.2 Reno Aerosol Optics Study (RAOS)

The RAOS was designed and conducted to compare the performance of many existing and new instruments for the in-situ measurement of aerosol optical properties with a focus on the determination of aerosol b_{abs} (Sheridan et al., 2005). The RAOS was conducted from 6/3/02 to 6/28/02 in the Optics and Acoustics Laboratory of DRI. This study generated simple test aerosols of black and white particles, combined them into external mixtures under low RH conditions, and delivered the mixtures to various measurement instruments. The aerosol mixing and delivery system was constantly monitored using particle counters and nephelometers to ensure that the same aerosol number concentration and amount reached the different instruments. Four types of black aerosols (diesel generator soot, kerosene soot, carbon black, and graphite vane pump exhaust) were tested during the study. An eductor system was fabricated to dilute the black aerosols with filtered air by up to 100 times. White aerosols used in most of the intercomparisons were ammonium sulfate [$(NH_4)_2SO_4$] generated with an ultrasonic humidifier (UH). Source air for the UH was filtered, and the output was directed into a preliminary mixing/drying chamber.

Table 6-1 shows the measurements, instruments, wavelengths, and institutions that participated in RAOS. Measurements of in-situ b_{abs} were made using two primary methods, which were the PA, and the difference between aerosol light extinction (b_{ext}) by transmissometer and b_{scat} by nephelometer (i.e., b_{ext}–b_{scat}). In addition, filter-based light-attenuation measurements were made using two 7-AEs (370, 470, 521, 590, 660, 880, and 950 nm), a single wavelength (565 nm) and a three wavelength (467, 530 and 660 nm) PSAP (Arnott et al., 2005a), and the MAAP (670 nm) (Petzold and Schönlinner, 2004) to derive b_{abs}. One of the 7-AE had three of the light emitting diodes (LEDs) replaced so that different regions of the visible spectrum (370, 430, 470, 521, 565, 700, 950 nm) were covered. The three-wavelength PSAP was operated at wavelengths matching those of a folded-path optical extinction cell (OEC).

The PA b_{abs} and transmissometer minus nephelometer (b_{ext}–b_{scat}), showed excellent agreement on mixed black/white aerosols. When all stable mixed kerosene soot and $(NH_4)_2SO_4$ experiments were considered, the agreement was within 2–4% based on regression slopes (with the PA absorption slightly lower) for absorption levels in the visible wavelength region up to ~800 Mm^{-1}. If one high absorption test was excluded, the difference in the two sets of measurements increased to ~3–7%, depending on wavelength. The average of these two measurements (adjusted to 530 nm) was taken as the reference b_{abs}. Good agreement was also observed between the filter-based PSAP b_{abs} and the reference b_{abs} for atmospherically relevant levels of b_{abs} (<25 Mm^{-1}) under the controlled laboratory conditions of these comparison tests. It is not clear if similar agreement could be expected from ambient atmospheric aerosols, where changes in aerosol composition, concentration, and RH could influence the comparisons. For test aerosols exhibiting higher b_{abs} (and a lower single-scattering albedo [ω]), the agreement between the methods worsened with decreasing ω, presumably because of an inadequate filter loading correction. The Bond et al. (1999) correction scheme appeared to do a good job of correcting the PSAP b_{abs} for aerosol mixtures in this study at $\omega > 0.80 - 0.85$, which represents most atmospheric aerosols. The MAAP, which uses a two-stream radiative transfer model to account for the filter and aerosol scattering effects, agreed with the reference b_{abs} closely (linear

regression slope of ~0.99) for all experimental tests on externally mixed kerosene soot and $(NH_4)_2SO_4$. The comparisons are summarized in Table 6-2.

The wavelength dependence of absorption was investigated for all three types of light-absorbing particles. For the kerosene and diesel soot, measurements from most instruments showed a wavelength dependence near λ^{-1}, the theoretical small-particle limit. The large, irregularly shaped graphite particles showed widely variable wavelength dependencies over several graphite runs. This could be due to changing size distributions of the graphite caused by sample line efficiency or an unsteady source of the particles. The σ_{abs} at $\lambda = 530$ nm for pure kerosene soot with a number size distribution peak near 0.3 μm diameter was found to be 7.5 ± 1.2 m^2/g.

6.1.3 Big Bend Regional Aerosol and Visibility Observational Study (BRAVO)

The EPA, National Park Service (NPS), and Texas Commission on Environmental Quality (TCEQ) sponsored BRAVO with technical support from Electric Power Research Institute (EPRI). The BRAVO Study involved a four-month IOP from July through October 1999, followed by a four-year data analysis and modeling effort to assess the causes of haze in Big Bend National Park, TX. At Big Bend, b_{abs} was measured by both a PA at 532 nm and a single wavelength aethalometer at 880 nm (1-AE; Model AE-16). Both instruments operated simultaneously for one month (mid-September to mid-October), enabling comparison of their measurements.

Figure 6-1 shows a time series of the PA and 1-AE measurements, as 12-hour averages. The time series shows the maximum b_{abs} was 2.1 Mm^{-1}, and the maximum BC concentration was 0.2 $\mu g/m^3$, consistent with other measurements in the arid southwest USA (Pinnick et al., 1993). Between 9/20/99 and 9/23/99, the temporal variation of the measurements was very similar. On 9/25/99 and 10/2/99 both measurements indicated low values, and the 1-AE measurements were smoother than the PA measurements. From 10/8/99 to 10/16/99, the PA b_{abs} was proportionally lower than the 1-AE BC concentration. In summary, there were periods of agreement and disagreement in the relative trends of b_{abs} and BC measurements, perhaps due to size and compositional changes of the particles and to the difference in the MDLs of the methods (During this study, the 1-AE MDL was 71 ng/m^3 for a 1-hr average and the PA MDL was less than 0.1 Mm^{-1} for a 12-hr average).

The PA instrument used here was less sensitive than later versions. Larger signal variations around 10/12/99 could be related to this issue. The noise limiting factor in the PA measurements was identified as ambient or sampling derived acoustic noise, rather than microphone or other electronic noise.

Hourly-averaged 738 PA b_{abs} measurements were plotted against 1-AE BC measurements in Figure 6-2. The slopes of the linear models are 8.4 m^2/g and 9.9 m^2/g, depending on whether the entire data set was considered (solid line), or just the data corresponding to BC > 0.15 $\mu g/m^3$ (dashed line), respectively. The first slope (8.4 m^2/g) indicates the values that can occur when measurements are near the noise levels of the instruments. The correlation coefficient of the data in Figure 6-2 is relatively low ($r = 0.67$). It appears that the 1-AE BC data never went to zero,

suggesting that a small fraction of its response was due to contamination by scattering aerosol. A prior study comparing versions of these two instruments at an urban aerosol-dominated site in Brighton, CO (located in a semi-rural environment about 30 km northeast of downtown Denver, CO; Moosmüller et al., 1998) indicated an efficiency of 10.0 m^2/g, which agrees with the value obtained at Big Bend when the BC concentration was greater than 0.15 $\mu g/m^3$. It also agrees with the conventional value of 10 m^2/g that is used in the IMPROVE network for estimating extinction from EC concentrations (Watson, 2002). These slopes can be interpreted as σ_{abs} used in estimating BC from aethalometer transmittance. Note that 1-AE BC concentrations in this study were themselves derived from apparent filter absorption by using a σ_{abs} of 19 m^2/g, as discussed by Bodhaine (1995). Thus, the multiple-scattering filter substrate tends to amplify light absorption beyond the in-situ value.

6.1.4 Northern Front Range Air Quality Study (NFRAQS)

The goals of NFRAQS (Watson et al., 1998) were: 1) to attribute the air pollution in the Denver urban region to a source or source category; and 2) to collect data necessary to support informed decisions leading to attainment of federal air quality standards. NFRAQS (Watson et al., 1998) offered the opportunity to compare the routine measurement methods for ambient aerosol light absorption, such as the integrating plate. The instruments were operated at Brighton, CO, during the period from December 1996 to January 1997.

Continuous instruments deployed at Brighton included: 1) 1-AE (AE 10IM) at 880 nm; and 2) the DRI PA instrument at 532 and 685 nm. These measurements were compared with b_{abs} from six- or 12-hour filter samples on Teflon-membrane filters determined by densitometer, an integrating plate method (Tobias TBX-10), and EC from quartz-fiber filters following the IMPROVE_TOR protocol. The densitometer operates with "white" light, however; the effective spectral weighting (i.e., convolution of source and detector spectrum) is not known.

For the PA operated at 532 and 685 nm, the contribution of gaseous light absorption can be neglected for rural environments (Arnott et al., 1999). Measurements of PA were averaged over each sampling period for comparison. Results of linear regression analysis are summarized in Table 6-3.

Relatively good correlation (r = 0.92) was found between IMPROVE_TOR EC and PA b_{abs} (685 nm) with a slope of 3.58 m^2/g and a zero offset of 0.17 Mm^{-1}. Reasonable correlation (0.85) was found between the filter b_{abs} and PA (685 nm) b_{abs} measurements with a large slope (3.00) and intercept (3.43 Mm^{-1}). The correlation improved to 0.93, if one single filter measurement (i.e., $b_{abs} = 0.0$) was excluded.

For PA at 532 nm vs. 1-AE at 880 nm measurements, linear regression analysis indicates good correlation (0.94) with a σ_{abs} of 10 m^2/g and an intercept of 0.80 Mm^{-1}. The time series generally showed good agreement between the two instruments, although at certain times results were different by up to a factor of two. Disagreements were more frequent during short spikes which often encompassed only a single data point. This could be due to spatial inhomogeneities in aerosol properties, temporal changes in σ_{abs}, and/or inaccurate measurements by one or both of

the instruments. Measurements for PA at 685 nm were quite similar to those at 532 nm with good correlations (0.95) between the two time series, with the exception of the σ_{abs}, which was ~50% lower than PA σ_{abs} at 532 nm.

Comparisons of PA b_{abs} measurements and 1-AE BC concentrations have resulted in a BC σ_{abs} of 10 m^2/g at 532 nm and ~5 m^2/g at 685 nm. In addition, the IMPROVE_TOR EC σ_{abs} was determined to be ~3.6 m^2/g at 685 nm, somewhat smaller than the BC efficiency at the same wavelength. Recent reviews of aerosol light absorption have summarized values for σ_{abs} ranging from 2 m^2/g to 17 m^2/g (Liousse et al., 1993; Horvath, 1993a; Bond and Bergstrom, 2006). This large range has been attributed mainly to the diversity of methods used for measuring aerosol b_{abs} and EC, internal scattering in different filter media, and the variability of the aerosols encountered. The range of σ_{abs} can be narrowed if only measurements of aerosol b_{abs} by the PA method and the wavelengths (for the visible and near-visible spectral region) at which the PA instruments operate are considered as shown in Figure 6-3. At each wavelength the aerosol absorption efficiencies for different aerosols are quite close to each other. The σ_{abs} decreases toward longer wavelengths. The values determined as part of NFRAQS fit nicely with previously published values. Fitting a simple power law to the experimental data indicates that the σ_{abs} is proportional to $\lambda^{-2.7}$ with a correlation coefficient of 0.97, where λ is the wavelength used for the PA measurement of b_{abs}. A meaningful evaluation that seeks closure of measured and theoretical light absorption is difficult as refractive indices are only poorly known at these wavelengths, aerosol size distribution is generally unknown, and aerosol shape is generally non-spherical.

6.1.5 Southern Nevada Air Quality Study (SNAQS)

The Clark County (Nevada) Department of Air Quality Management and the U.S. Federal Transit Administration sponsored SNAQS during winter 2003 to better understand source category contributions to carbonaceous compounds in the Las Vegas urban region. Based on previous studies and a general knowledge of sources and activity levels within the Las Vegas Valley, gasoline vehicles, on-road diesel vehicles and non-road diesel engines, such as construction equipment, were expected to be major contributors to fine carbonaceous aerosol and haze. Minor carbon sources included wood burning (local RWC in winter, and some forest fire smoke transported into the valley in summer) and meat cooking.

SNAQS acquired ambient measurements at four sites in the Las Vegas urban region. A PA at 532 nm was deployed at the East Charleston site (~50 meters north of East Charleston Street, a secondary thoroughfare). Land use along East Charleston includes a Mexican restaurant, which is east of the site, and apartment buildings and detached houses that are north of the site. The objective of this experiment was to establish the relationship between b_{abs} and EC by using only the temperature set up of the IMPROVE_TOT and NIOSH_TOT protocols (See Table A-1 of Appendix A). The hypothesis was that the variation in the OC/EC split is due to differences in the temperature program between the two protocols, as applied using a Sunset Laboratory Carbon Aerosol Analysis Field Instrument that sampled onto a quartz-fiber filter and then analyzed using TOT following the short residence time set up in the NIOSH protocol. During this study, the Sunset instrument was operated (with an annular denuder for gas-phase organics)

on the IMPROVE temperature program for about two weeks in January, 2003 and then changed to the NIOSH method for about two weeks in February 2003. Samples were collected for 95 minutes, followed by an analysis time of just under 25 minutes, except for midday when concentrations were lower, when a 3-hour sample was collected. The PA measurements were made across the two periods to be compared with the EC results from the two different protocols.

Figure 6-4 compares EC concentrations from each method to the PA b_{abs}. Both methods showed EC was highly correlated ($r > 0.98$) with b_{abs}, but the slope was 16.3 m^2/g for NIOSH_TOT compared to 11.7 m^2/g for IMPROVE_TOT. The intercepts of 3.6 to 4.9 $\mu g/m^3$ are thought to be a TOT artifact. σ_{abs} higher than 10 m^2/g are seldom reported for diesel exhaust. However, in ambient samples they may be reasonable since EC σ_{abs} increases with the increasing OC/TC ratio (e.g., Martins et al., 1998). The EC/TC ratio ranged from 5 – 35% in the Las Vegas urban region and varied by time of the day. Figure 6-5 shows the diurnal pattern of TC to daily average TC ratio and EC to TC ratio for each method. The EC/TC ratio peaked during morning hours, likely due to increased diesel emissions. It reached a minimum during mid-day, as greater vertical mixing caused more regional rather than urban influence to be imposed. TC peaked in the evening, as vertical mixing was suppressed and wood smoke from RWC impacted the site. Carbon speciation analyses were used to apportion carbon to sources such as diesel vehicles, gasoline vehicles, wood smoke and meat cooking (Green et al., 2004).

6.1.6 Gasoline/Diesel Split Study

The Department of Energy (DOE) Gasoline/Diesel PM Split Study was conducted during summer 2001 to assess the source of uncertainties in quantifying the relative contributions of tailpipe emissions from gasoline- and diesel-powered motor vehicles to ambient concentrations of $PM_{2.5}$ (Fujita et al., 2006a). Gasoline- and diesel-powered vehicles were tested on dynamometers over prescribed driving cycles (i.e., the Federal Test Procedure) to characterize variations in the emission rates and PM composition. All vehicles tested, including late model spark ignition vehicles, had BC emissions. Ambient measurements in metropolitan Los Angeles and surrounding areas were obtained using both mobile and stationary sampling platforms. A PA at 1047 nm was used in this study. This same instrument suite was previously evaluated in measurements of emissions from light duty diesel trucks on a dynamometer (Moosmüller et al., 2001a; 2001b). A σ_{abs} of 5 m^2/g was used to convert b_{abs} to BC concentration. Filter samples were analyzed for OC and EC following IMPROVE_TOR and STN_TOT protocols.

Figure 6-6 shows the comparison of EC measurements obtained via IMPROVE_TOR and STN_TOT protocols to the PA BC measurements for heavy-duty diesel vehicles. The agreement between BC and EC by both protocols is within ±10%. Diesel carbonaceous material contains little OP and the OC/EC split is not influenced by the uncertainty in charring correction. Figure 6-6 also indicates that a σ_{abs} of 5 m^2/g might be appropriate for diesel EC. For the IMPROVE_TOR analysis, EC2 (the high temperature carbon faction evolved through oxidation in 98% He/2% O_2 at 700 °C) is the dominant carbon fraction, accounting for ~80% of EC.

Figure 6-7 shows similar comparisons for emissions from spark ignition vehicles. Note that EC is larger than BC for both protocols and that PA measurements agree better with EC2

measurements obtained by the IMPROVE_TOR protocol than with total EC. One way to reconcile the BC and EC is to use a lower σ_{abs} (<5 m^2/g) for gasoline vehicle samples. Fujita et al. (2006a) hypothesized that gas-phase organics adsorbed onto the quartz-fiber filter or biases in the optical charring correction cause the overestimation of EC, since the filters were exposed to sample air at ambient temperature; additionally, gasoline-powered vehicles typically have a higher ratio of vapor phase organics to EC than do diesel powered vehicles. EC2 is not expected to be influenced by the charring correction.

Ambient measurements of carbonaceous aerosol were obtained at two fixed sites: North Main Street near downtown Los Angeles, and at Azusa, east of Los Angeles. They were also obtained from an instrumented vehicle that traveled on the freeways of Los Angeles. Figure 6-8 shows a comparison of IMPROVE_TOR EC and STN_TOT EC to PA BC. The correlations of EC with BC by both protocols is very high ($r > 0.99$), although they differ in proportion. The slope of the IMPROVE_TOR curve, 1.21, is between the value found for diesel vehicles (1.07) and that found for gasoline vehicles (1.39).

6.1.7 Missoula Forest Fire Characterization Study

The pilot study conducted at the United States Forest Service Fire Science Laboratory (Missoula, MT) from 11/19/03 to 11/26/03 (Chakrabarty et al., 2006; Chen et al., 2006b) had three objectives: 1) to quantify emission factors from burning various wild-land fuels; 2) to characterize optical, physical, and chemical properties of these individual fire emissions; and 3) to test innovative measurement techniques. Emphasis was placed on fuels commonly burned in mid-latitude forests and Savanna/grassland. This experiment was designed to simulate isolated burning events that proceed through ignition, flaming, smoldering, and extinction stages. Trace gas concentration and particle mass and size distribution were continuously monitored. Optical properties of the smoke that were directly related to its radiative effects were also measured in-situ with the PA and cavity ring-down instruments. Time-integrated filter samples were collected and analyzed for elements, OC, EC, and organic species. OC and EC from both the IMPROVE_TOR and STN_TOT protocols were reported.

Both 532 nm and 1047 nm PA instruments were used to measure the smoke from vegetative burning. During this study, the PAs measured b_{abs} at 10 sec time resolution with a MDL of 1 to 2 Mm^{-1}. The response of the PA to light scattering and RH is negligible (Arnott et al., 2003), but NO_2 produced during combustion interferes with the absorption at 532 nm ($\approx$ 0.306 Mm^{-1} per ppb of NO_2; Arnott et al., 2000). Filter samples represented time-integrated averages throughout three to four replicate burns so that contributions from different combustion phases could not be separated.

Table 6-4 shows the linear regression of PA b_{abs} against the IMPROVE_TOR and STN_TOT EC for all burns. High correlations ($r > 0.96$) were found, indicating the consistency of EC and b_{abs} in the wood/grass smokes. The interference of NO_2 was minor. On average, the IMPROVE_TOR EC was ~15% higher than the STN_TOT EC, compared with a ±10% measurement uncertainty. The σ_{abs} were close to the default values for the PA instruments; i.e., 5 m^2/g at 1047 nm and 10 m^2/g at 532 nm. The intercept of b_{abs} versus IMPROVE_TOR EC was

always negative, while the b_{abs} versus STN_TOT EC intercept was always positive. Absorption should be at a minimum, when EC is absent. At very low concentrations, the IMPROVE_TOR protocol overestimated EC but the STN_TOT protocol underestimated EC.

The EC sub-fractions, based on the IMPROVE_TOR definition, varied dramatically between different fuels (Figure 6-9). Ponderosa pine wood burning resembled the kerosene flame, emitting EC that was dominated by the high temperature EC2. Dambo grass also produced a higher EC2 fraction, but EC1 was favored in many other burns. EC2 is used as a marker for diesel soot (e.g., Watson et al., 1994; Kim and Hopke, 2004; Kim et al., 2004). Due to a lower combustion temperature, gasoline vehicle and RWC are not expected to produce abundant EC2. This experiment, however, demonstrated that EC sub-fractions depend on the fuel and burning conditions. If combustion temperature is the key factor controlling the production rate of EC fractions, Ponderosa pine wood and Dambo grass burning might have a relatively high combustion temperature in their flaming phase. Other possibilities include the matrix effect; i.e., catalytic and oxidizing compounds that change the thermal behavior of EC. For OC sub-fractions, the majority were high-temperature OC3 and OC4 in all the biomass combustion PM (except kerosene soot), in contrast to diesel soot where OC3 and OC4 are minor fractions (Chow et al., 2004b; Chow et al., 2005b; Fujita et al., 2006b). OC3 and OC4 likely represent polar and high-molecular-weight organic compounds. The amount of OP also tends to increase with the increasing OC3 and OC4 content.

6.1.8 Summary of Past Studies by Regression Analysis

The σ_{abs} is the most important parameter that converts b_{abs} into BC concentration and vice-versa. This conversion factor is known to depend on wavelength and sample type. σ_{abs} of 10 and 5 m^2/g are commonly used to convert b_{abs} to BC at 532 and 1047 nm, respectively. Table 6-5 compares the regression of the PA b_{abs} measurement, a light absorption benchmark, with different BC and EC measurements across the seven studies summarized in this section. For both source and ambient samples, 5 m^2/g appears to be at the high end of the EC σ_{abs} at 1047 nm, if EC is determined by the IMPROVE_TOR protocol. This factor is more likely between 3 and 5 m^2/g, though values as low as 2.4 were also observed at the Fresno Supersite during winter. The OC/EC ratio is generally higher for ambient samples (especially winter at Fresno), and therefore a larger bias in EC measurement due to charring correction is expected. The conversion factor is 20 to 39% higher for EC determined from the STN_TOT protocol, but within 20% for wood smoke samples and 5% for diesel and gasoline samples.

For 532 nm, 10 m^2/g appears to an appropriate conversion factor for ambient samples analyzed with the IMPROVE_TOR protocol or aethalometer. However, for ambient samples the IMPROVE and STN (or NIOSH) protocols tend to determine a different OC/EC split. A higher conversion factor, such as 15 m^2/g, is needed for the STN_TOT EC. The Missoula fire study indicates that the conversion factor at 532 nm is slightly lower than 10 m^2/g for fresh wood smoke. Whether this is due to different internal mixing warrants further investigations. The absorption exponent often exceeded unity (Table 6-5).

6.2 Carbon Fractions of Source and Ambient Samples

This section discusses the OC and EC fractions within the source and ambient samples. As mentioned in Section 4.4.3 portions of the quartz-fiber filters were analyzed by three commonly used thermal evolution protocols: IMPROVE_A_TOR/TOT, STN_TOT, and the French two-temperature method. These protocols represent a wide range of variability in thermal and optical parameters including temperature plateaus, residence times, combustion atmospheres, heating rates, and optical pyrolysis monitoring by TOR and TOT that can be used to assess the impact of these variables on the determination of OC and EC.

Thermal methods involving TOR and TOT to monitor pyrolysis are most commonly used in the United States. Johnson et al. (1981) and Yang and Yu (2002) pointed out that such partitioning assumes that: 1) charred OC evolves before the original EC in the thermal analysis, and 2) charred OC and original OC equally attenuate reflectance (R) and transmittance (T). These assumptions are likely valid only under certain conditions (sample type, loading etc.) This section also discusses the influence of salt on thermal analysis, the distribution of thermally-resolved carbon fractions, and the organic sampling artifacts (i.e., carbon loading on backup filters).

6.2.1 Source Samples

Table 6-6 summarizes the number of samples, by source, analyzed by the IMPROVE_A, STN and French two-step protocols. Selected backup quartz-fiber filters were also submitted for analysis with the IMPROVE_A protocol to quantify the organic sampling artifacts.

6.2.1a OC/EC Fractions by Source Category and by Thermal Method

The samples were varied in loading, controlled by the dilution ratio in the dilution sampling system. Different current levels of 300 and 950 a.u. were applied to the electric arc soot generator, but produced little difference with respect to the EC/TC ratio. Table 6-7 compares the average carbon loadings (OC, EC, and TC) and EC/TC ratios by source as determined by the IMPROVE_A_TOR protocol. The sum of OC and EC approximates the TC but are not always the same (i.e., ([EC] + [OC])/[TC] ≠ 100%). This is due to blank correction that automatically zeros a concentration if it is negative after the blank subtraction (i.e., measurement is less than the blank level).

The average EC/TC ratio was highest for the acetylene flame (0.98 ± 0.05), followed by carbon black (0.94 ± 0.055), graphite (0.91 ± 0.095), diesel (0.65 ± 0.11), electric arc (0.50 ± 0.11), and wood smoke (0.26 ± 0.12). The EC/TC ratio appeared to be consistent within each source category, except for wood combustion, where the EC fraction was relatively low and variable. Emissions from wood combustion are sensitive to burning conditions, such as air flow rate and flame intensity.

Two diesel soot samples were excluded from the calculation of the EC/TC ratio. One sample (Filter ID STRQQF090), which was a pure combustion run, contained a higher NaCl

concentration (Na^+ = 11.8 ± 2.8 μg/m^3 and Cl^- = 15.5 ± 3.5 μg/m^3) than the other pure diesel combustion experiments (typically, less than 0.8 μg/m^3 Na^+ and 1.9 μg/m^3 for Cl^-). The NaCl likely resulted from incomplete flushing of the system after the experiments (electric arc soot mixed with NaCl) conducted the previous day. Even though the NaCl concentration (Na^+ = 11.7 ± 2.3 μg/m^3 and Cl^- = 15.5 ± 3.2 μg/m^3) was lower than that in the experiments with intentional NaCl introduction (Na^+ = 45 to 111 μg/m^3; Cl^- = 69 to 265 μg/m^3), it still shifted the carbon fractions (see Section 6.2.1c). The second diesel soot sample (Filter ID STRSQ016) that was excluded showed abnormally high charring (~60% of TC) likely due to changes in laser baseline during that particular thermal analysis.

Dilution of the source emissions changed the carbon concentration and loading on the filters, but it did not appear to affect the EC/TC ratio, as observed from this experiment. Figure 6-10 indicates good correlation (r = 0.92) between IMPROVE_A_TOR EC and TC for diesel samples. The EC/TC ratio increases for the lowest TC samples (the highest dilution ratio ~165), possibly due to the change in particle/gas-phase distribution of semi-volatile organics, i.e., the high dilution ratio shifts particle-phase organics to gas phase (Lipsky and Robinson, 2006). For wood smoke, the correlation of EC with TC is weaker (r = 0.85).

To compare the EC/TC ratio determined by different thermal protocols, a subset of samples were selected and analyzed by the STN_TOT and French two-step protocols in addition to the IMPROVE_A protocol. The STN_TOT protocol uses the transmittance charring correction while the French two-step protocol does not use any optical correction. The EC in the French two-step protocol consisted of the residual carbon remaining after baking for two hours in pure O_2. Since, the TC determined from the IMPROVE_A protocol was used to calculate OC for the French two-step protocol (OC = TC – EC), the IMPROVE_A and French two-step TC are the same in the results presented here. Table 6-8 shows the comparisons of EC/TC ratios by source and by thermal protocol.

TC measured by the IMPROVE_A and STN_TOT protocols agree with each other within 10% most of the time. This confirms that TC is independent of the method, although the STN_TOT protocol heats the sample to a higher temperature. With respect to EC, all three protocols agree within ~5% for diesel, acetylene flame, and electric arc samples, and within 10 to 15% for carbon black and graphite. The large variability in EC/TC ratio for graphite samples is due to an outlier (Filter ID RESQ1742) that has EC/TC ~ 0.58. This sample has a relatively low loading and was possibly contaminated. For wood smoke, both STN_TOT and French two-step protocols measured lower EC (by 46% and 86%, respectively) than the IMPROVE_A_TOR protocol. Wood smoke contains salts like KCl from wood, and therefore a larger matrix effect is expected. These comparisons are presented in Figure 6-11.

6.2.1b Distribution of Temperature-Resolved Carbon Fractions

The IMPROVE_A protocol reports a total of eight carbon fractions: four OC fractions (OC1 – OC4 evolved in an inert 100% He), three EC fractions (EC1 – EC3 evolved in an oxidative 98%He/2%O_2), and an OP (by TOR/TOT) fraction. Table 6-9 presents the means and standard deviations of the eight carbon fractions in TC, for each source category (pure aerosol and mixed

with NaCl or CH_3OH). EC2 accounted for a major fraction of TC: 65%, 94%, and 98% of TC in diesel, carbon black, and acetylene flame, respectively. More than 56% of graphite evolved as EC3, followed by 35% as EC2. The electric arc samples contained ~50% EC. Even so, a large OP (49% of TC) appears for the electric arc samples. Whether the cathode in the electric arc soot generator contains oxygenated organic compounds or the electric arc soot morphology leads to the charring warrants further investigation. In all other samples, OP was small (0.2% to 1.3% of TC) except for wood smoke (8.2% of TC).

The carbon black samples obtained from resuspension is dominated by EC2 (93 ± 4% of TC). EC2 also dominates the carbon black samples obtained from nebulization using methanol/water as solvent, but in this case EC is higher than TC after the blank subtraction, leading to an unusual EC/TC ratio of 3.48±4.78. The blank levels for this experiment were determined with 10% methanol solution while a 5% methanol solution was used for nebulizing carbon black particles. There were difficulties in producing consistent aerosol concentration using this experimental setup (Section 5.4.5). As a result, the nebulizer blank might overcorrect OC and TC.

Most of the OC in diesel samples evolves in the OC1 (20% of TC) and OC2 (12% of TC) fractions. This indicates that diesel EC is accompanied by volatile organic compounds (VOCs). In contrast, wood smoke contains higher OC3 (30% of TC) and OC4 (12% of TC) content. These high temperature OC fractions are semi-volatile or non-volatile hydrocarbons that usually char during thermal analysis. Approximately 6% of TC is OC3 for electric arc samples. In other samples (acetylene flame, carbon black and graphite), the OC fractions are very minor (OC1-OC4 <3% of TC).

6.2.1c Matrix Effect on Thermal/Optical Carbon Analysis

It has been reported (Lin and Friedlander, 1988a; 1988b) that salt and other catalysts increase EC oxidation at lower temperatures. NaCl was nebulized and injected into the dilution chamber to mix with the combustion particles during the source testing. Figure 6-12 shows amount of Na^+ in the samples relative to TC. Without NaCl injection, the Na^+ concentrations were lower than 1 $\mu g/m^3$ except for wood smoke where Na^+ ranged between 0.36 ± 2.7 $\mu g/m^3$ and 9.7 ± 7.0 $\mu g/m^3$. This is consistent with the chemical composition of biomass, i.e., rich in Na^+ and K^+. With NaCl injection, the Na^+ concentration was between 20 and 200 $\mu g/m^3$.

Changes in IMPROVE_A carbon fractions due to NaCl are summarized in Table 6-9. Figure 6-13 compares the changes in EC/TC ratio for different sources by the three thermal protocols. The EC/TC ratio from the IMPROVE_A_TOR and STN_TOT protocols are not strongly influenced by the NaCl. The inert atmosphere for OC combustion in the IMPROVE_A_TOR and STN_TOT limits EC oxidation kinetics, and changes in charring characteristics are compensated for with optical monitoring. Neither inert atmosphere nor optical correction was applied to the French two-step protocol; as a result, substantial EC evolved during the pre-combustion phase when samples were heated in pure O_2 at 340 °C for two hours. The French two-step protocol underestimates EC in such cases; 60 to 90% lower EC was detected in diesel and electric arc samples with the French two-step protocol (Figure 6-13). The influence of additional NaCl on wood smoke samples is expected to be minor, since the wood smoke already

contains KCl and NaCl. The higher EC/TC ratio in wood smoke with NaCl, as measured by the French two-step protocol, likely resulted from variations in wood burning conditions.

A large variability of the EC/TC ratio was found for the electric arc combined with NaCl. Figure 6-14 shows that the electric arc samples exhibit a distinct thermogram that contains a sharp EC1 peak. The peak is so narrow in time (10 – 15 sec) and intense in amplitude that the OC/EC split error due to transit time becomes important. It was found that the transit time in one of the carbon analyzer was off by two seconds. Such small biases are unlikely to influence the OC/EC split in most analyses, since the peak carbon evolution rate is much lower than that seen in the electric arc sample. Due to the very sharp EC1 peak in electric arc samples, the slight change in the transit time influences the amount of carbon assigned to OP and hence the OC/EC split.

Although the EC/TC ratios by the IMPROVE_A_TOR and STN_TOT protocols was not influenced by NaCl, the carbon fractions were. As shown in Figure 6-15, most of the EC2 in diesel and acetylene flame samples shifted to EC1 upon the inclusion of NaCl, while EC3 in the acetylene flame samples shifted to EC2. NaCl likely lowers the activation energy for soot oxidation and therefore increases its combustion rate at lower temperatures. This is, however, limited by the presence of O_2. With the addition of NaCl, the fractions of OC3 and OC4 in electric arc and wood smoke samples also increased. Whether NaCl could suppress charring in an inert atmosphere requires further investigation.

The early combustion of EC could be triggered by other salts as well, such as KCl or KBr, although these are not as commonly found in ambient air as NaCl. HCl, NH_4, NO_3, $(NH_4)_2SO_4$, and H_2SO_4 leave the sample at < 300 °C and probably have negligible effects on EC evolution. This matrix effect is important when using carbon fractions derived from thermal analysis to develop source profiles for source apportionment.

6.2.1d Organic Sampling Artifacts

Adsorption of vapor phase organic compounds on quartz-fiber filters are known to inflate the particulate OC concentration (Turpin et al., 1994; Watson and Chow, 2002b; Chow et al., 2006d). The magnitude of this positive sampling artifact depends on the amount of organic vapor in each source and also depends on the sampling duration since the quartz-fiber filters are eventually saturated (Chow et al., 1996). Backup quartz-fiber filters have been typically used to estimate the sampling artifact (Subramanian et al., 2004; Chow et al., 2006d). It is assumed that only organic vapor (not particles) can penetrate the front filter and be intercepted by the backup filter and, therefore, the particulate OC concentration may be obtained by subtracting OC on the backup filter from that on the front filter. This assumption is probably valid for solid particles, but not for liquid particles or solutions (e.g., sugars such as levoglucosan or sucrose) that can wick throughout primary and backup filters.

In Table 6-10, the average carbon fractions on front and backup filters are presented by source type (note: these values are not blank subtracted). EC on backup filters were generally low, consistent with EC's presence only in the particle phase. A higher EC level found on backup filters for wood smoke implies the bias in optical charring correction when the EC concentration

or EC/TC ratio is very low. OC on the backup filters is large, ranging from ~25% to ~90% of OC on front filters (Table 6-10). OC on backup filter behind Teflon (TB) is usually higher than that behind quartz (QB), since front quartz (QF) filters adsorb and retain the organic vapors on the front filter, thus reducing the vapor concentration in the sampling stream available for adsorption on QB. Turpin et al. (1994) suggest using the OC on TB as a more accurate estimate of the positive sampling artifact. However, this may not apply for electric arc samples, where unusually higher OC was found on QB than TB, implying possible attachment of some organic compounds from the electric arc samples to Teflon-membrane rather than quartz-fiber filters. The electric arc samples showed unique properties throughout the experiment, including a high OC and OP (charring) content, an extremely sharp EC1 peak, and unusual organic vapor distribution. The chemical composition and morphology of particles in electric arc samples need to be examined further.

Since the backup OC represents VOCs that are expected to evolve at lower heating temperature, OC1 and OC2 should be the dominating carbon fractions on backup filters. For acetylene flame and wood smoke samples, OC1 on TB were 70 to 107% of OC1 on QF, suggesting that most of OC1 could be artifact. For diesel samples, OC1 on QF was 5 to 6 times higher than that on backup filters. Diesel samples may contain more liquid-phase volatile phase particles such as those from lube oil (Brandenberger et al., 2005). OC3 was also found to be substantial (~30% of TC) on backup filters, especially for wood smoke and electric arc samples with or without the addition of NaCl. Each quartz-fiber filter may have different capacity for organic vapor adsorption (Kirchstetter et al., 2001). Overall, substantial uncertainty still exists in OC quantification owing to variable amounts of adsorbed organic vapors. This does not appear to significantly influence the EC measurement.

6.2.2 Ambient Samples

Twenty-four hour ambient samples were collected from the Fresno Supersite during the summer and winter IOPs using FRM, Hi-Vol and RAAS samplers. Filter samples from the FRM sampler were not analyzed by STN_TOT and French two-step protocols; hence, they are not included in the discussion in this section. As explained in Section 4.4, the RAAS contains six channels, three of which are used for carbon analysis: Channel 1 with a non-denuded Teflon-quartz sequential filter pack; Channel 2 with a non-denuded quartz-quartz filter pack; and Channel 4 with a denuded quartz-quartz filter pack. Table 6-11 summarizes the number of samples analyzed by each of the three thermal protocols.

The Fresno samples showed TC loadings ranging from 2 to 22 $\mu g/m^3$. Figure 6-16 compares 25 EC and TC measurements from the Hi-Vol sampler, including 18 from the summer IOP and 7 from the winter IOP. The IMPROVE_A_TOR protocol shows an EC/TC slope of 0.32 with high correlation ($r = 0.98$). The STN_TOT protocol showed a lower EC concentration (slope = 0.05) and a weaker correlation ($r = 0.77$) between EC and TC. The EC/TC ratio by the French two-step protocol is 0.1. Table 6-12 summarizes the inter-method comparison using the average and standard deviation of EC/TC ratio by method and by season. Average TC in winter was about twice as high as that in summer. The EC/TC ratio was 0.21 and 0.26 in summer and winter, respectively, as determined by the IMPROVE_A protocol. The STN_TOT protocol, not only

shows a low EC/TC ratio, but also shows an inverse seasonal trend; i.e., lower in winter (0.1) than summer (0.17). The French two-step protocol determined EC/TC ratio similar to (within ±10%) the IMPROVE_A_TOR protocol in summer, but deviates by more than 100% in winter. The French two-step protocol also determined a lower EC/TC ratio in winter.

Table 6-13 compares the measurements from Hi-Vol and RAAS samplers. The RAAS samples shown here correspond to carbon concentrations determined on the front quartz-fiber filter after field blank subtraction. For the IMPROVE_A_TOR analysis, the RAAS Channel 2 and Hi-Vol EC/TC ratios were within 10% during the winter IOP (Table 6-13). In summer, however, the RAAS EC/TC ratio was ~25% lower than the Hi-Vol EC/TC ratio. The organic sampling artifact is more pronounced in summer than in winter (Chow et al., 2006d). Artifacts may vary by sampler because of different sampling flow rates. In addition, the artifacts influence not only OC but also EC measurement to some degree (Chen et al., 2004) when the EC concentration is low. The STN_TOT analysis on RAAS Channel 2 samples measured 48% higher TC but a 28% lower EC/TC ratio in summer, relative to the Hi-Vol. In winter, the STN_TOT analysis showed a much wider range of EC/TC ratio from the RAAS sampler (0.12 ± 0.08), compared with those determined by the IMPROVE_A_TOR protocol (0.237 ± 0.019).

The RAAS Channel 4 samples are expected to show lower OC and TC, since the denuder removes a fraction of organic sampling artifacts. Table 6-13 confirms 40 to 45% lower OC in Channel 4 relative to Channel 2 of the RAAS in summer, leading to higher EC/TC ratios by both the IMPROVE_A_TOR and STN_TOT protocols. The denuder not only lowered the TC concentration but also lowered the EC concentration slightly (Figure 6-17). Based on Table 6-13, the lower EC mostly occurred in summer. The only way EC is influenced by denuder is through the optical charring correction, which could be biased by the sampling artifact. In contrast, STN_TOT appears to determine a higher EC with denuders. The organic sampling artifact influences the STN_TOT and IMPROVE_A results differently, due to the different optical corrections (i.e., transmittance versus reflectance), as suggested in Chow et al. (2004a).

The RAAS sampler provides multiple channels and filter configurations by which the organic sampling artifact can be assessed. The TB measures higher OC (60% to >200%) than QB; most of the artifact appears in the OC2 and OC3 fractions (Table 6-14). This is consistent with the wood-smoke source samples (Table 6-10), although the degree of artifact appears to be lower for the ambient samples (mostly <25% of TC). The artifact, as estimated by TB, is similar between summer and winter, despite a higher TC concentration in winter. The denuded backup quartz filter (dQB) shows very low carbon concentration (<0.1 $\mu g/m^3$), mostly below the LQL. This confirms the efficiency of the denuder for removing VOCs. For winter, the difference of TC between QF and TB is 8.63 $\mu g/m^3$, which is in good agreement with that from front quartz behind denuder (dQF; 9.42 $\mu g/m^3$). For summer, the difference is 3.5 $\mu g/m^3$, compared to 2.94 $\mu g/m^3$ from dQF. The subtraction of TB from QF may not completely compensate the sampling artifact during summer when the fraction of artifact in TC is larger.

6.2.3 Summary of Carbon Fractions in Source and Ambient Samples

Major findings from the filter sample intercomparisons include:

- The IMPROVE_A_TOR protocol determined a EC/TC ratio of 0.65±0.11, 0.98±0.05, 0.50±0.11, 0.26±0.12, 0.94±0.06, and 0.91±0.10 for diesel, acetylene flame, electric arc, wood smoke, carbon black, and graphite samples, respectively.
- The EC/TC ratio at the Fresno Supersite was 0.22±0.04 and 0.26±0.05 for summer and winter IOPs (based on Hi-Vol samples), respectively. These are closest to the wood-smoke source samples.
- The STN_TOT and French two-step protocols determined EC/TC ratios similar (within 5%) to the IMPROVE_A_TOR protocol for diesel, acetylene flame, and electric arc samples and within 5 to 15% for carbon black and graphite samples. A larger difference was found for wood smoke samples. STN_TOT and French two-step protocols are significantly low-biased (46% and 86%, respectively) for EC in wood smoke compared to the IMPROVE_A_TOR protocol.
- For ambient samples, the STN_TOT and the French two-step protocols are also low-biased for EC/TC ratio compared to the IMPROVE_A_TOR protocol. This trend is especially clear during the winter IOP. This corroborates strong wood-smoke influence at Fresno during winter.
- EC2 is the dominant carbon fraction in TC, for diesel (62 ± 8.7%), acetylene flame (81 ± 15%) and carbon black (93 ± 4.4%). EC3 dominates the graphite samples (56±13%). The electric arc and wood smoke samples contain higher levels of OC (>50%) and EC1 (59% and 30% respectively).
- EC1 and OC3 are also dominant carbon fractions in TC at Fresno during winter IOP. This confirms the influence of RWC. In summer, however, the percentage of EC2 in TC (12%) is higher than in winter (8%), possibly due to a more dominant influence of mobile sources, especially those from diesel exhaust.
- For source samples, most of OC1 and OC2 could be sampling artifacts, except for electric arc and diesel samples where there are likely real particles evolved in OC1 and OC2. These particles/fractions are not observed on backup filters.
- The denuder used in the RAAS sampler removes most of the sampling artifact. OC determined from the difference of QF and TB are close to that from denuded channel.
- Salts, such as NaCl, increase the evolution rate of EC at lower temperatures. With NaCl, EC2 in source samples is mostly shifted to EC1 while EC3 is shifted to EC2. It appears that the presence of salts may also suppress the charring of OC in an inert atmosphere; however more work is needed to confirm this.
- Although the addition of NaCl shifts the carbon fractions, it does not affect the EC/TC ratio or the OC/EC split determined by the IMPROVE_A_TOR and STN_TOT protocols. For the French two-step protocol, however, lower EC (>60 to 90%) was determined in the presence of NaCl. Since the effect of the catalyst is limited by the presence of oxidants, it is apparent that the French two-step protocol (that operates in 100% O_2) without charring correction is more influenced by the sample matrix.

6.3 Laboratory Source Testing Carbon Measurements

This section summarizes the intercomparisons of laboratory source measurements. Paired comparisons are summarized in Tables 6-15 and 6-16. Table 6-17 summarizes the results of the intercomparisons in terms of equivalence, comparability, and predictability. Regression slopes and intercepts with OLS (Bevington, 1969) and effective variance (EV) (Watson et al., 1984) weighting, with their standard errors, provide one measure. The OLS regression does not weight measurements when computing linear regression statistics, whereas EV regression accounts for measurement uncertainties in both independent (x) and dependent (y) variables to make the dataset less likely to be biased by extreme values. Other useful statistics are averages of y/x, standard deviations of the average ratios, and the distribution of the data pairs whose difference (y minus x) is less than 1σ (σ is the measurement uncertainty of $y–x$, which is the square root of the sum of the squared uncertainties $[\sigma^2_x+\sigma^2_y]$, where σ_x and σ_y are the one standard deviation precisions for the x and y observables, respectively), between 1 and 2σ, between 2 and 3σ, and greater than 3σ. Other performance statistics presented in Tables 6-15 and 6-16 are: 1) the average of the paired differences ($y–x$); and 2) the RMS precision (the square root of the mean squared precisions), which is essentially the average measurement uncertainty of "$y–x$." The equivalence, comparability, and predictability (or lack thereof) among different carbon measurements are defined in Section 5.1.1 (Watson and Chow, 2002b).

6.3.1 Comparison between 7-AE and PA Measurements

Comparison of b_{abs} between 7-AE (at 880 and 950 nm) and PA at 1047 nm were predictable ($r>0.9$) only for the following sources: electric arc, carbon black, acetylene + NaCl and electric arc + NaCl (Table 6-15). Figures 6-18 and 6-16 represent the data graphically. The disagreement between the EV/OLS slope and the average ratio is caused by the large intercepts of the regressions (diesel ~1,100, diesel + NaCl ~1000, and acetylene ~350 Mm^{-1}). The 7-AE b_{abs} was higher than the PA b_{abs} by two times for diesel, 1.1 to 1.4 times for acetylene and electric arc, and 3.7 times for wood smoke. Samples mixed with NaCl showed similar average ratios.

Comparison of BC between 7-AE at 880 nm and PA at 1047 nm showed a general trend of slope < 0.5 with the exception of carbon black (slope 0.7 and r = 1.0) and wood smoke + NaCl samples (slope = 1.2, r = 0.73), as shown in Figure 6-20. As shown in Table 6-15, the best comparison is found for the nebulized carbon black, with a slope of 0.73, average y/x ratio of 0.86, and correlation of one. High correlations (r = 0.91 to 0.95) were also found for the electric arc samples, but with lower slopes (0.31 to 0.44). Similar observations were found for acetylene flame with moderate to good correlations (r = 0.78 to 0.97) and low slopes (0.25 to 0.30). Correlations were moderate (r = 0.72) for diesel samples with slopes of 0.23 to 0.25. The effect of NaCl on BC was not apparent, but correlations improved for acetylene (from 0.78 to 0.97) and wood smoke (from 0.65 to 0.73) experiments. Paired comparisons show large variations between the 7-AE and PA measurements. Only 22 out of 125 samples (with 19 from the wood smoke and wood smoke + NaCl samples) have differences (y-x) which were less than or equal to ±2σ. Laboratory-generated test aerosol had an unusually high BC content. The AE quickly (~4 minutes) reached its tape advance set point and needed to be reinitialized before startup of the instrument. This yielded data for only 20% of the sampling period. However, data recovery

reached ~50% for the low BC wood-smoke samples. The differences between the 7-AE and the PA measurements may be reduced if better data recovery for the AE could be achieved. Therefore, the following section uses PA measurements as a benchmark for filter EC comparison.

6.3.2 Comparison between Filter EC and PA BC

In order to elucidate the variations between the PA BC and filter EC by thermal methods and by source type, a σ_{abs} of 5 m^2/g was used to convert PA b_{abs} (Mm^{-1}) to BC ($\mu g/m^3$). The comparison is made for thermal EC acquired from quartz-fiber filter samples following three protocols: 1) IMPROVE_A (Chow et al., 1993; 2001; 2004a) via TOR and TOT; 2) STN_TOT; and 3) the French two-step protocol (Cachier et al., 1989a; 1989b).

6.3.2a Comparison between IMPROVE_A EC by TOR/TOT and PA BC

As shown in Figure 6-21a, the comparison between IMPROVE_A_TOR EC and PA BC varies by source type. The best comparison is found for carbon black samples with high correlation (r = 0.99), near unit average ratio and ratio of averages, and all sample pairs within ±1σ. Even though only three samples were tested, the comparison between IMPROVE_A_TOR EC and PA BC raised confidence that both methods measure light absorbing carbon.

Since the PA σ_{abs} of 5 m^2/g is derived from limited diesel and kerosene tests and IMPROVE_A_TOR EC, comparable results for diesel samples are expected (Arnott et al., 2000) with an average ratio of y/x = 0.96 ± 0.15, slope varying from 0.85 to 0.93, and correlation of 0.90. Similar findings were determined for IMPROVE_A_TOT EC (Table 6-16 and Figure 6-21b). 97% of the 35 sample paired-comparison lie within ±1σ for both IMPROVE_A_TOR and IMPROVE_A_TOT. Better comparisons were found for the mixture of diesel and NaCl samples with 100% of the y-x distribution lying within ±1σ. The regression statistics show a closer to unit slope for TOR (1.00 to 1.05) than TOT (1.19 to 1.22) with good correlations (r = 0.95 to 0.97). This shows that the empirical σ_{abs} of 5 m^2/g is an appropriate estimate for diesel particles and the Cabot carbon black particles. The effect of salt on the OC/EC split by the IMPROVE_A protocol is not important for diesel samples.

For acetylene flame samples, moderate correlations (r = 0.88 to 0.89) were observed with slopes between 1.10 and 1.15, and high y/x ratios (1.5 ± 0.07). About 60 to 70% of the samples showed differences within ±1σ and 30 to 40% between ±1σ and ±2σ. Even though the ratio of y/x stayed within ±10% (1.54 to 1.57) for the acetylene + NaCl samples, the slope ranged from 1.20 to 1.58. The distribution of y-x also shows higher data variations with ~33 to 45% within ±1σ, and 55 to 67% between ±1σ and ±2σ.

A high correlation (r = 0.96) was found for the electric arc samples with average ratios and slopes ranging from 1.48 to 1.56. These correlations decreased to (r ~0.60) for the electric arc + NaCl samples. The average ratio was also reduced to 1.3 ± 0.49.

The pure wood smoke samples showed slopes ranging from 1.16 to 1.25 with reasonable correlations (r=0.7 to 0.9). Wood smoke + NaCl showed moderate correlation (r=0.7) with slopes ranging from 0.60 to 1.05. The wood smoke + NaCl samples show unit slopes and an average ratio within measurement uncertainty, with the IMPROVE_A_TOT EC measurements. The average ratio suggests that the IMPROVE_A_TOR/TOT EC was 1.8 to 2.7 times the PA BC for pure wood smoke, and from 1 to 1.2 times PA BC for wood smoke + NaCl. The wood smoke samples were not as reproducible as other sources. A more uniform set of wood pieces (e.g., cut 2×4 studs) may yield more reproducible results in future experiments.

Not much variability was found between IMPROVE_A_TOR and IMPROVE_A_TOT EC. It appears that the PA σ_{abs} of 5 m^2/g is appropriate for the diesel (and potentially the carbon black powder), but is too high for the other sources.

6.3.2b Comparison between STN_TOT EC and PA BC

As shown in Figure 6-22, the comparison of STN_TOT EC with PA BC for diesel and diesel + NaCl samples shows high correlations (r = 0.90 to 0.96) with near unit slopes (1.04 to 1.09) and average y/x ratios (0.99 to 1.01). High correlations (r = 0.97 to 0.99) were found for the acetylene and acetylene + NaCl samples, with slopes between 1.3 and 1.5 and high average y/x ratios (1.5 to 1.6). All (100%) acetylene samples showed y-x distribution > ±3σ. High correlations (r = 0.97 to 1) were also found for the electric arc and electric arc + NaCl samples, but all samples, except one, exceeded 3σ. The y/x ratios (1.4) and slopes (1.5) were high. The wood smoke and the wood smoke + NaCl samples have high correlations (r = 0.91 to 0.99), but have less than unity slopes (0.71 to 0.84), and average y/x ratios above unity (1.17) for wood smoke, and below unity (0.84) for wood smoke + NaCl.

6.3.2c Comparison between French two-step EC and PA BC

The effect of NaCl is apparent in all the samples following the French two-step protocol. While the pure source samples (except wood smoke) showed good correlations (r> 0.97) between PA and the French two-step protocol, Figure 6-23 shows a reduction in slope and correlation as NaCl is added to the samples. Section 6.2.1c showed that the French two-step protocol that operated in pure O_2 without a charring correction was highly influenced by the sample matrix. The majority of the pure source samples (18 out of 21) were within ±2σ. On the other hand, only five out of 19 source + NaCl (with four from the wood smoke + NaCl) samples were within ±2σ.

6.3.3 Comparison between PA and Filter b_{abs}

The PA b_{abs} was compared to b_{abs} measured using densitometry on a Teflon-membrane filter and the dependence on the source types is shown in Figure 6-24. Filter b_{abs} is consistently higher than PA b_{abs}. The influence of light scattering by the filter substrate and the particle deposits may artificially increase the b_{abs} measurement. The correlation varied by source, with the lowest (r = 0.52 to 0.75) found for wood-smoke samples, and the highest (r = 1.0) for carbon black samples. Average differences showed that 94% (118 out of 125) of the samples had uncertainties > ±3σ. Slopes were greater than unity for all sources. The slopes for the diesel and

diesel + NaCl samples varied from 1.3 to 1.8. The slopes for the acetylene samples varied from 1.0 to 2.5. The highest slope was found for the pure and mixed electric arc (2.3 to 2.7) and wood smoke (2.6 to 3.0) samples. The nebulized carbon black samples have a slope of 1.9.

Table 6-17 summarizes the results of intercomparisons in terms of their equivalence, comparability, and predictability. None of the methods were equivalent. The IMPROVE_A EC versus PA BC comparison was comparable for pure and mixed diesel samples using the assumed σ_{abs}. The STN_TOT EC was either comparable to or predictable of PA BC for all sources tested. Some of the IMPROVE_A EC versus PA BC comparisons showed correlations < 0.9, making the comparisons non-related. On the other hand, the STN_TOT comparisons showed correlations >0.90 making it comparable to PA BC with the assumed σ_{abs}. As noted in Section 6.3.2a, the PA σ_{abs} (1047) of 5 m^2/g appears to be high for sources other than diesel and carbon black.

6.3.4 σ_{abs} for each Source

The σ_{abs} (1047 nm) was calculated by comparing the PA b_{abs} (1047 nm) with the filter EC concentration, for each source (pure and the mixture) and is summarized in Table 6-18. For all of the experiments (pure and mixture samples) using diesel (~5.1 m^2/g), acetylene flame (~3.3 m^2/g), electric arc (~3.3 m^2/g), and carbon black (~5.0 m^2/g), the σ_{abs} are consistent across the different thermal protocols and are similar for each source, with the exception of the source + NaCl samples analyzed by the French two-step protocol. As discussed earlier, the French two-step protocol was the only protocol where the presence of NaCl influenced the amount of EC (Section 6.2.1c). The σ_{abs} for the wood-smoke samples were highly variable within (i.e., high standard deviation) and between the thermal protocols. This is probably due to the highly variable EC emissions during the course of the wood combustion, as well as the lower EC fractions, as compared to the other sources. In addition, the matrix effect due to presence of salts such as K^+ and Cl^- in wood smoke may also cause this discrepancy.

As seen above, the σ_{abs} is variable depending on the source analyzed. This would make it inaccurate to use one σ_{abs} value for all sources. It is also important to recognize that these are fresh emissions and, as aerosols are aged in the atmosphere, the σ_{abs} values could change.

6.3.5 Test of the Absorption Exponent (α) in the Angstrom Power Law ($\lambda^{-\alpha}$)

Both light and mass absorption efficiencies convert light absorption (i.e., the Angstrom Power Law [$\lambda^{-\alpha}$], assuming $\alpha = 1$) to BC and both are wavelength dependent (Park et al., 2006). The absorption by spherical BC particles is expected to change inversely with wavelength (λ^{-1}) (Bond, 2001). The presence of certain organic compounds enhances absorption at visible and UV wavelengths, thus changing the relationship between b_{abs} and λ (Kirchstetter et al., 2004). The spectral dependence of aerosol light absorption is described by the Angstrom Power Law ($\sigma_{abs} = K \lambda^{-\alpha}$), where '$\alpha$' is the Angstrom absorption exponent and 'K' is a constant. Since b_{abs} is proportional to σ_{abs}, the above relationship could also be applied with b_{abs} (i.e., $b_{abs} = K \lambda^{-\alpha}$). The value of α is derived using:

$$\ln (b_{abs}) = -\alpha \ln \lambda + \ln K \quad (6\text{-}1)$$

The multi-wavelength b_{abs} measurements by the 7-AE were used to estimate α for each source. The assumption that these efficiencies vary with inverse wavelength is tested for each source (pure and mixture) and calculated in Table 6-19. The correlations are high ($r > 0.96$) for all sources except the electric arc + NaCl samples ($r = 0.89$). The addition of NaCl did not alter many of the α values. Both diesel and diesel + NaCl, and acetylene and acetylene + NaCl samples have α between 0.79 and 0.86. The electric arc and electric arc + NaCl and wood smoke and wood smoke + NaCl samples both have α values greater than 1.15. The lower α values in diesel and acetylene samples also corresponded to higher (>0.5) EC/TC ratios, while the electric arc and wood smoke samples corresponded to lower ($\leq$ 0.5) EC/TC ratios. Samples with a higher fraction of BC are expected to have α closer to unity, while the presence of organics is expected to increase α greater than unity (Kirchstetter et al., 2004).

6.4 Summer IOP Carbon Measurements at Fresno

This section presents: 1) intercomparison of continuous and integrated b_{abs} and BC measurements at Fresno during the summer IOP, 2) evaluates the range of uncertainty involved in the σ_{abs} (m^2/g) estimates due to the different measurement and analysis methods, and 3) determines the Angstrom absorption exponent, α, for the aerosol at Fresno during the summer, 2005 period. Comparisons presented here include data between 08/01/05 and 09/30/05.

Continuous data were converted to hourly (for continuous instrument comparison) and 24-hr (for continuous vs. integrated filter comparison) averages. Default factors for each instrument were used to convert b_{abs} (Mm^{-1}) to BC ($\mu g/m^3$) concentrations or vice-versa. No default factor was available for the PSAP, and hence comparisons were made in Mm^{-1}. A combination of performance measures is considered in paired comparison.

6.4.1 Intercomparison of b_{abs} (Mm^{-1}) Measurements

As shown in Table 6-20, intercomparison of hourly b_{abs} measurements were made at similar wavelengths measured by the different instruments. To compare the instruments at a common wavelength, the b_{abs} measured by the 2-AE, 7-AE, PSAP and the PA were scaled to 670 nm, the wavelength of the MAAP. The scaling was done as follows:

$$b_{abs}(670\text{ nm}) = b_{abs}(\lambda)\left(\frac{670}{\lambda}\right)^{-\alpha} \quad (6\text{-}2)$$

where:

b_{abs} (670 nm) = b_{abs} scaled to 670 nm

b_{abs} (λ) = b_{abs} at a specific wavelength, λ,

α = Angstrom absorption exponent

The b_{abs} at 660 nm for the 7-AE and the PSAP measurements, at 532 nm for PA, and at 880 nm for 2-AE were scaled to 670 nm. To estimate the measurement uncertainty at 670 nm, it was assumed that the ratio of measurement uncertainty to b_{abs} would remain similar to that at 660 nm for the 7-AE and PSAP measurements. For the 2-AE and PA, the maximum of the ratios at the two wavelengths of the respective instruments was used.

For 7-AE and PSAP,

$$b_{abs}\,UNC\,(670\,nm) = b_{abs}\,(670\,nm)\left(\frac{b_{abs}\,UNC(660\,nm)}{b_{abs}\,(660\,nm)}\right) \qquad (6\text{-}3)$$

where:

b_{abs} (670 nm) = b_{abs} scaled to 670 nm

b_{abs} UNC(670 nm) = Uncertainty of b_{abs} (670 nm)

b_{abs} (660 nm) = b_{abs} at 660 nm

b_{abs} UNC(660 nm) = uncertainty of b_{abs} (660 nm) measurement

For 2-AE and PA,

$$b_{abs}\,UNC\,(670\,nm) = b_{abs}\,(670\,nm) * \max\left(\frac{b_{abs}\,UNC(\lambda_i)}{b_{abs}\,(\lambda_i)}\right)_{i=1to2} \qquad (6\text{-}4)$$

where: 'max', refers to the maximum ratio:

λ_i = 370 and 880 nm for 2-AE

λ_i = 532 and 1047 nm for PA

Intercomparisons of all continuous b_{abs} measurements (except the filter b_{abs} comparison against the PA) showed correlations (r) exceeding 0.90. All continuous instruments satisfied the criteria for predictability. Similar to those found by Watson and Chow (2002b), high correlations were found between the 2-AE and 7-AE, for both the 370 nm (r = 0.96) and 880 nm (r = 0.98). The average ratio showed that the 7-AE measured 7% higher b_{abs} compared to the 2-AE at both wavelengths. When weighted by uncertainties of each instrument, the EV slopes showed similar

values, ranging from 1.04 to 1.08. More than 98% of the paired differences were within ±2σ. As expected, similar results were found for BC comparisons. The 24-hr averaged filter b_{abs} was well correlated (r = 0.93) with the 2-AE and 7-AE b_{abs} and satisfied the criteria for predictability. Comparison of filter b_{abs} and 2-AE showed unit slopes within one standard error.

Measurements of b_{abs} from the 7-AE at 470, 520, and 660 nm were compared with PSAP (adj) b_{abs} at 467, 530, and 660 nm, MAAP at 670 nm, and PA at 532 nm. At comparable wavelengths, the 7-AE measured ~3.5 to 9 times higher b_{abs} than PSAP (adj), MAAP or PA. When scaled to 670 nm, the 2-AE and 7-AE b_{abs} were 8.5 to 9 times higher than the PSAP (adj), 3 to 3.5 times higher than the MAAP, and ~5 times higher than the PA. This could be due to possible enhancement of absorption caused by multiple scattering effects within the filter matrix and by aerosols on the quartz-fiber filter of the AE (Kirchstetter et al., 2004; Arnott et al., 2005a). This is also reflected in the average difference, where more than 75% of the values were greater than ±3σ. Using the PA (670 nm) as the benchmark (x-axis), the PSAP (raw) b_{abs} were approximately two times higher than the PA, while the PSAP (adj) b_{abs} (670 nm) was 0.6 ± 0.20 times that of PA b_{abs} (670 nm). It could be that the calibration proposed by Virkkula et al. (2005) and applied in this study to adjust PSAP b_{abs}, may overcorrect for the filter loading and light-scattering effects, causing the PSAP (adj) b_{abs} to be lower than the PA b_{abs}. The regression slope between PSAP (adj) and PA is close to unity (0.94 ± 0.03) so the bias is more like a constant offset. The MAAP b_{abs} (670 nm) is 1.5 (±0.35) times higher than PA b_{abs} (670 nm). As seen in Figure 6-25, the MAAP diverges from PA with increasing b_{abs}, suggesting a discrepancy in the current MAAP algorithm for higher BC concentrations.

Figure 6-26 compares the average b_{abs} by the different instruments during the summer IOP. Decreasing b_{abs} were found with increasing wavelengths. While the PSAP (adj), MAAP, and PA all showed b_{abs} less than 10 Mm^{-1}, the 2-AE and 7-AE ranged from 15 to 38 Mm^{-1} depending on wavelength. Both PSAP and MAAP account for the interferences due to filter- and aerosol-scattering effects, whereas the PA is not subject to filter matrix effects. Different correction algorithms have been proposed to correct the scattering effect in AE (Weingartner et al., 2003; Arnott et al., 2005a), that might minimize the differences. Although a straight line is used for the 2-AE and the PA to connect b_{abs} at the two wavelengths (Figure 6-26), it must be realized that b_{abs} varies non-linearly with wavelength, as seen in the 7-AE curve.

Similar to the AE, the filter b_{abs} was 2.8 to 9.4 times higher than the PSAP, MAAP, and PA with more than 80% of the paired difference being greater than ±3σ. This suggests that the filter b_{abs} may also be subject to absorption enhancement due multiple scattering effects by the embedded particles. Although they are based on different filter substrates (Teflon-membrane for the filter b_{abs}, while quartz-fiber filter for the AE), it appears that absorption enhancement might be present in both cases.

6.4.2 Intercomparison of BC Concentration (μg/m^3)

Table 6-21 shows average paired difference for BC to be less than ±0.73 μg/m^3 with correlations ranging from 0.73 to 0.99 among the 2-AE, 7-AE, MAAP, PA, and Sunset optical measurements. The 2-AE and 7-AE 880 nm BC measurements would be equivalent, if not for

the collocated precision of 0.15 $\mu g/m^3$ (or 15% of the average concentration). More than 98% of the paired differences were within ±2σ. Filter EC concentrations determined by the IMPROVE_A_TOR/TOT, STN_TOR, and French two-step protocols, showed average ratios ranging from 0.80 ± 0.19 to 1.11 ± 0.22 in comparison with the 880 nm 2-AE and 7-AE BC concentration. The STN_TOT EC was biased 35 to 50% lower than the 2-AE and 7-AE BC at 880 nm. The EV slope suggests that only IMPROVE_A_TOR/TOT EC and STN_TOR EC were within 15 to 20% of the 2-AE and 7-AE BC concentrations.

The BC concentration measured by the MAAP at 670 nm showed unit slope, within measurement uncertainty, in comparison with the 7-AE BC at 660 nm (1.02 ± 0.014) and 880 nm (1.01 ± 0.014). While 7-AE b_{abs} (670 nm) was approximately 3.5 times higher than MAAP (670 nm) their BC concentrations were comparable (average ratio = 1.05 ± 0.12). The conversion factor (σ_{abs} = 14,625/λ) used by the AE indirectly accounts, in part, for the absorption enhancement in the b_{abs} measurements, and thus reports concentrations which are similar to that reported by the MAAP. Using an algorithm similar to that of an AE, the MAAP-A BC (denoted in Table 6-21) was 10% (based on slope) to 20% (based on average ratio) higher than the MAAP BC at 670 nm. This implies that the correction for scattering effects made by the MAAP, effectively lowers the concentration by ~10 to 20%. The Sunset optical BC (660 nm) was ~50% of the MAAP BC concentration, even though it was highly correlated (r = 0.98). About 30%, 74% and 98% of the paired differences were within ±1σ, 1-2σ, and ±3σ, respectively, suggesting that while the data still followed a bell-shaped curve, they were widely distributed. Previous comparisons (Park et al., 2006) of AE and MAAP at the Fresno Supersite also showed similar slopes (OLS slopes ranging from 0.92 to 0.99) for summer months (July and August 2004). The IMPROVE_A_TOR EC showed the best agreement with MAAP BC (670 nm) concentration, with unit average ratio (0.994 ± 0.18) and slopes (by both EV and OLS) ranging from 1.05 ± 0.06 to 1.07 ± 0.16. All paired differences between IMPROVE_A_TOR EC and MAAP BC (100% of data) were within ±1σ, with a negligible average difference (0.013 ± 0.124 $\mu g/m^3$). STN_TOT EC was biased lower than MAAP BC by 40 to 50%.

Compared to the PA benchmark, the BC concentration measured by the 7-AE at 880 nm and the MAAP at 670 nm were, respectively, 1.7 (±0.39) and 1.6 (±0.43) times that of the PA at 532 nm and 2.4 (±0.39) and 2.3 (±0.41) times that of the PA at 1047 nm. The 40% difference in performance relative to the two PAs (for example, ratio of 7-AE to PAs were 1.7 and 2.4) is reflected by the difference between BC by PA (532 nm) and PA (1047 nm), which have a ratio of 1.4 ± 0.24. The EV slopes for AE and MAAP vs. PA ranged from 2.2 to 2.7. The Sunset optical BC was 0.9 (±0.28) times that of PA (532 nm) and 1.3 (±0.32) times BC by PA (1047 nm). The EV slope was 1.3 and 1.5 for comparisons against the PA at 532 nm and 1047 nm, respectively. At least 50% of the paired differences were within ±2σ for PA at 532 nm, while being between ±1σ and ±3σ in the comparisons with PA at 1047 nm, suggesting a wider distribution for PA at 1047 nm. Filter EC determined by IMPROVE_A_TOR/TOT, STN_TOR and French two-step protocols were all higher than the PA, with average ratios ranging between 1.4 ± 0.41 to 1.9 ± 0.53 against PA at 532 nm and from 2.0 ± 0.45 to 2.7 ± 0.54 against PA at 1047 nm. In contrast, STN_TOT EC was within 3 and 50% of the PA BC at 532 and 1047 nm, respectively.

The Sunset thermal EC concentration correlated reasonably (r = 0.80 to 0.88) with the BC from 2-AE and 7-AE at 880 nm, MAAP at 670 nm, PA at 532 and 1047 nm, and Sunset optical at 660 nm. Approximately one-third of the Sunset thermal EC data was near zero, while the optical BC concentrations ranged from 0.1 to 0.5 $\mu g/m^3$. This resulted in high average ratios and standard deviations. Based on the EV slope, the Sunset optical BC (660 nm), and PA (532 nm and 1047 nm) were 38 to 63% lower than Sunset thermal EC, while the MAAP (670 nm) was 11% higher. The 2-AE and 7-AE (880 nm) BC were 1 to 10% lower than the Sunset thermal EC, while PA (532 and 1047 nm) were 57 to 63% lower. The consistent underestimation by the PA BC measurements shows that the conversion factors (10 m^2/g at 532 nm and 5 m^2/g at 1047 nm) used in these calculations are not appropriate for the Fresno aerosol. Filter EC vs. Sunset thermal EC showed an EV slope ranging from 0.82 to 1.17 for IMPROVE_A, indicating that IMPROVE_A_TOR/TOT EC were within 20% of Sunset thermal EC, although 17 to 50% of the paired differences were distributed between ±1 and ±2σ. STN_TOR was within 10% of Sunset thermal EC with an EV slope of 0.90 ± 0.26. Among the filter EC versus Sunset EC comparisons, STN_TOT EC showed the least average difference (-0.004 ± 0.163) with 94% of the differences being within ±1σ. This is expected, since similar temperature and residence protocols were used for the two methods.

Comparability was found between AE BC (880 nm) and MAAP BC (670 nm). The AE BC (880 nm), MAAP BC (670 nm) and the Sunset thermal EC were within 20% of each other. The PA BC at 532 nm and 1047 nm were lower than the Sunset thermal EC, the MAAP, and the AE. Filter EC measurements by IMPROVE_A_TOR and STN_TOT were within 10 to 20% of the continuous BC measurements, except for comparison against PA (532 and 1047 nm) and the Sunset optical BC. The STN_TOT EC was more than 35% lower than BC by 2-AE, 7-AE, and MAAP, except for comparisons against the PA, in which case it was 3 to 50% higher.

6.4.3 Estimate of σ_{abs} During Summer

The σ_{abs}, (in m^2/g) is estimated by comparing b_{abs} (Mm^{-1}) with the BC concentration ($\mu g/m^3$). Since the PA BC concentrations were biased significantly lower than other instruments, only the AE, MAAP, Sunset thermal EC, and filter EC by IMPROVE_A_TOR/TOT, STN_TOR/TOT, and French two-step protocols were used for BC/EC concentrations. The b_{abs} measured by the PSAP at 467, 530 and 660 nm, the MAAP at 670 nm, and the PA at 532 nm and 1047 nm, were compared against the BC/EC concentrations to determine σ_{abs} for the Fresno aerosol. Table 6-22 presents a detailed statistical summary of σ_{abs}, estimated using EV or OLS slopes and by the average ratio of the variables. In this discussion, the EV slope of b_{abs} against BC concentration was used to represent σ_{abs}, rather than the average ratio, to avoid the influence of low BC concentrations on these ratios (as seen in the Sunset thermal EC comparisons). However, if the Sunset thermal EC were eliminated from the average ratios, then the σ_{abs} estimated using the average ratio was within 7% of EV σ_{abs} for the 2-AE and 7-AE, 13% for the PSAP, 2% for the MAAP and 24 to 59% for the PA at 532 and 1047 nm

Table 6-22 shows that the σ_{abs} for MAAP (670 nm) ranged from 5.7 to 11.7 m^2/g with higher σ_{abs} for the STN_TOT protocol (11.7 m^2/g, respectively). The default value of 6.6 m^2/g for MAAP is closest to that determined using the 7-AE BC (6.4 m^2/g). Low σ_{abs} were found for PA (532 nm),

ranging from 2.9 to 7.3 m^2/g with an average of 4.5 m^2/g, and PA (1047 nm) ranging from 1.2 to 3.4 m^2/g with an average of 1.9 m^2/g. These σ_{abs} values are 55 to 62% lower than the default factors of 10 m^2/g at 532 nm and 5 m^2/g at 1047 nm for PA, which were derived from diesel emissions (Arnott et al., 2005b). The deviation from the default values suggests that the aerosol at Fresno was influenced by other sources, in addition to fresh diesel emissions. Using PA b_{abs} scaled to 670 nm, σ_{abs} of 2.2 to 5.0 m^2/g were derived. Similarly, the PSAP (adj) b_{abs} (670 nm) yielded σ_{abs} ranging from 2.4 to 5.2 m^2/g. The σ_{abs} of PSAP (adj) ranged from 3.9 to 8.5 m^2/g at 467 nm, 3.1 to 6.8 at 530 nm, and 2.4 to 5.4 m^2/g at 660 nm.

The PA vs. IMPROVE_TOR EC comparisons by Park et al. (2006) reported σ_{abs} (1047 nm) of 2.3 m^2/g, which is similar to the 1.9 m^2/g found in this study. Bond and Bergstrom (2006) suggested a σ_{abs} (550 nm) of 7.5 ± 1.2 m^2/g for uncoated (fresh) particles, based on an average of 17 studies. Sheridan et al. (2005) measured a σ_{abs} of 7.5 ± 1.2 m^2/g for pure kerosene soot particles. Based on the results presented here, it appears that the σ_{abs} (530 to 532 nm) ranges from 2.9 to 7.3 m^2/g, with an average of 4.4 m^2/g, during the summer season at the Fresno Supersite. This value is 41% lower than the 7.5 m^2/g (at 550 nm) suggested for fresh particles. This suggests that the particles at Fresno are relatively mixed and aged, with a particle structure different from fresh emissions.

6.4.4 Diurnal Variation of OC/BC/EC Concentrations

Figure 6-27 shows the average diurnal variation of OC, BC and EC concentrations during the summer IOP. Also shown are the $PM_{2.5}$ mass concentrations measured by the MetOne (Grants Pass, OR) BAM and the relative PAH concentrations measured by the EcoChem PAS-2000 instrument. The BC (and thermal EC) concentrations show a distinct diurnal pattern during the summer IOP. The BC concentration peaked between 0500 and 0900 hours PST, coinciding with morning rush hour. As the day progressed and the surface layer mixed with layers aloft, the BC (and thermal EC) concentration decreased and reached a minimum around 1600 to 1700 hours PST. The BC concentration rose again with a slight peak around 1900 to 2100 hours PST, coinciding with evening traffic. The formation of a shallow surface layer trapped the pollutants causing the concentrations to remain at that level throughout the night, until coupling with layers aloft occurred after sunrise on the following day. The OC concentration showed a pattern that was different from BC. The examination of each month separately (not shown) showed that, during August, OC increased continuously until 1100 hours PST and then decreased. During September 2005, the trend was similar, but not as distinct. $PM_{2.5}$ mass showed a distinct diurnal pattern, similar to BC, with higher mass concentrations during early morning hours. The PAH signal indicates a morning peak coinciding with the early morning traffic.

The EC/TC or EC/$PM_{2.5}$ mass ratio showed diurnal patterns similar to the absolute EC concentrations (Figure 6-28). Although the absolute OC concentrations decreased in August 2005 and stayed approximately constant in September 2005 (not shown), the fraction of OC in $PM_{2.5}$ mass consistently peaked between 1300 to 2000 hours PST. Concurrently, the EC/OC ratio decreased. The EC/OC ratio peak during morning traffic hours is indicative of the contribution of primary BC emissions from vehicle exhaust. During the afternoon, the EC/OC ratio decreased, with a concomitant increase in the OC/mass fraction (Figure 6-28). An increase

in the OC/mass ratio indicates an addition of OC in $PM_{2.5}$ mass compared to other species. This is consistent with contributions from secondary organic aerosols (SOA) that are produced through photochemical reactions (Watson et al., 2006).

6.4.5 Estimate of α During Summer IOP

The value of α was estimated using the procedure explained in Section 6.3.5. The presence of b_{abs} measurements by 7-AE and PSAP as a function of different λ allows the determination of 'α' for the Fresno Supersite during the summer IOP. The validity of α estimated from 2-AE and PA measurements may be limited due to the presence of only two wavelengths.

Table 6-23 and Figure 6-29 summarize the average value of α for each hour of the day during the summer IOP. While the α values determined from each instrument showed a similar trend without much diurnal variation, the absolute value varied from 0.88 to 1.71. The α ranged from 0.88 to 1.02 for 2-AE and 7-AE, and from 1.26 to 1.51 for PSAP and 1.33 to 1.71 for PA.

The average α were 0.94 to 0.95 for 2-AE and 7-AE, 1.38 ± 0.086 for PSAP (adj), and 1.47 ± 0.101 for PA during the summer IOP. These values are consistent with the findings of Park et al. (2006), who estimated α to be in the range of 1 to 2. As noted earlier, the AE does not correct for absorption enhancement due to multiple scattering effects. The lower value of α estimated by the 2-AE and 7-AE is possibly caused by different enhancements at the various wavelengths (see Section 6.7). Figure 6-29 shows a more distinct diurnal pattern for PA, with a dip from the average value around 0700 to 0800 hours PST and 2000 to 2100 hours PST, coinciding with vehicular traffic (similar to the trend in BC concentration, as shown in Figure 6-27) and an increase in the afternoon hours (1300 to 1600 hours PST) coinciding with peak photochemical activity and SOA formation. A value of 'α' close to 1.0 indicates weak spectral dependence; higher values indicate stronger spectral dependence. This is consistent with the findings of Kirchstetter et al. (2004), where the presence of organic compounds increased the spectral dependence, particularly at wavelengths shorter than 600 nm.

6.5 Winter IOP measurements at Fresno

This section presents calculations conducted for the winter IOP for 12/1/03 through 12/31/03.

6.5.1 Intercomparison of b_{abs} (Mm^{-1})

Table 6-24 summarizes the comparison statistics of b_{abs} (Mm^{-1}) measurements during the winter IOP. All b_{abs} measurements were predictable of each other ($r > 0.90$). The 2-AE and 7-AE showed high correlations ($r = 0.99$) at both the 370 nm and 880 nm wavelengths. The EV slope suggests that the 7-AE was 10% and 4% lower than 2-AE at 370 nm and 880 nm, respectively. More than 90% of the paired differences were within ±2σ. On the basis of the average ratio, the filter b_{abs} determined by densitometry on Teflon-membrane filters, was 11% to 16% higher than 2-AE and 7-AE b_{abs} at 880 nm. However, the EV slope was 0.6 ± 0.23 at both wavelengths, with large intercepts (12 Mm^{-1}), suggesting that AE may overestimate b_{abs} at high BC concentrations

(Figure 6-30), possibly due to absorption enhancement by particle light scattering as reported by previous studies (Kirchstetter et al., 2004; Arnott et al., 2005a).

When scaled to 670 nm, the 2-AE and 7-AE b_{abs} were 2.5 to 3 times higher than the MAAP. The filter b_{abs} was approximately 20% higher than the MAAP b_{abs} at 670 nm (EV slope of 1.19 ± 0.45) with an intercept of ~12 Mm^{-1}, in contrast to the summer period, when it showed an EV slope of 2.3 ± 0.27. The 7-AE b_{abs} at 950 nm was approximately 4 times higher than PA b_{abs} at 1047 nm during winter, while it was ~8 times higher during summer.

6.5.2 Intercomparison of BC Concentration (μg/m^3)

Table 6-25 compares the various BC concentration (μg/m^3) measurements. Although the R&P 5400 carbon monitor was in operation during the winter IOP, it is not included in the analysis here due to the following reasons: 1) frequent instrument failure resulted in low data capture (43% during 2003); 2) previous comparisons have shown that the R&P 5400 EC measurements were not comparable to, or predictable of, other continuous BC and integrated EC measurements (Watson and Chow, 2002b; Park et al., 2006); and 3) this instrument experienced malfunctions during the summer IOP.

The 2-AE and 7-AE BC measurements at 880 nm showed high correlations (r = 0.99) with OLS slopes of unity within one standard error. Similar to the summer IOP, the measurements would have been equivalent except for the collocated precision (0.178 μg/m^3, or 10% of mean concentration) being greater than 5% of the mean concentration. About 92% of the paired differences were within ±1σ, suggesting a narrow distribution.

Filter EC concentrations determined by IMPROVE_A_TOR were 26% (based on EV slope) to 55% (based on average ratio) higher than 2-AE and 7-AE BC at 880 nm. Among the filter EC versus continuous BC comparisons, STN_TOR showed correlations greater than 0.9 in all cases. EC by STN_TOR protocol was within 3% (based on EV slope and average ratio) to 12% (based on OLS slope) of the 2-AE and 7-AE BC, with 100% of the differences within ±1σ. Filter EC concentrations determined by the French two-step and STN_TOT protocols were biased 30 to 45% lower than the 2-AE and 7-AE BC at 880 nm, based on the average ratios.

The MAAP BC (670 nm) concentrations were higher than the 2-AE and 7-AE at 880 nm, PA at 1047 nm, and the Sunset thermal EC and optical BC concentrations. The BC concentrations measured by the 2-AE and 7-AE at 880 nm were 21 to 26% lower than those measured by the MAAP (670 nm). The PA (1047 nm) BC was 45% lower than the MAAP (670) BC. Similarly, the Sunset thermal EC was 40% lower than the MAAP BC. IMPROVE_A_TOR EC was 16% higher based on the average ratio. While the summer intensive comparisons showed that the MAAP and AE agreed closely, the winter intensive measurements showed that the MAAP BC was higher (based on average ratio, and EV and OLS regression slopes). This is consistent with the findings of Park et al. (2006), which also showed that the MAAP (670 nm) BC concentration was 10 to 20% higher than 7-AE (660 nm) from December 2003 through February 2004, while agreeing within 3% from May through August 2004. It appears that the loading correction by MAAP is inaccurate at high BC concentrations during winter and may affect the agreement

between the AE and the MAAP. This could imply that the σ_{abs} used by the MAAP (6.6 m^2/g), while being appropriate for the summer period, is underestimated for the winter period. Filter EC concentration determined by the French two-step and STN_TOT protocols were 42 to 57% lower than the MAAP BC at 670 nm, based on the average ratios.

Using PA (1047 nm) BC as a benchmark, the 2-AE (880 nm) and 7-AE (880 nm) BC concentrations were 35 to 45% higher. The EV slopes were 1.4 when compared to AE and 1.7 when compared to MAAP. At least 50% of the paired differences were between ±1σ and ±3σ, indicating a wide distribution. Sunset thermal EC was within 16% of PA (1047 nm) BC. Filter EC determined by IMPROVE_A_TOR, IMPROVE_A_TOT and STN_TOR were 1.4 ± 0.15 to 2.1 ± 0.78 times the PA (1047 nm) BC. Filter EC by STN_TOT was within 19% (based on EV slope) of the PA BC.

The Sunset thermal EC concentration showed a high correlation (r = 0.97 to 0.98) with the 2-AE and 7-AE BC at 880 nm, the MAAP BC at 670 nm, the PA BC at 1047 nm and the Sunset optical BC at 660 nm. Based on the EV slope, the 2-AE and 7-AE BC were within 21 to 25% of the Sunset thermal EC. The PA BC was biased 9% lower than the Sunset thermal EC. While the MAAP BC showed unit slope (within one standard error) against the Sunset thermal EC during summer IOP, it was biased 57% higher during the winter IOP. At least 87% of the paired differences were within ±2σ for comparisons of 2-AE, 7-AE and the PA against Sunset thermal EC. The comparison of MAAP BC versus Sunset thermal EC showed 60% of the paired differences within ±2σ and 36% between ±2σ and ±3σ. This suggests that the distribution of paired differences of MAAP BC versus Sunset thermal EC was wider than that of AE and PA versus the Sunset thermal EC. The IMPROVE_A_TOR EC was twice that Sunset thermal EC, while the IMPROVE_A_TOT and STN_TOR showed EV regression slopes of 1.37 ± 0.4 against the Sunset thermal EC.

Winter IOP measurements show that the 2-AE and 7-AE BC (880 nm) were within 27% of the filter EC by IMPROVE_A_TOR and within 3% by STN_TOR protocol. The loading correction by MAAP is inaccurate at high BC concentrations during the winter season affecting the agreement of the MAAP with the AE BC and thus, the σ_{abs} used by the MAAP is not appropriate for the winter-time aerosol at Fresno. Filter EC measurements by IMPROVE_A_TOR and STN_TOR were within ~25% of the AE and MAAP BC measurements. EC estimates using STN_TOT protocol were more than 30% lower than BC by the 2-AE, 7-AE and the MAAP.

6.5.3 Estimate of σ_{abs} during the Winter IOP

The σ_{abs} was estimated by EV slope for the winter period as shown in Table 6-26. Comparison of 2-AE and 7-AE b_{abs} at 880 nm against filter EC concentrations, suggested a σ_{abs} ranging from 8.5 ± 1.23 to 21.9 ± 5.7 m^2/g, with an average of 14.4 m^2/g. This is within 13% of the default value of 16.6 m^2/g used by the 2-AE and 7-AE.

The σ_{abs} for the MAAP at 670 nm ranged from 3.9 ± 0.68 to 10.8 ± 3.1 m^2/g, with an average of 7.7 m^2/g (~17% higher than the default value of 6.6 m^2/g). The average σ_{abs} (1047 nm) for the

PA was 3.5 m^2/g (~30% lower than the default value of 5 m^2/g) and ranged from 1.6 ± 0.31 to 5.8 ± 1.41 m^2/g.

6.5.4 Estimate of α during the Winter IOP

The 2-AE and 7-AE were the only instruments with multi-wavelength measurements that were in operation during the winter IOP. The average α, as estimated using the 2-AE and 7-AE measurements (Table 6-27), were 1.32 ± 0.125 and 1.2 ± 0.108, respectively. These are much higher than the corresponding α values estimated for the summer IOP (0.93 to 0.95), suggesting a difference in aerosol composition between winter and summer seasons.

The diurnal variation in α is more pronounced during the winter season (Figure 6-31) than that observed in summer (Figure 6-29). The α decreased between 8 and 10 am PST coinciding with the morning traffic, suggesting the influence of fresh BC emissions from mobile sources. The apparent rise during the evening period, which persisted through the night to evolve the next morning, suggests the influence of RWC. This phenomenon is similar to that found by Watson and Chow (2002a). An average value of α greater than unity confirms that the wintertime aerosol at Fresno is, in general, mixed and is probably influenced to a greater extent by RWC.

6.6 Summary of Summer and Winter IOP Comparisons

Table 6-28 summarizes the intercomparisons for the summer and winter IOPs. The 2-AE and 7-AE overestimated b_{abs} (670 nm) by 150 to 200% during both summer and winter compared to the MAAP, and is not suitable for b_{abs} measurements. However, in terms of BC concentrations, the AE BC was within 21% of the MAAP BC, the Sunset thermal EC, and the IMPROVE_A_TOR/TOT EC concentrations during summer. Similar trends were observed in winter, except for comparisons with MAAP, where the AE was within 26%. This could be due to the overestimation of BC by the MAAP during the winter IOP, as discussed earlier. The MAAP BC agreed within 7% of the AE, the Sunset thermal EC, and the IMPROVE_A_TOR EC during the summer IOP, while being within 26% during winter IOP. It appears that BC measurements by the AE were not affected between summer and winter periods, indicating that the σ_{abs} used by the AE (14625/λ) was valid during both seasons. The σ_{abs} (670 nm) for the MAAP (6.6 m^2/g) while being consistent with the calculated BC for summer, was not appropriate for the winter period, suggesting that the MAAP needs to use a different σ_{abs} for each season. The results presented here suggest a σ_{abs} (670 nm) of 7.7 m^2/g for the MAAP during the winter season. The PA BC differed by more than 17% in all cases. The calculations suggest an average σ_{abs} of 1.9 m^2/g and 3.5 m^2/g for PA at 1047 nm for the Fresno aerosol during summer and winter, respectively. The IMPROVE_A_TOR was within 15% of AE, MAAP BC, and Sunset thermal EC concentrations during summer. The IMPROVE_A_TOT was within 25% during summer, and within 35% during winter. The STN_TOT differed by more than 35% during both seasons. It appears that the difference in composition between summer and winter, affected the response of the MAAP, the PA, and the thermal/optical EC methods. The AE appeared to be unaffected between seasons.

6.7 Optical Model for b_{abs} and EC Measurements with the Thermal/Optical Method

EC or BC has a chemical structure loosely related to graphite and is emitted directly into the atmosphere during incomplete combustion (Bond and Bergstrom, 2006). EC is believed to be the dominant contributor to atmospheric light absorption in the visible region (e.g., Horvath, 1993b; Watson, 2002), although EC is nearly always mixed with organic matter (OM) and possibly other particle constituents that may change its optical properties. Pure crystalline forms of EC, such as graphite and diamond, are not commonly found in ambient aerosols. As shown in the experiments described above, none of the other source materials showed thermal or optical properties similar to the pure graphite powder.

Previous studies and this work collectively indicate that results from different methods (e.g., the IMPROVE_A, STN, and French two-step protocols) differ, sometimes, by more than an order of magnitude (Watson et al., 2005). This section examines the fundamentals of thermal/optical carbon analysis particularly the charring correction, introduce the recent improvements in both theory and instrumentation, and suggest refined approaches for quantifying EC and b_{abs}.

6.7.1 Filter-Based b_{abs} Measurement

Both the AE and PSAP instruments continuously collect aerosol particles on a filter and monitor the attenuation of light transmitted through the filter (up to 1-min time resolution). Lindberg et al. (1999) suggest that the attenuation is linearly related to particle light absorption under most conditions with a diffuse illumination. Therefore, the apparent light absorption coefficient [$b_{abs(ATN)}$] of the air that originally contains the particles can be determined, assuming that b_{abs} is conserved during the sampling and deposition process (e.g., Hansen et al., 1984; Bond et al., 1999; Hansen et al., 1999):

$$b_{abs(ATN)} = \frac{A}{V}\tau_{L,ATN} \tag{6-5}$$

$$\tau_{L,ATN} = -\ln(\frac{T_F}{T_F^{(0)}}) \tag{6-6}$$

where T_F and $T_F^{(0)}$ represent the transmitted light intensity for particle-loaded and blank filters, respectively, A is the filter cross section, and V is the volume of air drawn through that cross section. $\tau_{L,\,ATN}$ is the apparent optical depth of aerosol layer on the filter; the subscript "*ATN*" indicates that it is determined from light attenuation. The AE and PSAP differ in incident light wavelength and filter material, i.e., quartz-fiber vs. glass-fiber, respectively, both of which are optically diffusive. In addition, the AE uses a filter tape (instead of individual filters used by PSAP) that automatically advances to a new/blank spot once the original spot exceeds a pre-set bustion</IDText><MDL Remulation of particles. In this manner, the AE may perform months of ambient monitoring without operator attention.

Other investigations (e.g., Bond et al., 1999; Petzold et al., 2003; Arnott et al., 2005a) indicate three potential artifacts in the filter-based methods. First, the highly-diffusive filter material substantially enhances the absorption by particles due to strong multiple scattering that does not occur in the air. This leads to an overestimation of "true" light absorption. Second, the multiple-scattering effect is gradually shadowed by increasing particle loading and absorption on the filter. As a result, the ratio of apparent and true light absorption coefficient is neither unity nor a constant. Moreover, part of the incident radiation is lost via reflection from the filter rather than absorption within the filter, but Eqs. 6-5 and 6-6 based only on light transmission tends to misattribute all the radiation loss to absorption. It has been found that the AE and PSAP respond to "white" aerosol that has a single scattering albedo (ω) of nearly one (i.e., no absorption).

Empirical corrections to multiple scattering and shadowing effects were formulated by Arnott et al. (2005a) and Bond et al. (1999) for the AE and PSAP, respectively. Their corrections, however, are situation specific; i.e., they require additional information of the aerosol ω. They are limited by the fact that only light transmitted through the filter is measured. Petzold and Schönlinner (2004) and Petzold et al. (2005) demonstrate that aerosol absorption and ω can be retrieved simultaneously by detecting both reflected and transmitted light, so they developed the MAAP. Petzold and Schönlinner (2004) demonstrate that the fraction of light reflected from and transmitted through a filter sample are different for diffuse or collimated illumination and should be treated differently.

As shown in Figure 6-32, it is assumed that the particle loaded quartz-fiber filter is treated as a two-layer system: an uppermost "aerosol-filter" layer (noted by "*L*") that occupies 10-15% of the filter thickness and the remaining particle-free (blank) filter matrix (noted by "*M*"). The whole filter is referred to as "*F*". The light transmitted through the aerosol-filter layer, $T_{L,}$ is divided into two parts, the penetration (P_L) and forward scattered (F_L) light. Light back scattered by the two layers is noted as R_{L} and R_{M}, respectively. P_L is related to optical properties of the aerosol-filter layer by:

$$\sigma_{L,a} = \sigma_{a,p}\,;\ \sigma_{L,s} = \sigma_{s,p} + \sigma_{s,f} \tag{6-7}$$

$$-\ln(P_L) = \tau_L = \tau_{L,a} + \tau_{L,s} = \sigma_{L,a} \times L + \sigma_{L,s} \times L \tag{6-8}$$

$$SSA_L = \frac{\tau_{L,s}}{\tau_{L,a} + \tau_{L,s}} \tag{6-9}$$

$$b_{abs} = \frac{A}{V}\tau_{L,a} \tag{6-10}$$

where $\sigma_{a,p,}$ $\sigma_{s,p}$, and $\sigma_{s,f}$ are absorption coefficient of aerosol, scattering coefficient of aerosol, and scattering coefficient of filter fibers within the layer, respectively (fibers only scatter light). SSA_L denotes the ω of the layer. Eq. (6-10) calculates the average absorption coefficient of the

sampled air. As the incident radiation strikes the aerosol-filter layer first, it should be treated as collimated illumination. Diffuse illumination is assumed for light propagating inside the filter. Petzold and Schönlinner (2004) use the radiative transfer scheme developed by Hänel (1987):

$$\frac{T_F}{T_F^{(0)}} = \frac{P_L + F_L}{1 - R_L^* R_M} \tag{6-11}$$

$$\frac{R_F}{R_F^{(0)}} = T_L^* \frac{P_L + F_L}{1 - R_L^* R_M} + \frac{R_L}{R_M} \tag{6-12}$$

to relate P_L to measurable quantities, i.e., the transmitted (T_F, $T_F^{(0)}$) and reflected (R_F, $R_F^{(0)}$) light intensities. The superscript (*) in Eqs. (6-11) and (6-12) indicates the values derived from diffuse illumination. Details on calculations of F_L, T_L^*, R_L, R_L^*, and R_M from P_L and SSA_L can be found in Petzold and Schönlinner (2004). With measured $T_F / T_F^{(0)}$ and $R_F / R_F^{(0)}$, Eqs. (6-10) and (6-11) can be solved numerically to obtain P_L and SSA_L and subsequently $\tau_{L,a}$ and b_{abs} following Eqs. (6-8) – (6-10).

Although Eqs. (6-11) and (6-12) are much more complex than Eq. (6-5) and (6-6), they still do not provide an exact description of radiative transfer within the filter. F_L and R_L are calculated for collimated illumination. However, according to diffusion theory (Wang et al., 1998a), the layer thickness within which collimated illumination can be applied depends on the photon mean free path, which decreases with increasing particle loading. It is oversimplified to apply the collimated F_L and R_L to an aerosol-filter layer of any loading. Moreover, Petzold and Schönlinner (2004) assume that $R_M = R_M^*$ and $P_M = P_M^*$ to simplify calculation. They also assume a scattering phase function (i.e., angular distribution of scattered light) following the Henyen-Greenstein approximation with an anisotropy of 0.75. Considering all these approximations and instrumental noise, the uncertainty in b_{abs} measurement by MAAP is estimated to be ~12% (Petzold and Schönlinner, 2004).

6.7.2 Thermal/Optical Method for EC

Thermal methods separate EC from OM according to their different thermal resistances. In an oxidative environment, such as the 100% O_2 imposed by Novakov et al. (1982) and Cachier et al. (1989a), EC is expected to evolve through oxidation at a higher temperature than OM, but the split is method-dependent. It is also demonstrated in Section 6.2.1 that the dominant EC fraction varies with source of EC; e.g., EC2 in diesel soot versus EC1 in wood smoke (see also Kirchstetter et al., 2001; Nguyen et al., 2001). Heating the sample in an inert atmosphere slows EC evolution for temperatures <~700 °C, and this approach was adopted by the IMPROVE and thermal protocol.

A fraction of OM pyrolyzes to form dark and non-volatile char at temperatures >~275 °C in an inert atmosphere. The fraction that chars is highly variable, depending on the OM composition, as well as on temperature steps and ramping rate. Extended heating at lower initial temperatures

assists the volatilization of OM, so there is less available to char at higher temperatures (Chow et al., 2004a). Flash heating (rapid temperature rise) is suggested to minimize charring (Lavanchy et al., 1999). To avoid OP being measured as EC, the filter darkening due to charring is monitored. This is achieved by introducing a laser (collimated) light source and detecting the light reflected from (Chow et al., 1993) or transmitted through (Birch and Cary, 1996a) the filter during thermal analysis. As pyrolysis is completed, the analysis environment turns oxidative, OP and EC start to evolve, and filter darkness is reduced. EC is defined as the residue carbon after the reflected or transmitted signal returns to its initial value, assuming that by then OP is completely removed from the filter.

Even with an identical temperature protocol, charring corrections based on reflectance and transmittance often produce different results (Chen et al., 2004; Chow et al., 2004a). One of the major conclusions of the source characterization experiments conducted for this study is that the STN_TOT and the French two-step protocols determined EC/TC ratios similar to the IMPROVE_A protocol for all sources except wood smoke. The STN_TOT and French two-step protocols returned lower EC (46% and 86% respectively) for wood smoke compared to the IMPROVE_A protocol. For ambient samples, the STN_TOT and the French two-step protocols also yielded lower EC/TC ratios compared to the IMPROVE_A protocol. The trend was especially clear during the winter IOP. This is consistent with a strong wood-smoke influence at Fresno during winter.

Chen et al. (2004) attributes the difference between the reflectance and transmittance charring corrections to nonequivalent light absorption efficiencies between OP and EC and their different distributions within the filter. Unlike EC that exists only on the top 10-15% of filter thickness, OP forms throughout the filter, consistent with at least part of OP deriving from charring of semi-volatile organic vapors adsorbed within the quartz fibers. For the charring correction, intensity of reflected light mostly depends on the darkness of filter surface, while intensity of transmitted light is sensitive to light-absorbing material at any depth. The calculations in Chen et al. (2004) are confirmed by microscopic examinations of filter cross-sections at various stages of thermal analysis (Chow et al., 2004a).

The configuration of thermal/optical method with transmittance charring correction resembles those of the AE and the PSAP; i.e., an incident collimated light source at the normal angle and 180° from a photo-detector beneath the filter (Figure 6-33). The apparent light absorption coefficient can be determined prior to and during thermal analysis using Eqs. (6-5) and (6-6) with the laser intensity detected at the end of analysis (equivalent to a blank filter) used as $T_F^{(0)}$. $\tau_{L,ATN}$ is routinely reported by some commercial carbon analyzers as an indicator for EC (e.g., the Sunset Laboratory instrument reports this as "optical EC"). The relation between $\tau_{L,ATN}$ and absorption caused by OP and EC, however, is not just influenced by multiple-scattering and shadowing effects; it also depends on the distribution of OP and EC within the filter (Chen et al., 2004).

The DRI Model 2001 thermal/optical carbon analyzer (Atmoslytic, Inc., Calabasas, CA) allows reflectance and transmittance charring correction to be carried out simultaneously in one instrument. To do so, reflected and transmitted light is collected and delivered to a detector by

two quartz light pipes normal to and ~3 to 5 mm from the filter (Chow et al., 2001; 2004a). This configuration is similar to MAAP but with the following differences:

- Photodetectors are placed further away from the filter in MAAP without light pipes in between. Only light scattered at specific angles can be detected. The Model 2001 detects all light collected by the light pipes (3 mm diameter) that subtend a large angular range.
- Multiple photodetectors at reflection angles of 130° and 165° are used in MAAP to quantify diffuse reflectance. Model 2001 has one detector connected to the reflection light pipe. Both MAAP and Model 2001 have only one detector at the transmission side (front hemisphere) of the filter.

It is shown by Petzold and Schönlinner (2004) that both reflected and transmitted light have a diffuse component. In the back hemisphere, the angular distribution of reflected light depends on the aerosol *SSA* (or ω). Due to the different configurations, the Model 2001 and MAAP likely detect different amounts of reflected radiation and their ratios could vary with aerosol type and loading.

In principle, monitoring reflected and transmitted radiation simultaneously allows more accurate quantification of aerosol light absorption by the Model 2001, although the radiative transfer scheme in Eqs. 6-7 to 6-12 needs to be refined to compensate for the different detector geometries between Model 2001 and MAAP and the distinct OP and EC distributions within a filter. Besides the light absorption measurement, such an effort could improve the charring correction if contributions from OP and EC to light absorption can be distinguished.

6.7.3 Monte Carlo Radiative Transfer Simulation

Solving radiative transfer equations analytically for optically-diffusive medium is challenging, especially when the system contains finite geometry (e.g., sizes, detection angles, etc.). One alternative is the Monte Carlo simulation, in which propagation of individual photons within the medium is simulated in a stochastic manner. This method describes local rules of photon propagation that are expressed, in the simplest case, as probability distributions describing the step size of photon movement between sites of photon-medium interaction, and the angles of deflection in a photon's trajectory when a scattering event occurs (Wang et al., 1995; Chen and Bai, 1998). Monte Carlo methods can be applied to problems with very complex geometry and achieve very high accuracy. However, since the method is statistical in nature, it relies on calculating the propagation of a large number of photons and requires a large amount of computation time.

The Monte Carlo code developed by Wang and Jacques (1993; 1995), referred to as MCML, deals with radiative transfer in multi-layer turbid medium where each layer is characterized by a unique absorption ($\tau_{L,a}$) and scattering ($\tau_{L,s}$) optical depth and scattering phase function. The default illumination is a collimated beam with infinitesimal diameter. After a photon enters the medium, each step between photon positions equals $-\ln(\xi)L/(\tau_{L,a} + \tau_{L,s})$ where ξ is a random number between 0 – 1 and L represents the layer-characteristic thickness. The weight of the photon is decreased from an initial value (1 for the first layer) as it moves through the layer, and

drops "$(SSA_L)^n$-fold" after n steps. When the photon strikes the air-medium interfaces, a fraction of the photon weight escapes as reflectance or transmittance, and the remaining weight is internally reflected and continues to propagate. Eventually, the photon weight drops below a threshold level and the simulation for that photon is terminated. Many photon trajectories (10^4 to 10^6) are typically calculated to yield a statistical description of photon distribution in the medium.

By tracking photon propagation in three dimensions, MCML is able to record spatial absorption, angular-resolved reflection and transmission at any resolution specified by the user. However, total absorption, reflection, and transmission are independent of the choice of resolution. They should not depend on the incident beam diameter, either, if the medium extends horizontally to infinity. Although L, $\sigma_{L,a}$ and $\sigma_{L,s}$ (see Eq. [6-7]) are the actual model inputs, only their products, $\tau_{L,a}$ and $\tau_{L,s}$, influence the results. The accuracy of the MCML for different SSA_L has been examined against diffusion theory (Wang et al., 1998b; 1998c). Excellent agreement was achieved by allowing for a sufficient number of photons. The uncertainty of various output parameters can be estimated from the standard deviations of results from replicate runs with the same number of photons.

Figure 6-34 compares the reflectance and transmittance of a two layer aerosol-filter system, calculated by the Kubelka-Munk (Kubelka and Munk, 1931; McNeil and French, 2001), MAAP, and MCML algorithms. The top and bottom layers are 0.004 cm and 0.04 cm in thickness, respectively, chosen to model a typical quartz-fiber filter (Pallflex 7202, Pall Laboratory, Ann Arbor, MI; filter average thickness of ~0.044 cm). Both layers have a uniform σ_s of 2000 cm^{-1} for quartz fibers. σ_a varies from 0 to 500 cm^{-1} for the top layer, but remains zero for the second layer. This simulates a range of absorption optical depths $\tau_{L,a}$ from 0 to 2. Kubelka-Munk (K-M) theory assumes totally diffuse (Lambertian) illumination compared to collimated illumination for MAAP and MCML. Both MAAP and MCML algorithms use a Henyen-Greenstein scattering phase function with anisotropy =0.75.

The MAAP algorithm reproduces reflectance determined by MCML over a wide dynamic range of $\tau_{L,a}$ while the K-M theory fails for high-loading cases (Figure 6-34a). Reflectance is dominated by the response of the top layer to the collimated beam, for which the equation of radiative transfer in Hänel (1987) appears to be adequate. For transmittance calculations that involve collimated incident radiation and diffusive propagation within the filter, however, both K-M and MAAP overestimate the attenuation by 5% at low loadings to ~20% at high loadings (Figure 6-34b). Irrespective of the algorithm, $\tau_{a,ATN}$ estimated from $-\ln(T_F / T_F^{(0)})$ would overestimate $\tau_{L,a}$, and this corroborates the multiple-scattering effect. In such an optically-thick medium, transmittance only accounts for a small fraction (<7%) of the incident radiation. Despite the bias in transmittance, MAAP is able to quantify the absorbance ($1 - R_F - T_F$) with an accuracy <5% for $\tau_{L,a} > 0.3$.

6.7.4 Optical Model Development

In a Model 2001 carbon analyzer, red light from a He-Ne laser (632.8 nm) is guided to a filter punch via the reflectance light pipe (Figure 6-33). Part of the light scattered back is collected by the same light pipe and detected as the operational reflectance, R_{op}. Radiation that penetrates the

filter or forward scattered off the filter may be collected by the transmittance light pipe and detected as the operational transmittance, T_{op}. In the current setup, both light pipes are quartz rods of 3-mm diameter, separated from the filter by 5 mm (Figure 6-33). To simulate the incident beam of a finite size, the original MCML code was modified to launch photons at random sites within a 3-mm-diameter projection area on the upper surface of the filter. As a photon exits the filter after multiple scattering and enters the reflectance/transmittance light pipe, its weight is added to R_{op}/T_{op}. The final R_{op} or T_{op} is then calculated from the ratio of accumulated weight and the total number of photons launched. R_F and T_F that include full back and front hemisphere scattering, respectively, are determined simultaneously.

The $\sigma_{s,f}$ is a function of refractive indexes, thickness, and density of quartz fibers; it may vary between individual filters. The cross section of quartz fibers is estimated at 500 – 1,000 cm^2/cm^3. A nominal $\sigma_{s,f}$ of 2,200 cm^{-1} leads to $\tau_L^{(0)}$ of 96.8 for a blank filter; MCML determines the R_{op} and T_{op} at 7.9×10^{-2} and 5.7×10^{-3}, respectively (g = 0.75; 1 million photons), which agree with those measured in Chen et al. (2004). Figure 6-35 shows that R and T come close to R_F and T_F, respectively as the light pipes contact the filter but decrease sharply with increasing light pipe-filter distance. The R/T ratio is around 14 for light pipe-filter distance >0.5 cm and increases to 15.5 when the distance approaches zero (Figure 6-35). This is consistent with different angular distributions of reflected and transmitted radiation (Kopp et al., 1999). $\tau_L^{(0)}$ is directly related to the multiple scattering effect and should be quantified more precisely. Figure 6-36 shows the reflectance and transmittance as a function $\tau_L^{(0)}$, by which $\tau_L^{(0)}$ can be determined from reflectance/transmittance measurements.

For filters with an aerosol deposit, it is important to characterize particle distribution within the filter, since that influences $\tau_{L,s}$ and $\tau_{L,a}$ of each layer. Chen et al. (2004) use a single parameter, penetration depth (d_e), to describe the particle distribution; d_e could range from zero (monolayer deposit atop the filter) to infinity (uniform deposit throughout the filter). For ambient samples d_e is found to be consistent with a specific sampling configuration but varies between 0.014 and 0.38 for different configurations. For OP that forms during thermal analysis, d_e is much larger, at 6 – 8. The current optical modeling uses a simplified scheme: a uniform OP layer superimposed on the typical aerosol-filter system (e.g., Petzold and Schönlinner, 2004), creating a new two-layer system where $\tau_{L,s}$ and $\tau_{L,a}$ of both layers could vary. In this new system, the top layer (*L1*) receives contributions from aerosol and OP while the bottom layer (*L2*) is only influenced by OP. Assigning τ_{L1}/SSA_{L1} and τ_{L2}/SSA_{L2}, the optical depth/ω of *L1* and *L2*, respectively, results in:

$$\tau_{L1,a} = (1 - SSA_{L1})\tau_{L1} \tag{6-13}$$

$$\tau_{L2,a} = (1 - SSA_{L2})\tau_{L2} \tag{6-14}$$

Two special cases: 1) only aerosol (SSA_{L2} = 1), and 2) only OP ($SSA_{L1} = SSA_{L2}$) are investigated first. In Case 1, it is assumed that $\tau_{L2} = {}^{10}\!/_{11}\,\tau_L^{(0)}$ for a reasonably thin *L1*, but adjustments may be made with known penetration depth. SSA_{L1} is not likely below 0.80 as long as τ_{L1} is still

dominated by filter scattering (i.e., low to medium aerosol loading). In Case 2, SSA_{L1} or SSA_{L2} could be much higher since absorbing material is spread throughout the filter.

Figures 6-37a and 6-37b demonstrate R_{op} and T_{op} as functions of $\tau_{L1,a}$ at various τ_{L1} for Case 1. Note that $\tau_{L1,a}$ represents the total absorption since $\tau_{L2,a}$ equals 0. $\tau_{L1,a}$ is limited for each τ_{L1} so that SSA_{L1} is always greater than ~0.8. In this range, R_{op} and T_{op} only depend on absorption ($\tau_{L1,a}$). The effect of τ_{L1} is minor, especially for $0.1 < \tau_{L1,a} < 0.7$. Although aerosols of different *SSA* may alter the filter scattering and absorption coefficients differently, the aerosol absorption is the dominant factor that determines the filter reflectance and transmittance. Therefore, the response of the AE transmittance to white aerosol of *SSA* ~1 (Arnott et al., 2005a) likely results from changes in scattering anisotropy which is modeled neither in the current simulation nor in Petzold and Schönlinner (2004). Figure 6-37b confirms that τ_{ATN} (i.e., $-\ln[T_{op}/T_{op}^{(0)}]$) is 3-4 times the actual absorption $\tau_{L1,a}$ and the ratio decreases with increased particle loading on the filter (the shadowing effect).

The same simulation is performed for Case 2 as shown in Figures 6-37c and 6-37d. Note that $\tau_{L,a}$ represents the total absorption since absorption is uniformly distributed throughout the filter. In this case R_{op} and T_{op} also do not depend on τ_L as much as on $\tau_{L,a}$. A comparison between Figure 6-37a and Figure 6-37c indicates that R_{op} is much higher for Case 2, providing the same filter loading. An aerosol deposit near the surface attenuates reflectance more efficiently. If visual investigations were made, the Case 1 filter would look darker than the Case 2 filter. Since transmittance represents light going through the filter, it is assumed that the aerosol distribution within the filter is not important. However, for a uniform distribution in Case 2, aerosol absorption attenuates the transmittance much more efficiently (Figure 6-37d versus Figure 6-37c). One explanation is a weaker shadowing effect in Case 2 due to a lower concentrated aerosol distribution and a higher SSA_L that enhances the apparent absorption efficiency of each absorber.

For equally light-absorptive OP and EC that distribute in the filter following Cases 1 and 2, respectively, they produce different filter reflectance and transmittance, whether the reflectance and transmittance are referred to total diffusive R_F and T_F or operationally defined R_{op} and T_{op}. During thermal analysis, the initial reflectance and transmittance are only influenced by EC, but at the optical split point they reflect absorption by both OP and EC. The optical charring correction based on reflectance, such as the IMPROVE_A protocol, may overestimate the EC content since at the split point much more OP is required to compensate for the increase in reflectance owing to the loss of EC. In contrast, the transmittance charring correction may underestimate the EC content, since a small amount of OP needs much more EC to compensate for the attenuation by transmittance. The bias of reflectance and transmittance charring correction depends on the relative amounts of OP and EC.

6.7.5 Further Discussion

Figure 6-37 conveys an important message: aerosol absorption within a filter may be retrieved from either a reflectance or transmittance measurement, but the distribution of aerosol within the

filter needs to be known, since it affects the SSA_L of the aerosol-filter matrix. If the filter contains dual distribution, such as OP and EC during thermal analysis, information from reflectance and transmittance should be combined to achieve a better estimate of light absorption and OC/EC split. The following simulation assumes a constant *SSA* for aerosol OP and EC. Although in reality OP and EC could have different *SSA*, only their light absorption matters and *SSA* generally does not influence the relationship between the absorption and filter reflectance/transmittance (Figure 6-37). If $\tau_{OP,a}$ and $\tau_{EC,a}$ represent the absorption caused by OP and EC respectively, the current two-layer system becomes:

$$\tau_{L1,a} = \tau_{EC,a} + x\tau_{OP,a} \tag{6-15}$$

$$\tau_{L2,a} = (1-x)\tau_{OP,a} \tag{6-16}$$

where x is the fraction of OP formed in the top layer and coexists with EC. The responses of R_{op} and T_{op} to changing $\tau_{L1,a}$ and $\tau_{L2,a}$ are shown in Figure 6-38, which demonstrates that R_{op} is very sensitive to $\tau_{L1,a}$ but almost independent of $\tau_{L2,a}$. R_{op} provides a good measure of absorption in the top layer caused by OP and EC. In contrast, T_{op} is influenced by both $\tau_{L1,a}$ and $\tau_{L2,a}$, though $\tau_{L2,a}$ has a stronger impact since the SSA_{L2} is generally higher than SSA_{L1}. Because of this imbalance, T_{op} cannot provide an accurate measure of total absorption within the filter by itself. It is possible, however, to combine T_{op} with R_{op} to achieve a better description of the total absorption. The reversed relation of R_{op} /T_{op} with $\tau_{L1,a}$ /$\tau_{L2,a}$ is shown in Figure 6-39. $\tau_{L1,a}$ and $\tau_{L2,a}$ can be uniquely retrieved from R_{op} and T_{op} measurements in this simulation. The special cases of pure OP and EC are represented by the edges of the modeled domain (Figure 6-39). The Model 2001 carbon analyzer measures filter reflectance and transmittance simultaneously and therefore absorption caused by OP and EC can be retrieved continuously. For the optical charring correction, the split should be made when the total absorption ($\tau_{L1,a}$ + $\tau_{L2,a}$), rather than reflectance or transmittance, returns to its initial value.

Figure 6-40 shows the total absorption as a function of R_{op} and T_{op}. Assuming a filter sample begins the thermal analysis with $\tau_{L1,a}$ = $\tau_{EC,a}$ = 0.6 (point O in Figure 6-40). When charring occurs during analysis, both R_{op} and T_{op} decrease and the sample moves to point M with a total absorption of 0.8. The contribution from OP is thereby 0.2. OP and EC start to evolve as O_2 is introduced into the analyzer, and both R_{op} and T_{op} increase rapidly. Since EC leaves the filter earlier (i.e., $\tau_{L2,a}$ is nearly constant; see Figure 6-39), the filter moves to R_s, the reflectance split point first, at which the total absorption is ~0.7. In other words, the reflectance charring correction overestimates the EC by ~17%. As the analysis continues, the sample passes the accurate split point "A" (total absorption = 0.6) and then finally arrives at the transmittance split point T_s. At T_s the total absorption is only 0.2, and the transmittance charring correction underestimates the EC by 67%. Actual situations may vary from sample to sample, but with a reasonable amount of OP, the transmittance charring correction generally causes a larger bias.

Although R_{op} and T_{op} do not respond to the sample absorption linearly, accurate absorption measurements may be made following Figure 6-40. Further, the charring correction based on this absorption provides more reasonable EC measurements, which are usually somewhere between the reflectance and transmittance corrected values. Major uncertainties in this approach

include: 1) $\tau_L^{(0)}$ for blank filters, 2) particle penetration depth into a filter, and 3) the change of scattering anisotropy caused by particle deposits. The first two parameters can be determined experimentally for different types of samples, and Figure 6-40 must be modified accordingly. Variations between individual samples are not expected to be more than 10%. The change in scattering anisotropy is difficult to evaluate either experimentally or theoretically. Angularly-resolved reflectance and transmittance are required to calculate the asymmetric g-factor, but they cannot be measured under the current instrumental configuration. Light-scattering behaviors for soot particles attached to rod-like quartz fibers have never been investigated. With the modern advancements in light-scattering calculation software, such as FDTD, T-matrix, and Monte Carlo methods, how the scattering g-factor changes with filter loading will become more clear in the near future. Petzold and Schönlinner (2004) report that absorption is only overestimated by 2% and 6%, respectively, if g = 0.65 and 0.5 are used instead of 0.75.

6.7.6 Summary of Optical Modeling

The new generation of carbon analyzer is equipped with dual optical detectors that monitor both filter reflectance and transmittance. This configuration is intended for charring correction, but it also allows a more precise measurement of light absorption within the filter to be determined. This study demonstrates that filter-based absorption measurements, such as the AE and MAAP, still do not fully address the multiple scattering and shadowing effects. The Monte-Carlo simulation represents a precise method to determine the radiative transfer within a filter.

A filter sample can be described as a two-layer model during thermal analysis. The top layer contains OP and EC, while the second layer contains exclusively OP. The reflectance is insensitive to absorption in the second layer, and therefore absorption by the top and bottom layer can be retrieved separately from the reflectance and transmittance measurements. It has been demonstrated that the optical charring correction based on absorption is more accurate. Reflectance and transmittance charring corrections generally overestimate and underestimate the EC fraction, respectively.

Although the model explains the observations during thermal analysis well, more extensive comparisons with experimental results are needed. Particularly, the optical depth of blank filter and particle penetration depth should be quantified more accurately. Reflectance and transmittance of various samples during thermal analysis should be plotted as those shown in Figure 6-40 and the retrieved absorption should be compared with in-situ measurements (e.g., photoacoustic). As part of another project (U.S. EPA STAR grant), this model will be applied to more samples to confirm these hypotheses and suggest better EC and b_{abs} quantification methods.

6.8 Synthesis of Results from Laboratory Source Testing and Ambient Measurements

The objective of Phase I of this study was to compare different BC and b_{abs} measurements of emissions generated in the laboratory under controlled conditions and apply those results in interpreting the measurements conducted at the Fresno Supersite. Estimates of σ_{abs} and α were also determined for the source and ambient measurements. This section synthesizes the results in order to obtain a broader understanding of the measurement equivalency and comparability.

The PA represents an accurate and quick-response method for b_{abs} measurements (Sheridan et al., 2005). Particularly, it is not influenced by light scattering and RH in the sampled air (Arnott et al., 2000; 2003). In its current configuration, it is limited to a single wavelength, and scaling to other wavelengths depends on the aerosol composition, size distribution, and shape. The filter-based b_{abs} measurement methods, such as the AE, are subject to artifacts. The ratios of AE b_{abs} to PA b_{abs} for the source and ambient samples are summarized in Table 6-29. They vary from 1.05 to 7.2. The ratio does not appear to depend on EC/TC ratio directly; e.g., acetylene flame and carbon black contain over 90% of EC in TC but the $b_{abs(AE)}/b_{abs(PA)}$ are very different. The ratio is influenced by BC concentration; lower EC/TC ratios generally occur during sampling air with high BC concentrations. For Fresno summer samples, the BC concentration was low (<1 $\mu g/m^3$) and the $b_{abs(AE)}/b_{abs(PA)}$ was as high as 7.2. This confirms the shadowing effect (Section 6.7.4); i.e., multiple-scattering enhancement is gradually weakened with increasing filter loading. Although the AE advances the tape when an attenuation of 25% is reached, for ambient samples the tape is lightly loaded, resulting in a tape advance typically every four hours. For source samples, the tape reaches the critical loading quickly (typically within four minutes) and multiple scattering becomes less-pronounced.

The shadowing effect is not accounted for in the AE. A constant conversion factor ($14625/\lambda$) is used to translate b_{abs} to BC concentrations. PSAP was adjusted for filter loading (Virkkula et al., 2005). The adjustment algorithm was shown to work well for particles of high albedo (>0.8; Sheridan et al., 2005). The adjusted PSAP absorption at Fresno agrees closely (within ±5%) with PA during the summer intensive (Section 6.4.1). MAAP also considers the loading effect. Non-linear fittings are used to retrieve total absorption from filter reflectance and transmittance (Petzold and Schönlinner, 2004). The MAAP absorption is still higher by a factor of two relative to PA (scaled to 670 nm) during the Fresno summer intensive, although the correlation between the two measurements are high (r = 0.98). The current MAAP algorithm should be re-evaluated. Some of its discrepancies have been discussed in Section 6.7.

To convert b_{abs} to BC concentration or vice-versa, one needs to address the BC mass absorption efficiency, σ_{abs}. This σ_{abs} is controlled by: 1) size, 2) shape, 3) density, and 4) internal mixing of the BC-containing particles. Figure 6-41 shows the modeled σ_{abs} (at 1047 nm) of BC as a function of BC mass fraction and particle size, assuming spherical particles to which the Mie scattering theory applies. The refractive index and density for BC are assumed to be 1.96 – 0.66i and 1.7 g/cm^3, respectively (Chen et al., 2006a). The rest of the particle is modeled with a refractive index of 1.42 – 0.001i and density of 1.2 g/cm^3. σ_{abs} increases with imaginary refractive index and decreases with increasing particle density. The refractive index and density varies (e.g., Bond and Bergstrom, 2006), partly due to void volume in the particles.

Despite potential biases, Figure 6-41 is illustrative. For pure BC, σ_{abs} is ~ 2.5 m^2/g for particles less than 0.1 μm and increases gradually with particle diameter, maximizing (~ 3.5 m^2/g) at the size of ~0.3 μm. Higher σ_{abs} is found for lower BC fractions, due to enhancement through internal mixing (Jacobson, 2001). For large particles, this enhancement can be important with the σ_{abs} reaching 7 – 8 m^2/g (Figure 6-41). The ω remains nearly independent of the BC fraction up to a particle size of 0.4 μm. Therefore, ω is a good indicator for particle size.

From the source testing, it was found that the acetylene flame soot and carbon black samples primarily consist of EC (98% and 94% of TC, respectively). The volume-size distributions peak at 0.35 and 0.24 μm for the acetylene flame and carbon black samples, respectively, as shown in Figure 6-42. A σ_{abs} of ~3.5 m^2/g is expected for both types of particles based on Mie theory (see Figure 6-41). This σ_{abs} is confirmed for acetylene, but not for carbon black, as shown in Figure 6-43. Since carbon black was injected into the miniature dilution/residence chamber through nebulization using methanol as solvent, it is speculated that the carbon black particles are coated with organics when detected by the PA. The concentration of carbon black in the dilution system was low (24.3 $\mu g/m^3$) compared with that of the acetylene flame (290.4 $\mu g/m^3$) so the coating could lower the EC fraction substantially, leading to a higher σ_{abs} of EC (averages ~5.0 m^2/g). Thermal analysis indicates the existence of substantial OC (~4 times EC) in the carbon black samples, but it was removed after the blank subtraction.

For other source and ambient samples, the accuracy of σ_{abs} is limited by the accuracy of BC/EC measurements. It was demonstrated in Sections 6.2.1 and 6.2.2 that the IMPROVE_A, STN, and French two-step protocols yield different EC/TC ratios for wood smoke and ambient samples. In Section 6.7, it was shown that TOR could overestimate EC while TOT could underestimate EC owing to the charring correction. The wood-smoke particles appear to be relatively small in size (Figure 6-42) with a σ_{abs} of 2.72 ± 1.25 m^2/g (Figure 6-43). This value would be lower if EC is overestimated by the IMPROVE_A. For diesel samples, however, the EC/TC ratio is consistent (~0.6) across different protocols (Table 6-8), yielding a σ_{abs} of 5 m^2/g EC. Using the peak of the diesel volume-size distribution at ~0.2 μm, the model in Figure 6-41 suggests a σ_{abs} of 4.3 m^2/g that underestimates the actual value by ~15%. Thermal analyses indicate that the electric arc samples contain ~50% of OC, which should enhance the σ_{abs} of EC. In fact, the electric arc EC σ_{abs} is low, only ~3.4 m^2/gEC. This cannot be explained by the Mie scattering model. Mixing with salt does not appear to change σ_{abs} for diesel, acetylene, and electric arc samples.

The EC absorption efficiency in ambient samples is generally <3 m^2/g for the 1047 nm PA b_{abs}. The σ_{abs} (1047 nm) during summer (1.9 to 2.6 m^2/g EC) was lower than that observed for any of the sources. The EC concentration in the summer samples was low (average < 1 $\mu g/m^3$) with higher uncertainties. On the other hand, σ_{abs} (1047) during winter (2.5 to 3.8 m^2/g) was similar to that observed for pure wood smoke (2.7 and 3.1 m^2/g by IMPROVE_A_TOR and TOT respectively) and electric arc samples (3.4 and 3.2 m^2/g by IMPROVE_A_TOR and TOT respectively). This is consistent with the Fresno aerosol during winter being dominated by emissions from wood burning and consisting of particles that are similar in characteristics (such as surface area, particle size, and morphology).

Figure 6-43 shows that the σ_{abs} (1047 nm) varied by as much as ~50% among different source types, from 2.7 to 5.3 m^2/g. A universal conversion factor between b_{abs} and BC/EC concentration does not exist. In many cases, one has to consider other information in order to estimate the influence of BC particles on radiative forcing. This information includes: source type, particle size distribution, morphology, and internal or external mixing. More complex aerosol optical models that consider the fractal nature of soot particles need to be integrated into the source emission and aerosol dispersion models. Uncertainties in the filter-based light absorption and EC measurements (e.g., the thermal and optical methods) often present

challenges for reconciling the absorption and EC concentrations. Substantial progress in identifying these discrepancies has been made in this study, but efforts to improve the measurements should continue.

It has been shown that the wavelength dependence of b_{abs} and σ_{abs} differ for various types of samples (Kirchstetter et al., 2004; Chen et al., 2006a). One hypothesis is that some OC absorbs in the visible and UV region but not infrared region, and therefore increases the absorption exponent (α) (Kirchstetter et al., 2004). The morphology of particles could influence α (e.g., Bond et al., 2001; Sheridan et al., 2005), partly since it blurs the definition of particle size. α may be an indicator for the source and composition of particles. The 7-AE was the only instrument with multi-wavelength measurements that was available in both laboratory and field measurements. Hence the α estimates calculated using the 7-AE measurements are reported here. The effects of multiple scatter within the AE filter not only cause a bias in the absorption measurement but in α as well. This is because the filter optical depth and albedo depend on the wavelength of incident light and the degree of multiple scattering depends on the optical depth and SSA (see Section 6.7).

Figure 6-44 shows the wavelength dependence (i.e., α) of the 7-AE for the source and ambient aerosols. The important observation is that α varies significantly (by as much as 40%) for the different sources tested in the laboratory. The α during the summer IOP (0.95 ± 0.04) was 10 to 20% higher than that observed for diesel and acetylene samples (0.79 ± 0.09 to 0.86 ± 0.12), both pure and when mixed with NaCl. This indicates that the summer-time aerosol at Fresno, while being influenced by diesel emissions, might be mixed with aged or secondary aerosols. The α during the winter period (1.2 ± 0.11) was similar to that observed for emissions from wood combustion (1.2 ± 0.51). Previous studies have shown that RWC is a major source of $PM_{2.5}$ during the winter season (Schauer and Cass, 2000; Watson and Chow, 2002a). Despite the potential bias in the AE, this study confirms a higher α in wood smoke than in diesel samples. More importantly, these values differ from $\alpha = 1$ that is often used to scale the b_{abs} to different wavelengths. More complex aerosol optical models can be used to better understand these variations.

Overall, the results from the winter IOP are consistent with laboratory observations and the instrumental differences observed during the wood combustion experiments. The aerosol during summer IOP was more complex and difficult to explain with the laboratory data. The low EC concentration close to the detection limits of thermal/optical methods and the presence of secondary organic aerosol are important issues to be resolved in the future.

Table 6-1. Aerosol absorption measurements during the Reno Aerosol Optics Study (RAOS).

Measurement	Method	Instrument	Operating Wavelengths	Responsible Institution[a]
Aerosol light absorption coefficient, b_{abs}	Filter-based absorption	7-AE	370, 470, 521, 590, 660, 880, 950 nm	DRI
b_{abs}	Filter-based absorption	7-AE (with modified LEDs)	370, 430, 470, 521, 565, 700, 950 nm	NOAA/CMDL
b_{abs}	Filter-based absorption	PSAP*	565 nm	NOAA/CMDL
b_{abs}	Filter-based absorption	Three-wavelength PSAP	467, 530, 660 nm	University of Washington
b_{abs}	Filter-based absorption	MAAP	670 nm	Thermo Anderson
b_{abs}	Photoacoustic absorption	PA	532 nm	DRI
b_{abs}	Photoacoustic absorption	PA	1047 nm	DRI
b_{abs}	*in-situ* absorption (by difference)	Cavity ring-down transmissometer	690 nm	NASA/ARL
b_{abs}	*in-situ* absorption (by difference)	Optical extinction cell (OEC) and integrating nephelometer	467, 530, 660 nm	University of Washington and NOAA/CMDL

* 565 nm is the manufacturer's stated operating wavelength.

[a] DRI: Desert Research Institute
NOAA/CMDL: National Oceanic & Atmospheric Administration Climate Monitoring and Diagnostics Laboratory
NASA/ARL: National Aeronautics and Space Administration Air Resources Laboratory

Table 6-2. Results of linear regression analysis for the Reno Aerosol Optics Study (RAOS).

y	x	Slope	Intercept (Mm^{-1})	r
PA (467 nm)[a]	E-S[b] (467 nm)	0.984	3.630	0.998
PA (530 nm)[a]	E-S[b] (530 nm)	0.974	0.900	0.998
PA (660 nm)[a]	E-S[b] (660 nm)	0.980	-1.010	0.998
PA (467 nm)[a]	E-S[b] (467 nm) < 250 Mm^{-1}	0.996	4.480	0.987
PA (530 nm)[a]	E-S[b] (467 nm) < 250 Mm^{-1}	0.921	3.460	0.989
PA (660 nm)[a]	E-S[b] (467 nm) < 250 Mm^{-1}	0.933	0.720	0.992
PSAP (530 nm)[a]	Reference Absorption[c]	0.780	9.100	0.998
PSAP (530 nm)[a] < 200 Mm^{-1}	Reference Absorption[c]	0.860	4.900	0.995
PSAP (530 nm)[a] < 25 Mm^{-1}	Reference Absorption[c]	1.020	0.900	0.986
PSAP (530 nm)[a]	Reference Absorption[c]	0.990	2.900	0.995

[a] PA b_{abs} measurements were adjusted from 532 nm to the noted wavelengths using λ^{-1} wavelength dependence.
[b] E-S indicates the difference between extinction and scattering measurements.
[c] Reference absorption (b_{abs}) was the average of the 532 nm PA measurement (adjusted to 530 nm) and the difference of optical extinction cell OEC extinction and TSI nephelometer scattering, adjusted to 530 nm, as well.

Table 6-3. Results of linear regression analysis during the North Front Range Air Quality Study (NFRAQS).

Date(s)	y-axis (Mm^{-1})	x-axis	slope	zero-offset (Mm^{-1})	r
12/17/96	PA b_{abs} (532 nm)	Aethalometer BC (880 nm; $\mu g/m^3$)	12.10 m^2/g	0.19	0.95
12/18/96	PA b_{abs} (532 nm)	Aethalometer BC (880 nm; $\mu g/m^3$)	8.93 m^2/g	1.42	0.93
Avg. (12/17-18/96)	PA b_{abs} (532 nm)	Aethalometer BC (880 nm; $\mu g/m^3$)	10.51 m^2/g	0.80	0.94
1/3/97	PA b_{abs} (685 nm)	Aethalometer BC (880 nm; $\mu g/m^3$)	4.61 m^2/g	-0.31	0.92
1/6/97	PA b_{abs} (685 nm)	Aethalometer BC (880 nm; $\mu g/m^3$)	5.43 m^2/g	-0.22	0.94
1/7/97	PA b_{abs} (685 nm)	Aethalometer BC (880 nm; $\mu g/m^3$)	5.44 m^2/g	0.14	0.96
1/8/97	PA b_{abs} (685 nm)	Aethalometer BC (880 nm; $\mu g/m^3$)	4.14 m^2/g	0.08	0.95
1/9/97	PA b_{abs} (685 nm)	Aethalometer BC (880 nm; $\mu g/m^3$)	5.03 m^2/g	0.09	0.95
Avg. (1/3, 1/6/97-1/9/97)	PA b_{abs} (685 nm)	Aethalometer BC (880 nm; $\mu g/m^3$)	4.93 m^2/g	-0.05	0.95
1/3, 1/6-9/97	Filter b_{abs}	PA b_{abs} (685 nm; Mm^{-1})	3.00	3.43	0.85
1/3, 1/6-9/97	Corrected Filter b_{abs}	PA b_{abs} (685 nm; Mm^{-1})	1.68	-0.38	0.91
1/3, 1/6-9/97	PA b_{abs} (685 nm)	IMPROVE_TOR EC ($\mu g/m^3$)	3.58 m^2/g	0.17	0.92

Table 6-4. Results of linear regression analysis for the Missoula Forest Fire Characterization Study.

y	x	Number of Samples	Slope (m^2/g)	Intercept (Mm^{-1})	r
PA (532 nm)	IMPROVE_TOR EC	19	7.5 ± 0.4	-63.2 ± 55.8	0.97
PA (532 nm)	STN_TOT EC	19	8.9 ± 0.4	84.3 ± 38.5	0.98
PA (1047 nm)	IMPROVE_TOR EC	7	4.1 ± 0.5	-93.9 ± 83.5	0.97
PA (1047 nm)	STN_TOT EC	7	4.6 ± 0.3	50.2 ± 45.5	0.98

Table 6-5. Summary of intercomparisons by regression analysis.

	y-axis = PA (Mm^{-1})	x-axis					
Previous Study	**Type of Aerosol**	**Aethalometer BC ($\mu g/m^3$)**	**PSAP b_{abs} (Mm^{-1})**	**Filter b_{abs} (Mm^{-1})**	**IMPROVE EC ($\mu g/m^3$)**	**STN EC ($\mu g/m^3$)**	**Absorption Exponent, α**
Fresno	Ambient (winter)				y=2.3x + 0.07; r = 0.97; n=14 (PA at 1047 nm)		**1 - 2**
	Ambient (summer)				y=3.1x - 0.18; r = 0.99; n=16 (PA at 1047 nm)		
RAOS	Kerosene soot + $(NH_4)_2SO_4$ (all)		y=0.78x + 9.1; r = 0.999; n=~30 (PA at 532 nm)				**1**
	Kerosene soot + $(NH_4)_2SO_4$ (PSAP < 200 Mm^{-1})		y=0.86x + 4.9; r = 0.997; n=~29 (PA at 532 nm)				
	Kerosene soot + $(NH_4)_2SO_4$ (PSAP < 25 Mm^{-1})		y=1.02x + 0.9; r = 0.999; n=~6				
BRAVO	Ambient all	y=8.5x - 0.23; r = 0.67; n=738 (PA at 532 nm)					
	Ambient Aethalometer BC > 0.15 $\mu g/m^3$	y=9.9x - 0.45; r = 0.46; n=230 (PA at 532 nm)					
NFRAQS	Ambient	y=10.0x - 0.87; r = 0.93; n=~200 (PA at 532 nm)		y=0.33x-1.5; r=0.85; n=13 (PA at 685 nm)	y=3.58x + 0.17; r = 0.92; n=15 (PA at 685 nm)		**2.7**
SNAQS*	Ambient				y=11.7x + 3.6; r = 0.99; n=152 (PA at 532 nm)	y=16.3x + 4.9; r = 0.98; n=223 (PA at 532 nm)	
Gas/ Diesel Split	Heavy-duty diesel				y=4.67x + 0.00; r = 0.99; n=~50 (PA at 1047 nm)	y=4.55x + 0.00; r = 0.99; n=~50 (PA at 1047 nm)	
	Light-duty gasoline				y=3.60x + 0.00; r = 0.84; n=~40 (PA at 1047 nm)	y=3.47x + 0.00; r = 0.87; n=~40 (PA at 1047 nm)	
	Ambient (LA sea port)				y=4.13x + 0.00; r = 0.99; n=21 (PA at 1047 nm)	y=4.95x + 0.00; r = 0.99; n=21 (PA at 1047 nm)	
Missoula Fire Study	Wood smoke				y=4.1x - 93.9; r = 0.97; n=7 (PA at 1047 nm)	y=4.6x +50.20; r = 0.98; n=7 (PA at 1047 nm)	**0.9 - 2.4**
	Wood smoke				y=7.5x - 63.2; r = 0.97; n=19 (PA at 532 nm)	y=8.9x + 84.3; r = 0.98; n=19 (PA at 532 nm)	

* EC was determined by transmission with IMPROVE temperature protocol. Residence time was determined empirically from repetitive field tests by determining the time taken for fully-defined carbon fractions.

Table 6-6. Number of samples analyzed for the source testing program.

Source	Additive	IMPROVE_A Protocol	STN Protocol	French two-step Protocol
Diesel		35	7	7
Diesel	NaCl	9	6	6
Acetylene Flame		10	6	6
Acetylene Flame	NaCl	9	6	6
Electric Arc		13	4	4
Electric Arc	NaCl	9	3	3
Wood Smoke		23	6	6
Wood Smoke	NaCl	14	4	4
Carbon Black		9	3	3
Carbon Black	Methanol	3	1	1
Graphite	(CH_3OH)	9	3	4

Table 6-7. OC, EC, and TC measurements, by source, with the IMPROVE_A_TOR protocol.

Source	Protocol[a]	# of Samples	OC Avg. (µg/m^3)	EC Avg. (µg/m^3)	TC Avg. (µg/m^3)	EC/TC Avg.	± 1σ
Diesel	IMP	33*	95.1	155.3	250.4	0.653	0.111
Acetylene Flame	IMP	10	9.5	361.4	370.8	0.980	0.052
Electric Arc	IMP	13	569.4	474.4	1043.8	0.500	0.114
Wood Smoke	IMP	23	205.6	47.8	253.4	0.259	0.123
Carbon Black	IMP	9	791.2	20854.6	21645.8	0.941	0.055
Graphite	IMP	9	724.3	15182.6	15906.9	0.911	0.095

[a] IMP: IMPROVE_A_TOR

* Two outliers (Filter IDs STRSQ016 and STRQQF090) were removed.

Table 6-8. OC, EC, and TC measurements, by source and by thermal protocol.

Source	Protocol[a]	# of Samples[b]	OC Avg. (µg/m^3)	EC Avg. (µg/m^3)	TC Avg. (µg/m^3)	EC/TC Avg.	± 1σ
Diesel	IMP	7	125.8	175.2	301	0.59	0.078
	STN	7	119.8	183.1	302.9	0.606	0.044
	FM	7	126.4	174.5	301	0.587	0.058
Acetylene Flame	IMP	6	7.6	356.2	358.8	0.982	0.03
	STN	6	18.4	352.3	366.3	0.958	0.074
	FM	6	29.3	329.6	358.8	0.921	0.05
Electric Arc	IMP	4	532.4	476	1008.4	0.506	0.097
	STN	4	562.7	422.5	985.2	0.458	0.088
	FM	4	557.5	450.9	1008.4	0.497	0.142
Wood Smoke	IMP	6	188.5	52	240.5	0.266	0.118
	STN	6	225.9	27.7	253.6	0.143	0.084
	FM	6	234.2	6.3	240.5	0.036	0.024
Carbon Black	IMP	3	1348.5	22415.7	23764.2	0.905	0.072
	STN	3	1004.9	22625.6	23630.4	0.94	0.04
	FM	3	1785.9	21978.3	23764.2	0.855	0.12
Graphite	IMP	3	840.2	14899.7	15739.9	0.929	0.054
	STN	3	711.9	14584.9	15296.8	0.843	0.229
	FM	3	453.7	15286.2	15739.9	0.98	0.023

[a] IMP: IMPROVE_A_TOR protocol; STN: STN_TOT protocol; FM: French two-step protocol

[b] Only samples with all three analysis protocols are included in the averages shown here

Table 6-9. Averages and standard deviation of carbon fractions in TC by source. TC is presented in unit of μg/m^3.

Source	# of Samples	Average ± Standard Deviation of Carbon Fractions[a] in TC										
		OC1	OC2	OC3	OC4	OP	EC1	EC2	EC3	OC	EC	TC (μg/m^3)
Diesel	33	0.196 ± 0.050	0.116 ± 0.041	0.032 ± 0.018	0.006 ± 0.013	0.012 ± 0.036	0.041 ± 0.015	0.622 ± 0.087	0.001 ± 0.004	0.35 ± 0.11	0.65 ± 0.11	250 ± 89
Diesel + NaCl	9	0.249 ± 0.027	0.098 ± 0.034	0.032 ± 0.010	0.006 ± 0.006	0.011 ± 0.033	0.609 ± 0.038	0.007 ± 0.006	0 ± 0	0.4 ± 0.06	0.61 ± 0.06	307 ± 33
Acetylene Flame	10	0.006 ± 0.008	0.009 ± 0.011	0.015 ± 0.021	0.002 ± 0.003	0.003 ± 0.008	0.029 ± 0.046	0.813 ± 0.154	0.14 ± 0.168	0.03 ± 0.04	0.98 ± 0.05	371 ± 49
Acetylene Flame + NaCl	9	0.008 ± 0.010	0.008 ± 0.010	0.008 ± 0.009	0.002 ± 0.004	0.024 ± 0.069	0.857 ± 0.089	0.128 ± 0.100	0 ± 0	0.04 ± 0.06	0.96 ± 0.06	376 ± 63
Electric Arc	13	0.007 ± 0.012	0.013 ± 0.013	0.057 ± 0.035	0.014 ± 0.013	0.492 ± 0.094	0.587 ± 0.129	0.372 ± 0.112	0.032 ± 0.021	0.5 ± 0.11	0.5 ± 0.11	1044 ± 472
Electric Arc + NaCl	9	0 ± 0	0.003 ± 0.005	0.089 ± 0.017	0.053 ± 0.028	0.466 ± 0.167	0.855 ± 0.079	0.068 ± 0.020	0 ± 0.001	0.55 ± 0.17	0.46 ± 0.18	854 ± 366
Wood Smoke	23	0.13 ± 0.111	0.144 ± 0.039	0.303 ± 0.085	0.116 ± 0.042	0.082 ± 0.050	0.3 ± 0.126	0.04 ± 0.018	0 ± 0.001	0.75 ± 0.012	0.26 ± 0.012	253 ± 236
Wood Smoke + NaCl	14	0.047 ± 0.082	0.081 ± 0.060	0.514 ± 0.196	0.113 ± 0.064	0.043 ± 0.056	0.428 ± 0.252	0 ± 0.002	0 ± 0	0.64 ± 0.25	0.39 ± 0.28	38 ± 26
Carbon Black	9	0.007 ± 0.010	0.013 ± 0.010	0.025 ± 0.023	0.002 ± 0.004	0.013 ± 0.038	0.015 ± 0.014	0.932 ± 0.044	0.007 ± 0.007	0.06 ± 0.05	0.94 ± 0.05	21646 ± 17239
Carbon Black[b] + CH_3OH	3	0.016 ± 0.028	0.016 ± 0.027	1.301 ± 1.492	1.363 ± 1.670	0 ± 0	0.55 ± 0.775	2.912 ± 4.016	0.013 ± 0.023	0.25 ± 0.44	3.48 ± 4.78	29 ± 33
Graphite	9	0.011 ± 0.016	0.018 ± 0.019	0.043 ± 0.053	0.007 ± 0.010	0.011 ± 0.033	0.005 ± 0.004	0.352 ± 0.193	0.564 ± 0.129	0.09 ± 0.09	0.91 ± 0.09	15907 ± 12566

[a] Based on IMPROVE_A_TOR protocol

[b] TC in nebulizer blank is higher than TC in 2 out of 3 samples.

Table 6-10. Comparisons of front and backup filters of source samples.

			Carbon Concentration[b] by IMPROVE_A_TOR Analysis (µg/m^3)										
Source	**Type[a]**	**#**	**OC1**	**OC2**	**OC3**	**OC4**	**OP**	**EC1**	**EC2**	**EC3**	**OC**	**EC**	**TC**
Diesel	QF	1	94.95	31.72	17.67	7.2	2.97	11.2	211.18	0	154.5		373.9
	QB	1	16.63	7.35		4.15	0	0	0.02	0	35.1	0	35.1
	TB	1	20.09	5.91		3.67	0	0.72	0.24	0	37.1	219.4 1	38.1
Diesel + NaCl	QF	9	88.89	39.37 6.94	19.22	9.46	4.07	186.73	2.27	0	161	184.9	345.9
	QB	9	18.04	7.18 7.44			0	0.37	0.71	0	36.3	1.1	37.4
	TB	9	22.76	8.55	8.81	3	0.15			0	43.3	1.3	44.6
Acetylene Flame	QF	10	14.3	12.11 7.82	15.11 3.24	5.99	0.66	0.76	0.73	287.67	49.64	48.2	346.7	394.8
	QB	10	9.04	4.68	5.7	2.15	0.04			0.1	0.98	21.6	1	22.6
	TB	10	15.3	7.35			0	0.56			0.01	36	1.4	37.3
Acetylene Flame + NaCl	QF	9	15.5	12.04 8.64	12.67 4.67	6.83	7.31 10	0	0.78	44.01	0.03	54.3		415.6
	QB	9	7.87	4.85	7.4	2.93	0	0.13	0.46	0	23	0.6	23.6
	TB	9	12.05	7.51			0	324.54 0.36		0	34	361.3 1	35
Electric Arc + NaCl	QF	9	27.13	50.77 8.87	128.78 5.55	103.87	395.5		0.69	53.49	0.5	706.1	368.7	1074.7
	QB	9	43.75	35.84	36.92	11.8	0	0		0.31	0.01	128.3	0.3	128.6
	TB	9	14.2	17.32	16.54	0.3	0	710.17 0		0.51	0	48.4	0.5	48.9
Wood Smoke	QF	23	64.99	46.97	76.08	37.84	19.01	56.32	10.32	0.15	244.9	47.8	292.7
	QB	23	25.58	20.31	31.33	11.8	0.44	1.72	0.86	0	89.5	2.1	91.6
	TB	23	45.72	33.16	51.04	28.66	5.49	8.44	3.65	0	164.1	6.6	170.7
Wood Smoke + NaCl	QF	14	14.07	12.48	25.61	12.28	2.12	12.31	0.04	0	66.6	10.2	76.8
	QB	14	7.85	5.26	10	3.9	0.01	0.22	0.03	0	27	0.2	27.3
	TB	14	12.21	10.9	18.75	9.93	0	1.31	0.33	0	51.8	1.6	53.4

[a] QF, QB, and TB indicate front quartz, backup quartz behind quartz, and backup quartz behind Teflon, respectively.

[b] Dynamic blanks were not subtracted.

Table 6-11. Number of ambient filter samples analyzed for the summer and winter IOPs.

Season	Sampler	Channel	Protocol[a]	# of Samples
Summer	Hi-Vol	1	IMP	18
Summer	Hi-Vol	1	STN	18
Summer	Hi-Vol	1	FM	8
Summer	RAAS	1	IMP	25
Summer	RAAS	2	IMP	25×2[b]
Summer	RAAS	2	STN	8×2[b]
Summer	RAAS	4	IMP	25×2[b]
Summer	RAAS	4	STN	8×2[b]
Winter	Hi-Vol	1	IMP	7
Winter	Hi-Vol	1	STN	7
Winter	Hi-Vol	1	FM	7
Winter	RAAS	1	IMP	7
Winter	RAAS	1	STN	7
Winter	RAAS	2	IMP	7×2[b]
Winter	RAAS	2	STN	7×2[b]
Winter	RAAS	4	IMP	7×2[b]
Winter	RAAS	4	STN	7×2[b]

[a] IMP: IMPROVE_A protocol; STN: STN_TOT protocol; FM: French two-step protocol

[b] Including the analysis of backup samples.

Table 6-12. OC, EC, and TC measurements from Hi-Vol sampler.

SITE	Protocol[a]	Season	Sampler	# of Samples[b]	OC (µg/m^3)	EC (µg/m^3)	TC (µg/m^3)	EC/TC Avg. ± 1σ	
Fresno	IMP	Summer[c]	Hi-Vol	8	3.61	0.99	4.6	0.206	0.043
Fresno	STN	Summer	Hi-Vol	8	2.6	0.54	3.14	0.171	0.037
Fresno	FM	Summer	Hi-Vol	8	3.75	0.85	4.6	0.18	0.044
Fresno	IMP	Winter[d]	Hi-Vol	7	7.04	2.6	9.64	0.261	0.045
Fresno	STN	Winter	Hi-Vol	7	7.67	0.75	8.42	0.097	0.022
Fresno	FM	Winter	Hi-Vol	7	8.47	1.16	9.64	0.124	0.06

[a] IMP: IMPROVE_A_TOR protocol; STN: STN_TOT protocol; FM: French two-step protocol
[b] Only those analyzed by three thermal protocols are included.
[c] Summer samples include samples acquired from 8/1/05 to 9/30/05
[d] Winter samples include samples acquired from 12/1/03 to 12/31/03

Table 6-13. Comparisons of OC, EC, and TC measurements from the Hi-Vol and RAAS samplers.

Protocol[a]	Season	Sampler	Channel	# of Samples	OC ($\mu g/m^3$)	EC ($\mu g/m^3$)	TC ($\mu g/m^3$)	EC/TC Avg.	± 1σ
IMP	Summer	Hi-Vol	1	17	3.58	1.01	4.59	0.215	0.035
IMP	Summer	RAAS	2	17	3.94	0.88	4.81	0.163	0.059
IMP	Summer	RAAS	4	17	2.01	0.67	2.68	0.244	0.051
IMP	Winter	Hi-Vol	1	5	5.40	1.92	7.32	0.259	0.047
IMP	Winter	RAAS	2	5	5.12	1.63	6.75	0.237	0.019
IMP	Winter	RAAS	4	5	4.03	1.69	5.72	0.293	0.041
STN	Summer	Hi-Vol	1	8	2.60	0.54	3.14	0.171	0.037
STN	Summer	RAAS	2	8	4.08	0.59	4.66	0.123	0.023
STN	Summer	RAAS	4	8	2.39	0.46	2.85	0.159	0.036
STN	Winter	Hi-Vol	1	5	5.55	0.67	6.22	0.107	0.016
STN	Winter	RAAS	2	5	5.72	0.75	6.48	0.121	0.078
STN	Winter	RAAS	4	5	5.04	1.00	6.04	0.165	0.040

[a] IMP—IMPROVE_A_TOR protocol

Table 6-14. Comparisons of front and backup filters from RAAS sampler.

				Carbon Concentration by IMPROVE_A_TOR Analysis (µg/m^3)										
Season	**#**	**Ch**	**Type**[a]	**OC1**	**OC2**	**OC3**	**OC4**	**OP**	**EC1**	**EC2**	**EC3**	**OC**	**EC**	**TC**
Summer	25	2	QF	0.35	1.15	1.32	0.75	0.71	0.96	0.62	0.03	4.19	0.91	5.1
Summer	25	4	dQF	0.04	0.46	0.88	0.49	0.53	0.76	0.47	0	2.24	0.7	2.94
Summer	25	2	QB	0.07	0.22	0.14	0.09	0	0.02	0.03	0.04	0.39	0.09	0.48
Summer	25	4	dQB	0.01	0.05	0.07	0.02	0	0.01	0	0	0.09	0.01	0.09
Summer	25	1	TB	0.22	0.61	0.5	0.21	0.05	0.06	0.04	0	1.55	0.05	1.6
Winter	7	2	QF	0.74	1.54	2.55	1.58	1.45	3.23	0.85	0.01	7.77	2.63	10.41
Winter	7	4	dQF	0.25	1.42	2.27	1.44	1.45	3.33	0.81	0	6.73	2.7	9.42
Winter	7	2	QB	0.27	0.27	0.44	0.12	0.01	0.02	0.01	0	1	0.02	1.02
Winter	6	4	dQB	0.1	0.01	0.06	0.02	0	0.01	0	0	0.07	0.01	0.09
Winter	7	1	TB	0.33	0.39	0.59	0.26	0.07	0.15	0.1	0	1.6	0.18	1.78

[a] QF: Front quartz filter
dQF: Denuded front quartz
QB: Backup quartz behind quartz
dQB: Denuded backup quartz behind quartz
TB: Backup quartz behind Teflon

Table 6-15. Comparison between aethalometer and photoacoustic measurements of source samples.

Source	Unit	Instrument[a] y	Instrument[a] x	Averages y	Averages x	Effective Variance Weighted Regression[b] Slope	±	SE[c]	Intercept	±	SE[c]	Ordinary Least Squares Regression[d] Slope	±	SE[c]	Intercept	±	SE[c]	r[e]	Number of pairs	Ratio y/x Average	±	SD[f]	Ratio Avg y/Avg	Difference y-x Averge	±	SD[f]	RMS[g] Precision	Distribution of y-x[h] (%) <1σ[i]	1σ-2σ	2σ-3σ	>3σ
Diesel	µg/m^3	7-AE 880 nm	PA 1047 nm	115.8	191.1	0.23	±	0.033	69.82	±	6.164	0.24	±	0.040	70.24	±	8.023	0.72	35	0.66	±	0.212	0.61	-75.25	±	44.234	11.99	0.0	2.9	20.0	77.1
	Mm^{-1}	7-AE 880 nm	PA 1047 nm	1924.7	955.3	0.75	±	0.110	1160.40	±	102.450	0.79	±	0.134	1167.30	±	133.340	0.72	35	2.18	±	0.704	2.01	969.45	±	221.760	195.25	0.0	0.0	2.9	97.1
	Mm^{-1}	7-AE 950 nm	PA 1047 nm	1784.3	955.3	0.67	±	0.102	1097.80	±	95.642	0.71	±	0.125	1102.10	±	124.670	0.70	35	2.03	±	0.666	1.87	829.02	±	215.410	181.02	0.0	0.0	5.7	94.3
Acetylene	µg/m^3	7-AE 880 nm	PA 1047 nm	96.5	290.4	0.25	±	0.110	22.86	±	31.581	0.26	±	0.073	21.48	±	21.374	0.78	10	0.33	±	0.022	0.33	-193.89	±	22.166	14.71	0.0	0.0	0.0	100.0
	Mm^{-1}	7-AE 880 nm	PA 1047 nm	1604.5	1452.2	0.84	±	0.365	380.43	±	524.800	0.86	±	0.244	356.93	±	355.220	0.78	10	1.11	±	0.072	1.10	152.32	±	101.210	170.39	50.0	50.0	0.0	0.0
	Mm^{-1}	7-AE 950 nm	PA 1047 nm	1516.4	1452.2	0.80	±	0.345	340.08	±	495.900	0.82	±	0.220	324.73	±	320.480	0.80	10	1.05	±	0.065	1.04	64.16	±	93.108	162.03	90.0	10.0	0.0	0.0
PALAS	µg/m^3	7-AE 880 nm	PA 1047 nm	174.0	381.1	0.40	±	0.025	12.96	±	6.973	0.44	±	0.059	7.67	±	23.707	0.91	13	0.46	±	0.066	0.46	-207.15	±	81.462	18.92	0.0	0.0	0.0	100.0
	Mm^{-1}	7-AE 880 nm	PA 1047 nm	2891.2	1905.6	1.33	±	0.083	215.37	±	115.900	1.45	±	0.195	127.44	±	393.990	0.91	13	1.54	±	0.220	1.52	985.60	±	539.080	307.98	7.7	0.0	7.7	84.6
	Mm^{-1}	7-AE 950 nm	PA 1047 nm	2548.3	1905.6	1.18	±	0.073	194.29	±	102.480	1.27	±	0.172	135.52	±	345.710	0.91	13	1.36	±	0.194	1.34	642.75	±	428.920	271.35	7.7	7.7	53.8	30.8
Wood smoke	µg/m^3	7-AE 880 nm	PA 1047 nm	32.2	29.5	0.13	±	0.018	6.36	±	0.414	0.96	±	0.245	3.73	±	8.869	0.65	23	1.21	±	0.691	1.09	2.69	±	24.164	4.98	17.4	21.7	21.7	39.1
	Mm^{-1}	7-AE 880 nm	PA 1047 nm	534.9	147.5	0.43	±	0.059	105.71	±	6.883	3.21	±	0.813	62.03	±	147.390	0.65	23	4.02	±	2.298	3.63	387.39	±	466.440	75.26	4.3	8.7	0.0	87.0
	Mm^{-1}	7-AE 950 nm	PA 1047 nm	492.9	147.5	0.31	±	0.050	92.54	±	5.889	3.04	±	0.783	45.13	±	141.970	0.65	23	3.65	±	2.081	3.34	345.43	±	444.480	70.73	8.7	4.3	0.0	87.0
Carbon Black	µg/m^3	7-AE 880 nm	PA 1047 nm	20.6	24.3	0.73	±	0.229	2.94	±	5.299	0.73	±	0.030	2.92	±	0.760	1.00	3	0.86	±	0.039	0.85	-3.70	±	2.316	2.72	66.7	0.0	33.3	0.0
	Mm^{-1}	7-AE 880 nm	PA 1047 nm	342.3	121.5	2.42	±	0.760	48.89	±	88.058	2.42	±	0.100	48.47	±	12.633	1.00	3	2.85	±	0.130	2.82	220.84	±	60.141	36.28	0.0	0.0	0.0	100.0
	Mm^{-1}	7-AE 950 nm	PA 1047 nm	324.2	121.5	2.27	±	0.718	48.28	±	83.225	2.28	±	0.112	47.87	±	14.152	1.00	3	2.70	±	0.131	2.67	202.74	±	54.111	34.46	0.0	0.0	0.0	100.0
Diesel + NaCl	µg/m^3	7-AE 880 nm	PA 1047 nm	119.8	230.4	0.24	±	0.168	63.43	±	38.483	0.25	±	0.087	62.89	±	20.261	0.73	9	0.52	±	0.041	0.52	-110.61	±	19.755	12.32	0.0	0.0	0.0	100.0
	Mm^{-1}	7-AE 880 nm	PA 1047 nm	1990.4	1151.8	0.81	±	0.558	1053.80	±	639.630	0.82	±	0.291	1045.20	±	336.730	0.73	9	1.74	±	0.138	1.73	838.52	±	99.044	199.97	0.0	0.0	0.0	100.0
	Mm^{-1}	7-AE 950 nm	PA 1047 nm	1829.3	1151.8	0.72	±	0.514	987.09	±	589.620	0.74	±	0.270	979.94	±	312.440	0.72	9	1.60	±	0.130	1.59	677.46	±	95.361	183.86	0.0	0.0	0.0	100.0
Acetylene + NaCl	µg/m^3	7-AE 880 nm	PA 1047 nm	95.7	279.5	0.30	±	0.094	10.36	±	25.772	0.30	±	0.031	10.95	±	8.652	0.97	9	0.34	±	0.012	0.34	-183.84	±	26.677	15.30	0.0	0.0	0.0	100.0
	Mm^{-1}	7-AE 880 nm	PA 1047 nm	1589.9	1397.5	1.01	±	0.313	172.41	±	428.310	1.01	±	0.102	181.90	±	143.800	0.97	9	1.14	±	0.040	1.14	192.36	±	51.354	170.77	33.3	66.7	0.0	0.0
	Mm^{-1}	7-AE 950 nm	PA 1047 nm	1493.0	1397.5	0.97	±	0.294	140.62	±	402.320	0.96	±	0.094	155.67	±	132.360	0.97	9	1.07	±	0.036	1.07	95.50	±	47.957	161.68	88.9	11.1	0.0	0.0
PALAS + NaCl	µg/m^3	7-AE 880 nm	PA 1047 nm	115.7	334.0	0.31	±	0.029	9.60	±	7.804	0.32	±	0.040	7.21	±	14.022	0.95	9	0.35	±	0.036	0.35	-218.25	±	78.371	12.51	0.0	0.0	0.0	100.0
	Mm^{-1}	7-AE 880 nm	PA 1047 nm	1923.1	1669.8	1.04	±	0.095	159.47	±	129.690	1.08	±	0.133	119.81	±	233.040	0.95	9	1.16	±	0.119	1.15	253.28	±	206.600	202.43	44.4	22.2	33.3	0.0
	Mm^{-1}	7-AE 950 nm	PA 1047 nm	1705.8	1669.8	0.95	±	0.084	99.14	±	112.530	0.98	±	0.120	67.77	±	211.070	0.95	9	1.03	±	0.099	1.02	36.02	±	182.780	180.09	77.8	22.2	0.0	0.0
Wood smoke +NaCl	µg/m^3	7-AE 880 nm	PA 1047 nm	12.8	10.6	1.21	±	0.170	-0.16	±	1.685	1.17	±	0.319	0.43	±	3.595	0.73	14	1.21	±	0.432	1.21	2.24	±	4.609	2.19	57.1	14.3	7.1	21.4
	Mm^{-1}	7-AE 880 nm	PA 1047 nm	212.5	52.8	4.04	±	0.564	-2.66	±	28.008	3.89	±	1.060	7.08	±	59.749	0.73	14	4.02	±	1.437	4.03	159.78	±	96.388	25.21	0.0	0.0	0.0	100.0
	Mm^{-1}	7-AE 950 nm	PA 1047 nm	192.8	52.8	3.73	±	0.519	-5.50	±	25.755	3.58	±	0.979	3.88	±	55.168	0.73	14	3.64	±	1.315	3.65	140.02	±	87.836	23.20	0.0	0.0	7.1	92.9

[a] Refer to Table 4-2 for detailed instrumentation and measurements
[b] Effective variable weighted least squares linear regression (Watson et al., 1983) weights variable by precisions in both variables
[c] SE: Standard error defined as the standard deviation divided by the square root of the number of samples
[d] Ordinary least squares linear regression does not weight variables by their precision
[e] Correlation coefficient
[f] SD: Standard deviation
[g] RMS: Root mean squared precision
[h] Fraction of pairs in percent for which the difference is less than or greater than one, two, or three times the propagated measurement uncertainty
[i] Measurement uncertainty of y-x

Table 6-16. Comparison between filter and photoacoustic measurements of source samples.

Source	Unit	Instrument[a] y	Instrument[a] x	Averages y	Averages x	Effective Variance Weighted Regression[b] Slope ± SE[c]	Effective Variance Weighted Regression[b] Intercept ± SE[c]	Ordinary Least Squares Regression[d] Slope ± SE[c]	Ordinary Least Squares Regression[d] Intercept ± SE[c]	r[e]	Number of pairs	Ratio y/x Average ± SD[f]	Ratio Avg y/Avg x	Difference y-x Averge ± SD[f]	RMS[g] Precision	Distribution of y-x[h] (%) <1σ[i]	1σ-2σ	2σ-3σ	>3σ
Diesel	Mm^{-1}	Filter B_{abs}	PA 1047 nm	1803.1	955.3	1.83 ± 0.044	20.63 ± 35.866	1.76 ± 0.116	119.15 ± 115.200	0.94	35	1.89 ± 0.178	1.89	847.82 ± 281.350	100.09	0.0	0.0	0.0	100.0
	$\mu g/m^3$	IMP_A TOR EC	PA 1047 nm	182.4	191.1	0.85 ± 0.136	-34.85 ± 21.017	0.93 ± 0.077	4.23 ± 15.341	0.90	35	0.96 ± 0.152	0.95	-8.62 ± 24.923	64.80	97.1	0.0	0.0	2.9
	$\mu g/m^3$	IMP_A TOT EC	PA 1047 nm	186.6	191.1	0.75 ± 0.141	-106.74 ± 20.930	1.07 ± 0.081	-17.21 ± 16.164	0.92	35	0.97 ± 0.176	0.98	-4.51 ± 26.224	67.45	97.1	0.0	0.0	2.9
	$\mu g/m^3$	STN TOT EC	PA 1047 nm	218.2	220.1	1.04 ± 0.201	-13.16 ± 43.141	1.09 ± 0.233	-22.55 ± 51.660	0.90	7	0.99 ± 0.069	0.99	-1.91 ± 15.208	14.42	85.7	0.0	14.3	0.0
	$\mu g/m^3$	French 2-step EC	PA 1047 nm	207.9	220.1	0.75 ± 0.601	42.50 ± 130.460	0.78 ± 0.085	37.23 ± 18.833	0.97	7	0.95 ± 0.039	0.94	-12.21 ± 8.450	42.30	100.0	0.0	0.0	0.0
Acetylene	Mm^{-1}	Filter B_{abs}	PA 1047 nm	2191.3	1452.2	1.08 ± 0.287	606.21 ± 412.390	1.15 ± 0.366	517.35 ± 533.650	0.74	10	1.51 ± 0.106	1.51	739.11 ± 150.570	127.89	0.0	0.0	0.0	100.0
	$\mu g/m^3$	IMP_A TOR EC	PA 1047 nm	435.5	290.4	1.10 ± 1.636	114.59 ± 470.840	1.12 ± 0.202	111.51 ± 58.832	0.89	10	1.50 ± 0.071	1.50	145.03 ± 16.755	148.47	70.0	30.0	0.0	0.0
	$\mu g/m^3$	IMP_A TOT EC	PA 1047 nm	436.7	290.4	1.13 ± 1.654	106.33 ± 475.730	1.15 ± 0.215	101.67 ± 62.764	0.88	10	1.51 ± 0.072	1.50	146.30 ± 18.069	150.20	60.0	40.0	0.0	0.0
	$\mu g/m^3$	STN TOT EC	PA 1047 nm	424.8	284.5	1.50 ± 0.423	-1.25 ± 118.780	1.49 ± 0.204	-0.08 ± 58.426	0.96	6	1.49 ± 0.042	1.49	140.27 ± 20.485	29.43	0.0	0.0	0.0	100.0
	$\mu g/m^3$	French 2-step EC	PA 1047 nm	397.4	284.5	1.36 ± 1.057	10.55 ± 295.860	1.36 ± 0.154	9.08 ± 43.947	0.98	6	1.40 ± 0.038	1.40	112.88 ± 15.256	79.12	0.0	100.0	0.0	0.0
PALAS	Mm^{-1}	Filter B_{abs}	PA 1047 nm	4501.2	1905.6	2.35 ± 0.095	-2.18 ± 158.070	2.33 ± 0.132	66.15 ± 265.400	0.98	13	2.36 ± 0.137	2.36	2595.60 ± 954.250	296.82	0.0	0.0	0.0	100.0
	$\mu g/m^3$	IMP_A TOR EC	PA 1047 nm	570.6	381.1	1.48 ± 0.271	-4.53 ± 70.510	1.48 ± 0.132	7.93 ± 53.332	0.96	13	1.50 ± 0.142	1.50	189.44 ± 88.447	205.27	38.5	61.5	0.0	0.0
	$\mu g/m^3$	IMP_A TOT EC	PA 1047 nm	606.3	381.1	1.56 ± 0.294	4.74 ± 77.415	1.56 ± 0.129	10.25 ± 52.086	0.96	13	1.59 ± 0.135	1.59	225.15 ± 96.732	219.75	38.5	61.5	0.0	0.0
	$\mu g/m^3$	STN TOT EC	PA 1047 nm	511.7	368.0	1.42 ± 0.096	-17.46 ± 25.791	1.42 ± 0.264	-9.21 ± 102.480	0.97	4	1.38 ± 0.133	1.39	143.76 ± 80.590	35.68	0.0	0.0	25.0	75.0
	$\mu g/m^3$	French 2-step EC	PA 1047 nm	546.2	368.0	1.33 ± 0.323	55.87 ± 93.305	1.34 ± 0.030	54.29 ± 11.569	1.00	4	1.52 ± 0.120	1.48	178.24 ± 48.986	115.03	0.0	100.0	0.0	0.0
Wood smoke	Mm^{-1}	Filter B_{abs}	PA 1047 nm	622.3	147.5	2.98 ± 0.160	139.22 ± 21.533	2.59 ± 0.497	239.92 ± 90.080	0.75	23	5.47 ± 5.587	4.22	474.81 ± 299.330	81.56	0.0	4.3	13.0	82.6
	$\mu g/m^3$	IMP_A TOR EC	PA 1047 nm	57.4	29.5	1.24 ± 0.195	7.73 ± 3.545	1.25 ± 0.267	20.51 ± 9.695	0.71	23	2.69 ± 3.167	1.94	27.86 ± 26.941	23.35	13.0	78.3	8.7	0.0
	$\mu g/m^3$	IMP_A TOT EC	PA 1047 nm	45.5	29.5	1.16 ± 0.173	6.29 ± 3.080	1.19 ± 0.115	10.34 ± 4.175	0.91	23	1.83 ± 0.824	1.54	16.05 ± 12.113	18.49	47.8	47.8	4.3	0.0
	$\mu g/m^3$	STN TOT EC	PA 1047 nm	33.5	34.1	0.82 ± 0.066	5.45 ± 2.209	0.84 ± 0.055	4.84 ± 2.349	0.99	6	1.17 ± 0.311	0.98	-0.56 ± 5.550	4.76	50.0	33.3	16.7	0.0
	$\mu g/m^3$	French 2-step EC	PA 1047 nm	7.6	34.1	0.05 ± 0.222	5.05 ± 9.225	0.06 ± 0.061	5.66 ± 2.640	0.42	6	0.60 ± 0.874	0.22	-26.47 ± 27.449	17.09	50.0	16.7	0.0	33.3
Carbon Black	Mm^{-1}	Filter B_{abs}	PA 1047 nm	114.1	121.5	1.93 ± 1.279	-120.42 ± 162.870	1.92 ± 0.094	-119.48 ± 11.875	1.00	3	0.87 ± 0.307	0.94	-7.42 ± 39.204	76.12	100.0	0.0	0.0	0.0
	$\mu g/m^3$	IMP_A TOR EC	PA 1047 nm	24.1	24.3	0.73 ± 0.826	6.21 ± 18.965	0.73 ± 0.096	6.35 ± 2.420	0.99	3	1.01 ± 0.090	0.99	-0.21 ± 2.426	8.86	100.0	0.0	0.0	0.0
	$\mu g/m^3$	IMP_A TOT EC	PA 1047 nm	17.0	24.3	1.73 ± 0.768	-28.80 ± 16.503	1.30 ± 1.242	-14.67 ± 31.372	0.72	3	0.65 ± 0.577	0.70	-7.33 ± 10.809	7.78	66.7	0.0	0.0	33.3
Diesel + NaCl	Mm^{-1}	Filter B_{abs}	PA 1047 nm	2486.7	1151.8	1.43 ± 0.338	816.20 ± 386.210	1.30 ± 0.554	992.80 ± 641.670	0.66	9	2.17 ± 0.182	2.16	1334.90 ± 187.540	129.56	0.0	0.0	0.0	100.0
	$\mu g/m^3$	IMP_A TOR EC	PA 1047 nm	219.8	230.4	1.00 ± 1.008	-10.93 ± 227.950	1.05 ± 0.191	-23.02 ± 44.175	0.90	9	0.95 ± 0.052	0.95	-10.53 ± 12.727	75.15	100.0	0.0	0.0	0.0
	$\mu g/m^3$	IMP_A TOT EC	PA 1047 nm	224.7	230.4	1.19 ± 1.037	-50.17 ± 233.560	1.22 ± 0.113	-56.43 ± 26.273	0.97	9	0.97 ± 0.041	0.98	-5.71 ± 9.334	77.52	100.0	0.0	0.0	0.0
	$\mu g/m^3$	STN TOT EC	PA 1047 nm	237.3	234.5	1.07 ± 0.324	-13.60 ± 75.183	1.09 ± 0.153	-18.96 ± 35.897	0.96	6	1.01 ± 0.028	1.01	2.77 ± 6.641	15.55	100.0	0.0	0.0	0.0
	$\mu g/m^3$	French 2-step EC	PA 1047 nm	12.4	234.5	-0.12 ± 0.264	38.82 ± 62.268	-0.16 ± 0.257	48.85 ± 60.490	-0.29	6	0.05 ± 0.050	0.05	-222.16 ± 26.341	13.12	0.0	0.0	0.0	100.0
Acetylene + NaCl	Mm^{-1}	Filter B_{abs}	PA 1047 nm	2266.1	1397.5	2.46 ± 0.342	-1190.80 ± 469.110	2.34 ± 0.491	-1005.30 ± 691.650	0.87	9	1.61 ± 0.218	1.62	868.52 ± 354.890	134.18	0.0	0.0	0.0	100.0
	$\mu g/m^3$	IMP_A TOR EC	PA 1047 nm	430.0	279.5	1.58 ± 1.355	-20.60 ± 369.300	1.50 ± 0.428	9.86 ± 120.730	0.80	9	1.54 ± 0.162	1.54	150.51 ± 47.156	148.01	44.4	55.6	0.0	0.0
	$\mu g/m^3$	IMP_A TOT EC	PA 1047 nm	438.6	279.5	1.20 ± 1.396	99.14 ± 383.300	1.27 ± 0.301	82.59 ± 84.799	0.85	9	1.57 ± 0.110	1.57	159.13 ± 32.013	151.54	33.3	66.7	0.0	0.0
	$\mu g/m^3$	STN TOT EC	PA 1047 nm	430.8	277.1	1.33 ± 0.351	61.00 ± 95.551	1.31 ± 0.112	67.48 ± 31.272	0.99	6	1.56 ± 0.045	1.55	153.70 ± 15.606	30.03	0.0	0.0	0.0	100.0
	$\mu g/m^3$	French 2-step EC	PA 1047 nm	140.4	277.1	0.83 ± 0.329	-94.76 ± 87.654	0.80 ± 0.397	-81.34 ± 110.970	0.71	6	0.50 ± 0.126	0.51	-136.69 ± 33.337	33.08	0.0	16.7	0.0	83.3
PALAS + NaCl	Mm^{-1}	Filter B_{abs}	PA 1047 nm	4341.2	1669.8	2.68 ± 0.163	-155.07 ± 260.040	2.69 ± 0.217	-143.80 ± 381.250	0.98	9	2.59 ± 0.254	2.60	2671.40 ± 1021.400	297.47	0.0	0.0	0.0	100.0
	$\mu g/m^3$	IMP_A TOR EC	PA 1047 nm	438.6	334.0	0.21 ± 0.305	208.56 ± 97.076	1.29 ± 0.635	9.13 ± 222.960	0.61	9	1.33 ± 0.488	1.31	104.62 ± 195.500	167.81	33.3	55.6	0.0	11.1
	$\mu g/m^3$	IMP_A TOT EC	PA 1047 nm	430.1	334.0	0.18 ± 0.294	203.84 ± 93.829	1.32 ± 0.657	-9.36 ± 230.570	0.60	9	1.30 ± 0.504	1.29	96.09 ± 202.580	167.79	33.3	44.4	11.1	11.1
	$\mu g/m^3$	STN TOT EC	PA 1047 nm	471.5	327.8	1.54 ± 0.140	-33.65 ± 36.530	1.55 ± 0.056	-35.46 ± 19.542	1.00	3	1.42 ± 0.068	1.44	143.70 ± 74.343	33.13	0.0	0.0	0.0	100.0
	$\mu g/m^3$	French 2-step EC	PA 1047 nm	19.7	327.8	-0.04 ± 0.128	29.25 ± 46.540	-0.02 ± 0.059	27.13 ± 20.459	-0.36	3	0.08 ± 0.059	0.06	-308.13 ± 138.610	23.18	0.0	0.0	0.0	100.0
Wood smoke + NaCl	Mm^{-1}	Filter B_{abs}	PA 1047 nm	280.2	52.8	1.95 ± 0.596	174.55 ± 32.662	1.88 ± 0.902	181.04 ± 50.835	0.52	14	5.94 ± 2.564	5.31	227.45 ± 66.908	40.76	0.0	0.0	0.0	100.0
	$\mu g/m^3$	IMP_A TOR EC	PA 1047 nm	12.4	10.6	0.60 ± 0.306	4.52 ± 2.969	1.05 ± 0.283	1.26 ± 3.188	0.73	14	1.22 ± 0.370	1.17	1.83 ± 4.045	5.10	78.6	21.4	0.0	0.0
	$\mu g/m^3$	IMP_A TOT EC	PA 1047 nm	10.6	10.6	0.85 ± 0.293	-0.54 ± 2.745	0.99 ± 0.273	0.14 ± 3.080	0.72	14	1.03 ± 0.441	1.00	0.01 ± 3.903	4.57	78.6	14.3	0.0	7.1
	$\mu g/m^3$	STN TOT EC	PA 1047 nm	7.2	8.8	0.71 ± 0.357	0.90 ± 3.394	0.71 ± 0.228	0.91 ± 2.188	0.91	4	0.84 ± 0.214	0.81	-1.63 ± 1.912	2.92	75.0	25.0	0.0	0.0
	$\mu g/m^3$	French 2-step EC	PA 1047 nm	5.8	8.8	-0.36 ± 1.727	8.95 ± 16.497	-0.36 ± 0.081	8.95 ± 0.780	-0.95	4	0.90 ± 0.639	0.65	-3.03 ± 6.040	13.27	100.0	0.0	0.0	0.0

[a] Refer to Table 4-2 for detailed instrumentation and measurements

[b] Effective variable weighted least squares linear regression (Watson et al., 1983) weights variable by precisions in both variables

[c] SE: Standard error defined as the standard deviation divided by the square root of the number of samples

[d] Ordinary least squares linear regression does not weight variables by their precision

[e] Correlation coefficient

[f] SD: Standard deviation

Table 6-16. Continued

[g] RMS: Root mean squared precision
[h] Fraction of pairs in percent for which the difference is less than or greater than one, two, or three times the propagated measurement uncertainty
[i] Measurement uncertainty of y-x

Table 6-17. Summary of the equivalence, comparability, and predictability of the source samples.

Condition	Instrument (y)	Instrument (x)	Unit	Diesel	Acetylene	PALAS	Wood smoke	Carbon Black
Pure source	7-AE 880 nm	PA 1047 nm	mg/m^3	NonRelated	NonRelated	Predictable	NonRelated	Comparable
	7-AE 880 nm	PA 1047 nm	Mm^{-1}	NonRelated	NonRelated	Comparable	NonRelated	Comparable
	7-AE 950 nm	PA 1047 nm	Mm^{-1}	NonRelated	NonRelated	Comparable	NonRelated	Comparable
	Filter	PA 1047 nm	Mm^{-1}	Predictable	NonRelated	Predictable	NonRelated	Comparable
	IMP_A TOR EC	PA 1047 nm	mg/m^3	Comparable	NonRelated	Predictable	NonRelated	Comparable
	IMP_A TOT EC	PA 1047 nm	mg/m^3	Comparable	NonRelated	Predictable	Comparable	NonRelated
	STN TOT EC	PA 1047 nm	mg/m^3	Comparable	Comparable	Comparable	Comparable	Not applicable
	French two-step EC	PA 1047 nm	mg/m^3	Comparable	Comparable	Comparable	NonRelated	Not applicable
Source + NaCl	7-AE 880 nm	PA 1047 nm	mg/m^3	NonRelated	Predictable	Predictable	NonRelated	Not applicable
	7-AE 880 nm	PA 1047 nm	Mm^{-1}	NonRelated	NonRelated	Predictable	NonRelated	Not applicable
	7-AE 950 nm	PA 1047 nm	Mm^{-1}	NonRelated	Comparable	Comparable	NonRelated	Not applicable
	Filter	PA 1047 nm	Mm^{-1}	NonRelated	NonRelated	Predictable	NonRelated	Not applicable
	IMP_A TOR EC	PA 1047 nm	mg/m^3	Comparable	NonRelated	NonRelated	NonRelated	Not applicable
	IMP_A TOT EC	PA 1047 nm	mg/m^3	Comparable	NonRelated	NonRelated	NonRelated	Not applicable
	STN TOT EC	PA 1047 nm	mg/m^3	Comparable	Comparable	Predictable	Comparable	Not applicable
	French two-step EC	PA 1047 nm	mg/m^3	NonRelated	NonRelated	NonRelated	NonRelated	Not applicable

Table 6-18. The σ_{abs} for each pure and mixture source.

Source Condition	IMPROVE_A TOR	±	Stdev	IMPROVE_A TOT	±	Stdev	STN TOT	±	Stdev	French two-step	±	Stdev
Diesel	5.12		0.41	5.01		0.25	5.07	±	0.37	5.28	±	0.21
Diesel + NaCl	5.26		0.29	5.15		0.21	4.95	±	0.14	167.02	±	110.95
Acetylene Flame	3.33	±	0.16	3.32	±	0.16	3.35	±	0.10	3.58	±	0.10
Acetylene Flame + NaCl	3.28	±	0.37	3.19	±	0.22	3.21	±	0.09	10.44	±	2.18
Electric Arc	3.37	±	0.35	3.16	±	0.27	3.65	±	0.34	3.31	±	0.24
Electric Arc + NaCl	3.28	±	0.48	3.37	±	0.60	3.53	±	0.17	106.31	±	84.37
Wood Smoke	2.72	±	1.25	3.14	±	1.14	5.00	±	0.89	27.04	±	20.10
Wood Smoke + NaCl	4.47	±	1.44	4.51	±	1.81	6.20	±	1.46	9.07	±	6.63
Carbon Black	4.98	±	0.45	5.18	±	0.87						

Table 6-19. The summary of α for the Angstrom Power Law for each pure and mixed source.

Source Condition	a	±	stdev	r	±	stdev	N
Diesel	0.79	±	0.09	0.983	±	0.029	35
Diesel + NaCl	0.86	±	0.12	0.964	±	0.046	9
Acetylene Flame	0.80	±	0.03	0.990	±	0.002	10
Acetylene Flame + NaCl	0.85	±	0.04	0.989	±	0.005	9
Electric Arc	1.38	±	0.20	0.945	±	0.031	13
Electric Arc + NaCl	1.36	±	0.21	0.888	±	0.065	9
Wood Smoke	1.15	±	0.51	0.981	±	0.039	23
Wood Smoke + NaCl	1.22	±	0.29	0.995	±	0.004	14
Carbon Black	0.53	±	0.01	0.989	±	0.001	3

Table 6-20. Comparison statistics for b_{abs} measurements at Fresno between 8/1/05 and 9/30/05.

Instrument[a] y	Instrument[a] x	Averages y	Averages x	Effective Variance Weighted Regression[b] Slope ± SE[c]	Effective Variance Weighted Regression[b] Intercept ± SE[c]	Ordinary Least Squares Regression[d] Slope ± SE[c]	Ordinary Least Squares Regression[d] Intercept ± SE[c]	r[e]	Number of pairs	Ratio y/x Average ± SD[f]	Ratio Avg y/Avg x	Difference y-x Average ± SD[f]	RMS[g] Precision	Distribution of y-x[h] < 1σ[i]	1σ-2σ	2σ-3σ	>3σ
(Mm^{-1})	(Mm^{-1})	(Mm^{-1})	(Mm^{-1})	(Mm^{-1})		(Mm^{-1})						(Mm^{-1})	(Mm^{-1})	(%)			
7-AE 370 nm	2-AE 370 nm	38.19	35.59	1.044 ± 0.0101	0.265 ± 0.2816	1.110 ± 0.0080	-1.313 ± 0.3333	0.96	1459	1.073 ± 0.17	1.073	2.603 ± 7.016	7.098	76	22	3	0
7-AE 880 nm	2-AE 880 nm	17.27	16.01	1.081 ± 0.0099	-0.260 ± 0.1205	1.145 ± 0.0054	-1.056 ± 0.1022	0.98	1459	1.068 ± 0.11	1.079	1.259 ± 2.564	3.196	90	10	1	0
Filter babs	2-AE 880 nm	17.60	14.84	0.984 ± 0.0801	2.961 ± 1.1581	0.980 ± 0.0571	3.060 ± 0.8955	0.93	49	1.220 ± 0.20	1.186	2.756 ± 2.012	2.970	53	37	10	0
PSAP (adj) 467 nm	7-AE 470 nm	4.18	29.07	0.155 ± 0.0017	-0.416 ± 0.0427	0.159 ± 0.0019	-0.435 ± 0.0666	0.93	1124	0.137 ± 0.03	0.144	-24.893 ± 15.314	3.981	0	0	1	98
PSAP (raw) 467 nm	7-AE 470 nm	12.20	29.07	0.422 ± 0.0040	-0.078 ± 0.0893	0.398 ± 0.0028	0.640 ± 0.0954	0.97	1124	0.420 ± 0.05	0.420	-16.874 ± 11.064	4.123	0	2	10	88
PSAP (adj) 530 nm	7-AE 520 nm	3.36	27.00	0.133 ± 0.0012	-0.318 ± 0.0252	0.137 ± 0.0016	-0.337 ± 0.0523	0.93	1124	0.119 ± 0.03	0.125	-23.638 ± 14.645	3.654	0	0	1	99
PSAP (raw) 530 nm	7-AE 520 nm	10.49	27.00	0.393 ± 0.0036	-0.130 ± 0.0713	0.371 ± 0.0025	0.465 ± 0.0810	0.97	1124	0.388 ± 0.05	0.389	-16.507 ± 10.744	3.771	0	1	6	93
PSAP (adj) 660 nm	7-AE 660 nm	2.61	21.69	0.130 ± 0.0012	-0.273 ± 0.0190	0.135 ± 0.0017	-0.309 ± 0.0437	0.92	1125	0.114 ± 0.03	0.121	-19.074 ± 11.932	2.932	0	0	1	99
PSAP (raw) 660 nm	7-AE 660 nm	8.34	21.70	0.389 ± 0.0035	-0.098 ± 0.0553	0.369 ± 0.0024	0.326 ± 0.0625	0.98	1124	0.384 ± 0.05	0.384	-13.355 ± 8.752	3.027	0	1	6	93
MAAP 670 nm	7-AE 660 nm	7.06	24.64	0.285 ± 0.0039	0.036 ± 0.0803	0.271 ± 0.0015	0.371 ± 0.0452	0.99	946	0.288 ± 0.03	0.286	-17.582 ± 12.845	3.638	0	1	7	91
Filter babs	7-AE 880 nm	17.60	15.88	0.893 ± 0.0725	3.377 ± 1.1175	0.872 ± 0.0520	3.747 ± 0.8765	0.93	49	1.144 ± 0.19	1.108	1.714 ± 2.176	3.062	80	12	8	0
2-AE 670 nm*	PSAP (adj) 670 nm*	19.40	2.56	6.055 ± 0.0592	3.668 ± 0.1152	5.361 ± 0.0678	5.684 ± 0.2193	0.92	1119	8.571 ± 1.98	7.583	16.841 ± 9.721	2.683	0	0	1	98
7-AE 670 nm*	PSAP (adj) 670 nm*	21.39	2.57	6.751 ± 0.0633	3.559 ± 0.1191	6.326 ± 0.0800	5.165 ± 0.2589	0.92	1124	9.317 ± 2.36	8.339	18.827 ± 11.787	2.892	0	0	1	99
PSAP (raw) 670 nm*	PSAP (adj) 670 nm*	8.21	2.57	2.889 ± 0.0193	0.853 ± 0.0297	2.483 ± 0.0224	1.836 ± 0.0725	0.96	1124	3.491 ± 0.56	3.199	5.640 ± 3.286	0.833	0	0	0	100
PA 670 nm*	PSAP (adj) 670 nm*	3.79	2.48	0.898 ± 0.0315	1.534 ± 0.0994	0.909 ± 0.0116	1.535 ± 0.0362	0.92	1070	1.932 ± 0.94	1.527	1.309 ± 0.742	1.968	88	12	0	0
MAAP 670 nm	PSAP (adj) 670 nm*	6.31	2.45	2.129 ± 0.0367	1.040 ± 0.0786	1.927 ± 0.0292	1.596 ± 0.0937	0.94	622	2.890 ± 0.67	2.579	3.865 ± 2.450	1.357	2	27	28	44
Filter babs	PSAP (adj) 670 nm*	17.52	2.51	4.727 ± 0.3409	5.596 ± 0.8498	4.618 ± 0.2854	5.923 ± 0.7810	0.92	47	7.656 ± 2.02	6.978	15.007 ± 4.513	2.201	0	0	2	98
2-AE 670 nm*	PSAP (raw) 670 nm*	19.40	8.18	2.205 ± 0.0209	1.203 ± 0.1307	2.188 ± 0.0150	1.491 ± 0.1447	0.97	1119	2.440 ± 0.29	2.370	11.214 ± 6.612	2.782	0	2	11	87
7-AE 670 nm*	PSAP (raw) 670 nm*	21.39	8.21	2.459 ± 0.0223	0.858 ± 0.1347	2.587 ± 0.0170	0.169 ± 0.1645	0.98	1124	2.647 ± 0.33	2.607	13.187 ± 8.645	2.984	0	1	6	93
PSAP (adj) 670 nm*	PSAP (raw) 670 nm*	2.57	8.21	0.328 ± 0.0022	-0.215 ± 0.0114	0.369 ± 0.0033	-0.463 ± 0.0322	0.96	1124	0.294 ± 0.05	0.313	-5.640 ± 3.286	0.833	0	0	0	100
PA 670 nm*	PSAP (raw) 670 nm*	3.79	8.01	0.357 ± 0.0121	0.894 ± 0.1148	0.361 ± 0.0031	0.901 ± 0.0292	0.96	1070	0.536 ± 0.17	0.473	-4.222 ± 3.244	2.096	27	29	21	23
MAAP 670 nm	PSAP (raw) 670 nm*	6.31	7.99	0.770 ± 0.0128	0.134 ± 0.0887	0.765 ± 0.0048	0.201 ± 0.0464	0.99	622	0.800 ± 0.08	0.790	-1.680 ± 1.460	1.546	52	41	6	0
Filter babs	PSAP (raw) 670 nm*	17.52	7.96	1.647 ± 0.1174	4.315 ± 0.9238	1.635 ± 0.0930	4.497 ± 0.7955	0.93	47	2.332 ± 0.56	2.200	9.556 ± 2.805	2.316	0	2	11	87
2-AE 670 nm*	MAAP 670 nm	21.27	7.06	2.851 ± 0.0397	1.059 ± 0.2355	2.868 ± 0.0159	1.022 ± 0.1359	0.99	946	3.094 ± 0.35	3.013	14.206 ± 9.350	3.258	0	2	14	84
7-AE 670 nm*	MAAP 670 nm	24.30	7.06	3.363 ± 0.0461	0.332 ± 0.2703	3.536 ± 0.0194	-0.662 ± 0.1658	0.99	946	3.463 ± 0.40	3.442	17.239 ± 12.616	3.596	0	1	7	91
PA 670 nm*	MAAP 670 nm	3.87	6.17	0.475 ± 0.0212	0.908 ± 0.1567	0.479 ± 0.0042	0.913 ± 0.0312	0.98	598	0.723 ± 0.21	0.627	-2.301 ± 2.224	2.406	58	31	11	1
PSAP (adj) 670 nm*	MAAP 670 nm	2.45	6.31	0.422 ± 0.0070	-0.271 ± 0.0383	0.454 ± 0.0069	-0.420 ± 0.0525	0.94	622	0.361 ± 0.08	0.388	-3.865 ± 2.450	1.357	2	27	28	44
PSAP (raw) 670 nm*	MAAP 670 nm	7.99	6.31	1.268 ± 0.0210	-0.036 ± 0.1142	1.277 ± 0.0080	-0.069 ± 0.0608	0.99	622	1.261 ± 0.11	1.266	1.680 ± 1.460	1.546	52	41	6	0
Filter babs	MAAP 670 nm	17.12	6.25	2.336 ± 0.2689	2.474 ± 1.6466	2.320 ± 0.1301	2.612 ± 0.8820	0.96	28	2.848 ± 0.47	2.738	10.864 ± 3.938	2.536	0	4	14	82
7-AE 520 nm	PA 532 nm	26.15	5.23	6.262 ± 0.1538	-6.622 ± 0.8533	6.350 ± 0.0556	-7.050 ± 0.3226	0.96	1141	4.736 ± 1.08	5.002	20.921 ± 14.247	4.025	0	4	11	85
PSAP (adj) 530 nm	PA 532 nm	3.26	5.29	0.870 ± 0.0210	-1.315 ± 0.1191	0.881 ± 0.0118	-1.400 ± 0.0694	0.92	1070	0.563 ± 0.19	0.616	-2.031 ± 1.020	1.901	45	51	3	1
PSAP (raw) 530 nm	PA 532 nm	10.26	5.29	2.385 ± 0.0575	-2.278 ± 0.3262	2.381 ± 0.0240	-2.347 ± 0.1406	0.95	1070	1.833 ± 0.45	1.938	4.962 ± 4.003	2.110	24	26	20	31
MAAP 670 nm	PA 532 nm	6.06	5.38	1.468 ± 0.0495	-1.839 ± 0.2838	1.467 ± 0.0159	-1.825 ± 0.0960	0.96	653	1.045 ± 0.28	1.127	0.685 ± 1.684	2.385	87	12	1	0
Filter babs	PA 532 nm	17.37	5.21	3.144 ± 0.6511	1.172 ± 3.4943	3.188 ± 0.2698	0.771 ± 1.4571	0.87	47	3.340 ± 0.62	3.336	12.161 ± 4.123	2.873	0	11	9	81
2-AE 670 nm*	PA 670 nm*	18.95	3.76	5.857 ± 0.1957	-2.869 ± 0.8115	5.839 ± 0.0482	-2.979 ± 0.2026	0.97	1081	4.832 ± 0.97	5.046	15.195 ± 9.556	3.275	1	9	13	77
7-AE 670 nm*	PA 670 nm*	20.87	3.76	6.914 ± 0.2297	-4.991 ± 0.9548	6.939 ± 0.0486	-5.245 ± 0.2044	0.97	1086	5.241 ± 1.07	5.546	17.109 ± 11.546	3.437	1	6	13	80
PSAP (adj) 670 nm*	PA 670 nm*	2.48	3.79	0.942 ± 0.0308	-1.057 ± 0.1296	0.938 ± 0.0119	-1.072 ± 0.0505	0.92	1070	0.593 ± 0.20	0.655	-1.309 ± 0.742	1.968	88	12	0	0
PSAP (raw) 670 nm*	PA 670 nm*	8.01	3.79	2.592 ± 0.0846	-1.710 ± 0.3564	2.571 ± 0.0220	-1.734 ± 0.0931	0.96	1070	1.995 ± 0.46	2.114	4.222 ± 3.244	2.096	27	29	21	23
MAAP 670 nm	PA 670 nm*	6.17	3.87	2.005 ± 0.0882	-1.525 ± 0.3799	1.996 ± 0.0174	-1.555 ± 0.0762	0.98	598	1.481 ± 0.35	1.594	2.301 ± 2.224	2.406	58	31	11	1
Filter babs	PA 670 nm*	17.30	3.69	4.645 ± 1.1014	0.002 ± 4.1788	4.473 ± 0.3751	0.803 ± 1.4368	0.87	46	4.693 ± 0.84	4.690	13.609 ± 4.473	2.750	0	4	9	87
7-AE 950 nm	PA 1047 nm	14.69	1.98	8.154 ± 0.2328	-1.443 ± 0.4929	8.200 ± 0.0526	-1.514 ± 0.1197	0.98	1140	7.201 ± 1.20	7.434	12.711 ± 8.353	2.215	0	2	6	92
PA 532 nm	PA 1047 nm	5.25	1.94	2.181 ± 0.0794	0.999 ± 0.1732	2.180 ± 0.0189	1.015 ± 0.0424	0.96	1086	2.852 ± 0.49	2.702	3.309 ± 1.485	2.103	20	57	19	4
Filter babs	PA 1047 nm	18.90	2.05	6.790 ± 2.3087	4.944 ± 4.8533	6.810 ± 0.7692	4.910 ± 1.6366	0.86	30	9.411 ± 1.51	9.201	16.844 ± 4.008	2.417	0	0	0	100

[a] Refer to Table 4-2 for detailed instrumentation and measurements; Filter b_{abs} refers to light absorption measured by densitometry on Teflon filters; Data used here is an average of different integrated samplers. For 2-AE, 7-AE, and MAAP, BC ($\mu g/m^3$) was converted to b_{abs} (Mm^{-1}) based on manufacturer-supplied default values.

[b] Effective variance weighted least squares linear regression (Watson et al., 1984) weights variable by precisions in both variables

[c] SE: Standard error

[d] Ordinary least squares linear regression does not weight variables by their precisions

[e] Correlation coefficient

[f] SD: Standard deviation

[g] RMS: Root mean squared precision

Table 6-20. Continued.

[h] Fraction of pairs in percent for which the difference is less than or greater than one, two, or three times the propagated measurement uncertainty
[i] Measurement uncertainty of (y-x)
* b_{abs} scaled to 670 nm using wavelength dependence shown by the respective instrument

Table 6-21. Comparison statistics for BC concentration measurements at Fresno between 8/1/05 and 9/30/05.

Instrument[a]		Averages		Effective Variance Weighted Regression[b]		Ordinary Least Squares Regression[d]			Number	Ratio y/x		Ratio	Difference y-x		RMS[g]	Distribution of y-x (%)[h]			
y	x	y	x	Slope ± SE[c]	Intercept ± SE[c]	Slope ± SE[c]	Intercept ± SE[c]	r^2[e]	of pairs	Average ± SD[f]		Avg y/Avg x	Average ± SD[f]		Precision	< 1σ[i]	1σ-2σ	2σ-3σ	>3σ
(µg/m³)	(µg/m³)	(µg/m³)	(µg/m³)	(µg/m³)		(µg/m³)							(µg/m³)		(µg/m³)				
7-AE 370 nm	2-AE 370 nm	0.97	0.90	1.044 ± 0.0101	0.007 ± 0.0071	1.110 ± 0.0080	-0.033 ± 0.0084	0.96	1459	1.073 ± 0.17		1.073	0.066 ± 0.177		0.180	76	22	2	0
2-AE 370 nm	2-AE 880 nm	0.90	0.96	0.900 ± 0.0085	0.033 ± 0.0064	0.882 ± 0.0032	0.051 ± 0.0037	0.99	1459	0.951 ± 0.08		0.935	-0.063 ± 0.105		0.179	92	8	0	0
7-AE 880 nm	2-AE 880 nm	1.04	0.96	1.081 ± 0.0099	-0.016 ± 0.0073	1.145 ± 0.0054	-0.064 ± 0.0062	0.98	1459	1.068 ± 0.11		1.079	0.076 ± 0.154		0.192	90	10	1	0
7-AE 370 nm	7-AE 880 nm	0.97	1.04	0.885 ± 0.0082	0.043 ± 0.0064	0.870 ± 0.0036	0.062 ± 0.0046	0.99	1464	0.951 ± 0.10		0.930	-0.073 ± 0.135		0.193	85	15	0	0
Filter IMPROVE_A_ TOR	2-AE 880 nm	1.01	0.89	1.203 ± 0.1240	-0.116 ± 0.0872	1.186 ± 0.0819	-0.050 ± 0.0773	0.90	49	1.111 ± 0.22		1.129	0.115 ± 0.183		0.364	94	6	0	0
Filter IMPROVE_A_ TOT	2-AE 880 nm	0.76	0.89	0.858 ± 0.0858	-0.043 ± 0.0642	0.832 ± 0.0774	0.022 ± 0.0731	0.84	49	0.851 ± 0.20		0.856	-0.128 ± 0.172		0.251	73	22	4	0
Filter STN_ TOR	2-AE 880 nm	0.82	0.90	0.815 ± 0.1635	0.065 ± 0.1264	0.873 ± 0.0911	0.034 ± 0.0882	0.92	18	0.925 ± 0.14		0.912	-0.080 ± 0.139		0.276	94	6	0	0
Filter STN_ TOT	2-AE 880 nm	0.57	0.90	0.518 ± 0.1220	0.081 ± 0.0946	0.558 ± 0.0630	0.063 ± 0.0609	0.91	18	0.645 ± 0.11		0.628	-0.335 ± 0.183		0.231	39	39	22	0
HiVol by French	2-AE 880 nm	0.87	0.94	0.670 ± 0.1235	0.203 ± 0.1018	0.789 ± 0.1705	0.128 ± 0.1765	0.88	8	1.002 ± 0.27		0.925	-0.070 ± 0.218		0.196	75	13	13	0
Filter IMPROVE_A_ TOR	7-AE 880 nm	1.01	0.96	1.122 ± 0.1154	-0.115 ± 0.0864	1.049 ± 0.0760	0.006 ± 0.0771	0.90	49	1.043 ± 0.22		1.055	0.053 ± 0.181		0.367	92	8	0	0
Filter IMPROVE_A_ TOT	7-AE 880 nm	0.76	0.96	0.801 ± 0.0798	-0.042 ± 0.0635	0.742 ± 0.0695	0.056 ± 0.0705	0.84	49	0.799 ± 0.19		0.800	-0.191 ± 0.187		0.255	55	41	2	2
Filter STN_ TOR	7-AE 880 nm	0.82	0.98	0.729 ± 0.1455	0.084 ± 0.1216	0.765 ± 0.0817	0.070 ± 0.0867	0.92	18	0.852 ± 0.12		0.836	-0.161 ± 0.165		0.281	83	17	0	0
Filter STN_ TOT	7-AE 880 nm	0.57	0.98	0.468 ± 0.1110	0.088 ± 0.0933	0.494 ± 0.0532	0.081 ± 0.0565	0.92	18	0.596 ± 0.11		0.576	-0.417 ± 0.225		0.237	22	28	50	0
HiVol by French	7-AE 880 nm	0.87	1.04	0.577 ± 0.1079	0.226 ± 0.0981	0.675 ± 0.1590	0.168 ± 0.1830	0.87	8	0.914 ± 0.25		0.837	-0.169 ± 0.270		0.203	50	38	0	13
2-AE 880 nm	MAAP 670 nm	1.00	1.07	0.891 ± 0.0123	0.039 ± 0.0110	0.903 ± 0.0048	0.031 ± 0.0062	0.99	946	0.952 ± 0.11		0.932	-0.073 ± 0.128		0.253	95	5	0	0
7-AE 660 nm	MAAP 670 nm	1.11	1.07	1.015 ± 0.0139	0.016 ± 0.0124	1.067 ± 0.0059	-0.029 ± 0.0076	0.99	946	1.046 ± 0.12		1.040	0.043 ± 0.141		0.262	98	2	0	0
7-AE 880 nm	MAAP 670 nm	1.10	1.07	1.009 ± 0.0138	0.010 ± 0.0123	1.067 ± 0.0057	-0.041 ± 0.0074	0.99	946	1.033 ± 0.12		1.029	0.031 ± 0.138		0.261	98	2	0	0
PA 532 nm	MAAP 670 nm	0.54	0.92	0.416 ± 0.0143	0.155 ± 0.0150	0.418 ± 0.0045	0.154 ± 0.0050	0.96	653	0.686 ± 0.21		0.585	-0.381 ± 0.373		0.281	47	28	19	6
PA 1047 nm	MAAP 670 nm	0.40	0.96	0.369 ± 0.0141	0.048 ± 0.0148	0.375 ± 0.0029	0.044 ± 0.0033	0.98	622	0.456 ± 0.10		0.420	-0.555 ± 0.409		0.280	26	32	25	17
Sunset Thermal EC	MAAP 670 nm	0.65	1.05	0.655 ± 0.0195	-0.056 ± 0.0196	0.625 ± 0.0128	-0.003 ± 0.0160	0.88	665	0.586 ± 0.36		0.622	-0.397 ± 0.339		0.335	39	46	14	1
Sunset Optical BC	MAAP 670 nm	0.52	0.99	0.560 ± 0.0151	-0.031 ± 0.0158	0.566 ± 0.0040	-0.035 ± 0.0048	0.98	734	0.516 ± 0.06		0.531	-0.463 ± 0.303		0.296	30	44	24	2
Filter IMPROVE_A_ TOR	MAAP 670 nm	0.96	0.95	1.072 ± 0.1554	-0.076 ± 0.1209	1.047 ± 0.0597	-0.031 ± 0.0613	0.96	28	0.994 ± 0.18		1.013	0.013 ± 0.124		0.376	100	0	0	0
Filter IMPROVE_A_ TOT	MAAP 670 nm	0.73	0.95	0.758 ± 0.1072	-0.016 ± 0.0871	0.753 ± 0.0698	0.012 ± 0.0717	0.90	28	0.759 ± 0.17		0.766	-0.222 ± 0.175		0.288	71	25	4	0
Filter STN_ TOR	MAAP 670 nm	0.83	0.98	0.699 ± 0.1717	0.125 ± 0.1482	0.738 ± 0.0893	0.105 ± 0.0954	0.92	14	0.877 ± 0.15		0.845	-0.153 ± 0.175		0.323	86	14	0	0
Filter STN_ TOT	MAAP 670 nm	0.58	0.98	0.502 ± 0.1322	0.078 ± 0.1113	0.517 ± 0.0595	0.076 ± 0.0636	0.93	14	0.614 ± 0.10		0.594	-0.400 ± 0.227		0.288	36	50	14	0
HiVol by French	MAAP 670 nm	0.89	1.07	0.632 ± 0.1339	0.185 ± 0.1290	0.727 ± 0.1715	0.118 ± 0.2018	0.88	7	0.919 ± 0.27		0.838	-0.173 ± 0.253		0.259	71	14	14	0
7-AE 660 nm	MAAP-A 670 nm	1.11	1.25	0.872 ± 0.0115	0.004 ± 0.0116	0.913 ± 0.0078	-0.029 ± 0.0118	0.97	946	0.889 ± 0.14		0.890	-0.137 ± 0.215		0.278	74	25	1	0
MAAP-A 670 nm	MAAP 670 nm	1.25	1.07	1.098 ± 0.0174	0.064 ± 0.0161	1.109 ± 0.0093	0.063 ± 0.0121	0.97	946	1.197 ± 0.18		1.168	0.180 ± 0.225		0.316	76	24	0	0
2-AE 880 nm	PA 532 nm	0.88	0.52	2.030 ± 0.0500	-0.179 ± 0.0277	2.035 ± 0.0195	-0.185 ± 0.0113	0.95	1136	1.600 ± 0.37		1.680	0.355 ± 0.308		0.223	36	32	21	10
7-AE 520 nm	PA 532 nm	0.93	0.52	2.227 ± 0.0547	-0.236 ± 0.0303	2.258 ± 0.0198	-0.251 ± 0.0115	0.96	1141	1.684 ± 0.38		1.778	0.407 ± 0.358		0.227	32	32	21	15
7-AE 880 nm	PA 532 nm	0.94	0.52	2.296 ± 0.0563	-0.263 ± 0.0312	2.328 ± 0.0201	-0.279 ± 0.0117	0.96	1141	1.690 ± 0.39		1.794	0.415 ± 0.375		0.228	33	32	19	16
MAAP 670 nm	PA 532 nm	0.92	0.54	2.225 ± 0.0750	-0.279 ± 0.0430	2.222 ± 0.0241	-0.277 ± 0.0145	0.96	653	1.583 ± 0.43		1.708	0.381 ± 0.373		0.281	47	28	19	6
MAAP-A 670 nm	PA 532 nm	1.09	0.54	2.453 ± 0.0824	-0.237 ± 0.0472	2.460 ± 0.0352	-0.236 ± 0.0212	0.94	653	1.902 ± 0.52		2.020	0.549 ± 0.466		0.293	37	22	23	18
PA 1047 nm	PA 532 nm	0.39	0.53	0.846 ± 0.0311	-0.055 ± 0.0176	0.848 ± 0.0074	-0.057 ± 0.0043	0.96	1086	0.721 ± 0.12		0.740	-0.136 ± 0.072		0.269	97	3	0	0
Sunset Thermal EC	PA 532 nm	0.62	0.55	1.485 ± 0.0509	-0.208 ± 0.0286	1.470 ± 0.0351	-0.181 ± 0.0211	0.80	1015	1.043 ± 0.66		1.139	0.076 ± 0.307		0.319	69	30	1	0
Sunset Optical BC	PA 532 nm	0.51	0.52	1.300 ± 0.0400	-0.171 ± 0.0226	1.305 ± 0.0154	-0.176 ± 0.0089	0.93	1133	0.899 ± 0.28		0.969	-0.016 ± 0.151		0.285	94	6	0	0
Filter IMPROVE_A_ TOR	PA 532 nm	1.00	0.52	2.403 ± 0.5724	-0.270 ± 0.2950	2.332 ± 0.2317	-0.212 ± 0.1251	0.83	47	1.874 ± 0.53		1.924	0.481 ± 0.297		0.391	34	64	2	0
Filter IMPROVE_A_ TOT	PA 532 nm	0.77	0.52	1.794 ± 0.4141	-0.171 ± 0.2158	1.767 ± 0.1784	-0.149 ± 0.0964	0.83	47	1.445 ± 0.41		1.480	0.250 ± 0.206		0.290	53	47	0	0
Filter STN_ TOR	PA 532 nm	0.81	0.53	1.829 ± 0.6497	-0.171 ± 0.3432	1.849 ± 0.2151	-0.174 ± 0.1199	0.91	17	1.484 ± 0.27		1.522	0.278 ± 0.204		0.314	76	24	0	0
Filter STN_ TOT	PA 532 nm	0.55	0.53	1.124 ± 0.4413	-0.051 ± 0.2291	1.176 ± 0.1381	-0.071 ± 0.0770	0.91	17	1.029 ± 0.18		1.043	0.023 ± 0.096		0.275	100	0	0	0
HiVol by French	PA 532 nm	0.82	0.55	1.642 ± 0.6405	-0.073 ± 0.3631	1.673 ± 0.3497	-0.096 ± 0.2057	0.91	7	1.485 ± 0.27		1.497	0.273 ± 0.237		0.246	57	29	14	0

Table 6-21. Continued.

Instrument[a] y	Instrument[a] x	Averages y	Averages x	Effective Variance Weighted Regression[b] Slope ± SE[c]	Effective Variance Weighted Regression[b] Intercept ± SE[c]	Ordinary Least Squares Regression[d] Slope ± SE[c]	Ordinary Least Squares Regression[d] Intercept ± SE[c]	r[e]	Number of pairs	Ratio y/x Average ± SD[f]	Ratio Avg y/Avg x	Difference y-x Average ± SD[f]	RMS[g] Precision	Distribution of y-x (%)[h] < 1σ[i]	1σ-2σ	2σ-3σ	>3σ
(μg/m³)	(μg/m³)	(μg/m³)	(μg/m³)		(μg/m³)		(μg/m³)					(μg/m³)	(μg/m³)				
2-AE 880 nm	PA 1047 nm	0.90	0.39	2.367 ± 0.0679	-0.031 ± 0.0287	2.351 ± 0.0177	-0.024 ± 0.0080	0.97	1135	2.247 ± 0.38	2.290	0.508 ± 0.332	0.228	16	33	30	22
7-AE 880 nm	PA 1047 nm	0.96	0.40	2.673 ± 0.0763	-0.093 ± 0.0323	2.688 ± 0.0173	-0.098 ± 0.0079	0.98	1140	2.365 ± 0.39	2.440	0.569 ± 0.402	0.233	13	31	28	27
7-AE 950 nm	PA 1047 nm	0.95	0.40	2.648 ± 0.0756	-0.094 ± 0.0320	2.663 ± 0.0171	-0.098 ± 0.0078	0.98	1140	2.339 ± 0.39	2.415	0.559 ± 0.397	0.232	14	32	28	26
MAAP 670 nm	PA 1047 nm	0.96	0.40	2.603 ± 0.0979	-0.092 ± 0.0423	2.576 ± 0.0197	-0.079 ± 0.0093	0.98	622	2.276 ± 0.41	2.380	0.555 ± 0.409	0.280	26	32	25	17
MAAP-A 670 nm	PA 1047 nm	1.13	0.40	2.916 ± 0.1093	-0.044 ± 0.0471	2.887 ± 0.0316	-0.031 ± 0.0149	0.96	622	2.728 ± 0.52	2.811	0.728 ± 0.506	0.293	16	27	23	34
PA 532 nm	PA 1047 nm	0.53	0.39	1.091 ± 0.0397	0.100 ± 0.0173	1.090 ± 0.0095	0.102 ± 0.0042	0.96	1086	1.426 ± 0.24	1.351	0.136 ± 0.072	0.269	97	3	0	0
Sunset Thermal EC	PA 1047 nm	0.64	0.41	1.742 ± 0.0643	-0.097 ± 0.0278	1.699 ± 0.0376	-0.062 ± 0.0177	0.82	1025	1.445 ± 0.89	1.550	0.228 ± 0.315	0.324	60	37	3	0
Sunset Optical BC	PA 1047 nm	0.52	0.39	1.508 ± 0.0509	-0.073 ± 0.0220	1.507 ± 0.0151	-0.071 ± 0.0069	0.95	1132	1.261 ± 0.32	1.326	0.128 ± 0.161	0.289	88	11	2	0
Filter IMPROVE_A_ TOR	PA 1047 nm	1.12	0.41	2.704 ± 1.0396	-0.013 ± 0.4244	2.625 ± 0.3518	0.042 ± 0.1497	0.82	30	2.723 ± 0.54	2.727	0.709 ± 0.279	0.421	3	80	17	0
Filter IMPROVE_A_ TOT	PA 1047 nm	0.83	0.41	1.773 ± 0.6793	0.088 ± 0.2793	1.759 ± 0.3070	0.112 ± 0.1306	0.73	30	2.043 ± 0.45	2.033	0.424 ± 0.203	0.304	20	77	3	0
Filter STN_ TOR	PA 1047 nm	0.91	0.43	2.085 ± 1.0939	-0.003 ± 0.4674	2.073 ± 0.5200	0.019 ± 0.2362	0.83	9	2.107 ± 0.46	2.118	0.481 ± 0.272	0.332	22	56	22	0
Filter STN_ TOT	PA 1047 nm	0.63	0.43	1.118 ± 0.6791	0.133 ± 0.2834	1.173 ± 0.2646	0.121 ± 0.1202	0.86	9	1.494 ± 0.25	1.454	0.195 ± 0.112	0.286	89	11	0	0
HiVol by French	PA 1047 nm	1.16	0.51	2.205 ± 1.6768	0.026 ± 0.8692	2.230 ± 0.3768	0.015 ± 0.2018	0.99	3	2.270 ± 0.14	2.259	0.644 ± 0.251	0.265	0	33	33	33
2-AE 880 nm	Sunset Thermal EC	0.97	0.65	0.896 ± 0.0177	0.356 ± 0.0112	0.986 ± 0.0198	0.332 ± 0.0160	0.83	1120	25.165 ± 78.03	1.498	0.323 ± 0.320	0.292	41	39	17	3
7-AE 880 nm	Sunset Thermal EC	1.05	0.65	0.987 ± 0.0194	0.360 ± 0.0122	1.139 ± 0.0236	0.307 ± 0.0192	0.82	1125	26.833 ± 82.50	1.609	0.397 ± 0.389	0.297	35	38	22	5
MAAP 670 nm	Sunset Thermal EC	1.05	0.65	1.111 ± 0.0310	0.287 ± 0.0199	1.253 ± 0.0256	0.232 ± 0.0208	0.88	665	21.304 ± 65.98	1.608	0.397 ± 0.339	0.335	39	46	14	1
MAAP-A 670 nm	Sunset Thermal EC	1.23	0.65	1.245 ± 0.0342	0.374 ± 0.0218	1.406 ± 0.0313	0.313 ± 0.0253	0.87	665	25.617 ± 76.00	1.886	0.578 ± 0.433	0.347	25	39	29	7
PA 532 nm	Sunset Thermal EC	0.55	0.62	0.431 ± 0.0154	0.274 ± 0.0112	0.432 ± 0.0103	0.278 ± 0.0080	0.80	1015	18.641 ± 53.21	0.878	-0.076 ± 0.307	0.319	69	30	1	0
PA 1047 nm	Sunset Thermal EC	0.41	0.64	0.383 ± 0.0152	0.164 ± 0.0112	0.392 ± 0.0087	0.162 ± 0.0069	0.82	1025	12.113 ± 35.88	0.645	-0.228 ± 0.315	0.324	60	37	3	0
Sunset Optical BC	Sunset Thermal EC	0.56	0.65	0.616 ± 0.0179	0.154 ± 0.0129	0.645 ± 0.0124	0.144 ± 0.0100	0.84	1125	13.194 ± 40.56	0.866	-0.087 ± 0.264	0.340	82	18	0	0
Filter IMPROVE_A_ TOR	Sunset Thermal EC	1.03	0.59	1.174 ± 0.2070	0.293 ± 0.1115	1.192 ± 0.1083	0.329 ± 0.0705	0.85	47	2.384 ± 2.39	1.751	0.441 ± 0.212	0.432	45	51	4	0
Filter IMPROVE_A_ TOT	Sunset Thermal EC	0.78	0.59	0.816 ± 0.1405	0.267 ± 0.0784	0.821 ± 0.0962	0.299 ± 0.0627	0.79	47	1.867 ± 1.97	1.330	0.194 ± 0.189	0.339	79	17	4	0
Filter STN_ TOR	Sunset Thermal EC	0.85	0.59	0.896 ± 0.2632	0.299 ± 0.1451	0.963 ± 0.1149	0.279 ± 0.0765	0.91	17	2.012 ± 2.13	1.433	0.257 ± 0.139	0.358	71	29	0	0
Filter STN_ TOT	Sunset Thermal EC	0.59	0.59	0.497 ± 0.1850	0.273 ± 0.1011	0.579 ± 0.0810	0.246 ± 0.0540	0.88	17	1.516 ± 1.88	0.994	-0.004 ± 0.163	0.324	94	6	0	0
HiVol by French	Sunset Thermal EC	0.94	0.66	0.696 ± 0.2429	0.436 ± 0.1570	0.830 ± 0.3070	0.389 ± 0.2280	0.77	7	3.159 ± 4.93	1.420	0.277 ± 0.262	0.304	71	14	14	0
2-AE 880 nm	Sunset Optical BC	0.92	0.53	1.495 ± 0.0302	0.124 ± 0.0171	1.499 ± 0.0115	0.125 ± 0.0074	0.97	1242	1.841 ± 0.31	1.734	0.389 ± 0.236	0.249	25	52	21	2
7-AE 660 nm	Sunset Optical BC	1.00	0.53	1.683 ± 0.0339	0.101 ± 0.0193	1.729 ± 0.0146	0.082 ± 0.0094	0.96	1247	1.975 ± 0.33	1.883	0.469 ± 0.328	0.255	19	46	27	9
7-AE 880 nm	Sunset Optical BC	0.99	0.53	1.684 ± 0.0339	0.091 ± 0.0193	1.732 ± 0.0143	0.071 ± 0.0092	0.96	1247	1.952 ± 0.33	1.865	0.459 ± 0.327	0.254	21	46	25	8
MAAP 670 nm	Sunset Optical BC	0.99	0.52	1.721 ± 0.0461	0.085 ± 0.0259	1.704 ± 0.0121	0.094 ± 0.0079	0.98	734	1.968 ± 0.25	1.885	0.463 ± 0.303	0.296	30	44	24	2
MAAP-A 670 nm	Sunset Optical BC	1.16	0.52	1.903 ± 0.0508	0.161 ± 0.0284	1.902 ± 0.0206	0.165 ± 0.0134	0.96	734	2.369 ± 0.41	2.217	0.637 ± 0.414	0.309	16	37	33	14
PA 532 nm	Sunset Optical BC	0.52	0.51	0.660 ± 0.0205	0.185 ± 0.0123	0.661 ± 0.0078	0.187 ± 0.0048	0.93	1133	1.243 ± 0.46	1.032	0.016 ± 0.151	0.285	94	6	0	0
PA 1047 nm	Sunset Optical BC	0.39	0.52	0.592 ± 0.0204	0.084 ± 0.0122	0.596 ± 0.0060	0.083 ± 0.0038	0.95	1132	0.847 ± 0.24	0.754	-0.128 ± 0.161	0.289	88	11	2	0
Filter IMPROVE_A_ TOR	Sunset Optical BC	1.01	0.52	1.672 ± 0.3075	0.114 ± 0.1543	1.602 ± 0.1328	0.181 ± 0.0749	0.87	48	1.992 ± 0.45	1.950	0.493 ± 0.241	0.406	27	73	0	0
Filter IMPROVE_A_ TOT	Sunset Optical BC	0.77	0.52	1.141 ± 0.2064	0.150 ± 0.1059	1.108 ± 0.1214	0.194 ± 0.0684	0.80	48	1.533 ± 0.40	1.481	0.250 ± 0.185	0.308	58	42	0	0
Filter STN_ TOR	Sunset Optical BC	0.82	0.53	1.154 ± 0.3200	0.201 ± 0.1636	1.176 ± 0.1254	0.202 ± 0.0738	0.92	18	1.686 ± 0.36	1.558	0.294 ± 0.142	0.327	67	33	0	0
Filter STN_ TOT	Sunset Optical BC	0.57	0.53	0.668 ± 0.2144	0.194 ± 0.1075	0.713 ± 0.1048	0.191 ± 0.0616	0.86	18	1.185 ± 0.30	1.074	0.039 ± 0.136	0.290	94	6	0	0
HiVol by French	Sunset Optical BC	0.87	0.55	1.112 ± 0.3264	0.249 ± 0.1856	1.169 ± 0.2061	0.231 ± 0.1289	0.92	8	1.887 ± 0.69	1.592	0.323 ± 0.174	0.260	25	63	13	0

[a] Refer to Table 4-2 for detailed instrumentation and measurements; MAAP-A refers to BC concentration estimated using aethalometer algorithm of 14625/λ. Filter EC data used here is an average of different integrated samplers, analyzed by the protocol indicated in the Table: Interagency Monitoring of Protected Visual Environments (IMPROVE) Thermal Optical Reflectance (TOR) and Transmittance (TOT) and Speciation Trends Network (STN) Thermal Optical Reflectance (TOR) and Transmittance (TOT) protocols. Cachier's French two-step protocol (Cachier et al., 1989a; Cachier et al., 1989b) was used only on samples from Andersen high volume (HiVol) sampler.

[b] Effective variance weighted least squares linear regression (Watson et al., 1984) weights variable by precisions in both variables

[c] SE: Standard error

[d] Ordinary least squares linear regression does not weight variables by their precisions

[e] Correlation coefficient

[f] SD: Standard deviation

[g] RMS: Root mean squared precision

[h] Fraction of pairs in percent for which the difference is less than or greater than one, two, or three times the propagated measurement uncertainty

[i] Measurement uncertainty of (y-x)

* b_{abs} scaled to 670 nm using wavelength dependence shown by the respective instrument

Table 6-22. Comparison between b_{abs} and BC concentrations measurements at Fresno between 8/1/05 and 9/30/05.

Instrument[a]		Averages		Effective Variance Weighted Regression[b]				Ordinary Least Squares Regression[d]					Number	Ratio y/x	Ratio
y	x	y	x	Slope ± SE[c]		Intercept ± SE[c]		Slope ± SE[c]		Intercept ± SE[c]		r^2	of pairs	Average ± SD[f]	Avg y/Avg x
(Mm^{-1})	($\mu g/m^3$)	(Mm^{-1})	($\mu g/m^3$)	(m^2/g)		(Mm^{-1})		(m^2/g)		(Mm^{-1})				(m^2/g)	(m^2/g)
2-AE 880 nm	Filter IMPROVE_A_ TOR	14.84	1.01	11.996 ±	1.2003	2.755 ±	0.9224	11.449 ±	0.7910	3.295 ±	0.8585	0.90	49	15.716 ±	4.05	14.716
2-AE 880 nm	Filter IMPROVE_A_ TOT	14.84	0.76	15.324 ±	1.4680	2.966 ±	0.9227	14.197 ±	1.3203	3.983 ±	1.0855	0.84	49	20.799 ±	5.88	19.406
2-AE 880 nm	Filter STN_ TOR	15.00	0.82	18.287 ±	3.5339	0.026 ±	2.4568	16.205 ±	1.6911	1.668 ±	1.4997	0.92	18	18.306 ±	2.49	18.233
2-AE 880 nm	Filter STN_ TOT	15.00	0.57	27.192 ±	6.0123	-0.431 ±	2.8999	24.741 ±	2.7912	0.967 ±	1.6923	0.91	18	26.439 ±	4.42	26.446
2-AE 880 nm	HiVol by French	15.61	0.87	19.408 ±	3.3882	-1.487 ±	2.5260	16.456 ±	3.5566	1.312 ±	3.3849	0.88	8	17.793 ±	5.27	17.966
7-AE 880 nm	Filter IMPROVE_A_ TOR	15.88	1.01	12.762 ±	1.2715	2.996 ±	0.9699	12.707 ±	0.9202	3.068 ±	0.9987	0.90	49	16.806 ±	4.43	15.749
7-AE 880 nm	Filter IMPROVE_A_ TOT	15.88	0.76	16.345 ±	1.5569	3.174 ±	0.9716	15.865 ±	1.4861	3.749 ±	1.2218	0.84	49	22.254 ±	6.56	20.768
7-AE 880 nm	Filter STN_ TOR	16.35	0.82	20.504 ±	3.9395	-0.465 ±	2.7268	18.369 ±	1.9606	1.240 ±	1.7387	0.92	18	19.850 ±	2.64	19.876
7-AE 880 nm	Filter STN_ TOT	16.35	0.57	29.636 ±	6.5487	-0.551 ±	3.1516	28.355 ±	3.0531	0.269 ±	1.8511	0.92	18	28.755 ±	5.10	28.829
7-AE 880 nm	HiVol by French	17.24	0.87	21.434 ±	3.7412	-1.684 ±	2.7631	18.467 ±	4.3478	1.199 ±	4.1379	0.87	8	19.645 ±	6.28	19.848
MAAP 670 nm	2-AE 880 nm	7.06	1.00	7.219 ±	0.1003	-0.158 ±	0.0837	7.119 ±	0.0374	-0.039 ±	0.0450	0.99	946	7.014 ±	0.73	7.081
MAAP 670 nm	7-AE 660 nm	7.06	1.11	6.318 ±	0.0871	0.036 ±	0.0803	6.014 ±	0.0331	0.371 ±	0.0452	0.99	946	6.384 ±	0.68	6.348
MAAP 670 nm	7-AE 880 nm	7.06	1.10	6.364 ±	0.0878	0.067 ±	0.0800	6.024 ±	0.0322	0.430 ±	0.0437	0.99	946	6.466 ±	0.69	6.414
MAAP 670 nm	Sunset Thermal EC	6.93	0.65	7.334 ±	0.2046	1.891 ±	0.1314	8.266 ±	0.1691	1.530 ±	0.1370	0.88	665	140.620 ±	435.48	10.611
MAAP 670 nm	Filter IMPROVE_A_ TOR	6.25	0.96	5.746 ±	0.8309	0.736 ±	0.6508	5.815 ±	0.3318	0.670 ±	0.3493	0.96	28	6.878 ±	1.43	6.513
MAAP 670 nm	Filter IMPROVE_A_ TOT	6.25	0.73	7.322 ±	1.0340	0.868 ±	0.6480	7.166 ±	0.6647	1.055 ±	0.5297	0.90	28	9.198 ±	2.39	8.620
MAAP 670 nm	Filter STN_ TOR	6.50	0.83	8.459 ±	2.0310	-0.524 ±	1.4742	7.605 ±	0.9195	0.173 ±	0.8242	0.92	14	7.709 ±	1.21	7.813
MAAP 670 nm	Filter STN_ TOT	6.50	0.58	11.675 ±	2.9926	-0.355 ±	1.4993	11.023 ±	1.2690	0.054 ±	0.7982	0.93	14	11.023 ±	1.73	11.115
MAAP 670 nm	HiVol by French	7.04	0.89	8.270 ±	1.7504	-0.429 ±	1.3935	7.100 ±	1.6740	0.692 ±	1.6458	0.88	7	7.778 ±	2.45	7.874
PA 532 nm	2-AE 880 nm	5.22	0.88	4.461 ±	0.1136	1.273 ±	0.1119	4.453 ±	0.0426	1.314 ±	0.0438	0.95	1136	6.655 ±	1.92	5.952
PA 532 nm	7-AE 520 nm	5.23	0.93	4.102 ±	0.1038	1.402 ±	0.1086	4.073 ±	0.0357	1.441 ±	0.0393	0.96	1141	6.310 ±	1.75	5.623
PA 532 nm	7-AE 880 nm	5.23	0.94	3.990 ±	0.1007	1.473 ±	0.1068	3.959 ±	0.0342	1.514 ±	0.0382	0.96	1141	6.301 ±	1.77	5.574
PA 532 nm	MAAP 670 nm	5.38	0.92	4.157 ±	0.1428	1.547 ±	0.1504	4.179 ±	0.0454	1.539 ±	0.0505	0.96	653	6.856 ±	2.14	5.855
PA 532 nm	Sunset Thermal EC	5.46	0.62	4.310 ±	0.1536	2.740 ±	0.1119	4.316 ±	0.1029	2.777 ±	0.0801	0.80	1015	186.420 ±	532.15	8.781
PA 532 nm	Filter IMPROVE_A_ TOR	5.21	1.00	2.887 ±	0.7598	2.283 ±	0.7918	2.969 ±	0.2949	2.231 ±	0.3184	0.83	47	5.965 ±	2.55	5.196
PA 532 nm	Filter IMPROVE_A_ TOT	5.21	0.77	3.751 ±	0.9775	2.272 ±	0.7947	3.879 ±	0.3918	2.216 ±	0.3250	0.83	47	7.752 ±	3.44	6.754
PA 532 nm	Filter STN_ TOR	5.32	0.81	4.568 ±	1.6798	1.606 ±	1.3937	4.496 ±	0.5227	1.680 ±	0.4584	0.91	17	6.920 ±	1.08	6.571
PA 532 nm	Filter STN_ TOT	5.32	0.55	7.268 ±	2.9108	1.279 ±	1.6063	7.045 ±	0.8281	1.411 ±	0.4926	0.91	17	10.043 ±	2.04	9.589
PA 532 nm	HiVol by French	5.48	0.82	5.035 ±	2.0869	1.275 ±	1.8538	4.905 ±	1.0246	1.456 ±	0.9328	0.91	7	6.952 ±	1.41	6.678
PA 670 nm*	2-AE 880 nm	3.76	0.89	3.351 ±	0.1148	0.756 ±	0.1186	3.361 ±	0.0273	0.775 ±	0.0283	0.97	1081	4.673 ±	1.25	4.235
PA 670 nm*	7-AE 880 nm	3.76	0.95	2.991 ±	0.1015	0.911 ±	0.1134	2.993 ±	0.0207	0.931 ±	0.0233	0.98	1086	4.436 ±	1.14	3.977
PA 670 nm*	MAAP 670 nm	3.87	0.94	3.135 ±	0.1401	0.908 ±	0.1567	3.164 ±	0.0276	0.913 ±	0.0312	0.98	598	4.769 ±	1.38	4.140
PA 670 nm*	Sunset Thermal EC	3.92	0.63	3.252 ±	0.1495	1.875 ±	0.1137	3.257 ±	0.0762	1.886 ±	0.0596	0.81	973	132.340 ±	382.06	6.268
PA 670 nm*	Filter IMPROVE_A_ TOR	3.69	1.00	2.162 ±	0.6231	1.556 ±	0.6328	2.154 ±	0.2066	1.540 ±	0.2224	0.84	46	4.244 ±	1.81	3.698
PA 670 nm*	Filter IMPROVE_A_ TOT	3.69	0.77	2.822 ±	0.8041	1.536 ±	0.6371	2.821 ±	0.2750	1.526 ±	0.2272	0.84	46	5.520 ±	2.43	4.813
PA 670 nm*	Filter STN_ TOR	3.70	0.80	3.340 ±	1.4134	1.049 ±	1.1386	3.154 ±	0.3994	1.186 ±	0.3464	0.90	16	4.897 ±	0.77	4.642
PA 670 nm*	Filter STN_ TOT	3.70	0.55	5.037 ±	2.2460	0.962 ±	1.2125	4.985 ±	0.6121	0.976 ±	0.3599	0.91	16	7.095 ±	1.40	6.772
PA 670 nm*	HiVol by French	3.76	0.84	3.888 ±	1.6856	0.540 ±	1.4538	3.727 ±	0.4573	0.620 ±	0.4306	0.97	6	4.610 ±	0.59	4.462
PA 1047 nm	2-AE 880 nm	1.97	0.90	1.984 ±	0.0583	0.174 ±	0.0573	1.999 ±	0.0150	0.166 ±	0.0159	0.97	1135	2.301 ±	0.47	2.183
PA 1047 nm	7-AE 880 nm	1.98	0.96	1.779 ±	0.0518	0.257 ±	0.0549	1.777 ±	0.0114	0.263 ±	0.0131	0.98	1140	2.182 ±	0.42	2.049
PA 1047 nm	7-AE 950 nm	1.98	0.95	1.796 ±	0.0523	0.259 ±	0.0549	1.793 ±	0.0115	0.265 ±	0.0131	0.98	1140	2.206 ±	0.43	2.071
PA 1047 nm	MAAP 670 nm	2.01	0.96	1.847 ±	0.0703	0.241 ±	0.0742	1.873 ±	0.0143	0.219 ±	0.0166	0.98	622	2.280 ±	0.48	2.101
PA 1047 nm	Sunset Thermal EC	2.07	0.64	1.916 ±	0.0761	0.819 ±	0.0558	1.961 ±	0.0434	0.812 ±	0.0346	0.82	1025	60.559 ±	179.40	3.226
PA 1047 nm	Filter IMPROVE_A_ TOR	2.05	1.12	1.235 ±	0.5339	0.666 ±	0.6070	1.268 ±	0.1698	0.633 ±	0.1997	0.82	30	1.928 ±	0.52	1.834
PA 1047 nm	Filter IMPROVE_A_ TOT	2.05	0.83	1.508 ±	0.7020	0.786 ±	0.6014	1.535 ±	0.2678	0.772 ±	0.2346	0.73	30	2.596 ±	0.73	2.460
PA 1047 nm	Filter STN_ TOR	2.15	0.91	1.721 ±	0.9952	0.573 ±	0.9266	1.674 ±	0.4198	0.626 ±	0.4120	0.83	9	2.461 ±	0.45	2.361
PA 1047 nm	Filter STN_ TOT	2.15	0.63	3.394 ±	2.1193	0.026 ±	1.2968	3.141 ±	0.7101	0.187 ±	0.4662	0.86	9	3.434 ±	0.58	3.440
PA 1047 nm	HiVol by French	2.56	1.16	2.209 ±	1.6994	0.006 ±	1.9889	2.181 ±	0.3675	0.039 ±	0.4447	0.99	3	2.209 ±	0.14	2.214
PSAP (adj) 467 nm	2-AE 880 nm	4.17	0.91	5.035 ±	0.0561	-0.493 ±	0.0435	5.271 ±	0.0638	-0.616 ±	0.0677	0.93	1119	4.346 ±	0.92	4.592
PSAP (adj) 467 nm	7-AE 880 nm	4.18	0.97	4.571 ±	0.0505	-0.335 ±	0.0413	4.645 ±	0.0559	-0.327 ±	0.0644	0.93	1124	4.137 ±	0.91	4.308
PSAP (adj) 467 nm	MAAP 670 nm	4.02	0.96	4.518 ±	0.0814	-0.368 ±	0.0704	4.772 ±	0.0666	-0.542 ±	0.0770	0.94	622	3.984 ±	0.76	4.206
PSAP (adj) 467 nm	Sunset Thermal EC	4.42	0.65	4.781 ±	0.0998	1.166 ±	0.0645	5.192 ±	0.1304	1.060 ±	0.1043	0.78	1016	91.767 ±	300.97	6.830
PSAP (adj) 467 nm	Filter IMPROVE_A_ TOR	4.10	1.01	3.855 ±	0.4033	0.180 ±	0.3198	3.925 ±	0.2705	0.144 ±	0.2941	0.91	47	4.149 ±	0.94	4.068
PSAP (adj) 467 nm	Filter IMPROVE_A_ TOT	4.10	0.76	5.028 ±	0.4994	0.202 ±	0.3229	4.991 ±	0.4324	0.286 ±	0.3558	0.86	47	5.490 ±	1.43	5.365
PSAP (adj) 467 nm	Filter STN_ TOR	3.94	0.81	5.641 ±	1.1274	-0.651 ±	0.7829	5.353 ±	0.6684	-0.405 ±	0.5871	0.90	17	4.697 ±	1.04	4.854
PSAP (adj) 467 nm	Filter STN_ TOT	3.94	0.56	8.519 ±	1.9573	-0.869 ±	0.9406	8.422 ±	0.9519	-0.776 ±	0.5717	0.92	17	6.756 ±	1.55	7.035
PSAP (adj) 467 nm	HiVol by French	4.26	0.89	6.478 ±	1.1126	-1.525 ±	0.8610	6.208 ±	0.5754	-1.291 ±	0.5656	0.98	7	4.345 ±	1.26	4.763
PSAP (adj) 530 nm	2-AE 880 nm	3.35	0.91	3.999 ±	0.0376	-0.367 ±	0.0261	4.245 ±	0.0503	-0.501 ±	0.0533	0.93	1119	3.493 ±	0.72	3.693
PSAP (adj) 530 nm	7-AE 880 nm	3.36	0.97	3.664 ±	0.0339	-0.272 ±	0.0245	3.739 ±	0.0441	-0.266 ±	0.0508	0.93	1124	3.325 ±	0.71	3.465
PSAP (adj) 530 nm	MAAP 670 nm	3.23	0.96	3.613 ±	0.0603	-0.286 ±	0.0499	3.837 ±	0.0530	-0.441 ±	0.0612	0.95	622	3.194 ±	0.59	3.376
PSAP (adj) 530 nm	Sunset Thermal EC	3.55	0.65	3.808 ±	0.0756	0.950 ±	0.0479	4.180 ±	0.1043	0.850 ±	0.0834	0.78	1016	73.676 ±	241.38	5.493
PSAP (adj) 530 nm	Filter IMPROVE_A_ TOR	3.30	1.01	3.097 ±	0.2768	0.145 ±	0.1961	3.145 ±	0.2126	0.128 ±	0.2311	0.91	47	3.339 ±	0.74	3.272
PSAP (adj) 530 nm	Filter IMPROVE_A_ TOT	3.30	0.76	4.058 ±	0.3414	0.145 ±	0.2011	3.986 ±	0.3450	0.252 ±	0.2839	0.86	47	4.420 ±	1.15	4.316
PSAP (adj) 530 nm	Filter STN_ TOR	3.17	0.81	4.542 ±	0.8631	-0.523 ±	0.5844	4.298 ±	0.5264	-0.315 ±	0.4624	0.90	17	3.786 ±	0.82	3.910
PSAP (adj) 530 nm	Filter STN_ TOT	3.17	0.56	6.794 ±	1.4826	-0.666 ±	0.6992	6.749 ±	0.7546	-0.605 ±	0.4532	0.92	17	5.447 ±	1.24	5.667
PSAP (adj) 530 nm	HiVol by French	3.42	0.89	5.204 ±	0.8276	-1.222 ±	0.6123	4.938 ±	0.4915	-0.993 ±	0.4831	0.98	7	3.499 ±	1.01	3.828
PSAP (adj) 660 nm	2-AE 880 nm	2.61	0.91	3.153 ±	0.0294	-0.336 ±	0.0203	3.391 ±	0.0427	-0.470 ±	0.0453	0.92	1120	2.688 ±	0.63	2.873
PSAP (adj) 660 nm	7-AE 880 nm	2.61	0.97	2.891 ±	0.0264	-0.263 ±	0.0190	2.988 ±	0.0374	-0.284 ±	0.0431	0.92	1125	2.558 ±	0.61	2.696
PSAP (adj) 660 nm	MAAP 670 nm	2.50	0.96	2.839 ±	0.0473	-0.274 ±	0.0391	3.055 ±	0.0461	-0.425 ±	0.0533	0.94	622	2.437 ±	0.51	2.611
PSAP (adj) 660 nm	Sunset Thermal EC	2.77	0.65	3.016 ±	0.0597	0.699 ±	0.0377	3.334 ±	0.0857	0.611 ±	0.0685	0.77	1017	55.769 ±	184.04	4.279

Table 6-22. Continued.

Instrument[a] y	Instrument[a] x	Averages y	Averages x	Effective Variance Weighted Regression[b] Slope ± SE[c]	Effective Variance Weighted Regression[b] Intercept ± SE[c]	Ordinary Least Squares Regression[d] Slope ± SE[c]	Ordinary Least Squares Regression[d] Intercept ± SE[c]	r^2[e]	Number of pairs	Ratio y/x Average ± SD[f]	Ratio Avg y/Avg x
(Mm^{-1})	($\mu g/m^3$)	(Mm^{-1})	($\mu g/m^3$)	(m^2/g)	(Mm^{-1})	(m^2/g)	(Mm^{-1})			(m^2/g)	(m^2/g)
PSAP (adj) 660 nm	Filter IMPROVE_A_ TOR	2.56	1.01	2.449 ± 0.2170	0.069 ± 0.1526	2.495 ± 0.1658	0.049 ± 0.1802	0.91	47	2.581 ± 0.57	2.544
PSAP (adj) 660 nm	Filter IMPROVE_A_ TOT	2.56	0.76	3.206 ± 0.2673	0.070 ± 0.1565	3.142 ± 0.2762	0.163 ± 0.2272	0.86	47	3.419 ± 0.90	3.355
PSAP (adj) 660 nm	Filter STN_ TOR	2.47	0.81	3.605 ± 0.6836	-0.468 ± 0.4623	3.432 ± 0.4022	-0.318 ± 0.3533	0.91	17	2.928 ± 0.66	3.040
PSAP (adj) 660 nm	Filter STN_ TOT	2.47	0.56	5.362 ± 1.1682	-0.565 ± 0.5505	5.364 ± 0.5876	-0.536 ± 0.3529	0.92	17	4.217 ± 1.01	4.406
PSAP (adj) 660 nm	HiVol by French	2.65	0.89	4.072 ± 0.6465	-0.981 ± 0.4771	3.841 ± 0.4359	-0.779 ± 0.4284	0.97	7	2.706 ± 0.82	2.969
PSAP (adj) 670 nm*	2-AE 880 nm	2.56	0.91	3.092 ± 0.0288	-0.330 ± 0.0199	3.327 ± 0.0420	-0.462 ± 0.0445	0.92	1119	2.635 ± 0.61	2.818
PSAP (adj) 670 nm*	7-AE 880 nm	2.57	0.97	2.836 ± 0.0259	-0.258 ± 0.0186	2.932 ± 0.0368	-0.279 ± 0.0424	0.92	1124	2.508 ± 0.59	2.644
PSAP (adj) 670 nm*	MAAP 670 nm	2.45	0.96	2.784 ± 0.0463	-0.271 ± 0.0383	2.998 ± 0.0454	-0.420 ± 0.0525	0.94	622	2.386 ± 0.51	2.559
PSAP (adj) 670 nm*	Sunset Thermal EC	2.71	0.65	2.956 ± 0.0586	0.686 ± 0.0370	3.271 ± 0.0843	0.598 ± 0.0674	0.77	1016	54.608 ± 180.29	4.195
PSAP (adj) 670 nm*	Filter IMPROVE_A_ TOR	2.51	1.01	2.403 ± 0.2127	0.063 ± 0.1496	2.446 ± 0.1617	0.045 ± 0.1758	0.91	47	2.527 ± 0.56	2.491
PSAP (adj) 670 nm*	Filter IMPROVE_A_ TOT	2.51	0.76	3.146 ± 0.2620	0.065 ± 0.1534	3.078 ± 0.2702	0.159 ± 0.2223	0.86	47	3.348 ± 0.88	3.286
PSAP (adj) 670 nm*	Filter STN_ TOR	2.41	0.81	3.531 ± 0.6695	-0.458 ± 0.4527	3.361 ± 0.3930	-0.311 ± 0.3452	0.91	17	2.868 ± 0.64	2.978
PSAP (adj) 670 nm*	Filter STN_ TOT	2.41	0.56	5.246 ± 1.1424	-0.550 ± 0.5382	5.250 ± 0.5766	-0.522 ± 0.3463	0.92	17	4.132 ± 0.99	4.316
PSAP (adj) 670 nm*	HiVol by French	2.60	0.89	3.984 ± 0.6319	-0.956 ± 0.4661	3.755 ± 0.4280	-0.757 ± 0.4208	0.97	7	2.651 ± 0.80	2.908
PSAP (raw) 467 nm	2-AE 880 nm	12.17	0.91	13.572 ± 0.1292	-0.177 ± 0.0906	13.243 ± 0.0831	0.146 ± 0.0881	0.98	1119	13.345 ± 1.41	13.404
PSAP (raw) 467 nm	7-AE 880 nm	12.20	0.97	12.496 ± 0.1169	0.104 ± 0.0855	11.672 ± 0.0723	0.874 ± 0.0833	0.98	1124	12.688 ± 1.53	12.572
PSAP (raw) 467 nm	MAAP 670 nm	11.90	0.96	12.302 ± 0.2061	0.121 ± 0.1712	12.231 ± 0.0680	0.203 ± 0.0786	0.99	622	12.492 ± 1.12	12.443
PSAP (raw) 467 nm	Sunset Thermal EC	12.84	0.65	12.514 ± 0.2499	4.428 ± 0.1586	13.200 ± 0.2680	4.299 ± 0.2144	0.84	1016	305.180 ± 987.82	19.844
PSAP (raw) 467 nm	Filter IMPROVE_A_ TOR	11.84	1.01	10.257 ± 0.9313	1.461 ± 0.6684	10.256 ± 0.6822	1.504 ± 0.7415	0.91	47	12.324 ± 2.99	11.749
PSAP (raw) 467 nm	Filter IMPROVE_A_ TOT	11.84	0.76	13.251 ± 1.1349	1.587 ± 0.6767	12.683 ± 1.1917	2.149 ± 0.9805	0.85	47	16.333 ± 4.60	15.496
PSAP (raw) 467 nm	Filter STN_ TOR	11.66	0.81	16.042 ± 3.0463	-1.347 ± 2.0673	14.545 ± 1.6059	-0.132 ± 1.4106	0.92	17	14.138 ± 2.60	14.382
PSAP (raw) 467 nm	Filter STN_ TOT	11.66	0.56	23.046 ± 5.0446	-1.333 ± 2.3830	22.229 ± 2.6334	-0.775 ± 1.5816	0.91	17	20.477 ± 4.48	20.844
PSAP (raw) 467 nm	HiVol by French	12.21	0.89	16.384 ± 2.6299	-2.418 ± 1.9574	15.153 ± 2.1846	-1.330 ± 2.1474	0.95	7	13.044 ± 2.91	13.664
PSAP (raw) 530 nm	2-AE 880 nm	10.47	0.91	11.736 ± 0.1078	-0.222 ± 0.0736	11.524 ± 0.0732	0.004 ± 0.0776	0.98	1119	11.441 ± 1.20	11.528
PSAP (raw) 530 nm	7-AE 880 nm	10.49	0.97	10.835 ± 0.0976	-0.004 ± 0.0693	10.160 ± 0.0633	0.634 ± 0.0729	0.98	1124	10.875 ± 1.29	10.813
PSAP (raw) 530 nm	MAAP 670 nm	10.23	0.96	10.634 ± 0.1761	0.034 ± 0.1452	10.629 ± 0.0617	0.058 ± 0.0713	0.99	622	10.695 ± 0.95	10.690
PSAP (raw) 530 nm	Sunset Thermal EC	11.05	0.65	10.832 ± 0.2145	3.757 ± 0.1357	11.471 ± 0.2351	3.623 ± 0.1880	0.84	1016	260.860 ± 843.32	17.070
PSAP (raw) 530 nm	Filter IMPROVE_A_ TOR	10.18	1.01	8.841 ± 0.7746	1.229 ± 0.5394	8.870 ± 0.5899	1.245 ± 0.6412	0.91	47	10.590 ± 2.57	10.105
PSAP (raw) 530 nm	Filter IMPROVE_A_ TOT	10.18	0.76	11.445 ± 0.9436	1.319 ± 0.5483	10.946 ± 1.0360	1.820 ± 0.8524	0.84	47	14.039 ± 3.98	13.328
PSAP (raw) 530 nm	Filter STN_ TOR	10.03	0.81	13.899 ± 2.6208	-1.241 ± 1.7718	12.629 ± 1.3690	-0.207 ± 1.2025	0.92	17	12.146 ± 2.24	12.374
PSAP (raw) 530 nm	Filter STN_ TOT	10.03	0.56	19.868 ± 4.3147	-1.176 ± 2.0320	19.252 ± 2.2776	-0.737 ± 1.3679	0.91	17	17.604 ± 3.91	17.935
PSAP (raw) 530 nm	HiVol by French	10.50	0.89	14.126 ± 2.2373	-2.120 ± 1.6501	13.031 ± 1.9245	-1.149 ± 1.8917	0.95	7	11.206 ± 2.53	11.745
PSAP (raw) 660 nm	2-AE 880 nm	8.32	0.91	9.384 ± 0.0861	-0.236 ± 0.0587	9.288 ± 0.0607	-0.112 ± 0.0643	0.98	1119	9.061 ± 0.97	9.165
PSAP (raw) 660 nm	7-AE 880 nm	8.34	0.97	8.669 ± 0.0779	-0.065 ± 0.0552	8.193 ± 0.0518	0.392 ± 0.0597	0.98	1124	8.611 ± 1.01	8.597
PSAP (raw) 660 nm	MAAP 670 nm	8.13	0.96	8.504 ± 0.1407	-0.032 ± 0.1160	8.560 ± 0.0531	-0.062 ± 0.0613	0.99	622	8.466 ± 0.76	8.495
PSAP (raw) 660 nm	Sunset Thermal EC	8.78	0.65	8.681 ± 0.1718	2.936 ± 0.1087	9.229 ± 0.1916	2.812 ± 0.1533	0.83	1016	205.760 ± 664.64	13.574
PSAP (raw) 660 nm	Filter IMPROVE_A_ TOR	8.10	1.01	7.033 ± 0.6159	0.968 ± 0.4284	7.093 ± 0.4729	0.949 ± 0.5140	0.91	47	8.413 ± 2.05	8.034
PSAP (raw) 660 nm	Filter IMPROVE_A_ TOT	8.10	0.76	9.102 ± 0.7500	1.042 ± 0.4354	8.732 ± 0.8345	1.424 ± 0.6866	0.84	47	11.156 ± 3.18	10.596
PSAP (raw) 660 nm	Filter STN_ TOR	7.99	0.81	11.139 ± 2.0999	-1.054 ± 1.4193	10.157 ± 1.0767	-0.251 ± 0.9458	0.93	17	9.649 ± 1.79	9.847
PSAP (raw) 660 nm	Filter STN_ TOT	7.99	0.56	15.869 ± 3.4458	-0.972 ± 1.6225	15.435 ± 1.8249	-0.650 ± 1.0960	0.91	17	13.995 ± 3.17	14.273
PSAP (raw) 660 nm	HiVol by French	8.34	0.89	11.254 ± 1.7826	-1.710 ± 1.3139	10.378 ± 1.5618	-0.930 ± 1.5352	0.95	7	8.901 ± 2.03	9.337
PSAP (raw) 670 nm*	Filter IMPROVE_A_ TOR	7.96	1.01	6.917 ± 0.6059	0.952 ± 0.4215	6.977 ± 0.4651	0.931 ± 0.5055	0.91	47	8.273 ± 2.01	7.901
PSAP (raw) 670 nm*	Filter IMPROVE_A_ TOT	7.96	0.76	8.952 ± 0.7379	1.024 ± 0.4284	8.588 ± 0.8211	1.400 ± 0.6756	0.84	47	10.971 ± 3.13	10.420
PSAP (raw) 670 nm*	Filter STN_ TOR	7.85	0.81	10.958 ± 2.0655	-1.038 ± 1.3959	9.993 ± 1.0573	-0.250 ± 0.9287	0.93	17	9.490 ± 1.76	9.685
PSAP (raw) 670 nm*	Filter STN_ TOT	7.85	0.56	15.601 ± 3.3876	-0.953 ± 1.5950	15.179 ± 1.7963	-0.639 ± 1.0788	0.91	17	13.765 ± 3.12	14.037
PSAP (raw) 670 nm*	HiVol by French	8.20	0.89	11.059 ± 1.7516	-1.677 ± 1.2912	10.198 ± 1.5378	-0.910 ± 1.5116	0.95	7	8.753 ± 1.99	9.180

[a] Refer to Table 4-2 for detailed instrumentation and measurements; Filter EC data used here is an average of different integrated samplers, analyzed by the protocol indicated in the Table: Interagency Monitoring of Protected Visual Environments (IMPROVE) Thermal Optical Reflectance (TOR) and Transmittance (TOT) and Speciation Trends Network (STN) Thermal Optical Reflectance (TOR) and Transmittance (TOT) protocols. Cachier's French two-step protocol (Cachier et al., 1989a; Cachier et al., 1989b) was used only on samples from Andersen high volume (HiVol) sampler.

[b] Effective variance weighted least squares linear regression (Watson et al., 1984) weights variable by precisions in both variables

[c] SE: Standard error

[d] Ordinary least squares linear regression does not weight variables by their precisions

[e] Correlation coefficient

[f] SD: Standard deviation

* b_{abs} scaled to 670 nm using wavelength dependence shown by the respective instrument

Table 6-23. Angstrom absorption exponent at Fresno (8/1/05-9/30/05).

	Angstrom Absorption Exponent, α, for 8/1/05-9/30/05							
Instrument[a]=>>	**2-AE**		**7-AE**		**PSAP**		**PA**	
Hour	**Average**	**± SD[b]**	**Average**	**± SD[b]**	**Average**	**± SD[b]**	**Average**	**± SD[b]**
0	0.93	± 0.094	0.95	± 0.102	1.33	± 0.078	1.39	± 0.213
1	0.94	± 0.071	0.94	± 0.095	1.31	± 0.087	1.43	± 0.192
2	0.93	± 0.067	0.92	± 0.090	1.29	± 0.087	1.44	± 0.243
3	0.91	± 0.080	0.92	± 0.095	1.27	± 0.100	1.46	± 0.182
4	0.91	± 0.076	0.90	± 0.091	1.26	± 0.079	1.48	± 0.187
5	0.92	± 0.083	0.91	± 0.100	1.27	± 0.088	1.47	± 0.218
6	0.91	± 0.080	0.92	± 0.094	1.27	± 0.107	1.37	± 0.178
7	0.89	± 0.083	0.91	± 0.099	1.26	± 0.118	1.33	± 0.219
8	0.88	± 0.073	0.88	± 0.094	1.32	± 0.096	1.34	± 0.220
9	0.89	± 0.097	0.91	± 0.114	1.38	± 0.116	1.39	± 0.214
10	0.91	± 0.110	0.95	± 0.113	1.38	± 0.114	1.45	± 0.211
11	0.95	± 0.109	0.97	± 0.112	1.41	± 0.136	1.42	± 0.195
12	0.96	± 0.087	0.98	± 0.111	1.45	± 0.151	1.52	± 0.275
13	0.96	± 0.102	1.00	± 0.121	1.49	± 0.196	1.53	± 0.329
14	0.95	± 0.110	1.02	± 0.110	1.51	± 0.169	1.59	± 0.270
15	0.95	± 0.140	1.02	± 0.113	1.51	± 0.193	1.63	± 0.254
16	0.96	± 0.117	1.01	± 0.127	1.51	± 0.162	1.59	± 0.252
17	0.97	± 0.102	0.98	± 0.111	1.49	± 0.122	1.62	± 0.291
18	0.98	± 0.095	0.96	± 0.107	1.43	± 0.076	1.71	± 0.242
19	0.96	± 0.086	0.93	± 0.103	1.39	± 0.081	1.55	± 0.239
20	0.98	± 0.093	0.93	± 0.105	1.38	± 0.083	1.38	± 0.220
21	0.97	± 0.088	0.95	± 0.123	1.38	± 0.060	1.37	± 0.239
22	0.96	± 0.084	1.00	± 0.116	1.37	± 0.072	1.42	± 0.268
23	0.94	± 0.079	0.98	± 0.099	1.36	± 0.092	1.42	± 0.198
Average ± SD[b]	0.94	± 0.030	0.95	± 0.041	1.38	± 0.086	1.47	± 0.101

[a] Refer to Table 4-2 for detailed instrumentation and measurements

[b] SD: Standard deviation

Table 6-24. Comparison statistics for b_{abs} measurements at Fresno from 12/1/03 to 12/31/03.

Instrument[a]		Averages		Effective Variance Weighted Regression[b]				Ordinary Least Squares Regression[d]					Number	Ratio y/x		Ratio	Difference y-x		RMS[g]	Distribution of y-x[h]			
y	x	y	x	Slope ± SE[c]		Intercept ± SE[c]		Slope ± SE[c]		Intercept ± SE[c]		r^e	of pairs	Average ± SD[f]		Avg y/Avg x	Average ± SD[f]		Precision	< 1σ[i]	1σ-2σ	2σ-3σ	>3σ
(Mm^{-1})	(Mm^{-1})	(Mm^{-1})	(Mm^{-1})			(Mm^{-1})				(Mm^{-1})							(Mm^{-1})		(Mm^{-1})	(%)			
7-AE 370 nm	2-AE 370 nm	84.52	93.12	0.904 ±	0.0080	-1.051 ±	0.3690	0.916 ±	0.0057	-0.788 ±	0.7077	0.99	741	0.896 ±	0.15	0.908	-8.606 ±	14.511	17.426	61	31	7	0
7-AE 880 nm	2-AE 880 nm	28.50	29.68	0.957 ±	0.0089	-0.239 ±	0.1404	0.996 ±	0.0041	-1.061 ±	0.1634	0.99	741	0.945 ±	0.08	0.960	-1.178 ±	2.924	5.770	92	7	1	0
MAAP 670 nm	7-AE 660 nm	14.88	40.14	0.356 ±	0.0040	0.402 ±	0.0945	0.364 ±	0.0017	0.276 ±	0.0915	0.99	741	0.388 ±	0.07	0.371	-25.259 ±	23.338	6.241	3	4	7	86
Filter b_{abs}	2-AE 880 nm	30.16	30.07	0.591 ±	0.2227	11.887 ±	7.6422	0.589 ±	0.1021	12.460 ±	3.4921	0.92	8	1.114 ±	0.27	1.003	0.089 ±	8.405	11.345	75	25	0	0
Filter b_{abs}	7-AE 880 nm	30.16	29.17	0.600 ±	0.2257	12.213 ±	7.5264	0.599 ±	0.1020	12.693 ±	3.3994	0.92	8	1.157 ±	0.30	1.034	0.992 ±	8.133	11.327	88	13	0	0
2-AE 670 nm*	MAAP 670 nm	42.32	14.88	2.869 ±	0.0322	-0.033 ±	0.2847	2.730 ±	0.0129	1.692 ±	0.2594	0.99	741	2.853 ±	0.37	2.844	27.439 ±	23.692	6.432	3	3	6	88
7-AE 670 nm*	MAAP 670 nm	39.43	14.88	2.705 ±	0.0302	-0.751 ±	0.2646	2.658 ±	0.0123	-0.129 ±	0.2461	0.99	741	2.594 ±	0.34	2.649	24.545 ±	22.696	6.150	3	4	8	85
PA 1047 nm	MAAP 670 nm	6.86	16.15	0.429 ±	0.0046	-0.121 ±	0.0470	0.446 ±	0.0029	-0.345 ±	0.0642	0.99	552	0.417 ±	0.07	0.425	-9.286 ±	8.224	2.827	2	8	20	70
Filter b_{abs}	MAAP 670 nm	30.16	15.22	1.191 ±	0.4526	11.637 ±	7.7135	1.186 ±	0.1610	12.101 ±	2.7955	0.95	8	2.181 ±	0.46	1.981	14.937 ±	3.895	10.853	13	88	0	0
7-AE 950 nm	PA 1047 nm	28.45	6.86	4.085 ±	0.0351	0.284 ±	0.1426	3.926 ±	0.0256	1.506 ±	0.2447	0.99	552	4.209 ±	0.66	4.145	21.585 ±	19.883	4.058	1	2	2	95
Filter b_{abs}	PA 1047 nm	30.38	6.34	2.777 ±	0.9351	12.516 ±	7.2021	2.789 ±	0.2919	12.689 ±	2.1724	0.97	7	5.386 ±	1.18	4.789	24.038 ±	8.004	10.657	0	29	57	14

[a] Refer to Table 4-2 for detailed instrumentation and measurements; Filter b_{abs} refers to light absorption measured by densitometry on Teflon filters; Data used here is an average of different integrated samplers.

[b] Effective variance weighted least squares linear regression (Watson et al., 1984) weights variable by precisions in both variables

[c] SE: Standard error

[d] Ordinary least squares linear regression does not weight variables by their precisions

[e] Correlation coefficient

[f] SD: Standard deviation

[g] RMS: Root mean squared precision

[h] Fraction of pairs in percent for which the difference is less than or greater than one, two, or three times the propagated measurement uncertainty

[i] Measurement uncertainty of (y-x)

* b_{abs} scaled to 670 nm using wavelength dependence shown by the respective instrument

Table 6-25. Comparison statistics for BC concentration measurements at Fresno from 12/1/03 to 12/31/03.

Instrument[a]		Averages		Effective Variance Weighted Regression[b]		Ordinary Least Squares Regression[d]			Number	Ratio y/x		Ratio	Difference y-x		RMS[g]	Distribution of y-x (%)[h]			
y	x	y	x	Slope ± SE[c]	Intercept ± SE[c]	Slope ± SE[c]	Intercept ± SE[c]	r[e]	of pairs	Average ± SD[f]		Avg y/Avg x	Average ± SD[f]		Precision	< 1σ[i]	1σ-2σ	2σ-3σ	>3σ
(μg/m³)	(μg/m³)	(μg/m³)	(μg/m³)	(μg/m³)		(μg/m³)							(μg/m³)		(μg/m³)				
7-AE 370 nm	2-AE 370 nm	2.14	2.36	0.904 ± 0.0080	-0.027 ± 0.0093	0.916 ± 0.0057	-0.020 ± 0.0179	0.99	741	0.896 ± 0.15		0.908	-0.218 ± 0.367		0.441	61	31	7	0
7-AE 880 nm	2-AE 880 nm	1.71	1.79	0.957 ± 0.0089	-0.014 ± 0.0084	0.996 ± 0.0041	-0.064 ± 0.0098	0.99	741	0.945 ± 0.08		0.960	-0.071 ± 0.176		0.347	92	7	1	0
Filter IMPROVE_A_ TOR	2-AE 880 nm	2.67	1.80	1.259 ± 0.1854	0.111 ± 0.2505	1.331 ± 0.4296	0.265 ± 0.8751	0.76	9	1.477 ± 0.52		1.478	0.862 ± 1.185		0.500	33	44	11	11
Filter IMPROVE_A_ TOT	2-AE 880 nm	1.73	1.80	0.864 ± 0.1571	-0.006 ± 0.2078	0.915 ± 0.2190	0.083 ± 0.4459	0.84	9	0.958 ± 0.31		0.961	-0.071 ± 0.586		0.478	56	44	0	0
Filter STN_ TOR	2-AE 880 nm	1.73	1.80	0.970 ± 0.2034	-0.014 ± 0.2684	0.877 ± 0.0623	0.149 ± 0.1270	0.98	9	0.966 ± 0.08		0.960	-0.072 ± 0.206		0.558	100	0	0	0
Filter STN_ TOT	2-AE 880 nm	0.98	1.80	0.300 ± 0.1162	0.225 ± 0.1670	0.590 ± 0.1383	-0.084 ± 0.2816	0.85	9	0.550 ± 0.16		0.544	-0.823 ± 0.550		0.448	0	67	22	11
HiVol by French	2-AE 880 nm	1.12	1.56	0.567 ± 0.1327	0.042 ± 0.1795	1.039 ± 0.3325	-0.499 ± 0.5530	0.81	7	0.708 ± 0.32		0.719	-0.439 ± 0.460		0.271	43	14	0	43
Filter IMPROVE_A_ TOR	7-AE 880 nm	2.67	1.73	1.270 ± 0.1887	0.157 ± 0.2457	1.307 ± 0.4656	0.400 ± 0.9137	0.73	9	1.551 ± 0.60		1.538	0.933 ± 1.239		0.497	33	44	11	11
Filter IMPROVE_A_ TOT	7-AE 880 nm	1.73	1.73	0.867 ± 0.1599	0.029 ± 0.2041	0.909 ± 0.2413	0.157 ± 0.4737	0.82	9	1.006 ± 0.35		1.000	0.000 ± 0.629		0.475	56	44	0	0
Filter STN_ TOR	7-AE 880 nm	1.73	1.73	0.996 ± 0.2096	0.005 ± 0.2655	0.892 ± 0.0789	0.186 ± 0.1548	0.97	9	1.009 ± 0.10		0.999	-0.001 ± 0.229		0.555	100	0	0	0
Filter STN_ TOT	7-AE 880 nm	0.98	1.73	0.304 ± 0.1198	0.234 ± 0.1657	0.606 ± 0.1419	-0.069 ± 0.2784	0.85	9	0.575 ± 0.16		0.566	-0.752 ± 0.531		0.445	11	56	22	11
HiVol by French	7-AE 880 nm	1.12	1.49	0.575 ± 0.1373	0.060 ± 0.1784	1.063 ± 0.3809	-0.463 ± 0.6041	0.78	7	0.744 ± 0.36		0.752	-0.369 ± 0.495		0.267	43	14	0	43
2-AE 880 nm	MAAP 670 nm	1.79	2.25	0.805 ± 0.0090	-0.013 ± 0.0120	0.760 ± 0.0038	0.072 ± 0.0116	0.99	741	0.791 ± 0.11		0.792	-0.469 ± 0.531		0.466	49	47	4	0
7-AE 660 nm	MAAP 670 nm	1.81	2.25	0.820 ± 0.0092	-0.034 ± 0.0122	0.806 ± 0.0037	-0.005 ± 0.0113	0.99	741	0.787 ± 0.10		0.803	-0.443 ± 0.445		0.470	48	50	2	0
7-AE 880 nm	MAAP 670 nm	1.71	2.25	0.778 ± 0.0087	-0.034 ± 0.0116	0.763 ± 0.0036	-0.005 ± 0.0109	0.99	741	0.744 ± 0.10		0.761	-0.540 ± 0.522		0.463	33	59	9	0
MAAP-A 670 nm	MAAP 670 nm	2.56	2.25	1.097 ± 0.0139	0.049 ± 0.0192	1.134 ± 0.0081	0.006 ± 0.0247	0.98	741	1.156 ± 0.17		1.136	0.307 ± 0.526		0.599	73	26	1	0
PA 1047 nm	MAAP 670 nm	1.37	2.45	0.567 ± 0.0061	-0.024 ± 0.0094	0.589 ± 0.0039	-0.069 ± 0.0128	0.99	552	0.550 ± 0.09		0.561	-1.074 ± 0.940		0.430	3	18	34	44
Sunset Thermal EC	MAAP 670 nm	1.44	2.41	0.570 ± 0.0118	0.026 ± 0.0194	0.590 ± 0.0053	0.019 ± 0.0172	0.98	612	0.606 ± 0.22		0.598	-0.969 ± 0.928		0.601	21	39	36	4
Sunset Optical BC	MAAP 670 nm	1.10	2.35	0.483 ± 0.0078	-0.041 ± 0.0153	0.489 ± 0.0025	-0.050 ± 0.0081	0.99	630	0.446 ± 0.06		0.467	-1.254 ± 1.109		0.479	7	22	30	41
Filter IMPROVE_A_ TOR	MAAP 670 nm	2.67	2.29	1.050 ± 0.1757	0.023 ± 0.3113	1.017 ± 0.3529	0.343 ± 0.9103	0.74	9	1.163 ± 0.45		1.167	0.381 ± 1.185		0.584	89	0	0	11
Filter IMPROVE_A_ TOT	MAAP 670 nm	1.73	2.29	0.717 ± 0.1426	-0.061 ± 0.2465	0.714 ± 0.1773	0.103 ± 0.4573	0.84	9	0.753 ± 0.25		0.759	-0.551 ± 0.698		0.566	22	67	11	0
Filter STN_ TOR	MAAP 670 nm	1.73	2.29	0.775 ± 0.1765	-0.040 ± 0.3039	0.680 ± 0.0691	0.179 ± 0.1782	0.97	9	0.761 ± 0.09		0.758	-0.553 ± 0.468		0.635	44	56	0	0
Filter STN_ TOT	MAAP 670 nm	0.98	2.29	0.280 ± 0.1021	0.160 ± 0.1840	0.484 ± 0.0971	-0.124 ± 0.2505	0.88	9	0.430 ± 0.12		0.430	-1.303 ± 0.732		0.540	0	11	56	33
HiVol by French	MAAP 670 nm	1.12	1.94	0.450 ± 0.1218	0.075 ± 0.2094	0.857 ± 0.3391	-0.539 ± 0.6928	0.75	7	0.570 ± 0.27		0.579	-0.817 ± 0.533		0.366	29	29	0	43
2-AE 880 nm	PA 1047 nm	1.92	1.37	1.370 ± 0.0117	0.042 ± 0.0095	1.263 ± 0.0091	0.184 ± 0.0173	0.99	552	1.445 ± 0.23		1.397	0.545 ± 0.450		0.273	9	22	46	23
7-AE 880 nm	PA 1047 nm	1.84	1.37	1.324 ± 0.0114	0.018 ± 0.0093	1.272 ± 0.0084	0.099 ± 0.0160	0.99	552	1.365 ± 0.22		1.344	0.472 ± 0.447		0.268	15	28	47	10
7-AE 950 nm	PA 1047 nm	1.85	1.37	1.327 ± 0.0114	0.019 ± 0.0093	1.275 ± 0.0083	0.098 ± 0.0159	0.99	552	1.367 ± 0.21		1.346	0.475 ± 0.449		0.269	14	27	47	11
MAAP 670 nm	PA 1047 nm	2.45	1.37	1.716 ± 0.0186	0.074 ± 0.0160	1.658 ± 0.0109	0.171 ± 0.0209	0.99	552	1.859 ± 0.29		1.783	1.074 ± 0.940		0.430	3	18	34	44
MAAP-A 670 nm	PA 1047 nm	2.78	1.37	1.896 ± 0.0206	0.114 ± 0.0174	1.912 ± 0.0142	0.156 ± 0.0272	0.99	552	2.126 ± 0.39		2.026	1.408 ± 1.293		0.492	2	13	24	61
Sunset Thermal EC	PA 1047 nm	1.53	1.42	0.969 ± 0.0198	0.087 ± 0.0193	0.980 ± 0.0111	0.138 ± 0.0220	0.97	497	1.162 ± 0.45		1.077	0.110 ± 0.342		0.459	76	21	2	0
Sunset Optical BC	PA 1047 nm	1.16	1.40	0.830 ± 0.0111	-0.004 ± 0.0146	0.817 ± 0.0059	0.021 ± 0.0115	0.99	508	0.821 ± 0.13		0.832	-0.235 ± 0.311		0.256	69	24	6	2
Filter IMPROVE_A_ TOR	PA 1047 nm	2.67	1.25	1.767 ± 0.2349	0.129 ± 0.2246	1.821 ± 0.6340	0.395 ± 0.9176	0.76	8	2.135 ± 0.78		2.137	1.420 ± 1.375		0.448	0	0	50	50
Filter IMPROVE_A_ TOT	PA 1047 nm	1.75	1.25	1.318 ± 0.2234	-0.058 ± 0.2021	1.289 ± 0.2958	0.143 ± 0.4280	0.87	8	1.388 ± 0.41		1.404	0.504 ± 0.610		0.425	63	13	25	0
Filter STN_ TOR	PA 1047 nm	1.67	1.25	1.295 ± 0.2770	0.045 ± 0.2544	1.164 ± 0.1153	0.222 ± 0.1669	0.97	8	1.365 ± 0.15		1.342	0.426 ± 0.256		0.496	50	50	0	0
Filter STN_ TOT	PA 1047 nm	1.05	1.25	0.814 ± 0.2053	-0.005 ± 0.1846	0.896 ± 0.0637	-0.070 ± 0.0922	0.99	8	0.833 ± 0.10		0.840	-0.200 ± 0.147		0.396	75	25	0	0
HiVol by French	PA 1047 nm	0.96	1.00	0.421 ± 0.1839	0.263 ± 0.1726	1.324 ± 0.6837	-0.358 ± 0.7222	0.70	6	0.983 ± 0.52		0.965	-0.035 ± 0.538		0.176	17	33	17	33

Table 6-25. (continued).

Instrument[a]		Averages		Effective Variance Weighted Regression[b]				Ordinary Least Squares Regression[d]					Number	Ratio y/x		Ratio	Difference y-x		RMS[g]	Distribution of y-x (%)[h]			
y	x	y	x	Slope	± SE[c]	Intercept	± SE[c]	Slope	± SE[c]	Intercept	± SE[c]	r[e]	of pairs	Average	± SD[f]	Avg y/Avg x	Average	± SD[f]	Precision	< 1σ[i]	1σ-2σ	2σ-3σ	>3σ
(μg/m³)	(μg/m³)	(μg/m³)	(μg/m³)	(μg/m³)				(μg/m³)									(μg/m³)		(μg/m³)				
2-AE 880 nm	Sunset Thermal EC	1.90	1.44	1.247	± 0.0237	0.080	± 0.0229	1.221	± 0.0132	0.142	± 0.0256	0.97	612	3.041	± 11.62	1.320	0.461	± 0.513	0.506	47	40	12	1
7-AE 880 nm	Sunset Thermal EC	1.84	1.44	1.212	± 0.0230	0.051	± 0.0223	1.230	± 0.0129	0.061	± 0.0251	0.97	612	2.840	± 10.73	1.272	0.393	± 0.513	0.504	55	36	8	1
MAAP 670 nm	Sunset Thermal EC	2.41	1.44	1.569	± 0.0315	0.090	± 0.0307	1.615	± 0.0145	0.082	± 0.0282	0.98	612	4.575	± 19.17	1.672	0.969	± 0.928	0.601	21	39	36	4
PA 1047 nm	Sunset Thermal EC	1.42	1.53	0.909	± 0.0175	0.007	± 0.0182	0.959	± 0.0109	-0.047	± 0.0225	0.97	497	1.717	± 10.87	0.928	-0.110	± 0.342	0.459	76	21	2	0
Sunset Optical BC	Sunset Thermal EC	1.13	1.44	0.780	± 0.0174	-0.012	± 0.0198	0.795	± 0.0072	-0.019	± 0.0140	0.98	612	1.770	± 6.75	0.782	-0.314	± 0.353	0.498	74	25	1	0
Filter IMPROVE_A_ TOR	Sunset Thermal EC	2.67	1.31	2.024	± 0.5282	-0.099	± 0.5817	1.741	± 0.6416	0.384	± 0.9475	0.72	9	2.025	± 0.83	2.034	1.355	± 1.335	0.591	0	44	44	11
Filter IMPROVE_A_ TOT	Sunset Thermal EC	1.73	1.31	1.367	± 0.3887	-0.147	± 0.4194	1.248	± 0.3176	0.098	± 0.4690	0.83	9	1.305	± 0.45	1.323	0.423	± 0.631	0.573	78	11	11	0
Filter STN_ TOR	Sunset Thermal EC	1.73	1.31	1.372	± 0.4275	-0.054	± 0.4578	1.177	± 0.1477	0.190	± 0.2181	0.95	9	1.325	± 0.22	1.322	0.422	± 0.309	0.641	78	22	0	0
Filter STN_ TOT	Sunset Thermal EC	0.98	1.31	0.601	± 0.2410	0.075	± 0.2560	0.875	± 0.1541	-0.165	± 0.2275	0.91	9	0.741	± 0.21	0.749	-0.329	± 0.307	0.548	89	0	11	0
HiVol by French	Sunset Thermal EC	1.12	1.11	1.008	± 0.3777	-0.020	± 0.3861	1.455	± 0.7283	-0.487	± 0.8420	0.67	7	1.003	± 0.49	1.015	0.016	± 0.611	0.380	43	43	14	0
2-AE 880 nm	Sunset Optical BC	1.85	1.10	1.604	± 0.0239	0.101	± 0.0224	1.537	± 0.0093	0.166	± 0.0142	0.99	630	1.766	± 0.20	1.687	0.755	± 0.620	0.356	17	25	40	18
7-AE 880 nm	Sunset Optical BC	1.79	1.10	1.569	± 0.0235	0.062	± 0.0219	1.545	± 0.0090	0.090	± 0.0137	0.99	630	1.670	± 0.20	1.627	0.689	± 0.625	0.353	21	28	40	11
MAAP 670 nm	Sunset Optical BC	2.35	1.10	2.035	± 0.0330	0.110	± 0.0300	2.013	± 0.0104	0.140	± 0.0159	0.99	630	2.293	± 0.40	2.141	1.254	± 1.109	0.479	7	22	30	41
PA 1047 nm	Sunset Optical BC	1.40	1.16	1.175	± 0.0155	0.029	± 0.0170	1.193	± 0.0086	0.011	± 0.0140	0.99	508	1.264	± 0.34	1.203	0.235	± 0.311	0.256	69	24	6	2
Filter IMPROVE_A_ TOR	Sunset Optical BC	2.67	1.05	1.898	± 0.3946	0.401	± 0.3717	1.761	± 0.7573	0.824	± 0.9208	0.66	9	2.681	± 1.25	2.548	1.620	± 1.408	0.498	0	0	56	44
Filter IMPROVE_A_ TOT	Sunset Optical BC	1.73	1.05	1.323	± 0.3250	0.175	± 0.2927	1.283	± 0.3921	0.391	± 0.4767	0.78	9	1.722	± 0.68	1.657	0.687	± 0.706	0.476	44	33	11	11
Filter STN_ TOR	Sunset Optical BC	1.73	1.05	1.456	± 0.3953	0.188	± 0.3472	1.281	± 0.1739	0.393	± 0.2115	0.94	9	1.724	± 0.28	1.656	0.686	± 0.354	0.556	33	56	11	0
Filter STN_ TOT	Sunset Optical BC	0.98	1.05	0.524	± 0.2197	0.253	± 0.1890	0.933	± 0.1892	0.006	± 0.2300	0.88	9	0.972	± 0.27	0.938	-0.065	± 0.332	0.445	89	0	11	0
HiVol by French	Sunset Optical BC	1.12	0.86	1.192	± 0.3791	-0.013	± 0.3182	1.563	± 0.7918	-0.226	± 0.7260	0.66	7	1.336	± 0.72	1.301	0.260	± 0.621	0.288	29	57	0	14

[a] Refer to Table 4-2 for detailed instrumentation and measurements; Filter EC data used here is an average of different integrated samplers, analyzed by the protocol indicated in the Table: Interagency Monitoring of Protected Visual Environments (IMPROVE) Thermal Optical Reflectance (TOR) and Transmittance (TOT) and Speciation Trends Network (STN) Thermal Optical Reflectance (TOR) and Transmittance (TOT) protocols. Cachier's French two-step protocol (Cachier et al., 1989a; Cachier et al., 1989b) was used only on samples from Andersen high volume (HiVol) sampler.

[b] Effective variance weighted least squares linear regression (Watson et al., 1984) weights variable by precisions in both variables

[c] SE: Standard error

[d] Ordinary least squares linear regression does not weight variables by their precisions

[e] Correlation coefficient

[f] SD: Standard deviation

[g] RMS: Root mean squared precision

[h] Fraction of pairs in percent for which the difference is less than or greater than one, two, or three times the propagated measurement uncertainty

[i] Measurement uncertainty of (y-x)

* b_{abs} scaled to 670 nm using wavelength dependence shown by the respective instrument

Table 6-26. Comparison between b_{abs} and BC concentration measurements at Fresno from 12/1/03 to 12/31/03.

Instrument[a]		Averages		Effective Variance Weighted Regression[b]		Ordinary Least Squares Regression[d]			Number	Ratio y/x	Ratio
y	x	y	x	Slope ± SE[c]	Intercept ± SE[c]	Slope ± SE[c]	Intercept ± SE[c]	r^2[e]	of pairs	Average ± SD[f]	Avg y/Avg x
(Mm^{-1})	($\mu g/m^3$)	(Mm^{-1})	($\mu g/m^3$)	(m^2/g)	(Mm^{-1})	(m^2/g)	(Mm^{-1})			(m^2/g)	(m^2/g)
2-AE 880 nm	Filter IMPROVE_A_ TOR	29.99	2.67	9.074 ± 1.3000	5.019 ± 2.4645	7.221 ± 2.3318	10.742 ± 7.3140	0.76	9	12.119 ± 2.88	11.249
2-AE 880 nm	Filter IMPROVE_A_ TOT	29.99	1.73	14.404 ± 2.4605	4.888 ± 2.9228	12.969 ± 3.1047	7.508 ± 6.2486	0.84	9	18.667 ± 4.72	17.300
2-AE 880 nm	Filter STN_ TOR	29.99	1.73	16.717 ± 3.4782	0.704 ± 4.4212	18.298 ± 1.3003	-1.709 ± 2.5051	0.98	9	17.297 ± 1.35	17.312
2-AE 880 nm	Filter STN_ TOT	29.99	0.98	21.948 ± 5.7411	6.982 ± 4.0346	20.344 ± 4.7647	10.023 ± 5.6244	0.85	9	35.138 ± 20.69	30.554
2-AE 880 nm	HiVol by French	25.95	1.12	11.619 ± 2.3759	10.229 ± 2.3139	10.578 ± 3.3896	14.076 ± 4.5416	0.81	7	30.712 ± 20.18	23.114
7-AE 880 nm	Filter IMPROVE_A_ TOR	28.81	2.67	8.509 ± 1.2311	5.101 ± 2.3441	6.735 ± 2.3985	10.854 ± 7.5234	0.73	9	11.664 ± 2.89	10.806
7-AE 880 nm	Filter IMPROVE_A_ TOT	28.81	1.73	13.671 ± 2.3470	4.837 ± 2.7969	12.242 ± 3.2487	7.587 ± 6.5383	0.82	9	17.983 ± 4.84	16.618
7-AE 880 nm	Filter STN_ TOR	28.81	1.73	16.130 ± 3.3588	0.541 ± 4.2699	17.665 ± 1.5615	-1.794 ± 3.0085	0.97	9	16.596 ± 1.45	16.630
7-AE 880 nm	Filter STN_ TOT	28.81	0.98	21.022 ± 5.5082	6.679 ± 3.8775	19.822 ± 4.6427	9.353 ± 5.4805	0.85	9	33.777 ± 20.25	29.350
7-AE 880 nm	HiVol by French	24.80	1.12	10.785 ± 2.2313	9.948 ± 2.2034	9.525 ± 3.4142	14.104 ± 4.5746	0.78	7	29.439 ± 19.03	22.086
MAAP 670 nm	2-AE 880 nm	14.88	1.79	8.002 ± 0.0898	0.262 ± 0.0960	8.525 ± 0.0428	-0.341 ± 0.1014	0.99	741	8.545 ± 1.51	8.334
MAAP 670 nm	7-AE 880 nm	14.88	1.71	8.306 ± 0.0932	0.424 ± 0.0949	8.513 ± 0.0402	0.283 ± 0.0933	0.99	741	9.089 ± 1.73	8.678
MAAP 670 nm	Sunset Thermal EC	15.92	1.44	10.355 ± 0.2079	0.592 ± 0.2027	10.659 ± 0.0959	0.542 ± 0.1864	0.98	612	30.194 ± 126.51	11.035
MAAP 670 nm	Filter IMPROVE_A_ TOR	15.08	2.67	3.905 ± 0.6821	3.766 ± 1.4094	3.522 ± 1.2224	5.692 ± 3.8343	0.74	9	6.128 ± 1.37	5.657
MAAP 670 nm	Filter IMPROVE_A_ TOT	15.08	1.73	6.739 ± 1.3111	3.086 ± 1.6563	6.459 ± 1.6045	3.884 ± 3.2291	0.84	9	9.439 ± 2.32	8.699
MAAP 670 nm	Filter STN_ TOR	15.08	1.73	8.069 ± 1.8174	0.843 ± 2.3828	9.053 ± 0.9196	-0.602 ± 1.7718	0.97	9	8.779 ± 0.99	8.705
MAAP 670 nm	Filter STN_ TOT	15.08	0.98	10.845 ± 3.0688	3.723 ± 2.2260	10.642 ± 2.1364	4.636 ± 2.5220	0.88	9	17.539 ± 9.32	15.364
MAAP 670 nm	HiVol by French	12.81	1.12	5.096 ± 1.3254	5.813 ± 1.4080	4.320 ± 1.7105	7.955 ± 2.2919	0.75	7	15.648 ± 10.83	11.405
PA 1047 nm	2-AE 880 nm	6.86	1.92	3.530 ± 0.0298	-0.052 ± 0.0346	3.851 ± 0.0277	-0.521 ± 0.0709	0.99	552	3.586 ± 0.97	3.579
PA 1047 nm	7-AE 880 nm	6.86	1.84	3.655 ± 0.0310	0.030 ± 0.0343	3.839 ± 0.0253	-0.219 ± 0.0637	0.99	552	3.809 ± 1.18	3.720
PA 1047 nm	Sunset Thermal EC	7.11	1.53	4.542 ± 0.0875	0.036 ± 0.0909	4.794 ± 0.0545	-0.233 ± 0.1127	0.97	497	8.589 ± 54.37	4.642
PA 1047 nm	Filter IMPROVE_A_ TOR	6.24	2.67	2.104 ± 0.2512	0.851 ± 0.4796	1.589 ± 0.5534	2.004 ± 1.7665	0.76	8	2.527 ± 0.60	2.340
PA 1047 nm	Filter IMPROVE_A_ TOT	6.24	1.75	3.063 ± 0.4776	0.968 ± 0.5690	2.947 ± 0.6764	1.081 ± 1.3933	0.87	8	3.828 ± 0.88	3.563
PA 1047 nm	Filter STN_ TOR	6.24	1.67	3.665 ± 0.7663	0.046 ± 0.9491	4.056 ± 0.4020	-0.549 ± 0.7598	0.97	8	3.705 ± 0.41	3.728
PA 1047 nm	Filter STN_ TOT	6.24	1.05	5.751 ± 1.4093	0.288 ± 1.0351	5.416 ± 0.3855	0.564 ± 0.4788	0.99	8	6.089 ± 0.78	5.954
PA 1047 nm	HiVol by French	4.99	0.96	1.636 ± 0.3062	3.399 ± 0.2762	1.826 ± 0.9436	3.230 ± 1.1039	0.70	6	6.906 ± 4.53	5.183

[a] Refer to Table 4-2 for detailed instrumentation and measurements; Filter EC data used here is an average of different integrated samplers, analyzed by the protocol indicated in the Table: Interagency Monitoring of Protected Visual Environments (IMPROVE) Thermal Optical Reflectance (TOR) and Transmittance (TOT) and Speciation Trends Network (STN) Thermal Optical Reflectance (TOR) and Transmittance (TOT) protocols. Cachier's French two-step protocol (Cachier et al., 1989a; Cachier et al., 1989b) was used only on samples from Andersen high volume (HiVol) sampler.

[b] Effective variance weighted least squares linear regression (Watson et al., 1984) weights variable by precisions in both variables

[c] SE: Standard error

[d] Ordinary least squares linear regression does not weight variables by their precisions

[e] Correlation coefficient

[f] SD: Standard deviation

* b_{abs} scaled to 670 nm using wavelength dependence shown by the respective instrument

Table 6-27. Angstrom absorption exponent at Fresno (12/1/03-12/31/03).

	Angstrom Absorption Exponent, α, for Dec 2003					
Instrument[a]=>>	2-AE			7-AE		
Hour	Average	±	SD[b]	Average	±	SD[b]
0	1.47	±	0.254	1.30	±	0.271
1	1.43	±	0.335	1.28	±	0.288
2	1.43	±	0.296	1.30	±	0.231
3	1.42	±	0.311	1.28	±	0.217
4	1.45	±	0.289	1.31	±	0.280
5	1.39	±	0.255	1.25	±	0.243
6	1.25	±	0.187	1.11	±	0.219
7	1.16	±	0.175	1.08	±	0.176
8	1.12	±	0.188	1.09	±	0.185
9	1.10	±	0.199	1.04	±	0.162
10	1.14	±	0.189	1.02	±	0.187
11	1.19	±	0.270	1.08	±	0.230
12	1.20	±	0.292	1.06	±	0.213
13	1.19	±	0.297	1.07	±	0.244
14	1.24	±	0.300	1.14	±	0.262
15	1.32	±	0.338	1.18	±	0.344
16	1.34	±	0.321	1.21	±	0.287
17	1.38	±	0.324	1.30	±	0.295
18	1.41	±	0.265	1.33	±	0.236
19	1.40	±	0.259	1.29	±	0.219
20	1.43	±	0.235	1.30	±	0.187
21	1.44	±	0.209	1.30	±	0.254
22	1.41	±	0.206	1.26	±	0.191
23	1.46	±	0.243	1.32	±	0.269
Average ± SD[b]	1.32	±	0.125	1.20	±	0.108

[a] Refer to Table 4-2 for detailed instrumentation and measurements
[b] SD: Standard deviation

Table 6-28. Summary of carbon comparison between the summer and winter IOPs.

Observable	Comparison (y vs. x)	Summer IOP	Winter IOP
b_{abs}	2-AE (670) vs. MAAP (670)	200% (3 times) higher than MAAP	200% (3 times) higher than MAAP
b_{abs}	7-AE (670) vs MAAP (670)	250% (3.5 times) higher than MAAP	150% (2.5 times) higher than MAAP
b_{abs}	7-AE (950) vs. PA (1047)	620% (7.2 times) higher than PA	320% (4.2 times) higher than PA
BC	2-AE (880) vs MAAP (670)	5% lower than MAAP	21% lower than MAAP
BC	2-AE or 7-AE (880) vs PA (1047)	~100% (~ 2 times) higher than PA	~40% (~1.4 times) higher than PA
BC	2-AE (880) vs Sunset Thermal EC	20% lower than Sunset	16% higher than Sunset
BC	7-AE (880) vs MAAP (670)	3% higher than MAAP	26% lower than MAAP
BC	7-AE (880) vs Sunset Thermal EC	16% lower than Sunset	10% higher than Sunset
BC	MAAP (670) vs PA (1047)	~150% (~ 2.5 times) higher than PA	~70% (~1.7 times) higher than PA
BC	MAAP (670) vs Sunset Thermal EC	2% lower than Sunset	38% higher than Sunset
BC	PA (1047) vs MAAP (670)	54% lower than MAAP	45% lower than MAAP
BC	PA (1047) vs Sunset Thermal EC	63% lower than Sunset	18% lower than Sunset
BC	IMPROVE_A_TOR vs 2-AE or 7-AE (880)	15% higher than 2-AE and 7-AE	12% higher than 2-AE and 7-AE
BC	IMPROVE_A_TOR vs MAAP (670)	5 to 7% higher than MAAP	8% lower than MAAP
BC	IMPROVE_A_TOR vs PA (1047)	170% (2.7 times) higher than PA	110% (2.1 times) higher than PA
BC	IMPROVE_A_TOR vs Sunset Thermal EC	10% higher than Sunset	~100% (~ 2 times) higher than Sunset
BC	IMPROVE_A_TOT vs 2-AE or 7-AE (880)	15% lower than 2-AE and 7-AE	23% lower than 2-AE and 7-AE
BC	IMPROVE_A_TOT vs MAAP (670)	25% lower than MAAP	35% lower than MAAP
BC	IMPROVE_A_TOT vs PA (1047)	100% (2 times) higher than PA	40% (1.4 times) higher than PA
BC	IMPROVE_A_TOT vs Sunset Thermal EC	21% lower than Sunset	32% higher than Sunset
BC	STN_TOT vs 2-AE or 7-AE (880)	35 to 40% lower than 2-AE and 7-AE	~45% lower than 2-AE and 7-AE
BC	STN_TOT vs MAAP (670)	40% lower than MAAP	57% lower than MAAP
BC	STN_TOT vs PA (1047)	50% higher than PA	17% lower than PA
BC	STN_TOT vs Sunset Thermal EC	58% lower than Sunset	54% lower than Sunset
BC	French two-step vs 2-AE or 7-AE (880)	0 to 10% lower than 2-AE and 7-AE	26 to 30% lower than 2-AE and 7-AE
BC	French two-step vs MAAP (670)	9% lower than MAAP	43% lower than MAAP
BC	French two-step vs PA (1047)	130% (2.3 times) higher than PA	2% lower than PA
BC	French two-step vs Sunset Thermal EC	17 to 47% lower than Sunset	54 to 102% lower than Sunset

Table 6-29. Comparison of b_{abs} from AE (950 nm) and PA (1047 nm).

Sample Type	Average BC ($\mu g/m^3$) from PA[a]	Average $b_{abs(AE)}/b_{abs(PA)}$	EC/TC Ratio (IMPROVE_A_TOR)
Diesel	191.1	2.03 ± 0.67	0.65 ± 0.11
Acetylene Flame	290.4	1.05 ± 0.07	0.98 ± 0.05
Electric Arc	381.1	1.36 ± 0.19	0.5 ± 0.11
Wood Smoke	29.5	3.65 ± 2.08	0.26 ± 0.12
Carbon Black	24.3	2.70 ± 0.13	0.94 ± 0.06
Fresno (Summer)	0.40	7.2 ± 1.2	0.21 ± 0.04
Fresno (Winter)	1.37	4.21 ± 0.66	0.26 ± 0.05

[a] The average BC is determined from PA b_{abs} assuming a σ_{abs} of 5 m^2/g.

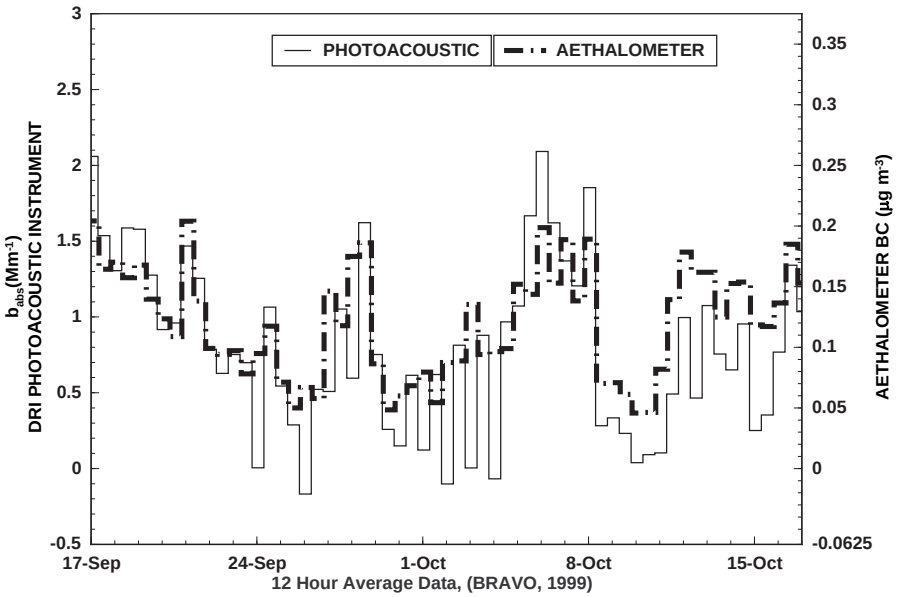

Figure 6-1. Time series of 12-hr averages of photoacoustic b_{abs} and aethalometer BC during BRAVO. The BC concentration was scaled to the pressure and temperature of the site for direct comparison with photoacoustic data.

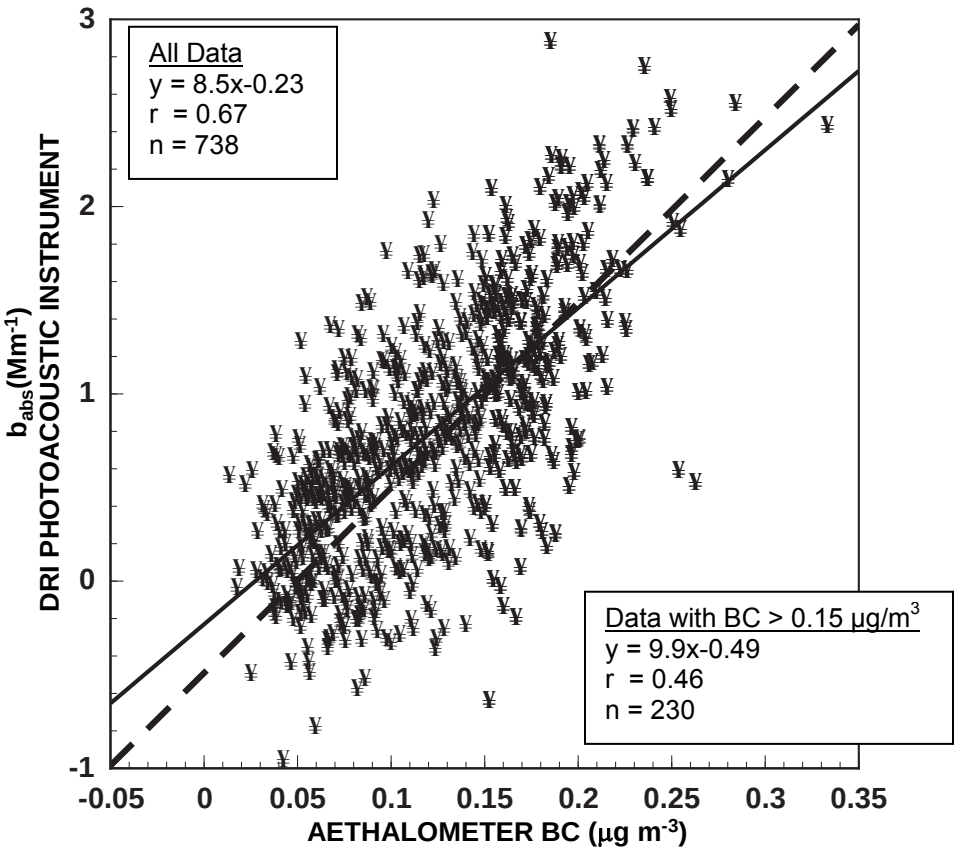

Figure 6-2. Correlation of hourly averaged b_{abs} and BC obtained during BRAVO during September/October 1999. Linear regression lines are shown for the entire data set (solid) and also for the data where BC > 0.15 µg/m^3.

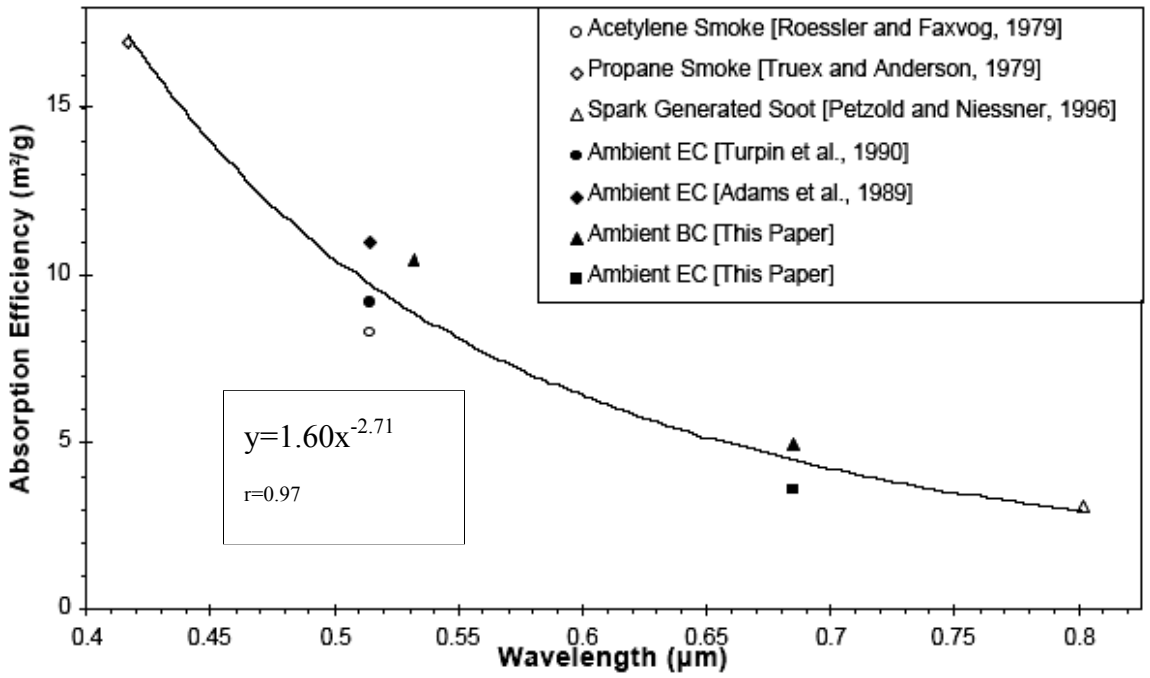

Figure 6-3. Absorption efficiency (σ_{abs}) of light absorbing aerosols as a function of wavelength. Values for laboratory generated aerosols are shown with open symbols and ambient aerosols are shown with solid symbols (Moosmüller et al., 1998).

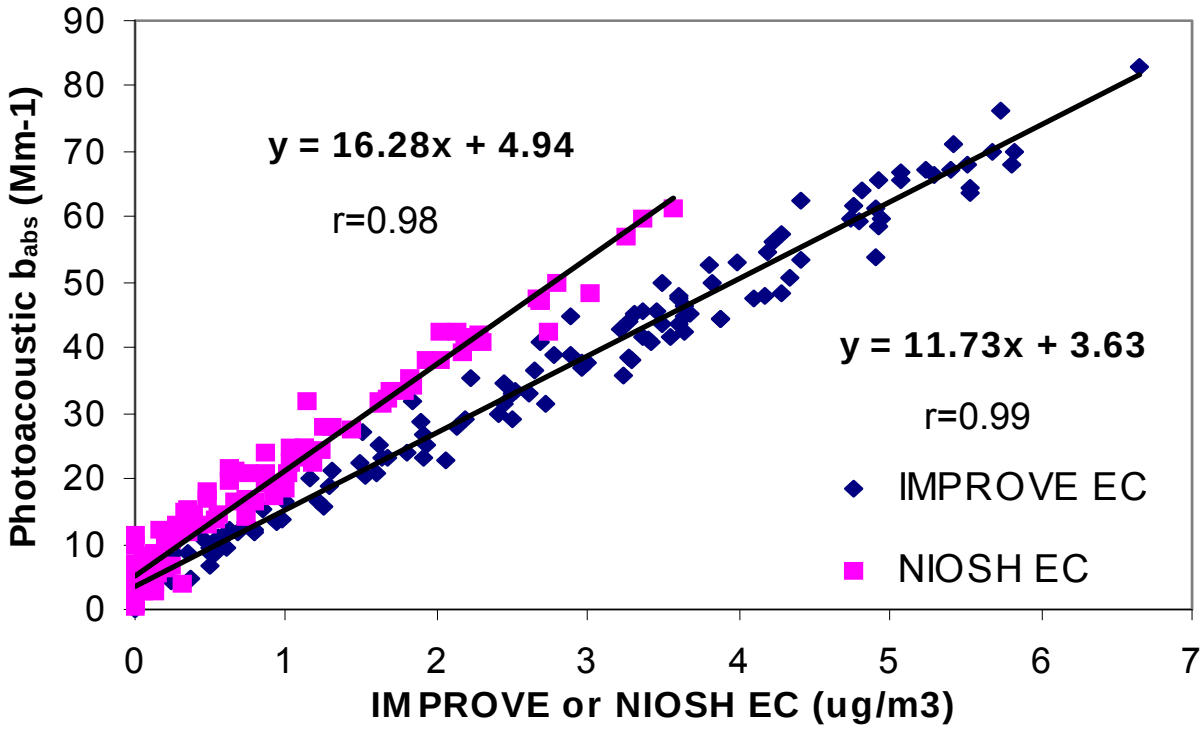

Figure 6-4. Comparison of photoacoustic b_{abs} with IMPROVE_TOT* and NIOSH_TOT EC during SNAQS for winter 2003.

*The IMPROVE temperature set up was used with NIOSH residence time.

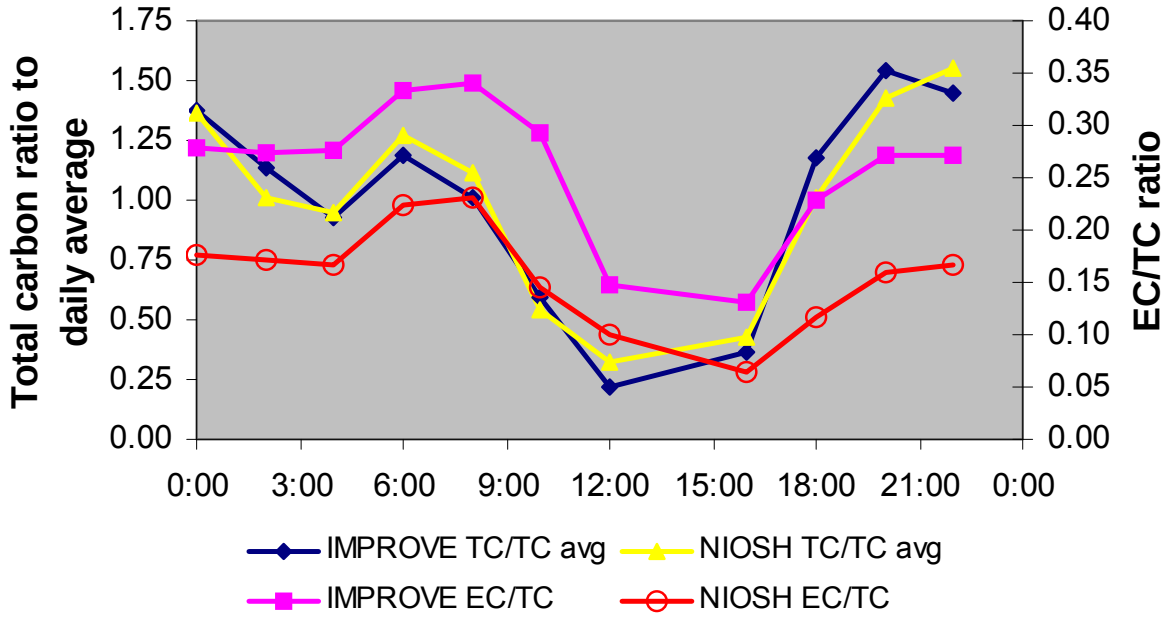

Figure 6-5. Comparison of TC to daily average TC and EC/TC ratios by time, using the semi-continuous Sunset Carbon Analyzer following the IMPROVE and NIOSH temperature protocols during SNAQS.

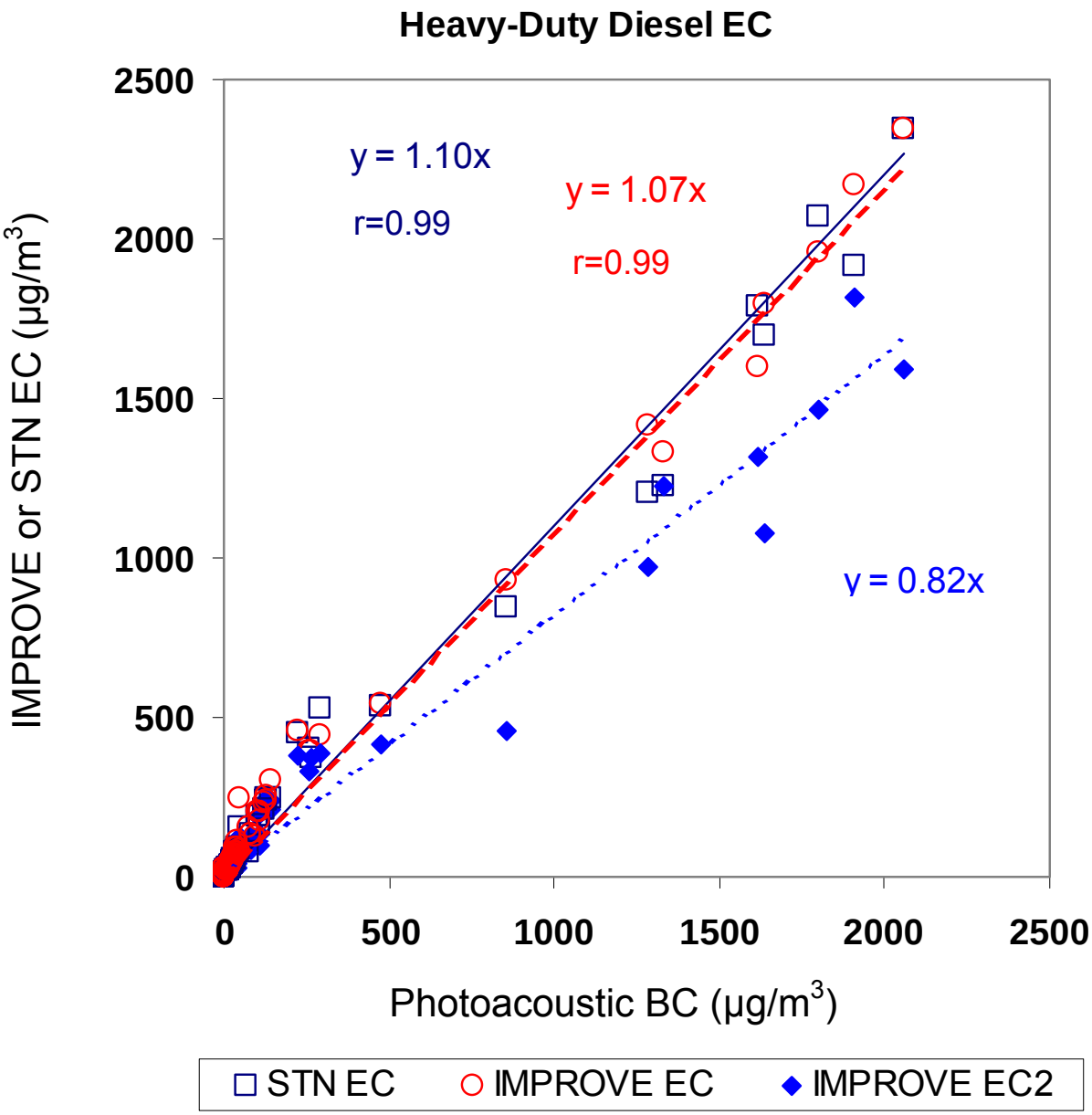

Figure 6-6. Scatter plot of IMPROVE_TOR EC and STN_TOT EC vs. photoacoustic BC concentration* for the diesel-vehicle dynamometer testing. (*σ_{abs} of 5 m^2/g is used to covert photoacoustic b_{abs} to BC concentrations.)

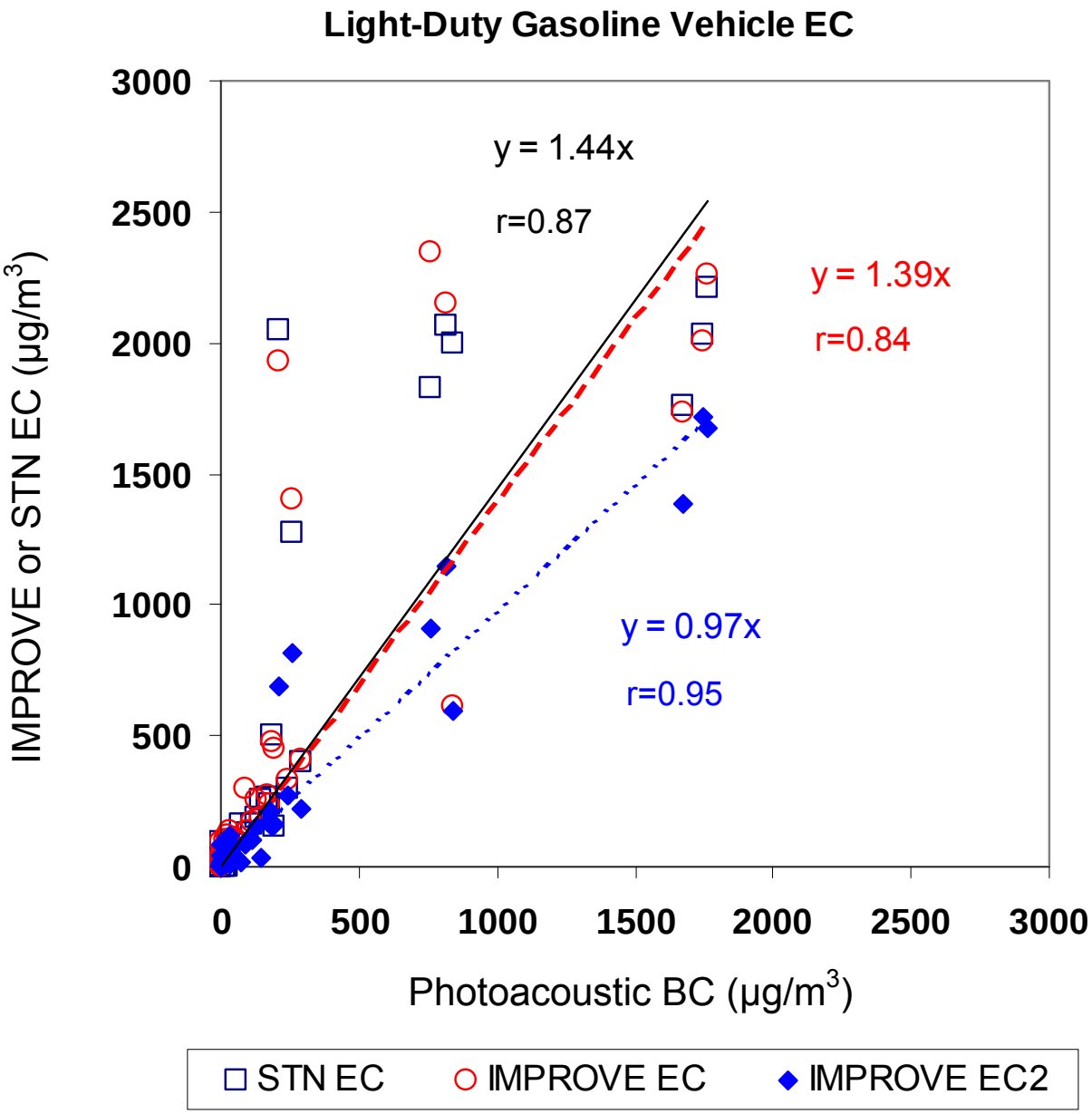

Figure 6-7. Scatter plot of IMPROVE_TOR EC and STN_TOT EC vs. photoacoustic BC concentration* for the gasoline-vehicle dynamometer testing. (*σ_{abs} of 5 m^2/g is used to covert photoacoustic b_{abs} to BC concentrations.)

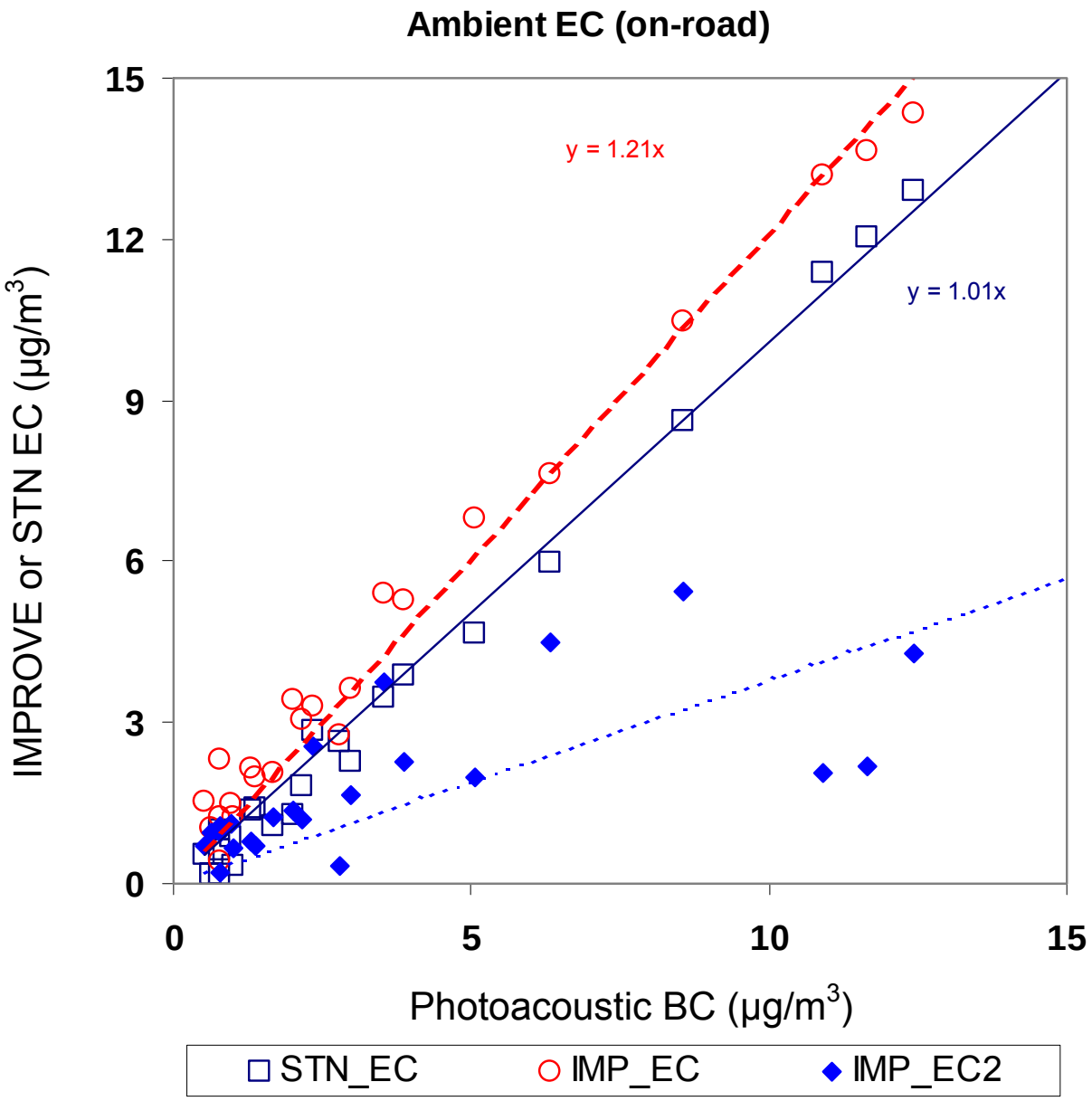

Figure 6-8. Scatter plot of IMPROVE_TOR EC and STN_TOT EC vs. photoacoustic BC concentration* for measurements made at various vehicle-exhaust dominated and regional background locations using an instrumented vehicle. (*σ_{abs} of 5 m^2/g is used to covert photoacoustic b_{abs} to BC concentrations.)

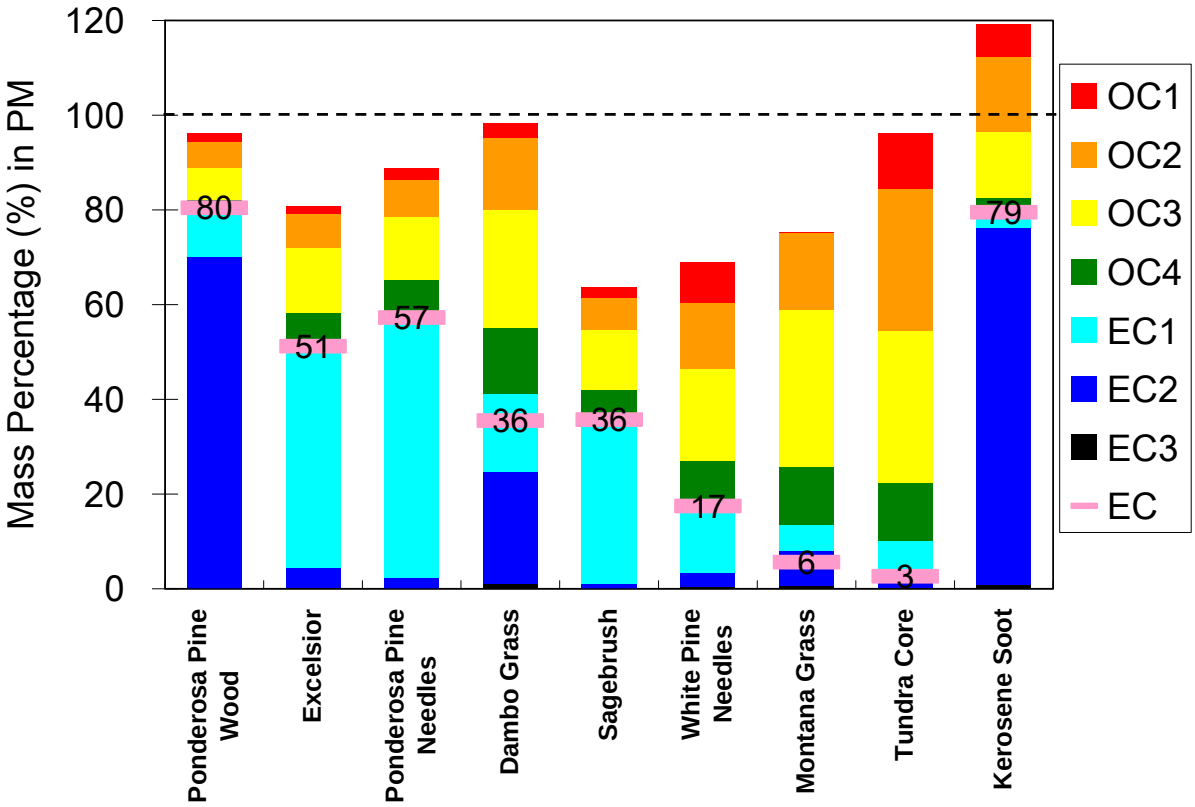

Figure 6-9. Mass percentage of thermally separated carbon fractions in PM. The numbers indicate the mass percentage of EC.

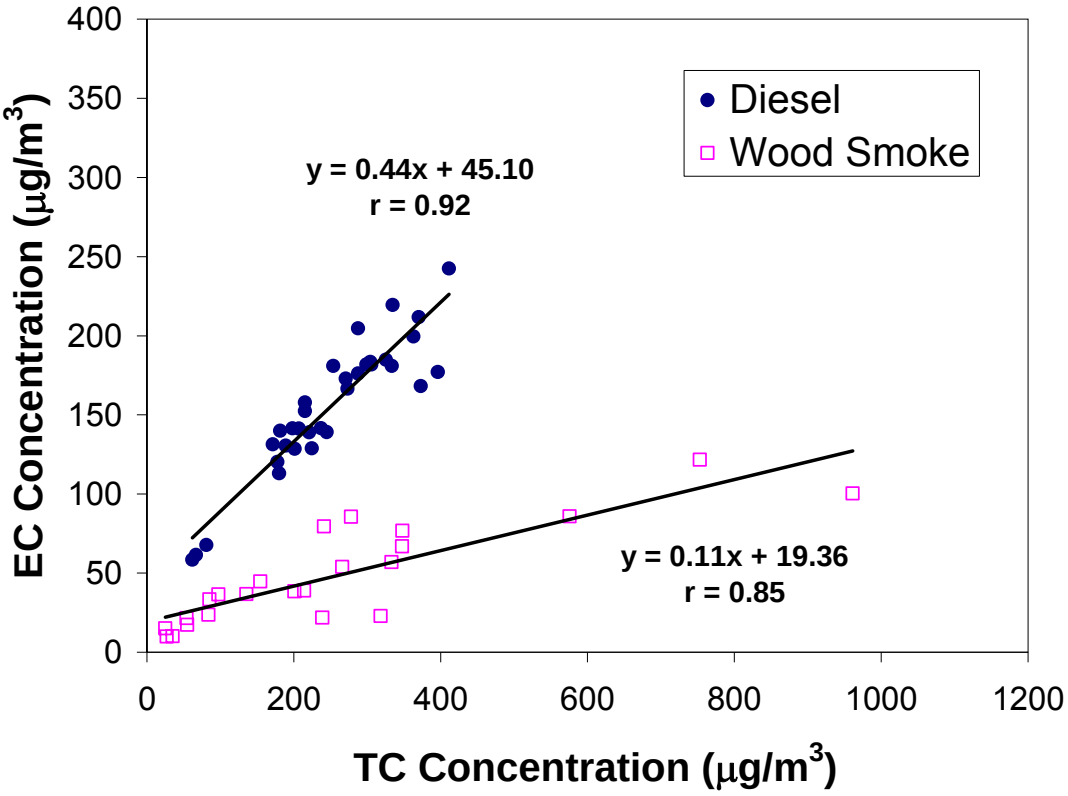

Figure 6-10. EC as a function of TC loading on filters for the diesel and wood smoke samples. Analysis is made by the IMPROVE_A_TOR protocol. Lines indicate the linear regression.

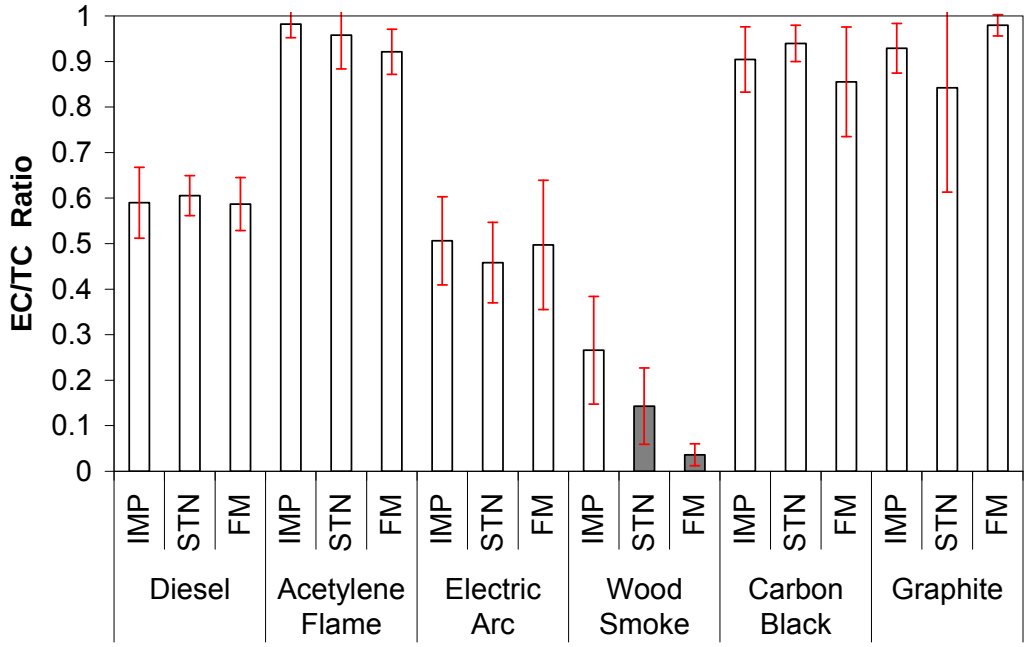

Figure 6-11. EC/TC ratio by source and by thermal method. Error bars determined from the standard deviation across replicate samples. IMP refers to the IMPROVE_A_TOR protocol, STN refers to the STN_TOT protocol, and FM refers to the French two-step protocol.

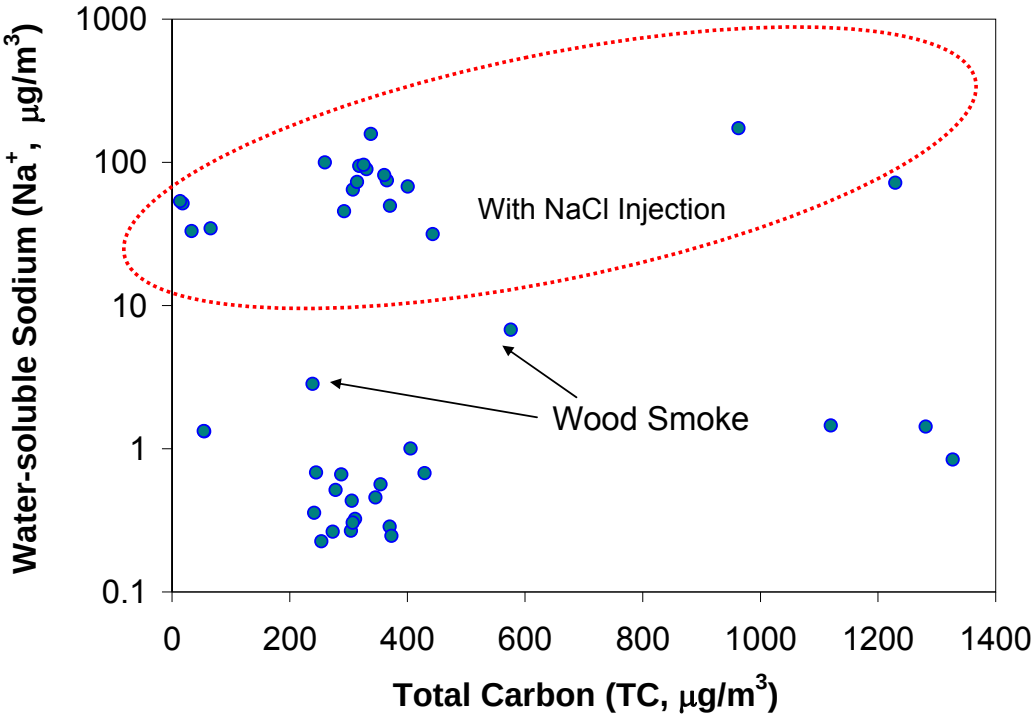

Figure 6-12. Amount of Na^+ in the source samples relative to total carbon (TC). Samples with NaCl injection are enclosed within the circle.

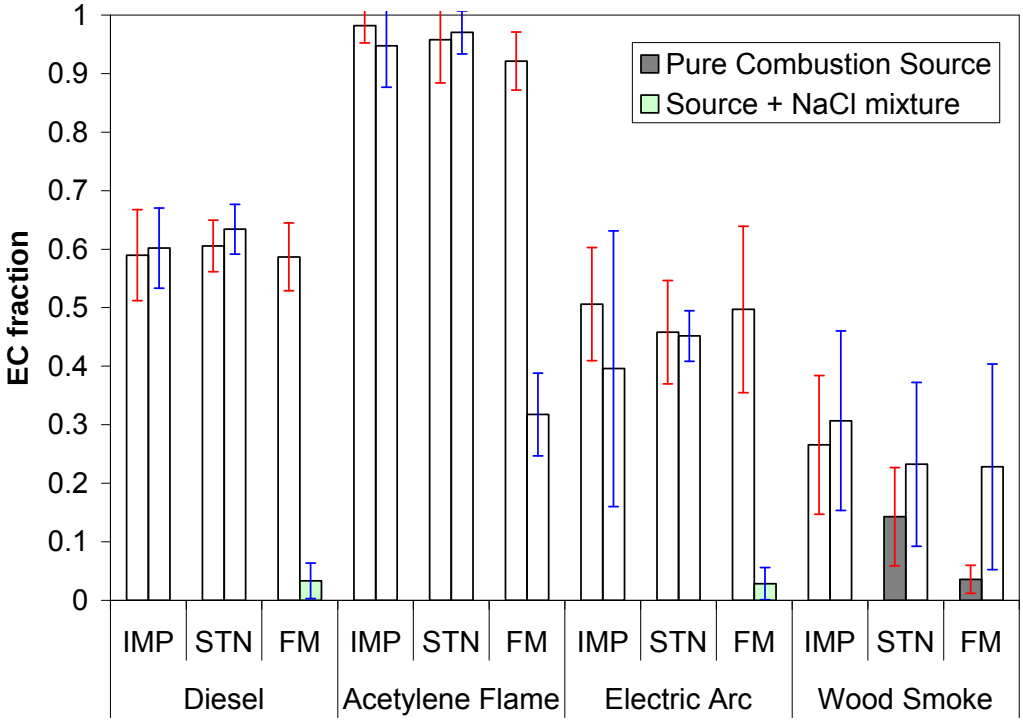

Figure 6-13. EC fraction in TC as a function of source, thermal method, and addition of NaCl. IMP refers to the IMPROVE_A_TOR protocol; STN refers to the STN_TOT protocol; and FM refers to the French two-step protocol.

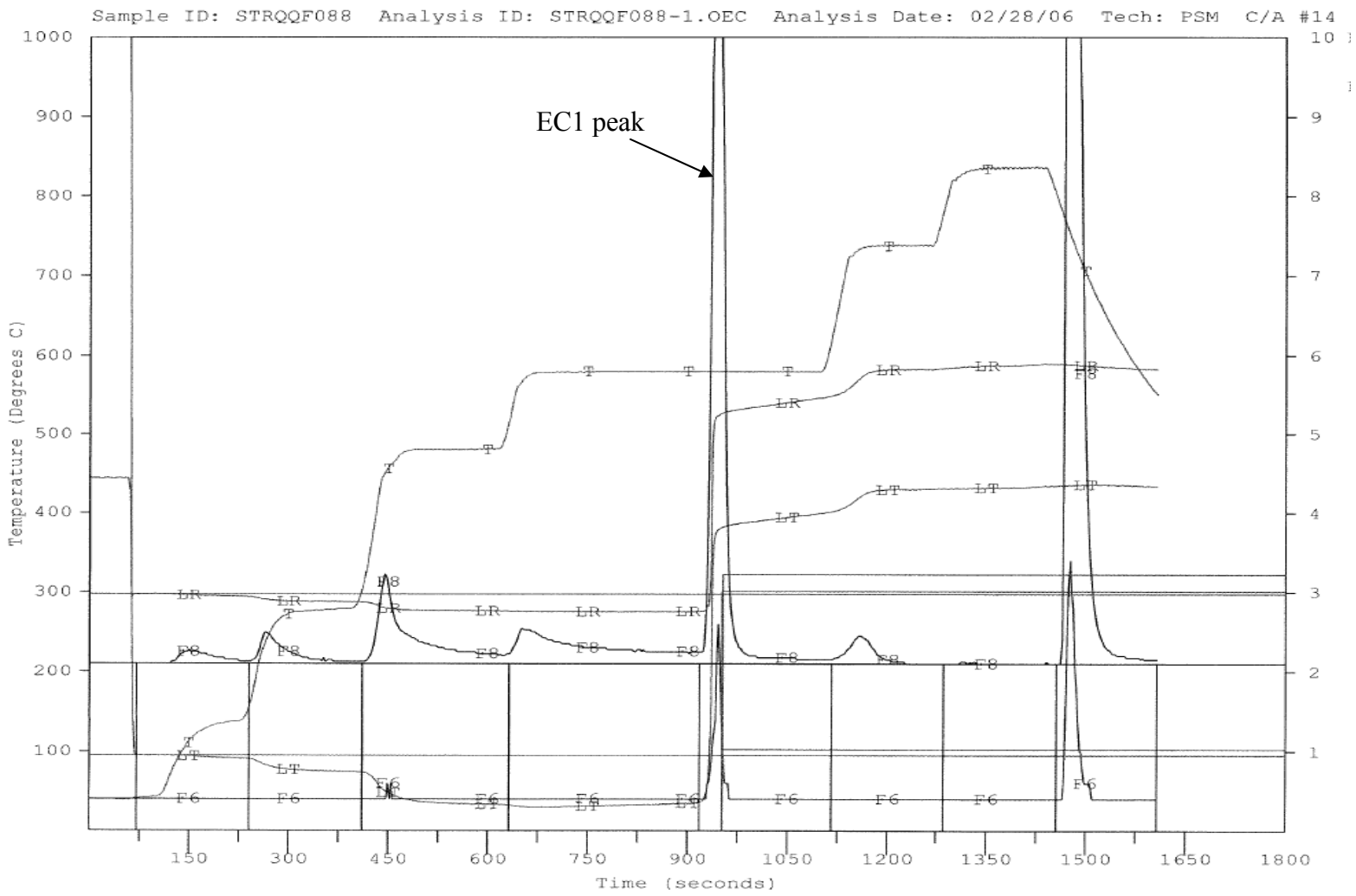

Figure 6-14. Example thermogram of IMPROVE_A analysis on one electric arc + NaCl sample (STRQQF088).

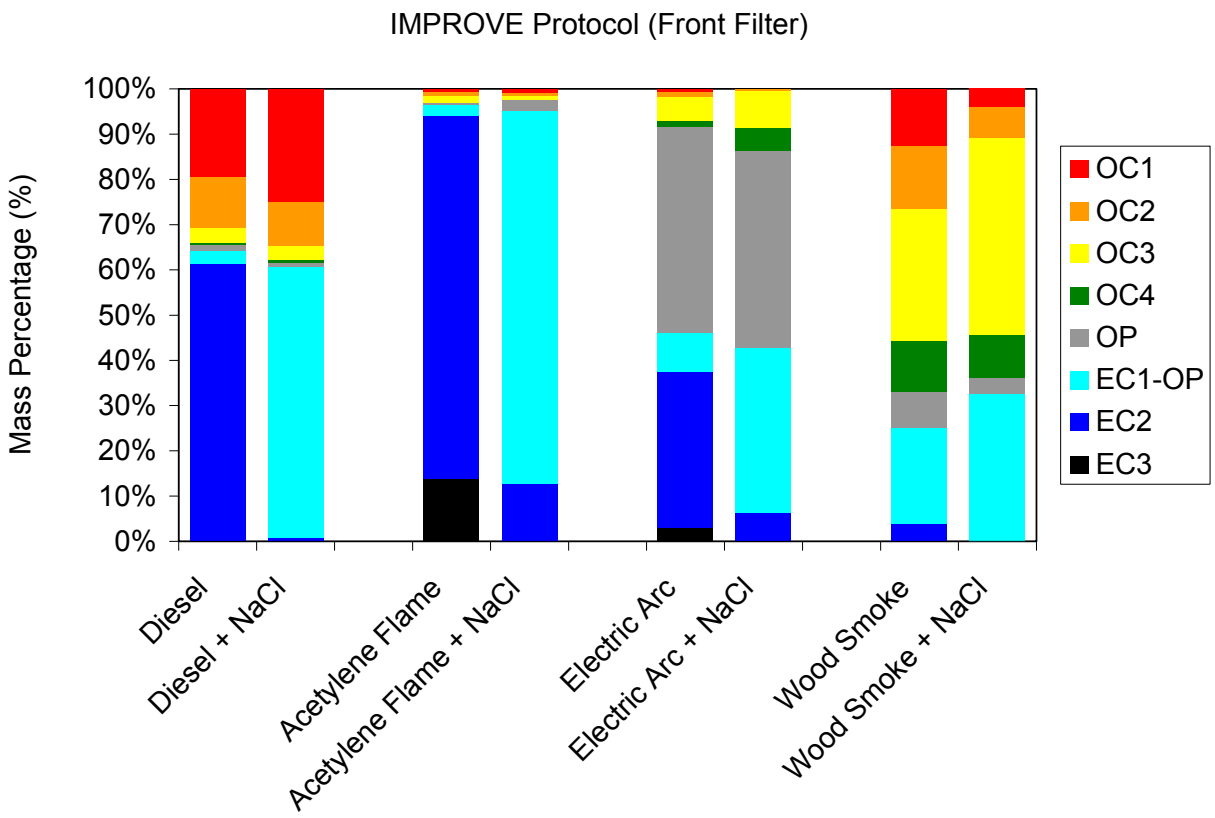

Figure 6-15. Comparisons of carbon fractions (in TC) by IMPROVE_A_TOR protocol of different samples with or without additional NaCl.

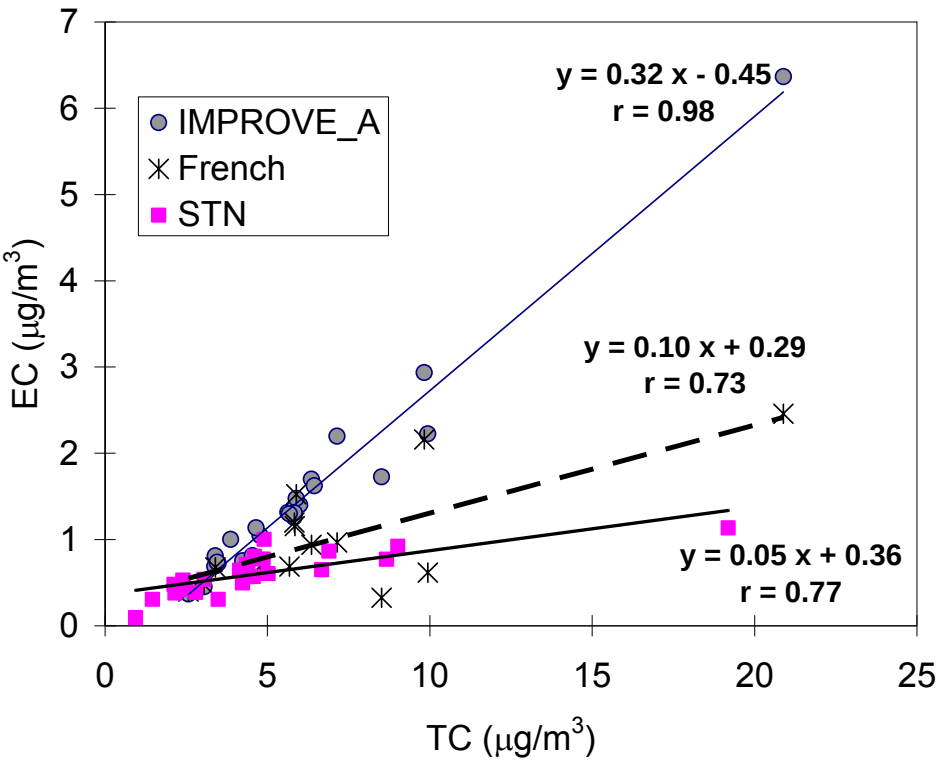

Figure 6-16. Comparisons of 25 EC vs. TC measurements of the Hi-Vol samples from the Fresno Supersite. TC for French two-step protocol was determined by IMPROVE_A.

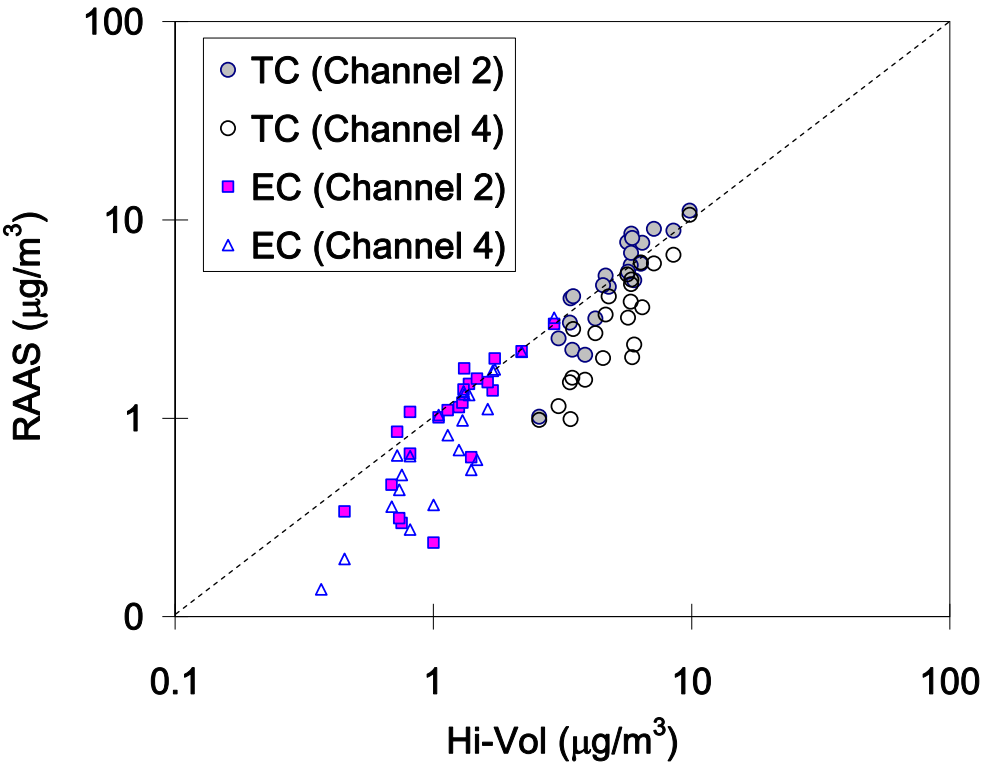

Figure 6-17. Comparisons of EC and TC from the IMPROVE_A analysis of concurrent Hi-Vol and RAAS (Channels 2 and 4) samples. The dashed line indicates the 1:1 line.

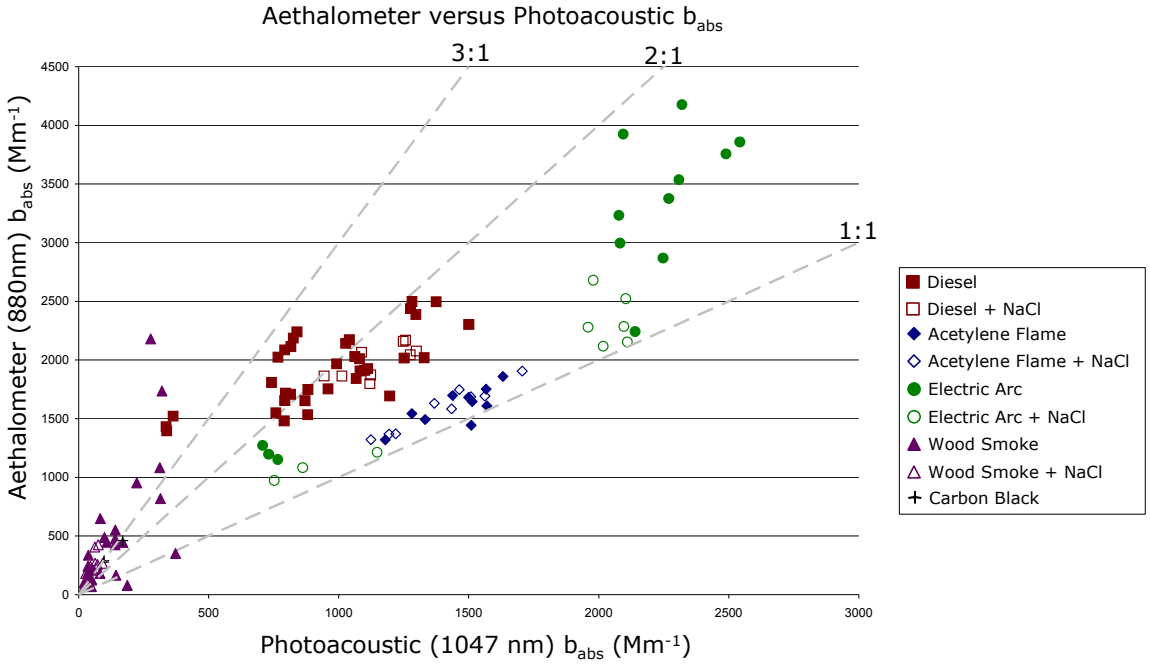

Figure 6-18. Scatter plot of 7-AE (880 nm) and PA (1047 nm) b_{abs} for different sources.

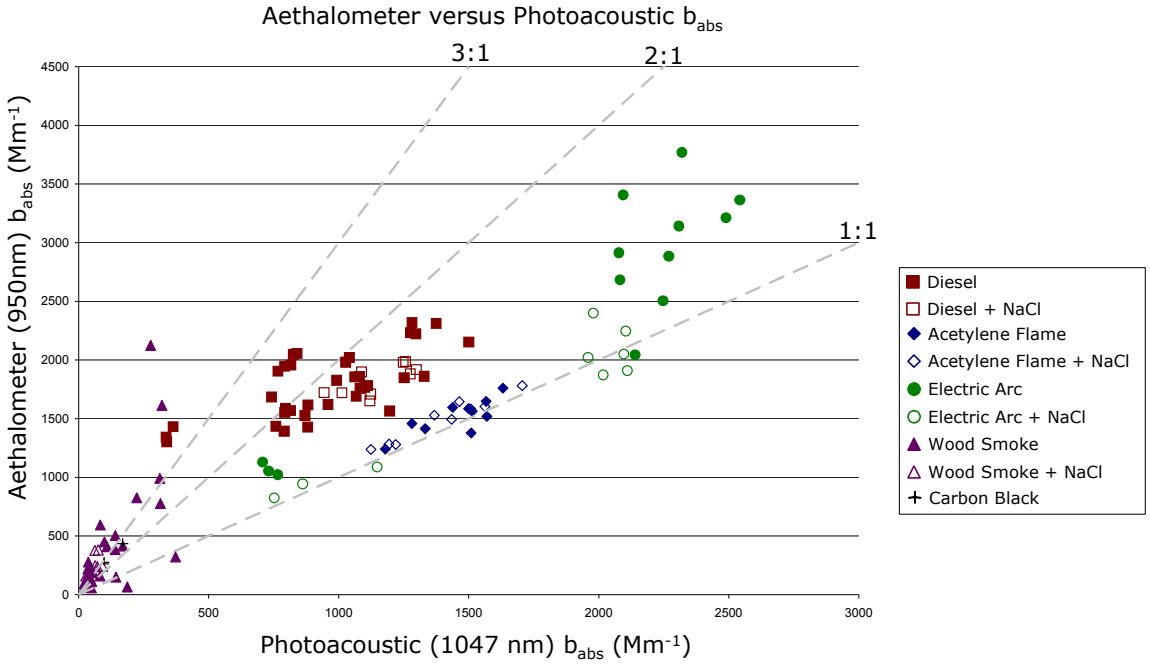

Figure 6-19. Scatter plot of 7-AE (950 nm) and PA (1047 nm) b_{abs} measurements for different sources.

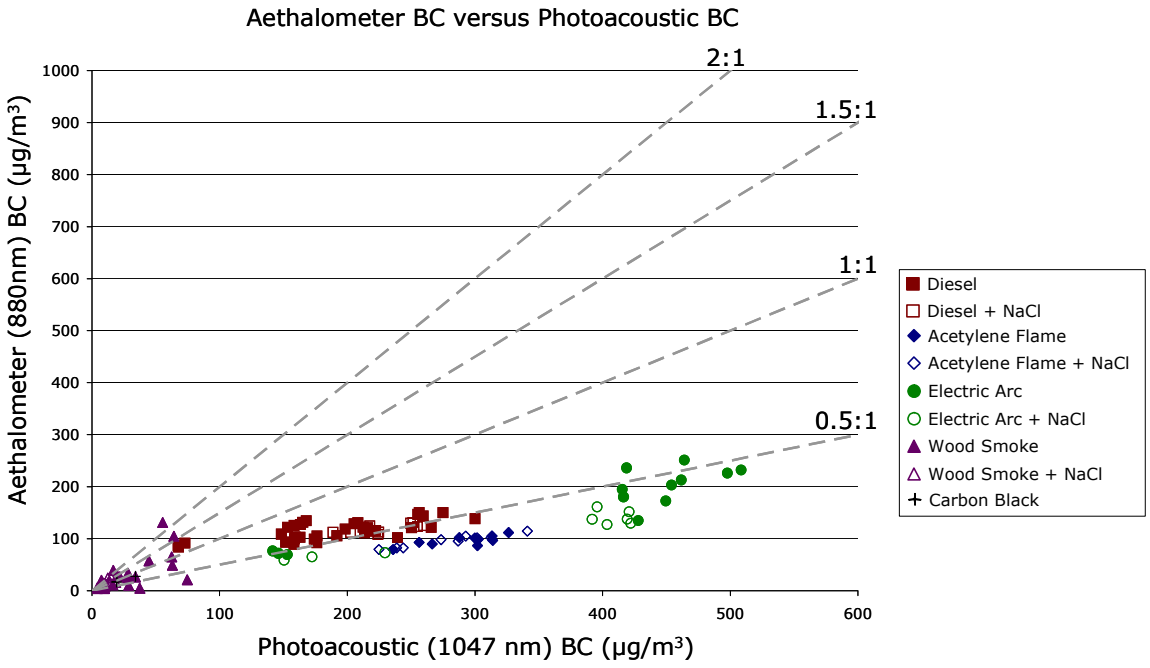

Figure 6-20. Scatter plot of 7-AE (880 nm) and PA (1047 nm) BC concentrations for different sources.

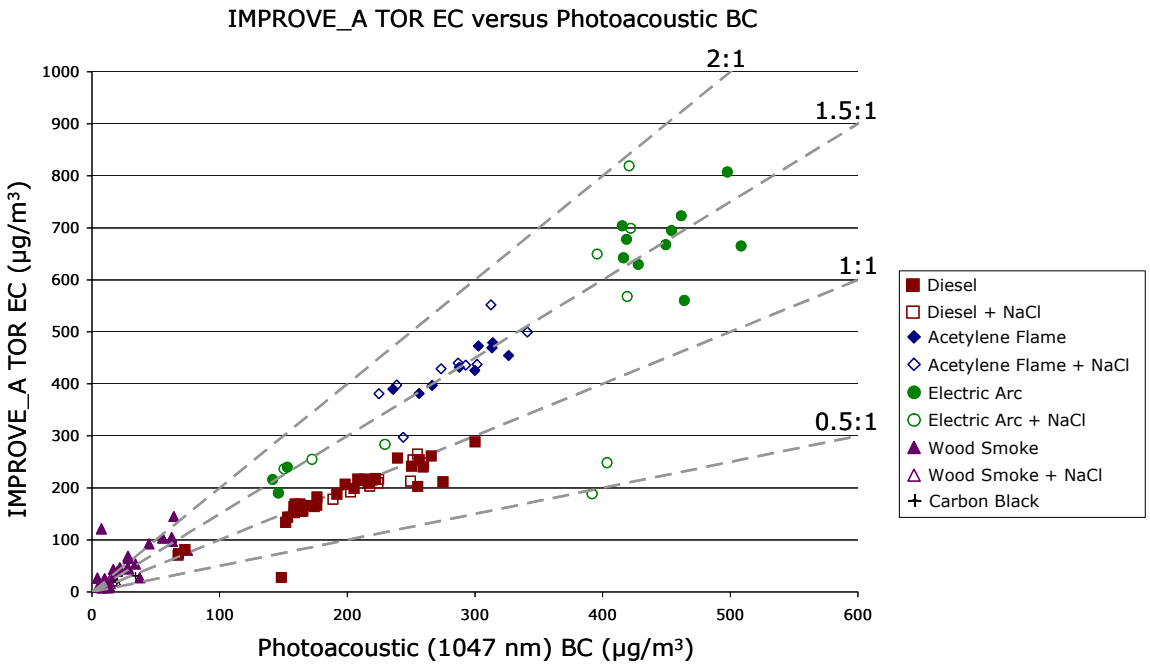

(a)

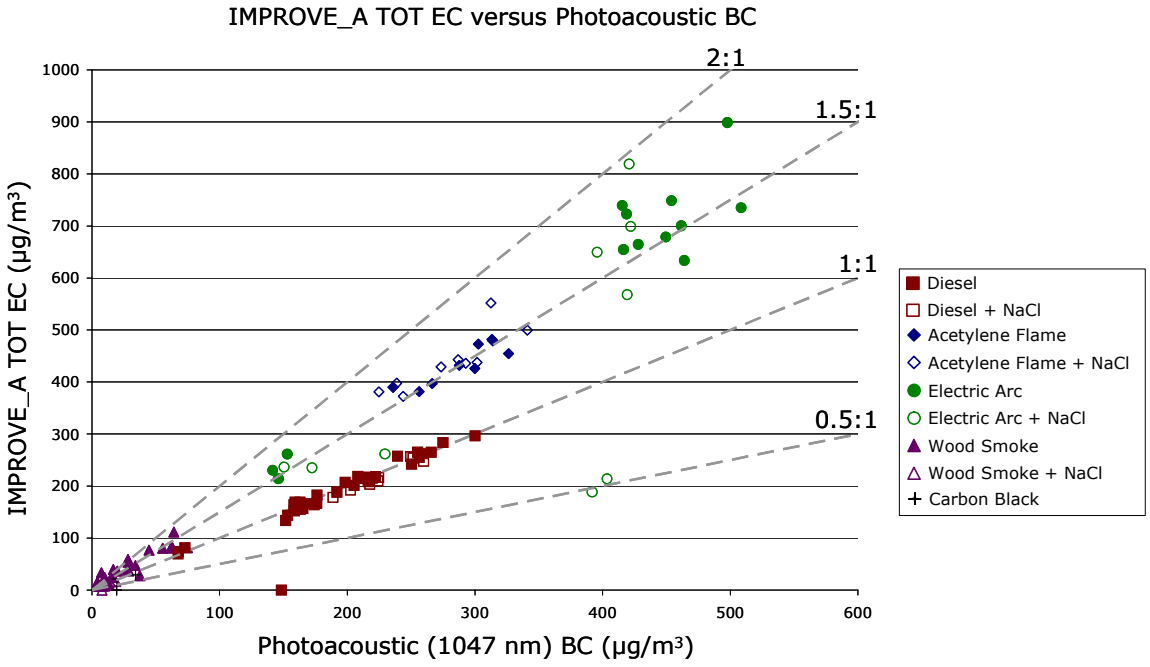

(b)

Figure 6-21. Scatter plot of IMPROVE_A EC and PA (1047 nm) BC concentrations by: a) reflectance; and b) transmittance for different sources.

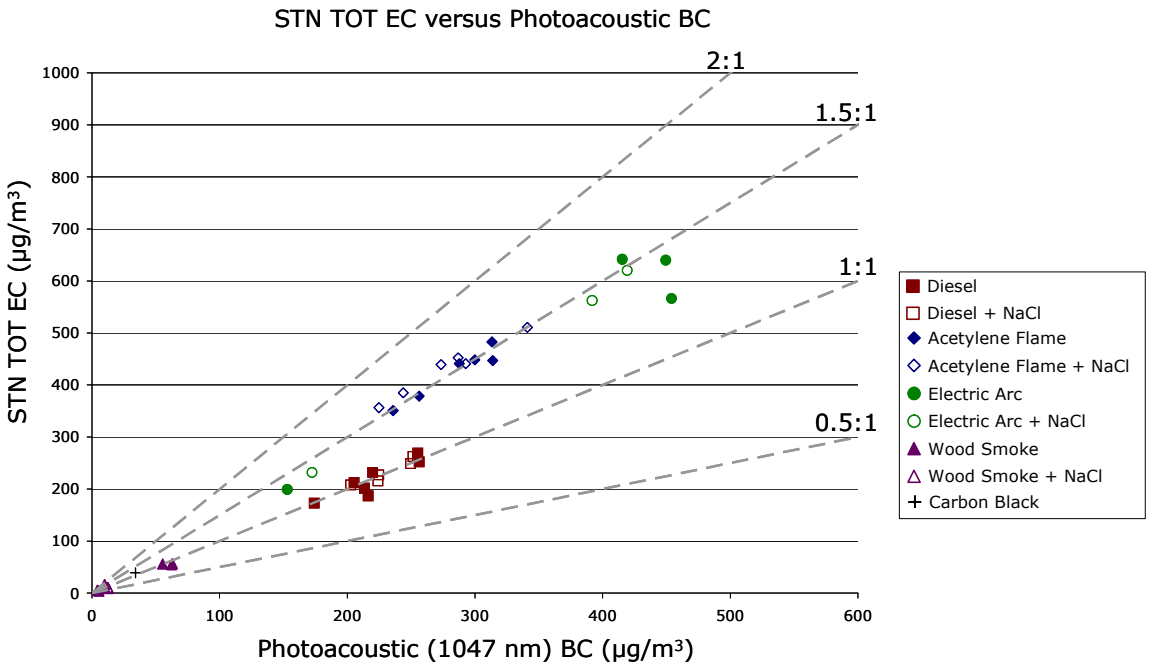

Figure 6-22. Scatter plot of STN_TOT EC and PA (1047 nm) BC concentrations for different sources.

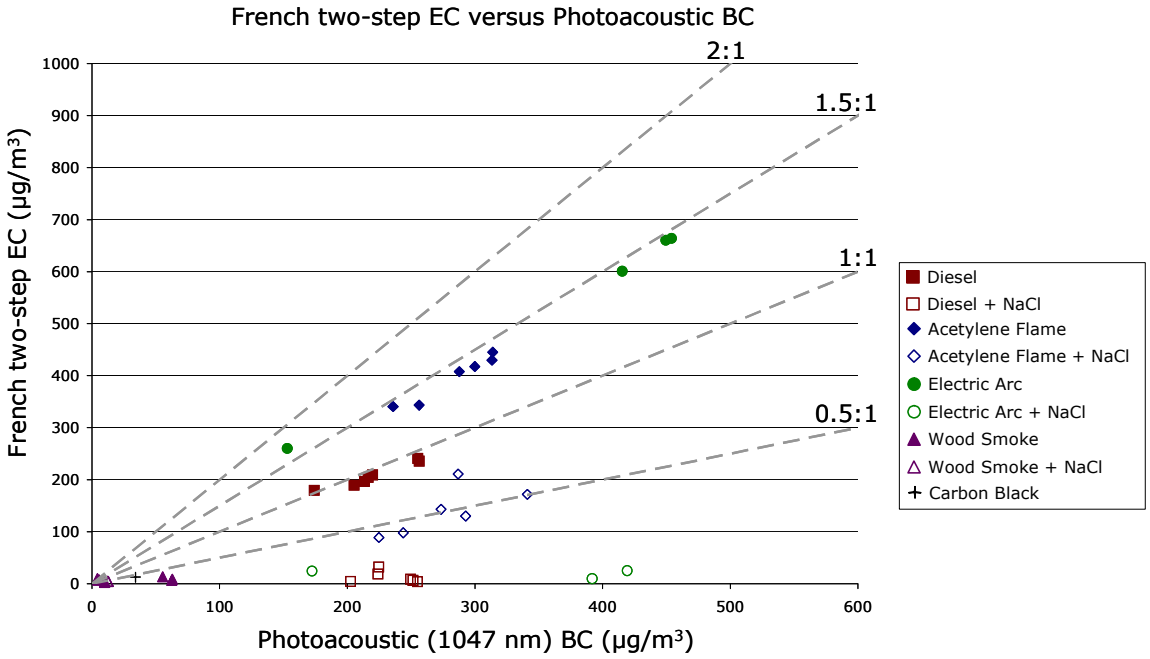

Figure 6-23. Scatter plot of French two-step EC and PA (1047 nm) BC concentrations for different sources.

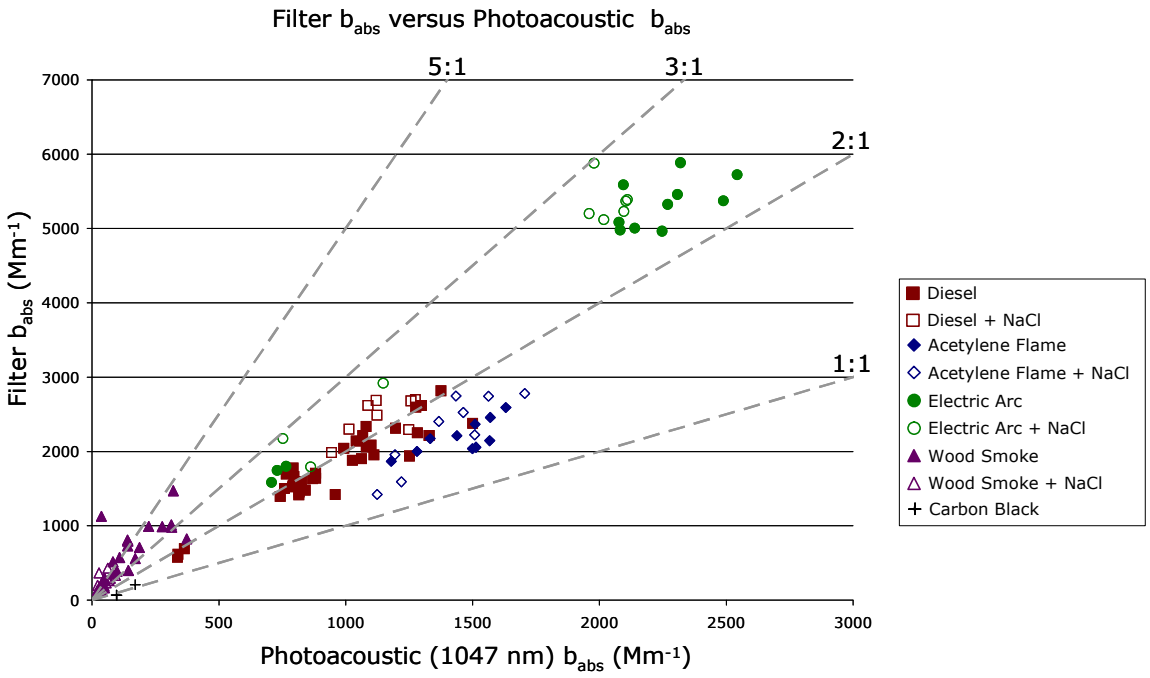

Figure 6-24. Scatter plot of filter b_{abs} and PA (1047 nm) b_{abs} measurements for different sources.

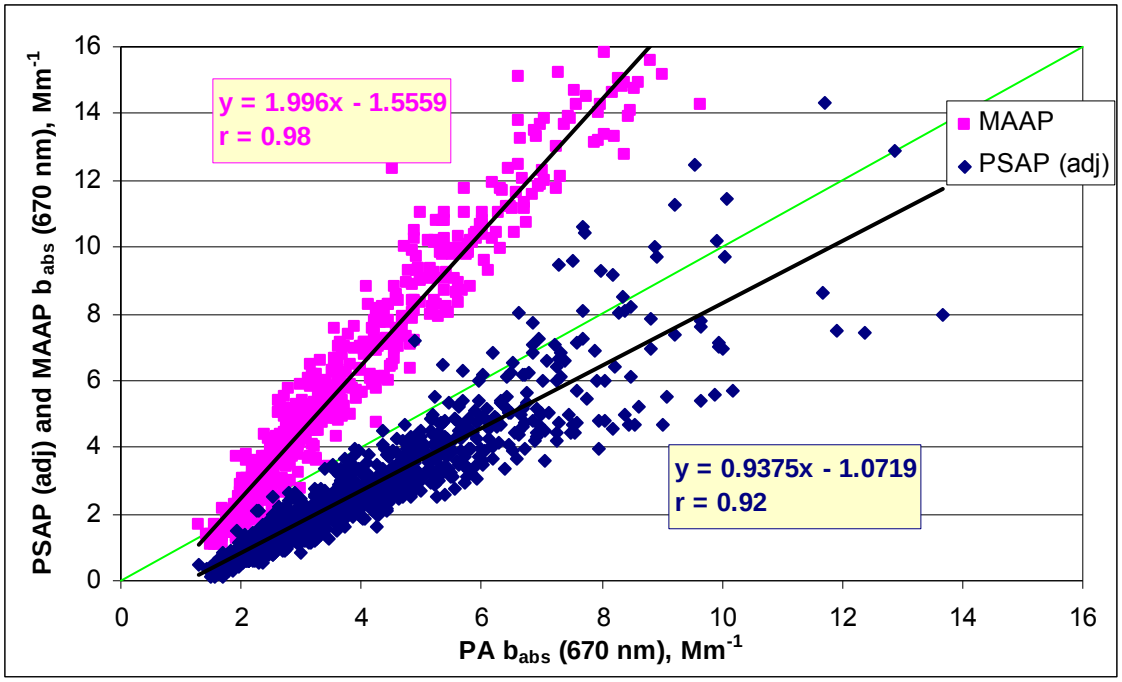

Figure 6-25. Comparison of PSAP(adj), MAAP, PSAP, and PA b_{abs} (measurements normalized to 670 nm) for samples acquired at the Fresno Supersite during 8/1/05 to 9/30/05.

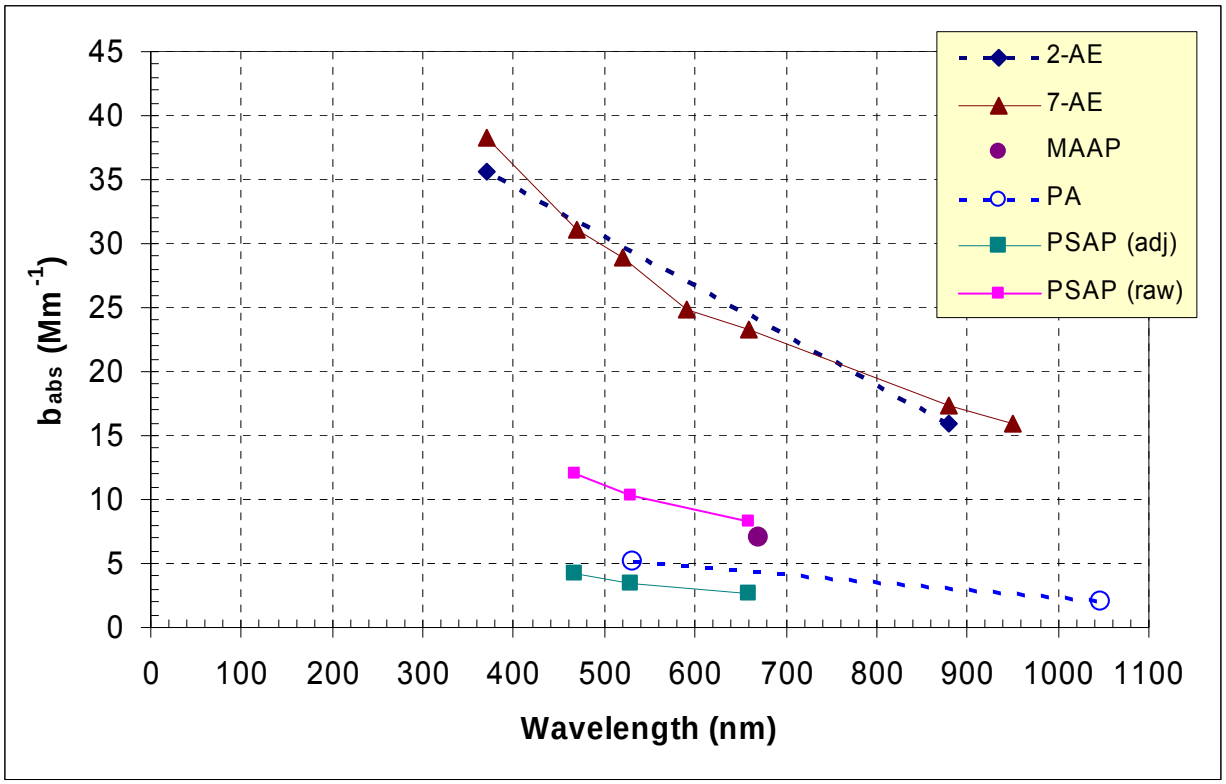

Figure 6-26. Average b_{abs} (Mm^{-1}) measured by different instruments at the Fresno Supersite during 8/1/05 to 9/30/05.

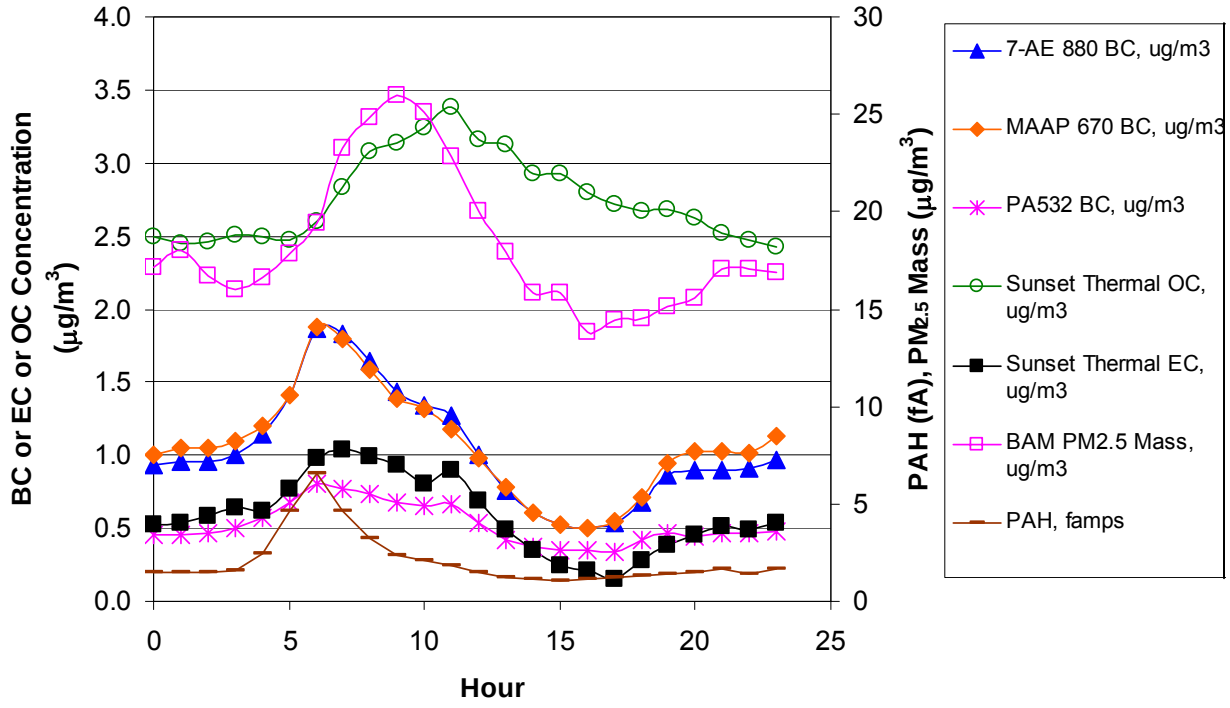

Figure 6-27. Diurnal variation of BC, EC, OC and $PM_{2.5}$ mass at the Fresno Supersite during 08/01/05-09/30/05.

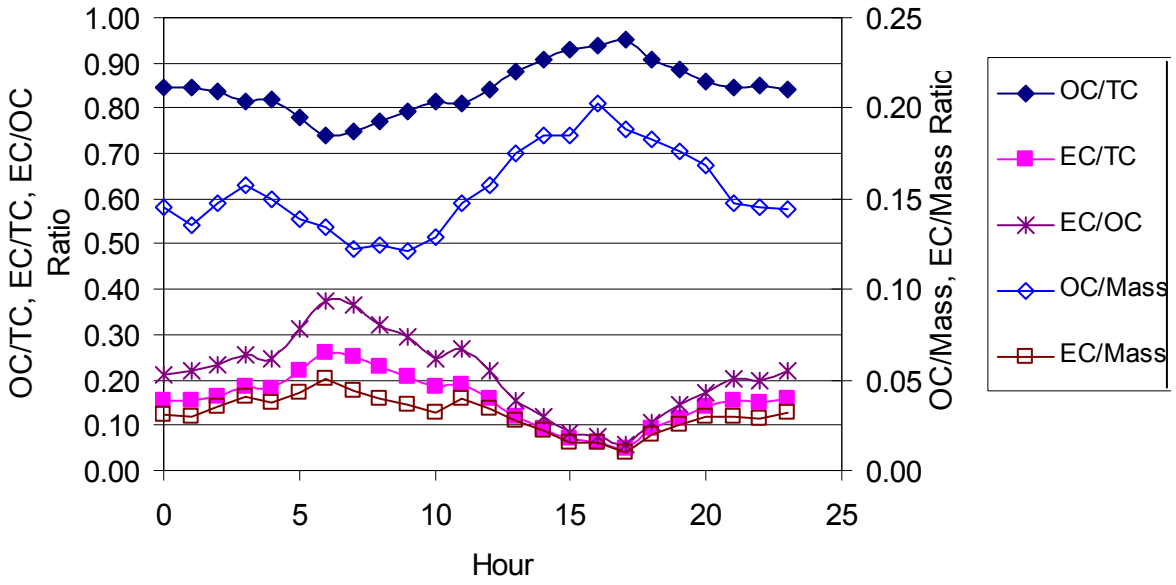

Figure 6-28. Diurnal variation of BC, EC, OC as fraction of TC and $PM_{2.5}$ mass at the Fresno Supersite during 08/01/05-09/30/05.

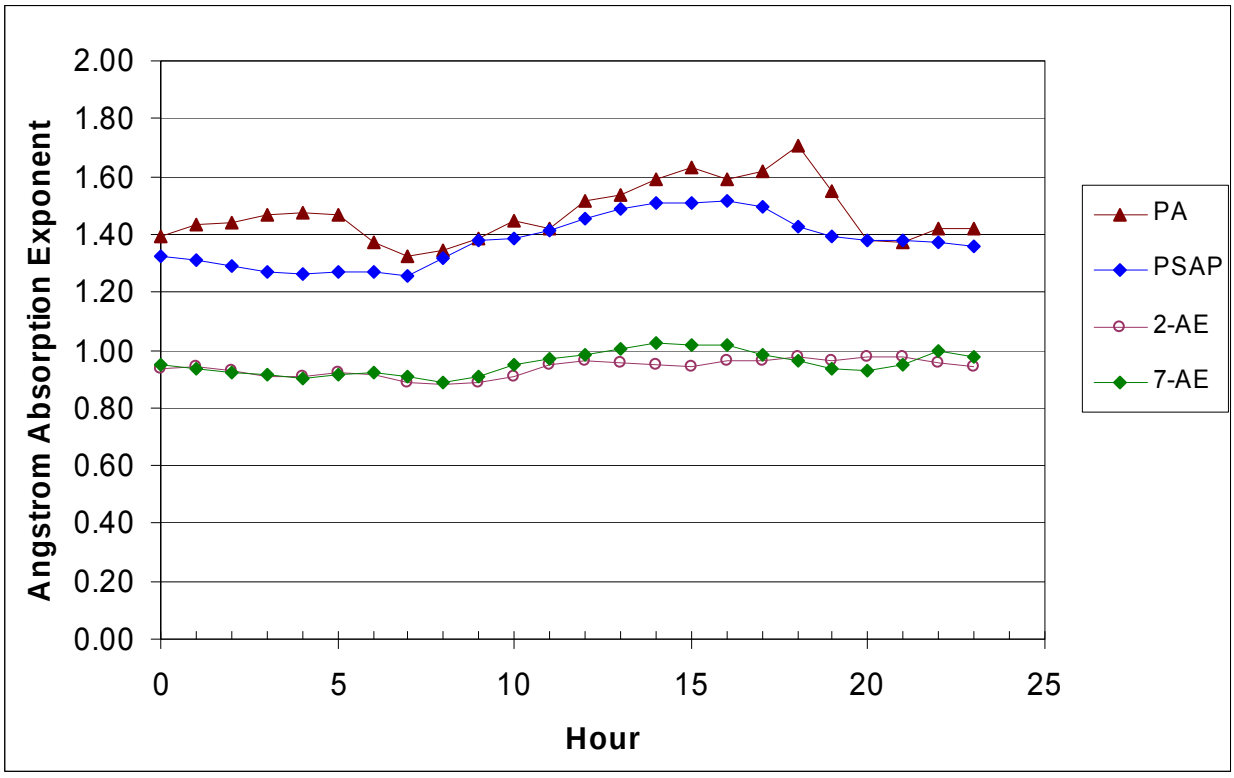

Figure 6-29. Diurnal variation of Angstrom absorption exponent, α, at the Fresno Supersite during 08/01/05-09/30/05. α was not estimated for the MAAP because the MAAP only measures at one wavelength (670 nm)

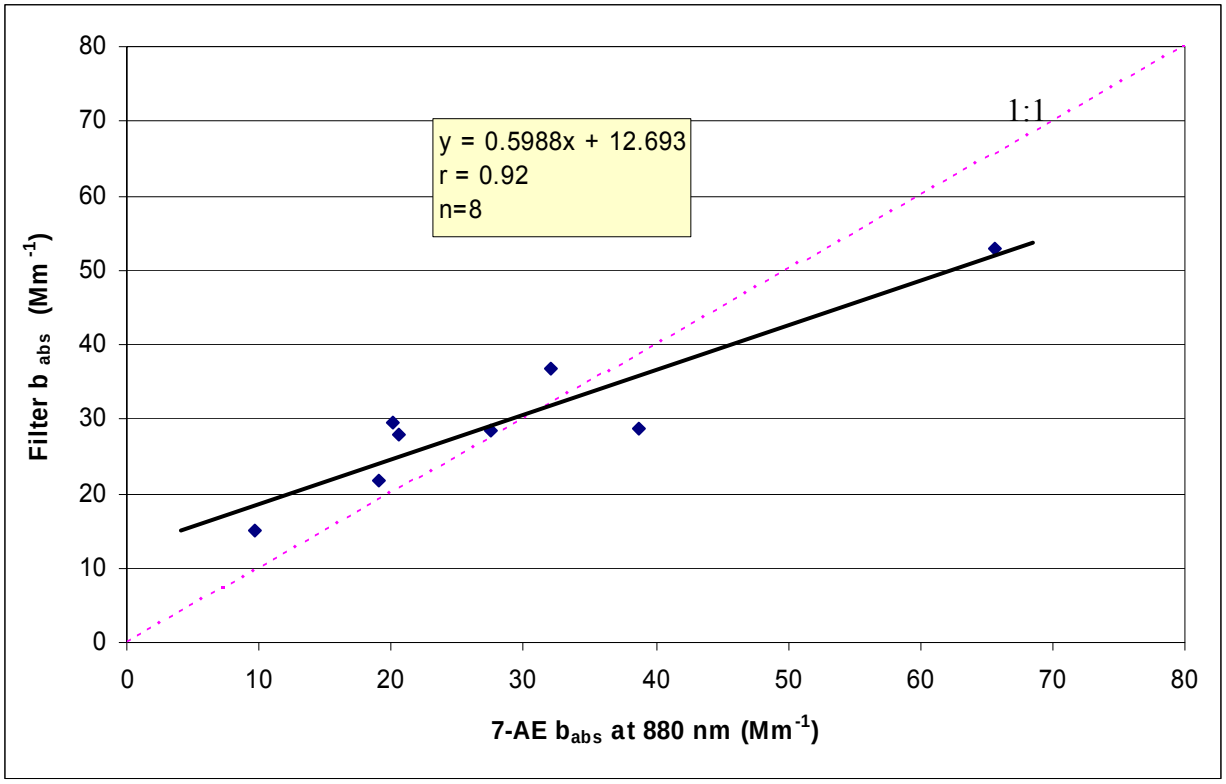

Figure 6-30. Comparison of filter b_{abs} vs. 7-AE b_{abs} at 880 nm during 12/1/03 to 12/31/03.

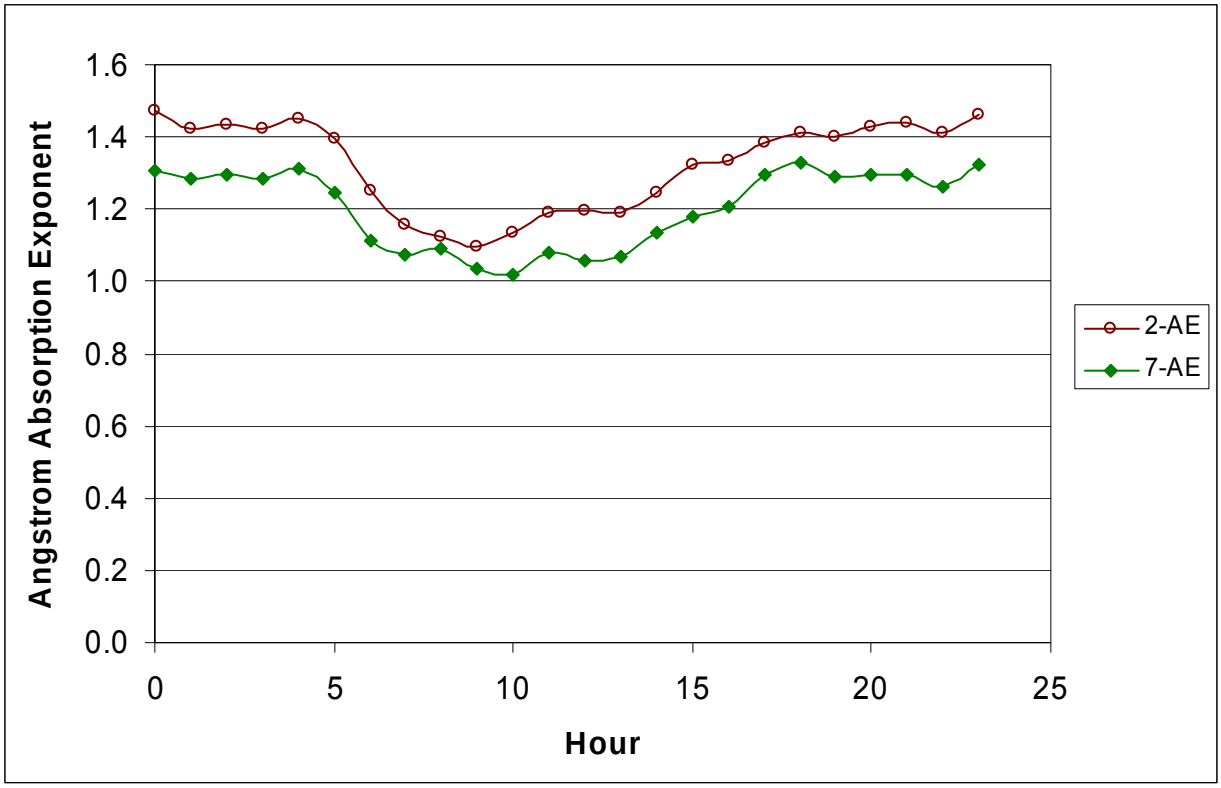

Figure 6-31. Diurnal variation of the Angstrom absorption exponent during 12/1/03 to 12/31/03.

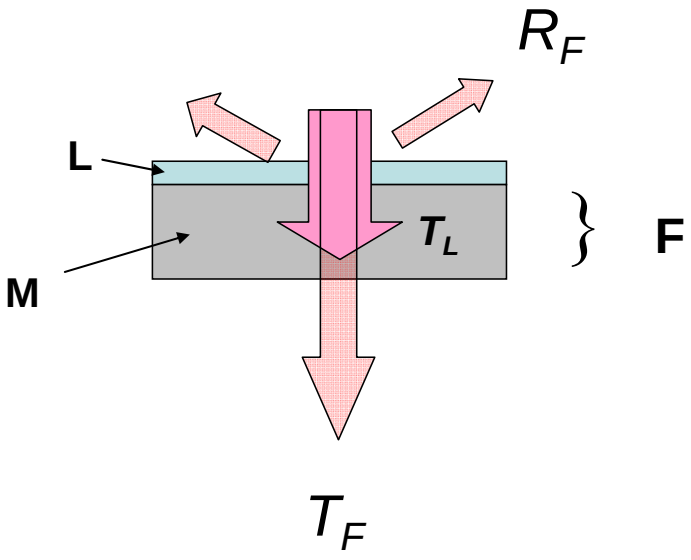

Figure 6-32. Schematic diagram of radiative transfer in a two-layer filter. L and M indicate the aerosol-filter and filter-only layer, respectively; T and R indicate reflectance and transmittance, respectively.

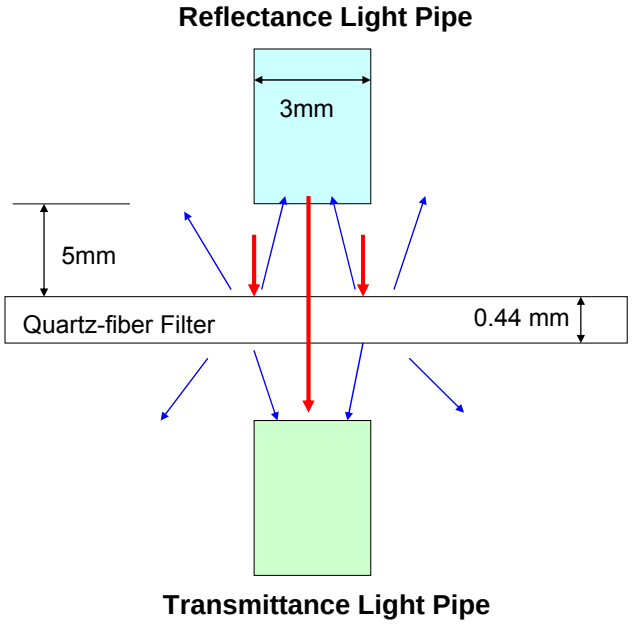

Figure 6-33. Configuration of optical measurements for thermal/optical analysis.

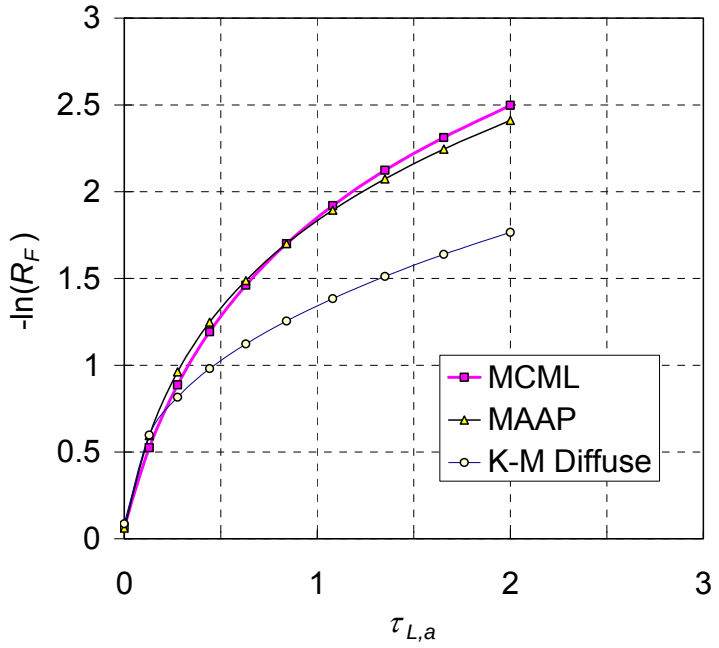

(a)

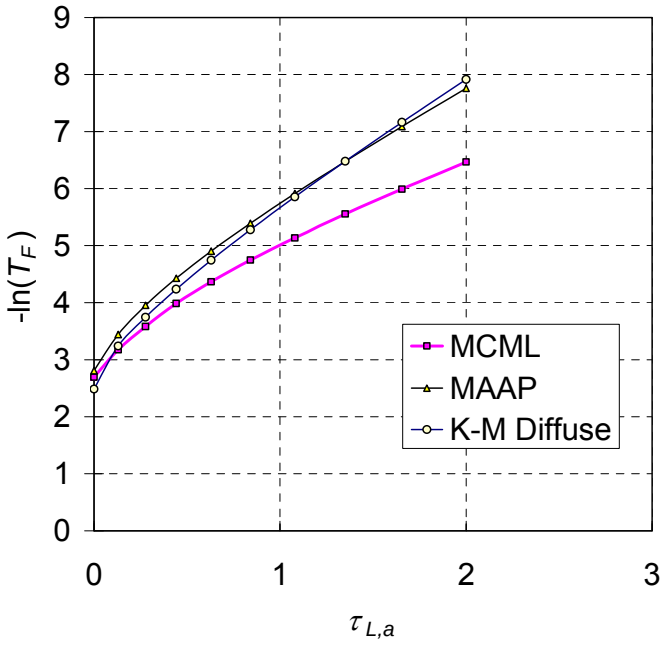

(b)

Figure 6-34. Filter (a) reflectance and (b) transmittance as a function of filter loading ($\tau_{L,a}$). Calculations are made by MCML, MAAP, and Kubelka-Munk algorithms.

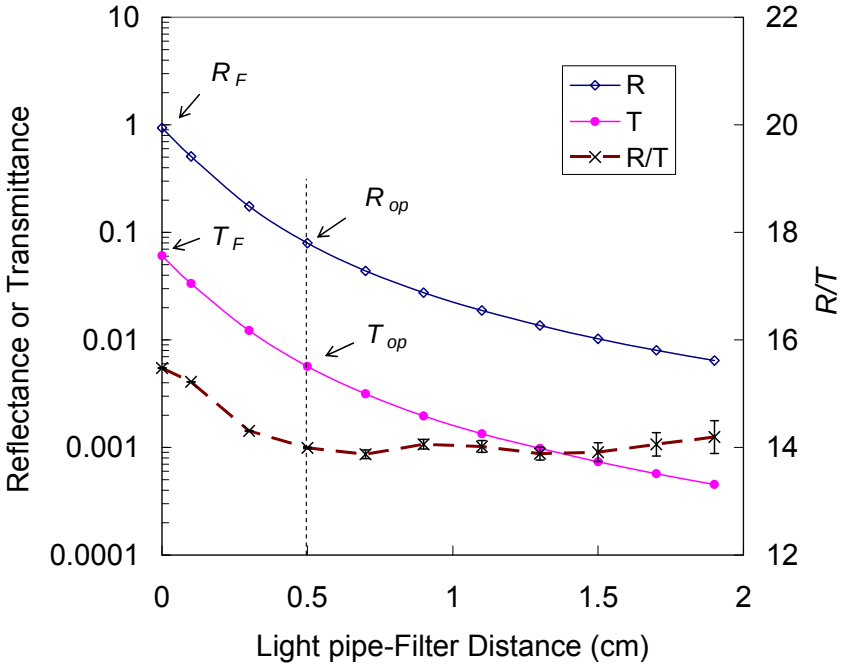

Figure 6-35. Filter reflectance and transmittance as a function of light pipe-filter distance.

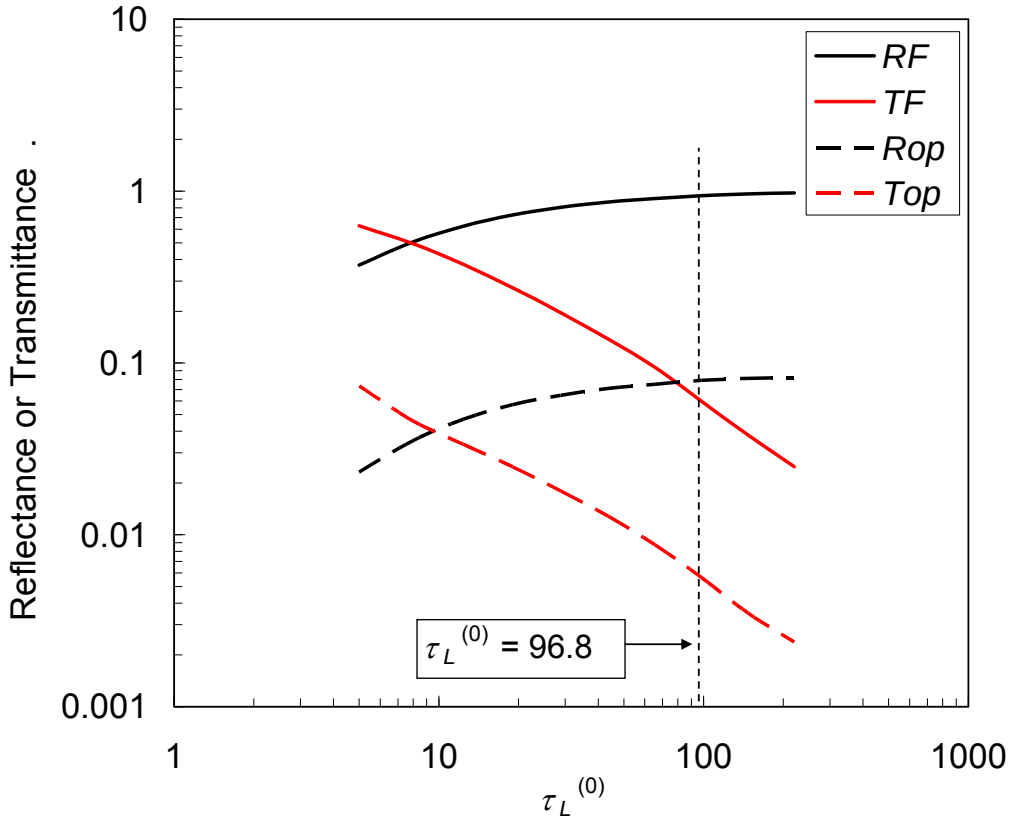

Figure 6-36. Reflectance and Transmittance as a function of filter optical depth ($\tau_{L(0)}$). R_F and T_F are the theoretical hemispheric reflectance and transmittance, respectively. R_{op} and T_{op} are operational reflectance and transmittance determined from experiments.

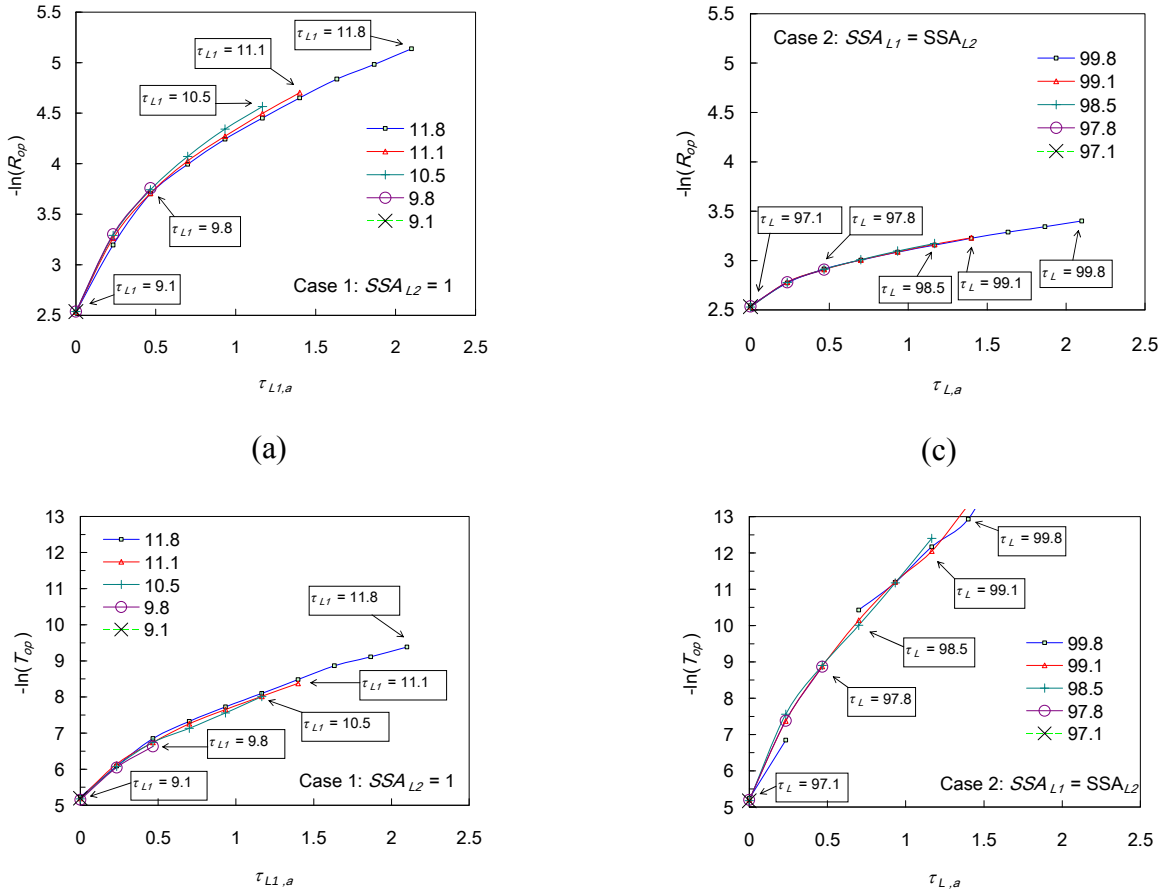

Figure 6-37. Operational reflectance and transmittance as a function of particle absorption ($\tau_{L,a}$), determined for Case 1 (two layers) and Case 2 (one layer). The total filter optical depth (τ_L or $\tau_{L,1}$) represents another parameter in the calculation.

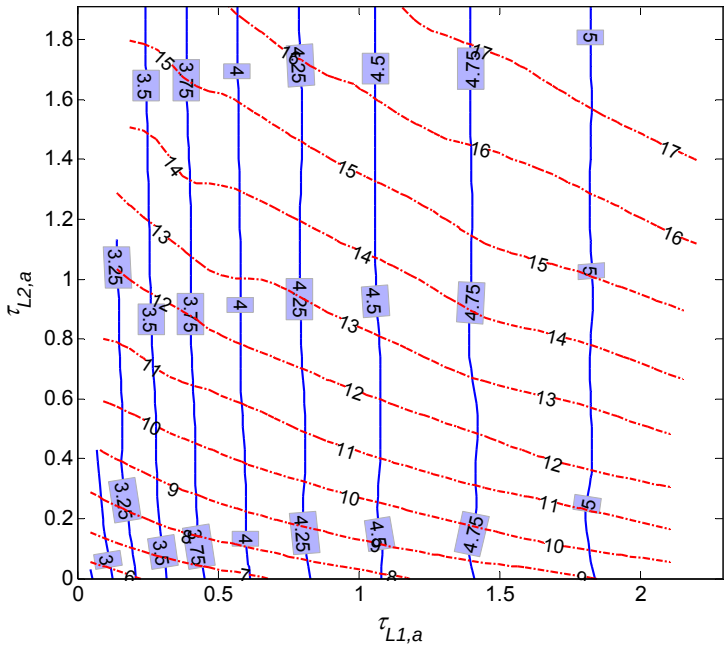

Figure 6-38. -ln(R_{op}) (blue lines) and -ln(T_{op}) (red lines) as functions of absorption at the top layer ($\tau_{L1,a}$) and bottom layer ($\tau_{L2,a}$) of a filter.

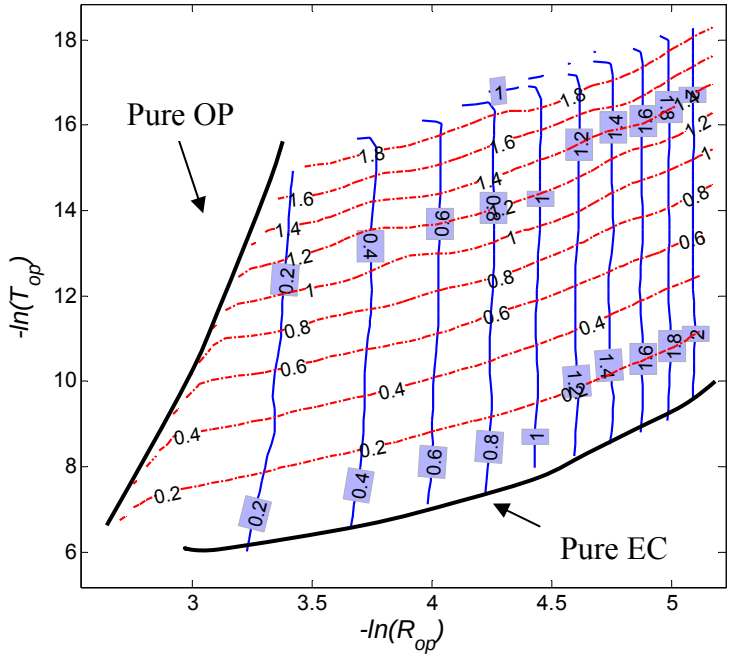

Figure 6-39. Absorption at the top layer ($\tau_{L1,a}$) and bottom layer ($\tau_{L2,a}$) of a filter can be retrieved from the measurements of operational reflectance (R_{op}) and transmittance (T_{op}). Two special cases are pure OP and pure EC for which absorption only occurs on the top filter layer or uniform throughout the filter.

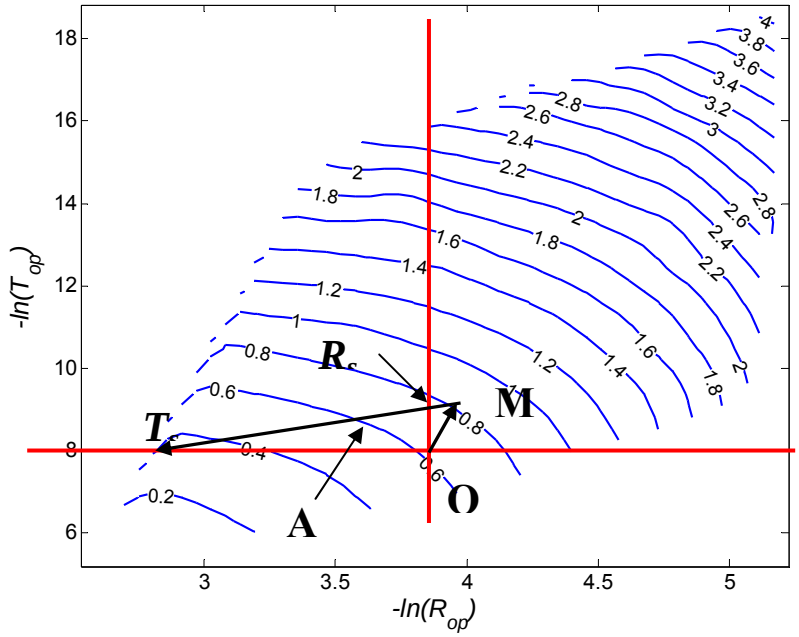

Figure 6-40. Total absorption ($\tau_{L1,a} + \tau_{L2,a}$) can be determined from the measurements of operational reflectance (R_{op}) and transmittance (T_{op}). The arrows indicate the change of filter absorption during thermal analysis. Point O (the origin) denotes the point at which the filter sample begins the thermal analysis. Point M (maximum) is the maximum occurrence of charring. R_s is the OC/EC split point by reflection, and T_s is the OC/EC split point by transmittance. Point A is the actual split point.

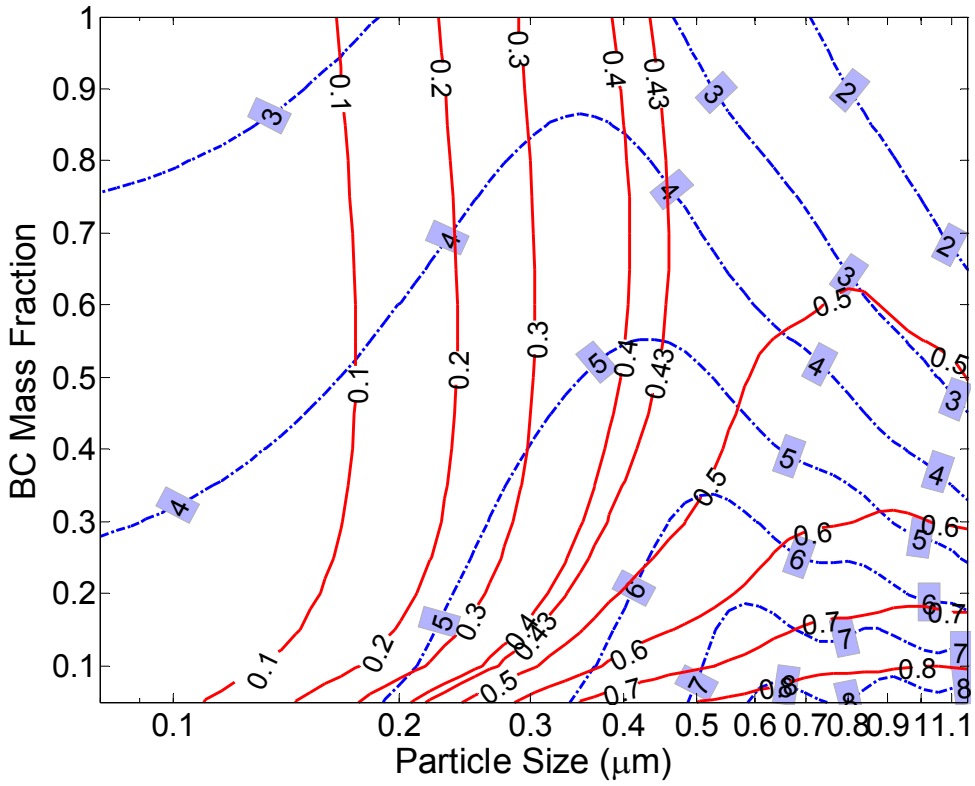

Figure 6-41. Optical properties of signal spherical particles calculated with Mie theory. The blue dashed lines indicate BC σ_{abs} at 1047 nm in m^2/g and the red solid lines indicate the single scattering albedo, ω.

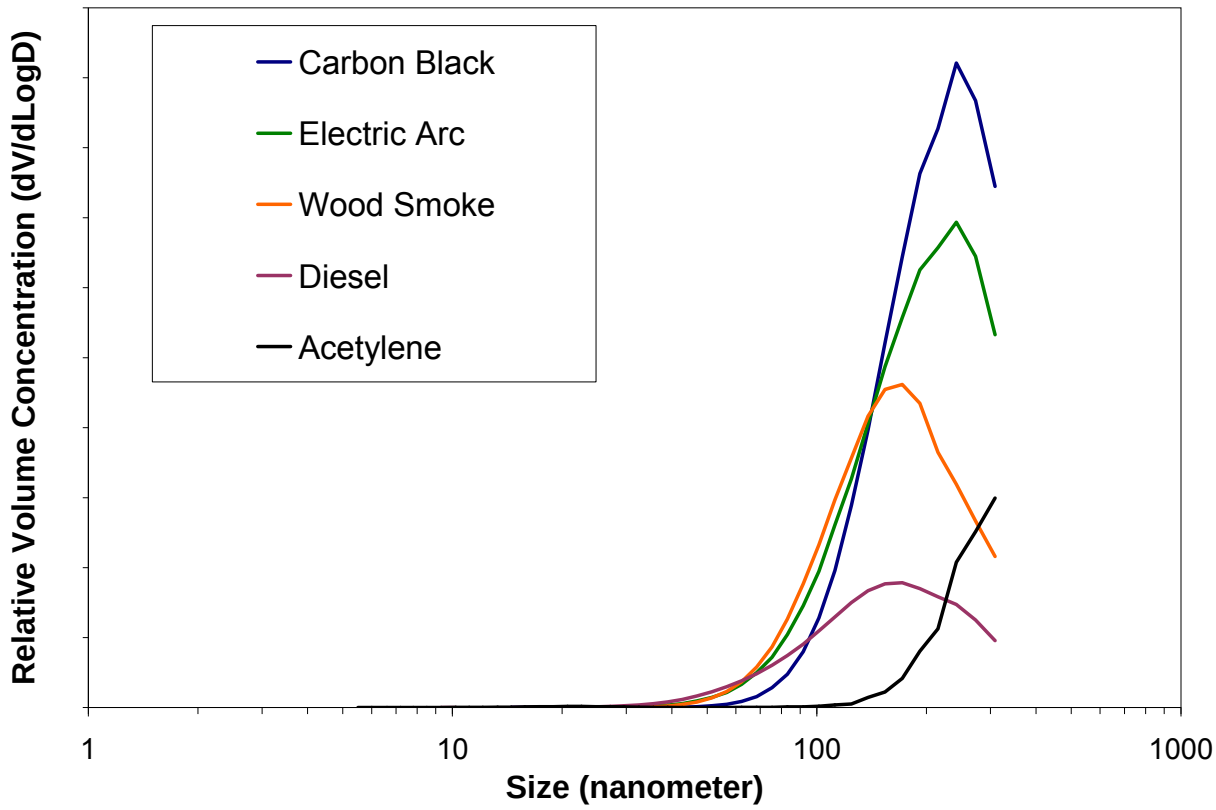

Figure 6-42. Typical volume-size distribution of particles generated in the laboratory.

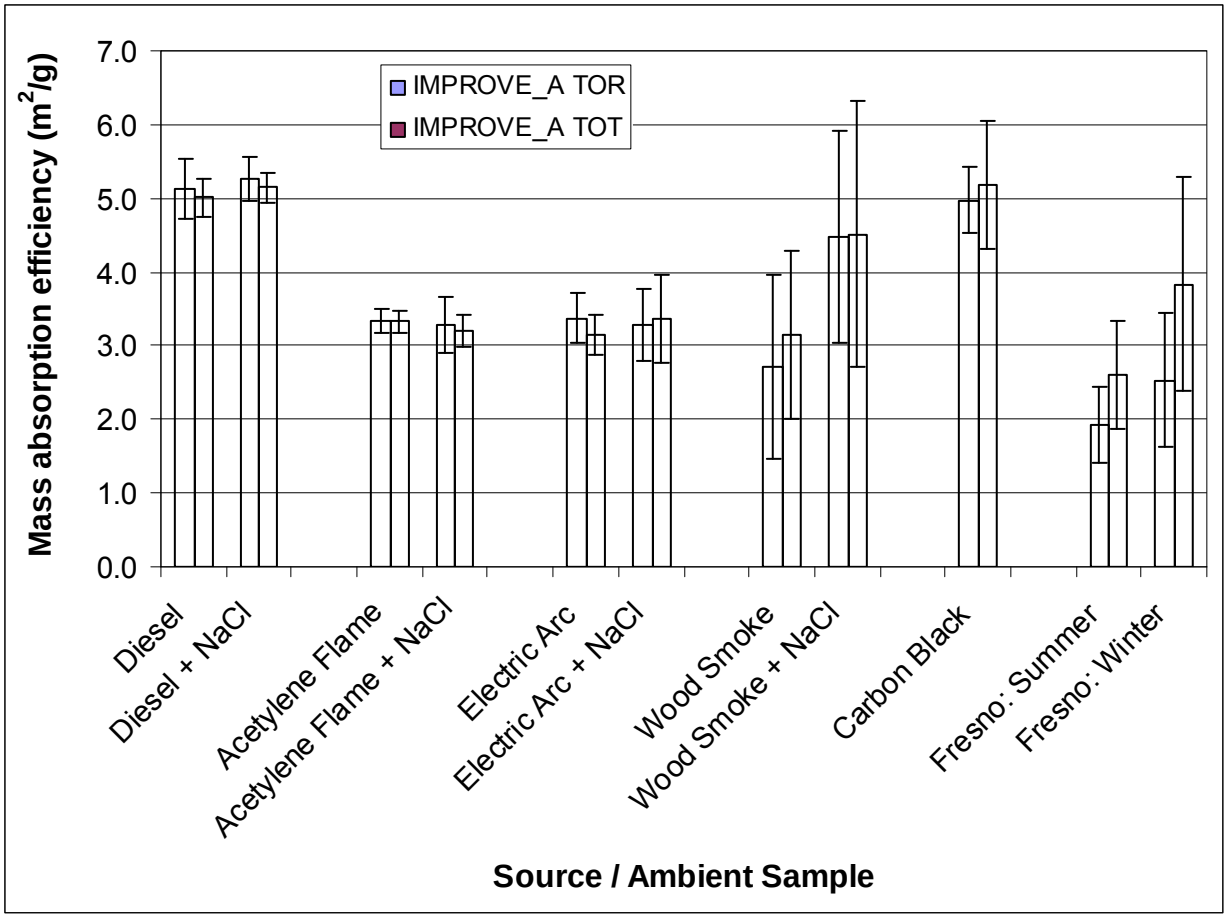

Figure 6-43. Estimate of σ_{abs} (1047) for the PA for different source and ambient samples. Error bars shown are one standard deviation from the mean. σ_{abs} are represented by the ratio of PA (1047 nm) b_{abs} to thermal EC.

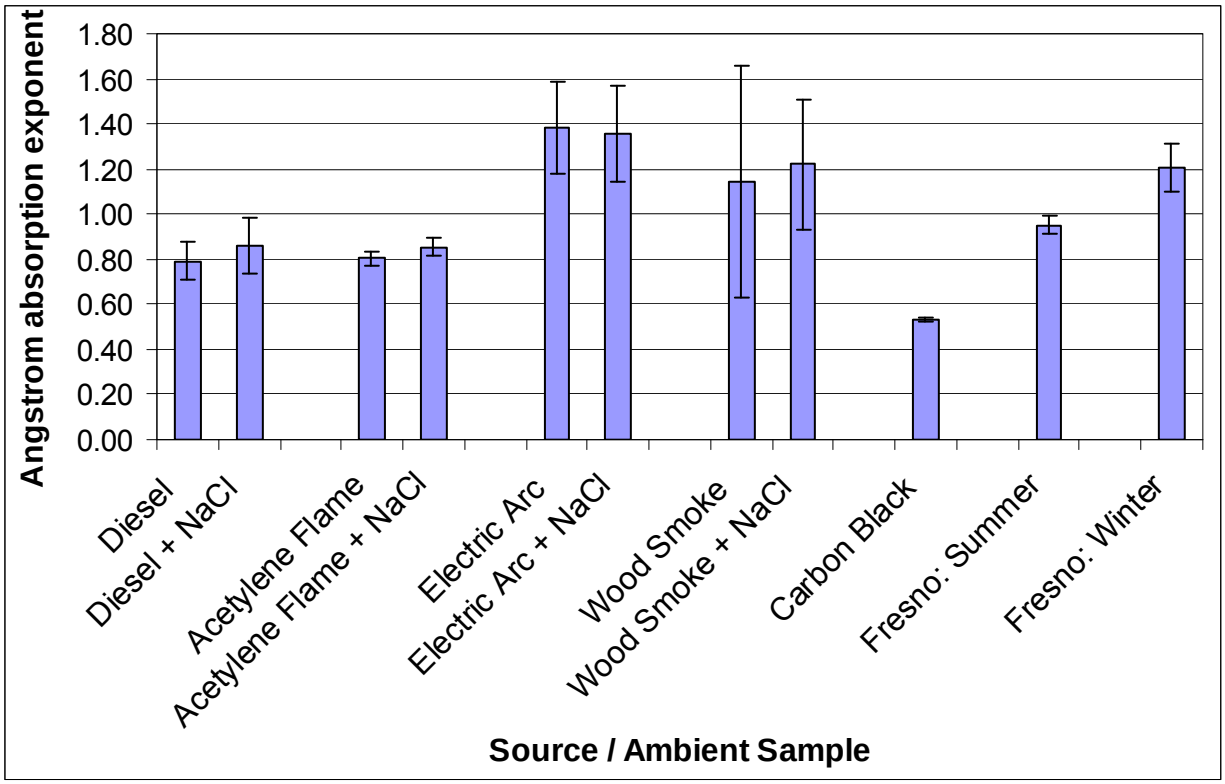

Figure 6-44. Estimate of the Angstrom absorption exponent, α, using 7-AE measurements for different source and ambient samples. Error bars shown are one standard deviation from the mean.

7. CONCLUSIONS

This study intends to improve BC emission inventories by understanding and characterizing BC and EC measurement methods, and by measuring emission rates and profiles from BC-emitting sources. *Phase I: Method Intercomparison* of the study, consisted of four major tasks (Tasks 1a to 4a): 1) conduct a critical review of literature (Task 1a); 2) create carbon analysis QA/QC plans (Task 2a); 3) generate source-sample aerosols and inter-compare methods (Task 3a); and 4) conduct a field comparison at Fresno (Task 4a). The findings from the laboratory intercomparisons were applied to the results observed at Fresno to gain an overall understanding of the causes of measurement differences.

7.1 Task 1a: Critically Review Literature on Carbon Analysis Methods and Comparisons

A review of 19 different carbon analysis methods and 42 carbon intercomparison studies was completed and published by Watson et al. (2005). An additional 38 carbon intercomparison studies that were not included in Watson et al. (2005) were reviewed and are included in Appendix B. This review focused on method development and validation of BC/EC measurements, inter-method or inter-laboratory comparisons; and investigation on fundamental BC/EC properties, including the development of reference materials. The important findings from the review include the following:

- The review identified possible biases in thermal and optical methods. For filter-based thermal/optical analyses, charring correction represented the most important uncertainty in thermal methods (Chow et al., 2004a). This was followed by the early combustion of EC in an inert atmosphere due to trace oxidants in the sample, thereby biasing the OC/EC split.

- The photoacoustic (PA) absorption compared well (within ±3%) with a standard light absorption measurement, i.e., the difference between extinction by optical extinction cell (OEC) and scattering by nephelometer, for pure soot sample or soot mixed with salts (Sheridan et al., 2005).

- The PA absorption at 1047 nm was least-affected by gaseous interferences such as those from NO_2.

- A mass absorption efficiency (σ_{abs}) of 10 and 5 m^2/g is commonly used to convert PA b_{abs} at 532 and 1047 nm to EC concentration, respectively. The review showed that σ_{abs} ranged from 3 to 5 m^2/g with a 5 m^2/g appeared to be at the high end of the EC σ_{abs} at 1047 nm, using the IMPROVE thermal/optical protocol for EC. For 532 nm, 10 m^2/g appeared to be appropriate for ambient samples analyzed with the IMPROVE protocol; but a higher conversion factor, such as 15 m^2/g, is needed for the STN EC.

- Several studies pointed out the need for correcting filter-based absorption methods for particle light scattering effects, the uncertainty involved in σ_{abs} estimates and its effect on b_{abs} measurements, the influence of organic aerosols on b_{abs}, and its influence on the Angstrom absorption exponent, α. Kirchstetter et al. (2004) showed that α = 2.5

approximated the strong spectral dependence of the biomass burning aerosols and $\alpha = 1.0$ described the weak spectral dependence of motor vehicle aerosols.

7.2 Task 2a: Create Carbon Analysis QA/QC Methods and Plans

A QAPP was developed which includes 49 SOPs for methods applied to this study (Volume II). An important outcome was the standardization of thermal/optical carbon analyses for the DRI Model 2001 Thermal/Optical Carbon Analyzer (Atmoslytic, Inc., Calabasas, CA).

- It included the development of multi-point temperature calibrations, characterization of analysis atmosphere, and calibration of laser intensity using neutral density filters.

- It improved the precision of OC/EC and carbon fraction measurements (Chow et al., 2005a). The temperature calibration corrects the difference between thermocouple and sample temperature, which is typically biased high by 14 to 22 °C, causing up to a 30% change in carbon fraction concentrations.

- It developed new auditing procedures as part of the carbon analysis SOP (DRI SOP# 2-216.4).

7.3 Task 3a: Conduct a Laboratory Comparison of b_{abs}, BC, EC, and OC Measurement Methods

A carbon source characterization laboratory generated carbon aerosols from different combustion sources, simulated atmospheric aging through a dilution sampling system, and permitted simultaneous continuous measurements and integrated sample collection. Filter samples were collected for: diesel exhaust (35 pure, 9 mixed with NaCl), acetylene flame (10 pure and 9 mixed with NaCl), electric arc (13 pure, 9 mixed with NaCl) and wood smoke (23 pure, 14 mixed with NaCl). NaCl was added to evaluate the catalytic effects of a mixed aerosol on b_{abs}, BC, and EC measurements. Three carbon black samples were also nebulized using the DRI monomodal aerosol generator. In addition, carbon black and graphite were collected using the DRI resuspension chamber. Portions of the quartz-fiber filters were analyzed by three commonly used thermal evolution protocols: IMPROVE_A_TOR/TOT, STN_TOT, and the French two-step protocols. These protocols represent a wide range of variability in thermal and optical parameters, including temperature plateaus, analysis times, combustion atmospheres, heating rates, and optical pyrolysis monitoring by reflectance (TOR) and transmittance (TOT). The following results were observed:

- The STN_TOT and French two-step protocols determined EC/TC ratios similar to (within 5%) that of the IMPROVE_A_TOR protocol for diesel soot EC/TC ~60%), acetylene flame (~96%), and electric arc (~50%) samples and within 5 to 15% for carbon black (~90%) and graphite (~93%) samples.
- Larger differences were found for wood smoke samples. The STN_TOT and French two-step protocols yielded lower EC (46% and 86%, respectively) for wood smoke compared to the IMPROVE_A_TOR protocol.
- High temperature EC2 (at 740 °C) is the dominant carbon fraction for diesel (62 ± 8.7%), acetylene flame (81 ± 15%) and carbon black (93 ± 4.4%) samples. EC3 (840 °C)

dominated the graphite samples (56 ± 13%). The electric arc and wood smoke samples contained higher (>50%) amounts of OC and EC1 at 580 °C (59% and 30% respectively).

- Although NaCl altered the abundance of EC fractions for a given source type, it did not affect EC/TC ratio determined by the IMPROVE_A and STN protocols. For the French two-step protocol, however, lower EC (>60% to 90%) was determined in the presence of NaCl. It is apparent that the French two-step protocol, which operates in pure O_2 without charring corrections, is influenced more by the matrix effect.
- Comparison of PA b_{abs} (1047 nm) to IMPROVE_A_TOR/TOT EC, showed that the EC σ_{abs} varied by as much as ~50% among different source types in the range of 2.7 to 5.3 m^2/g. Therefore, a universal conversion factor between b_{abs} and BC/EC concentration does not exist. Other information, such as source type, particle size distribution, morphology, and internal or external mixing, needs to be considered in order to estimate the influence of BC particles on radiative forcing.
- The ratios of AE to PA b_{abs} (1047 nm) for the source samples varied from 1.05 to 3.7. The ratio did not appear to depend on the EC/TC ratio directly (e.g., acetylene flame and carbon black samples contain >90% EC in TC], but the $b_{abs(AE)}/b_{abs(PA)}$ were very different). Rather, the $b_{abs(AE)}/b_{abs(PA)}$ ratio was influenced by the BC concentration; lower ratios were found to be associated with higher BC concentrations.
- Using a factor of 5 m^2/g to convert PA b_{abs} at 1047 nm to BC concentration resulted in BC comparable to IMPROVE_A_TOR/TOT EC only for diesel samples. Different conversion factors should be used for other types of samples (~3.3 m^2/g for acetylene flame and electric arc, 2.7 to 4.5 m^2/g for wood smoke, and ~5 m^2/g for carbon black).
- Although biased, α estimated by 7-AE showed higher values (i.e., greater than unity) for wood smoke samples (1.2) and lower values for diesel (0.79 to 0.86) samples.
- The optical modeling demonstrated that filter-based absorption measurements, such as the AE and MAAP, still do not fully address the multiple scattering and loading effects. The Monte-Carlo simulation represents a precise method to determine the radiative transfer within a filter of finite dimensions. A filter sample can be described as a two-layer model during thermal analysis. The top layer contains pyrolyzed organics, charring (OP and EC), while the second layer contains exclusively OP. The reflectance is insensitive to absorption in the second layer, and therefore absorption by the top and bottom layer can be retrieved separately from the reflectance and transmittance measurements. This model of the filters, combined with the Monte-Carlo simulation, explained well the observations during thermal analysis (i.e., the darkening and whitening of the filters and the observed changes in filter reflectance and transmittance). The simulation also suggested that an accurate charring correction should be made when the absorption, rather than reflectance or transmittance, returns to its initial value. This absorption can be estimated from simultaneous measurements of reflectance and transmittance.

7.4 Task 4a: Perform a Field Comparison at the Fresno Supersite

The field measurements at Fresno during the summer and winter IOPs intended to: 1) inter-compare the continuous and integrated b_{abs} and BC measurements at Fresno; 2) evaluate the range of uncertainty involved in the σ_{abs} (m^2/g) estimates due to the different measurement and

analysis methods; and 3) determine the Angstrom absorption exponent, α, for the IOPs. Continuous b_{abs} was acquired by 2-AE, 7-AE, PSAP (summer only), MAAP, PA at 532 nm (summer only) and PA at 1047 nm. Twenty-four-hour filter samples acquired by the Hi-Vol and Anderson RAAS samplers were used in the analysis. A total of 18 and 25 samples collected by Hi-Vol and RAAS, respectively, during the summer IOP, and a total of 14 filters acquired by Hi-Vol and RAAS (7 and 7, respectively) during the winter IOP, were analyzed by the IMPROVE_A and STN protocols, and a subset of the Hi-Vol samples (8 during summer and 7 during winter) were analyzed by the French two-step protocol. The following are the key conclusions from this task:

- The EC/TC ratio at the Fresno Supersite was 0.215 ± 0.035 and 0.259 ± 0.047 for summer and winter IOPs, respectively (based on Hi-Vol samples using the IMPROVE_A_TOR protocol). These are close to that in wood smoke samples (0.259 ± 0.123, using IMPROVE_A_TOR), especially for the winter period.
- The STN_TOT and French two-step protocols showed lower EC/TC ratios (13 to 17% during summer, 52 to 63% during winter) compared to the IMPROVE_A_TOR protocol.
- High temperature OC3 (at 480 °C, 24%) and EC1 (at 580 °C, 31%) were the dominant carbon fractions at Fresno during the winter IOP. This is consistent with the influence of residential wood combustion. In summer, however, the percentage of high temperature EC2 (at 740 °C) in TC (12%) was higher than in winter (8%), consistent with a larger contribution from diesel vehicles.
- The denuder used in the RAAS sampler removed most of the sampling artifact. OC determined from the difference of front quartz-fiber filter and backup quartz-fiber filter behind Teflon values are close to that of front quartz-fiber filter from the denuded channel.
- The 2-AE and 7-AE overestimated b_{abs} (670 nm) by 150 to 200% during both summer and winter compared to the MAAP. However, in terms of BC concentrations, the AE BC was within 20% of the MAAP BC, the Sunset thermal EC, and the IMPROVE_A EC during summer. A similar result was observed in winter, except for comparisons of AE with MAAP, where the AE was within 26%. It appears that the σ_{abs} used by the AE using $14625/\lambda$ was valid for ambient conditions (i.e., typically low EC concentration compared to source samples).
- The default σ_{abs} (670 nm) for the MAAP (6.6 m^2/g) was appropriate for the summer period, while it appeared to be underestimated by 17% for the winter period. This study suggests a σ_{abs} (670 nm) of 7.7 m^2/g for the MAAP during the winter season.
- At Fresno, the default σ_{abs} for the PA was overestimated at both the 532 nm and 1047 nm (in contrast to the literature review which suggested that 532 nm σ_{abs} of 10 m^2/g may be valid for ambient samples analyzed by the IMPROVE protocol). This study suggests an average PA σ_{abs} (532 nm) of 4.5 m^2/g during summer, and a σ_{abs} (1047 nm) of 1.9 and 3.5 m^2/g during the summer and winter, respectively.
- The IMPROVE_A_TOR EC was within 20% of AE and MAAP BC and Sunset thermal EC concentrations during summer, while the STN_TOT EC differed by more than 35% during both seasons.

- The ratios of AE b_{abs} to PA b_{abs} for the ambient samples ranged from 4.2 to 7.2. These ratios were influenced by BC concentrations, especially at low BC concentrations. For the Fresno summer samples, the BC concentration was low (<1 $\mu g/m^3$) resulting in the $b_{abs(AE)}/b_{abs(PA)}$ ratio as high as 7.2. The loading effect is not accounted for in the AE and a constant conversion factor of $14{,}625/\lambda$ is used to translate b_{abs} to BC concentrations.
- The 7-AE was the only instrument with multi-wavelength measurements that was available in both laboratory and field measurements. Hence the α in the Angstrom Power Law ($b_{abs} = K\ \lambda^{-\alpha}$) derived from 7-AE were used for comparisons. It was found that α varied by as much as 40% for the different sources tested in the laboratory. The α during the summer IOP (0.95 ± 0.04) was 10 to 20% higher than that observed for diesel and acetylene flame samples (0.79 ± 0.09 to 0.86 ± 0.12), for both pure and mixed (with NaCl) aerosols. This would indicate that the summer-time aerosol at Fresno, while being influenced by diesel emissions, might be mixed with transformed (aged or secondary) aerosols. The α during the winter period (1.2 ± 0.11) was similar to that observed for emissions from wood combustion (1.2 ± 0.51). More importantly, these values differ from $\alpha = 1$ that is typically used in the literature to scale the b_{abs} to different wavelengths. More complex aerosol optical models are needed to explain these discrepancies.
- Overall, the results from the winter IOP were consistent with laboratory observations during the wood combustion experiments. The aerosol during summer IOP was more complex and difficult to explain with the laboratory data. The low EC concentration close to the detection limit of thermal/optical methods and the presence of secondary and biogenic organic aerosol are important issues to be resolved in the future.

8. REFERENCES

Adams, K.M.; Turpin, B.J.; and Huntzicker, J.J. (1989). Intercomparison of photoacoustic and thermal-optical methods for the measurement of atmospheric elemental carbon. Presentation at the 82nd Annual Meeting in Anaheim, CA, June 25, 1989. Air & Waste Management Association, Pittsburgh, PA.

Arnott, W.P.; Hamasha, K.; Moosmüller, H.; Sheridan, P.J.; and Ogren, J.A. (2005a). Towards aerosol light-absorption measurements with a 7-wavelength Aethalometer: Evaluation with a photoacoustic instrument and 3-wavelength nephelometer. *Aerosol Sci. Technol.*, **39**(1):17-29. ISI:000225877400002.

Arnott, W.P.; Moosmüller, H.; Rogers, C.F.; Jin, T.; and Bruch, R. (1999). Photoacoustic spectrometer for measuring light absorption by aerosol: Instrument description. *Atmos. Environ.*, **33**(17):2845-2852.

Arnott, W.P.; Moosmüller, H.; Sheridan, P.J.; Ogren, J.A.; Raspet, R.; Slaton, W.V.; Hand, J.L.; Kreidenweis, S.M.; and Collett, J.L., Jr. (2003). Photoacoustic and filter-based ambient aerosol light absorption measurements: Instrument comparison and the role of relative humidity. *J. Geophys. Res.*, **108**(D1):AAC 15-1-AAC 15-11.

Arnott, W.P.; Moosmüller, H.; and Walker, J.W. (2000). Nitrogen dioxide and kerosene-flame soot calibration of photoacoustic instruments for measurement of light absorption by aerosols. *Rev. Sci. Instrum.*, **71**(12):4545-4552.

Arnott, W.P.; Zielinska, B.; Rogers, C.F.; Sagebiel, J.; Park, K.; Chow, J.C.; Moosmüller, H.; Watson, J.G.; Kelly, K.; Wagner, D.; Sarofim, A.; Lighty, J.; and Palmer, G. (2005b). Evaluation of 1047 nm photoacoustic instruments and photoelectric aerosol sensors in source-sampling of black carbon aerosol and particle bound PAH's from gasoline and diesel powered vehicles. *Environ. Sci. Technol.*, **39**(14):5398-5406.

Bae, M.S.; Schauer, J.J.; Deminter, J.T.; Turner, J.R.; Smith, D.; and Cary, R.A. (2004). Validation of a semi-continuous instrument for elemental carbon and organic carbon using a thermal-optical method. *Atmos. Environ.*, **38**(18):2885-2893. ISI:000221422400011.

Bennett, C.A., Jr.; and Patty, R.R. (1982). Monitoring particulate carbon collected on Teflon filters: An evaluation of photoacoustic and transmission techniques. *Appl. Opt.*, **21**(3):371-374.

Berkson, J. (1950). Are there two regressions? *J. Am. Stat. Assoc.*, **45**:164-180.

Bevington, P.R. (1969). *Data Reduction and Error Analysis for the Physical Sciences*. McGraw Hill, New York, NY.

Birch, M.E. (1998). Analysis of carbonaceous aerosols: Interlaboratory comparison. *Analyst*, **123**(5):851-857.

Birch, M.E.; and Cary, R.A. (1996a). Elemental carbon-based method for monitoring occupational exposures to particulate diesel exhaust. *Aerosol Sci. Technol.*, **25**(3):221-241.

Birch, M.E.; and Cary, R.A. (1996b). Elemental carbon-based method for occupational monitoring of particulate diesel exhaust: Methodology and exposure issues. *Analyst*, **121**:1183-1190.

Bodhaine, B.A. (1995). Aerosol absorption measurements at Barrow, Mauna Loa and the South Pole. *J. Geophys. Res.*, **100**(D5):8967-8975.

Bolleter, W.T.; Bushman, C.J.; and Tidwell, P.W. (1961). Spectrophotometric determination of ammonia as indophenol. *Anal. Chem.*, **33**(4):592-594.

Bond, D.W.; Zhang, R.Y.; Tie, X.X.; Brasseur, G.; Huffines, G.; Orville, R.E.; and Boccippio, D.J. (2001). NO_x production by lightning over the continental United States. *J. Geophys. Res.*, **106**(D21):27701-27710.

Bond, T.C. (2001). Spectral dependence of visible light absorption by carbonaceous particles emitted from coal combustion. *Geophys. Res. Lett.*, **28**(21):4075-4078.

Bond, T.C.; Anderson, T.L.; and Campbell, D.E. (1999). Calibration and intercomparison of filter-based measurements of visible light absorption by aerosols. *Aerosol Sci. Technol.*, **30**(6):582-600.

Bond, T.C.; and Bergstrom, R.W. (2006). Light absorption by carbonaceous particles: An investigative review. *Aerosol Sci. Technol.*, **40**(1):27-67.

Brandenberger, S.; Mohr, M.; Grob, K.; and Neukomb, H.P. (2005). Contribution of unburned lubricating oil and diesel fuel to particulate emission from passenger cars. *Atmos. Environ.*, **39**(37):6985-6994. ISI:000233473900004.

Bray, E.E.; and Evans, E.D. (1961). Distribution of n-paraffins as a clue to recognition of source beds. *Geochimica et Cosmochimica Acta*, **22**:2-15.

Cachier, H.; Bremond, M.P.; and Buat-Ménard, P. (1989a). Determination of atmospheric soot carbon with a simple thermal method. *Tellus*, **41B**(3):379-390.

Cachier, H.; Bremond, M.P.; and Buat-Ménard, P. (1989b). Thermal separation of soot carbon. *Aerosol Sci. Technol.*, **10**(2):358-364.

Chakrabarty, R.K.; Moosmüller, H.; Garro, M.A.; Arnott, W.P.; Walker, J.; Susott, R.A.; Babbitt, R.E.; Wold, C.E.; Lincoln, E.N.; and Hao, W.M. (2006). Emissions from the laboratory combustion of wildland fuels: Particle morphology and size. *J. Geophys. Res.*, **111**:D07204.

Chen, L.-W.A.; Chow, J.C.; Watson, J.G.; Lowenthal, D.H.; and Chang, M.C. (2006a). Quantifying PM2.5 source contributions for the San Joaquin Valley with multivariate receptor models. *Environ. Sci. Technol.*, submitted.

Chen, L.-W.A.; Chow, J.C.; Watson, J.G.; Moosmüller, H.; and Arnott, W.P. (2004). Modeling reflectance and transmittance of quartz-fiber filter samples containing elemental carbon particles: Implications for thermal/optical analysis. *J. Aerosol Sci.*, **35**(6):765-780.

Chen, L.-W.A.; Moosmüller, H.; Arnott, W.P.; Chow, J.C.; Watson, J.G.; Susott, R.A.; Babbitt, R.E.; Wold, C.; Lincoln, E.; and Hao, W.M. (2006b). Particle emissions from laboratory combustion of wildland fuels: In situ optical and mass measurements. *Geophys. Res. Lett.*, **33**(L04804):1-4.

Chen, N.G.; and Bai, J. (1998). Monte Carlo approach to modeling of boundary conditions for the diffusion equation. *Phys. Rev. Lett.*, **80**(24):5321-5325.

Chow, J.C.; and Watson, J.G. (1999). Ion chromatography in elemental analysis of airborne particles. In *Elemental Analysis of Airborne Particles, Vol. 1*, S. Landsberger and M. Creatchman, Eds. Gordon and Breach Science, Amsterdam, pp. 97-137.

Chow, J.C.; Watson, J.G.; Chen, L.W.A.; Paredes-Miranda, G.; Chang, M.-C.O.; Trimble, D.; Fung, K.K.; Zhang, H.; and Yu, J.Z. (2005a). Refining temperature measures in thermal/optical carbon analysis. *Atmos. Chem. Physics*, **5**(4):2961-2972.

Chow, J.C.; Watson, J.G.; and Chen, L.-W.A. (2006a). Contemporary inorganic and organic speciated particulate matter source profiles for geological material, motor vehicles, vegetative burning, industrial boilers, and residential cooking - Draft Report 2. Prepared for Pechan and Associates, Inc., Springfield, VA, by Desert Research Institute, Reno, NV.

Chow, J.C.; Watson, J.G.; Chen, L.-W.A.; Arnott, W.P.; Moosmüller, H.; and Fung, K.K. (2004a). Equivalence of elemental carbon by Thermal/Optical Reflectance and Transmittance with different temperature protocols. *Environ. Sci. Technol.*, **38**(16):4414-4422.

Chow, J.C.; Watson, J.G.; Crow, D.; Frazier, C.A.; and Pritchett, L.C. (2006b). Thermal carbon analysis procedures for organic carbon, elemental carbon, and carbonate carbon in airborne materials collected on filters. In *Methods of Air Sampling and Analysis,* 4th ed.,

J.P. Lodge, Ed. Air & Waste Management Association, Pittsburgh, PA, In preparation, p. in preparation.

Chow, J.C.; Watson, J.G.; Crow, D.; Lowenthal, D.H.; and Merrifield, T.M. (2001). Comparison of IMPROVE and NIOSH carbon measurements. *Aerosol Sci. Technol.*, **34**(1):23-34.

Chow, J.C.; Watson, J.G.; and Divita, F., Jr. (1996). Particulate matter with aerodynamic diameters smaller than 10 μm: Measurement methods and sampling strategies. In *Principles of Environmental Sampling, 2nd Ed.,* 2nd ed., L.H. Keith, Ed. American Chemical Society, Washington, DC, pp. 539-573.

Chow, J.C.; Watson, J.G.; Ho, S.S.H.; and Yu, J. (2006c). A review of recent applications of the thermal desorption method in analysis of aerosol samples. *Anal. Chem.*, in preparation.

Chow, J.C.; Watson, J.G.; Houck, J.E.; Pritchett, L.C.; Rogers, C.F.; Frazier, C.A.; Egami, R.T.; and Ball, B.M. (1994). A laboratory resuspension chamber to measure fugitive dust size distributions and chemical compositions. *Atmos. Environ.*, **28**(21):3463-3481.

Chow, J.C.; Watson, J.G.; Kuhns, H.D.; Etyemezian, V.; Lowenthal, D.H.; Crow, D.J.; Kohl, S.D.; Engelbrecht, J.P.; and Green, M.C. (2004b). Source profiles for industrial, mobile, and area sources in the Big Bend Regional Aerosol Visibility and Observational (BRAVO) Study. *Chemosphere*, **54**(2):185-208.

Chow, J.C.; Watson, J.G.; Louie, P.K.K.; Chen, L.-W.A.; and Sin, D. (2005b). Comparison of PM2.5 carbon measurement methods in Hong Kong, China. *Environ. Poll.*, **137**(2):334-344.

Chow, J.C.; Watson, J.G.; Lowenthal, D.H.; Chen, L.W.A.; and Magliano, K.L. (2006d). Particulate carbon measurements in California's San Joaquin Valley. *Chemosphere*, **62**(3):337-348. ISI:000234793500002.

Chow, J.C.; Watson, J.G.; Lowenthal, D.H.; Chen, L.W.A.; Tropp, R.J.; Park, K.; and Magliano, K. (2006e). PM2.5 and PM10 mass measurements in California's San Joaquin Valley. *Aerosol Sci. Technol.*, **40**(10):796-810.

Chow, J.C.; Watson, J.G.; Pritchett, L.C.; Pierson, W.R.; Frazier, C.A.; and Purcell, R.G. (1993). The DRI Thermal/Optical Reflectance carbon analysis system: Description, evaluation and applications in U.S. air quality studies. *Atmos. Environ.*, **27A**(8):1185-1201.

Countess, R.J. (1990). Interlaboratory analyses of carbonaceous aerosol samples. *Aerosol Sci. Technol.*, **12**:114-121.

Currie, L.A.; Benner, B.A., Jr.; Cachier, H.; Cary, R.; Chow, J.C.; Druffel, E.R.M.; Eglinton, T.I.; Gustafsson, Ö.; Hartmann, P.C.; Hedges, J.I.; Kessler, J.D.; Kirchstetter, T.W.; Klinedinst, D.B.; Klouda, G.A.; Marolf, J.V.; Masiello, C.A.; Novakov, T.; Pearson, A.; Prentice, K.M.; Puxbaum, H.; Quinn, J.G.; Reddy, C.M.; Schmid, H.; Slater, J.F.; Watson, J.G.; and Wise, S.A. (2002). A critical evaluation of interlaboratory data on total, elemental, and isotopic carbon in the carbonaceous particle reference material, NIST SRM 1649a. *J. Res. National Bureau Standards*, **107**(3):279-298.

Dzubay, T.G. (1977). X-Ray Fluorescence Analysis of Environmental Samples, T.G. Dzubay, Ed. Ann Arbor Science Publ. Inc., Ann Arbor, MI, pp. 289-306.

Eglinton, G.; and Hamilton, R.J. (1963). The distribution of alkanes. In *Chemical Plat Taxonomy*. Academic Press, New York, pp. 187-208.

Falkovich, A.H.; and Rudich, Y. (2001). Analysis of semivolatile organic compounds in atmospheric aerosols by direct sample introduction thermal desorption GC/MS. *Environ. Sci. Technol.*, **35**(11):2326-2333.

Fujita, E.M.; Zielinska, B.; Arnott, W.P.; Campbell, D.E.; Reinhart, L.; Sagebiel, J.C.; and Chow, J.C. (2006a). Gasoline/Diesel PM Split Study: Source and ambient sampling, chemical analysis, and apportionment phase, final report. Report No. NREL Subcontract Nos. ACL-1-31046-01 and ACL-1-31046-02. Prepared for National Renewable Energy Laboratory, Golden, CO, by Desert Research Institute, Reno, NV.

Fujita, E.M.; Zielinska, B.; Campbell, D.E.; Arnott, W.P.; Sagebiel, J.C.; Reinhart, L.; Chow, J.C.; Gabele, P.A.; Crews, W.; Snow, R.; Clark, N.N.; and Wayne, W.S. (2006b). Variations in speciated emissions from spark-ignition and compression-ignition motor vehicles in California's South Coast Air Basin. *J. Air Waste Manage. Assoc.*, submitted.

Gogou, A.; Stephanou, E.G.; Stratigakis, N.; Grimalt, J.O.; Simo, R.; Aceves, M.; and Albaiges, J. (1994). Differences in lipid and organic salt constituents of aerosols from eastern and western Mediterranean coastal cities. *Atmos. Environ.*, **28**:1301-1310.

Gogou, A.; Stratigakis, N.; Kanakidou, M.; and Stephanou, E.G. (1996). Organic aerosol in eastern Mediterranean: Components source reconciliation by using molecular markers and atmospheric back trajectories. *Org. Geochem.*, **25**:79-96.

Green, M.C.; Chang, M.C.; Chow, J.C.; Kuhns, H.; Chen, L.-W.A.; Nussbaum, N.J.; Nikolic, D.; Arnott, W.P.; Kumar, S.; and Etyemezian, V. (2004). Las Vegas carbon source apportionment study, final report. Prepared for Clark County Department of Air Quality Management, Las Vegas, NV, by Desert Research Institute, Reno, NV.

Grimmer, G.; Jacob, J.; Naugack, R.W.; and Deltbarn, G. (1983). Determination of polycyclic aromatic compounds emitted from brown coal fired residential stoves by GC/MS. *Anal. Chem.*, **55**:892-900.

Hänel, G. (1987). Radiation budget of the boundary layer: Part II, Simultaneous measurement of mean solar volume absorption and extinction coefficients of particles. *Beitr. Phys. Atmos.*, **60**:241-247.

Hansen, A.D.A.; and McMurry, P.H. (1990). An intercomparison of measurements of aerosol elemental carbon during the 1986 Carbonaceous Species Method Comparison Study. *J. Air Waste Manage. Assoc.*, **40**(6):894-895.

Hansen, A.D.A.; Rosen, H.; and Novakov, T. (1984). The aethalometer - An instrument for the real-time measurement of optical absorption by aerosol particles. *Sci. Total Environ.*, **36**:191-196.

Hansen, B.; Wyers, G.P.; Nornberg, P.; Nemitz, E.; and Sutton, M.A. (1999). Intercalibration of a passive wind-vane flux sampler against a continuous-flow denuder for the measurements of atmospheric ammonia concentrations and surface exchange fluxes. *Atmos. Environ.*, **33**(27):4379-4388.

Hays, M.D.; Smith, N.D.; Kinsey, J.; Dong, Y.; and Kariher, P. (2003). Polycyclic aromatic hydrocarbon size distributions in aerosols from appliances of residential wood combustion as determined by direct thermal desorption - GC/MS. *J. Aerosol Sci.*, **34**(8):1061-1084.

Helmig, D.; Bauer, A.; Muller, J.; and Klein, W. (1990). Analysis of particulate organics in a forest atmosphere by thermodesorption GC/MS. *Atmos. Environ.*, **24A**(1):179-184.

Hidy, G.M. (1985). Jekyll Island meeting report: George Hidy reports on the acquisition of reliable atmospheric data. *Environ. Sci. Technol.*, **19**(11):1032-1033.

Hildemann, L.M.; Cass, G.R.; and Markowski, G.R. (1989). A dilution stack sampler for collection of organic aerosol emissions: Design, characterization and field tests. *Aerosol Sci. Technol.*, **10**(10-11):193-204.

Hitzenberger, R.; Dusek, U.; and Berner, A. (1996). Black carbon measurements using an integrating sphere technique. *J. Geophys. Res.*, **101**(D14):19601-19606.

Hitzenberger, R.; Jennings, S.G.; Larson, S.M.; Dillner, A.; Cachier, H.; Galambos, Z.; Rouc, A.; and Spain, T.G. (1999). Intercomparison of measurement methods for black carbon aerosols. *Atmos. Environ.*, **33**(17):2823-2833.

Ho, S.S.H.; and Yu, J.Z. (2004). In-injection port thermal desorption and subsequent gas chromatography-mass spectrometric analysis of polycyclic aromatic hydrocarbons and *n*-alkanes in atmospheric aerosol samples. *J. Chromatogr. A*, **1059**(1-2):121-129.

Horvath, H. (1993a). Atmospheric light absorption - A review. *Atmos. Environ.*, **27A**(3):293-317.

Horvath, H. (1993b). Comparison of measurements of aerosol optical absorption by filter collection and a transmissometric method. *Atmos. Environ.*, **27A**(3):319-325.

Huebert, B.J.; and Charlson, R.J. (2000). Uncertainties in data on organic aerosols. *Tellus*, **52B**(5):1249-1255.

Huntzicker, J.J.; Johnson, R.L.; Shah, J.J.; and Cary, R.A. (1982). Analysis of organic and elemental carbon in ambient aerosols by a thermal-optical method. In *Particulate Carbon: Atmospheric Life Cycle*, G.T. Wolff and R.L. Klimisch, Eds. Plenum Press, New York, NY, pp. 79-88.

IPCC (2001a). Climate change 2001 - Synthesis report. Prepared by Cambridge University Press, Cambridge, UK.

IPCC (2001b). *Climate Change 2001: The Scientific Basis,* J.T. Houghton, Ed. Cambridge University Press, Cambridge.

Jacobson, M.C.; Hansson, H.C.; Noone, K.J.; and Charlson, R.J. (2000). Organic atmospheric aerosols: Review and state of the science. *Rev. Geophys.*, **38**(2):267-294.

Jacobson, M.Z. (2001). Strong radiative heating due to the mixing state of black carbon in atmospheric aerosols. *Nature*, **409**:695-697.

Johnson, R.L. (1981). Development and evaluation of a thermal/optical method for the analysis of carbonaceous aerosol. M.S. Thesis, Oregon Graduate Center, Beaverton, OR.

Johnson, R.L.; Shah, J.J.; Cary, R.A.; and Huntzicker, J.J. (1981). An automated thermal-optical method for the analysis of carbonaceous aerosol. In *Atmospheric Aerosol: Source/Air Quality Relationships*, E.S. Macias and P.K. Hopke, Eds. American Chemical Society, Washington, DC, pp. 223-233.

Kendall, M.G. (1951). Regressions, structure and functional relationship, Part I. *Biometrika*, **39**:96-108.

Kim, E.; and Hopke, P.K. (2004). Source apportionment of fine particles at Washington, DC, utilizing temperature-resolved carbon fractions. *J. Air Waste Manage. Assoc.*, **54**(7):773-785.

Kim, E.; Hopke, P.K.; and Edgerton, E.S. (2004). Improving source identification of Atlanta aerosol using temperature resolved carbon fractions in positive matrix factorization. *Atmos. Environ.*, **38**(20):3349-3362. ISI:000221838500021.

Kirchstetter, T.W.; Corrigan, C.E.; and Novakov, T. (2001). Laboratory and field investigation of the adsorption of gaseous organic compounds onto quartz filters. *Atmos. Environ.*, **35**(9):1663-1671.

Kirchstetter, T.W.; Novakov, T.; and Hobbs, P.V. (2004). Evidence that the spectral dependence of light absorption by aerosols is affected by organic carbon. *J. Geophys. Res.*, **109**(D21):D21208. ISI:000225190500010.

Kopp, C.; Petzold, A.; and Niessner, R. (1999). Investigation of the specific attenuation cross-section of aerosols deposited on fiber filters with a polar photometer to determine black carbon. *J. Aerosol Sci.*, **30**(9):1153-1163.

Kubelka, P.; and Munk, F. (1931). Ein beitrag zur optik der farbanstriche. *Z. Tekn. Physik.*, **12**:593-601.

Lavanchy, V.M.H.; Gäggeler, H.W.; Nyeki, S.; and Baltensperger, U. (1999). Elemental carbon (EC) and black carbon (BC) measurements with a thermal method and an aethalometer at the high-alpine research station Jungfraujoch. *Atmos. Environ.*, **33**(17):2759-2769.

Lin, C.; and Friedlander, S.K. (1988a). Soot oxidation in fibrous filters. 1. Deposit structure and reaction mechanisms. *Langmuir*, **4**(4):891-898.

Lin, C.; and Friedlander, S.K. (1988b). Soot oxidation in fibrous filters. 2. Effects of temperature, oxygen partial pressure, and sodium additives. *Langmuir*, **4**(4):898-903.

Lindberg, J.D.; Douglass, R.E.; and Garvey, D.M. (1999). Atmospheric particulate absorption and black carbon measurement. *Appl. Opt.*, **38**(12):2369-2376.

Liousse, C.; Cachier, H.; and Jennings, S.G. (1993). Optical and thermal measurements of black carbon aerosol content in different environments: Variation of the specific attenuation cross-section, sigma (σ). *Atmos. Environ.*, **27A**(8):1203-1211.

Lipsky, E.M.; and Robinson, A.L. (2006). Effects of dilution on fine particle mass and partitioning of semivolatile organics in diesel exhaust and wood smoke. *Environ. Sci. Technol.*, **40**(1):155-162. ISI:000234421400030.

Lloyd, A.C.; and Cackette, T.A. (2001). Critical review - Diesel engines: Environmental impact and control. *J. Air Waste Manage. Assoc.*, **51**(6):809-847.

Madansky, A. (1959). The fitting of straight lines when both variables are subject to error. *J. Am. Stat. Assoc.*, **54**:173-205.

Martins, J.V.; Artaxo, P.; Liousse, C.; Reid, J.S.; Hobbs, P.V.; and Kaufman, Y.J. (1998). Effects of black carbon content, particle size, and mixing on light absorption by aerosols from biomass burning in Brazil. *J. Geophys. Res.*, **103**(D24):32041-32050.

McDonald, J.D.; Zielinska, B.; Fujita, E.M.; Sagebiel, J.C.; Chow, J.C.; and Watson, J.G. (2000). Fine particle and gaseous emission rates from residential wood combustion. *Environ. Sci. Technol.*, **34**(11):2080-2091.

McNeil, L.E.; and French, R.H. (2001). Light scattering from red pigment particles: Multiple scattering in a strongly absorbing system. *J. Appl. Phys.*, **89**(1):283.

Moosmüller, H.; Arnott, W.P.; and Rogers, C.F. (1997). Methods for real-time, *in situ* measurement of aerosol light absorption. *J. Air Waste Manage. Assoc.*, **47**(2):157-166.

Moosmüller, H.; Arnott, W.P.; Rogers, C.F.; Bowen, J.L.; Gillies, J.A.; Pierson, W.R.; Collins, J.F.; Durbin, T.D.; and Norbeck, J.M. (2001a). Time resolved characterization of diesel particulate emissions 1. Instruments for particle mass measurements. *Environ. Sci. Technol.*, **35**(4):781-787.

Moosmüller, H.; Arnott, W.P.; Rogers, C.F.; Bowen, J.L.; Gillies, J.A.; Pierson, W.R.; Collins, J.F.; Durbin, T.D.; and Norbeck, J.M. (2001b). Time resolved characterization of diesel particulate emissions 2. Instruments for elemental and organic carbon measurements. *Environ. Sci. Technol.*, **35**(10):1935-1942.

Moosmüller, H.; Arnott, W.P.; Rogers, C.F.; Chow, J.C.; Frazier, C.A.; Sherman, L.E.; and Dietrich, D.L. (1998). Photoacoustic and filter measurements related to aerosol light absorption during the Northern Front Range Air Quality Study (Colorado 1996/1997). *J. Geophys. Res.*, **103**(D21):28149-28157.

Mulik, J.D.; Puckett, R.; Williams, D.; and Sawicki, E. (1976). Ion chromatographic analysis of sulfate and nitrate in ambient aerosols. *Anal. Lett.*, **9**(7):653-663.

Nguyen, H.T.H.; Takenaka, N.; Bandow, H.; Maeda, Y.; de Oliva, S.T.; Botelho, M.M.F.; and Tavares, T.M. (2001). Atmospheric alcohols and aldehydes concentrations measured in Osaka, Japan and in Sao Paulo, Brazil. *Atmos. Environ.*, **35**(18):3075-3083.

Nielsen, T. (1996). Traffic contribution of polycyclic aromatic hydrocarbons in the center of a large city. *Atmos. Environ.*, **30**(20):3481-3490.

Novakov, T. (1982). Soot in the atmosphere. In *Particulate Carbon: Atmospheric Life Cycle*, G.T. Wolff and R.L. Klimisch, Eds. Plenum Press, New York, NY, pp. 19-41.

Park, K.; Chow, J.C.; Watson, J.G.; Trimble, D.L.; Doraiswamy, P.; Arnott, W.P.; Stroud, K.R.; Bowers, K.; Bode, R.; Petzold, A.; and Hansen, A.D.A. (2006). Comparison of continuous and filter-based carbon measurements at the Fresno Supersite. *J. Air Waste Manage. Assoc.*, **56**(4):474-491.

Peterson, M.R.; and Richards, M.H. (2002). Thermal-optical-transmittance analysis for organic, elemental, carbonate, total carbon, and OCX2 in PM2.5 by the EPA/NIOSH method. In *Proceedings, Symposium on Air Quality Measurement Methods and Technology-2002*, E.D. Winegar and R.J. Tropp, Eds. Air & Waste Management Association, Pittsburgh, PA, pp. 83-1-83-19.

Petzold, A.; Kramer, H.; and Schönlinner, M. (2002). Continuous measurement of atmospheric black carbon using a multi-angle absorption photometer. *Environ. Sci. & Pollut. Res.*, (Special Issue 4):78-82.

Petzold, A.; and Niessner, R. (1995). Method comparison study on soot-selective techniques. *Mikrochimica Acta*, **117**:215-237.

Petzold, A.; Schloesser, H.; Sheridan, P.J.; Arnott, W.P.; Ogren, J.A.; and Virkkula, A. (2005). Evaluation of multiangle absorption photometry for measuring aerosol light absorption. *Aerosol Sci. Technol.*, **39**(1):40-51. ISI:000225877400004.

Petzold, A.; and Schönlinner, M. (2004). Multi-angle absorption photometry - A new method for the measurement of aerosol light absorption and atmospheric black carbon. *J. Aerosol Sci.*, **35**(4):421-441.

Petzold, A.; Stein, C.; Nyeki, S.; Gysel, M.; Weingartner, E.; Baltensperger, U.; Giebl, H.; Hitzenberger, R.; Döpelheuer, A.; Vrchoticky, S.; Puxbaum, H.; Johnson, M.; Hurley, C.D.; Marsh, R.; and Wilson, C.W. (2003). Properties of jet engine combustion particles during the PartEmis experiment: Microphysics and chemistry. *Geophys. Res. Lett.*, **30**(13):52-1-52-4.

Pinnick, R.G.; Fernandez, G.; Martinez-Andazola, E.; Hinds, B.D.; Hansen, A.D.A.; and Fuller, K. (1993). Aerosol in the arid southwest United States: Measurements of mass loading, volatility, size distribution, absorption characteristics, black carbon content, and vertical structure to 7km above sea level. *J. Geophys. Res.*, **98**(D2):2651-2666.

Reid, J.S.; Hobbs, P.V.; Liousse, C.; Martins, J.V.; Weiss, R.E.; and Eck, T.F. (1998). Comparisons of techniques for measuring shortwave absorption and black carbon content of aerosols from biomass burning in Brazil. *J. Geophys. Res.*, **103**(D24):32031-32040.

Rodes, S.R.; Guinn, V.P.; and Thompson, R.J. (1989). General atomic absorption procedure for trace metals in airborne material collected on filters. In *Methods of Air Sampling and Analysis*, J.P. Lodge, Ed. Lewis Publishers, Chelsea, NY, pp. 608-618.

Rogge, W.F.; Hildemann, L.M.; Mazurek, M.A.; Cass, G.R.; and Simoneit, B.R.T. (1994). Sources of fine organic aerosol - 6. Cigarette smoke in the urban atmosphere. *Enivron. Sci. Technol.*, **28**(7):1375-1388.

Rogge, W.F.; Mazurek, M.A.; Hildemann, L.M.; Cass, G.R.; and Simoneit, B.R.T. (1993). Quantification of urban organic aerosols at a molecular level: Identification, abundance and seasonal variation. *Atmos. Environ.*, **27A**(8):1309-1330.

Sadler, M.; Charlson, R.J.; Rosen, H.; and Novakov, T. (1981). An intercomparison of the integrating plate and the laser transmission methods for determination of aerosol absorption coefficients. *Atmos. Environ.*, **15**(7):1265-1268.

Schauer, J.J. (1999). Source contributions to atmospheric organic compound concentrations: Emissions measurements and model predictions. Ph.D. Dissertation, California Institute of Technology, Pasadena, CA.

Schauer, J.J.; and Cass, G.R. (2000). Source apportionment of wintertime gas-phase and particle-phase air pollutants using organic compounds as tracers. *Environ. Sci. Technol.*, **34**(9):1821-1832.

Schmid, H.P.; Laskus, L.; Abraham, H.J.; Baltensperger, U.; Lavanchy, V.M.H.; Bizjak, M.; Burba, P.; Cachier, H.; Crow, D.; Chow, J.C.; Gnauk, T.; Even, A.; ten Brink, H.M.; Giesen, K.P.; Hitzenberger, R.; Hueglin, C.; Maenhaut, W.; Pio, C.A.; Puttock, J.; Putaud, J.P.; Toom-Sauntry, D.; and Puxbaum, H. (2001). Results of the "Carbon Conference" international aerosol carbon round robin test: Stage 1. *Atmos. Environ.*, **35**(12):2111-2121.

Sharma, S.; Brook, J.R.; Cachier, H.; Chow, J.; Gaudenzi, A.; and Lu, G. (2002). Light absorption and thermal measurements of black carbon in different regions of Canada. *J. Geophys. Res.*, **107**(D24). ISI:000181253900005.

Sheridan, P.J.; Arnott, W.P.; Ogren, J.A.; Andrews, E.; Atkinson, D.B.; Covert, D.S.; Moosmüller, H.; Petzold, A.; Schmid, B.; Strawa, A.W.; Varma, R.; and Virkkula, A. (2005). The Reno Aerosol Optics Study: An evaluation of aerosol absorption measurement methods. *Aerosol Sci. Technol.*, **39**(1):1-16. ISI:000225877400001.

Sicre, M.A.; Marty, J.C.; Saliot, A.; Aparicio, X.; Grimalt, J.; and Albaiges, J. (1987). Aliphatic and aromatic hydrocarbons in different sized aerosols over the Mediterranean Sea: Occurrence and origin. *Atmos. Environ.*, **21**:2247-2259.

Simoneit, B.R.T. (1984). Organic matter of the troposphere - III. Characterization and sources of petroleum and pyrogenic residues in aerosols over the western United States. *Atmos. Environ.*, **18**(1):51-67.

Simoneit, B.R.T. (1985). Application of molecular marker analysis to vehicular exhaust for source reconciliations. *Int. J. Environ. Anal. Chem.*, **22**:203-233.

Simoneit, B.R.T.; and Mazurek, M.A. (1982). Organic matter of the troposphere II - Natural background of biogenic lipid matter in aerosols over the rural western United States. *Atmos. Environ.*, **16**(9):2139-2159.

Subramanian, R.; Khlystov, A.Y.; Cabada, J.C.; and Robinson, A.L. (2004). Positive and negative artifacts in particulate organic carbon measurements with denuded and undenuded sampler configurations. *Aerosol Sci. Technol.*, **38**(Suppl 1):27-48.

Turpin, B.J.; Huntzicker, J.J.; and Adams, K.M. (1990). Intercomparison of photoacoustic and thermal-optical methods for the measurement of atmospheric elemental carbon. *Atmos. Environ.*, **24A**(7):1831-1835.

Turpin, B.J.; Huntzicker, J.J.; and Hering, S.V. (1994). Investigation of organic aerosol sampling artifacts in the Los Angeles Basin. *Atmos. Environ.*, **28**(19):3061-3071.

U.S.EPA (1997). Revised requirements for designation of reference and equivalent methods for $PM_{2.5}$ and ambient air surveillence for particulate matter - final rule. *Federal Register*, **62**(138):38763-38854. http://www.epa.gov/ttn/amtic/files/cfr/recent/pm-mon.pdf.

U.S.EPA (1998). EPA guidance for quality assurance project plans: EPA QA/G-5. Report No. EPA/600/R-98/018. Prepared by U.S. Environmental Protection Agency, Washington, D.C.

U.S.EPA (1999a). EPA requirements for quality assurance project plans: EPA QA/R-5. Prepared by U.S. Environmental Protection Agency, Washington, D.C.

U.S.EPA (1999b). EPA requirements for quality management plans: EPA QA/R-2. Prepared by U.S. Environmental Protection Agency, Washington, D.C.

U.S.EPA (1999c). SPECIATE: EPA's repository of total organic compound and particulate matter speciated profiles for a variety of sources for use in source apportionment studies. Prepared by U.S. Environmental Protection Agency, Office of Air Quality Planning and

Standards, Research Triangle Park, NC. http://www.epa.gov/ttn/chief/software/speciate/.

VDI (1996). Measurement of soot (immission) - Chemical analysis of elemental carbon by extraction and thermal desorption of organic carbon. Report No. 2465 Part 1. Prepared by Verein Deutscher Ingenieure, Dusseldorf, Germany.

VDI (1999). Measurement of soot (ambient air) - Thermographic determination of elemental carbon after thermal desorption of organic carbon. Report No. 2465 Part 2. Prepared by Verein Deutscher Ingenieure, Dusseldorf, Germany.

Virkkula, A.; Ahlquist, N.C.; Covert, D.S.; Arnott, W.P.; Sheridan, P.J.; Quinn, P.K.; and Coffman, D.J. (2005). Modification, calibration and a field test of an instrument for measuring light absorption by particles. *Aerosol Sci. Technol.*, **39**(1):68-83. ISI:000225877400006.

Wang, C.F.; Chin, C.J.; and Chiang, P.C. (1998a). Multielement analysis of suspended particulates collected with a beta-gauge monitoring system by ICP atomic emission spectrometry and mass spectrometry. *Anal. Sci.*, **14**(4):763-768. ISI:000075270100017.

Wang, I.T.; Chico, T.; Huang, Y.H.; and Farber, R.J. (1998b). Development, evaluation, and application of a primary aerosol model. In *Proceedings, $PM_{2.5}$: A Fine Particle Standard*, J.C. Chow and P. Koutrakis, Eds. Air & Waste Management Association, Pittsburgh, PA, pp. 759-770.

Wang, L.H.; and Jacques, S.L. (1993). Analysis of diffusion theory and smiliary relations. In *Photon Migration and Imaging in Random Media and Tissues*, B. Chance and R.R. Alfano, Eds. Proc. SPIE, pp. 107-116.

Wang, L.H.; Jacques, S.L.; and Zheng, L.Q. (1995). MCML - Monte Carlo modeling of photon transport in multi-layered tissues. *Computer Methods and Programs in Biomedicine*, **47**:131-146.

Wang, L.-H.; Jacques, S.L.; and Zheng, L.-Q. (1998c). MCML-Monte Carlo modeling of photon transport in multi-layered tissues. *Computer Methods and Programs in Biomedicine*, **47**:131-146.

Watson, J.G. (2002). Visibility: Science and regulation. *J. Air Waste Manage. Assoc.*, **52**(6):628-713.

Watson, J.G.; and Chow, J.C. (2001). Ambient air sampling. In *Aerosol Measurement: Principles, Techniques, and Applications, Second Edition,* 2nd ed., P. Baron and K. Willeke, Eds. John Wiley & Sons, New York, NY, pp. 821-844.

Watson, J.G.; and Chow, J.C. (2002a). A wintertime $PM_{2.5}$ episode at the Fresno, CA, supersite. *Atmos. Environ.*, **36**(3):465-475.

Watson, J.G.; and Chow, J.C. (2002b). Comparison and evaluation of in-situ and filter carbon measurements at the Fresno Supersite. *J. Geophys. Res.*, **107**(D21):ICC 3-1-ICC 3-15.

Watson, J.G.; Chow, J.C.; Bowen, J.L.; Lowenthal, D.H.; Hering, S.; Ouchida, P.; and Oslund, W. (2000a). Air quality measurements from the Fresno Supersite. *J. Air Waste Manage. Assoc.*, **50**(8):1321-1334. ISI:000089085700005.

Watson, J.G.; Chow, J.C.; and Chen, L.-W.A. (2005). Summary of organic and elemental carbon/black carbon analysis methods and intercomparisons. *Aerosol and Air Quality Research*, **5**(1):65-102. http://aaqr.org/.

Watson, J.G.; Chow, J.C.; and Fitz, D.R. (2000b). Quality assurance project plan - Fresno Supersite (Revision 0). Prepared for U.S. Environmental Protection Agency, Office of Air Quality Planning and Standards, Research Triangle Park, NC, by Desert Research Institute, Reno, NV.

Watson, J.G.; Chow, J.C.; and Frazier, C.A. (1999). X-ray fluorescence analysis of ambient air samples. In *Elemental Analysis of Airborne Particles, Vol. 1*, S. Landsberger and M. Creatchman, Eds. Gordon and Breach Science, Amsterdam, pp. 67-96.

Watson, J.G.; Chow, J.C.; and Houck, J.E. (2001). $PM_{2.5}$ chemical source profiles for vehicle exhaust, vegetative burning, geological material, and coal burning in northwestern Colorado during 1995. *Chemosphere*, **43**(8):1141-1151.

Watson, J.G.; Chow, J.C.; Lowenthal, D.H.; Pritchett, L.C.; Frazier, C.A.; Neuroth, G.R.; and Robbins, R. (1994). Differences in the carbon composition of source profiles for diesel- and gasoline-powered vehicles. *Atmos. Environ.*, **28**(15):2493-2505.

Watson, J.G.; Chow, J.C.; Park, K.; and Lowenthal, D.H. (2006). Nanoparticle and ultrafine particle events at the Fresno Supersite. *J. Air Waste Manage. Assoc.*, **56**(4):417-430.

Watson, J.G.; Cooper, J.A.; and Huntzicker, J.J. (1984). The effective variance weighting for least squares calculations applied to the mass balance receptor model. *Atmos. Environ.*, **18**(7):1347-1355.

Watson, J.G.; Fujita, E.M.; Chow, J.C.; Zielinska, B.; Richards, L.W.; Neff, W.D.; and Dietrich, D. (1998). Northern Front Range Air Quality Study. Final report. Prepared for Colorado State University, Fort Collins, CO, by Desert Research Institute, Reno, NV. http://charon.cira.colostate.edu/DRIFinal/ZipFiles/.

Watson, J.G.; Lioy, P.J.; and Mueller, P.K. (1983). The measurement process: Precision, accuracy and validity. In *Air Sampling Instruments for Evaluation of Atmospheric Contaminants, Sixth Edition,* 6th ed., P.J. Lioy and M.J.Y. Lioy, Eds. American Conference of Governmental Industrial Hygienists, Cincinnati, OH, p. L-1-L-7.

Watson, J.G.; Lioy, P.J.; and Mueller, P.K. (1989). The measurement process: Precision, accuracy, and validity. In *Air Sampling Instruments for Evaluation of Atmospheric Contaminants, Seventh Edition,* 7th ed., S.V. Hering, Ed. American Conference of Governmental Industrial Hygienists, Cincinnati, OH, pp. 51-57.

Watson, J.G.; Lioy, P.J.; and Mueller, P.K. (1995). The measurement process: Precision, accuracy, and validity. In *Air Sampling Instruments for Evaluation of Atmospheric Contaminants,* 8th ed., B.S. Cohen and S.V. Hering, Eds. American Conference of Governmental Industrial Hygienists, Cincinnati, OH, pp. 187-194.

Weingartner, E.; Saathoff, H.; Schnaiter, M.; Streit, N.; Bitnar, B.; and Baltensperger, U. (2003). Absorption of light by soot particles: Determination of the absorption coefficient by means of aethalometers. *J. Aerosol Sci.*, **34**(10):1445-1463.

Willermet, P.A. (1998). Some engine oil additives and their effects on antiwear film formation. *Tribology Letters*, **5**(1):41-47.

Yang, H.; and Yu, J.Z. (2002). Uncertainties in charring correction in the analysis of elemental and organic carbon in atmospheric particles by thermal/optical methods. *Environ. Sci. Technol.*, **36**(23):5199-5204.

9. PUBLISHED PAPERS

9.1 Watson et al., 2005

Watson et al., Aerosol and Air Quality Research, Vol. 5, No.1, pp. 65-102, 2005

Summary of Organic and Elemental Carbon/Black Carbon Analysis Methods and Intercomparisons

John G. Watson*, Judith C. Chow, and L.-W. Antony Chen

Desert Research Institute, 2215 Raggio Parkway, Reno, NV, 89512-1095, USA

Abstract

Many different thermal, optical, and thermal/optical carbon analysis methods for organic carbon (OC), elemental carbon (EC) or black carbon (BC) have been applied throughout the world to evaluate visibility and the Earth's radiation balance. Dozens of intermethod and interlaboratory comparison studies have been conducted. Several of these studies are catalogued and summarized here. BC or EC concentrations are found to differ by up to a factor of 7 among different methods; factor of 2 differences are common. Differences between methods are not consistent among comparison studies, with some methods showing higher BC for one set of samples and lower BC for other sets relative to a common benchmark. The absorption efficiency relating light absorption (b_{abs}) to EC that is derived from collocated optical and chemical measurements can vary by a factor of 10, depending on the collocated b_{abs} and EC measurement methods. Future intermethod and interlaboratory comparisons must include components that seek to understand the causes of these differences.

Keywords: Black carbon, elemental carbon, organic carbon, thermal/optical analysis, water-soluble organics, aerosol, light scattering/absorption efficiency.

1. Introduction

Elemental carbon (EC) and black carbon (BC) are operationally defined by the measurement method applied, although EC and BC are often used interchangeably. The objective of this paper is to: 1) summarize filter methods used to measure organic carbon (OC) and EC; 2) assemble interlaboratory and intermethod comparisons; and 3) identify knowledge gaps and research needs.

EC occurs as the mineral graphite or as diamond in its purest forms, but these structures of more than 0.1 micrograms (μg) are seldom found in ambient particulate matter (PM). Freshly emitted diesel soot consists of agglomerates of small spherical graphitic particles consistent in size from 20 to

*Corresponding author. Tel: +775-674-7046; Fax: +775-674-7009.
E-mail address: johnw@dri.edu

30 nanometers (nm). Even the soot from incomplete combustion contains non-carbon components and has a non-crystalline structure (Akhter et al., 1984, 1985). It has a large surface-to-volume ratio and reactive surfaces, so it attracts condensable materials (e.g., polycyclic aromatic hydrocarbon [PAH] gases) soon after emission into ambient air.

Of the major components of $PM_{2.5}$ and PM_{10}, OC and EC are the most uncertain with respect to sampling and analysis (Huebert and Charlson, 2000; Jacobson et al., 2000; Turpin et al., 1994). Most EC and BC characterization involves collecting PM on filters and measuring either the carbon content on the filter or the attenuation of light reflected from or transmitted through the filter. Filter-based optical techniques include the British Smoke Shade method (Hill, 1936), the coefficient of haze (COH) (Hemeon et al., 1953), the integrating plate method (IPM) (Lin et al., 1973), the aethalometer (Hansen et al., 1984), and the particle soot absorption photometer (PSAP) (Bond et al., 1999). The scattering and absorption properties of particles distributed on top of and throughout a filter are not the same as they are in the atmosphere. Light absorption coefficients (b_{abs}) determined from these methods are often biased (Horvath, 1993).

It is generally agreed that EC is the major contributor to b_{abs} (e.g., Horvath, 1993; Watson, 2002). EC absorbs light due to conduction electrons associated with the graphitic structure. EC is, therefore, often referred to as BC. However, the specific mass absorption efficiency of EC has been estimated to range from 2 to 20 m^2/g (Liousse et al., 1993). Particle light absorption depends on the wavelength (λ) of the incident light. Moosmüller (1998) reported that EC absorption efficiency varied as $\lambda^{-2.7}$ near Denver, CO, while Horvath et al. (1997) reported that absorption efficiency for aerosols in Santiago, Chile, varied as $\lambda^{-0.92}$. Kirchstetter et al. (2004) found that b_{abs} from engine exhaust varied as λ^{-1} whereas b_{abs} from biomass burning varied as λ^{-2}. Carbonaceous material from different sources (e.g., diesel versus wood burning) has different structures and compositions. A small quantity of carbonates (e.g., $CaCO_3$) is found in some fine particulate samples, but this is rarely comparable to the EC content (Chow and Watson, 2002; Cao et al., 2005). The remainder of the carbonaceous material is organic matter that is a complex mixture of hundreds of organic compounds covering a wide range of molecular forms and volatilities (Jacobson et al., 2000). Organic matter can be emitted directly from combustion sources with EC, or it can be formed in the atmosphere through condensation of low-volatility oxidation products of hydrocarbons (i.e., secondary organic aerosol [SOA]). Some components of OC may be weakly light-absorbing in the visible spectrum, but OC mainly influences direct radiative forcing through light-scattering or through mixing with EC to enhance the EC absorption efficiency (e.g., Fuller et al., 1999).

Particles change when they are extracted from the air onto a filter, on which most EC or BC measurements are made. The rate at which the material evaporates depends on how the filter is handled and stored between sampling and analysis. Quartz-fiber filters used for thermal carbon analysis absorb some organic vapors throughout their thickness; these vapors are often interpreted as OC by thermal methods and possibly as a portion of EC if the OC is charred.

Fuller et al. (1999) hypothesized that differences among estimates for soot extinction efficiencies are due to: 1) different wavelength dependencies; 2) deviations from spherical particles; 3) mischaracterization of the soot refractive index; 4) inaccurate densities; and 5) mixtures of graphitic material with other compounds. By applying radiative transfer models for non-spherical particles of non-homogeneous composition, Fuller et al. (1999) found that for the same quantity of EC, b_{abs} decreased rapidly for particles >0.1 μm, the particle size of most of the aged EC in the atmosphere. Up to 60% higher efficiencies were calculated for long chain aggregates relative to the same amount of EC in a sphere. Absorption efficiencies >10 m^2/g—exceeding 25 m^2/g in some situations—were estimated for soot imbedded in a sulfate particle. Efficiency decreased as the EC fraction in the particle increased, implying that a lower EC concentration may yield a higher contribution per EC mass to light absorption under some circumstances. Efficiencies decreased by nearly 1 order of magnitude as an EC core at the center of a concentric sphere migrated through the sphere to its surface.

Martins et al. (1998) found similar results, with maximum soot absorption efficiencies approaching 30 m^2/g when the carbon constituted 0.5% of the volume of a 0.5 μm diameter particle. Empirically derived soot extinction efficiencies are usually greater at non-urban than urban monitors (Horvath, 1993). This is consistent with an aged aerosol in which more of the fresh emissions become coated with condensed, absorbed, and adsorbed material. Horvath (1993, 1997) shows how light transmission through a filter varies depending on the filter loading, the presence or absence of light-scattering particles, and the location of particles within a filter. These results imply that constant conversion factors used to infer EC from b_{abs}, such as the 10 m^2/g often used in visibility studies (Watson, 2002), are subject to large uncertainties.

OC and EC are measured directly by thermal evolution methods that quantify the amount of carbon that leaves the filter at different temperatures (Currie et al., 2002; Schmid et al., 2001). These methods use different combinations of temperature and analysis atmospheres to evaporate, pyrolyze, and combust the carbon-containing compounds on a filter sample, then detect the evolved carbon gases. The separation of OC from EC is ambiguous because some of the EC combusts in the presence of oxygen, and some of the OC chars (turns to EC) in an oxygen-deficient atmosphere. Light reflected from (Johnson et al., 1981; Huntzicker et al., 1982; Chow et al., 1993) or transmitted through (Turpin et al., 1990; Birch and Cary, 1996a, 1996b; Chow et al., 2001) the filter during the analysis is used to monitor and correct for this charring. Interlaboratory and intermethod comparisons (e.g., Chow et al., 2001; Countess, 1990; Currie et al., 2002; Schmid et al., 2001) show EC differences of a factor of 2 or more among thermal methods, depending on the protocol and type of sample. Analysis methods alone can account for the large differences in EC emission rates among inventories. In addition to OC and EC, carbon that evolves at several different temperatures has been found useful for source apportionment studies (Watson et al., 1994; Kim and Hopke, 2004).

2. Thermal Organic and Elemental Carbon Analysis Methods

Table 1 summarizes several of the thermal methods that have been applied to estimating total carbon (TC), OC, and EC. All of these produce OC and EC concentrations that are defined by the method rather than by an absolute standard. Many of these methods use a two-step temperature in which the carbon evolving below the temperature (~350 to 550 °C) is termed OC and the remaining carbon evolving at a higher temperature (~650 to 1100 °C) is termed EC. Between different methods, lower OC temperatures are used in an oxidizing atmosphere for which the combustion rate of EC is assumed to be low; higher OC temperatures are usually applied in a non-oxidizing atmosphere, with an oxidizer added at a time after which most of the OC is assumed to have left the sample. The evolved carbon is converted to carbon dioxide (CO_2), which can be detected directly or converted to methane (CH_4) for more sensitive detection.

As Table 1 shows, many of the methods employ thermal/optical reflectance (TOR) and/or thermal/optical transmission (TOT) to monitor the conversion of OC to EC as part of the analysis. Since EC is not volatile, it is released only by oxidation (typically in an oxygen [O_2] atmosphere at a temperature below 800°C) and is thereby separated from OC. Heating in an O_2-free environment, however, causes certain OC components to pyrolyze and form non-volatile, light-absorbing, "charred," material that can be mistaken for atmospheric EC. Light reflected from or transmitted through the sample monitors the darkening of the particle deposit on the filter due to OC charring. When O_2 is added to the analysis atmosphere (i.e., carrier gas) at a sufficiently high temperature (e.g., >350 °C), this black char combusts along with the original EC on the filter, and the filter becomes whiter. When the reflected or transmitted light attains its original intensity, the charred, or pyrolyzed, OC (POC) is considered to have been removed. All of the remaining carbon is associated with the EC that was originally on the filter. Therefore, a partitioning can be made by assigning carbon evolved before this split point to OC and after this point to EC. Johnson et al. (1981) and Yang and Yu (2002) pointed out that such partitioning assumes that: 1) charred OC evolves before the original EC in the thermal analysis, and 2) charred OC and original OC equally attenuate reflectance (R) and transmittance (T). Several of the thermal methods appear to be similar, but they contain subtle differences with respect to: 1) analysis atmospheres, 2) temperature ramping rates, 3) temperature plateaus, 4) residence time at each plateau, 5) optical pyrolysis monitoring configuration and wavelength, 6) standardization, 7) oxidation and reduction catalysts, 8) sample aliquot and size, 9) evolved carbon detection method, 10) carrier gas flow through or across the sample, 11) location of the temperature monitor relative to the sample, and 12) oven flushing conditions. These differences are not always well characterized or reported along with analysis results, but this information is critical to interpret variability in the results. For example, Chow et al. (2005a) demonstrate the influence of temperature calibration on TOR analysis for temperature-resolved carbon fractions. Chow et al. (2004) and Chen et al. (2004) discuss how TOR and TOT might determine different OC/EC splits for various types of samples.

Owing to differences in the form of EC and the methods that operationally separate OC from EC, there is no reason to expect a consistent relationship among samples measured in different laboratories. This is borne out by the summary of 40 different intermethod and interlaboratory comparisons studies in Table 2. These comparisons date from the early 1980s to the present and cover a wide range of samples, the thermal evolution methods described in Table 1, and types of sampled particles.

In some studies, several simulated and ambient samples were sent to different laboratories. These comparisons showed that TC was the same for well-calibrated instruments, but the OC/EC splits were different. Since EC usually constitutes the smallest fraction of TC, it shows the largest variation among laboratories (up to a factor of 7 as reported by Currie et al., 2002). Many of the methods agreed on EC from diesel exhaust or powdered graphite samples, but they often disagreed for ambient and biomass burning samples. Schmid et al. (2001) showed that biases were not consistent from sample to sample for paired measurements from several thermal/optical protocols. This demonstrated that differences depend on the samples analyzed as well as on the instruments and methods used for the analyses. Potential sample biases include: 1) non-uniform particle deposits on the filter; 2) particle deposits that are too light or too dark, which make R and T charring corrections uncertain; 3) organic vapor filter adsorption and its charring during heating; 4) catalytic and oxidation interactions between OC, EC, and non-carbonaceous material in the sampled particles; and 5) changes in optical properties of the particles during thermal evolution.

It is doubtful that future carbon comparisons will add much information to those already completed unless they include components that systematically quantify the effects of sample properties and the analysis variables cited above. This degree of systematization is lacking in most of the studies. While it is possible to observe differences, it is not possible to explain why.

As an example, Chow et al. (2004) examined charring of the filter backside and microscopic cross-sections of a filter punch at different parts of the temperature cycle during thermal analysis. It appeared that R was dominated by charring of OC that co-existed with EC in particles on the surface of the filter, while T was dominated by the charring of organic vapors distributed throughout the filter. When oxygen was added to the analysis atmosphere, the surface EC (original EC and charred OC) evolved before the charred OC that was distributed throughout the filter. Hence, T achieved its initial value later than R. Using a radiative transfer model, Chen et al. (2004) showed that this explanation is plausible, and that simultaneous R and T measurements can be used to estimate contributions to charring from the surface particulate OC and the charred vapors adsorbed throughout the filter.

Table 1. Summary of organic and elemental carbon thermal analysis protocols.

Protocol	Carrier gas for OC	Carrier gas for EC	Temperature plateaus for OC (°C)	Residence time at each temperature for OC (s)	Temperature plateaus for EC (°C)	Residence time at each temperature for EC (s)	Optical charring correction	Converter and detector
IMPROVE[1]	He	98%He 2%O_2	120,250,450, 550	150 – 580[a]	550,700,800	150 – 580[a]	Reflectance	Methanator; FID/CH_4
TMO[2]	He[b]	98%He 2%O_2	525	300[c]	750	180	N/A	Methanator; FID/CH_4
OGI[3]	He[d]	98%He 2%O_2	600	Varies[a]	400, 500, 600	100,120,>200	Reflectance	Methanator; FID/CH_4
NIOSH[4] 5040	He	98%He 2%O_2	250,500,650, 850	60,60,60, 90	650,750,850, 940	30,30,30, >120	Transmittance	Methanator; FID/CH_4
STN[5,e]	He	98%He 2%O_2	310,480,615, 900	60,60,60, 90	600,675,750, 825,920	45,45,45, 45,120	Transmittance	Methanator; FID/CH_4
HKGL[6] (Hong Kong)	He	95%He 5%O_2	350,550,850	70,70,110	550,600,700, 750,800,850	10,50,40, 30,30,70	Transmittance	Methanator; FID/CH_4
HKUST-3[7] (Hong Kong)	He	99%He 1%O_2	250,500,650, 850	150,150,15 0, 150	650,750,850, 890	150,150,150, 150	Transmittance	Methanator; FID/CH_4
CalTech[8] (ACE-Asia)	He	90%N_2 10%O_2	310,450,575, 870	60,60,60, 90	550,625,700, 775,850,900	45,45,45, 45,45,120	Transmittance	Methanator; FID/CH_4
MSC1[9] (Canada)	He	90%He 10%O_2	250,450,550, 900	150,150,18 0,90	550,700,800	240,210,150	Transmittance	Methanator; FID/CH_4
RU/OGI[10] (Atlanta)	He	90%He 10%O_2	Stepwise to 700[e]	N/A	Stepwise to 850	N/A	Transmittance	Methanator; FID/CH_4
LBL[11]	O_2	O_2	Continuous (25 – 825)[f]	10 °C per minute	Continuous (25 – 825)	10 °C per minute	Transmittance	NDIR/CO_2
CNRS-CEA[12] (France 2-Step)	O_2	O_2	340	7200	1100	~600a	Assume 10% of OC is charred; assume EC decomposition rate of ~0.22% per min during OC analysis.	Coulometric titration/CO_2
U. Berne[13] (Switzerland 2-Step)	O_2	O_2	650[e],340[e]	60, 2520	650	1920	N/A	NDIR/CO_2
BNL[14]	He	90%He 10%O_2	400	300 or 900 g	700	300 or 900[g]	N/A	NDIR/CO_2
GM[15] Research Laboratory	He[h]	Ambient air	650	~100[a]	650	~120[a]	N/A	NDIR/CO_2
VDI[16] 2465/1 (Germany)	N/A[i]	O_2	N/A	N/A	200,650,200	60,420,120	N/A	Coulometric titration/CO_2
VDI[17] 2465/2 (Germany)	He	80%He 20%O_2	80,350,620, 400	12,72,108, 18	300,700[j]	30,54	N/A	Coulometric titration/CO_2
RCOP[18] (Japan)	N_2	92%N_2 8%O_2	450	600[k]	850	300	N/A	Methanator; FID/CH_4
R&P 5400[19] (continuous analyzer)	Ambient air	Ambient air	340	~600[l]	750	~600[l]	N/A	Low-volume IR CO_2 Meter

Table 1. (Continued)

[a] Advance from one temperature to the next when a well-defined carbon peak has evolved.

[b] Sample is acidified with 30 µl of 0.02N hydrochloric acid (HCl) and preheated at 120 °C in contact with a bed of granulated manganese dioxide (MnO_2) in helium (He) for 180 s to remove volatile OC and carbonate. The sample remains in contact with MnO_2 throughout analysis.

[c] Temperature change is accomplished by moving the sample from a lower-temperature oven to a higher-temperature oven.

[d] Sample is preheated at 350°C in 98% He/2% oxygen (O_2) environment until all volatile OC is removed.

[e] Cool to ~ 350 °C before the introduction of O_2 (Turpin et al., 1990).

[f] The third of four carbon dioxide (CO_2) peaks evolving during thermal analysis is assigned to EC; this peak is usually accompanied by an increasing filter transmittance.

[g] Residence times for loadings < 50 µgC and > 50 µgC per cm^2 are 300 s and 900 s each, respectively, for both 400 °C and 700 °C temperature stages.

[h] Sample is preheated at 350 °C in ambient air for ~ 450 s to remove volatile OC.

[i] OC on half a filter is extracted with 10 ml of a 50:50 volume %–mixture of toluene and 2-propanol for 24 hr, and the half-filter is dried in pure nitrogen (N_2) before thermal analysis. OC is estimated from the difference between TC and EC acquired from two separated filter halves.

[j] The sample is cooled to 80 °C from 700 °C. Carbon evolved during cooling is also counted as EC.

[k] Temperature changes are accomplished by moving the sample through an increasing temperature gradient in the oven.

[l] The overall analysis time is adjustable but should not be > 30 min.

References

1 Interagency Monitoring of Protected Visual Environments, Chow et al., 1993, 2001, 2004

2 Thermal Magnesium Dioxide, Fung, 1990; Fung et al., 2002

3 Oregon Graduate Institute, Huntzicker et al., 1982

4 National Institute of Occupational Safety and Health, Birch, 1998; Birch and Cary, 1996a, 1996b; NIOSH 1996, 1999

5 Speciation Trends Network, Peterson and Richards, 2002

6 Hong Kong Governmental Laboratory, Sin et al., 2002; Chow et al., 2005b

7 Hong Kong University of Science and Technology, Yang and Yu, 2002; Yu et al., 2002

8 California Institute of Technology, Mader et al., 2001

9 Meteorological Service of Canada, Version I, Sharma et al., 2002

10 Rutgers University/Oregon Graduate Institute, Lim et al., 2003

11 Lawrence Berkeley Laboratory, Novakov, 1982; Ellis et al., 1984; Kirchstetter et al., 2001

12 Laboratoire des Sciences du Climat et de l'Environnement, Cachier et al., 1989a, 1989b

13 University of Berne, Switzerland, Lavanchy et al., 1999

14 Brookhaven National Laboratory, Tanner, 1982; Gaffney et al., 1984

15 General Motors Research Laboratory, Cadle et al., 1980, 1983

16 VDI, 1996

17 VDI, 1999

18 Radiation Center of Osaka Prefecture, Mizohata and Ito, 1985

19 Rupprecht and Patashnick, Rupprecht et al., 1995

Table 2. Summary of carbon intercomparison studies.

Study/Period/Location/Type	Sampling and Analytical Method[a]	Summary of Major Findings
A Comparison of Integrating Plate Method and Transmission Method (Sadler et al., 1981) • Location: Five sampling sites in the western part of Washington state, from a highly congested site in a highway tunnel to a remote site on a western foothill of the Olympic Mountains. • Type: Rural ambient aerosol and urban traffic emission aerosol.	• This study compares absorption on three different sampling substrates (Nuclepore, Millpore, and quartz-fiber). – Integrating plate method (IPM) for measuring absorption coefficient through transmission. – Laser transmission method (LTM) for measuring absorption. This was the early development of PSAP. The LTM compared the transmission of a 633 nm He-Ne laser beam through a loaded Millipore filter relative to a blank filter to calculate the absorption caused by the particle deposit. – A total combustion/CO_2 evolution method on quartz-fiber filters for total carbon (TC) (Mueller et al., 1971).	• A total of 44 filters of each type were used in this comparison. The correlation coefficient between IPM and LTM measurements was 0.95, and the absorption coefficient determined by LTM was a factor of ~2.5 greater than that determined by the IPM. This difference was attributed to the filter material. • The correlation coefficient found between TC and IPM measurements for the urban data was 0.96. The absorption of urban aerosol was similar to that of a pure graphitic particle of 0.1 μm diameter and 0.66 imaginary refractive index.
Colorado State University Aerosol Workshop (Bennett and Patty, 1982) • Sample: Black carbon (BC) and white ammonium sulfate [$(NH_4)_2SO_4$] particles generated during the Colorado State University Aerosol Workshop. • Type: Artificial standard aerosol.	• Particles were deposited on the Teflon-membrane filter substrates at a flow rate of 16.7 L/min. The deposits were analyzed by: – IPM operated at 633 nm. – Photoacoustic detection (PAD) operated at 633 nm for measuring absorption coefficient based on absorptive and thermal properties of the sample.	• After a pure carbon deposit was analyzed by IPM and PAD, an overload of $(NH_4)_2SO_4$ was placed on top of the carbon, and the IPM and PAD measurements were repeated. The perturbation of salt to the IPM measurements was much larger (5 – 10 times) than expected, indicating that multiple scattering was apparently taking place within the samples. The perturbation to PAD measurements was much less. • IPM overestimated absorption when interfered with by scattering particles, but the opposite trend was found in PAD.

Table 2. (Continued)

Study/Period/Location/Type	Sampling and Analytical Method	Summary of Major Findings
General Motors Intercomparison Study I (Cadle and Groblicki, 1982) • Location: Three ambient sampling sites: Denver, CO, rural areas near Picas, SD, and Abbeville, LA. Source particulate samples were obtained from gasoline and diesel passenger cars run on a chassis dynamometer, and from residential fireplace wood combustion. • Type: Ambient and source emissions.	• Samples were collected on a glass-fiber filter or a quartz-fiber filter. The analytical methods for EC included: – General Motors Research (GMR) thermal analysis protocol. OC removed from the sample by heating at 650 °C under He. – Solvent or Fluorinert FC-78 extraction for 8 hrs before thermal analysis. – Nitric acid (6N HNO_3) digestion for 24 hrs before thermal analysis. – Vacuum Stripping (1 torr, 180 °C or 350 °C) before thermal analysis. – IPM operated at 550 nm for measuring absorption.	• Heating at 180 °C removed only 30% of the carbon compared to 62% at 350 °C in a vacuum. Heating in air at 350 °C removed even more carbon (67%). • Both 350 °C oxidation and 2 hr HNO_3 extraction removed 67-68% of the carbon compared to a maximum of 54% removal by the most effective solvent. Thus, a maximum of 14% of the organic matter was not extractable by solvent. • The amount of charring at 650 °C under He depended on the type of organic material present and percent of EC in the samples. Errors were small in automotive diesel particulate samples where charring is limited. The error can be large in samples susceptible to charring, such as wood burning. • The IPM absorption showed a good correlation with EC from thermal method ($r = 0.93$), resulting in an absorption efficiency of ~ 10 m^2/g.
General Motors Intercomparison Study II (Cadle et al., 1983) • Location: One ambient sampling site near Luray, VA. Additional ambient samples were acquired at Warren, MI, during the winter and spring of 1981. Source particulate samples were obtained from diesel passenger cars run on a chassis dynamometer. Wood smoke was collected from a fireplace burning either softwood or hardwood. • Type: Ambient and source aerosol.	• Samples were collected on quartz-fiber filters. The analytical methods for EC included: – GMR thermal analysis protocol. OC was removed from the sample by heating at 650 °C under He. Other heating temperatures were tested. – Three digestion methods were used to remove OC before thermal analysis. In one method, the filters were immersed in a 1.4 M H_2SO_4, 0.13 M $K_2S_2O_8$, 0.6%W/V $AgNO_3$ solution. In another method, the filters were immersed in a 1:1 solution of ethanol and 4N KOH for ~ 18 hrs. The third method consisted of immersion in a 30% H_2O_2 solution and irradiation with a 200W Xe-Hg arc lamp for 0.75 hr.	• The absorption of organic vapor on glass- and quartz-fiber filters and silver-membrane filters may be a major problem. With some samples, the amount of carbon adsorbed by a backup filter was 30% of that on the front filter. • Thermal methods have the advantage of being rapid, but can cause charring of OC, even at 950 °C. The optimum thermal method varies with different samples. A two-step separation procedure employing heating at 350 °C in air followed by a 950 °C pyrolysis under He should be used for samples of unknown compositions. • The digestion methods investigated removed some EC and showed no advantage over the thermal methods.

Table 2. (Continued)

Study/Period/Location/Type	Sampling and Analytical Method	Summary of Major Findings
Comparison of British Smoke Shade (BSS) with Elemental Carbon Concentration (Edwards et al., 1983) • Location: Two aerosol sampling sites: the University of Washington campus provided a typical urban setting while a highway tunnel (U.S. 99) provided a high concentration of vehicle exhaust. • Type: Urban ambient fine aerosol and traffic emissions ($D_p < 1.6$ μm).	• Particles were collected on quartz-fiber and Nuclepore polycarbonate-membrane filters. • EEL reflectometer (OECD, 1964) for British Smoke Shade (BSS) measurement. • IPM operated at 550 nm. • OGI_TOR (Johnson et al., 1981) protocol on quartz-fiber filters for EC.	• b_{abs} determined by reflectometer and IPM transmittance were well correlated to each other, but the slope varied with filter medium and face velocity of sampling. This was probably due to penetration of particles into the filters, causing them to be more reflective and transmit less light for a given aerosol loading than they would have if particles were retained on the surface. • The transmission of a sample on a fiber filter was always less than that for a Nuclepore filter, while the reflectance was either greater or less than that of the Nuclepore, likely due to multiple scattering effects. • The absorption efficiency of EC ranged from 7 – 12 m^2/g in this study. • A correction factor of 1.3 was applied to the BC calculated from BSS for a comparison with the EC. The data suggested that BSS might be used to estimate EC within about a factor of two.
Allegheny Mountain Tunnel Study (Szkarlat and Japar, 1983) • Period: 7/14/1981 – 7/18/1981. • Location: Allegheny Mountain Tunnel on the Pennsylvania Turnpike. The tunnel is located in southwestern Pennsylvania with the closest population center being Somerset, 21 km to the west. • Type: Highway traffic emissions.	• High volume samplers (Misco Model 680, 5.5 μm size cutoff) were set up in the east portal of the eastbound tunnel. Particles were collected on glass-fiber and Teflon-membrane filters (4 – 7.5 hrs duration). The vehicle composition was monitored. • The organic-soluble fraction of the particulate emission was determined by 16 hr Soxhlet extractions of filter samples in 1:1 (v/v) mixtures of toluene/1-propanol. • The carbon content of extracted, nonextracted, and blank filters was determined by combustion (Spang Microanalytical Laboratory, Eagle Harbor, MI). • IPM operated at 500 nm. • Integrating nephelometer operated at 550 nm for particle scattering. • A He-Ne laser (632.8 nm) was used for total extinction measurements.	• The non-extractable carbon was assumed to be EC. Chemical analyses showed that: 1) 24% of the vehicle aerosol was extractable material, 2) 75% of the total mass was carbon, 3) 55% of the total mass was EC, and 4) the stoichiometry of extractable fraction of the diesel particle emissions was $C_nH_{1.70}N_{0.05n}$. • The mass absorption efficiency of particulate emissions was estimated at 6.0 ± 1.0 m^2/g for diesel vehicles and at 6 ± 24 m^2/g for spark-ignition vehicles. • The measurement of mass fraction of EC in particulate emissions allowed the calculation of the mass absorption efficiency of EC, and it was determined to average 10.9 ± 1.8 m^2/g at 500 nm. • In terms of light extinction per km driven, diesel particle emissions were at least 1 order of magnitude more important than those of spark-ignition vehicles.

Table 2. (Continued)

Study/Period/Location/Type	Sampling and Analytical Method	Summary of Major Findings
Ford Motor Company Dynamometer Study (Japar et al, 1984) • Vehicles tested: A 1979 2.3 L Opal and a 1980 2.3 L Peugeot were tested. Both of them used diesel engines. • Driving cycle tested: Over a series of cruises between 20 mph and 60 mph, as well as over a portion of the Federal test procedure (FTP) driving cycle including cold start, hot stabilized, and hot start phases. • Type: Diesel emission fine PM.	• Samples were collected on Teflon-membrane and glass-fiber filters. Total particulate mass was determined by weighing Teflon filter. • The organic-soluble fraction of the particulate emission was determined by 20 hr Soxhlet extractions of Teflon filter samples in 1:1 (v/v) mixtures of toluene/1-propanol. • The quartz-fiber filters were analyzed for OC, EC, and TC by the OGI_TOR protocol (Johnson et al., 1981).	• The non-extractable mass can be assumed an upper limit to EC. The average ratio of EC to unextractable mass was 1.03 ± 0.06 for all filters. The regression gave a slope of 1.05 ± 0.04 when three outliers were excluded. • Outliers were attributed to dust components (Al, Si, Ca, Fe, S) in the non-extractable mass. • The ratio of OC to extractable mass was 0.7 ± 0.05. The regression gave a slope of 0.75. • The fraction of solvent extractable mass in total emission mass varied strongly (23 – 63%) with the vehicle operating conditions.
Ford Photoacoustic Spectroscopy Validation (Adams et al., 1989) • Period: 9/29/1986 – 11/10/1986. • Location: in a mobile office trailer located adjacent to Ford Motor Company's Scientific Research Laboratory in Dearborn, MI. • Type: Rural ambient PM_5.	• A high-volume sampler equipped with a 5 µm pre-separator was used to collect particles on quartz-fiber filters (5 – 6 hr duration), followed by TOT analysis. Samples were extracted overnight in a 50/50 (v/v) mixture of n-propanol and toluene. Thermal analysis included 250, 385, 580, and 680 °C in He and 600 and 750 °C in $2\%O_2$/98%He. The OC/EC split was determined by transmittance. • Photoacoustic instrument (Ford Motor Company) operated at 514.5 nm (30 sec average).	• A mass absorption efficiency (10 m^2/g) was applied to obtain BC concentrations. Agreement between photoacoustic BC and thermal/optical EC were excellent (r = 0.926, slope = 1.10 ± 0.13, intercept = -0.1 ± 0.22 $\mu g/m^3$). • The photoacoustic instrument showed a detection limit ~ 0.3 $\mu gC/m^3$ (5 – 6 hr average). The instrument signal was sensitive to temperature and humidity, so frequent calibration was necessary as the ambient conditions changed. No influence from atmospheric light scattering species was observed.
Southern California Air Quality Study I (SCAQS) (Adams et al., 1990) • Period: 6/19, 6/24-25, 7/13-15, 8/27-29, 9/2-3 in 1987 (ozone or PM_{10} episode days). • Location: at Claremont, CA. • Type: Suburban ambient $PM_{2.5}$.	• A high-volume sampler equipped with a 5 µm pre-separator was used to collect particles on quartz-fiber filters (5 – 6 hr average) for OC, EC, and TC by TOT protocol. Samples were extracted overnight in a 50/50 (v/v) mixture of n-propanol and toluene. The thermal analysis included 250, 385, 580, and 680°C in He and 600 and 750°C in $2\%O_2$/98%He. The split of OC and EC was determined by transmittance. • Photoacoustic instrument (Ford Motor Company) operated at 514.5 nm (30 sec average).	• Correlation was good for the optical absorption measured photoacoustically with EC concentration determined by extraction/thermal analysis (r = 0.945). The EC mass absorption efficiency was estimated at 10.06 ± 0.56 m^2/g at 514.5 nm. • The correlation between photoacoustic measurements and the thermal technique (no extraction) yielded greater uncertainty (10%). • This study confirmed that EC is the dominant source of aerosol optical absorption in the visible region.

Table 2. (Continued)

Study/Period/Location/Type	Sampling and Analytical Method	Summary of Major Findings
Southern California Air Quality Study II (SCAQS) (Turpin et al., 1990) • Period: 6/19, 6/24-25, 7/13-15, 8/27-29, 9/2-3 in 1987 (ozone or PM_{10} episode days). • Location: at Claremont, CA. • Type: Suburban ambient $PM_{2.5}$.	• OGI dual-filter/time-resolved thermal-optical carbon analyzer (80-min average followed by 40-min analysis). OC was evolved at 650 °C in a pure He atmosphere and EC was evolved at 750 °C in a 98%He/2%O_2 atmosphere. • Photoacoustic instrument (Ford Motor Company, 30 s average) operated at 514.5 nm.	• The comparison over the concurrent sampling periods indicated good agreements between OGI_EC and Ford absorption (b_{abs}). • When converting b_{abs} to BC concentration using an absorption efficiency of 10 m^2/g, the two methods yielded a correlation coefficient of 0.905. The ratio of the mean Ford BC value to the mean OGI_EC value was 1.01, and a two-sided t-test showed no significant difference between Ford and OGI values at the 95% confidence level.
Carbonaceous Species Methods Comparison Study I (CSMCS) (Cadle and Mulawa, 1990; Countess, 1990; Hering et al., 1990; Lawson and Hering, 1990) • Period: 9 days from 8/12/1986 to 8/20/1986. • Location: at Citrus College in Glendora, CA, located in the north-eastern portion of the Los Angeles Basin. • Type: Urban ambient fine PM ($PM_{1.9}$ to $PM_{2.8}$, varied between groups).	• Ambient samples (4 – 12 hr average) were collected and analyzed for OC, EC, and TC by: – OGI_TOR protocol (Johnson et al., 1981) with backup-filter correction. – Two-step (He and He/O_2) thermal evolution methods without optical charring correction: by U.S. EPA, Environmental Monitoring and Service, Inc. (EMSI), and GMR. – Optical absorption measurement for EC plus one-step combustion for TC by Air Industrial Hygiene Laboratory (AIHL). – Samples were analyzed for EC by oxidation in He over an MnO_2 catalyst (Thermal Manganese Dioxide Oxidation [TMO] method, 525 °C for OC and 850 °C for EC) (Fung, 1990). – Forward alpha scattering technique (FAST, Cahill et al., 1984) for TC by the University of California at Davis. This is a nuclear technique which does not distinguish between OC and EC.	• Consistently higher OC concentrations were reported by the AIHL undenuded quartz-fiber filter and the AeroVironment (AV; Monrovia, CA) denuded quartz-fiber filter. Lower OC was reported by the adsorption corrected quartz-fiber filter by OGI. The lowest OC were from University of Minnesota (UM) and GMR, both of which used impactors to collect particles. • The differences in OC were mostly attributed to sampling methods rather than to analytical methods, but much of the difference in EC was attributed to analytical methods. • The TC on Teflon-fiber filters determined by UCD FAST was consistently below (~ 64%) the mean of all other methods. • The adsorption of gaseous vapors onto quartz-fiber filters was a significant sampling artifact. For systems employing tandem filters, the TC found on the backup filters was 14% to 53% of the five-sampler mean for TC.

Table 2. (Continued)

Study/Period/Location/Type	Sampling and Analytical Method	Summary of Major Findings
Carbonaceous Species Methods Comparison Study II (CSMCS) (Countess, 1990; Lawson and Hering, 1990) • Period: 10 days in August, 1986. • Location: suburban Los Angeles, CA. • Type: Reference samples including suburban/urban ambient aerosol, gasoline/diesel source samples, wood smoke samples, a pure secondary organic carbon sample (generated from the photolysis of trimethylbenzene), and a blank (PM_{10} or less).	• Quartz-fiber samples were analyzed for OC, EC, and TC by: – IMPROVE_TOR protocol. – OGI_TOR protocol. – Sunset_TOT method (top temperature 700°C for OC). – Two-Step thermal methods: Global Geochemistry Corporation (GGC), U.S. EPA, EMSI, GMR, and Oregon Department of Environmental Quality (DEQ). – Pure oxygen/continuous ramping. – Optical absorption measurement plus one-step combustion (AIHL). – The samples were analyzed for EC by oxidation in He over an MnO_2 catalyst by TMO method (525 °C for OC and 850 °C for EC).	• All laboratories agreed well on TC analyses, with a pooled coefficient of variation for all reference samples of 9%. • The coefficient of variation for OC and EC were 25.8% and 52.3%, respectively. • The range of EC/TC ratios for the ambient PM_{10} samples varied by a factor of three from a low of 0.1 (from U.S. EPA) to a high of 0.3 (from GGC) with a mean of 0.22. • Overall, U.S. EPA had the lowest average EC/TC ratio while the IMPROVE_TOR had the highest EC/TC ratio of 0.5. U.S. EPA's EC values might be low due to their methodology of switching carrier gases during operation (O_2 contamination). • Three of the four laboratories (except Sunset_TOT) that attempted to correct for charring gave higher EC values than those without charring corrections.
Carbonaceous Species Methods Comparison Study III (CSMCS) (Hansen and McMurry, 1990; McMurry and Hansen, 1990) • Period: 10 days in August 1986. • Location: suburban Los Angeles, CA. • Type: suburban ambient aerosol ($PM_{2.5}$).	• Five-stage (2.5, 1.0, 0.6, 0.23, and 0.1 μm) impactors with aluminum foil substrates with quartz-fiber backup filter (University of Minnesota) (12-hr). • One-stage (0.1 μm) impactor with aluminum foil substrates with quartz-fiber backup filter (University of Minnesota) (12 hr). • Samples were analyzed for EC by oxidation in He over an MnO_2 catalyst by TMO method (525°C for OC and 850 °C for EC). • Aethalometer (University of California at Berkeley) (1 min).	• The aethalometer was calibrated against a chemical determination of EC by solvent extraction pretreatment followed by thermal evolved gas analysis (Gundel et al., 1984). • The results of the intercomparison yielded a slope (EC/BC) of 1.02 ± 0.04 and a correlation coefficient of $r^2 = 0.973$, within the limits of accuracy of actual determinations.

Table 2. (Continued)

Study/Period/Location/Type	Sampling and Analytical Method	Summary of Major Findings
Carbonaceous Species Methods Comparison Study IV (CSMCS) (Hansen and Novakov, 1990) • Period: 9 days from 8/12/1986 to 8/20/1986. • Location: at Citrus College in Glendora, CA, located in the northeastern portion of the Los Angeles Basin. • Type: Urban ambient total suspended particulate matter.	• Aethalometer (632 nm, minutely resolution) (6 hr) • IPM was used to calibrate the aethalometer.	• The 6-hr average BC concentration ranged from 1.1 to 6.5 $\mu g/m^3$, with the highest concentration for each day usually shown by the filter collected during period 0800-1400 Pacific Daylight Time (PDT). • Examination of minute-by-minute data showed definite events in which individual vehicles in an adjacent property emitted plumes contributing up to 5 $\mu g/m^3$. • The aethalometer filters were subsequently analyzed in the laboratory for BC by an IPM that had been calibrated against the solvent extraction/quantitative thermal analysis of EC. The comparison of these analyses confirmed the calibration of the aethalometer.
DLR Research Center Aethalometer Intercomparison Study (Ruoss et al., 1992) • Period: Winter 1990-1991. • Location: The field station of the Meteorological Institute at Garching, located about 20 km north of Munich, Germany. • Type: Artificial black (graphite) and white (salt) samples and ambient fine aerosols.	• Using DLR and Magee aethalometers (Magee Scientific Inc.), white light was emitted from a source on the downstream side of the filter. Light passing through the filter was detected by four photodiodes, two of them sensitive in the green range (550 nm) and two in the infrared range (950 nm). Two photodiodes measured the reference signals, and the other two detected the measuring signals.	• The response of the DLR aethalometer was critical to the ratio of the mass of absorbing and non-absorbing materials as compared with an optical absorption technique (Hänel, 1987; 1988). • During the field experiments, the measured soot concentration differed by ~ 50% on average between the DLR aethalometer and the Magee aethalometer. The results of the Magee aethalometer agreed with the absorption technique (Hänel, 1987; 1988) very well.

Table 2. (Continued)

Study/Period/Location/Type	Sampling and Analytical Method	Summary of Major Findings
Comparison of Filter Absorption and Transmissometer Methods (Horvath, 1993) • Samples: Pure carbon particles and transparent salt particles. • Type: Artificial black, white, and mixture fine aerosols (D_p < 0.05 μm).	• An aerosol consisting of pure carbon was produced by a spark discharge between carbon electrodes in an inert atmosphere. This aerosol was mixed with an aerosol consisting of particles produced by spraying a sugar solution from a constant output atomizer. Particles were collected by a cascade impactor. • Long-path transmissometers were used to measure extinction by pure carbon and sugar aerosols separately. • IPM for measuring absorption of particle deposit on Nuclepore filter.	• For pure carbon aerosol, when transmission of Nuclepore filter was between 0.4 and 0.95 (the filter has light- to medium-gray appearance), the light absorption coefficient measured with IPM was on the average 22% higher than the transmissometric measurements, assuming scattering is negligible. Agreements were obtained for transmission < 0.2. • Transparent particle deposit produced limited changes in IPM, but the change became significant if the sugar particle was replaced by latex particles. This is due to a stronger backscattering. • On a filter which already had carbon particles, an additional deposition of transparent particles onto it always decreased its transmission. Depositing sugar particles that had a scattering coefficient amounting to 50% of the absorption of the carbon particles caused a change in IPM of 14% on average.
German Intercomparison Study I (Petzold and Niessner, 1995a) • Locations: Long-term field studies were located at two sites of different pollution levels in Munich and Berlin, Germany, respectively. Additional short-term studies were conducted at two rural sites. • Type: Urban and rural PM_{10}.	• OC, EC, and TC were determined by the German VDI solvent extraction/thermal oxidation protocol. Volatile organic components were gasified in nitrogen (N_2) atmosphere at 500 °C. This method determined non-extractable carbon (NEC: only solvent extraction), non-volatilizable carbon (NVC: only thermal desorption), and apparent EC (AEC: thermal desorption and solvent extraction). • Aethalometer (AE-9, Magee Scientific) operated at 880 nm. • Black smoke method (Christolis et al., 1992). • Photoelectric aerosol sensor (PAS) (Niessner and Wilbring, 1989).	• The method yielded AEC fractions of TC from 9% to 30% at rural sites and from 18% to 53% at urban sites. The NEC fraction of TC was 68–78%. The EC-overestimation by removing OC only with solvent extraction was 35–135%. • Aethalometer BC showed a good correlation to AEC at all sites ($r = 0.81 - 0.97$) with AEC varying from < 2 μg/m^3 to > 10 μg/m^3. The regression slopes showed strong site dependence, indicating a variation of mass absorption efficiency of EC. • The black smoke method correlated well with NEC and AEC, but it was not possible to detect a mass concentration of < 5 μg/m^3. • The PAS was found to be much more sensitive to fresh soot than aged ambient EC.

Table 2. (Continued)

Study/Period/Location/Type	Sampling and Analytical Method	Summary of Major Findings
German Intercomparison Study II (Petzold and Niessner, 1995b) • Period: 4/1992 – 4/1993. • Location: Two long-term field studies were located in Munich (Site 1: 4/1992 - 10/1992; Site 2: 11/1992 - 4/1993). Site 1 was in a residential district without industrial plants. Site 2 was at a traffic-impacted street crossing with a traffic volume of > 100,000 vehicles per day. Additional short-term studies were conducted at two rural sites. • Type: Urban and suburban ambient PM_{10}.	• A tandem filter design was used in this study. Sampling started at 7 a.m. daily (24 hr). • OC, EC, and TC were determined by the German VDI solvent extraction/thermal oxidation protocol. Volatile organic components were gasified in N_2 atmosphere at 500 °C. This method determined NEC, NVC, and AEC. • Aethalometer (AE-9, Magee Scientific) operated at 880 nm. • Smoke shade method (Christolis et al., 1992). • PAS, which makes use of photoelectron emission from particles when irradiated with UV light.	• The method yielded AEC fraction of TC between 40% and 50% and NEC fraction of TC between 75% and 78%. • Aethalometer BC and NEC yielded site-dependent mass absorption efficiencies (Site 1: 8.4 m^2/g; Site 2: 13.7 m^2/g) with respect to non-extractable carbon. • For the smoke shade method based on reflectometer, a detection limit of 4.2 $\mu g/m^3$ with respect to EC was determined. Reliable NEC determination was not possible for NEC < 5 $\mu g/m^3$. • The PAS showed complex dependences in its response to a given soot concentration on the age of aerosol. Hence, the PAS was found not to be a useful stand-alone technique for soot monitoring. But in combination with an EC measurement, the ratio of PAS signal to EC might allow an estimate of mobile source contribution to particulate carbon.
Intercomparison of Black Carbon Measurement (Hitzenberger et al., 1996; 1999) • Sample: Resuspended carbon black samples and ambient samples from a rural site (Bondville, IL). • Type: Artificial BC standards and rural ambient $PM_{2.5}$ far away from source regions.	• The test aerosol was generated by nebulizing a suspension of carbon black (Elftex 124, Cabot Corp.) in a mixture of 80% ultrapure water and 20% analytic grade isopropanol and sampled by quartz-fiber and polycarbonate filters. Ambient samples acquired by micro-orifice uniform deposit impactor (MOUDI) and dichotomous samplers. • BC standards were analyzed by the pure O_2/2-step protocol (Cachier et al., 1989a, 1989b); ambient samples by the NIOSH 5040 protocol. • Integrating Sphere (IS) method (Hitzenberger et al., 1996). • Aethalometer (Magee Scientific) operated at 880 nm.	• b_{abs} measured through aethalometer and IS agreed well (r = 0.943; slope = 0.998; intercept = 0.001 m^{-1}). • For standards, the BC mass concentrations determined by aethalometer were only 30% of those from IS. When compared to the thermal method, the IS overestimated BC by 21%. The absorption efficiency (19 m^2/g) for the aethalometer might be too high. • For ambient samples, BC determined by thermal/optical method and IS agreed within 5% of the 1:1 slope. • For ambient samples, a calibration factor of 6.8 m^2/g yielded a slope of aethalometer vs. thermal/optical results of 0.99, very close to the expected 1:1 line, but there was a considerable offset.

Table 2. (Continued)

Study/Period/Location/Type	Sampling and Analytical Method	Summary of Major Findings
IMPROVE Network EC/Absorption Comparison (Huffman, 1996) • Period: 1988 – 1993. • Locations: Several rural sites (Pinnacles National Monument, CA; Bandelier National Monument, NM, etc.) • Type: Rural ambient $PM_{2.5}$.	• Quartz-fiber filters were analyzed for OC, EC, and TC using the IMPROVE_TOR protocol. • Teflon-fiber filters were analyzed by laser IPM (LIPM) for b_{abs} at the University of California at Davis.	• The ratio of b_{abs} to EC measured by IMPROVE_TOR consistently indicates an absorption efficiency that was twice the accepted value of 10 m^2/g. Correlations between b_{abs} and TOR carbon fractions strongly suggest that the discrepancy was due to an underestimate of light-absorbing carbon rather than an overestimation of b_{abs} or due to a real, higher value of the absorption efficiency. • The potential errors in the current interpretation of TOR analysis included: 1) The pyrolysis correction based on optical reflectance monitoring; and 2) the carbon evolving between 450 and 550 °C in a pure He atmosphere, which was well-correlated with b_{abs} and appeared to be light absorbing as EC.
Measurement of Haze and Visual Effects (MOHAVE) (Turpin et al., 1997) • Period: 7/15/1992 – 8/30/1992. • Location: at Meadview, AZ, located 905 m above sea level on the western edge of Grand Canyon National Park, 95 km east of Las Vegas, NV, and 120 km northeast of the MOHAVE coal-fire power plant. • Type: Desert ambient $PM_{2.5}$.	• Size-resolved PM was measured with MOUDIs by the University of Minnesota from 0700 to 1900 Pacific Standard Time (PST) using aluminum foil substrates and then analyzed by TMO method, in which samples were heated in He over an MnO_2 catalyst (525°C for OC and 850 °C for EC). • $PM_{2.5}$ samples were collected by a standard IMPROVE four-module sampler and then analyzed by the IMPROVE TOR protocol.	• Average MOUDI TC concentrations were 88% greater than IMPROVE TC, with 95% confidence limits, and the data were uncorrelated (n = 22). • OC on backup quartz-fiber filter was 50 ± 20% of the front filter loading. Subtracting the backup filter OC averaged over all sites caused Meadview OC concentrations to be underestimated by 60% on average. • The TMO reported an EC mass fraction of < 10% in TC while the IMPROVE_TOR reported an EC mass fraction of ~ 17% in TC.
Southwestern Pennsylvania Air Pollution Health Effect Study (Allen et al., 1999) • Period: Summer 1990, 11 weeks. • Location: at a school 2 km north of the center of Uniontown, PA, in a residential area. Uniontown is located in Fayette County, 60 km south-southwest of Pittsburgh, PA, and 90 km east of the Ohio River. • Type: Rural ambient $PM_{2.5}$.	• Samples for OC and EC were collected (3 hr) using a parallel plate denuder/filter pack system. Quartz-fiber filters were analyzed by IMPROVE_TOR protocol. • Aethalometer (AE-9, Magee Scientific Inc.) operated at 880 nm. • Coefficient of Haze (COH; RAC 5000) operated at 400 nm.	• Ten-min average aethalometer BC data were averaged into 3-hr values to match the 63 OC and EC samples. The two methods were found to be highly correlated ($r^2 = 0.925$). The regression equation is BC = (0.95 ± 0.4) EC – (0.2 ± 0.4). The range of EC was 0.6 – 9.4 $\mu g/m^3$. • Collocated COH and aethalometer measurements were conducted in Philadelphia, PA, and showed comparable results. There was a linear relationship between the two measurements ($r^2 = 0.98$ with p-value < 0.001).

Table 2. (Continued)

Study/Period/Location/Type	Sampling and Analytical Method	Summary of Major Findings
NIOSH Interlaboratory Comparison Study (Birch, 1998) • Location: Source dominated samples were collected from four sites: at a construction site (where diesel-powered compressors were used) near downtown; at a diesel truck loading dock; in the bay of a fire engine house; and from wood smoke. Cigarette smoke was collected in the laboratory. • Type: Various combustion source samples.	• Quartz-fiber filter samples were analyzed for OC, EC, and TC by: – NIOSH 5040_TOT protocols. – TOR (similar to IMPROVE_TOR but the residence times were estimates based on scale shown in thermograms). – C1: 800°C, 10 min in N_2 for OC; 800°C, 7 min in O_2 for EC. – C2A: 200°C (2 min), 400°C (4 min), and 560°C (6 min) in N_2 for OC; 800°C (4.5 min) and 1200°C (2 min) in O_2 for EC. – C2B, C3, C4: 200°C (2 min), 400°C (2 min), and 550°C (4 min) in N_2 for OC; 800°C (4.5 min) in O_2 for EC. – C1-C4 detect carbon using coulometric methods.	• Good agreement (relative standard deviation [RSD] < 15%) between the TC results were reported by all laboratories. Reasonable within-method agreement was found for EC results. • For EC, all coulometric method results were positively biased relative to thermal/optical results. About 52% and 70% of the carbon found in sucrose and EDTA solutions, respectively, was quantified as EC by coulometric methods, while thermal/optical methods found < 3% of EC for these standards. • The NIOSH 5040_TOT method reported only 2% of EC in cigarette smoke, while the coulometric method reported an average EC fraction of 40% in cigarette smoke. • The coulometric method without charring correction overestimated EC due to inadequate removal of OC in the first part of the analysis.
Northern Front Range Air Quality Study (NFRAQS) (Moosmüller et al., 1998) • Period: 12/17/1996 – 1/9/1997 • Location: at Brighton, CO, located in a semi-rural environment about 30 km northeast of downtown Denver. • Type: Suburban ambient $PM_{2.5}$.	• Particles were acquired for 6- or 12-hr periods on: 1) quartz-fiber filters for OC, EC, and TC by the IMPROVE_TOR protocol; and 2) Teflon-membrane filters followed by light-transmission analysis (filter b_{abs}) using a Tobias TBX-10 Densitometer. • Aethalometer (AE-10IM, Magee Scientific) (10-min average). • Photoacoustic instrument (532 nm and 685 nm) (10-min average).	• The aethalometer BC was well correlated with photoacoustic b_{abs} ($r^2 = 0.87 – 0.92$). The comparison resulted in an absorption efficiency for BC of ~ 5 m^2/g at 685 nm and ~ 10 m^2/g at 532 nm. • The TOR EC also showed a good correlation with photoacoustic b_{abs} ($r^2 = 0.85$). Large variations occurred when the EC concentration was low. The comparison resulted in a absorption efficiency for EC of ~ 3.6 m^2/g • The correlation of photoacoustic b_{abs} and filter b_{abs} was fair ($r^2 = 0.74$). A correction method (Horvath, 1997) may be used to improve agreement.

Table 2. (Continued)

Study/Period/Location/Type	Sampling and Analytical Method	Summary of Major Findings
Smoke, Clouds, and Radiation-Brazil (SCAR-B) Experiment (Reid et al., 1998; Martins et al., 1998) • Period: 8/17/1995 – 9/20/1995. • Location: Samples were obtained from *in-situ* instrumentation or filters collected aboard the University of Washington Convair C-131A research aircraft flying over mountainous and Amazon forest regions of Brazil. • Type: Aloft fine aerosol dominated by smoke from biomass burning.	• Optical extinction cell (OEC), which is a 6.4 m long transmissometer operated at 538 nm. • IPM (Radiance Research), operated at 550 nm. • PSAP (Radiance Research) at 550 nm (1-min average) • Optical reflectance (OR) (Diffusion Systems), operated in a broadband visible mode to determine the absorption coefficient. • Pure O_2/2-Step thermal evolution (TE) method (Cachier et al., 1989a, 1989b). • Remote sensing (RS) techniques acquired measurements from satellite or Sun photometer combined with irradiance data to obtain estimates of the columnar-averaged, single-scattering albedo using SPCTRAL2 (Bird and Riordan, 1986) radiative transfer model.	• The IPM and OR methods produced data that scatter around 1:1 line; the mean residuals for IPM and OR were –3% and –0.5%, respectively. The uncertainties in IPM and OR methods were estimated at 40% and 17%, respectively. • There was a variance of 45% between the PSAP and the OR techniques. The uncertainty in PSAP was estimated ~±40%. This translated into uncertainties of ±0.05 in single scattering albedo for 1-min samples. • Combining of the scattering measurements from nephelometer, the OEC produced single scattering albedo for smoke particles that varied from 0.35 – 0.9. • The TE method produced data lying well below the 1:1 line with OEC ($r = 0.45$); the mean residual for TE was –49% relative to OEC, indicating systematic errors. The uncertainty of TE was estimated at 31%. BC in biomass burning aerosol was poorly correlated with b_{abs}. This might lead to biases in BC absorption efficiency estimates. • SPCTRAL2 model yielded single-scattering albedos slightly higher (by 0.01) than the columnar-averaged values derived from *in-situ* optical measurements on the aircraft.
Free Troposphere Research Station Jungfraujoch (Lavanchy et al., 1999) • Period: 7/1995 – 6/1997. • Location: at the Jungfraujoch high-alpine research station in Switzerland (3454 m above surface level). • Type: Free troposphere fine PM.	• Filter samples were analyzed by the Switzerland pure O_2/2-Step (340 and 650°C) TE protocol with flash heating. • Aethalometer (AE-10, Magee Scientific Inc.), operated at 880 nm (19 – 360 hr sampling duration). • PM_{10} samples were acquired from a roadside location in Brene with heavy traffic and from a suburban site at Dübendorf. • Standards for OC were obtained by dissolution of starch, tri-sodium citrate 2-hydrate, glucose, and humic acid in pure water, and by pipetting a known volume of these standards onto quartz-fiber filters. EC standards were acquired by using flame soot 101 (Degussa) ultra-sonically suspended in pure water.	• The recovery of model organic compounds glucose and starch as OC was ~ 100% while charring was negligible. The recovery of humic acid as OC was 84% on average and artifact formation of EC due to charring was found to be 14%. • The correlation of the EC from TE method and BC from aethalometer was high ($r^2 = 0.91$), exhibiting an average absorption efficiency of 9.3 ± 0.4 m^2/g. • Results confirmed that the aethalometer underestimates the true BC at remote sites when the manufacturer's calibration is used. • No significant seasonal cycle in absorption efficiency was found. Shorter term variability (days to weeks) was attributed to: 1) the EC/TC composition, and 2) a combination of the aethalometer filter temporal resolution and the fraction of air mass sampled.

Table 2. (Continued)

Study/Period/Location/Type	Sampling and Analytical Method	Summary of Major Findings
Harvard/EPRI Intercomparison Study (Babich et al., 2000) • Periods and Locations: – Riverside CA, 8/15/1997–9/20/1997 – Boston, MA, 9/10/1997–9/30/1997 – Chicago, IL, 10/10/1997–11/15/1997 – Dallas, TX, 12/5/1997–1/20/1998 – Phoenix, AZ, 12/10/1997–1/25/1998 – Bakersfield, CA, 2/10/1998–3/25/1998 – Philadelphia, PA, 8/1/1998–9/1/1998 – Bakersfield, CA, 1/8/1999–1/29/1999 • 2. Type: Urban ambient $PM_{2.5}$.	• Particles were collected on quartz-fiber filters (24-hr average) for OC, EC, and TC by the IMPROVE_TOR protocol. • Aethalometer (AE-16U, Magee Scientific) at all cities except for Boston (5-min average). • Dual channel aethalometer (AE-20UV, Magee Scientific) operated at 325 nm and 880 nm (5-min average).	• For six cities combined, the EC measured by TOR and BC measured by aethalometer (880 nm) were highly correlated (r^2 = 0.94; 187 24-hr samples), but the BC values were consistently ~ 24% less than the EC across all six cities, using the aethalometer manufacturer's absorption efficiency (19.2 m^2/g). • The ratios of BC and EC ranged from 0.62 to 0.81. The lowest ratio was obtained in Dallas, which had the smallest dynamic range of EC concentrations and minimum influence on the overall regression.
Kyoto Intercomparison (Japan) (Tohno and Hitzenberger, 2000) • Location: at Kyoto University, Uji campus, Kyoto, Japan. • Type: Urban ambient $PM_{2.5}$.	• R&P 5400 ambient carbon particulate monitor (ACPM) (0.14 - 2.5 μm) (1-hr average) • IS method (Hitzenberger et al., 1996). Atmospheric particles were collected on Nuclepore filters (3-hr average) downstream of a size-selective Anderson impactor. The exposed filters were dissolved in chloroform, then acetone, to produce liquid suspensions of the collected particles, and the blackness of the suspensions was determined in terms of BC content using the calibration curve of IS.	• Poor agreement was found for EC from ACPM and BC from IS. • BC mass fraction for particles less than 0.14 μm in diameter ranged from 0.5 to 0.7 in the measurements. Excluding particles below 0.14 μm from IS, the agreement between IS BC and ACPM EC improved. It was found that ACPM underestimated the real BC concentration without corrections.

Table 2. (Continued)

Study/Period/Location/Type	Sampling and Analytical Method	Summary of Major Findings
Comparison of IMPROVE and NIOSH temperature protocols for OC and EC (Chow et al., 2001) • Period: Samples were acquired from a variety of sampling sites during 1997 – 1998. These included 41 ambient samples and 19 source samples. • Location: in CA; NV; CO; DC; VA; NC; TX; and Mexico. • Type: Urban (commercial, residential, and industrial), suburban agriculture, and rural ambient $PM_{2.5}$; resuspended dry lake soil and road dust; motor vehicle exhaust and chicken rotisserie cooking emissions.	• Pallflex quartz-fiber filter samples were analyzed for OC, EC, and TC by: – IMPROVE_TOR protocol. – NIOSH 5040_TOT protocol.	• The IMPROVE and NIOSH thermal evolution protocols were equivalent for TC sampled on quartz-fiber filters. • NIOSH_TOT EC was typically less than half of IMPROVE_TOR EC. The primary difference was the allocation of carbon evolving at the NIOSH high (850°C) temperature in He atmosphere to the OC rather than EC fraction. When this portion of NIOSH OC was added to NIOSH_TOT EC, the IMPROVE and NIOSH analyses were in good agreement. • The pyrolysis adjustment to the EC fraction was always higher for transmittance than reflectance regardless of the protocols used. The difference was most pronounced for very dark samples on which neither reflectance nor transmittance was able to accurately detect further blackening due to pyrolysis.
Vehicle Emissions Research Laboratory (VERL) Dynamometer Study (Moosmüller et al, 2001b) • Vehicles tested: 1996 Dodge Ram 2500 (29509 km), and 1999 Ford F250 SD (32401 km). • Driving cycle tested: Typical FTP driving cycle including cold start, hot stabilized, and hot start phases. • Type: Diesel emission $PM_{2.5}$.	• Time-integrated emissions were acquired on quartz-fiber filters followed by IMPROVE_TOR protocol for OC and EC analysis (1 – 10 min average). • TEOM (R&P 1105) (1-sec average). • Nephelometer (TSI DustTrak 8520) (1-sec average). • Aethalometer (Anderson RTAA-800) (1-sec average). • Photoacoustic Instrument (532 nm) (1-sec average). • Smoke Meter (DRI SM) (633 nm) (1-sec average).	• Aethalometer, photoacoustic, and smoke meter showed the best correlations with the IMPROVE_TOR EC (r^2 = 0.92, 0.92, and 0.91, respectively). The aethalometer overestimated TOR EC by ~ 40%. Photoacoustic estimated an EC absorption efficiency of ~ 8.5 m^2/g. • TEOM and nephelometer had better correlations with TC (r^2 = 0.92 and 0.84, respectively). • OC can be reasonably estimated by the difference between TEOM/nephelometer total mass measurements and EC can be estimated from aethalometer, photoacoustic, or smoke meter.

Table 2. (Continued)

Study/Period/Location/Type	Sampling and Analytical Method	Summary of Major Findings
Carbon Conference International Aerosol Carbon Round-Robin Test (Schmid et al., 2001) • Period: 11/7,8,10/1998 for 24-hr average sampling. • Location: Frankfurter Allee Street in the city of Berlin, Germany. The traffic volume is approximately 58,000 cars per day with a proportion of trucks of ~ 5%. • Type: Urban/traffic ambient PM_{10}.	• Particles were collected by a high-volume sampler (Digitel DHA80) with a PM_{10} inlet and analyzed for OC, EC (or BC), and TC by various thermal protocols: – German VDI 2465 part 1 (solvent extraction, coulometry). – German VDI 2465 part 2 (thermal). – France CNRS-CEA two-step flash heating. – Thermal linear temperature method (20°C/min) in pure O_2. – TOT methods (various temperature programs). – IMPROVE_TOR protocol. – Shimadzu TOC 5000. – Elemental Analyzer CE 440; BC: optical transmissometry. – Modified IS method transmission mode.	• A good agreement was shown for the analysis of TC by all laboratories (7 and 9% interlaboratory RSD). • For EC, the within-laboratory RSD was ~5% and the interlaboratory RSD was 37% for the low load and 46% for the high load samples. • Thermal/optical methods obtained, on average, lower EC values than laboratories using only thermal methods, likely due to the charring correction. However, a relatively high RSD was found for the highest loaded sample with thermal/optical methods. • Agreements between thermal/optical methods (TOR/TOT) and methods that reduce charring (extraction, two-step flash method) were better. • Optical transmissometry and modified IS did not report exact BC since the sample was too dark.
Soil BC Content Measurements (Schmidt et al., 2001) • Location: The eight Australian soils investigated originated from the surface horizons of Vertisols, Mollisols, Alfisols, and Oxisols. • Type: Sieved rural soil samples (coarse particles > 2 mm).	• The sieved soil samples were analyzed for BC using various methods: – Thermal oxidation method in which OC is removed at 375 °C for 24 hours, and EC is determined by C, N-elemental analysis using mass difference. – Additional acid extraction (with or without hydrofluoric acid [HF]) before thermal oxidation to remove OC. – Chemical oxidation with HNO_3 (65%) at 170 °C for 8 hrs to remove OC. EC is determined by GC/FID using benzene carboxylic acids as markers.	• Thermal oxidation resulted in BC concentrations exhibiting only small differences (41.8 – 58.7 g BC/kg) between samples compared to the other methods. When it was combined with extraction/hydrolysis as a pretreatment, measured values of BC were lower by factors of 8 – 10. • Pure chemical oxidation methods often resulted in higher BC concentrations (37.2 – 109.0 g BC/kg soil). Differences between samples were also larger. • BC concentrations generally decreased with increasing intensity of chemical attack. • BC measured for individual samples varied over 2 orders of magnitude (up to a factor of 571).
Maryland Aerosol Research and Characterization (MARCH-Atlantic) Study (Chen et al., 2002) • Period: 7/1999 – 7/2002 • Location: at Fort Meade Army base, near the middle of the Baltimore-Washington corridor. • Type: Suburban ambient $PM_{2.5}$.	• Samples were collected on quartz-fiber filters (24 hr). Tandem quartz/quartz and Teflon/quartz filter packs were employed. The quartz-fiber filers were analyzed for OC, EC, and TC by the IMPROVE_TOR protocol. • PSAP (Radiance Research) operated at 550 nm was deployed in 1/2001 for measuring absorption coefficient. (1 min).	• The backup quartz-fiber filters behind the quartz-fiber filters reported average OC 23 ± 12% of those on the front quartz-fiber filters. The backup quartz-fiber filters behind Teflon-membrane filters reported average OC 49 ± 19% of those on the front quartz-fiber filters. • The PSAP absorption coefficient showed a strong correlation with the IMPROVE_TOR EC ($r^2 = 0.87$). This comparison produced an EC absorption efficiency of 7.1 m^2/g at 550 nm.

Table 2. (Continued)

Study/Period/Location/Type	Sampling and Analytical Method	Summary of Major Findings
NIST Reference Material Study (Currie et al., 2002) • Period: Bulk Standard Reference Material (SRM1649a) resulted from atmospheric sampling in 1976-1977. • Location: at Washington, DC, Navy Yard. • Type: Resuspended urban dust $PM_{2.5}$.	• The SRM were resuspended and sampled by quartz-fiber filters using URG filter packs and analyzed for carbon by various methods: – Aethalometer. – 375°C thermal oxidation method followed by flash/combustion/GC to determine residue EC. – Pure O_2/2-Step TE method (Cachier et al., 1989a, 1989b). – LBL pure O_2/continuous ramping. – NIOSH_TOT protocol with maximum temperatures of 900°C for both OC and EC. – IMPROVE_TOR protocol. – TOT protocol with linear temperature ramping. – Thermal kinetic oxidation/intercept method. – Thermal oxidation method with various acid pretreatments. – Pure chemical oxidation methods (no heating). – Isotope carbon (C^{14}, C^{13}) speciation for TC and EC.	• A good agreement was shown in the analysis of TC by all laboratories (<1 % variation in TC mass fraction). • The EC/TC ratios resulted from all analytical methods varied by about one order of magnitude (7% - 52%). Thermal method results cover the full range of EC/TC values, whereas results from pure chemical oxidation methods were restricted to the upper regions. • Particle loss may accompany chemical processing of very small samples. • The transmittance measurements for samples with EC > $10\mu g/cm^2$ are unreliable due to saturation. • EC/TC ratios by TOR were higher than those by TOT. • From the isotope study, about 38% of the SRM particulate carbon was derived from modern carbon. The modern carbon fraction of EC ranged from 2.8 - 11.3%. Fossil fuel combustion generally produced a higher EC/TC ratio.
Comparisons of IMPROVE_TOR and TMO Methods (Fung et al., 2002) • Location: 60 samples from the U.S. IMPROVE Network, 16 from urban South Korea, 10 from Hong Kong, and 14 synthetic BC (or soot) samples. • Type: Urban (industrial and traffic) and rural ambient $PM_{2.5}$; reference BC samples (Cabot Monarch 120).	• Quartz-fiber filter samples were analyzed for OC, EC, and TC by: – IMPROVE_TOR protocol. – TMO method.	• TMO and IMPROVE protocols provided equivalent results of OC, EC, and TC values within ± 25% for a wide variety of samples. • EC biases were not consistent among different sample sets. EC levels were: 1) consistent for synthetic soot samples (no OC), 2) higher by TMO in heavily loaded Hong Kong urban samples, and 3) higher by IMPROVE_TOR for lightly loaded IMPROVE network and urban South Korea samples. • TMO method can effectively reduce charring in pure He environment.

Table 2. (Continued)

Study/Period/Location/Type	Sampling and Analytical Method	Summary of Major Findings
Canada Black Carbon Study (Sharma et al., 2002) • Period: Different time periods from 11/1998 to 8/2000 • Locations: Six sites across Canada: Alert (remote/continental); Egbert (rural); Downsview (suburban); Evans Avenue, Toronto (urban, roadside); Winchester (urban, school yard); and Palmerston (urban, school yard). • Type: Remote, rural, suburban, and urban ambient $PM_{2.5}$.	• Ambient $PM_{2.5}$ sampler (averaging time from 12 hrs to 2 weeks). • Quartz-fiber filter samples were analyzed for OC, EC, and TC by IMPROVE_TOR, MSC1_TOT, and France CNRS-CEA 2-Step flash heating TE protocols. • Aethalometer (AE-11, Magee Scientific) (1-hr average). • PSAP (Radiance) (1-hr average).	• EC determined from MSC1_TOT and France TE protocols were similar with ~ 10% lower concentration from IMPROVE_TOR. • The aethalometer and PSAP BC agreed with each other but underestimated thermal EC by as much as 76% at all sites except for remote Alert, where all measurements agreed well. • The range of median site-specific absorption efficiency of EC for aethalometer and PSAP ranged from 6.4 - 28.3 m^2/g and from 3.2 - 11.6 m^2/g, respectively. • The highest absorption efficiency at the most remote site, Alert, was likely due to the more aged, internally mixed aerosols.
Fresno Supersite Experiment (Watson and Chow, 2002) • Time: 1/1/2000 – 12/16/2000 • Location: at the Fresno Supersite, CA (3425 North First Street), ~ 5.5 km north northeast of the downtown Fresno commercial district. • Type: Urban ambient $PM_{2.5}$.	• Single-channel RAAS-100 FRM (24-hr) • Six-channel RAAS-400 (with and without organic gas denuders) (24-hr) • Dual-channel sequential filter sampler (SFS) (24-hr) • Teflon-membrane filters were analyzed for b_{abs} using densitometer. • Quartz-fiber filter samples were analyzed for OC, EC, and TC by IMPROVE_TOR protocol. • R&P 5400 Ambient Carbon Particulate Monitor (1-hr average). • Single- and seven- wavelength aethalometer (AE-14U and AE-30S, Magee Scientific) (1-hr average). • PAS 2000 particle-bound polycyclic aromatic hydrocarbon (PAH) monitor (10-min average)	• Equivalence was found for $PM_{2.5}$ mass, b_{abs}, TC, OC, and EC among RAAS-100 FRM, RAAS-400, and SFS samplers, and for front filter TC between denuded and non-denuded channels in the RASS-400 samplers. • The average positive OC artifact was 1.62 ± 0.5 $\mu g/m^3$ for the non-denuded Teflon/quartz channel and 1.12 ± 0.91 $\mu g/m^3$ for the non-denuded quartz/quartz channel. With preceding denuders, the average negative artifact was 0.61 ± 0.5 $\mu g/m^3$, ~ 9% of the front filter OC. • R&P 5400 TC was 40%-60% higher than filter carbon. • A high correlation ($r>0.9$) was found between b_{abs} and EC. The absorption coefficient ranged from 11.4 ± 0.7 to 12.0 ± 0.7 m^2/g among FRM, RASS, and SFS. • Two aethalometer measurements showed a high correlation coefficient of 1, but an average of 0.11 $\mu g/m^3$ less BC was measured by the seven-wavelength aethalometer for the 880 nm channel. • IMPROVE_TOR EC was consistently 20–25% higher than aethalometer BC. Particle-bound PAH were correlated with BC and EC, but not sufficiently to be considered predictable.

Table 2. (Continued)

Study/Period/Location/Type	Sampling and Analytical Method	Summary of Major Findings
Big Bend Regional Aerosol and Visibility Observation Study (BRAVO) (Arnott et al., 2003) • Period: 9/17/1999 – 10/17/1999 • Location: at Big Bend National Park near the Rio Grande River in South Texas. • Type: Rural ambient $PM_{2.5}$.	• Photoacoustic instrument operated at 532 nm (1-hr average). • Aethalometer (AE-16, Magee Scientific) (1-hr average).	• The aethalometer BC was weakly correlated with photoacoustic b_{abs} ($r^2 = 0.21 – 0.45$) at low ambient absorption coefficients (<2.1 Mm^{-1}). The comparison resulted in an absorption efficiency for BC of 8.4 – 9.9 m^2/g at 532 nm. • The aethalometer BC data never went to zero, suggesting that a small fraction of its response was due to contamination by scattering aerosol.
Southern Great Plains Intensive Operating Period (Arnott et al., 2003) • Period: March and April 2000. • Location: at the Department of Energy Cloud and Radiation Testbed site in northern Oklahoma. • Type: Rural ambient $PM_{2.5}$.	• PSAP (Radiance) operated at 550 nm. • PSAP (Radiance) downstream of a humidifier operated at 550 nm. • Photoacoustic instrument downstream of a humidifier operated at 532 nm. • Humidified (i.e., 1 hr cycle for humidification) nephelometer (TSI Model 3563).	• The photoacoustic BC correlated well with the dry PSAP measurements ($r^2 = 0.96$), but the slope of the correlation was close to 1.61, meaning that PSAP might overestimate the absorption. • The photoacoustic BC showed weak dependence of light absorption on relative humidity (RH). • The humidified PSAP showed erroneously high light absorption as the RH increased.
Atlanta Supersite Experiment (Lim et al., 2003) • Period: 8/3/1999 – 9/1/1999 • Location: at the Atlanta Supersite, GA, (Jefferson Street), located in a mixed industrial-residential area ~ 4 km northwest of downtown Atlanta, GA. • Type: Urban ambient $PM_{2.5}$.	• Rutgers/OGI *in-situ* Thermal/Optical Carbon Analyzer (1-hr average every other hour). • R&P 5400 Ambient Carbon Particulate Monitor (1-hr average). • Aethalometer (Magee Scientific) (1-hr average) • PSAP (Radiance) (1-hr average) • Aerosol Dynamics Inc. (ADI) Flash Vaporization Carbon Analyzer (10-min cycle; flash temperature unknown) • MOUDI Impactor samples (12-hr average; analyzed by IMPROVE_TOR) • Integrated Filter Samples (Anderson RASS, Met One SASS, URG MASS, the FRM, R&P Speciation, BYU PC-BOSS, TVA PC-BOSS, ARA PCM, CIT PCM, and URG-VAPS) (24 hr). Filters were analyzed by IMPROVE_TOR or TOT methods.	• The "inter-sampler precisions" with which semicontinuous particulate TC, OC, and EC were measured were 7%, 13%, and 26%, expressed as pooled coefficients of variations of 2, 3, and 4 instruments, respectively. • Correlations (r^2) between pairs of OC measurements were 54 – 73% and between pairs of EC measurements were 74 - 97%. • OC and EC measured by R&P 5400 were 8% lower and 20% higher than RU/OGI OC and EC, respectively. • The best correlation for EC measurements was found between the PSAP and aethalometer ($R^2 = 0.97$), but PSAP measured only ~ 50% of aethalometer BC. • For time-integrated filter and MOUDI measurements, OC, EC, and TC had pooled coefficients of variation of 28%, 66%, and 25% (9 instruments), respectively.

Table 2. (Continued)

Study/Period/Location/Type	Sampling and Analytical Method	Summary of Major Findings
Regional Visibility Experimental Assessment in the Lower Fraser Valley (REVEAL II) (Nejedlý et al., 2003) • Period: 4/1994 – 6/1995. • Locations: Two sampling sites at the Abbotsford Airport in southern British Columbia, Canada, and near the Huntsman Marine Science Center at St. Andrews, New Brunswick, Canada. • Type: Rural ambient $PM_{2.5}$.	• Ambient particles were collected by IMPROVE samplers Module A, B, and C, with an additional IMPROVE sampler Module A. • Particles were collected on quartz-fiber filters (24 hr) in the IMPROVE sampler Module C and then analyzed for OC, EC, and TC by the IMPROVE_TOR protocol. • Particles were collected on Teflon-membrane filters in the additional Model A and then analyzed by LIPM for BC at the University of Guelph.	• A correction factor "R" for converting b_{abs} measured by LIPM to BC was empirically determined from values of absorption b_{abs}, concentration of EC, and BC mass absorption efficiency. • A polynomial fit of "R" as a function of areal concentration "s" yielded the new correction "R(s)". • The correction was retrospectively applied to the LIPM data and compared to the EC. The BC data derived from the LIPM measurements explained about 81% of the variability of the TOR EC. • The absolute value of the correction factor "R" at the two sites agreed for high filter loadings but differed by up to 50% in the case of the low filter loadings, highlighting the influences of aerosol composition.
Reno Aerosol Optics Study (Sheridan et al., 2005) Period: 6/3/2002 – 6/28/2002. Location: at Reno, Nevada. Type: Kerosene soot (largely BC), white $(NH_4)_2NO_3$ aerosols, and mixtures thereof, as well as ambient $PM_{2.5}$.	• Cavity Ring-Down (CRD) Extinction (DRI, NASA, and Portland State University [PSU] CRD). • Classic extinction cell operated at 467, 530, and 660 nm. • Integrating nephelometers operated at 530 nm. • Photoacoustic instrument operated at 532 nm. • Aethalometer operated at 880 nm. • PSAP (Radiance) operated at 565 nm. • Multi-Angle Absorption Photometer (MAAP).	• Photoacoustic absorption and absorption by the difference of extinction and scattering agreed with each other within about 10% for aerosols with scattering albedos ranging from ~ 0.3 – 1, yielding two quasi-equivalent primary standards for aerosol light absorption. • The CRD was capable of measuring atmospheric extinction down to below 1 Mm^{-1}. • Uncorrected filter-based absorption methods such as aethalometer and PSAP showed substantial systematic errors. • Filter-based methods corrected for scattering interference (e.g., MAAP) generally compared well (after empirical calibration) with primary standards such as the photoacoustic method. However, their dynamic range was limited.

[a] See Table 1 for detailed thermal/optical analysis protocols for most of the methods. Less commonly applied methods are summarized in the table to the extent that they could be interpreted from the intercomparison reports.

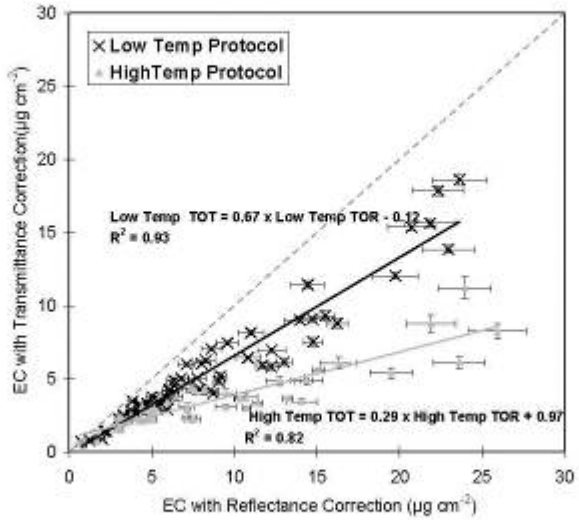

Figure 1. Comparison of EC derived from transmittance (TOT) and reflectance (TOR) charring corrections for low (IMPROVE in Table 1) and high (STN in Table 1) temperature protocols for 58 samples taken at the Fresno, California supersite from 08/23/2002 to 04/26/2003 (adapted from Chow et al., 2004). The dashed line indicates the 1:1 correspondence and the trend lines are derived from unweighted least squares fits.

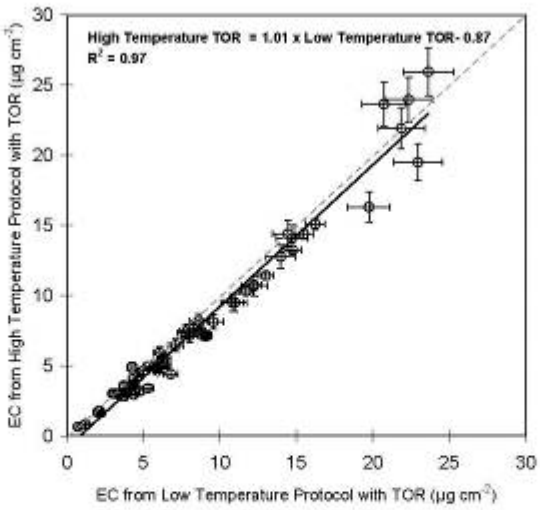

Figure 2. Comparison of Fresno supersite EC for the high and low temperature protocols with a TOR pyrolysis correction applied to both. The dashed line indicates the 1:1 correspondence (adapted from Chow et al., 2004).

Figure 1 shows how EC determined by TOT compared with EC by TOR for a high and low temperature analysis protocol. EC by TOT was lower than that by TOR in both cases, with the high temperature protocol yielding much lower EC values. Chow et al. (2004) hypothesized that much of the organic vapors adsorbed throughout the filter is desorbed at the 120 °C and 250 °C plateaus of the low temperature protocol, leaving less to char during the remainder of the analysis. The high initial temperature protocol begins analysis at 310 °C, and charring is immediately observed before volatilization is possible.

Figure 2 compares EC from the high temperature and low temperature protocols using the TOR correction. The values are in good agreement for this case. The correction is less sensitive to the temperature protocol than is the transmittance correction.

Carbonate carbon present with the OC and EC may interfere with the analysis if it decomposes during the analysis. For the high temperature protocol used in Figures 1 and 2, temperatures exceed 850 °C during the OC step, while for the low temperature protocol the temperature does not reach 800 °C until the EC step. Chow and Watson (2002) demonstrated that calcium carbonate is uncommon in many atmospheric samples and is not measured by thermal methods with temperatures <800 °C. Chow et al. (2001) showed that high temperatures (e.g., 800 °C) in the OC step may also oxidize EC via reactions with O_2-containing minerals in the sample (Fung, 1990; Fung et al., 2002).

While most air quality studies in the U.S. have measured OC and EC by thermal/optical methods, the two-temperature method of Cachier et al. (1989a, 1989b) is most widely used in global inventories and ambient studies. Owing to their widespread use, similarities and differences between the IMPROVE, STN, and CNRS-CEA protocols in Table 1 need special attention with respect to their comparability.

3. Optical Light Absorption Measurements

Also summarized in Table 2 are comparisons of thermal EC measurements with *in-situ* or filter-based optical BC measurements. A fundamental measurement of *in-situ* aerosol b_{abs} can be achieved by the photoacoustic instrument (Arnott et al., 1999; Moosmüller et al., 1997), which quantifies minute changes in the speed of sound in response to heating and cooling of PM by a modulated laser beam. It may be possible to relate EC or BC measurements to their absorption properties by collocating filter-based samplers with photoacoustic measurements.

Photoacoustic instruments have been used to measure BC in engine exhaust for more than two decades (Faxvog and Roessler, 1979; Killinger et al., 1980; Japar et al., 1982, 1984; Roessler, 1984), though it has only been recently that lasers have become adequately compact and powerful so that practical portable instruments can be fielded. The large dynamic range of the photoacoustic photometer allows it to measure b_{abs} over a wide range of BC concentrations in source and ambient samples (Moosmüller et al., 2001a, 2001b). For BC size distributions with mass median diameter < 0.3 μm, the BC mass absorption efficiency (b_{abs}/BC) is stable (Killinger et al., 1980). As explained

in the introduction, b_{abs} can be translated into a BC or EC concentration with an appropriate mass absorption efficiency. Consistent with other studies cited above, Table 2 shows that mass absorption efficiencies differ from study to study. These differences result from variability in the shape, density, material refractive index, and internal mixing of particles as well as inconsistencies in quantification EC by other methods.

A more common method of b_{abs} and BC (or EC) measurement is filter-based absorption using an aethalometer. The aethalometer measures optical aerosol absorption by quantifying the attenuation of light transmitted through a filter tape on which aerosol particles are collected (Hansen et al., 1984). Once the spot monitored on the filter tape exceeds a certain optical density, the aethalometer automatically advances the tape to a new spot. In this manner, the aethalometer can perform months of ambient monitoring without operator attention. The measured attenuation is reported as BC concentration after conversion with an empirically determined factor. The aethalometer also obtains its calibration by comparison with thermal EC measurements (Hansen et al., 1984; Hansen and Novakov, 1990). Arnott et al. (2005) suggested that a filter-loading correction is needed to account for the multiple scattering effects of filter material in the aethalometer. A 50% reduction occurs between when the filter is pristine and white after a filter change, and when it is dark right before a filter change. Time averaged aethalometer data tends to average out this variation if the source of BC is sufficiently steady. Otherwise, the aethalometer b_{abs} would not be linearly related to BC. This correction was not made in the earlier studies summarized in Table 2, and a wide range of b_{abs}/BC ratios is observed.

Similar to the aethalometer, the integrating plate method (IPM, Lin et al., 1973), measures the transmission of diffused light through a polycarbonate-membrane, Teflon-membrane, or quartz-fiber filter. Quartz-fiber filters have more internal scattering than the thin polycarbonate- or Teflon-membrane filters, and the transmittance is usually double that for a given deposit on the membrane filters. This method can be applied to 47 millimeter (mm) Teflon-membrane filters with a photographer's densitometer for filter transmission that is calibrated with photographers' neutral density filters (Wratten Kodak, Rochester, NY). Filter transmission is highly correlated with the aethalometer measurement and has been used as a surrogate for BC in several studies (e.g., Chow et al., 1997; Watson and Chow, 2002). Bond et al. (1999) note the importance of correcting for particle scattering when a mixed aerosol is sampled and measured by filter transmission as with the IPM.

4. Conclusions and Knowledge Gaps

This summary documents and compares many OC and EC measurement methods and the efforts made to determine the equivalence among them. OC and EC are operationally defined by these methods, but they are often not sufficiently documented to allow the methods to be repeated outside of the laboratory origin. In seeking to determine equivalence, samples have been prepared from organic chemicals, graphite, diesel exhaust, and wood smoke. Ambient samples have also been

circulated among laboratories or taken in parallel in a variety of environments. Measurements of particle absorption have been compared with thermal evolution and photoacoustic methods. The general conclusion is that different studies give different results for method comparisons, and that citation of a single comparison study is insufficient to establish comparability. More systematic comparisons are needed that hold most variables constant while varying only a few. These variables apply to the type of sample analyzed as well as to the analysis method.

Future comparison studies need to:

- Evaluate the sensitivity of OC and EC concentrations to variations in thermal evolution temperatures, pyrolysis corrections, analysis atmosphere compositions, presence or absence of oxidizing minerals and catalysts, vapor adsorption, and optical pyrolysis correction methods.
- Create reproducible and well characterized samples with homogeneous deposits of light, medium and heavy particle loadings that represent simple (e.g., graphite powder, organic compounds, carbon arc emission) and complex (diesel exhaust, wood smoke, mixtures with inorganic minerals and salts) situations that might be found in the environment.
- Implement the methods in Table 1 on a single instrument so that variables can be systematically changed for analysis of the prepared samples and selected ambient samples.
- Develop and apply methods to calibrate and audit temperatures, analysis atmospheres, and optical monitoring that can be applied to a variety of hardware to determine that analysis assumptions are met in practice.

Interpreting the data from comparisons that incorporate these features will provide the basis for determining why different methods give different results.

Acknowledgements

This work was jointly supported by the U.S. Environmental Protection Agency (EPA) STAR Grant No. RD-83108601-0, EPA Contract #R-82805701 for the Fresno Supersite, and California Air Resources Board Contract #04-307. The conclusions are those of the authors and do not necessarily reflect the views of the sponsoring agencies. Mention of commercially available products and supplies does not constitute an endorsement of these products and supplies. The authors wish to thank Eric Dieterle and Jo Gerrard of the Desert Research Institute for assembling and editing the manuscript.

References

Adams, K.M., Turpin, B.J. and Huntzicker, J.J. (1989), Intercomparison of photoacoustic and

thermal-optical methods for the measurement of atmospheric elemental carbon. Presentation at the 82nd Annual meeting of the Air & Waste Management Association in Anaheim, CA, Jun. 1989. Air & Waste Management Association, Pittsburgh, PA.

Adams, K.M., Davis, L.I., Jr., Japar, S.M., Finley, D.R. and Cary, R.A. (1990), Measurement of atmospheric elemental carbon: Real-time data for Los Angeles during summer 1987. *Atmos. Environ.* 24A(3):597-604.

Akhter, M.S., Chughtai, A.R. and Smith, D.M. (1984), Reactions of hexane soot with NO_2/N_2O_4. *Journal of Physical Chemistry*. 88:5334-5342.

Akhter, M.S., Chughtai, A.R. and Smith, D.M. (1985), The structure of hexane soot I. Spectroscopic studies. *Applied Spectroscopy*. 39(1):143-153.

Allen, G.A., Lawrence, J.E. and Koutrakis, P. (1999), Field validation of a semi-continuous method for aerosol balck carbon (aethalometer) and temporal patterns of summertime hourly black carbon measurements in southwestern PA. *Atmos. Environ.* 33(5):817-823.

Arnott, W.P., Moosmüller, H., Rogers, C.F., Jin, T. and Bruch, R. (1999), Photoacoustic spectrometer for measuring light absorption by aerosol: Instrument description. *Atmos. Environ.* 33(17):2845-2852.

Arnott, W.P., Moosmüller, H., Sheridan, P.J., Ogren, J.A., Raspet, R., Slaton, W.V., Hand, J.L., Kreidenweis, S.M. and Collett, J.L., Jr. (2003), Photoacoustic and filter-based ambient aerosol light absorption measurements: Instrument comparison and the role of relative humidity. *J. Geophys. Res.* 108(D1):AAC 15-1-AAC 15-11.

Arnott, W.P., Hamasha, K., Moosmuller, H., Sheridan, P.J. and Ogren, J.A. (2005). Towards aerosol light-absorption measurements with a 7-wavelength Aethalometer: Evaluation with a photoacoustic instrument and 3-wavelength nephelometer. *Aerosol Sci. Technol.* 39(1):17-29.

Babich, P., Davey, M., Allen, G. and Koutrakis, P. (2000), Method comparisons for particulate nitrate, elemental carbon, and $PM_{2.5}$ mass in seven U.S. cities. *JAWMA*. 50(7):1095-1105.

Bennett, C.A., Jr. and Patty, R.R. (1982), Monitoring particulate carbon collected on Teflon filters: An evaluation of photoacoustic and transmission techniques. *Appl. Opt.* 21(3):371-374.

Birch, M.E. (1998), Analysis of carbonaceous aerosols: Interlaboratory comparison. *Analyst*. 123 (5):851-857.

Birch, M.E. and Cary, R.A. (1996a), Elemental carbon-based method for monitoring occupational exposures to particulate diesel exhaust. *Aerosol Sci. Technol.* 25(3):221-241.

Birch, M.E. and Cary, R.A. (1996b), Elemental carbon-based method for occupational monitoring of particulate diesel exhaust: Methodology and exposure issues. *Analyst*. 121:1183-1190.

Bird, R.B. and Riordan, C. (1986), Simple solar model for direct and diffuse irradiance on horizontal and tilted planes at the Earth's surface for cloudless atmospheres. *J. Climate Appl. Meteorol.* 25:87-97.

Bond, T.C., Anderson, T.L. and Campbell, D.E. (1999), Calibration and intercomparison of filter-based measurements of visible light absorption by aerosols. *Aerosol Sci. Technol.* 30(6):582-600.

Cachier, H., Bremond, M.P. and Buat-Ménard, P. (1989a), Thermal separation of soot carbon. *Aerosol Sci. Technol.* 10(2):358-364.

Cachier, H., Bremond, M.P. and Buat-Ménard, P. (1989b), Determination of atmospheric soot carbon with a simple thermal method. *Tellus*. 41B(3):379-390.

Cadle, S.H. and Groblicki, P.J. (1982), An evaluation of methods for the determination of organic and elemental carbon in particulate samples. In *Particulate Carbon: Atmospheric Life Cycles*, G.T. Wolff and R.L. Klimisch, Eds. Plenum Press, New York, NY, pp. 89-109.

Cadle, S.H. and Mulawa, P.A. (1990), Atmospheric carbonaceous species measurement methods comparison study: General Motors results. *Aerosol Sci. Technol.* 12:128-131.

Cadle, S.H., Groblicki, P.J. and Stroup, D.P. (1980), An automated carbon analyzer for particulate samples. *Anal. Chem.* 52(13):2201-2206.

Cadle, S.H., Groblicki, P.J. and Mulawa, P.A. (1983), Problems in the sampling and analysis of carbon particulate. *Atmos. Environ.* 17(3):593-600.

Cahill, T.A., Matsuda, Y., Shadoan, D.J., Eldred, R.A. and Kusko, B.H. (1984). Forward alpha scattering techniques (FAST) for elements hydrogen through fluorine. *Nuclear Instruments and Methods in Physics Research*, 263.

Cao, J.J., Wang, Y.Q., Zhang, X.Y., Lee, S.C., Ho, K.F., Cao, Y.N. and Li, Y. (2005). Analysis of carbon isotope in airborne carbonate: Implications for aeolian sources. *Chinese Science Bulletin.* accepted.

Chen, L.W., Doddridge, B.G., Dickerson, R.R., Chow, J.C. and Henry, R.C. (2002), Origins of fine aerosol mass in the Baltimore-Washington corridor: Implications from observation, factor analysis, and ensemble air parcel back trajectories. *Atmos. Environ.* 36(28):4541-4554.

Chen, L.W., Chow, J.C., Watson, J.G., Moosmüller, H. and Arnott, W.P. (2004), Modeling reflectance and transmittance of quartz-fiber filter samples containing elemental carbon particles: Implications for thermal/optical analysis. *J. Aerosol Sci.* 35(6):765-780.

Chow, J.C. and Watson, J.G. (2002), $PM_{2.5}$ carbonate concentrations at regionally representative Interagency Monitoring of Protected Visual Environment sites. *J. Geophys. Res.* 107(D21):ICC 6-1-ICC 6-9. doi: 10.1029/2001JD000574.

Chow, J.C., Watson, J.G., Pritchett, L.C., Pierson, W.R., Frazier, C.A. and Purcell, R.G. (1993), The DRI Thermal/Optical Reflectance carbon analysis system: Description, evaluation and applications in U.S. air quality studies. *Atmos. Environ.* 27A(8):1185-1201.

Chow, J.C., Watson, J.G., Lowenthal, D.H., Richards, L.W., Solomon, P.A. and Magliano, K.L. (1997). Size-resolved particle and light extinction measurements during IMS95. In: *Proceedings. Visual Air Quality: Aerosols and Global Radiation Balance*. Tombach, I.H., Ed., Air and Waste Management Association: Pittsburgh, PA, p. 80-85.

Chow, J.C., Watson, J.G., Crow, D., Lowenthal, D.H. and Merrifield, T. (2001), Comparison of IMPROVE and NIOSH carbon measurements. *Aerosol Sci. Technol.* 34(1):23-34.

Chow, J.C., Watson, J.G., Chen, L.W., Arnott, W.P., Moosmüller, H. and Fung, K. (2004),

Equivalence of elemental carbon by the IMPROVE and STN Thermal/Optical Carbon Analysis Methods. *Environ. Sci. Technol.*, in press.

Chow, J.C., Watson, J.G., Chen, L.W.A. , Paredes-Miranda, G., Chang, M.C., Trimble, D., Fung, K., Zhang, J. and Yu, J.Z. (2005a). Refining temperature measures in thermal optical carbon analysis. *Atmos. Chem. and PhysicsDiscuss.* 5:1-29.

Chow, J.C., Watson, J.G., Louie, P.K.K., Chen, L.W.A. and Sin, D. (2005b). Comparison of $PM_{2.5}$ carbon measurement methods in Hong Kong, China. *Environ. Poll.* in press, 2005.

Christolis, M., Clayton, P., Hecq, P., Payrissat, M. and Petti-Coviaux, P. (1992), Instruction Manual for Air Pollution Monitoring - Vol. II: Black Smoke Monitoring. Report No. EUR 14550/II EN. Joint Research Center, Commission for the European Communities, Ispra.

Countess, R.J. (1990), Interlaboratory analyses of carbonaceous aerosol samples. *Aerosol Sci. Technol.* 12:114-121.

Currie, L.A., Benner, B.A., Jr., Cachier, H., Cary, R., Chow, J.C., Druffel, E.R.M., Eglinton, T.I., Gustafsson, Ö., Hartmann, P.C., Hedges, J.I., Kessler, J.D., Kirchstetter, T.W., Klinedinst, D.B., Klouda, G.A., Marolf, J.V., Masiello, C.A., Novakov, T., Pearson, A., Prentice, K.M., Puxbaum, H., Quinn, J.G., Reddy, C.M., Schmid, H., Slater, J.F., Watson, J.G. and Wise, S.A. (2002), A critical evaluation of interlaboratory data on total, elemental, and isotopic carbon in the carbonaceous particle reference material, NIST SRM 1649a. *J. Res. National Bureau Standards*. 107(3):279-298.

Edwards, J.D., Ogren, J.A., Weiss, R.E. and Charlson, R.J. (1983), Particulate air pollutants: A comparison of British 'Smoke' with optical absorption coefficients and elemental carbon concentration. *Atmos. Environ.* 17(11):2337-2341.

Ellis, E.C.; Novakov, T.; and Zeldin, M.D. (1984), Thermal characterization of organic aerosols. *Sci. Total Environ.* 36(Jun.):261-270.

Faxvog, F.R. and Roessler, D.M. (1979). Optoacoustic measurements of diesel particulate emissions. *J. Appl. Phys.* 50:7880-7882.

Fuller, K.A., Malm, W.C. and Kreidenweis, S.M. (1999), Effects of mixing on extinction by carbonaceous particles. *J. Geophys. Res.* 104(D13):15941-15954.

Fung, K.K. (1990), Particulate carbon speciation by MnO_2 oxidation. *Aerosol Sci. Technol.* 12(1):122-127.

Fung, K.K., Chow, J.C. and Watson, J.G. (2002), Evaluation of OC/EC speciation by thermal manganese dioxide oxidation and the IMPROVE method. *J. Air & Waste Manage. Assoc.* 52(11):1333-1341.

Gaffney, J.S., Tanner, R.L. and Phillips, M. (1984), Separating carbonaceous aerosol source terms using thermal evolution, carbon isotopic measurements, and C/N/S determinations. *Sci. Total Environ.* 36:53-60.

Gundel, L.A., Dod, R.L., Rosen, H. and Novakov, T. (1984). The relationship between optical attenuation and black carbon concentration for ambient and source particles. *Sci. Total Environ.*

36:197-202. 169.

Hansen, A.D. A. and McMurry, P.H. (1990). An intercomparison of measurements of aerosol elemental carbon during the 1986 Carbonaceous Species Method Comparison Study. *JAWMA* 40(6):894-895.

Hansen, A.D.A. and Novakov, T. (1990), Real-time measurement of aerosol black carbon during the Carbonaceous Species Methods Comparison Study. *Aerosol Sci. Tecnol.* 12: 194-199.

Hansen, A.D.A., Rosen, H. and Novakov, T. (1984), The aethalometer - An instrument for the real-time measurement of optical absorption by aerosol particles. *Sci. Total Environ.* 36:191-196.

Hänel, G. (1987). Radiation budget of the boundary layer: Part II, Simultaneous measurement of mean solar volume absorption and extinction coefficients of particles. *Beitr. Phys. Atmos.* 60:241-247.

Hänel, G. (1988). Single scattering albedo, asymmetry parameter, apparent refractive index, and apparent soot content of dry atmospheric particles. *Appl. Opt.* 27(11):2287-2294.

Hemeon, W.C., Haines, G.F., Jr. and Ide, H.M. (1953), Determination of haze and smoke concentrations by filter paper samples. *Air Repair.* 3:22-28.

Hering, S.V., Appel, B.R., Cheng, W., Salaymeh, F., Cadle, S.H., Mulawa, P.A., Cahill, T.A., Eldred, R.A., Surovik, M., Fitz, D.R., Howes, J.E., Knapp, K.T., Stockburger, L., Turpin, B.J., Huntzicker, J.J., Zhang, X. and McMurry, P.H. (1990), Comparison of sampling methods for carbonaceous aerosols in ambient air. *Aerosol. Sci. Tecnol.* 12:200-213.

Hill, A.S.G. (1936), Measurement of the optical densities of smokestains of filter papers. *Trans. Faraday Soc.* 32:1125-1131.

Hitzenberger, R., Dusek, U. and Berner, A. (1996), Black carbon measurements using an integrating sphere technique. *J. Geophys. Res.* 101(D14):19601-19606.

Hitzenberger, R., Jennings, S.G., Larson, S.M., Dillner, A., Cachier, H., Galambos, Z., Rouc, A. and Spain, T.G. (1999), Intercomparison of measurement methods for black carbon aerosols. *Atmos. Environ.* 33(17):2823-2833.

Horvath, H. (1993), Atmospheric light absorption - A review. *Atmos. Environ.* 27A(3):293-317

Horvath, H. (1997), Experimental calibration for aerosol light absorption measurements using the integrating plate method - Summary of the data. *J. Aerosol Sci.* 28(7):1149-1161.

Horvath, H., Catalan, L. and Trier, A. (1997), A study of aerosol of Santiago de Chile III: Light absorption measurements. *Atmos. Environ.* 31(22): 3737-3744.

Huebert, B.J. and Charlson, R.J. (2000), Uncertainties in data on organic aerosols. *Tellus.* 52B (5):1249-1255.

Huffman, H.D. (1996), Comparison of the light absorption coefficient and carbon measures for remote aerosols: An independent analysis of data from the IMPROVE NETWORK – I. *Atmos. Environ.* 30(1):73-83.

Huntzicker, J.J., Johnson, R.L., Shah, J.J. and Cary, R.A. (1982), Analysis of organic and elemental carbon in ambient aerosols by a thermal-optical method. In *Particulate Carbon: Atmospheric Life*

*Cycle.*G.T. Wolff and R.L. Klimisch, Eds. Plenum Press, New York, NY, pp. 79-88.

Jacobson, M.C., Hansson, H.C., Noone, K.J. and Charlson, R.J. (2000), Organic atmospheric aerosols: Review and state of the science. *Rev. Geophys.* 38(2):267-294.

Japar, S.M., Moore, J., Killinger, D.K. and Szkarlat, A.C. (1982), Spectrophone measurements of diesel vehicle particulate material. In: *Light Absorption by Aerosol Particles.* Gerber, H.E. and Hindman, E.E., Eds., Spectrum Press: Hampton, VA, p. 275-278.

Japar, S.M., Szkarlat, A.C., Gorse, R.A., Jr., Heyerdahl, E.K., Johnson, R.L., Rau, J.A. and Huntzicker, J.J. (1984). Comparison of solvent extraction and thermal-optical carbon analysis methods: Application to diesel vehicle exhaust aerosol. *Environ. Sci. Tecnol.* 18(4):231-234.

Johnson, R.L., Shah, J.J., Cary, R.A. and Huntzicker, J.J. (1981), An automated thermal-optical method for the analysis of carbonaceous aerosol. In *Atmospheric Aerosol: Source/Air Quality Relationships.* E.S. Macias and P.K. Hopke, Eds. American Chemical Society, Washington, DC, pp. 223-233.

Killinger, D.K., Moore, J. and Japar, S.M. (1980). The use of photoacoustic spectroscopy to characterize and monitor soot in combustion processes. ACS Symposium Series No. 134: Laser Probes for Combustion Chemistry. Crosley, D.R., Ed.. American Chemical Society: Washington, DC, p. 457-462.

Kim, E. and Hopke, P.K. (2004), Source apportionment of fine particles at Washington, DC, utilizing temperature-resolved carbon fractions. *JAWMA.* 54(7):773-785.

Kirchstetter, T.W., Corrigan, C.E. and Novakov, T.(2001), Laboratory and field investigation of the adsorption of gaseous organic compounds onto quartz filters. *Atmos. Environ.* 35(9):1663-1671.

Kirchstetter, T.W., Novakov, T. and Hobbs, P.V. (2004), Evidence that the spectral dependence of light absorption by aerosols is affected by organic carbon. *J. Geophys. Res.* 109(D21):D21208. doi:10.1029/2004JD004999.

Lavanchy, V.M.H., Gäggeler, H.W., Nyeki, S. and Baltensperger, U. (1999), Elemental carbon (EC) and black carbon (BC) measurements with a thermal method and an aethalometer at the high-alpine research station Jungfraujoch. *Atmos. Environ.* 33(17):2759-2769.

Lawson, D.R. and Hering, S.V. (1990), The Carbonaceous Species Method Comparison Study: An overview. *Aerosol. Sci. Tecnol.* 12:1-2.

Lim, H.J., Turpin, B.J., Edgerton, E., Hering, S.V., Allen, G., Maring, H. and Solomon, P.A. (2003), Semicontinuous aerosol carbon measurements: Comparison of Atlanta Supersite measurements. *J. Geophys. Res.* 108(D7):SOS 7-1-SOS 7-12. doi: 10.1029/2001JD001214.

Lin, C.I., Baker, M.B. and Charlson, R.J. (1973), Absorption coefficient of atmospheric aerosol: A method for measurement. *Appl. Opt.* 12(6):1356-1363.

Liousse, C., Cachier, H. and Jennings, S.G. (1993), Optical and thermal measurements of black carbon aerosol content in different environments: Variation of the specific attenuation cross-section, sigma ( ). *Atmos. Environ.* 27A(8):1203-1211.

Mader, B.T., Flagan, R.C. and Seinfeld, J.H. (2001), Sampling atmospheric carbonaceous aerosols

using a particle trap impactor/denuder sampler. *Environ. Sci. Technol.* 35(24):4857-4867.

Martins, J.V., Artaxo, P., Liousse, C., Reid, J.S., Hobbs, P.V. and Kaufman, Y.J. (1998), Effects of black carbon content, particle size, and mixing on light absorption by aerosols from biomass burning in Brazil. *J. Geophys. Res.* 103(D24):32041-32050.

McMurry, P.H. and Hansen, A.D.A. (1990), An intercomparison of measurements of aerosol elemental carbon during the 1986 Carbonaceous Species Method Comparison Study. *JAWMA.* 40(6):894-895.

Mizohata, A. and Ito, N. (1985), Analysis of organic and elemental carbon in atmospheric aerosols by thermal method. *Annual Report of the Radiation Center of Osaka Prefecture.* 26(0):51-55.

Moosmüller, H., Arnott, W.P. and Rogers, C.F. (1997), Methods for real-time, *in situ* measurement of aerosol light absorption. *J. Air & Waste Manage. Assoc.* 47(2):157-166.

Moosmüller, H., Arnott, W.P., Rogers, C.F., Chow, J.C., Frazier, C.A., Sherman, L.E. and Dietrich, D.L. (1998). Photoacoustic and filter measurements related to aerosol light absorption during the Northern Front Range Air Quality Study (Colorado 1996/1997). *J. Geophys. Res.* 103(D21):28149-28157.

Moosmüller, H., Arnott, W.P., Rogers, C.F., Bowen, J.L., Gillies, J.A., Pierson, W.R., Collins, J.F., Durbin, T.D. and Norbeck, J.M. (2001a). Time resolved characterization of diesel particulate emissions 1. Instruments for particle mass measurements. *Environ. Sci. Technol.* 35(4):781-787.

Moosmüller, H., Arnott, W.P., Rogers, C.F., Bowen, J.L., Gillies, J.A., Pierson, W.R., Collins, J.F., Durbin, T.D. and Norbeck, J.M. (2001b), Time resolved characterization of diesel particulate emissions 2. Instruments for elemental and organic carbon measurements. *Environ. Sci. Technol.* 35(10):1935-1942.

Mueller, P.K., Mosley, R.W. and Pierce, L.B. (1971). Carbonate and noncarbonate carbon in atmospheric particles. In *Proceedings of the Second International Clean Air Congress.* Englund, H.M. and W.T. Beery, Eds. Academic Press, New York, NY, p. 532-539.

Nejedlý, Z., Campbell, J.L., Brook, J.R., Vet, R. and Eldred, R. (2003), Evaluation of elemental and black carbon measurements from the GAViM and IMPROVE networks. *Aerosol. Sci. Tecnol.* 37(1):96-108.

Niessner, R. and Wilbring, P. (1989). Ultrafine particles as trace catchers for PAHs: The photelectric aerosol sensor as a tool for in-situ sorption and desorption studies. *Anal. Chem.* 61(7):708-714.

NIOSH (1996), Method 5040 Issue 1 (Interim): Elemental carbon (diesel exhaust). In *NIOSH Manual of Analytical Methods,* 4th ed. National Institute of Occupational Safety and Health, Cincinnati, OH.

NIOSH (1999), Method 5040 Issue 3 (Interim): Elemental carbon (diesel exhaust). In *NIOSH Manual of Analytical Methods,* 4th ed. National Institute of Occupational Safety and Health, Cincinnati, OH.

Novakov, T. (1982), Soot in the atmosphere. In *Particulate Carbon: Atmospheric Life Cycle.* G.T. Wolff and R.L. Klimisch, Eds. Plenum Press, New York, NY, pp. 19-41.

Peterson, M.R. and Richards, M.H. (2002), Thermal-optical-transmittance analysis for organic, elemental, carbonate, total carbon, and OCX2 in $PM_{2.5}$ by the EPA/NIOSH method (Session 5, Paper #83). Presentation at the Symposium on Air Quality Measurement Methods and Technology in San Francisco, CA, Nov., 2002. Air & Waste Management Association, Pittsburgh, PA.

Petzold, A. and Niessner, R. (1995a), Intercomparison Study on soot-selective methods – Field study results from several polluted areas in Germany. *J. Aeosol. Sci.* 26(S1):S393-S394.

Petzold, A. and Niessner, R. (1995b), Method comparison study on soot-selective techniques. *Mikrochimica Acta*, 117:215-237.

Reid, J.S., Hobbs, P.V., Liousse, C., Martins, J.V., Weiss, R.E. and Eck, T.F. (1998), Comparisons of techniques for measuring shortwave absorption and black carbon content of aerosols from biomass burning in Brazil. *J. Geophys. Res.* 103(D24):32031-32040.

Roessler, D.M. (1984). Photoacoustic insights on diesel exhaust particles. *Appl. Opt.* 23(8):1148-1155.

Ruoss, K., Dlugi, R., Weigl, C. and Hänel, G. (1992), Intercomparison of different aethalometers with an absorption technique: Laboratory calibrations and field measurements. *Atmos. Environ.* 26A(17):3161-3168.

Rupprecht, E.G., Patashnick, H., Beeson, D.E., Green, R.E. and Meyer, M.B. (1995), A new automated monitor for the measurement of particulate carbon in the atmosphere. In *Proceedings, Particulate Matter: Health and Regulatory Issues*. J.A.Cooper and L.D.Grant, Eds. Air and Waste Management Association, Pittsburgh, PA, pp. 262-267.

Sadler, M., Charlson, R.J., Rosen, H. and Novakov, T. (1981), An intercomparison of the integrating plate and the laser transmission methods for determination of aerosol absorption coefficients. *Atmos. Environ.* 15(7):1265-1268.

Schmid, H.P., Laskus, L., Abraham, H.J., Baltensperger, U., Lavanchy, V.M.H., Bizjak, M., Burba, P., Cachier, H., Crow, D.J., Chow, J.C., Gnauk, T., Even, A., ten Brink, H.M., Giesen, K.P., Hitzenberger, R., Hueglin, C., Maenhaut, W., Pio, C.A., Puttock, J., Putaud, J.P., Toom-Sauntry, D. and Puxbaum, H. (2001), Results of the "Carbon Conference" international aerosol carbon round robin test: Stage 1. *Atmos. Environ.* 35(12):2111-2121.

Schmidt, M.W.I., Skjemstad, J.O., Czimczik, C.I., Glaser, B., Prentice, K.M., Gelinas, Y. and Kuhlbusch, T.K. (2001), Comparative analysis of black carbon in soils. *Global Biogeochemical Cycles*. 15(1):163-167.

Sharma, S., Brook, J.R., Cachier, H., Chow, J.C., Gaudenzi, A. and Lu, G. (2002), Light absorption and thermal measurements of black carbon in different regions of Canada. *J. Geophys. Res.* 107(D24):4771. doi: 10.1029/2002JD002496.

Sheridan, P.J., Arnott, W.P., Ogren, J.A., Andrews, E., Atkinson, D.B., Covert, D.S., Moosmuller, H., Petzold, A., Schmid, B., Strawa, A.W., Varma, R. and Virkkula, A. (2005), The Reno aerosol optics study: An evaluation of aerosol absorption measurement methods. *Aerosol Sci. Tech.*

39(1):1-16.

Sin, D.W.M., Fung, W.H. and Lam, C.H. (2002),Measurement of carbonaceous aerosols: Validation and comparison of a solvent extraction - gas chromatographic method and a thermal optical transmittance method. *Analyst*.127(5):614-622.

Szkarlat, A.C. and Japar, S.M. (1983), Optical and chemical properties of particle emissions from on-road vehicles. *JAPCA*. 33(6):592-597.

Tanner, R.L. (1982), An ambient experimental study of phase equilibrium in the atmospheric system: aerosol H^+, NH_4^+, SO_4^{-2}, NO_3^-, NH_3(g), HNO_3(g). *Atmos. Environ.* 16(12):2935-2942.

Tohno, S. and Hitzenberger, R. (2000), Comparison of ambient carbon particulate monitor and filter sampling for black carbon measurement. *J. Areosol. Sci.* 31(S1):S315-S316.

Turpin, B.J., Cary, R.A. and Huntzicker, J.J. (1990), An *in-situ*, time-resolved analyzer for aerosol organic and elemental carbon. *Aerosol Sci. Technol.* 12(1):161-171.

Turpin, B.J., Huntzicker, J.J. and Hering, S.V. (1994), Investigation of organic aerosol sampling artifacts in the Los Angeles Basin. *Atmos. Environ.* 28(19):3061-3071. Research & Development.

Turpin, B.J., Saxena, P., Allen, G.A., Koutrakis, P., McMurry, P.H. and Hildemann, L.M. (1997), Characterization of the southwestern desert aerosol, Meadview, AZ. *JAWMA*. 47(3):344-356.

VDI (1996). Measurement of soot (immission) - Chemical analysis of elemental carbon by extraction and thermal desorption of organic carbon. Report No. 2465 Part 1. Verein Deutscher Ingenieure, Dusseldorf, Germany.

VDI (1999), Measurement of soot (ambient air) - Thermographic determination of elemental carbon after thermal desorption of organic carbon. Report No. 2465 Part 2. Verein Deutscher Ingenieure, Dusseldorf, Germany.

Watson, J.G. (2002), Visibility: Science and regulation. *J. Air and Waste Manage. Assoc.* 52(6):628-713.

Watson, J.G. and Chow, J.C. (2002). Comparison and evaluation of in-situ and filter carbon measurements at the Fresno Supersite. *J. Geophys. Res.* 107(D21):ICC 3-1-ICC 3-15.

Watson, J.G., Chow, J.C., Lowenthal, D.H., Pritchett, L.C., Frazier, C.A., Neuroth, G.R. and Robbins, R. (1994), Differences in the carbon composition of source profiles for diesel- and gasoline-powered vehicles. *Atmos. Environ.* 28(15):2493-2505.

Yang, H. and Yu, J.Z. (2002), Uncertainties in charring correction in the analysis of elemental and organic carbon in atmospheric particles by thermal/optical methods. *Environ. Sci. Technol.* 36(23):5199-5204.

Yu, J.Z., Xu, J.H., and Yang, H. (2002), Charring characteristics of atmospheric organic particulate matter in thermal analysis. *Environ. Sci. Technol.* 36(4):754-761.

Received for review, March 31,2005
Accepted, June 13, 2005

9.2 Park et al., 2006

TECHNICAL PAPER

ISSN 1047-3289 *J. Air & Waste Manage. Assoc.* 56:474–491

Comparison of Continuous and Filter-Based Carbon Measurements at the Fresno Supersite

Kihong Park, Judith C. Chow, John G. Watson, Dana L. Trimble, and Prakash Doraiswamy
Desert Research Institute, Reno, NV

Kihong Park
Gwangju Institute of Science and Technology, Gwangju, Korea

W. Pat Arnott
University of Nevada, Reno, NV

Kenneth R. Stroud, Kenneth Bowers, and Richard Bode
California Air Resources Board, Sacramento, CA

Andre Petzold
Deutsches Zentrum fur Luft—und Raumfahrt Oberpfaffenhofen, Institut fur Physik der Atmosphare, Wessling, Germany

Anthony D.A. Hansen
Lawrence Berkeley National Laboratory, Berkeley, CA

ABSTRACT

Results from six continuous and semicontinuous black carbon (BC) and elemental carbon (EC) measurement methods are compared for ambient samples collected from December 2003 through November 2004 at the Fresno Supersite in California. Instruments included a multi-angle absorption photometer (MAAP; λ = 670 nm); a dual-wavelength (λ = 370 and 880 nm) aethalometer; seven-color (λ = 370, 470, 520, 590, 660, 880, and 950 nm) aethalometers; the Sunset Laboratory carbon aerosol analysis field instrument; a photoacoustic light absorption analyzer (λ = 1047 nm); and the R&P 5400 ambient carbon particulate monitor. All of these acquired BC or EC measurements over periods of 1 min to 1 hr. Twenty-four-hour integrated filter samples were also acquired and analyzed by the Interagency Monitoring of Protected Visual Environments (IMPROVE) thermal/optical reflectance carbon analysis protocol. Site-specific mass absorption efficiencies estimated by comparing light absorption with IMPROVE EC concentrations were 5.5 m^2/g for the MAAP, 10 m^2/g for the aethalometer at a wavelength of 880 nm, and 2.3 m^2/g for the photoacoustic analyzer; these differed from the default efficiencies of 6.5, 16.6, and 5 m^2/g, respectively. Scaling absorption by inverse wavelength did not provide equivalent light absorption coefficients among the instruments for the Fresno aerosol measurements. Ratios of light absorption at 370 nm to those at 880 nm from the aethalometer were nearly twice as high in winter as in summer. This is consistent with wintertime contributions from vehicle exhaust and from residential wood combustion, which is believed to absorb more shorter-wavelength light. To reconcile BC and EC measurements obtained by different methods, a better understanding is needed of the wavelength dependence of light-absorption and mass-absorption efficiencies and how they vary with different aerosol composition.

IMPLICATIONS

BC can be measured in situ and continuously by optical, thermal, and photoacoustic methods. The results of these measurements are highly correlated but have different absolute values. Relationships differ with changes in the sampled particles (e.g., winter vs summer). Both light- and mass-absorption efficiencies convert light absorption (i.e., the Angstrom Power Law [$\lambda^{-\alpha}$], assuming α = 1) to BC, and both are wavelength dependent. The assumption that these efficiencies scale with inverse wavelength is not true at the Fresno Supersite and probably not at other locations.

INTRODUCTION

Black carbon (BC), or elemental carbon (EC), particles originate mostly from incomplete combustion of fuels and are major contributors to aerosol light absorption (b_{abs}, units of inverse megameters [Mm^{-1}]) in exhaust emissions and ambient air. Both BC and EC affect visibility, health, and the earth's radiation balance.[1–6] The terms BC, EC, light-absorbing carbon, and soot have been used interchangeably by many researchers, depending on the material sampled, the method used for quantification, and the uses of the data. This imprecise usage, coupled

with method-dependent definitions for BC or EC, has resulted in much confusion about their comparability.[5]

The most commonly used methods for determining BC and EC extract particles from the air onto a filter, followed by optical and/or thermal analyses.[5] In optical methods, the attenuation of light (b_{abs}) with wavelength (λ) reflected from, or transmitted through, the particle deposit relative to the blank filter is used to estimate $b_{abs}(\lambda)$. The $b_{abs}(\lambda)$ is divided by a mass absorption efficiency, $\sigma_{abs}(\lambda)$ (units of m^2/g), to obtain the BC concentration in $\mu g/m^3$. The wavelength dependence for b_{abs} and σ_{abs} is often scaled as λ^{-1}, following the Angstrom Power Law (λ^{α}) where $\alpha = 1$, but α depends on the chemical and physical properties of the sampled aerosol and the filter medium. Kirchstetter et al.[7] found that the λ^{-1} scaling approximated the behavior of fresh vehicle exhaust, but that a λ^{-2} scaling was more appropriate for biomass burning aerosol.

In addition to λ, light scattering in the filter medium, light-scattering particles deposited on the filter, and filter loading influence the accurate determination of BC concentrations.[6,8–10] Fuller et al.[11] and Martins et al.[12] applied advanced optical models to different particle compositions, sizes, and shapes to estimate σ_{abs} ranging from 2 to 30 m^2/g. Empirical measurements of σ_{abs} have been reported in a range of 2 to 17 m^2/g.[6,13] Bond and Bergstrom[14] suggested a $\sigma_{abs}(550\ nm)$ of $7.5 \pm 1.2\ m^2/g$ for freshly emitted particles.

In thermal methods for measuring EC, the filter is heated so that carbon evolves at specified temperatures in both nonoxidizing and oxidizing carrier gases. These methods are intended to separate organic carbon (OC) from EC. Carbonate carbon, typically in the form of calcite ($CaCO_3$), may also be classified as OC or EC at high temperatures (>800 °C), but it is found only when erosion of non-weathered crustal material is a large contributor to the sample.[15,16] Although EC will combust in an oxidizing atmosphere, it is stable at high temperatures (<700 °C) in inert atmospheres (e.g., helium [He]).

Some thermal methods use optical monitoring to correct for the charring of OC to EC in nonoxidizing atmospheres. Different temperature and charring-correction protocols have resulted in different values of EC even within the same thermal evolution method.[17,18] Currie et al.[19] found that the lowest and highest EC reported by different laboratories for the same standard filter sample differed by a factor of 7.

Photoacoustic detection[20–22] measures $b_{abs}(\lambda)$ on particles that have not been changed by filter collection. The photoacoustic analyzer draws particle-laden air into an acoustic resonator through which a high-intensity, modulated, monochromatic light beam is directed. A sound wave is produced at the modulation frequency by expansion of the air when particles absorb energy from light. Matching the modulation frequency to the resonator frequency reinforces the acoustic wave for measurement with a sensitive microphone; $b_{abs}(\lambda)$ is proportional to the sound energy, and particle absorption is divided by an empirically derived $\sigma_{abs}(\lambda)$ to attain a BC concentration.

Recent studies have compared and evaluated several current optical, thermal, and photoacoustic BC and EC measurement methods under controlled laboratory conditions.[23–26] Saathoff et al.[24] generated diesel soot, graphite electric arc soot, organic-coated soot, and mixtures of soot and ammonium sulfate during the Aerosols, Interactions and Dynamics in the Atmosphere (AIDA) soot aerosol campaign in 1999. They found that optical methods required different $\sigma_{abs}(\lambda)$ for diesel-soot and arc-soot aerosols to determine BC concentrations. The $\sigma_{abs}(\lambda)$ determined by optical techniques varied depending on the source type, wavelengths used, and measurement method. Schnaiter et al.[25] reported a $\sigma_{abs}(450\ nm)$ value of 10.6 m^2/g for diesel soot and 5.6 m^2/g for the graphite electric arc generator. The difference was attributed to different particle structures. These experiments showed higher a $\sigma_{abs}(450\ nm)$ for coated BC particles, similar to the theoretical findings of Fuller et al.[11] Sheridan et al.[26] used laboratory-generated diesel soot and kerosene and found reasonable agreements among (1) photoacoustic $b_{abs}(532\ nm)$; (2) the difference between particle light extinction and scattering; and (3) filter-based b_{abs}.

Watson et al.[5] summarized nearly 40 published intercomparison studies of optical, thermal, and photoacoustic measures of BC and EC. Some comparisons showed good agreement among the different methods, whereas others showed wide disagreements for the same methods applied to different samples. Agreement was typically better for laboratory-generated particles than for ambient air samples. Watson et al.[5] concluded that citation of a single BC or EC comparison study is insufficient to justify comparability among the different measurement methods. Lacking a more systematic understanding of the differences, aerosol- and instrument-specific comparisons are needed to use measurements interchangeably.

For this study, eight continuous or semicontinuous and integrated BC or EC measurement methods, as detailed in Table 1, were used to sample air at the Fresno Supersite.[27,28] In addition to these continuous and time-integrated carbon measurements, the Supersite provides continuous data of 1-hr or less for particle number concentration (3–407 nm), particle light scattering (b_{scat} [530 nm], units of Mm^{-1}), fine particulate matter ($PM_{2.5}$) mass, nitrate (NO_3^-), and gaseous nitrogen oxides (NO_x), carbon monoxide (CO), and ozone (O_3) that can be used to better understand differences among these BC and EC measurements. The analysis approach taken here can be applied at other sites that use similar measurements.

EXPERIMENTAL APPROACH

Fresno is located in California's San Joaquin Valley (SJV), which is in nonattainment of the $PM_{2.5}$ National Ambient Air Quality Standards. Air pollution in central California is affected by different types of emissions, including point sources (e.g., steam generators and natural gas combustion), area sources (e.g., residential wood combustion [RWC] and cooking), on-road and non-road mobile sources (e.g., gasoline- and diesel-fueled vehicles, high emitters, and cold starts in winter), agricultural sources (e.g., tillage, field burning, and fertilizers), and biogenic sources (e.g., plants and crops).[27] OC and EC are important components of $PM_{2.5}$ in the SJV,[29,30] and the relative abundances of OC and EC are used to evaluate source contributions for emission reduction strategies. The

Table 1. Summary of BC and EC measurement methods.

Instruments[a]	Observable (units)	Measurement Principle[b]	Wavelength (nm)	Inlet	Collection Medium	Flow Rate (L/min)	Averaging Time
MAAP	b_{abs} (Mm^{-1}) BC ($\mu g/m^3$)	Light reflected from the filter at 130° and 165° from the illumination direction are used in a radiative transfer model to estimate b_{abs} and is converted to BC using σ_{abs} of 6.5 m^2/g.	670	$PM_{2.5}$ cyclone	Glass-fiber filter tape	16	1 min
2-AE	b_{abs} (Mm^{-1}) BC ($\mu g/m^3$)	Attenuation of light transmitted through the filter tape is measured and converted to BC using σ_{abs} of 14,625/λ (m^2/g).	370,880	$PM_{2.5}$ cyclone	Quartz-fiber filter tape	6.8	5 min
7-AE	b_{abs} (Mm^{-1}) BC ($\mu g/m^3$)		370, 470, 520, 590, 660, 880, 950	$PM_{2.5}$ cyclone	Quartz-fiber filter tape	6.8	5 min
Photoacoustic	b_{abs} (Mm^{-1}) BC ($\mu g/m^3$)	Light absorption by particles in air results in heating of the surrounding air. The expansion of the heated air produces an acoustic (sound wave) signal that is detected by a microphone to determine b_{abs}, which is converted to BC using σ_{abs} = 5 m^2/g	1047	TSP[c]	Acoustic resonator	3	5 min
Sunset	OC, EC ($\mu g/m^3$)	Particles collected on a quartz-fiber filter are subjected to different temperature ramps following the NIOSH 5040 TOT protocol, and the resulting CO_2 is analyzed by NDIR. Pyrolysis correction is by laser transmittance.	660	$PM_{2.5}$ cyclone	Quartz-fiber filter tape	8.5	1 hr
	BC ($\mu g/m^3$)	Light transmitted through the filter is monitored during the collection phase to quantify BC.	660	$PM_{2.5}$ cyclone	Quartz-fiber filter tape	8.5	1 hr
R&P 5400	OC, EC, and TC ($\mu g/m^3$)	Particles collected on an impactor are heated to 275 °C for OC and to 750 °C for TC, and the resulting CO_2 is measured by NDIR. EC is obtained by the difference between TC and OC.	NA	$PM_{2.5}$ cyclone	Impactor	16.7	1 hr
PAS-PAH	Particle-bound PAH (IA)	The air stream is exposed to UV radiation, which ionizes the particle-bound PAH molecules. The charged particles are collected on a filter element, and the pizeoelectric current is proportional to the particle-bound PAH.	225	$PM_{2.5}$ impactor	Filter element mounted in a Faraday cage	2	5 min
FRM filter samples analyzed by IMPROVE TOR[d]	OC, EC, and TC ($\mu g/m^3$)	Particles collected on a quartz-fiber filter are subjected to different temperature ramps following the IMPROVE TOR protocol. The resulting CO_2 is converted to CH_4 and analyzed by FID. Pyrolysis correction is by laser reflectance.	632.8	$PM_{2.5}$ impactor	Quartz-fiber filter	16.7	24 hr

Notes: [a]MAAP, model 5012, Thermo-Electron, Waltham, MA); 2-AE, model AE-21, Magee Scientific, Berkeley, CA); 7-AE, model AE-31, Magee Scientific, Berkeley, CA); photoacoustic, photoacoustic analyzer (DRI, Reno, NV); Sunset, semicontinuous Sunset Laboratory Carbon Aerosol Analysis Field Instrument (Sunset Laboratory, Tigard, OR) following the National Institute for Occupational Safety and Health (NIOSH) TOT 5040 protocol; R&P 5400, ambient carbon particulate monitor (Rupprecht & Patashnick, Albany, NY); PAS-PAH, particle-bound PAH monitor (model PAS2000, EcoChem Analytics, League City, TX); FRM, Federal Reference Monitor (Andersen Instruments, Smyrna, GA); [c]TSP = total suspended particles; NA = not applicable; PAS = photoelectric aerosol sensor; FID = flame-ionization detector; [d]IMPROVE TOR as in ref. 5.

Fresno Supersite (3425 First Street, Fresno, CA) is located near commercial buildings, restaurants, churches, schools, and residential areas and is ~5.5 km northeast of the downtown Fresno commercial district. First Street is a four-lane artery with moderate traffic levels; sampling inlets are on the rooftop of a two-story building on the

west side of the street. This analysis examines measurements from December 2003 through November 2004.

For the Magee Scientific dual-wavelength (2-AE) and seven-color (7-AE) aethalometers,[31,32] particles are deposited on a quartz-fiber filter tape and the change of light transmission through the filter tape measured by light source and detector is used to calculate 5-min average BC concentrations. The filter tape is automatically advanced when its optical density attains 0.75. The attenuation is converted to a BC mass concentration, using a σ_{abs} of 14625/λ (m^2/g). In normal operation, corrections are not made for filter loading, filter scattering, or aerosol scattering.[8]

For the Thermo multi-angle absorption photometer (MAAP), samples are deposited on a filter tape similar to the process in the aethalometer.[10,33,34] The MAAP measures reflectance of 670 nm light at 130° and 165° from the projected light beam. Use of these as inputs to a two-stream-approximation radiative transfer model minimizes filter- and aerosol-scattering biases, returning a b_{abs}(670 nm) comparable to that of the photoacoustic analyzer for kerosene smoke and electric arc graphite.[34] An empirical σ_{abs}(670 nm) of 6.5 m^2/g was applied to convert 1-min b_{abs} to BC. Comparison of the MAAP samples with EC derived from the German extraction/thermal desorption method[35] yielded σ_{abs}(670 nm) values of 6.4 ± 1 m^2/g for urban Berlin aerosol, 6.5 ± 0.7 m^2/g for urban Bad Korzingen aerosol, and 4.8 ± 1.2 m^2/g for non-urban Mount Kleiner Feldberg aerosol with EC <0.5 $\mu g/m^3$. The VDI method reports higher fractions of EC than many other methods,[36] including the Interagency Monitoring of Protected Visual Environments (IMPROVE) thermal/optical reflectance (TOR) protocol[17,37,38] applied to $PM_{2.5}$ filter samples at the Fresno Supersite.

The Desert Research Institute (DRI) photoacoustic analyzer measures 5-min average b_{abs}(1047 nm).[20,39,40] An empirical σ_{abs}(1047 nm) of 5 m^2/g was applied to convert photoacoustic b_{abs}(1047 nm) to BC, based on comparison samples from IMPROVE EC and photoacoustic BC measurements of diesel emissions.[40]

The Sunset analyzer,[41,42] which is based on thermal/optical transmittance (TOT), draws air through a quartz-fiber filter for 45 min at 8.5 L/min to obtain the sample. The sampling port is then sealed for 15 min, and the sample is heated to 250, 500, 650, and 850 °C in 100% He, then to 650, 750, 850, and 940 °C in 98% He/2% oxygen (O_2) that backflows through the filter. The evolved carbon is oxidized to carbon dioxide (CO_2), then quantified by a nondispersive IR (NDIR) detector. Charred OC is monitored by transmittance at λ = 660 nm. The carbon that evolves after the transmittance achieves its original value is classified as EC. The filter is presumably free of carbon after the analysis. The sampling inlet is opened, and the cycle begins again for the next hour. This unit also monitors the transmitted laser signal during the collection phase to obtain a BC measurement by the same principle as applied in the aethalometer.

For the R&P 5400 carbon monitor,[43] particles are drawn through a $PM_{2.5}$ inlet, deposited on an impactor, and heated by a Xenon lamp to 275 °C in air, combusted to CO_2, and measured with an NDIR to determine 1-hr average OC. The temperature is increased to 750 °C to measure total carbon (TC). EC is determined based on the difference between TC and OC.

The EcoChem particle-bound polycyclic aromatic hydrocarbon (PAH) monitor[44] uses a photoelectric sensor with an excimer lamp that produces UV radiation (225 nm) to photo-ionize the sampled particles. This photon energy minimizes ionization of gas molecules. The charged particles are collected on a filter element mounted in a Faraday cage, and the electric current is measured with an electrometer. The photoelectric current is proportional to the concentration of particle-bound PAHs, weighted according to an average ionization response. This is a relative measure of particle-bound PAH; therefore, the results are reported in terms of the electrometer output in femptoamps (fA).

These continuous BC measurements are compared with each other and with EC determined by IMPROVE-TOR analysis[17,37,38] of 24-hr quartz-fiber filters from a $PM_{2.5}$ Federal Reference Monitor (FRM)[45] operated every sixth day. Filters were baked at 900 °C for 4 hr before sampling to remove adsorbed organic vapors.[46] For IMPROVE_TOR analysis, the sample is heated in successive steps of 120 °C (OC1), 250 °C (OC2), 450 °C (OC3), and 550 °C (OC4) in He and 550 °C (EC1), 700 °C (EC2), and 800 °C (EC3) in 98% He/2% O_2. Evolved carbon is oxidized to CO_2 and then reduced to methane (CH_4) for detection by a flame-ionization detector (FID). The pyrolyzed (i.e., charred) OC is monitored by reflectance at λ = 632.8 nm. Until the laser signal returns to its initial value, the portion of EC1 is assigned to pyrolyzed OC (OP). The OC is defined by the sum of OC1, OC2, OC3, OC4, and OP, whereas the EC is defined by EC1 + EC2 + EC3 − OP.

Other continuous measurements examined in this analysis include (1) ultrafine and fine particle numbers from nano (3–84 nm) and standard (84–407 nm) scanning mobility particle sizers (SMPS; models 3936N25A and 3936L10, TSI, Shoreview, MN);[5,47] (2) b_{scat}(530 nm) by nephelometer (Radiance Research M903, Seattle, WA);[48] (3) $PM_{2.5}$ mass concentration by tapered element oscillating microbalance (TEOM; model 1400a, Rupprecht and Patashnick, Albany, NY);[49] (4) NO_3^- by flash volatilization (model R&P 8400N, Rupprecht and Patashnick, Albany, NY);[50] (5) NO_x by chemiluminescence (model TEI 42, Thermo Electron Inc., Franklin, MA); (6) CO by IR gas filter correlation (model DASIBI 3008, Environmental Corp., Glendale, CA); (7) O_3 by UV absorption (model API 400, API Inc., San Diego, CA); and (8) meteorology measurements (i.e., wind speed and direction [model 05305L high-sensitivity wind vane and anemometer, Met One, Grants Pass, OR], temperature [model CS500L platinum resistance sensor, Met One], relative humidity [RH; model CS capacitance sensor, Met One], solar radiation [model LI200X-L pyranometer, Li-Cor, Lincoln, NE], and atmospheric pressure [model Met One piezofilm sensor, Met One]).

RESULTS

Comparison of BC and EC Measurements

Table 2 lists comparability statistics, obtained with the assumed $\sigma_{abs}(\lambda)$, for the different BC and EC measurements. These statistics reflect the differences evident in

Table 2. Comparison statistics for collocated BC and EC measurements between December 1, 2003, and November 30, 2004

Sampling period	Methods[a]		No. of Pairs	Average of Ratios ($y/x \pm$ SD)	Distribution of Differences[b] (%)				Average Difference of $y - x$ ($\mu g/m^3$)	Correlation (r)	Regression Slope ± Standard Error	Intercept ± Standard Error ($\mu g/m^3$)
	y	x			$<1\sigma$[c]	1σ–2σ	2σ–3σ	$>3\sigma$				
	DRI/OGC	Photoacoustic at 1047 nm										
Dec 2003–Feb 2004	IMPROVE EC		14	2.24 ± 0.40	0	0	7	93	1.28	0.97	2.09 ± 0.14	0.09 ± 0.18
June 2004–Aug 2004	IMPROVE EC		16	1.82 ± 0.24	13	38	38	13	0.33	0.99	1.59 ± 0.07	0.07 ± 0.03
	MAAP at 670 nm	Photoacoustic at 1047 nm										
Dec 2003			491	1.99 ± 0.80	17	26	12	45	1.19	0.99	1.78 ± 0.01	0.14 ± 0.02
Jan 2004			696	1.83 ± 0.27	6	26	24	44	0.88	0.99	1.81 ± 0.01	0.00 ± 0.02
Feb 2004			672	1.83 ± 0.39	19	26	13	42	0.67	0.99	1.80 ± 0.01	0.00 ± 0.01
Mar 2004			719	1.80 ± 0.39	11	18	21	50	0.46	0.98	1.68 ± 0.01	0.04 ± 0.01
Apr 2004			673	1.75 ± 0.54	17	26	18	39	0.25	0.97	1.55 ± 0.02	0.04 ± 0.01
May 2004			730	1.70 ± 0.54	18	25	18	39	0.17	0.96	1.49 ± 0.02	0.03 ± 0.01
Jun 2004			714	1.71 ± 0.43	11	22	23	44	0.19	0.97	1.52 ± 0.02	0.03 ± 0.01
Jul 2004			743	1.67 ± 0.37	9	21	29	41	0.25	0.96	1.44 ± 0.02	0.07 ± 0.01
Aug 2004			168	1.63 ± 0.43	12	35	15	32	0.20	0.95	1.45 ± 0.04	0.04 ± 0.02
	7-AE at 880 nm	Photoacoustic at 1047 nm										
Dec 2003			514	1.45 ± 0.62	27	21	13	33	0.50	0.99	1.33 ± 0.01	0.06 ± 0.01
Jan 2004			697	1.42 ± 0.22	19	30	17	33	0.42	0.98	1.35 ± 0.01	0.04 ± 0.01
Feb 2004			672	1.96 ± 0.71	17	18	11	53	0.77	0.96	1.89 ± 0.02	0.05 ± 0.03
Mar 2004			720	1.61 ± 0.33	15	18	18	48	0.35	0.97	1.50 ± 0.01	0.05 ± 0.01
Apr 2004			695	1.54 ± 0.47	21	22	19	37	0.18	0.96	1.38 ± 0.02	0.03 ± 0.01
May 2004			714	1.61 ± 0.51	18	20	19	43	0.15	0.96	1.42 ± 0.01	0.03 ± 0.01
Jun 2004			695	1.67 ± 0.58	12	21	18	49	0.17	0.95	1.56 ± 0.02	0.01 ± 0.01
Jul 2004			743	1.58 ± 0.36	14	24	23	39	0.22	0.95	1.40 ± 0.02	0.05 ± 0.01
Aug 2004			743	1.46 ± 0.37	25	31	16	28	0.23	0.96	1.37 ± 0.02	0.02 ± 0.01
	Sunset optical at 660 nm	Photoacoustic at 1047 nm										
Dec 2003			297	0.91 ± 0.19	79	19	1	0	−0.15	0.99	0.92 ± 0.01	−0.04 ± 0.01
Jan 2004			717	0.82 ± 0.13	59	25	11	5	−0.19	0.98	0.86 ± 0.01	−0.04 ± 0.01
Feb 2004			540	0.79 ± 0.17	48	28	8	14	−0.19	0.99	0.78 ± 0.01	0.00 ± 0.01
Mar 2004			394	0.89 ± 0.22	60	27	4	6	−0.10	0.98	0.79 ± 0.01	0.03 ± 0.01
Apr 2004			682	0.89 ± 0.27	55	27	11	7	−0.06	0.97	0.82 ± 0.01	0.01 ± 0.00
May 2004			712	0.94 ± 0.35	55	28	9	8	−0.04	0.90	0.78 ± 0.01	0.03 ± 0.01
Jun 2004			694	0.92 ± 0.32	57	31	7	4	−0.04	0.96	0.89 ± 0.01	−0.01 ± 0.00
Jul 2004			717	0.98 ± 0.31	69	20	4	7	−0.02	0.85	0.90 ± 0.02	0.02 ± 0.01
Aug 2004			441	1.00 ± 0.32	66	26	4	3	−0.02	0.95	0.95 ± 0.01	0.01 ± 0.01
	Sunset thermal	Photoacoustic at 1047 nm										
Dec 2003			287	1.18 ± 0.42	72	19	3	2	0.18	0.97	1.09 ± 0.02	0.05 ± 0.03
Jan 2004			691	1.21 ± 0.39	62	28	7	3	0.16	0.95	1.08 ± 0.01	0.07 ± 0.02
Feb 2004			448	1.27 ± 0.37	59	27	5	5	0.21	0.96	1.10 ± 0.01	0.11 ± 0.02
Mar 2004			373	1.28 ± 0.56	52	34	6	2	0.12	0.93	1.02 ± 0.02	0.11 ± 0.02
Apr 2004			319	1.05 ± 0.35	54	33	4	3	0.00	0.89	0.82 ± 0.02	0.11 ± 0.02
May 2004			307	1.34 ± 0.79	43	24	6	19	0.06	0.77	0.82 ± 0.04	0.12 ± 0.02
Jun 2004			396	1.00 ± 0.51	41	27	9	15	0.00	0.87	0.94 ± 0.03	0.02 ± 0.01
Jul 2004			579	1.22 ± 0.71	35	29	13	19	0.05	0.62	0.71 ± 0.04	0.18 ± 0.02
Aug 2004			286	1.08 ± 0.35	59	29	4	2	0.02	0.91	0.88 ± 0.02	0.11 ± 0.02
	R&P thermal	Photoacoustic at 1047 nm										
Dec 2003			322	0.57 ± 0.64	17	16	4	57	−0.96	0.81	0.22 ± 0.01	0.21 ± 0.02
Jan 2004			697	0.77 ± 0.84	25	20	13	42	−0.49	0.24	0.15 ± 0.02	0.44 ± 0.03
Feb 2004			665	0.96 ± 1.46	28	21	10	41	−0.37	0.25	0.18 ± 0.03	0.31 ± 0.03
Mar 2004			703	0.81 ± 0.86	28	19	17	36	−0.17	0.13	0.40 ± 0.11	0.27 ± 0.08
Apr 2004			671	0.95 ± 0.62	39	26	12	22	−0.13	0.69	0.26 ± 0.01	0.16 ± 0.01
May 2004			707	1.13 ± 0.72	43	29	12	15	−0.04	0.43	0.29 ± 0.02	0.16 ± 0.01
Jun 2004			367	1.07 ± 0.81	36	30	8	19	−0.07	0.43	0.31 ± 0.03	0.14 ± 0.01

Table 2. Cont.

Sampling period	Methods[a] y	Methods[a] x	No. of Pairs	Average of Ratios ($y/x \pm$ SD)	Distribution of Differences[b] (%) <1σ[c]	1σ–2σ	2σ–3σ	>3σ	Average Difference of $y - x$ (μg/m³)	Correlation (r)	Regression Slope ± Standard Error	Intercept ± Standard Error (μg/m³)
	PAH	Photoacoustic at 1047 nm										
Dec 2003			323	NA NA	NA	NA	NA	NA	NA	0.91	11.42 ± 0.29	1.34 ± 0.51
Jan 2004			NA	NA NA	NA	NA	NA	NA	NA	NA	NA ± NA	NA ± NA
Feb 2004			632	NA NA	NA	NA	NA	NA	NA	0.95	9.49 ± 0.13	−0.78 ± 0.14
Mar 2004			720	NA NA	NA	NA	NA	NA	NA	0.81	8.64 ± 0.24	−1.36 ± 0.17
Apr 2004			683	NA NA	NA	NA	NA	NA	NA	0.76	5.25 ± 0.17	−0.07 ± 0.08
May 2004			706	NA NA	NA	NA	NA	NA	NA	0.77	4.54 ± 0.14	0.22 ± 0.05
Jun 2004			695	NA NA	NA	NA	NA	NA	NA	0.78	3.52 ± 0.11	0.30 ± 0.04
Jul 2004			720	NA NA	NA	NA	NA	NA	NA	0.70	4.06 ± 0.16	−0.07 ± 0.08
Aug 2004			720	NA NA	NA	NA	NA	NA	NA	0.73	4.56 ± 0.16	−0.41 ± 0.11
	2-AE at 880 nm	7-AE at 880 nm										
Dec 2003			719	1.07 ± 0.12	87	9	3	1	0.07	0.99	0.99 ± 0.00	0.09 ± 0.01
Jan 2004			750	1.03 ± 0.11	89	9	2	1	0.03	0.99	0.99 ± 0.01	0.03 ± 0.01
Feb 2004			672	1.04 ± 0.11	89	8	3	1	0.01	0.99	0.96 ± 0.00	0.05 ± 0.01
Mar 2004			720	1.04 ± 0.09	94	5	1	0	0.02	0.99	0.99 ± 0.01	0.03 ± 0.01
Apr 2004			527	1.04 ± 0.21	88	8	2	1	0.01	0.98	1.01 ± 0.01	0.01 ± 0.01
May 2004			252	1.09 ± 0.11	83	13	1	2	0.03	0.99	1.09 ± 0.01	0.00 ± 0.00
Jun 2004			696	1.07 ± 0.10	86	10	3	1	0.03	0.98	1.00 ± 0.01	0.03 ± 0.00
Jul 2004			744	1.09 ± 0.11	81	15	2	1	0.05	0.98	1.05 ± 0.01	0.02 ± 0.01
Aug 2004			744	1.09 ± 0.10	84	11	3	2	0.07	0.99	1.08 ± 0.01	0.01 ± 0.01
Sep 2004			702	1.07 ± 0.12	82	14	3	1	0.05	0.98	1.01 ± 0.01	0.04 ± 0.01
Oct 2004			629	1.14 ± 0.19	73	18	7	2	0.13	0.99	1.03 ± 0.01	0.09 ± 0.01
Nov 2004			660	1.12 ± 0.13	77	16	4	3	0.20	0.99	1.08 ± 0.01	0.05 ± 0.01
	2-AE at 370 nm	7-AE at 370 nm										
Dec 2003			719	1.16 ± 0.26	71	18	6	4	0.22	0.99	1.06 ± 0.01	0.09 ± 0.02
Jan 2004			750	1.10 ± 0.22	71	20	6	3	0.12	0.98	1.02 ± 0.01	0.08 ± 0.02
Feb 2004			672	1.10 ± 0.24	75	18	4	2	0.07	0.99	0.99 ± 0.01	0.08 ± 0.01
Mar 2004			720	1.07 ± 0.16	68	24	5	3	0.05	0.97	1.01 ± 0.01	0.05 ± 0.01
Apr 2004			527	1.07 ± 0.18	72	18	5	3	0.02	0.96	1.02 ± 0.01	0.01 ± 0.01
May 2004			252	1.14 ± 0.16	69	23	2	4	0.04	0.98	1.08 ± 0.01	0.01 ± 0.01
Jun 2004			696	1.12 ± 0.15	67	23	6	4	0.04	0.97	1.00 ± 0.01	0.04 ± 0.01
Jul 2004			744	1.13 ± 0.16	62	26	8	4	0.07	0.96	1.05 ± 0.01	0.04 ± 0.01
Aug 2004			744	1.14 ± 0.15	67	20	8	6	0.09	0.97	1.10 ± 0.01	0.02 ± 0.01
Sep 2004			702	1.12 ± 0.17	64	22	9	5	0.08	0.97	1.02 ± 0.01	0.06 ± 0.01
Oct 2004			629	1.18 ± 0.23	62	22	10	6	0.16	0.98	1.05 ± 0.01	0.10 ± 0.01
Nov 2004			660	1.17 ± 0.20	64	22	8	5	0.29	0.99	1.11 ± 0.01	0.06 ± 0.02
	PAH	7-AE at 370 nm										
Dec 2003			543	NA NA	NA	NA	NA	NA	NA	0.91	7.03 ± 0.14	−0.41 ± 0.40
Jan 2004			NA	NA NA	NA	NA	NA	NA	NA	NA	NA ± NA	NA ± NA
Feb 2004			632	NA NA	NA	NA	NA	NA	NA	0.92	4.70 ± 0.08	−0.40 ± 0.17
Mar 2004			720	NA NA	NA	NA	NA	NA	NA	0.84	5.62 ± 0.13	−1.44 ± 0.15
Apr 2004			696	NA NA	NA	NA	NA	NA	NA	0.74	3.71 ± 0.13	−0.16 ± 0.09
May 2004			719	NA NA	NA	NA	NA	NA	NA	0.71	2.80 ± 0.11	0.33 ± 0.06
Jun 2004			696	NA NA	NA	NA	NA	NA	NA	0.79	2.50 ± 0.07	0.25 ± 0.04
Jul 2004			719	NA NA	NA	NA	NA	NA	NA	0.73	3.17 ± 0.11	−0.24 ± 0.07
Aug 2004			719	NA NA	NA	NA	NA	NA	NA	0.71	3.59 ± 0.13	−0.45 ± 0.12
	DRI/OGC	MAAP at 670 nm										
Dec 2003–Feb 2004	IMPROVE EC	MAAP	13	1.18 ± 0.18	31	23	23	23	0.98	0.33	1.16 ± 0.07	0.01 ± 0.16
June 2004–Aug 2004	IMPROVE EC	MAAP	12	1.12 ± 0.13	67	25	8	0	0.98	0.05	0.94 ± 0.06	0.09 ± 0.03
	DRI/OGC	7-AE at 880 nm										
Dec 2003–Feb 2004	IMPROVE EC	7-AE	15	1.64 ± 0.32	7	7	33	53	0.95	0.88	1.49 ± 0.14	0.13 ± 0.24
June 2004–Aug 2004	IMPROVE EC	7-AE	16	1.23 ± 0.2	69	25	6	0	0.97	0.12	1.08 ± 0.07	0.06 ± 0.05
	Photoacoustic at 1047 nm	MAAP at 670 nm										
Dec 2003			491	0.53 ± 0.09	17	26	12	45	0.99	−1.19	0.55 ± 0.00	−0.05 ± 0.01
Jan 2004			696	0.56 ± 0.08	6	26	24	44	0.99	−0.88	0.54 ± 0.00	0.03 ± 0.01

Table 2. Cont.

Sampling period	Methods[a] y	Methods[a] x	No. of Pairs	Average of Ratios ($y/x \pm$ SD)	Distribution of Differences[b] (%) <1σ[c]	1σ–2σ	2σ–3σ	>3σ	Average Difference of $y - x$ ($\mu g/m^3$)	Correlation (r)	Regression Slope ± Standard Error	Intercept ± Standard Error ($\mu g/m^3$)
Feb 2004			672	0.57 ± 0.17	19	26	13	42	0.99	−0.67	0.54 ± 0.00	0.01 ± 0.01
Mar 2004			719	0.57 ± 0.10	11	18	21	50	0.98	−0.46	0.57 ± 0.00	0.00 ± 0.00
Apr 2004			673	0.62 ± 0.17	17	26	18	39	0.97	−0.25	0.60 ± 0.01	0.01 ± 0.01
May 2004			730	0.64 ± 0.17	18	25	18	39	0.96	−0.17	0.62 ± 0.01	0.00 ± 0.00
Jun 2004			714	0.62 ± 0.15	11	22	23	44	0.97	−0.19	0.61 ± 0.01	0.00 ± 0.00
Jul 2004			743	0.62 ± 0.12	9	21	29	41	0.96	−0.25	0.64 ± 0.01	−0.01 ± 0.01
Aug 2004			168	0.65 ± 0.15	12	35	15	32	0.95	−0.20	0.63 ± 0.02	0.01 ± 0.01
	7-AE at 880 nm	MAAP at 670 nm										
Dec 2003			645	0.75 ± 0.08	46	24	11	19	0.99	−0.63	0.72 ± 0.00	0.04 ± 0.01
Jan 2004			720	0.77 ± 0.08	42	32	14	13	0.99	−0.44	0.74 ± 0.00	0.05 ± 0.01
Feb 2004			672	0.82 ± 0.10	55	21	9	15	0.99	−0.31	0.77 ± 0.00	0.04 ± 0.01
Mar 2004			720	0.90 ± 0.09	80	13	3	4	0.98	−0.10	0.88 ± 0.01	0.03 ± 0.01
Apr 2004			696	0.89 ± 0.10	71	23	3	3	0.99	−0.07	0.88 ± 0.00	0.00 ± 0.00
May 2004			720	0.96 ± 0.14	85	10	3	2	0.98	−0.02	0.91 ± 0.01	0.02 ± 0.00
Jun 2004			695	0.96 ± 0.12	87	11	1	1	0.98	0.02	1.02 ± 0.01	−0.03 ± 0.00
Jul 2004			743	0.95 ± 0.14	83	14	3	1	0.97	−0.03	0.95 ± 0.01	0.00 ± 0.01
Aug 2004			168	0.92 ± 0.08	84	10	4	3	0.99	−0.05	0.86 ± 0.01	0.02 ± 0.01
	7-AE at 660 nm	MAAP at 670 nm										
Dec 2003			645	0.79 ± 0.08	52	23	10	15	0.99	−0.53	0.76 ± 0.00	0.04 ± 0.01
Jan 2004			720	0.81 ± 0.08	51	31	12	7	0.99	−0.36	0.80 ± 0.00	0.02 ± 0.01
Feb 2004			672	0.89 ± 0.11	69	19	6	6	0.99	−0.20	0.85 ± 0.00	0.03 ± 0.01
Mar 2004			720	0.94 ± 0.09	92	6	1	0	0.98	−0.06	0.92 ± 0.01	0.02 ± 0.01
Apr 2004			696	0.94 ± 0.11	83	13	3	1	0.99	−0.04	0.92 ± 0.01	0.01 ± 0.00
May 2004			720	1.00 ± 0.13	86	9	3	2	0.98	0.00	0.93 ± 0.01	0.03 ± 0.00
Jun 2004			695	1.01 ± 0.11	90	8	1	1	0.98	0.01	1.05 ± 0.01	−0.02 ± 0.00
Jul 2004			743	1.00 ± 0.16	86	11	2	1	0.97	0.00	0.99 ± 0.01	0.01 ± 0.01
Aug 2004			168	0.97 ± 0.08	90	6	4	0	0.99	−0.02	0.92 ± 0.01	0.02 ± 0.01
	Sunset optical at 660 nm	MAAP at 670 nm										
Dec 2003			559	0.45 ± 0.05	14	27	17	42	0.99	−1.40	0.49 ± 0.00	−0.06 ± 0.01
Jan 2004			717	0.44 ± 0.05	3	24	26	46	0.99	−1.09	0.48 ± 0.00	−0.04 ± 0.01
Feb 2004			452	0.42 ± 0.05	2	29	21	48	0.99	−1.11	0.43 ± 0.00	−0.01 ± 0.01
Mar 2004			397	0.48 ± 0.06	6	22	25	48	0.98	−0.62	0.47 ± 0.01	0.01 ± 0.02
Apr 2004			361	0.51 ± 0.07	6	23	27	44	0.96	−0.45	0.53 ± 0.01	−0.02 ± 0.01
May 2004			711	0.55 ± 0.07	8	37	22	33	0.97	−0.28	0.57 ± 0.01	−0.01 ± 0.01
Jun 2004			694	0.51 ± 0.07	1	19	43	38	0.98	−0.31	0.61 ± 0.01	−0.05 ± 0.00
Jul 2004			716	0.59 ± 0.10	5	42	32	21	0.95	−0.26	0.69 ± 0.01	−0.05 ± 0.01
Aug 2004			167	0.75 ± 0.17	51	28	12	9	0.90	−0.15	0.72 ± 0.03	0.01 ± 0.02
	Sunset thermal	MAAP at 670 nm										
Dec 2003			559	0.63 ± 0.20	33	22	16	28	0.98	−1.05	0.59 ± 0.01	0.03 ± 0.02
Jan 2004			691	0.65 ± 0.17	27	32	16	25	0.96	−0.74	0.60 ± 0.01	0.05 ± 0.02
Feb 2004			448	0.67 ± 0.19	32	29	19	20	0.98	−0.67	0.61 ± 0.01	0.08 ± 0.02
Mar 2004			373	0.69 ± 0.22	31	29	19	21	0.94	−0.40	0.61 ± 0.01	0.01 ± 0.01
Apr 2004			319	0.58 ± 0.25	17	31	20	32	0.88	−0.38	0.56 ± 0.02	0.03 ± 0.02
May 2004			331	0.68 ± 0.39	26	36	16	22	0.88	−0.19	0.89 ± 0.03	−0.12 ± 0.02
Jun 2004			369	0.63 ± 0.26	20	27	25	28	0.88	−0.25	0.59 ± 0.02	0.02 ± 0.01
Jul 2004			572	0.73 ± 0.39	30	30	19	21	0.70	−0.23	0.54 ± 0.02	0.11 ± 0.02
Aug 2004			94	0.73 ± 0.37	33	27	22	18	0.77	−0.20	0.58 ± 0.05	0.09 ± 0.04

Notes: [a]7-AE (in $\mu g/m^3$) at 370, 660, or 880 nm, 7-AE BC (in $\mu g/m^3$) at λ = 370, 660, 880 nm, respectively; MAAP BC (in $\mu g/m^3$), at λ = 670 nm; R&P thermal, EC (in $\mu g/m^3$) thermally determined by R&P 5400 ambient carbon particulate monitor; IMPROVE EC (in $\mu g/m^3$), measured by the DRI/OGC TOR carbon analyzer following the IMPROVE protocol; Sunset optical, EC (in $\mu g/m^3$) optically determined (λ = 660 nm) with the Sunset Laboratory carbon analyzer; Sunset thermal, EC (in $\mu g/m^3$) determined by Sunset Laboratory carbon analyzer following the NIOSH 5040 protocol; PAH, particle-bound PAHs (in tA) measured by photoelectric aerosol sensor monitor; [b]Fraction of pairs in percent with which the difference ($y - x$) is less than or greater than one, two, or three times propagated measurement uncertainty (note that the precision interval, σ, is different from the mass absorption efficiency, σ_{abs}); [c]Measurement uncertainty of ($y - x$).

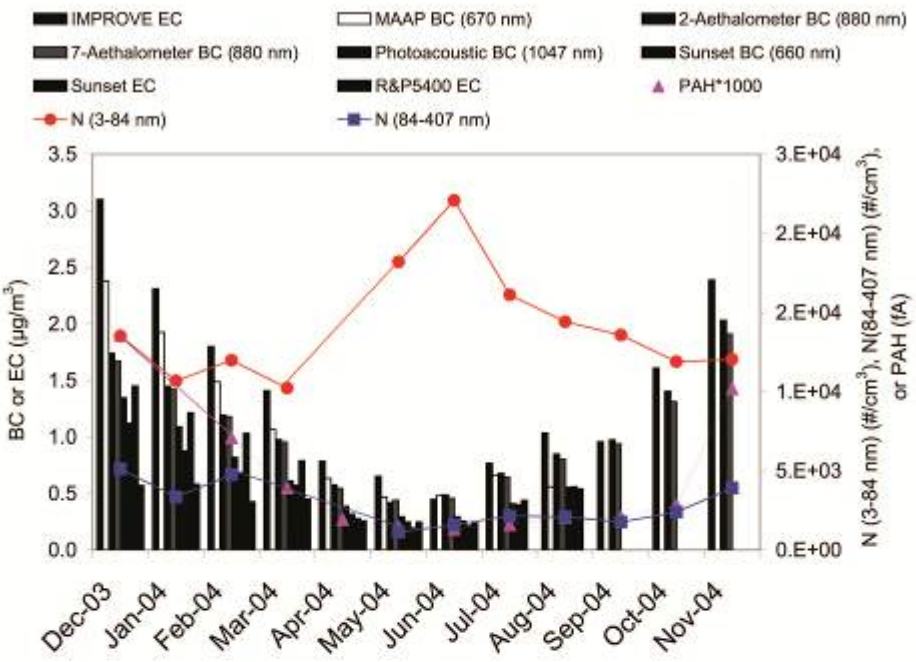

Figure 1. Monthly averages of BC or EC concentrations measured by eight carbon methods, particle-bound PAH, and particle number concentrations in two size ranges (3–84 nm and 84–407 nm) for ambient samples at the Fresno Supersite from December 2003 to November 2004.

Figure 1. The average of y/x with its standard deviation, the distribution of the difference $(y - x)$ between data pairs where σ is the measurement uncertainty (i.e., the square root of the sum of squared uncertainties), the average of the differences $(\overline{y - x})$, the linear correlation coefficient (r), and the regression slopes and intercepts with standard errors are calculated for each comparison.[28]

Data-pair requirements for carbon equivalence are met when the regression slope is 1 ± 0.05, the regression intercept is 0 ± 1 μg/m^3 ($r > 0.97$), and the collocated precision is 2 μg/m^3 or 5% (whichever is larger).[28] Comparability is attained when the regression slope equals unity within three standard errors, the regression intercept does not differ from zero by more than three standard errors, and r is >0.9. Predictability is attained when r is >0.9, but the slope and intercept exceeded those required for comparability. The equivalence criteria were established for $PM_{2.5}$ mass comparison by the U.S. Environmental Protection Agency and are too stringent for the comparison of $PM_{2.5}$ components.

As shown in Table 2, the average difference $(\overline{y - x})$ was typically <0.5 μg/m^3 with a few exceptions, and in no case did the $\overline{y - x}$ exceed 1.4 μg/m^3 of BC. The collocated 7-AE BC and 2-AE BC results met the equivalence criteria except during the months of May, August, and November 2004, when slopes were within ~10% of unity; hereafter, the 7-AE BC results are used to represent aethalometer BC. The filter-based IMPROVE EC results are highly correlated with the photoacoustic BC results ($0.97 < r < 0.99$), but the IMPROVE EC slope indicates a 1.5 to 2 times higher concentration than the photoacoustic analyzer, using the $\sigma_{abs}(1047) = 5$ m^2/g conversion. Compared with the photoacoustic BC results, the MAAP BC, 7-AE BC, Sunset optical (BC), Sunset thermal EC, and PAH values in winter also show high correlations ($r > 0.9$), but the slopes and average ratios differ from unity. The intercepts for these comparisons are well within 1 μg/m^3, but the slopes vary from unity within a factor of 2. Photoacoustic BC was much lower than either aethalometer or MAAP BC, as evidenced by the high slopes (1.3–2).

Sunset thermal EC results correlate better with the photoacoustic BC results in winter (December 2003 to February 2004; $0.95 < r < 0.97$) than in summer (June to August 2004; $0.62 < r < 0.91$), with slopes indicating a Sunset EC ~10% higher than the photoacoustic BC in winter and 5–30% lower than photoacoustic BC in summer. Compared with photoacoustic BC, the distribution of differences shows that ~80% of the Sunset thermal and ~85% of Sunset optical BC values are within ±3 precision intervals. Particle-bound PAH levels show higher correlations with photoacoustic BC for winter ($0.91 < r < 0.95$) than for summer ($0.70 < r < 0.78$). The R&P 5400 EC is not well correlated with the photoacoustic BC except for December 2003 ($r = 0.81$).

When the MAAP ($\lambda = 670$ nm) BC or 7-AE value is used as the benchmark, IMPROVE EC meets the requirements for comparability. The IMPROVE EC versus MAAP BC comparison almost meets the equivalence criteria in summer except for a lower slope (0.94 ± 0.06). The MAAP

Table 3. Comparisons of carbon measurement methods with overall averages of BC or EC for collocated periods between December 1, 2003, and November 30, 2004, at the Fresno Supersite.

Sampling Period	Methods: y[b]	Methods: x	No. of Pairs	Average of Ratios y/x ± SD	Distribution of Differences (%): <1σ[a]	1σ–2σ	2σ–3σ	>3σ	Correlation (r)	Average Difference of y − x	Regression Slope ± Standard Error	Intercept ± Standard Error
	IMPROVE EC	All methods average										
Winter			15	1.58 ± 0.22	20	67	7	7	0.98	0.85	1.50 ± 0.08	0.07 ± 0.15
Summer			15	1.38 ± 0.14	67	33	0	0	0.99	0.18	1.19 ± 0.03	0.08 ± 0.02
Dec 2003–Aug 2004			45	1.45 ± 0.21	62	20	13	4	0.98	0.42	1.53 ± 0.04	−0.07 ± 0.05
	7-AE at 880 nm	All methods average										
Winter			15	0.98 ± 0.09	100	0	0	0	0.99	−0.03	0.96 ± 0.04	0.03 ± 0.08
Summer			15	1.14 ± 0.01	93	7	0	0	0.99	0.08	1.15 ± 0.05	0.00 ± 0.03
Dec 2003–Aug 2004			45	1.08 ± 0.12	100	0	0	0	0.99	0.04	0.96 ± 0.02	0.08 ± 0.03
	Photoacoustic at 1047 nm	All methods average										
Winter			15	0.72 ± 0.06	71	21	7	0	0.99	−0.41	0.72 ± 0.02	0.01 ± 0.04
Summer			15	0.76 ± 0.06	87	13	0	0	0.99	−0.13	0.78 ± 0.02	−0.01 ± 0.02
Dec 2003–Aug 2004			44	0.74 ± 0.07	73	23	2	2	0.99	−0.24	0.72 ± 0.02	0.01 ± 0.02
	Sunset optical at 660 nm	All methods average										
Winter			14	0.57 ± 0.06	21	71	7	0	0.99	−0.66	0.69 ± 0.02	−0.16 ± 0.03
Summer			14	0.73 ± 0.12	86	14	0	0	0.98	−0.13	0.96 ± 0.06	−0.11 ± 0.04
Dec 2003–Aug 2004			41	0.66 ± 0.14	73	12	15	0	0.98	−0.34	0.64 ± 0.02	0.01 ± 0.03
	Sunset thermal	All methods average										
Winter			14	0.81 ± 0.08	86	14	0	0	0.99	−0.30	0.76 ± 0.03	0.08 ± 0.06
Summer			12	0.75 ± 0.18	92	8	0	0	0.98	−0.12	0.98 ± 0.06	−0.11 ± 0.04
Dec 2003–Aug 2004			35	0.78 ± 0.18	96	4	0	0	0.98	−0.21	0.81 ± 0.03	−0.01 ± 0.04
	MAAP at 670 nm	All methods average										
Winter			14	1.30 ± 0.07	57	36	7	0	1.00	0.50	1.35 ± 0.02	−0.05 ± 0.04
Summer			12	1.21 ± 0.06	100	0	0	0	1.00	0.10	1.27 ± 0.03	−0.02 ± 0.01
Dec 2003–Aug 2004			41	1.24 ± 0.10	71	15	12	2	1.00	0.26	1.34 ± 0.02	−0.05 ± 0.02

Notes: [a]The precision interval, σ, is different from the mass absorption efficiency, σ_{abs}. [b]See Table 2 for different measurement method specifications.

BC values are typically 30–50% higher than the photoacoustic and Sunset BC values, with small intercepts (≤0.1 ± 0.02 μg/m³). The best comparison is found for 7-AE values at λ = 660 or 880 nm and MAAP BC values, for which >70% of the samples are within ±2 precision intervals and >80% of the samples are within ±3 precision intervals.

Table 3 compares values from each instrument with the overall averages of all measurements, weighted by the number of available data points. BC or EC values from each method correlate well with the average ($r \geq 0.98$), but regression slopes range from 0.64 (Sunset optical BC) to 1.53 (IMPROVE EC). For the overall averages, Sunset optical BC and Sunset thermal EC meet the comparability criteria during summer, whereas 7-AE BC meets the criteria in both winter and summer seasons. Deviations from unity are 10–20% higher for winter (from −31% [Sunset optical] to +50% [IMPROVE EC]) than for summer (from −22% [photoacoustic] to +27% [MAAP]). The distribution of differences shows that >85% of the samples are within ±2 precision intervals and >90% of the samples are within ±3 precision intervals. All of the samples are within ±1 precision interval for the aethalometer in both the winter and annual periods and for the MAAP in summer.

Seasonal Variation

As shown in Figure 1, monthly averaged BC or EC concentrations were ~2.2 to 3.4 times higher during winter than summer. This is because of higher BC or EC contributions from traffic emissions in cold conditions, heating (including RWC), and accumulation of pollutants in a shallow surface layer during non-daylight hours. $PM_{2.5}$ BC and EC concentrations among different methods differed by as much as a factor of 5 during the winter, with IMPROVE EC being the highest and R&P 5400 EC being the lowest. Despite their similarities, the three thermal methods (IMPROVE, Sunset, and R&P 5400) yielded monthly EC concentrations ranging from 0.2 μg/m³ (Sunset) to 3.1 μg/m³ (IMPROVE), with 3-fold higher EC concentrations in winter (1.39 ug/m³) than in summer (0.46 μg/m³). Different temperature- and charring-correction protocols give different values of EC at Fresno.[17,29]

The three optical methods (MAAP, 7-AE, and Sunset optical) yielded monthly BC concentrations from 0.25 μg/m³ (Sunset) to 2.38 μg/m³ (15.5 Mm^{-1}; MAAP), also approximately three times higher in winter (1.42 ug/m³) than in summer (0.54 μg/m³). The monthly averaged PAH concentration was consistent with the variation of BC or EC concentrations, with PAH concentrations six times higher in winter than summer.

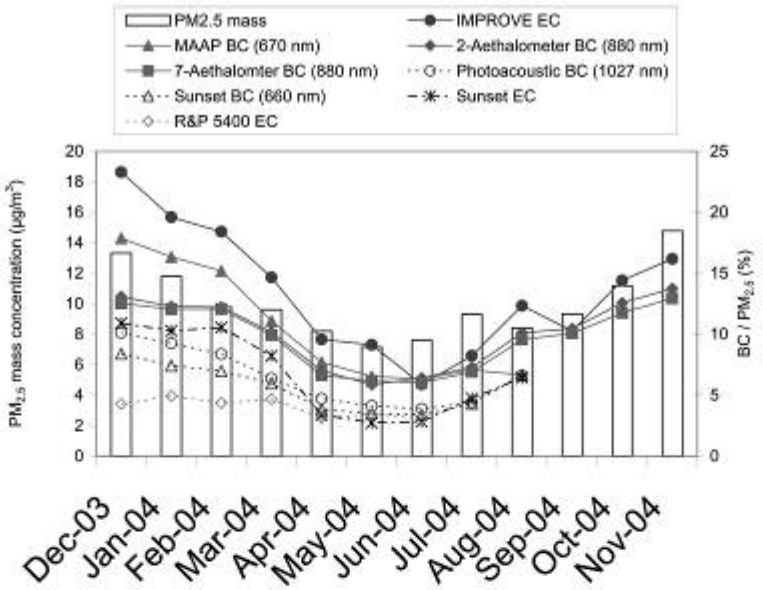

Figure 2. Monthly averages of $PM_{2.5}$ by TEOM and the ratio of BC or EC to $PM_{2.5}$ by IMPROVE, by MAAP (λ = 670 nm), by 2-AE (λ = 880 nm), by 7-AE (λ = 880 nm), by photoacoustic instrument (λ = 1047 nm), by Sunset optical (λ = 660 nm), by Sunset thermal, or by R&P 5400.

Ultrafine particle-number concentrations in the 3–84 nm size range [N(3–84 nm)] were higher during the summer, whereas the accumulation mode particle-number concentrations in the 84–407 nm range followed the BC or EC seasonal pattern. Watson et al.[47,51] observed frequent secondary ultrafine particle events during late spring through early fall. BC or EC are derived from primary emissions that accumulate during the winter when dispersion is low.[50]

Figure 2 shows how BC and EC concentrations varied with $PM_{2.5}$ throughout the year. The ratio of BC or EC to $PM_{2.5}$ ranged from 7% to 23% during winter and from 3% to 12% during summer (exclusive of the R&P 5400). Figure 3 shows how OC/EC ratios varied throughout the year. $PM_{2.5}$ OC/EC ratios were >78% higher during the summer (5.7) than during winter (3.2). This may result from (1) many EC concentrations during summer that were near the lower quantifiable limits, resulting in higher uncertainty in the denominator (EC concentrations were <1 μg/m^3 for ~75% of the days during summer); (2) higher contributions from secondary organic aerosol (SOA) during summer; (3) larger contributions from cold-vehicle starts during winter, which produce larger portions of EC in the exhaust; and (4) contributions from summertime forest fires in the surrounding mountains.

Ultrafine SOA[47,51] in relation to carbon levels is examined in Figure 4. N(84–407 nm) was reasonably correlated (r −0.75 to 0.78) with BC concentration regardless of the season. However, N(3–84 nm) was not related to BC levels in summer, consistent with condensation of organic vapors on sulfuric acid nuclei formed by photochemical.

Mass Absorption Efficiencies

The 24-hr averaged b_{abs} from the MAAP, the 7-AE, and the photoacoustic analyzer were compared with filter-based IMPROVE EC to estimate σ_{abs} applicable to the Fresno aerosol. As shown in Figure 5, σ_{abs} is 5.5 m^2/g for MAAP (670 nm), 10 m^2/g for 7-AE (880 nm), and 2.3 m^2/g for the photoacoustic analyzer (1047 nm); these values are substantially different from the assumed values of 6.5, 16.6, and 5 m^2/g for the MAAP, 7-AE, and photoacoustic analyzer, respectively. The wavelength dependence of $b_{abs}(\lambda)$ and $\sigma_{abs}(\lambda)$ and the different exponents (α) in the $\lambda^{-\alpha}$ scaling factor, owing to changing particle compositions and shapes, lead to different relationships between BC and b_{abs}. Table 4 compares σ(670 nm) for λ^{-1}, λ^{-2} (typical of biomass burning[7]), and $\lambda^{-2.7}$ (found in ambient Denver, CO, aerosol by Moosmüller et al.[52]) for these instruments. The σ_{abs}(670 nm) values for the 7-AE and photoacoustic analyzer increase by a factor of 3 with α increasing from 1 to 2.7. At α = 2, σ_{abs}(670 nm) values for the 7-AE and photoacoustic analyzer differ only by 4 and 12% from the default σ_{abs}, respectively. With λ^{-2} scaling, the MAAP and photoacoustic analyzer had similar σ_{abs}(670 nm) values of 5.5 and 5.6 m^2/g, respectively.

Comparison of daily averaged 7-AE values with BC values at λ = 370 nm versus λ = 880 nm (Figure 6) shows that the built-in λ^{-1} scaling is consistent during summer, whereas a $\lambda^{-1.3}$ better approximates the situation during winter. As shown in Table 2, aethalometer (λ = 880 nm) and photoacoustic analyzer (λ = 1047 nm) BC values were correlated (r = 0.95–0.99) for winter and summer. Comparison between the aethalometer BC value at λ = 950 nm and photoacoustic BC yielded similar results. Absorption at longer wavelengths is less prone to deviation than

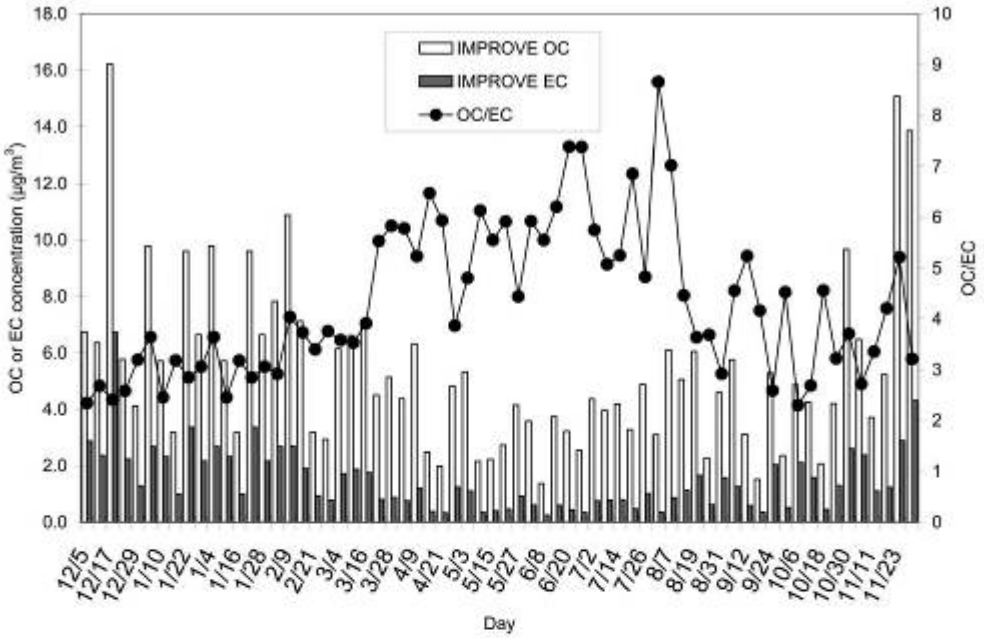

Figure 3. Twenty-four hour averages of OC and EC concentrations, and the OC/EC ratio measured by the DRI/OGC TOR carbon analyzer following the IMPROVE protocol for the period of December 2003 to November 2004.

absorption at shorter wavelengths. The assumed aethalometer σ_{abs}(880 nm) of 16.6 m^2/g may not apply because of a lack of consideration of multiple scattering effects in the aethalometer. This is evident in Figure 7a, as 7-AE b_{abs}(670 nm) ranges from 2.63 (winter) to 3.38 (summer) times higher than the MAAP b_{abs}, although they are highly correlated (r = 0.98–0.99). As shown in Figure 7b, MAAP b_{abs} is 1.52 (winter) to 1.23 (summer) times higher than the photoacoustic b_{abs}, still with a high correlation of 0.96–0.99. Better regression slopes of 1.33 (winter) and 1.07 (summer) can be obtained for the MAAP versus photoacoustic comparison if α = 1.3 is used (determined by Schnaiter et al.[25] with diesel exhaust).

As noted earlier, the σ_{abs}(1047 nm) of 5 m^2/g for the photoacoustic analyzer was derived from simultaneous measurements of diesel exhaust by IMPROVE EC.[40] As shown in Tables 2 and 3, this is not an appropriate assumption for the Fresno summer or winter aerosols. The 5 m^2/g assumption is also inconsistent with the suggestion of Bond and Bergstrom[14] cited above for fresh particle emissions, which yields a 1 SD range of 3.3–4.6 m^2/g at λ = 1047 nm assuming a λ^{-1} scaling. This range is 1.7–2.5 m^2/g with a λ^{-2} scaling. An α between 1 and 2 might be more appropriate for mixed and aged aerosol such as that found at the Fresno Supersite.

It is evident that wavelength has an important effect on the conversion of b_{abs} to BC. BC values obtained at different wavelengths might be useful in separating vegetative burning from other sources by use of receptor models.[53–55]

Diurnal Variations of the Single Scattering Albedo

The single scattering albedo ($\omega = b_{scat}/[b_{scat} + b_{abs}]$) was calculated using b_{scat}(530 nm) values obtained by nephelometer and b_{abs} (scaled from 1047 to 530 nm assuming λ^{-1}) values obtained by the photoacoustic analyzer. Higher values of daily ω were observed in winter (0.89) than in summer (0.80), consistent with particles containing more scattering species during winter. Higher RH in winter increases b_{scat} and therefore contributes to the higher ω. As shown in Figure 8, in winter the lowest ω occurred during the early morning rush hour of ~7:00 a.m. Pacific Standard Time (PST) and at ~8:00 p.m. PST. In summer, the lowest ω occurred at ~6:00 a.m. and at 7:00 p.m. PST. Times of low ω coincided with the peak b_{abs} occurrences. Although the evening b_{abs} peak was higher and broader than the morning b_{abs} peak in winter, the values of ω were comparable during both seasons.

Diurnal Variations of BC Concentrations

As shown in Figure 9, the dual peaks for hourly average BC levels were 7:00–8:00 a.m. PST and 8:00–10:00 p.m. PST in winter. The large evening peak persisted through midnight and early morning of the following day. This is consistent with increased emissions from morning and evening traffic and from RWC emissions that accumulate under the surface inversion during winter evenings.[50] In summer, the morning BC peak occurred at ~6:00 a.m. PST with a small evening peak at ~8:00 p.m. PST. The times of the peak concentrations of PAH, NO_x, and CO coincided

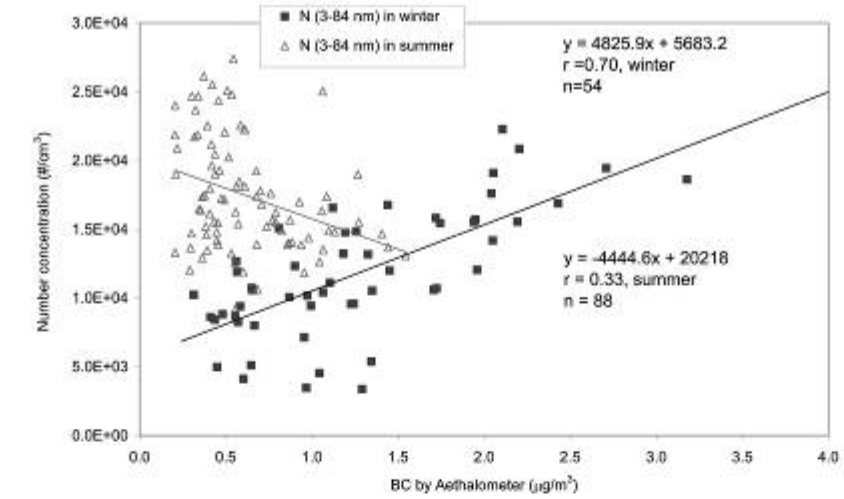

(a)

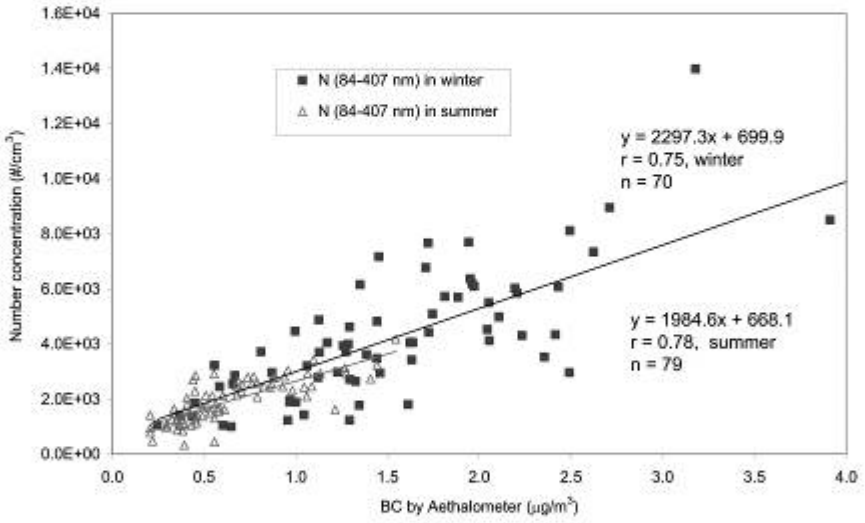

(b)

Figure 4. Particle number concentrations in the size ranges of (a) 3–84 nm and (b) 84–407 nm by the SMPS versus BC concentration by 7-AE (λ = 880 nm) for daily average in winter (December 2003 to February 2004) and summer (June to August 2004).

with the BC peak, and these followed similar seasonal patterns (i.e., the evening peak was more dominant in winter than in summer). The morning $PM_{2.5}$ peak lagged behind the BC peak by 1 to 2 hr. $PM_{2.5}$ NO_3^- levels increased after 7:00 a.m. PST in winter. The time for increasing NO_3^- is consistent with times for increasing temperature and decreasing BC, NO_x, and CO. This is consistent with NO_3^- formation above the surface layer with downward mixing when the layers couple.[50] During summer, the NO_3^- concentrations increased until ~8:00 a.m. PST and then decreased until the late afternoon, consistent with evaporation as temperatures increase.

CONCLUSIONS

$PM_{2.5}$ BC or EC concentrations at the Fresno Supersite are higher in winter than in summer. This is consistent with primary combustion emissions from traffic and home heating that accumulate under a shallow surface layer during winter nights. Similar seasonal patterns are observed for $PM_{2.5}$ mass, NO_3^-, PAH, NO_x, CO, ω, and

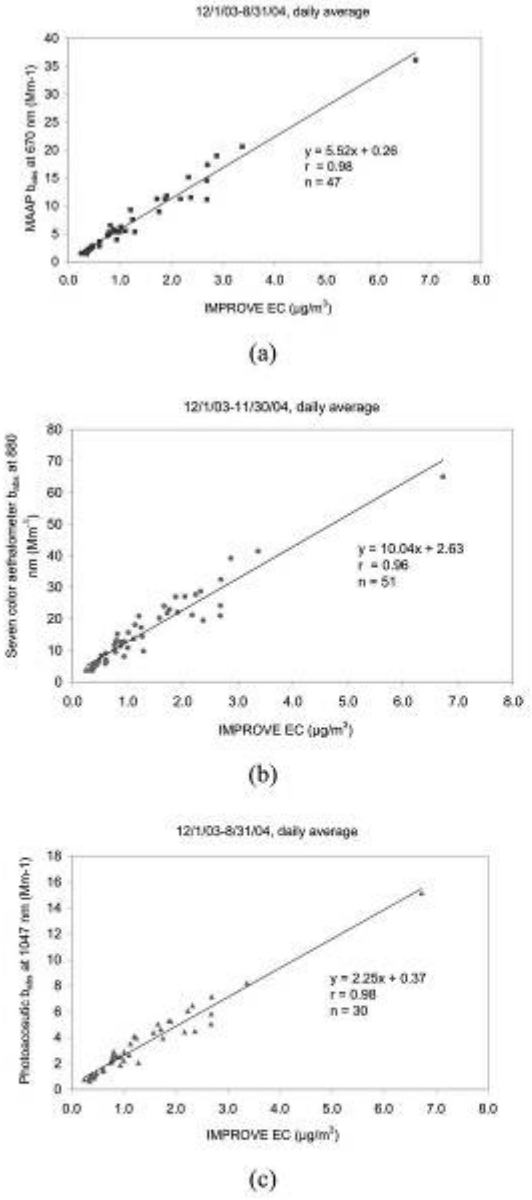

Figure 5. Mass absorption efficiencies calculated with (a) MAAP (λ = 670 nm), (b) 7-AE (λ = 880 nm), and (c) photoacoustic analyzer (λ = 1047 nm) versus IMPROVE EC concentrations. The aethalometer light attenuation is reported as light absorption without any calibration factor.

number concentration for particles in the accumulation mode [N(84–407 nm)]. The diurnal pattern of BC is consistent with those for PAH, NO_x, and CO, indicating that primary combustion emissions accumulate during early morning and night and decrease as the mixing layer increases, especially during the winter. Higher ratios of BC at λ = 370 nm to BC at λ = 880 nm occur during the winter, consistent with a larger contribution from RWC that absorbs more in the UV part of the spectrum. The number of ultrafine particles (3–84 nm) and the OC/EC ratio are lower during winter than summer, both of which are consistent with formation of SOA through vapor condensation.

Compared with IMPROVE EC, mass absorption efficiencies for Fresno are 5.5 m^2/g for the MAAP at 670 nm, 10 m^2/g for the aethalometer at 880 nm, and 2.3 m^2/g for the photoacoustic analyzer at 1047 nm. These differ from the assumed values of 6.5 m^2/g for the MAAP, 16.6 m^2/g for the aethalometer, and 5 m^2/g for the photoacoustic analyzer.

Intercomparisons show good correlations among all BC or EC measures except for the R&P 5400 EC, but with slopes ranging from 0.2 to 2. The degree of comparability differed between winter and summer, reinforcing the difference in aerosol composition with the season; σ_{abs} does not scale as λ^{-1} at Fresno.

ACKNOWLEDGMENTS

The Fresno Supersite is a cooperative effort between the California Air Resources Board (ARB) and the DRI. Sponsorship is provided by the U.S. Environmental Protection Agency through the Cooperative Institute for Atmospheric Sciences and Terrestrial Applications (CIASTA) of the National Oceanic and Atmospheric Administration and the California Regional Particulate Air Quality Study (CRPAQS) under the management of Ms. Karen Magliano of the ARB. This work was partially supported by U.S. Environmental Protection Agency STAR Grant No. RD-83108601-0. The conclusions are those of the authors and do not necessarily reflect the views of the sponsoring agencies. Any mention of commercially available products and supplies does not constitute an endorsement of those products and supplies. The authors thank Scott Scheller of the ARB and Dr. Susanne Hering of Aerosol Dynamics, Inc., for their efforts in maintaining the monitoring instruments. Dr. John Bowen, Steve Kohl, and Ms. Barbara Hinsvark of DRI assisted in field coordination, laboratory operations, and data processing of Supersite measurements. Ms. Jo Gerrard and Tim Richard of DRI assisted with assembling and editing the manuscript.

REFERENCES

1. Watson, J.G. Visibility: Science and Regulation; *J. Air & Waste Manage. Assoc.* **2002**, *52*, 628-713.
2. Watson, J.G. Visibility: Science and Regulation - A Summary of the 2002 Critical Review; *EM* **2002**, *8*, 36-43.
3. Jacobson, M.Z. Control of Fossil-Fuel Particulate Black Carbon plus Organic Matter, Possibly the Most Effective Method of Slowing Global Warming; *J. Geophys. Res.* **2002**, *107*, ACH 16-1-ACH 16-22.
4. Vedal, S. Critical Review - Ambient Particles and Health: Lines That Divide; *J. Air & Waste Manage. Assoc.* **1997**, *47*, 551-581.
5. Watson, J.G.; Chow, J.C.; Chen, L.-W.A. Summary of Organic and Elemental Carbon/Black Carbon Analysis Methods and Intercomparisons; *Aerosol Air Qual. Res.* **2005**, *1*, 69-102.
6. Horvath, H. Atmospheric Light Absorption - A Review; *Atmos. Environ.* **1993**, *27A*, 293-317.
7. Kirchstetter, T.W.; Novakov, T.; Hobbs, P.V. Evidence That the Spectral Dependence of Light Absorption by Aerosols Is Affected by Organic Carbon; *J. Geophys. Res.* **2004**, *109*, D21208.
8. Bond, T.C.; Anderson, T.L.; Campbell, D.E. Calibration and Intercomparison of Filter-based Measurements of Visible Light Absorption by Aerosols; *Aerosol Sci. Technol.* **1999**, *30*, 582-600.

Table 4. Comparisons of assumed absorption coefficients with measured values and wavelength-corrected absorption efficiencies.

Instruments	Assumed Absorption Efficiency (m^2/g)[a]	Fresno Absorption Efficiency at Instrument λ (m^2/g)[b]	Estimated Absorption Efficiency		
			Scaled by λ^{-1} to 670 nm[c]	Scaled by $\lambda^{-2.0}$ to 670 nm	Scaled by $\lambda^{-2.7}$ to 670 nm
MAAP (670 nm)	6.5	5.5	5.5	5.5	5.5
7-AE (880 nm)	16.6[d]	10.0	13.1	17.3	27.4
Photoacoustic analyzer (1047 nm)	5.0	2.3	3.5	5.6	11.7

Notes: [a]Conversion factors assumed to convert light absorption (for MAAP and photoacoustic analyzer) or light attenuation (for 7-AE) to BC concentration; [b]Regression slope from light absorption (for MAAP and photoacoustic analyzer) or light attenuation (for 7-AE) vs IMPROVE EC concentration; [c]Based on the Angstrom Power Law with different exponents ($b_{abs} \sim \lambda^{-\alpha}$): $\alpha = 1$ by Angstrom Power Law; $\alpha = 2$ by Kirchstetter et al.[7]; and $\alpha = 2.7$ by Moosmüller et al.[57]; [d]Based on 14,625/λ at 880 nm; the aethalometer light attenuation (Mm^{-1}) is reported as light absorption without any calibration factor in this study.

9. Lindberg, J.D.; Douglass, R.E.; Garvey, D.M. Atmospheric Particulate Absorption and Black Carbon Measurement; *Appl. Opt.* **1999**, *38*, 2369-2376.
10. Petzold, A.; Schönlinner, M. Multi-angle Absorption Photometry - A New Method for the Measurement of Aerosol Light Absorption and Atmospheric Black Carbon; *J. Aerosol Sci.* **2004**, *35*, 421-441.
11. Fuller, K.A.; Malm, W.C.; Kreidenweis, S.M. Effects of Mixing on Extinction by Carbonaceous Particles; *J. Geophys. Res.* **1999**, *104*, 15941-15954.
12. Martins, J.V.; Artaxo, P.; Liousse, C.; Reid, J.S.; Hobbs, P.V.; Kaufman, Y.J. Effects of Black Carbon Content, Particle Size, and Mixing on Light Absorption by Aerosols from Biomass Burning in Brazil; *J. Geophys. Res.* **1998**, *103*, 32041-32050.
13. Liousse, C.; Cachier, H.; Jennings, S.G. Optical and Thermal Measurements of Black Carbon Aerosol Content in Different Environments: Variation of the Specific Attenuation Cross-section, Sigma (σ); *Atmos. Environ.* **1993**, *27A*, 1203-1211.
14. Bond, T.C.; Bergstrom, R.W. Light Absorption by Carbonaceous Particles: An Investigative Review; *Aerosol Sci. Technol.* **2006**, *40*, 27-67.
15. Chow, J.C.; Watson, J.G. $PM_{2.5}$ Carbonate Concentrations at Regionally Representative Interagency Monitoring of Protected Visual Environment Sites; *J. Geophys. Res.* **2002**, *107*, ICC 6-1-ICC 6-9.
16. Cao, J.J.; Lee, S.C.; Zhang, X.Y.; Chow, J.C.; An, Z.S.; Ho, K.F.; Watson, J.G.; Fung, K.K.; Wang, Y.Q.; Shen, Z.X. Characterization of Airborne Carbonate over a Site near Asian Dust Source Regions during Spring 2002 and Its Climatic and Environmental Significance; *J. Geophys. Res.* **2005**, *110*, 1-8.
17. Chow, J.C.; Watson, J.G.; Chen, L.-W.A.; Arnott, W.P.; Moosmüller, H.; Fung, K.K. Equivalence of Elemental Carbon by Thermal/Optical Reflectance and Transmittance with Different Temperature Protocols; *Environ. Sci. Technol.* **2004**, *38*, 4414-4422.
18. Chen, L.-W.A.; Chow, J.C.; Watson, J.G.; Moosmüller, H.; Arnott, W.P. Modeling Reflectance and Transmittance of Quartz-Fiber Filter Samples Containing Elemental Carbon Particles: Implications for Thermal/Optical Analysis; *J. Aerosol. Sci.* **2004**, *35*, 765-780.
19. Currie, L.A.; Benner, B.A., Jr.; Cachier, H.; Cary, R.; Chow, J.C.; Druffel, E.R.M.; Eglinton, T.I.; Gustafsson, Ö.; Hartmann, P.C.; Hedges, J.I.; Kessler, J.D.; Kirchstetter, T.W.; Klinedinst, D.B.; Klouda, G.A.; Marolf, J.V.; Masiello, C.A.; Novakov, T.; Pearson, A.; Prentice, K.M.; Puxbaum, H.; Quinn, J.G.; Reddy, C.M.; Schmid, H.; Slater, J.F.; Watson, J.G.; Wise, S.A. A Critical Evaluation of Interlaboratory Data on Total, Elemental, and Isotopic Carbon in the Carbonaceous Particle Reference Material, NIST SRM 1649a; *J. Res. Natl. Bur. Stand. (U.S.)* **2002**, *107*, 279-298.
20. Arnott, W.P.; Moosmüller, H.; Rogers, C.F.; Jin, T.; Bruch, R. Photoacoustic Spectrometer for Measuring Light Absorption by Aerosol: Instrument Description; *Atmos. Environ.* **1999**, *33*, 2845-2852.
21. Bell, A.G. Production of Sound by Radiant Energy; *The Manufacturer and Builder*, **1881**, *15*, 156-158.
22. Bruce, C.W.; Pinnick, R.G. *In-Situ* Measurements of Aerosol Absorption with a Resonant CW Laser Spectrophone; *Appl. Opt.* **1977**, *16*, 1762-1764.
23. Saathoff, H.; Naumann, K.H.; Schnaiter, M.; Schöck, W.; Weingartner, E.; Baltensperger, U.; Krämer, L.; Bozoki, Z.; Pöschl, U.; Niessner, R.; Schurath, U. Carbon Mass Determinations during the AIDA Soot Aerosol Campaign 1999; *J. Aerosol Sci.* **2003**, *34*, 1399-1420.
24. Saathoff, H.; Moehler, O.; Schurath, U.; Kamm, S.; Dippel, B.; Mihelcic, D. The AIDA Soot Aerosol Characterisation Campaign 1999; *J. Aerosol Sci.* **2003**, *34*, 1277-1296.
25. Schnaiter, M.; Horvath, H.; Mohler, O.; Naumann, K.H.; Saathoff, H.; Schock, O.W. UV-VIS-NIR Spectral Optical Properties of Soot and Soot-containing Aerosols; *J. Aerosol. Sci.* **2003**, *34*, 1421-1444.
26. Sheridan, P.J.; Arnott, W.P.; Ogren, J.A.; Andrews, E.; Atkinson, D.B.; Covert, D.S.; Moosmüller, H.; Petzold, A.; Schmid, B.; Strawa, A.W.; Varma, R.; Virkkula, A. The Reno Aerosol Optics Study: An Evaluation of Aerosol Absorption Measurement Methods; *Aerosol. Sci. Technol.* **2005**, *39*, 1-16.
27. Watson, J.G.; Chow, J.C.; Bowen, J.L.; Lowenthal, D.H.; Hering, S.; Ouchida, P.; Oslund, W. Air Quality Measurements from the Fresno Supersite; *J. Air & Waste Manage. Assoc.* **2000**, *50*, 1321-1334.
28. Watson, J.G.; Chow, J.C. Comparison and Evaluation of In-Situ and Filter Carbon Measurements at the Fresno Supersite; *J. Geophys. Res.* **2002**, *107*, ICC 3-1-ICC 3-15.
29. Chow, J.C.; Watson, J.G.; Lowenthal, D.H.; Solomon, P.A.; Magliano, K.L.; Ziman, S.D.; Richards, L.W. PM_{10} and $PM_{2.5}$ Compositions in California's San Joaquin Valley; *Aerosol. Sci. Technol.* **1993**, *18*, 105-128.
30. Chow, J.C.; Chen, L.-W.A.; Watson, J.G.; Lowenthal, D.H.; Magliano, K.; Turkiewicz, K.; Lehrman, D. $PM_{2.5}$ Chemical Composition and Spatiotemporal Variability during the California Regional $PM_{10}/PM_{2.5}$ Air Quality Study (CRPAQS); *J. Geophys. Res.* **2006**, in press.
31. Hansen, A.D.A.; Rosen, H.; Novakov, T. The Aethalometer - An Instrument for the Real-Time Measurement of Optical Absorption by Aerosol Particles; *Sci. Total Environ.* **1984**, *36*, 191-196.
32. Arnott, W.P.; Hamasha, K.; Moosmüller, H.; Sheridan, P.J.; Ogren, J.A. Towards Aerosol Light-Absorption Measurements with a 7-Wavelength Aethalometer: Evaluation with a Photoacoustic Instrument and 3-Wavelength Nephelometer; *Aerosol Sci. Technol.* **2005**, *39*, 17-29.
33. Petzold, A.; Kramer, H.; Schönlinner, M. Continuous Measurement of Atmospheric Black Carbon Using a Multi-angle Absorption Photometer; *Environ. Sci. Pollut. Res.* **2002**, *Special Issue*, 478-82.
34. Petzold, A.; Schloesser, H.; Sheridan, P.J.; Arnott, W.P.; Ogren, J.A.; Virkkula, A. Evaluation of Multiangle Absorption Photometry for Measuring Aerosol Light Absorption; *Aerosol Sci. Technol.* **2005**, *39*, 40-51.
35. VDI Measurement of Soot (Ambient Air)—Thermographic Determination of Elemental Carbon after Thermal Desorption of Organic Carbon; Berein Deutscher: Dusseldorf, Germany, 1999, (2465 Patt 2).
36. Schmid, H.P.; Laskus, L.; Abraham, H.J.; Baltensperger, U.; Lavanchy, V.M.H.; Bizjak, M.; Burba, P.; Cachier, H.; Crow, D.; Chow, J.C.; Gnauk, T.; Even, A.; ten Brink, H.M.; Giesen, K.P.; Hitzenberger, R.; Hueglin, C.; Maenhaut, W.; Pio, C.A.; Puttock, J.; Putaud, J.P.; Toom-Sauntry, D.; Puxbaum, H. Results of the "Carbon Conference" International Aerosol Carbon Round Robin Test: Stage 1; *Atmos. Environ.* **2001**, *35*, 2111-2121.
37. Chow, J.C.; Watson, J.G.; Pritchett, L.C.; Pierson, W.R.; Frazier, C.A.; Purcell, R.G. The DRI Thermal/Optical Reflectance Carbon Analysis System: Description, Evaluation and Applications in U.S. Air Quality Studies; *Atmos. Environ.* **1993**, *27A*, 1185-1201.
38. Chow, J.C.; Watson, J.G.; Crow, D.; Lowenthal, D.H.; Merrifield, T.M. Comparison of IMPROVE and NIOSH Carbon Measurements; *Aerosol Sci. Technol.* **2001**, *34*, 23-34.
39. Arnott, W.P.; Moosmüller, H.; Sheridan, P.J.; Ogren, J.A.; Raspet, R.; Slaton, W.V.; Hand, J.L.; Kreidenweis, S.M.; Collett, J.L., Jr. Photoacoustic and Filter-based Ambient Aerosol Light Absorption Measurements: Instrument Comparison and the Role of Relative Humidity; *J. Geophys. Res.* **2003**, *108*, AAC 15-1-AAC 15-11.
40. Arnott, W.P.; Zielinska, B.; Rogers, C.F.; Sagebiel, J.; Park, K.; Chow, J.C.; Moosmüller, H.; Watson, J.G.; Kelly, K.; Wagner, D.; Sarofim, A.; Lighty, J.; Palmer, G. Evaluation of 1047 nm Photoacoustic Instruments and Photoelectric Aerosol Sensors in Source-Sampling of Black Carbon Aerosol and Particle Bound PAH's from Gasoline and Diesel Powered Vehicles; *Environ. Sci. Technol.* **2005**, *39*, 5398-5406.
41. Bae, M.S.; Schauer, J.J.; Deminter, J.T.; Turner, J.R.; Smith, D.; Cary, R.A. Validation of a Semi-continuous Instrument for Elemental Carbon and Organic Carbon Using a Thermal-Optical Method; *Atmos. Environ.* **2004**, *38*, 2885-2893.

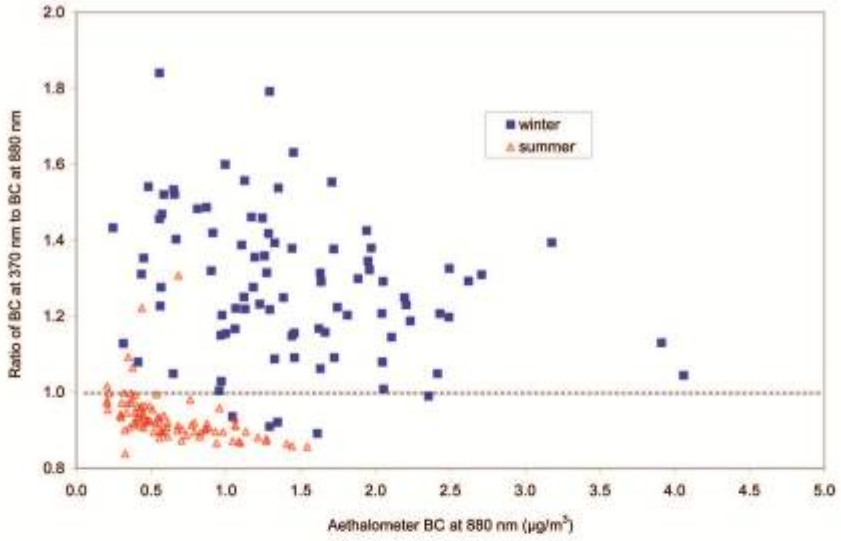

(a)

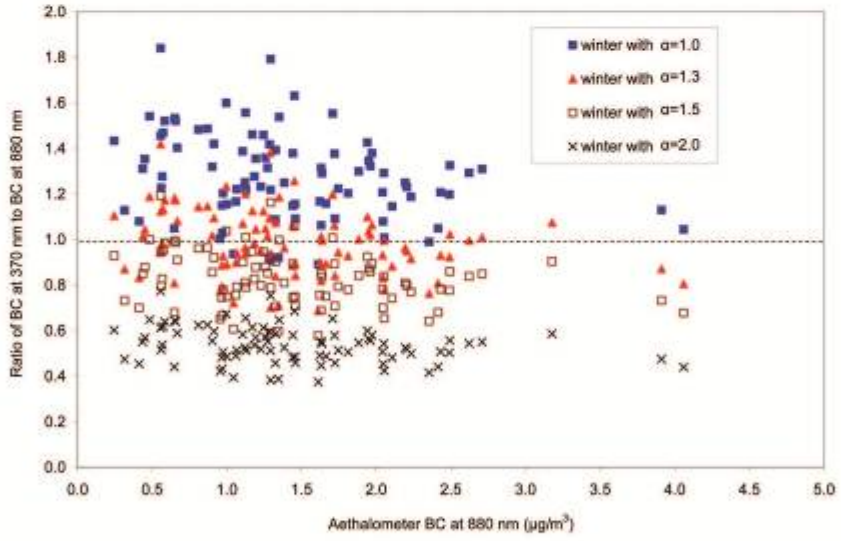

(b)

Figure 6. Ratio of daily averaged BC at the wavelength of 370 nm versus 880 nm as a function of the 7-AE BC concentration at λ = 880 nm in (a) winter (December 2003 to February 2004) and in summer (June to August 2004), and (b) in winter with different exponents (α) in the $\gamma-\alpha$ scaling factor.

42. Jeong, C.H.; Hopke, P.K.; Kim, E.; Lee, D.W. The Comparison between Thermal-Optical Transmittance Elemental Carbon and Aethalometer Black Carbon Measured at Multiple Monitoring Sites; *Atmos. Environ.* **2004**, *38*, 5193-5204.
43. Rupprecht, E.G.; Patashnick, H.; Beeson, D.E.; Green, R.E.; Meyer, M.B. A New Automated Monitor for the Measurement of Particulate Carbon in the Atmosphere. In *Proceedings, Particulate Matter: Health and Regulatory Issues*, April 4–6, 1995, Cooper, J.A. and Grant, L.D., Eds.; Air and Waste Management Association: Pittsburgh, PA, 1995, pp. 262-267.
44. Burtscher, H.; Schmidt-Ott, A. In Situ Measurement of Adsorption and Condensation of a Polyaromatic Hydrocarbon on Ultrafine Carbon

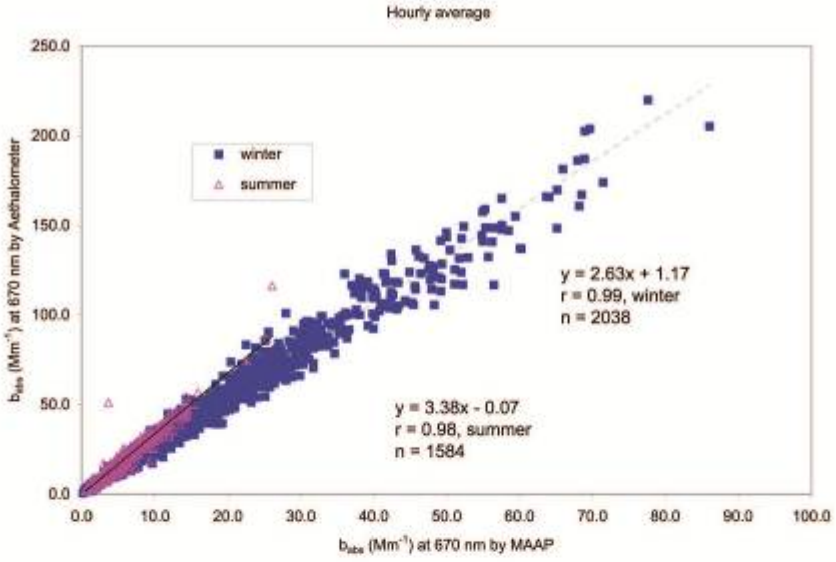

(a)

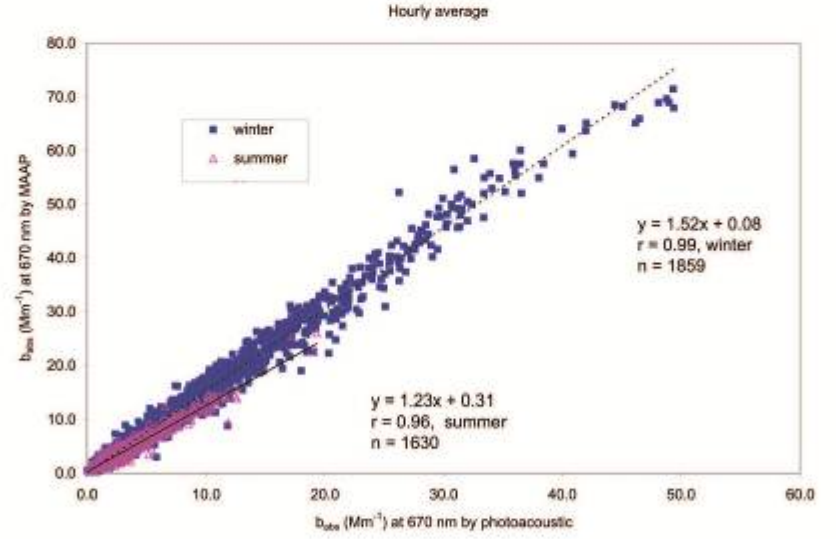

(b)

Figure 7. Hourly averaged (a) b_{abs} by 7-AE versus b_{abs} by MAAP at λ = 670 nm and (b) MAAP b_{abs} vs. photoacoustic b_{abs} at λ = 670 nm in winter (December 2003 to February 2004) and summer (June to August 2004)

Particles by Measurement of Photoemission; *J. Aerosol Sci.* **1986**, *18*, 699.

45. United States Environmental Protection Agency. Revised Requirements for Designation of Reference and Equivalent Methods for $PM_{2.5}$ and Ambient Air Surveillance for Particulate Matter—Final Rule; *Fed. Regist.* **1997**, *138*, 38763-38854.

46. Chow, J.C.; Watson, J.G.; Lowenthal, D.H.; Chen, L-W.A.; Magliano, K. Particulate Carbon Measurements in California's San Joaquin Valley; *Chemosphere*, **2006**, *62*, 337-348.

47. Watson, J.G.; Chow, J.C.; Lowenthal, D.H.; Kreisberg, N.; Hering, S.V.; Stolzenburg, M.R. Variations of Nanoparticle Concentrations at the Fresno Supersite. *Sci. Total Environ.* **2006**, *358*, 178-187.

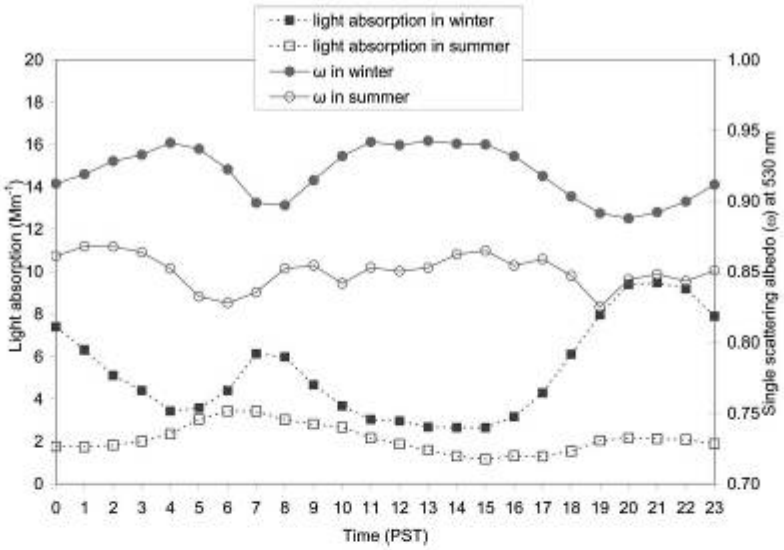

Figure 8. Diurnal variation of the single scattering albedo (ω) calculated by use of particle light scattering (b_{scat}) from the nephelometer (λ = 530 nm) and light absorption (b_{abs}) from the photoacoustic analyzer (λ = 1047 nm) averaged by the time of day in winter (December 2003 to February 2004) and summer (June to August 2004).

48. Richards, L.W.; Lehrman, D.E.; Weiss, R.E.; Bush, D.; Watson, J.G.; McDade, C.E.; Magliano, K. Light scattering measurements during the California Regional $PM_{10}/PM_{2.5}$ Air Quality Study. In *Proceedings, International Specialty Conference on Regional Haze and Global Radiation Balance—Aerosol Measurements and Models: Closure, Reconciliation and Evaluation*, Air & Waste Management Association/American Geophysical Union: Pittsburgh, PA/Washington, DC, 2001.
49. Patashnick, H.; Rupprecht, E.G. Continuous PM_{10} Measurements Using the Tapered Element Oscillating Microbalance; *J. Air & Waste Manage. Assoc.* **1991**, *41*, 1079-1083.
50. Watson, J.G.; Chow, J.C. A Wintertime $PM_{2.5}$ Episode at the Fresno, CA, Supersite; *Atmos. Environ.* **2002**, *36*, 465-475.
51. Watson, J.G.; Chow, J.C.; Park, K.; Lowenthal, D.H. Nanoparticle and Ultrafine Particle Events at the Fresno Supersite; *J. Air & Waste Manage. Assoc.* **2006**, *55*, 417-430.
52. Moosmüller, H.; Arnott, W.P.; Rogers, C.F.; Chow, J.C.; Frazier, C.A.; Sherman, L.E.; Dietrich, D.L. Photoacoustic and Filter Measurements Related to Aerosol Light Absorption during the Northern Front Range Air Quality Study (Colorado 1996/1997); *J. Geophys. Res.* **1998**, *103*, 28149-28157.
53. Watson, J.G.; Chow, J.C.; Houck, J.E. $PM_{2.5}$ Chemical Source Profiles for Vehicle Exhaust, Vegetative Burning, Geological Material, and Coal Burning in Northwestern Colorado during 1995; *Chemosphere*, **2001**, *43*, 1141-1151.
54. Watson, J.G.; Zhu, T.; Chow, J.C.; Engelbrecht, J.P.; Fujita, E.M.; Wilson, W.E. Receptor Modeling Application Framework for Particle Source Apportionment; *Chemosphere*, **2002**, *49*, 1093-1136.
55. Watson, J.G.; Chow, J.C. Receptor Models for Air Quality Management; *EM*, **2004**, *30*, 27-36.

About the Authors

Kihong Park was formerly an assistant research professor at the Desert Research Institute (DRI) and is currently an assistant professor at the Gwangju Institute of Science and Technology. Judith C. Chow and John G. Watson are research professors, Dana Trimble is an associate research scientist, and Prakash Doraiswamy is a post doctoral research associate at DRI. W. Pat Arnott is an associate professor at the University of Nevada, Reno. Kenneth R. Stroud is chief of the Air Quality Surveillance Branch, Kenneth Bowers is an air pollution specialist, and Richard D. Bode is chief of the Health and Exposure Assessment Branch of the California Air Resources Board. Andre Petzold is head of the Atmosphereic Group at the Instutue of Atmoshperic Physics (Deutsches Zentrum fur Luft - und Raumfahrt Oberpfaffenhofen, Institute fur Physic der Atmosphare). Anthony D. A. Hansen is a staff scientist for the Engineering Division of Lawrence Berkeley National Laboratory. Address correspondence to: Judith C. Chow, Division of Atmospheric Sciences, Desert Research Institute, 2215 Raggio Parkway, Reno, NV 89512; phone: +1-775-674-7050; fax: +1-775-674-7009; e-mail: judy.chow@dri.edu.

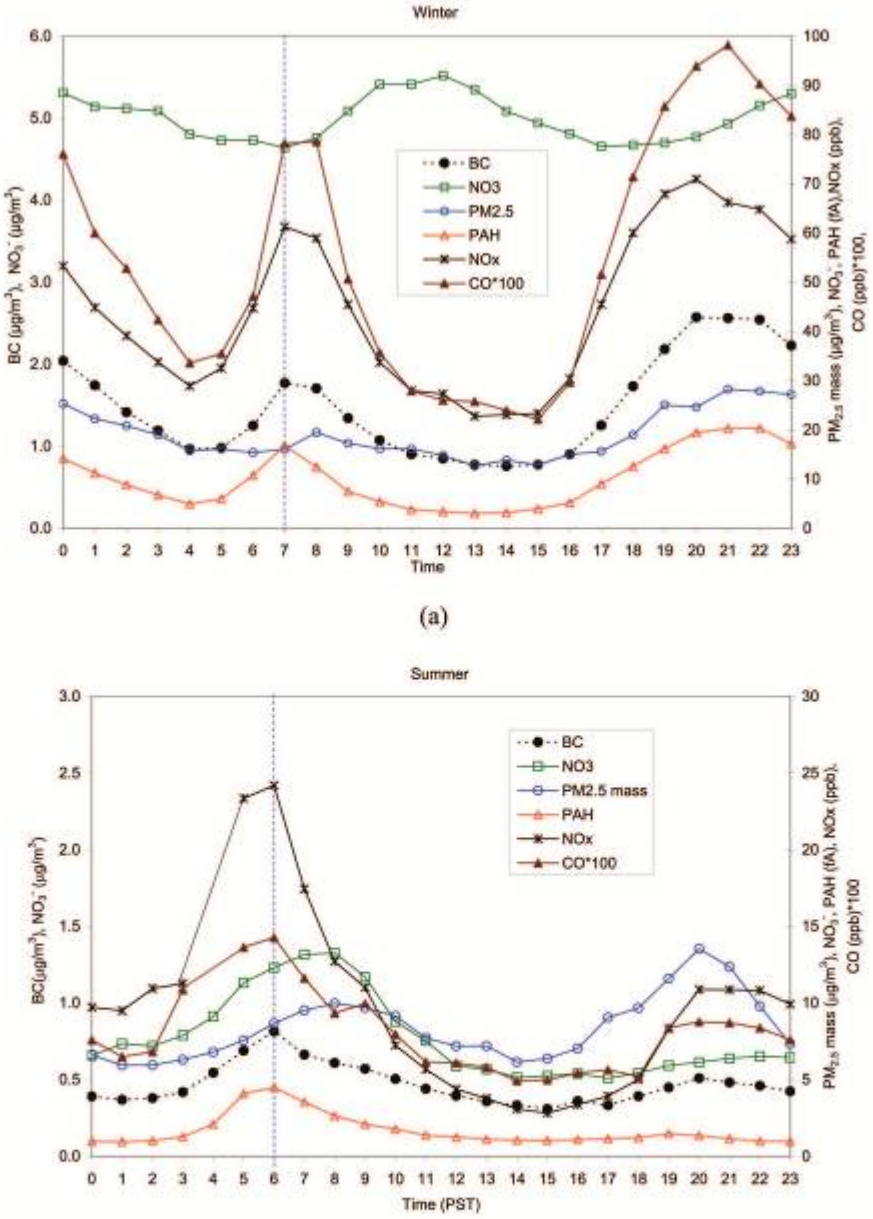

Figure 9. Diurnal variations of BC, NO_3^-, $PM_{2.5}$ mass, particle-bound PAHs, NO_x, and CO averaged by the time of day for (a) winter (December 2003 to February 2004) and (b) summer (June to August 2004)

10. GLOSSARY OF TERMS

10.1 Abbreviations

1-AE: Single wavelength aethalometer

2-AE: Dual wavelength aethalometer

7-AE: Seven color aethalometer

a.u.: arbitrary units

AAS: Atomic Absorption Spectrophotometry

AC: Automated Colorimetry

AE: Aethalometer

AIHL: Air industrial hygienic laboratory

ARB: California Air Resources Board

BAM: Beta attenuation monitor

BC: Black carbon

BRAVO: Big Bend Regional Aerosol and Visibility Study

BYU: Brigham Young University

CD: Compact Disc

CE: Capillary Electrophoresis

CIF: Charcoal-impregnated glass-fiber filter

CMB: Chemical Mass Balance model

CPC: Condensation Particle Counter

CPI: Carbon Performance Index: ratio of odd- to even-number carbon *n*-alkanes in a sample

CRPAQS: California Regional $PM_{10}/PM_{2.5}$ Air Quality Study

DCM: dichloromethane

DDW: Deionized distilled water

DMA: Differential mobility analyzer

DOE: U.S. Department of Energy

DRI: Desert Research Institute

EC: Elemental carbon

EV: Effective variance

EPA: U.S. Environmental Protection Agency

EPRI: Electric Power Research Institute

FACES: Fresno Asthmatic Children's Environment Study

FDMS: Filter dynamics mass balance system

FID: Flame ionization detector

French two-step: Two-step thermal analysis program to determine OC, EC, and TC

FEM: Federal equivalent method

FRM: Federal reference monitor

GC/MS: Gas Chromatography/Mass Spectrometry

GEEER: General Electric-Energy and Environmental Research Corporation

GHG: Greenhouse gases

HEPA: High efficiency particulate air

Hi-Vol: High volume sampler

HPLC: High Performance Liquid Chromatography

Hz: Hertz

IMPROVE: Interagency Monitoring of Protected Visual Environments

IC: Ion Chromatography

ICP/MS: Inductively coupled IC/Mass spectrometry

ID: Inner diameter

IOP: Intensive operating period

IR: Infrared

K-M: Kubelka-Munk theory

KHP: Potassium Hydrogen Phthalate

LOD: Limit of detection

LPS: Laser particle spectrometer

LQL: Lower quantifiable limit

LVPS: Las Vegas PM_{10} Study

MAAP: Multi-angle absorption photometer

MCML: Monte Carlo Code

MDL: Minimum detection limit

NAAQS: National ambient air quality standards

NDIR: Non-dispersive infrared

nDMA: nano-Differential mobility analyzer

NFRAQS: Northern Front Range Air Quality Study

NIOSH: National Institute of Safety and Health

NIST: National Institute of Standards and Technology

NASA/ARL: National Aeronautics and Space Administration Air Resources Laboratory

NOAA/CMDL: National Oceanic & Atmospheric Administration Climate Monitoring and Diagnostics Laboratory

NREL: National Renewable Energy Laboratory

NPS: National Park Service

OC: Organic carbon

OD: Outer diameter

OEC: Optical extinction cell

OLS: Ordinary least squares

OM: Organic matter

OP: Pyrolyzed organic carbon

OPC: Optical particle counter

PA: Photoacoustic analyzer

PAH: Polycyclic aromatic hydrocarbon

PCA: Principle Component Analysis

PC-BOSS: Particle concentrator-BYU organic sampling system

PM: Particulate matter

$PM_{2.5}$: PM with aerodynamic diameter or 2.5 micrometer (μm) or less

PM_{10}: PM with aerodynamic diameter or 10 μm or less

PMF: Positive Matrix Factorization

PMS: Particle Measuring Systems

PSAP: Particle soot absorption photometer

$PSAP_{raw}$: PSAP b_{abs} measurements reported by the instrument without any adjustments

$PSAP_{adj}$: PSAP b_{abs} measurements adjusted for scattering effects following procedure outlined by Virkkula et al. (2005)

PST: Pacific standard time

QA: Quality assurance

QAPP: Quality assurance project plan

QC: Quality control

RAAS: Reference Ambient Air Speciation Sampler

RAOS: Reno Aerosol Optics Study

RH: Relative humidity

RMS: Root mean square

RMSE: Root mean square error

RSD: Relative standard deviation

RWC: Residential wood combustion

SJV: San Joaquin Valley

SMPS: Scanning mobility particle sizer

SNAQS: Southern Nevada Air Quality Study

SOA: Secondary Organic Aerosols

SOPs: Standard Operating Procedures

SSA: Single scattering albedo

STAR: Science to achieve results program of EPA

STN: Speciation Trends Network

STP: Standard temperature and pressure, defined as 25 °C and 1 atm

SQL: Structured Query Language

SVOM: Semi-volatile organic matter

TC: Total Carbon

TCEQ: Texas Commission on Environmental Quality

TD: Thermal desorption

TEOM: Tapered element oscillating microbalance

TIGF: Teflon-impregnated Glass Fiber filter

TOR: Thermal optical reflectance

TOT: Thermal optical transmittance

TSP: Total Suspended Particulate Matter

UCM: Unresolved Carbon Matter

UCPC: Ultrafine Condensation Particle Counter

UH: Ultrasonic humidifier

UNC: Measurement uncertainty reported in literature in percent

U.S. United States of America

UV: Ultraviolet

VDI: Verein Deutscher Ingenieure, Germany

WINS: Well impactor ninety-six

WPS: Wide range particle spectrometer

XRF: X-ray Fluorescence

10.2 Symbols

A: Filter deposit area

ATN: Parameters determined through attenuation only

α: Angstrom absorption exponent

b_{abs}: light absorption in Mm^{-1} (inverse megameters)

B_i : average amount of species *i* on field blanks

B_{ij} : amount of species *i* found on field blank *j*

C_i : ambient concentration of species *i*

C_{max}: *n*-alkane that has the highest concentration among the *n*-alkane homologues

d_e: particle penetration depth into a filter

F : flow rate throughout sampling period

λ: Wavelength, in nm

σ_{abs}: mass absorption efficiency, in m^2/g

σ: precision or uncertainty

σ_{Bi} : blank precision for species *i*

σ_{Bij} : precision of the species *i* found on field blank *j*

σ_{Ci} : propagated precision for the concentration of species *i*

σ_{Mi} : precision of amount of species *i* on the substrate

σ_{RMSi} : root mean square precision for species *i*

σ_V : precision of sample volume

σ_x: uncertainty for the x-axis instrument

σ_y: uncertainty for the y-axis instrument

$\sigma_{L,a}$: local absorption coefficient within the loaded filter layer

$\sigma_{L,s}$: local scattering coefficient within the loaded filter layer

L: Thickness of a loaded filter layer

m/z: mass to charge ratio

M_i : amount of species *i* on the substrate

M_{ijf} : amount of species *i* on sample *j* from original analysis

M_{ijr} : amount of species *i* on sample *j* from replicate analysis

n : total number of samples

F_L/F_M: Fraction of forward scattering through a loaded/blank filter layer

P_L/P_M: Fraction of light penetration (non-scattered) through a loaded/blank filter layer

$R_L/R_M/R_F$: Hemisphere reflectance of a loaded/blank filter layer or whole filter

$T_L/T_M/T_F$: Hemisphere transmittance of a loaded/blank filter layer or whole filter

$R_F^{(0)}$ Hemisphere reflectance of a blank filter

R_{op}: Operational (detected) reflectance of a filter

SIG_{Bi} : root mean square error (RMSE), the square root of the averaged sum of the squared σ_{Bij}

SSA_L: Single scattering albedo of a loaded filter layer

STD_{Bi}: standard deviation of the blank

T = sample duration

$T_F^{(0)}$ Hemisphere transmittance of a blank filter

T_{op}: Operational (detected) transmittance of a filter

$\tau_{L,a}$: Absorption optical depth of a loaded filter layer

$\tau_{L,s}$: Scattering optical depth of a loaded filter layer

τ_L: Total optical depth of a loaded filter layer

$\tau_{EC,a}/\tau_{OP,a}$: Absorption optical depth cased by EC/OP

$\tau_{L,ATN}$: Apparent optical depth of a loaded filter (determined from attenuation)

V: Volume of air sampled

ξ : A random number between 0 – 1

ω: single-scattering albedo

10.3 Compounds/Species

^{147}Pm: Promethium-147, a radioactive isotope that emits beta rays

BC: Black carbon

BeP: benzo[e]pyrene

BghiP: benzo[g,h,i]perylene

Cor: Coronene

CH_4: Methane

Cl^-: Soluble Chloride ion

CO_2: Carbon dioxide

CO_3^{2-}: Soluble Carbonate

EC: Elemental carbon

Flu: Fluoranthene

H_2O: Water

He: Helium

HNO_3: Nitric acid

IcdP: indeno[1,2,3-cd]pyrene

K^+: Soluble potassium

KHP: Potassium Hydrogen Phthalate

MnO_2: Manganese oxide

Na: Total Sodium

Na^+: Soluble Sodium

NaCl: Sodium Chloride

NH_3: Ammonia

NH_4^+: Soluble Ammonium

$(NH_4)_2SO_4$: Ammonium Sulfate

NO_3^-: Soluble Nitrate

OC: Organic carbon

O_2: Oxygen

PO_4^{3-}: Soluble Phosphate

Pyr: Pyrene

SO_2: Sulfur Dioxide

$SO_4^=$: Soluble Sulfate

U: Total Uranium

10.4 Measurement Units

Distance or Length

nm: nanometer

µm: micrometer

mm: millimeter

cm: centimeter

km: kilometer

Concentration

ng/m^3: nanogram per cubic meter

µg/m^3: microgram per cubic meter

mg/m^3:milligram per cubic meter

Mass

µg: microgram

kg:: kilogram

Volume

µl: microliter

mL: milliliter

m^3: cubic meter

Flow rate

L/min: liters per minute

cm^3/min: cubic centimeters per minute

Mass absorption efficiency

m^2/g: square meter per gram

Light absorption

Mm^{-1}: Inverse megameters

Pressure

atm: atmospheres

psi: pounds per square inch

mbar millibar

kPa: kilopascal

Temperature

°C: degree Centigrade

K: degree Kelvin

°F: degree Fahrenheit

Time

sec: second

min: minute

hr: hour

Power

kW: kilowatt

Current

fA: femtoamps

mV: millivolts

APPENDIX A:

SUMMARY OF THERMAL/OPTICAL CARBON ANALYSIS PROTOCOLS AND PERFORMANCES

Table A-1. Summary of thermal/optical carbon analysis protocols and performances.

IMPROVE TOR Protocol

Procedure:

1) Liberating carbon compounds under different temperature and oxidation environments from sample punch taken from a quartz fiber filter, 2) converting these compounds to carbon dioxide (CO_2) by passing the volatized compounds through an oxidizer (MnO_2 at 912°C), 3) reduction of the CO_2 to methane (CH_4) by passing the flow through a methanator (firebrick impregnated with nickel catalyst at ~ 550°C in a stream of hydrogen, 4) quantification of CH_4 by FID, 5) calibrate the instrument with CH_4 standard.

References:
Chow et al., 1993; 2001; 2004

Contact person:
Judith Chow <judyc@dri.edu>

Studies using this technique:

IMPROVE Network: Malm et al., 1994; IMPROVE 2001

Chow et al., 1994; 1996

NFRAQS/BRAVO

MARCH-Atlantic: Chen et al., 2001; 2002

Working parameters in procedure (1):

Stage	T(°C)[1]	Time (s)[2]	Carrier gas	Note
0	25	240	He	Oven flush
1	120	80 – 580	He	OC1
2	250	80 – 580	He	OC2
3	450	80 – 580	He	OC3
4	550	80 – 580	He	OC4
5	550	80 – 850	2%O_2/98%He	EC1
6	700	80 – 580	2%O_2/98%He	EC2
7	800	80 – 580	2%O_2/98%He	EC3

[1] The temperature ramps as rapidly as possible when advancing to next stage; [2] Ramping to next stage begins when the FID response returns to baseline or a constant value.

Pyrolized OC adjustment:

The filter reflectance (in TOR)/transmittance (in TOT) is monitored continuously via a He-Ne laser at a wavelength of 632.8 nm and a photodetector. Laser signal typically decreases on stage 1 – 4 and increases after stage 4. The portion of EC1 until the laser signal returns to its initial value is assigned to pyrolized organic carbon (OP).

Carbonate adjustment:

Carbonate carbon is determined by measuring CO_2 evolved upon acidification of the sample punch with 20 µl of 0.4 M HCl before normal carbon analysis cycle.

OC and EC definition

OC = OC1 + OC2 + OC3 + OC4 + OP
EC = EC1 + EC2 + EC3 – OP
TC= OC + EC

Performances:

Lower detection limit (LDL):
0.2 µg carbon cm^{-2}.

Lower quantifiable limits (LQL)
OC: 0.5 – 1.0 µg carbon cm^{-2}
EC: 0.0 – 0.2 µg carbon cm^{-2}
Carbonate: 0.0 – 0.4 µg carbon cm^{-2}

Precision is determined by replicate analysis, typically within 10% for EC, OC and TC 10 times LDLs.

Potential artifacts for OC/EC split:

1) The pyrolysis-adjustment assumes that the light absorption per unit mass of pyrolytically produced carbon is equal to the light absorption per unit mass of carbon burned in restoring the reflectance or transmittance to its initial value. This is not fundamentally justified.

2) The volatilization of light-absorbing organic carbon could cause an increase in laser signal before the O_2 is introduced.

3) TOT results can be significantly different from TOR. The two methods could overlook the light scattering not in straight forward or backward direction. Un burned pyrolytic material beneath the filter surface can cause TOR to underestimate the pyrolysis.

Table A-1. Continued.

IMPROVE_A TOR and TOT protocol

References:
Chow et al., 2005

Contact Person
Judy Chow <judy.chow@dri.edu>

Stage	T(°C)[1]	Time (s)[2]	Carrier gas	Note
0		240	100% He	Oven flush
1	140	80 – 580	100% He	OC1
2	280	80 – 580	100% He	OC2
3	480	80 – 580	100% He	OC3
4	580	80 – 580	100% He	OC4
5	580	80 – 850	2%O_2/98%He	EC1
6	740	80 – 580	2%O_2/98%He	EC2
7	840	80 – 580	2%O_2/98%He	EC3

[1] The temperature ramps as rapidly as possible when advancing to next stage; [2] Ramping to next stage begins when the FID response returns to baseline or a constant value.

Table A-1. Continued

NIOSH 5040 TOT Method

Procedure①③:

1) Liberating carbon compounds under different temperature and oxidation environments from sample punch taken from a quartz fiber filter, 2) converting these compounds to carbon dioxide (CO_2) by passing the volatized compounds through a bed of granular MnO_2 (held ~ 900°C), 3) reduction of the CO_2 to methane (CH_4) by passing the flow through a methanator (firebrick impregnated with nickel catalyst at ~ 450°C in a stream of hydrogen, 4) quantification of CH_4 by FID, 5) calibrate the instrument with CH_4 standard.

References:
①NIOSH, 1996; Birch and Cary, 1996
②Birch, 1998
③NIOSH, 1999

Contact Person:
Eileen Birch <mib2@cdc.gov>

Studies using this technique:

Working parameters in procedure (1) ②:

Stage	T(°C)[1]	Time (s)	Carrier gas	Note
0	25	-	He	Oven flush
1	250	60	He	OC1
2	500	60	He	OC2
3	650	60	He	OC3
4	850[2]	90	He	OC4
5	-	20-30	He	Cool oven
6	650	30	2%O_2/98%He	EC1
7	750	30	2%O_2/98%He	EC2
8	850	30	2%O_2/98%He	EC3
9	940	>120	2%O_2/98%He	EC4

[1] The rate temperature increasing is 3 – 7°C/s when advancing to next stage②; [2] 750°C if EC loss is evident③.

Pyrolized OC adjustment:

The filter transmittance is monitored continuously via a He-Ne laser at a wavelength of 632.8 nm. Transmitted laser signal generally decreases on stage 1 – 4 and increases after stage 5. The portion on stage 6 until laser signal returns to its initial value (laser split) is assigned to pyrolized OC (OP) ①③.

Carbonate adjustment:

Carbonate carbon (CC) is estimated by exposing a second punch from the same filter to HCl vapor (PH ~ 2) for 1 hr before TOT analysis. The difference in total carbon (usually in OC4) between the two punches gives an estimate of carbonate carbon①③.

OC and EC definition:

OC = all the carbon evolved before laser split①②③.
EC = all the carbon evolved after laser split①②③.
TC = OC + EC

Performances:

Lower detection limit (LDL):
0.15 μg carbon cm^{-2} or 0.3 μg carbon (1.5 cm^2 filter punch)③.

Precision (S_r):
19% @ 1 μg carbon③
1% @ 10 – 72 μg carbon③

Potential biases for OC/EC split:

1) The pyrolysis-adjustment assumes that the light absorption per unit mass of pyrolytically produced carbon is equal to the light absorption per unit mass of carbon burned in restoring the reflectance or transmittance to its initial value. This is not fundamentally justified.

2) The volatilization of light-absorbing organic carbon could cause an increase in laser signal before the O_2 is introduced.

3) Residence time on each heating stage may not be long enough to allow FID response returning to the baseline, resulting in ill-defined carbon fractions.

4) EC may evolve on the 850 °C stage with pure He environment due to release of oxygen from complex mineral oxides at the high temperature. This may cause the laser signal returning before the introduction of O_2 and an underestimation of EC.

Table A-1. Continued

U.S. EPA STN TOT Method

Procedure:

1) Liberating carbon compounds under different temperature and oxidation environment from sample punch taken from a quartz fiber filter, 2) converting these compounds to carbon dioxide (CO_2) by passing the volatized compounds through a bed of granular MnO_2 (held ~ 867°C), 3) reduction of the CO_2 to methane (CH_4) by passing the flow through a methanator (firebrick impregnated with nickel catalyst at ~ 496°C in a stream of hydrogen, 4) quantification of CH_4 by FID, 5) calibrate the instrument with CH_4 standard.

References:
Peterson and Richards, 2002

Contact person
Max Peterson <mrp@rti.org>
Jewell Smiley
<Smiley.Jewell@epamail.epa.gov>

Studies using this technique:

Speciation Trend Network: USEPA, 2000; 2001

Working parameters in procedure (1):

Stage	T(°C)[1]	Time (s)	Carrier gas	Note
0	25	-	He	Oven flush
1	310	60	He	OC1
2	480	60	He	OC2
3	615	60	He	OC3
4	900	90	He	OC4
5	-	~30	He	Cool oven
7	600	45	2%O_2/98%He	EC1
8	675	45	2%O_2/98%He	EC2
9	750	45	2%O_2/98%He	EC3
10	825	45	2%O_2/98%He	EC4
11	920	120	2%O_2/98%He	EC5

[1] The temperature ramps as rapidly as possible when advancing to next stage.

Pyrolized OC adjustment:

The filter transmittance is monitored continuously via a He-Ne laser at a wavelength of 632.8 nm and a photodetector. After the introduction of O_2, the portion of EC until the laser signal returns to its initial value is assigned to pyrolized OC (OP). OP = 0 if laser signal returns to the initial value before turning on O_2.

Carbonate adjustment:

Same as the NIOSH TOT method.

OC and EC definition:

OC = all the carbon evolved before laser split (return to origin)
OP = OC - OC1 - OC2 - OC3 - OC4 or 0 if OC < sum of OC1–4.
EC = all the carbon evolved after laser split.
TC = OC + EC

Performances:

Lower detection limit (LDL):
0.2 μg carbon cm^{-2} or 0.3 μg carbon (1.5 cm^2 filter punch) for both OC and EC.

Precision:
4 – 6% for 5 – 400 μg OC cm^{-2} and 1 – 15 μg EC cm^{-2} (1.5 cm^2 filter punch).

Potential biases for OC/EC split:

1) The pyrolysis-adjustment assumes that the light absorption per unit mass of pyrolytically produced carbon is equal to the light absorption per unit mass of carbon burned in restoring the reflectance or transmittance to its initial value. This is not fundamentally justified.

2) The volatilization of light-absorbing organic carbon could cause an increase in laser signal before the O_2 is introduced.

3) Residence time at each heating stage may not be long enough to allow FID response returning to baseline, resulting in ill-defined carbon fractions.

4) EC may evolve at the 900 °C stage with pure He environment due to release of oxygen from complex mineral oxides at high temperature. This may cause the laser signal returning before the introduction of O_2 and an underestimation of OP and EC.

Table A-1. Continued

Lawrence Berkeley Laboratory TOT Method

Procedure:

1) Liberating carbon compounds under continuously increasing temperature and a pure oxygen environment from sample punch taken from a quartz fiber filter, 2) converting these compounds to carbon dioxide (CO_2) by passing the volatized compounds through annular CuO catalyst (held 850 – 900°C), 3) 3) quantification of CO_2 by a nondispersive infrared analyzer, 5) calibrate the instrument by releasing CO_2 into it.

References:
Novakov, 1982; Gundel et al., 1984

Contact person:
Tihomir Novakov
<TNovakov@lbl.gov>

Studies using this technique:

Rosen et al., 1980 (Science 208, p741); 1981 (AE 15, 1371-1374); 1983

Rosen and Novakov (Nature 306 768-770)

Pratsinis et al., 1983, AS&T, 2(2), 171.

Working parameters in procedure (1):

Stage	T(°C)	Time (s)	Carrier gas	Note
0	25	-	O_2	Oven flush
1	25-825[1]	~ 4800	O_2	TC

[1] The temperature is increased continuously at a rate of 10°C/min.

Pyrolized OC adjustment:

No estimate for pyrolized OC

OC and BC definition:

BC: The filter transmittance is monitored continuously during combustion via a He-Ne laser at a wavelength of 632.8 nm and a photodetector. Light transmission remains constant until a specific temperature at which it starts to increase. The area of the thermogram peak that corresponds to the increase in light transmission is assigned to BC. This can be crosschecked by converting the optical attenuation to BC with assumed mass absorption efficiency (20 m^2/g) of BC.

TC: Total carbon evolved before the laser signal returns to the value corresponding to that of a blank filter.

OC = TC - BC

Carbonate adjustment:

After the transmitted laser signal returns the value corresponding to that of a blank filter, carbon evolved (usually at > 600°C) is assigned to carbonate carbon.

Performances:

Lower detection limit (LDL):
~0.6μg cm^{-2} for BC.

Precision:
Precision is not available in the literature.

Potential biases for OC/EC split:

1) The entire thermal evolution process is in a pure oxygen environment. Both OC and EC combustion could occur in such an environment. If the laser signal increases continuously, there is no way to determine the EC/OC split point.

2) Crosscheck of BC depends on an empirical light absorption efficiency that, however, could vary significantly from one type of sample to another.

3) The method assumes that BC is the only light absorbing species. BC can actually include pyrolized OC, light-absorbing OC, and EC. This definition make results from this method difficult to be compared with the IMPROVE and NIOSH methods.

4) If carbonate carbon evolves before some of the combustible carbon, it could be mistaken as OC or BC and bias the OC/BC split.

Table A-1. Continued

France CNRS-CEA Thermal-evolution Method

Procedure:

1) Removing organic carbon compounds from a sample punch taken from a glass fiber filter in a furnace under a pure oxygen environment and a specific low heating temperature, 2) placing the sample punch in the furnace of a carbon analyzer (Coulomat 702) and liberating carbon under a pure oxygen environment and a specific high heating temperature, 3) converting the compounds to carbon dioxide (CO_2) by passing the volatized compounds through CuO catalyst (held ~ 1000°C), 4) quantification of CO_2 by means of coulometric titration to determine refractory carbon (soot), 5) taking another punch from the same filter and going through step 2 – 4 to determine total carbon.

References:
Cachier et al., 1989

Contact person:
Héléne Cachier
<cashier@lsce.cnrs.gif.fr>

Studies using this technique:
Cachier et al., 2001 (AE 35(2) 453-468)
SAFARI-92: Kuhllbusch et al., 1996

Working parameters in procedure (1) and (2):

Stage	T(°C)[1]	Time (s)	Carrier gas	Note
1	340[2]	> 7200[2]	O_2	OC1
2	1100	~ 600[3]	O_2	EC1

[1] The temperature ramps as rapidly as possible on each stage; [2] The temperature and time on stage 1 (precombustion) is optimized according to a preparation experiment; [3] until CO_2 signal returns to 0.

Pyrolized OC adjustment:

Charring rate was examined from literature and a 10% of OC is assumed to become pyrolized (OP) in this method.

Carbonate adjustment:

Carbonate carbon is removed by subjecting the filters to HCl fumes before normal carbon analysis cycle.

OC and BC definition:

BC: From the asymptotic line of carbon loss against baking time on stage 1, the decomposition rate of refractory carbon (BC) on stage one is estimated to be 0.22 ± 0.02%/min (K). Based on this rate and OP adjustment,

BC = EC1 - OP + K × Time on stage 1

TC: Total carbon is determined the same way as BC but use another punch and skip stage 1.

OC = TC - BC

Performances:

Lower detection limit (LDL):
< 1 μg for TC

Lower quantifiable limits (LQL):
< 0.5 μg carbon cm^{-2} (blank filter response)

Precision:
~ 5% for most of the sample

Potential biases for OC/EC split:

1) The heating is carried out in a pure oxygen environment. Both OC and EC could evolve under such an environment. This method assumes that oxidation rate of EC at Stage 1 is nearly a constant, which is not fundamentally justified.

2) Some high molecular weight organics that do not evolve at 340°C may be mistakenly classified as EC.

3) The method assumes that ~ 10% of organics is pyrolized on stage 1 and the pyrolized OC acts just like EC in the heating process. The pyrolized fraction, however, can vary for different types of samples and be significantly different from 10%.

4) TC and EC amounts are determined from different punches of the sample. The inhomogeneous loading on the sample surface could bias the EC/OC ratio.

Table A-1. Continued.

Brookhaven National Laboratory Thermo-evolution Method

Procedure:

1) Liberating carbon compounds under different temperature and oxidation environment from sample punch taken from a quartz fiber filter, 2) converting these compounds to carbon dioxide (CO_2) by passing the volatized compounds through a CuO catalyst (held ~ 650°C), 3) purifying the evolved gas using a gas chromatography column at 155 ± 5°C to remove gases such as SO_2 and NO_2, 4) quantification of CO_2 by a nondispersive infrared analyzer, 5) calibrate the instrument by with CO_2 standard.

References:
Tanner, 1982

Contact Person:
Roger Tanner <rltanner@tva.gov>

Studies using this technique:

Working parameters in procedure (1):

Stage	T(°C)[1]	Time (s)	Carrier gas	Note
0	25	-	He	Oven flush
1	400	300[2]	He	OC1
2	700	300[2]	10%O_2/90%He	EC1

[1] The temperature ramps as rapidly as ~ 600°C/min on each stage; [2] for load < 50 μg carbon cm^{-2} and 900 s for load of 50 – 100 μg carbon cm^{-2}.

Pyrolized OC adjustment:

No estimate for pyrolized OC, but flush heating rate to stage 1 is expected to minimize pyrolysis.

Carbonate adjustment:

No estimate for carbonate carbon

OC and BC definition:

The heating rate and temperature at stage 1 are designed to minimize pyrolysis, and therefore

OC = OC1

EC = EC1

TC = OC + EC

Performances:

Lower detection limit (LDL):
0.1 – 0.2 μg carbon (0.1 ppm CO_2)

Lower quantifiable limits (LQL):
~ 2 μg carbon cm^{-2} for OC (blank response)
~ 0.2 μg carbon cm^{-2} for EC

Precision:
~ 8% for organic carbon and ~ 12% for elemental carbon (standard deviation)

Potential biases for OC/EC split:

1) This method does not adjust for the pyrolized organic carbon in the baking process. Though pyrolysis can be minimized by quick temperature ramping, it could still be significant for heavily loaded sample and long baking time.

2) Some high molecular weight organics that do not evolve at 400°C may be mistakenly classified as EC.

3) Residence time on stage 1 may not be long enough to allow total volatilization of organics, leading to an underestimation of OC.

4) Lack of carbonate adjustment could bias EC/OC ratio for sample containing rich crustal material or fly ash.

Table A-1. Continued.

Oregon Graduate Institute TOR Method

Procedure:

1) Liberating carbon compounds under different temperature and oxidation environment from sample punch taken from a glass or quartz fiber filter, 2) converting these compounds to carbon dioxide (CO_2) by passing the volatized compounds through an oxidizer (MnO_2 at 950°C), 3) reduction of the CO_2 to methane (CH_4) by passing the flow through a methanator (firebrick impregnated with nickel catalyst at ~ 500°C in a stream of hydrogen, 4) quantification of CH_4 by FID, 5) calibrate the instrument by using CH_4.

References:
Huntzicker et al., 1982

Contact person:
James Huntzicker
<jimhz@admin.ogi.edu>

Studies using this technique:

Japar et al, 1984
Huntzicker et al., 1986, Ohio River Vallry

Working parameters in procedure (1):

Stage	T(°C)[1]	Time (s)[2]	Carrier gas	Note
0	350	-	2%O_2/98%He	Oven flush
1	350	-[2]	2%O_2/98%He	OC1
2	350	280	He	Oven flush
3	600	-[2]	He	OC2
4	-	-	He	Oven cool
5	400	100	2%O_2/98%He	EC1
6	500	120	2%O_2/98%He	EC2
7	600	>200[2]	2%O_2/98%He	EC3

[1] The temperature ramps as rapidly as possible when advancing to next stage; [2] Ramping to next stage begins when the FID response returns to baseline or a constant value.

Pyrolized OC adjustment:

The filter reflectance is monitored continuously via a He-Ne laser at a wavelength of 632.8 nm and a photodetector. Laser signal remains essentially constant on stage 1 but decreases on stage 2 and than increases since stage 5. The portion of EC1 until the laser signal returns to its initial value is assigned to pyrolized organic carbon (OP).

Carbonate adjustment:

Carbonate carbon is determined by measuring CO_2 (reduced to CH_4) evolved upon acidification of the sample punch with 1% aqueous H_3PO_4 in a separate system.

OC and EC definition

OC = OC1 + OC2 + OP
EC = EC1 + EC2 + EC3 – OP
TC= OC + EC

Performances:

Lower detection limit (LDL):
0.2 – 0.3 μg carbon cm^{-2}.

Lower quantifiable limits (LQL):
OC: 1.0 ± 0.5 μg carbon cm^{-2} (quartz filter)
EC: 0.3 ± 0.2 μg carbon cm^{-2} (quartz filter)

Precision: Upper limit of uncertainty is 20% for both OC and EC.

Potential biases for OC/EC split:

1) O_2 is released on stage 1 to avoid pyrolysis. However, this may cause oxidation of EC as well.

2) The pyrolysis-adjustment assumes that the light absorption per unit mass of pyrolytically produced carbon is equal to the light absorption per unit mass of carbon burned in restoring the reflectance or transmittance to its initial value. This is not fundamentally justified.

3) The volatilization of light-absorbing organic carbon could cause an increase in laser signal before the O_2 is introduced.

4) Residence time at stage 5 and 6 may not be long enough to allow FID response returning to baseline, resulting in ill-defined fraction in elemental carbon.

Table A-1. Continued.

Japan RCOP Thermo-evolution Method

Procedure:

1) Liberating carbon compounds at various positions of a quartz tube with a temperature gradient and under different oxidation environment from sample punch taken from a quartz fiber filter, 2) converting these compounds to carbon dioxide (CO_2) by passing the volatized compounds through an oxidizer (MnO_2 at 950°C), 3) reduction of the CO_2 to methane (CH_4) by passing the flow through a methanator (firebrick impregnated with nickel catalyst at 600°C in a stream of hydrogen, 4) quantification of CH_4 by FID-GC, 5) calibrate the instrument by releasing CO_2 or CH_4 into it.

References:
Mizohata and Ito, 1985

Contact person:
Akira Mizohata
<mizohata@riast.osakafu-u.ac.jp>

Studies using this technique:

Working parameters in procedure (1):

Stage	T(°C)[1]	Time (s)	Carrier gas	Note
0	25	~ 60	N_2	Oven flush
1	450	600	N_2	OC1
2	850	300	$8\%O_2/92\%N_2$	EC1

[1] The temperature change is accomplished by moving the sample from volatilization zone to combustion zero and is nearly immediate.

Pyrolized OC adjustment:

No estimate for pyrolized OC, but rapid temperature increase to stage 1 is expected to minimize pyrolysis.

Carbonate adjustment:

No estimate for carbonate carbon.

OC and EC definition:

OC = OC1

EC = EC1

TC= OC + EC

Performances:

Lower detection limit (LDL):
~ 0.3 μg carbon.

Precision:
~ 3% @ 40 μg carbon (0.78 cm^2 filter punch)

Potential biases for OC/EC split:

1) This method does not adjust for the pyrolized organic carbon in the baking process. Though pyrolysis can be minimized by moving the sample quickly in the temperature gradient baking tube, it could still be significant for heavily loaded sample and long baking time.

2) Residence time at stage 1 and 2 may not be long enough to allow total volatilization/oxidation of carbon, leading to ill-defined carbon fraction.

3) Some high molecular weight organics that do not evolve at 450°C may be mistakenly classified as EC.

4) Lack of carbonate adjustment could bias EC/OC ratio for sample containing rich crustal material or fly ash.

Table A-1. Continued

Rupprecht & Patashnick Continuous Carbon Analyzer

Procedure:

1) Collecting aerosols by passing air through a multi-hole impactor within a sealed, low volume clamshell envelope at 16.7 lpm for 1 hr, 2) liberating carbon compounds in a closed analysis loop (~ 100 cm^3) under two temperature stages from the sample impactor, 3) converting these compounds to carbon dioxide (CO_2) by passing the volatized compounds through an afterburner (750°C), 4) quantification of CO_2 by a low volume infrared CO_2 meter, 5) determining the baseline of the monitor by using a prefiltered air flow as blank.

References:
Rupprecht et al., 1995

Contact person:
Georg Rupprecht
<grupprecht@rpco.com>

Major Field Studies:

ACE-Asia surface measurement

Working parameters in procedure (2):

Stage	T(°C)[1]	Time (s)[2]	Carrier gas	Note
1	340	~ 600	Ambient air	OC1
2	750	~ 600	Ambient air	EC1

[1] The temperature ramps as rapidly as possible when advancing to next stage; [2] the entire analysis time are adjustable but should not be > 30 min.

Pyrolized OC adjustment:

No estimate for pyrolized OC, but rapid temperature increase to stage 1 is expected to minimize pyrolysis.

Carbonate adjustment:

No estimate for carbonate carbon.

OC and EC definition:

OC = OC1

EC = EC1 (soot)

TC= OC + EC

Performances:

Lower detection limit (LDL):
~0.2 μg carbon (0.1 μl CO_2) or ~0.1 μgC/m^3 ambient concentration for 3-hr average.

Precision:
~ 10% for TC and 20% for OC and EC.

Potential biases for OC/EC split:

1) This method does not adjust for the pyrolized organic carbon in the heating process. Though pyrolysis can be minimized in ambient air, it could still be produced over a long heating time.

2) The analysis uses ambient air that usually contains ~ 20% of oxygen. EC could be oxidized on stage 1 under such an environment, leading to an overestimation of OC.

3) Some high molecular weight organics that do not evolve at 340°C may be mistakenly classified as EC.

4) Lack of carbonate adjustment could bias EC/OC ratio for sample containing rich crustal material or fly ash.

5) Variations in ambient CO_2 concentration may influence the accuracy of carbon measurement.

Table A-1. Continued.

CalTech TOT method – ACE-Asian I

Procedure:

1) Liberating carbon compounds under different temperature and oxidation environment from sample punch taken from a quartz fiber filter (QFF) or carbon impregnated glass fiber filters (CIG, backup filter), 2) converting these compounds to carbon dioxide (CO_2) by passing the volatized compounds through a bed of granular MnO_2 (held ~ 900°C), 3) reduction of the CO_2 to methane (CH_4) by passing the flow through a methanator (firebrick impregnated with nickel catalyst at ~ 450°C in a stream of hydrogen, 4) quantification of CH_4 by FID, 5) calibrate the instrument by releasing CH_4 into it.

References:
Mader et al., 2001a; 2001b

Contact person:
Brain Mader
<bmader@cheme.caltech.edu>

Studies using this technique:

ACE-Asia aircraft carbon measurement, Mader et al., 2001b

Working parameters in procedure (1) for QFF:

Stage	T(°C)[1]	Time (s)	Carrier gas	Note
0	25	-	He	Oven flush
1	310	60	He	OC1
2	450	60	He	OC2
3	575	60	He	OC3
4	870	90	He	OC4
5	-	~60	He	Cool oven
6	550	45	10%O_2/90%He	EC1
7	625	45	10%O_2/90%He	EC2
8	700	45	10%O_2/90%He	EC3
9	775	45	10%O_2/90%He	EC4
10	850	45	10%O_2/90%He	EC5
11	900	120	10%O_2/90%He	EC6

Working parameters in procedure (1) for CIG

Stage	T(°C)[1]	Time (s)	Carrier gas	Note
0	25	-	He	Oven flush
1	250	60	He	OC1
2	300	60	He	OC2
3	350	60	He	OC3
4	400	90	He	OC4
5	450	30	He	OC5

[1] The rate temperature increasing is 3-7°C/s when advancing to next stage.

Pyrolized OC and carbonate adjustment:

Same as the NIOSH TOT method.

OC and EC definition (QFF):

OC = OC1 + OC2 + OC3 + OC4 + OP
EC = EC1 + EC2 + EC3 + EC4 + EC5 + EC6 - OP
TC= OC + EC

Performances:

Lower detection limit (LDL):
~ 0.15 μg carbon cm^{-2} or 0.24 – 0.3 μg carbon (1.45 cm^2 filter punch)

Precision (S_r):
~ 19% @ 1 μg carbon (NIOSH)
~ 1% @ 10 – 72 μg carbon (NIOSH)

Potential biases for OC/EC split:

1) The pyrolysis-adjustment assumes that the light absorption per unit mass of pyrolytically produced carbon is equal to the light absorption per unit mass of carbon burned in restoring the reflectance or transmittance to its initial value. This is not fundamentally justified.

2) The pyrolized OC adjustment is not applied to CIG filters.

3) Residence time at each heating stage may not be long enough to allow FID response returning to the baseline, resulting in ill-defined carbon fractions.

4) EC may evolve at the 870°C stage with pure He environment due to the release of oxygen from complex mineral oxides at high temperature. This may cause the laser signal returning before the introduction of O_2 and an underestimation of EC and OP.

Table A-1. Continued.

GM Research Laboratory Thermo-evolution Method

Procedure:

1) Liberating carbon compounds at a high temperature and various oxidation environments from 22-mm diameter glass disks from an impactor or sample punches (1.05 or 0.314 cm^2) from quartz fiber filters, 2) converting these compounds to carbon dioxide (CO_2) by passing the volatized compounds through an oxidizer (MnO_2 at ~ 950°C), 3) quantification of CO_2 by a nondispersive infrared analyzer, 4) (from ②, optional) preheating another sample punch from the same filter for several minutes and then repeating step 1 – 3 to determine EC.

References:

①Cadle et al., 1980
②Cadle et al., 1983

Contact person:
Steven Cadle
<SCADLE@cmsa.gmr.com>

Studies using this technique:

Working parameters in procedure (1):

Stage	T(°C)	Time (s)	Carrier gas	Note
0[1]	350	~450	Ambient air	
1	650[2]	~100[3]	He	OC
2	650	~120[3]	Ambient air	EC

[1] Optional step: This step is to minimize pyrolysis; [2] temperature change is accomplished by moving samples into the heating chamber and almost immediate; 3) Advancing to next stage begins when the NDIR response returns to baseline.

Pyrolized OC adjustment:

No estimate for pyrolized OC, but preheating the sample in ambient air (stage 0) is expected to minimize pyrolysis.

Carbonate adjustment:

Carbonate carbon is determined by measuring CO_2 (in He) evolved upon acidification of the sample punch with 0.1 mL, 25% aqueous H_3PO_4 for 30 minutes.

OC and EC definition:

If heating in stage 0 is not applied ① ,

OC = carbon evolved in stage 1
EC = carbon evolved in stage 2
TC = OC + EC

If stage 0 is included to reduce pyrolyzed OC ②,

TC is determined from the first case (i.e. no preheating)
EC = carbon evolved in stage 2
OC = TC - EC (e.g. OC and EC are determined on different sample punches)

Performances:

Lower detection limit (LDL):
~ 0.05 μg carbon

Lower quantifiable limits (LQL):
~ 1.8 μg carbon cm^{-2} for OC (blank correction)
~ 0.4 μg carbon cm^{-2} for EC

Precision:
Precision was determined by running duplicate or triplicate filter samples. Most results show a precision of ~ 2%.

Potential biases for OC/EC split:

1) This method does not adjust for the pyrolized organic carbon. Even if stage 0 is included to minimize pyrolysis, pyrolysis (filter blackening) could still be observed at stage 1, leading to an overestimation of EC.

2) When Stage 0 is included, OC and EC abundance are determined from different punches of the sample. The inhomogeneous deposition on the filter could bias the EC/OC ratio.

3) 650°C may not be high enough for complete combustion of some high-temperature elemental carbon.

Table A-1. Continued

German VDI 2465/1 Extraction and Thermo-evolution Method

Procedure:

0) Divide the exposed glass fiber filter (47 – 50 mm diameter) into two halves, 1) extracting organics on the filter half with 10 ml of a 50:50 vol.%-mixture of toluene and 2-propanol for 24 h, and then drying it with a pure N_2 flow, 2) heating the filter half in an inert environment (N_2) at 500°C to remove adhering solvent residues and non-extractable organic compounds, 3) liberating carbon compounds by heating the filter half in a pure O_2 environment and then 4) converting these volatile compounds to CO_2 by passing them through a CuO/Pt catalyst (held ~ 900°C), 5) removing evolved SO_2 and HCl by passing the gas stream through an oven packed with silver wool kept at 500°C, 6) quantification of CO_2 by coulometric titration (Coulomat 702; kept at PH = 9.6) to determine EC, 7) analyzing the other filter half through (3)-(6) to determine TC.

References:

VDI 2465/Part1, 1996;

Studies using this technique:

Laskus et al., 1999; 2001

Temperature program in procedure (2):

Stage	T(°C)[1]	Time (s)	Carrier gas	Note
0	-	120	N_2	Oven flush
1	200	60	N_2	
2	500	420	N_2	
3	200	120	N_2	

Temperature program in procedure (3):

Stage	T(°C)[1]	Time (s)	Carrier gas	Note
0	-	120	O_2	Oven flush
1	200	60	O_2	EC or TC
2	650	420	O_2	
3	200	120	O_2	

[1] The temperature-increasing rate is ____°C/s upon advancing to next stage.

Pyrolized OC adjustment:

No estimate for pyrolyzed OC. OC is removed by extraction to minimize pyrolysis.

Carbonate adjustment:

No estimate for carbonate carbon.

OC and EC definition:

EC and TC are determined on different filter halves and

OC = TC - EC

Performances:

Absolute detection limit:
~ 9 μg carbon

Precision:
The relative standard deviation for replicates is ~ 10% for all methods studied for separating off organic constitutes.

Potential biases for OC/EC split:

1) This method does not adjust for the pyrolized organic carbon. Whether the solvent can extract all the organic carbon but no elemental carbon is questionable.

2) TC and EC amounts are determined from different punches of the sample. The inhomogeneous loading on the sample surface could bias the EC/OC ratio.

3) Lack of carbonate adjustment could bias EC/OC ratio for sample containing rich crustal material or fly ash.

Table A-1. Continued.

German VDI 2465/2 Thermo-evolution Method

Procedure:

1) Liberating or pyrolyzing carbon compounds on a quartz fiber filter punch (diameter 8, 9, or 11 mm) under different temperature and oxidation environment, 2) converting the evolved carbon to CO_2 by passing the volatized compounds through a CuO/CeO_2 catalyst (held ~ 900°C), 3) quantification of CO_2 by a nondispersive infrared analyzer to determine OC and EC.

References:

VDI 2465/Part 2, 1999

Studies using this technique:

Schmid et al., 2001

Temperature program in procedure (1):

Stage	T(°C)*	Time (s)	Carrier gas	Note
0	-	-	He	Oven flush
1	80	12	He	OC
2	350[1]	72	He	
3	620[1]	108	He	
4	400[2]	18	He	
5	300[1]	30	20%O_2/80%He	
6	700[3]		20%O_2/80%He	EC
7	80[2]		20%O_2/80%He	

*The temperature-change rate is [1] 10, [2] 25 or [3] 6.7 °C/s from the previous stage. 54

End

Pyrolized OC adjustment:

No estimate for pyrolized OC. Flash heating in stage 2 is expected to minimize pyrolyzed.

Carbonate adjustment:

No estimate for carbonate carbon.

OC and EC definition:

OC = carbon evolved in stage 1-3
EC = carbon evolved in stage 6-7
TC = OC + EC

Performances:

Absolute detection limit (regarding blank correction):
~ 1.8 μg OC and ~0.3 μg EC

Relative detection limit:
~ 0.9 μg cm^{-3} for OC
~ 0.13 μg cm^{-3} for EC

Potential biases for OC/EC split:

1) This method does not adjust for the pyrolized organic carbon in the heating process. Though pyrolysis may be minimized by quickly ramping the temperature, it could still be significant for heavily loaded sample.

2) Lack of carbonate adjustment could bias EC/OC ratio for sample containing rich crustal material or fly ash.

3) For heavily loaded sample, the duration time at each stage may not be long enough for a complete evolution of carbon.

Table A-1. Continued.

AtmAA Thermal Manganese Dioxide Oxidation (TMO) Method

Procedure:

1) Acidifying sample punches of 0.07 cm^2 taken from quartz fiber filters, 2) liberating carbon compounds on the sample punches and converting them to CO_2 by heating the samples in contact with a bed of granulated MnO_2 through three temperature stages, 3) reducing CO_2 to methane (CH_4) by passing the flow through a methanator (firebrick impregnated with nickel catalyst at _____°C in a stream of hydrogen, 4) quantification of CH_4 by FID.

References:
Fung, 1990
Fung et al., 2002

Contact Person
Kochy Fung <kfung@earthlink.net>

Major Field Studies

SCAQS
Korea Institute of Science and Technology, Park et al., 2001; Kim et al., 2000

Temperature Program

Stage	T(°C)[1]	Time (s)	Carrier gas	Note
1	120	180	He	ARC
2	525	300	He	OC
3	750	180	2.5%O_2/97.5%He	EC

[1] The stage advancement is accomplished by moving the sample punch into next heating zone, and therefore the temperature change is instantaneous.

Pyrolized OC adjustment:

No estimate for pyrolized OC, but the constant availability of O_2 from MnO_2 at Stage 1 and the rapid temperature ramping rates all contribute to minimizing pyrolysis.

Carbonate adjustment:

Samples are acidified with 30 μL of 0.02N HCl prior to be heated for 180 s at Stage 1. This procedure removes water and CO_2 released by carbonate present. The carbon evolved at Stage 1 is defined as acid-released carbon (ARC).

OC and EC definition:

OC = carbon evolved at Stage 2.
EC = carbon evolved at Stage 3.
TC = OC +EC

Performances:

Lower detection limit (LDL):
0.08 μg OC carbon.

Lower quantifiable limits (LQL):
0.97 μg/cm^2 for ARC
1.57 μg/cm^2 for OC
0.39 μg/cm^2 for EC

Precision:
2.6% for OC at range 5.3 to 365.7 μg cm^{-2}
8.1% for EC at range 0.1 to 85.7 μg cm^{-2}

Remarks

1) Though pyrolysis during heating is expected to be minimized in the presence of MnO_2, the bias in OC/EC split due to pyrolysis is uncertain.

2) Semi-volatile OC may evolve at Stage 1 and be classified as ARC.

3) EC may evolve at Stage 2 due to O_2 released from MnO_2.

4) Heating time is limited, but it is usually long enough for a complete removal of OC before the introduction of oxygen.

5) The carbon analyzer is a modified Dohrmann DC-50 carbon analyzer and can be calibrated with a standard solution of potassium hydrogen phthalate (KHP).

Table A-1. Continued.

HONG KONG EPD TOT Method

Procedure:

1) Liberating carbon compounds under different temperature and oxidation environment from sample punch (1.5 cm^2) taken from a quartz fiber filter, 2) converting these compounds to carbon dioxide (CO_2) by passing the volatized compounds through a bed of granular MnO_2 (held ~ 900°C), 3) reduction of the CO_2 to methane (CH_4) by passing the flow through a methanator (firebrick impregnated with nickel catalyst at ~ 496°C in a stream of hydrogen, 4) quantification of CH_4 by FID, 5) calibrate the instrument by releasing CH_4 into it.

References:
①Sin et al., 2002

Contact Person
Della Sin <….>
Peter Louie <plouie@epd.gov.hk>

Studies using this technique:

Hong Kong 12 Month $PM_{2.5}$ Study

Working parameters in procedure (1) ❶:

Stage	T(°C)[1]	Time (s)	Carrier gas	Note
0	25	-	He	Oven flush
1	350	70	He	OC1
2	550	70	He	OC2
3	850	110	He	OC3
4	-	to 550°C	He	Cool oven
5	550	10	5%O_2/95%He	EC1
6	600	50	5%O_2/95%He	EC2
7	700	40	5%O_2/95%He	EC3
8	750	30	5%O_2/95%He	EC4
9	800	30	5%O_2/95%He	EC5
10	850	70	5%O_2/95%He	EC6

[1] The rate temperature increasing is 3 –7°C/s when advancing to next stage.

Pyrolized OC adjustment:

The filter transmittance is monitored continuously via a He-Ne laser at a wavelength of 632.8 nm. The portion after stage 6 until laser signal returns to its initial value (laser split) is assigned to pyrolized OC (OP).

Carbonate adjustment:

Carbonate carbon (CC) is estimated by exposing a second punch from the same filter to HCl vapor (PH ~ 2) for 1 hr before TOT analysis. The difference in total carbon (usually in OC4) between the two punches gives an estimate of carbonate carbon.

OC and EC definition:
OC = all the carbon evolved before laser split.
EC = all the carbon evolved after laser split.
TC = OC + EC

Performances:

Lower detection limit (LDL):
0.2 μg carbon cm^{-2} or 0.3 μg carbon (1.5 cm^2 filter punch) for both OC and EC.

Precision:
4 – 6% for 5 – 400 μg OC cm^{-2} and 1 – 15 μg EC cm^{-2} (1.5 cm^2 filter punch).

Potential biases for OC/EC split:

1) The pyrolysis-adjustment assumes that the light absorption per unit mass of pyrolytically produced carbon is equal to the light absorption per unit mass of carbon burned in restoring the reflectance or transmittance to its initial value. This is not fundamentally justified.

2) The volatilization of light-absorbing organic carbon could cause an increase in laser signal before O_2 is introduced.

3) Residence time at each heating stage may not be long enough to allow FID response returning to baseline, resulting in ill-defined carbon fractions.

4) EC may evolve at the 900 °C stage with pure He environment due to release of oxygen from complex mineral oxides at high temperature. This may cause the laser signal returning before the introduction of O_2 and an underestimation of EC and OP.

Table A-1. Continued.

HONG KONG UST-3 TOT Method

Procedure:

1) Liberating carbon compounds under different temperature and oxidation environment from sample strip (1×1.45 cm^2) taken from a quartz fiber filter, 2) converting these compounds to carbon dioxide (CO_2) by passing the volatized compounds through a bed of granular MnO_2 (held ~ 870°C), 3) reduction of the CO_2 to methane (CH_4) by passing the flow through a methanator (firebrick impregnated with nickel catalyst at ~ 496°C in a stream of hydrogen, 4) quantification of CH_4 by FID, 5) calibrate the instrument using standard CH_4.

References:
Yang and Yu, 2002
Yu et al., 2002

Contact Person
Jian Zhen Yu <chjianyu@ust.hk>

Studies using this technique:

Working parameters in procedure (1) ❶:

Stage	T(°C)[1]	Time (s)	Carrier gas	Note
0	25	-	He	Oven flush
1	250	150	He	OC1
2	500	150	He	OC2
3	650	150	He	OC3
4	850	150	He	OC4
5	-	to 650°C	He	Cool oven
6	650	150	1%O_2/99%He	EC1
7	750	150	1%O_2/99%He	EC2
8	850	150	1%O_2/99%He	EC3
9	890	150	1%O_2/99%He	EC4

[1] The rate temperature increasing is 3 –7°C/s when advancing to next stage.

Pyrolized OC adjustment:

The filter transmittance is monitored continuously via a He-Ne laser at a wavelength of 680 nm. The portion after stage 6 until laser signal returns to its initial value (laser split) is assigned to pyrolized OC (OP).

Carbonate adjustment:

No adjustment for carbonate compound.

OC and EC definition:

OC = all the carbon evolved before laser split.
EC = all the carbon evolved after laser split.
TC = OC + EC

Performances:

Lower detection limit (LDL):
0.2 μg carbon cm^{-2} or 0.3 μg carbon (1.5 cm^2 filter punch) for both OC and EC.

Precision:
4 – 6% for 5 – 400 μg OC cm^{-2} and 1 – 15 μg EC cm^{-2} (1.5 cm^2 filter punch).

Potential biases for OC/EC split:

1) The pyrolysis-adjustment assumes that the light absorption per unit mass of pyrolytically produced carbon is equal to the light absorption per unit mass of carbon burned in restoring the reflectance or transmittance to its initial value. This is not fundamentally justified.

2) The volatilization of light-absorbing organic carbon could cause an increase in laser signal before the O_2 is introduced.

3) Residence time at each heating stage may not be long enough to allow FID response returning to baseline, resulting in ill-defined carbon fractions.

4) EC may evolve at the 900 °C stage with pure He environment due to release of oxygen from complex mineral oxides at high temperature. This may cause the laser signal returning before the introduction of O_2 and an underestimation of EC and OP.

Table A-1. Continued.

Canada MSC1 TOT Method

Procedure:

1) Liberating carbon compounds under different temperature and oxidation environment from sample strip (1 cm^2) taken from a quartz fiber filter, 2) converting these compounds to carbon dioxide (CO_2) by passing the volatized compounds through a bed of granular MnO_2 (held ~ 900°C), 3) reduction of the CO_2 to methane (CH_4) by passing the flow through a methanator (firebrick impregnated with nickel catalyst at ~ 500°C in a stream of hydrogen, 4) quantification of CH_4 by FID, 5) calibrate the instrument using standard CH_4.

References:
Sharma et al., 2002

Contact Person
Sangeeta Sharma
<sangeeta.sharma@ec.gc.ca>

Studies using this technique:

Working parameters in procedure (1) :

Stage	T(°C)[1]	Time (s)	Carrier gas	Note
0	25	-	He	Oven flush
1	250	150	He	OC1
2	450	150	He	OC2
3	550	180	He	OC3
4	900	90	He	OC4
5	-	to 550°C	He	Cool oven
6	550	240	10%O_2/90%He	EC1
7	700	210	10%O_2/90%He	EC2
8	800	150	10%O_2/90%He	EC3

[1] The rate temperature increasing is 3 –7°C/s when advancing to next stage.

Pyrolized OC adjustment:

The filter transmittance is monitored continuously via a He-Ne laser at a wavelength of 680 nm. The portion after stage 6 until laser signal returns to its initial value (laser split) is assigned to pyrolized OC (OP).

Carbonate adjustment:

No adjustment for carbonate compound.

OC and EC definition:

EC (also called BC) = EC1 + EC2 +EC3 – OP + OC4
OC = OC1 + OC2 + OC3 + OP
TC = OC + EC

Performances:

Lower detection limit (LDL):
~ 0.17 μg carbon cm^{-2} or 3 μg carbon per filter (47 mm diameter) for both OC and EC.

Precision:
±10 %

Potential biases for OC/EC split:

1) The pyrolysis-adjustment assumes that the light absorption per unit mass of pyrolytically produced carbon is equal to the light absorption per unit mass of carbon burned in restoring the reflectance or transmittance to its initial value. This is not fundamentally justified.

2) The volatilization of light-absorbing organic carbon could cause an increase in laser signal before the O_2 is introduced.

3) Carbon evolved at the 900 °C stage (OC4) is assigned completely to EC. However, some pyrolyzed OC and carbonate material evolve at this stage as well. This could cause an overestimation of EC in some cases.

APPENDIX B

UPDATE OF LITERATURE REVIEW ON CARBON INTERCOMPARISON STUDIES

Table B-1. Summary of carbon intercomparison studies.

Study/Period/Location/Type	Sampling and Analytical Methods	Summary of Major Findings
Comparisons of shortwave absorption during SCAR-B Experiments (Reid et al., 1998) • Period: 8/17/1995 – 9/20/1995 • Location: Amazon area, Brazil. • Type: Wood smoke and regional haze.	• Six methods used to measure light-absorption coefficient: optical extinction cell (OEC), integrating plate (IP), optical reflectance (OR), particle soot/absorption photometer (PSAP), thermal evolution (TE), and remote sensing (RS). Except for RS, data all acquired from in-situ instruments or filters collected abroad an C-131A research aircraft, which flew over three main locations: Cuiabá, Porto Velho, and Marabá in Brazil. • OEC measured extinction with a 6.4 m long transmissometer. Absorption derived from the difference between extinction and scattering measured by nephelometer. • IP, OR, and PSAP determined light absorption by measuring attenuation through particles collected on filters. Appropriate corrections were applied to each method. • TE performed with France 2-step/pure oxygen thermal methods (Cachier et al., 1989). • Two radiative transfer algorithms (SPCTRAL2 and 6S) used to determine columnar-averaged single scattering albedo ($\omega 0$) from irradiance measurements by sun photometer and photosynthetically active radiation (PAR) sensor at the surface.	• For individual smoke plumes, IP and OR produced light-absorption measurements −3% and −0.5% difference from the OEC methods on average. OR compared best with OEC, with a variance less than 17%. • IP agreed better with OEC for filters with aerial densities >20 $\mu g\ m^{-2}$ with uncertainty < 30%. • TE showed poor agreements with OEC. Likely causes included the artifacts in the measurement and uncertainty in mass absorption efficiency of BC. (15 m^2/g was used in this study but other values were suggested in the literature.) • For regional haze events, there was a variance of 45% between PSAP and the OR techniques. This translates into an uncertainty in ω_0 of ±0.05 for a 1 min sample. • IP, OR, and PSAP gave mean values for ω_0 that agreed within ±0.02. However, much larger variance appeared in individual samples. • Application of the SPECTRAL2 to sun photometer and PAS dada yielded ω_0 slightly higher (by 0.01 – 0.02) than the columnar-averaged values derived from in-situ aircraft measurements. The 6S models showed varied results. The 6S model required the input of complex refractive index of aerosol, which might not be correctly parameterized. • This comparison study demonstrates the difficulty in deriving reliable absorption coefficient from TE. If errors in mass absorption efficiency could be overcome, the uncertainty in absorption coefficient from TE would be ~ 30%

Table B-1. Continued.

Study/Period/Location/Type	Sampling and Analytical Methods	Summary of Major Findings
Calibration of PSAP, Integrating Plate, and Hybrid Integrating Plate System (Bond et al., 1999) • Period: November 1996 – August 1997 • Location: University of Washington, Seattle. • Type: Synthesized light-absorbing and light-scattering aerosols.	• A common black pigment, nigrosin (C48N9H51), is used as reference light-absorbing material. Water solutions of nigrosin, ammonium sulfate, and their mixtures were nebulized using bubblers. The resulting droplets were dried, filtered out for supermicrometer particles, and transmitted to the measurement systems. • The measurement system consisted of: 1) optical extinction cell (6.37 m long OEC, Radiance Research); 2) Two nephelometers (TSI 3563); 3) PSAP (Radiance Research), integrating plate (IP), and IMPROVE sampler for subsequent Hybrid Integrating Plate System (HIPS) measurement. • PSAP and IP determined light absorption based on attenuation of laser through exposed filters. HIPS measured both reflectance (by integrating sphere) and transmittance (by integrating plate) of a filer to determine absorption. Absorption determined from the difference of OEC and nephelometer served as the reference. • Morphologies for each particle type were examined by transmission electron microscopy (TEM).	• Based on inter-unit comparisons, the precision of PSAP was estimated within ±6%. To reach the best precision, the corrections for flow rate and spot size need to be made. Precision appeared to be lower for low-absorbing aerosol. • All the particles generated were found to be spherical and internally uniform. Particle size ranged from 0.1 to 0.5 μm. • Response to light scattering and absorption were determined for each instrument. About 2%, 9%, and 4% of light scattering was interpreted as absorption by PASP, IP, and HIPS, respectively. • Without offline corrections, PSAP, IP, and HIPS overestimated absorption by 22, 23, and 33%, respectively; but their readings were highly correlated to absorption (r2 = 0.94, 0.91, and 0.82, respectively.) • Filter-based absorption must be corrected for light scattering effect. Correction formulas were given for each instrument used in this experiment.

Table B-1. Continued.

Study/Period/Location/Type	Sampling and Analytical Methods	Summary of Major Findings
Comparison of TOT and Aethalometer measurements for Diesel Particulate (Borak et al., 2003) • Period: Not indicated • Location: An automotive test track in Virginia. • Type: Diesel-powered school bus emission and DPM at industrial work sites.	• School buses were run on the track for 4 to 6 hours with measurements made at several locations on the test track. • Work sites included diesel repair workshop, diesel factory, and underground salt mine. • Three aethalometers (AE21) operated at a flow rate of 4 L/min and time resolution of 1 min. • NIOSH5040 thermal analysis performed on samples either open-faced or preceded by cyclones. • Filter sampling time were between 800 – 1,200 min for school buses and 200 – 500 min at work sites.	• There were statistically significant differences between measurements from two side-by-site aethalometers. A separate calibration was needed. • The aethalometer EC, determined by 1.32 × BC during the school bus survey, agreed closely ($r^2 = 0.91$) with NIOSH5040 EC from open-faced samples, though EC concentration was as low as undetectable to 1.9 μm^{-3}. • Comparison of results from workplace sampling also indicated that aethalometer EC agreed better with open-faced samples. EC might be associated with large particles at these work sites (e.g., > 4 μm). • Using aethalometer to monitor diesel emission is feasible, but there were two weaknesses. One was the inaccuracy of airflow. The other was the long cycle time required to advance the instrument's quartz tape, which prevented the aethalometer from monitoring moderate to high levels of DPM (> 50 $\mu m/m^3$).
ACE-Asia: EC Absorption in Asian Outflow (Chuang et al., 2003) • Period: 3/30/2001 – 5/2/2001 • Location: Gosan (Jeju Island), Korea • Type: Asian outflow.	• Twenty-four PM_1, $PM_{2.5}$, PM_{10}, and TSP were collected on quartz-fiber filters. • $PM_{2.5}$ was analyzed by two laboratories for EC using identical protocols (NIOSH5040). PM_1, PM_{10}, and TSP were analyzed by one of the laboratories. • Light-absorption at 565 nm was measured by PSAP and corrected to 550 nm. The PSAP measurements were alternated between PM_{10} and PM_1 in 6-min. intervals. • Light-absorption efficiency of internal and external mixtures of EC and dust were calculated with discrete dipole approximation. Three dust geometry and two EC geometry were considered.	• A significant amount of EC (39±11%) was present in the coarse-model particles. This indicated internal mixing of dust and EC. • Observed EC absorption efficiency was 12.6±2.6 m^2/g and 14.8±2.3 m^2/g for PM_{10} and PM_1, respectively. Absorption efficiency of coarse particles (PM_{10}-PM_1) was 5.7±1.6 m^2/g and 2.9±1.0 m^2/g for dust and non-dust days, respectively. These values could be high-biased since cyclones upstream of the filter samples removed more particles than those for PSAS during high RH days. • Model predicted the change in mass absorption efficiency of EC due to internal mixing of dust ranging from 15-37%, assuming an EC mass fraction of 0.4%. • The net change in shortwave absorption by polluted dust layers due to coagulation of EC with dust was predicted to range between -42% and 58%.

Table B-1. Continued.

Study/Period/Location/Type	Sampling and Analytical Methods	Summary of Major Findings
Optimization of Thermal-Optical Method with Reference Materials (Conny et al., 2003) • Period: SRM1649a was collected during 1976; other samples were collected particularly for this experiment. • Location: SRM 1649 was collected in Washington, DC. Other samples were collected in the laboratory. • Type: Urban dust material, wood smoke, etc.	• Three reference materials prepared: 1) urban dust (SRM1649a) resuspended on precleaned 37 mm quartz-fiber filters; 2) laboratory indoor particles < 0.95 μm in aerodynamic diameter collected on precleaned 20 × 25 cm quartz-fiber filter; 3) wood-smoke particles from the smoldering stage of a boreal forest fire collected on precleaned 20 × 25 cm quartz-fiber filter. • A Sunset Lab's Thermal Optical Carbon Analyzer deployed for carbon analysis. • Thermal methods modified from the NIOSH and IMPROVE protocol. Each method characterized by four factors: 1) temperature of step 4 in He; 2) duration of steps 1-4 in He; 3) temperature of steps 1-3 in He (varied proportionately; and 4) duration of step 1 in O_2-He. • Char examined with scanning electron microscopy (FEI-Phillips-Electroscan model 2020).	• The approaches to optimizing TOA were based on two goals: 1) to maximize OC char so that detection of residue OC as EC is minimized; 2) to minimize the loss of EC at high temperatures in He. The amount of OC char and EC loss was indicated by the maximum laser attenuation (*Lmax*) and laser attenuation at the end of He phase (*LHe4*), respectively. • The intersection between the *Lmax* and *LHe4* revealed the optimal TOA conditions, for sample types used in this study, in the fixed-step-duration TOT: step 1 in He, 190 ºC for 60 s; step 2 in He, 365 ºC for 60 s; step 3 in He, 610 ºC for 60 s; step 4 in He 835 ºC for 72 s. For steps 1-4 in O_2-He, the conditions are 550 ºC for 180 s, 700 ºC for 60 s, 850 ºC for 60 s and 900 ºC for 90 to 120 s, respectively. • SEM images revealed that smaller particles (< 1 μm in diameter) remained on filters following heating at 550, 700, or 800 ºC. Larger particles (> 2 μm diameter) were present only after 550 or 700 ºC treatments. The presence of larger particles, likely charred remains of non-agglomerated particles, suggested that 550 and 700 ºC treatments were inadequate to either volatilize the carbon or pyrolyze it in OC-rich particles. The fourth step in He has to be higher than 800 ºC.

Table B-1. Continued.

Study/Period/Location/Type	Sampling and Analytical Methods	Summary of Major Findings
Generation of Model EC Aerosol for Human Challenge Studies (Evans et al., 2003) • Period: Not indicated. • Location: University of Birmingham, UK. • Type: Synthesized soot.	• The Pals CGC 1000 generated fine and ultrafine carbonaceous aerosols by spark discharge between two graphite electrodes, followed by using argon as a inert shield over the arcing region. • The resulting soot was diluted through a dilution chamber and collected by quartz-fiber filters. • Particle size was monitored by a SMPS (TSI3071) and an ELPI (Dekati) fitted with aluminum foil and a thermophoretic precipitator (TTP). • Soot deposit on TPP was examined by a TEM (FEG TEM, Phillips, Technai F20). • Soot mass was quantified by a multiphase carbon determinator (RC-412, Leco) which burned carbon in pure oxygen.	• Number concentration increased linearly with spark frequency. Number distribution modes were shifted from 20 to 60 nm with increasing spark frequency. • TEM examination of a soot particle at 60 nm mobility diameter determined a total layer width of ~ 0.35 nm, agreeing with a reported C-C width between layers for graphite (0.335 nm). This supports that these particles were indeed elemental carbon. • The particles captured under conditions of low argon shielding flow had overall fractal dimensions of 1.09 and 1.07. The fractal dimension increased with the argon shielding flow. • The soot generated in this study was comparable to that from high-temperature combustion sources, in terms of fractal dimension. They differ markedly from those derived from combustion of hydrocarbon fuels.
Evaluation of EC and BC Measurements from GAVim and IMPROVE Networks (Nejedly et al., 2003) • Period: 06/1994 – 07/1997 • Location: Abbotsford, BC (06/1994 – 06/1995); St. Andrews, NB, Canada (12/1994 – 07/1997). • Type: Rural to remote ambient air.	• EC measured with standard IMPROVE sampling protocol and TOR methods. • Light-absorption coefficients determined by laser integrated plate method (LIPM) with exposed Teflon filters. • The Guelph LIPM based on 2mW Uniphase He/Ne laser (Model 1122P). The beam split into two with one as reference. The aerosol filter. Aerosol filters placed behind a diffuser and a collimator.	• The LIPM calibrated with 7 piece set of Oriel neutral density filters. Precision found within 1.5% (95% confidence level). • Assuming an BC absorption efficiency of 10 m^2/g, a correction coefficient R that converted LIMS BC at Abbotsford into TOR EC (EC = BC/R) was determined from a polynomial fit: R = 1.35 – 3.89 × 10-4s – 4.2 × 10-6s^2. S indicated the areal mass density of filter. • The same fitting was applied to two remote GAViM sites. The results implied that the light absorption coefficient measured by LIPM is generally higher than the true value by up to a factor of 1.3 and 1.8. LIPM would overestimate the black carbon content if no corrections were made.

Table B-1. Continued.

Study/Period/Location/Type	Sampling and Analytical Methods	Summary of Major Findings
AIDA Soot Aerosol Campaign 1999 (Schnaiter et al., 2003; Saathoff et al., 2003a; 2003b) • Period: 10/4-10/29/1999 • Location: AIDA Facility, Forschungszentrum Karlsruhe, Germany. • Type: Artificial and diesel soot, ammonium sulfate, and their mixtures.	• Soot aerosols were generated by: 1) a VW 4-cylinder turbo diesel engine: and 2) a commercial spark discharge generator (GfG 1000, Palas). • Soot aerosols were introduced into a reaction chamber 84.3 m^3 in volume where they were diluted by air and mixed with ammonium sulfate or secondary organic aerosol (from ozonolysis of α-pinene. • Soot was sampled with quartz-fiber filter, analyzed for TC by coulometric method (Coulomat 702, Ströhlein) and for OC and EC by the France 2-step method. • BC was measured in-situ by two aethalometers (AE30 and AE10) with a conversion factor of 16.6 and 19 m^2/g, respectively, by a photoacoustic soot sensor (PASS) with a conversion factor of 2.7 m^2/g (680 nm), and by a photoelectric aerosol sensor (PAS2000). • Aerosol extinction was determined in a extinction cell 5 m long using a deuterium/halogen lamp as light source. A nephelometer (TSI 2563) was used to measure light scattering. • Aerosol mass concentration was monitored by a betameter (FH 62-1-R, Eberline) which collects particles on filter tape.	• For pure diesel soot, good agreements were found among all EC, TC, and BC measurements except for aethalometers, which yield BC only 80% of 40% of the TC measurements. The diesel soot was dominated by EC (95%), but the conversion factors of aethalometers needed to be adjusted. • For pure “Palas" soot, agreements were found between TC and light extinction. EC and BC were significantly lower. PAS BC was correlated better with aerosol surface area than mass. “Palas” soot contained only ~ 60% EC with relatively large scatter, as indicated by thermal analysis. • Admixing $(NH_4)SO_4$ particles to diesel-soot aerosol did not affect carbon mass determinations significantly, not even at very high concentration. • SOA condensation: The BC signal of both aethalometer increased by 40% (AE10) and 54% (AE30) upon coating with SOA. SOA coating appeared to enhance the light absorption cress section of BC. • Coating diesel soot with SOA also reduced the PAS signal to a very low level (by a factor of 3), most likely due to the rapid reaction of ozone with surface functionalities and/or that the photoelectrons cannot penetrate the SOA surface film. • The total aerosol mass determined with betameter systematically exceeded the sum of TC/SOA/$(NH_4)SO_4$ mass concentrations (on average by 32%). A possible cause for part of this discrepancy was the remaining water content of the $(NH_4)SO_4$ particles.

Table B-1. Continued.

Study/Period/Location/Type	Sampling and Analytical Methods	Summary of Major Findings
ACE-Asia: Intercomparison Experiments for OC and EC Measurements (Schauer et al., 2003) • Period: Ace-Asia aircraft samples were obtained on 3/31/2001; other samples were collected at various times. • Location: Various locations. • Type: A wide variety of ambient and source samples.	• Nine samples and two blanks were prepared for round-ribbon intercomparisons among eight laboratories participating in the ACE-Asia study. These samples represented urban, rural, and remote environments. • Ten additional samples were prepared for testing temperature program effects. These samples represented urban atmosphere, wood smoke, fly ash, carbon black, secondary organic aerosol, etc. • Laboratory participating in the round-ribbon experiment used identical instrument (Sunset Lab Carbon Analyzer) and thermal protocol (NIOSH5040) for carbon analysis. • Three alterative temperature programs were used to test temperature effect on OC/EC split. These programs varied only in temperatures in He atmosphere (OC1–OC4).	• Average OC and EC content in the round-ribbon experiment ranged from 0.41 to 15.35 μg/cm^2 and 0.04 to 2.96 μg/cm^2, respectively. • Of the 72 valid OC and EC measurements, only one OC and three EC measurements deviated from consensus value by > 2 standard deviations. These outliers were reported by two laboratories, but the reasons were not fully identified. • The threshold uncertainty of EC measurements as the EC level approached zero was a factor of four higher than the level reported by the manufacturer (0.05 μg/cm^2). The slope of uncertainty curve for EC, as determined by this experiment, is close to 20%, but it reduced to ~ 5% if outlier measurements from the two laboratories were excluded. • An alternative temperature program that featured the lowest temperature in OC4 (550 ºC) reported EC 1.6-2.1 times greater than the base case. One possible explanation is that some OC that does not pyrolyze or volatilize at the low OC4 temperature is carried over to the EC fraction.
Light Absorption Measured by Aethalometer (Weingartner et al., 2003) • Period: Not Indicated • Location: at Paul Scherrer Institut, Villigen, Switzerland. • Type: Smog chamber.	• Smog maintained at typical atmospheric conditions (40% RH, 296K). • Model soot generated by graphite spark generates, diesel soot generated with a commercial turbo diesel engine, and $(NH_4)_2SO_4$ aerosol generated using an ultrasonic nebulizer and diffusion dryers. • Organic coatings prepared by addition of ozone and α-pinene into the chamber. • Two Magee aethalometers, AE10 (880 nm) and AE30 (7 wavelengths), used to measured light absorption at a time resolution of 2 min. • Extinction and scattering determined with a flow tube extinction spectrometer (230 – 1000 nm), a folded path cell (473 nm), and a three-color TSI integrating nephelometer (450, 550, and 700 nm). Absorption determined by the difference of extinction and scattering served as a reference.	• Light source in AE10 was found to emit a wide spectrum centered at 840 nm, and this made light absorption measurement a difficult task. • A shadowing effect was caused by reduction of multiple light scattering in the filter by the embedded light absorbing particles. For pure soot particles where a filter change caused an apparent increase of measured signals by 16%. • Another instrumental artifact is the enhanced light absorption of the filtered particles by multiple scattering. The average enhancement is at a factor of 2.14 ± 0.21, but as high as 3.6 ± 0.6 were observed during experiments where soot particles were coated with oxidation productions of α-pinene. • Correction factors were developed for aethalometer, based on the idea to convert all attenuation to that without shadowing effect. Without these corrections, the derived absorption coefficient will generally be too high.

Table B-1. Continued.

Study/Period/Location/Type	Sampling and Analytical Methods	Summary of Major Findings
Validation of Sunset Carbon Analyzer Field Instrument at the St. Louis Supersite (Bae et al., 2004) • Period: Year 2002 • Location: St. Louis, Missouri. • Type: Urban atmosphere.	• Two semi-continuous ECOC instruments (Sunset Lab., Forest Grove, OR) operated downstream of a $PM_{2.5}$ size inlet and a organic denuder with charcoal-impregnated filter strips. The time resolution is 1 h. • Two integrated sampler systems were deployed side-by-side with the ECOC instrument. Twenty-hour samples were acquired. • NIOSH 5040 thermal protocol was used for carbon analysis for integrated and semi-continuous measurements.	• Average TC and EC concentration for the entire year of 2002 were 3.88 and 0.70 $\mu g/m^3$, respectively, determined by integrated samplers. • TC measurements by semi-continuous analyzers agreed well with the integrated samples ($r^2 = 0.89$; slope = 0.97). • Good relations were also found for OC and EC with slopes of 0.93 ± 0.02 and 0.95 ± 0.04, respectively. • Correlation coefficients were 0.9 and 0.6 for OC and EC, respectively. The degraded EC statistics reflected dispersion inherent in the larger fraction of measurements near the EC detection limit.
OC Charring Behaviors within Filter Matrix and Impacts on Thermal/Optical Analysis (Chen et al., 2004) • Period: Various periods • Location: Carbon black samples were produced in the laboratory. Ambient samples were acquired from Hong Kong and the United States. • Type: Carbon black; urban and rural ambient samples.	• Twenty samples from 13 IMPROVE network sites represented remote to suburban environments in the United States. Eighteen samples from Hong Kong, China covered rural to urban environments. • The IMPROVE samples were on pure quartz-fiber filters while the Hong Kong samples were on quartz-fiber filters that contain 5% borosilicate glass as a binder. • Resuspended carbon black particles (~ 56 nm diameter) were sampled with quartz-fiber filters as an EC reference. • Carbon analysis were made with DRI Model 2001 Carbon Analyzer (Atmoslytic Inc., Calabasas, CA) following the IMPROVE protocol. Filter reflectance and transmittance were monitored at 1-s resolution.	• A radiative transfer model based on extended Kubelka-Munk theory was developed to explain the reflectance and transmittance observations prior to and during thermal/optical analysis. • The deposition depth of carbon black, IMPROVE, and Hong Kong samples were predicted to be 0.014, 0.25, and 0.42, respectively. The divergence was due to difference sampling configurations. Most particles in ambient samples deposited into the top half of the filter. • POC appeared to form uniformly within the filter during thermal analysis, evidenced by a much higher deposition depth (2 – 6) than EC. • When heated in oxygen, most EC evolved earlier than POC for IMPORVE samples, but not so for Hong Kong samples. This caused inconsistent OC/EC split. • EC mass absorption efficiency in the filter, estimated from attenuation and POC/EC content, was ~ 2.5 m^2/g EC for carbon black and > 15 m^2/gEC for ambient samples.

Table B-1. Continued.

Study/Period/Location/Type	Sampling and Analytical Methods	Summary of Major Findings
Equivalence of EC by TOR and TOT with Different Temperature Protocols (Chow et al., 2004) • Period: Samples were acquired from Fresno, CA between 8/24/2002 and 4/18/2003 and from the IMPROVE network at various periods. • Location: Various locations. • Type: Urban and rural atmospheres.	• Fifty-eight 24-hr samples were acquired from Fresno using a High-Vol sampler with 406 cm^2 quartz-fiber filters. Fresno is considered an urban environment. • Two batches of IMPROVE samples used in this study. Thirty samples contained in the first batch were from 16 sites divergent in source types and 68 samples contained in the second batch were from 25 sites. • Carbon analysis were made with DRI Model 2001 Carbon Analyzers (Atmoslytic Inc., Calabasas, CA) following the IMPROVE or STN temperature protocol. Reflection (TOR) and transmittance (TOT) charring corrections were made for each sample. • Microscopic examination performed on a subset of filter samples retrieved halfway of a typical analysis.	• For either the Fresno or IMPROVE samples, TOR corrections yield equivalent OC/EC splits for widely divergent temperature protocols. EC determined from IMPROVE and STN TOR mostly agreed within 10% and show correlations higher than 0.98. • For both Fresno and IMPROVE samples, EC results from IMPROVE TOT were ~ 30% lower than IMPROVE TOR. However, EC results from STN TOT were 70–80% lower than STN TOR. • Visual and microscopic examination showed that substantial charring took place within the filter besides on the filter surface. The within-filter char evolved earlier than the near-surface deposit when oxygen was introduced into the analysis atmosphere. • The partition of POC and EC was estimated from incremental absorbance. POC was found to have effective mass absorption efficiency much higher than EC (~ 50 vs. ~ 20 m^2/g). EC estimated from absorbance agreed better with TOR EC.
Santiago Air Quality Study (Gramsch et al., 2004) • Period: May 2000 to September 2000 • Location: Santiago de Chile. • Type: Urban aerosol.	• Light absorption was measured with SIMCA. Light attenuation through a filter which continuously collected $PM_{2.5}$ was monitored by a photodetector to infer the light absorption coefficient (σ_a). The light source was a broadband lamp (300–900 nm). The time resolution was set to ~ 20 min. • $PM_{2.5}$ mass was monitored with a TEOM (R&P1400). • OC and EC in $PM_{2.5}$ were determined with a continuous carbon analyzer (R&P 5400) with a two-step oxidation method in air (340 ºC for OC).	• High-correlation was found between all pairs of variables ($PM_{2.5}$, EC, and σa) during the colder months (May-August). Correlation (r^2) between σa and EC were 0.872 and 0.766 for May and July, but only 0.612 for September; likely due to the change in PM2.5 composition. • Mass absorption efficiency of EC was estimated between 4.21 and 4.78 m^2/g from May to August and only 3.23 m^2/g for September. Overall average σ_a was 4.46±0.1 m^2/g • The σ_a for $PM_{2.5}$ was estimated at 1.02±0.03 m^2/g. • The measured σa was at the low end of values in the literature. Potential uncertainties included the wavelength of light source and the precision of EC measurement.

Table B-1. Continued.

Study/Period/Location/Type	Sampling and Analytical Methods	Summary of Major Findings
Comparisons of TOT and Aethalometer Measurements during NE-OPS (Jeong et al., 2004) • Period: June 6, 2002 to August 2, 2002 • Location: Rochester Medical Center, Rochester, NY (6/6/2002 – 6/17/2002); NE-OPS site at Philadelphia, PA (7/1/2002 – 8/2/2002). • Type: Rural ambient air.	• A Sunset Lab OC/EC field instrument (Sunset Laboratory, Forest Grove, OR) deployed at a time resolution of two hrs. Temperature protocols modified from NIOSH5040 with two temperature steps in OC (600 ºC/90s; 870 ºC/90s) and one in EC (870 ºC/90s). • BC determined from the Sunset instrument (BCS) using variable light attenuation coefficient (65 – 15 m2/g depending on EC loading). • Aethalometer AE20 operated at 5 m in time resolution with two wavelengths (880/370nm). BC absorption efficiency at 880 nm was assumed to be 16.6 m^2/g (BCA). • $PM_{2.5}$ mass determined with a 30 ºC TEOM.	• At Rochester where $PM_{2.5}$ was dominated by local traffic, EC was correlated well with BCS and BCA , though BCS/EC slope (0.89) was much lower than BCA/EC slope (3.3). • Correlations of EC with BCS and BCA were weaker at NE-OPS site where OC and EC accounted for < 30% of $PM_{2.5}$ mass. The BCS/EC and BCA/EC slope are 0.99 and 2.7, respectively. • During a Canadian forest fire episode, the BCA/EC and BCS/EC slope at NE-OPS site dropped to 0.4 and 0.31, respectively. • Absorption efficiency of EC appeared to depend strongly on physical and chemical characteristics of EC and varied spatially and temporally. • The level of UV (370 nm) absorbing organics significantly increased during the Canadian fire episode.
Spectral Dependence of Light Absorption by EC and OC (Kirchstetter et al., 2004) • Period: Samples were collected at various periods but analyzed between February 2002 and February 2004. • Location: Samples were collected from various locations but analyzed at the Lawrence Berkeley National Laboratory (LBNL). • Type: Diesel, wood burning, and urban ambient samples.	• Archived filter samples used in this experiment were mostly from SAFARI (savanna fire), Caldecott Tunnel (diesel), and Berkeley, CA (road side). Particles were collected on quartz-fiber filters. • Spectral light absorption was determined using light transmission method. Measurements were made with commercial spectrometers (Perkin Elmer and Ocean Optics) or MULTI developed at LBNL. • Shadowing (loading) effect in transmittance measurement was not corrected. • EC and OC were determined with the LBNL thermal method (continuous ramping at 40ºC per min. to 800ºC.) • Replicate analyses were made on a subset of samples pretreated by solvent to remove OC.	• The Angstrom Exponent, $\alpha = 2.5$, approximated the strong spectral dependence of the biomass burning aerosols and $\alpha = 1.0$ described well the weak spectral dependence of motor vehicle aerosols. • Solvent-pretreatment reduced the spectral dependence of absorption of wood-burning aerosols, but not that of motor-vehicle aerosols. OC in wood-burning samples contributed significantly to light absorption in UV and visible regions. • The OC contribution to light absorption increased from 1% at 700 nm to 58% at 350 nm for one of the SAFARI samples. • The estimated imaginary refractive index of OC extracted from biomass smoke samples ranged from 0.001 at 700 nm to 0.168 at 350 nm, corresponding to light absorption efficiency of 0 and 5m^2/g, respectively. • Imaginary reflective index of BC in urban- and motor-vehicle aerosol remained relatively constant (0.71-0.77). The BC light absorption efficiency ranged from 11m^2/g at 700 nm to 14 m^2/g at 550 nm and 23 m^2/g at 350 nm.

Table B-1. Continued.

Study/Period/Location/Type	Sampling and Analytical Methods	Summary of Major Findings
RTI (Research Triangle Institute, RTP, NC) Integrating-Sphere Method for Determining BC and Environmental Tobacco Smoke (ETS) (Lawless et al., 2004) • Period: Not indicated. • Locations: Denver Exposure Study at Denver, CO. • Type: Personal exposure samples from indoor and outdoor environments.	• Samples collected daily from personal exposure monitors (PEMs) with Teflon filters. • Modified integrating-sphere method to determine light-absorption by BC and ETS with minimum influence of filter scattering. • Multiple wavelengths (940, 660, 587, and 430 nm) measurements achieved by using LEDs as light sources. • Mass on filter determined by gravimetric method. • Standard BC and ETS generated in the laboratory for calibration of light absorption.	• Filter material showed small and consistent absorbance within the same lot of filters. Apparent absorption of the experimental configuration ranged between 2 and 24%. • BC and ETS showed different spectral dependence of absorbance. At 940 nm, ETS and BC show mass-specific absorption coefficient of 0.22 and 9.1 m^2/g, respectively. At 587 nm they are 1.02 and 16.7 m^2/g, respectively. • Algorithms were developed to apportion particle mass into ETS, BC, and a non-absorbing component, using an assumption that their contributions to filter optical depth (OD) are additive. • The MDL for BC on a 37-mm filter, derived from synthetic data, was 0.3 μg and MDL for ETS is 1.7 μg.
Comparisons of Graphitic Carbon (GC) by Raman Spectroscopy and BC by PSAP at a Mountain Site (Mertes et al., 2004) • Period: Autumn 1998; early 1999 and spring 2000. • Location: Summit of Mt. Brocken, Germany. • Type: Remote ambient air.	• Ambient samples colleted by a PSAP and poly-carbonate filters side by side. PSAP had a size cut ~ 5 μm and time resolution of one min. • Monarch 71 carbon black particles prepared as the calibration standard for Raman GC measurement. • Raman spectra measured with Bruker IFS 55 spectrometer equipped with a FRA-106 Raman module. 1064 nm excitation wavelength (10 W/cm2) and liquid nitrogen cooled Ge-diode detector. • The spectral processing included subtraction of spectrum from a blank filter and baseline. GC determined by integrating the band from 1,510 to 1,736 cm-1 in the final spectrum. • Light absorption was derived from PSAP with corrections to flow rate, sample spot size, and light scattering.	• The calibration indicated a precision of 2% and a minimum detection limit of 0.08 $\mu g/cm^2$ GC (dynamic range 0 – 4 $\mu g/cm^2$). • Monarch 71 showed a Raman spectrum very similar to that of atmospheric GC especially in the merged G and D band region. • GC measured on PSAP and on poly-carbonate filters agreed well with an r^2 of 0.94 and slope of 0.93±0.03. • At Mt. Brocken, GC typically accounted for only 3–10% of total aerosol mass (PM_5). • Comparing GC and PSAP absorption measurement, mass absorption efficiency of GC at this remote site was estimated between 10 and 18 m^2/g with an average of 14.7 ± 2.8 m^2/g. • Variability in mass absorption efficiency was unlikely caused by experimental artifacts in quantifying mass concentration of GC, but could be assigned to relations between optical and physico-chemical aerosol properties, such as internally mixing of GC with light-scattering components.

Table B-1. Continued.

Study/Period/Location/Type	Sampling and Analytical Methods	Summary of Major Findings
RAOS – Evaluation of Multiangle Absorption Photometry (MAAP) (Petzold and Schönlinner, 2004) (Petzold et al., 2005) • Period: 6/3/2002 – 6/28/2002 • Location: Reno, Nevada. • Type: Kerosene soot (largely BC), white (NH4)2SO4 aerosols, and mixtures thereof, as well as ambient PM2.5.	• MAAP developed by measuring filter reflectance at 130º and 165º and transmittance at 0º to determine the total aerosol optical depth and single scattering albedo within the filter, and therefore the light absorption coefficient in the air. • The radiative transfer equation used by MAAP assuming an asymmetric g factor of 0.75 for aerosol-filter layer and back scattered fraction of 0.7 for blank filter. • During RAOS, MAAP were compared with filter transmittance, reflectance, photoacoustic, extinction/scattering methods for measuring pure BC, externally mixed, and pure "white" $(NH_4)_2SO_4$ aerosols.	• Combining uncertainties of 5% related to the asymmetry factor, 10% related to the blank filter back scattered fraction, and 5% related to the diffusely scattered fraction measurement, an overall uncertainty in the determination of the filter sample absorbance of 12% is obtained by MAAP. • The MDL of MAAP was estimated at ~ 3.5×10^{-4} absorbance unit. • MAAP showed close agreement with reference absorption measurement. The slopes of regression lines vary between 0.99 ± 0.01 and 1.07 ± 0.02 for pure BC and external mixtures with $(NH_4)_2SO_4$ to 1.03 ± 0.05 for ambient aerosol. No effects of the filter loading and aerosol single scattering albedo (ω_0) were observed. No correction function was needed. • The conventional reflection method absorbance had to be corrected for the filter loading, but did not require a correction for ω_0. The transmittance method absorbance requires corrections for both filter loading and ω0 effects. These correction functions were empirically determined. • Comparing with the German VDI method for EC, MAAP yielded an average mass absorption coefficient of 9.1 – 10.7 $\mu g\ m^{-3}$ at $\lambda = 550$ nm for atmospheric BC in urban air.
Comparisons of Integrated Filter and Automated Carbon Aerosol Measurements (Rice, 2004) • Period: Summer 2002 • Location: RTP, NC • Type: Rural ambient air.	• 24-hr filter samples collected by Thermo Andersen RAAS2.5-410 (FRM equivalent). • EC quantified by standard STN/NIOSH protocol. • Three-hour samples collected and analyzed by R&P Series 5400 ambient particulate monitor for TC, OC, and EC. • Ten-minute BC measurement made using Series AE-21 Magee Aethalometer. Light attenuation converted to EC with a fixed specific attenuation cross section of 16.6 m^2/g at 880 nm.	• Comparing the 5400 with filter-based TOT, the 5400 TC and OC measurements significantly understated the TOT TC and OC by 64 and 78%. Part of this could be attributed to positive sampling artifact of filters and/or different charring correction. Correlations were also poor (r2 = 0.64 – 0.67) • 5400 overestimated TOT EC by 89%. No correlation. • Aethalometer overestimated TOT EC by 30%, but the correlation was good (r = 0.86). Good agreements between the two measurements can be achieved using an specific absorption efficiency of 19.4 m^2/g. • The 5400 EC was compared with BC both with and without $PM_{2.5}$ size inlet, reaching a correlation of 0.92 and 0.55, respectively. The impact of size-cut inlet was unclear.

Table B-1. Continued.

Study/Period/Location/Type	Sampling and Analytical Methods	Summary of Major Findings
INTERCOMP2000: Method Comparison Study in Europe (ten Brink et al., 2004) • Period: 4/3/2000 – 4/14/2000 • Location: Melpitz, Germany. • Type: Rural aerosol.	• Twelve different samplers were used for TC/OC/EC measurements, including seven filter samplers, three cascade impactors (aluminum foil), and two in-situ monitors provided by six institutes. • Four thermal methods deployed for carbon analysis: VDI-2, France 2-step, TMS (similar to OGI method) and NIOSH TOT. • There was an ACPM (R&P 5400) operated at 3-hr time resolution. • BC was determined with a seven-wavelength aethalometer (AE-30) at a 5-min. resolution as well as with time-integrated reflectance and integrating sphere (IS) methods. BC A cohesion of 16.6 m2/g was used to convert absorption at 880 nm to BC mass. • OC was also monitored by an experimental semi-continuous instrument which collected aerosol in the water phase by condensing steam.	• The overall standard deviation of $PM_{2.5}$ TC measurements was 0.22 $\mu g/m^3$, corresponding to a standard deviation in the analysis of samples of 1.1 $\mu g/cm^2$. TC accounted for ~ 90% of $PM_{2.5}$ mass. • Evidence of organic adsorption artifact was provided by the presence of carbon on backup filters, in the amount up to 20% of the front filters. • The impactors collected less TC than filters (up to 30% difference); likely due to less sampling artifacts. • The difference in EC measurements was up to one order of magnitude between methods, though their correlations over the period were high; better than 0.9 (r^2). • Two institutes analyzed filters and impactors in the same way and found consistent EC values from filters that were a factor of 1.4 higher than those from impactors. • There was quite a difference in BC values obtained with different optical methods, though they were correlated to one another quite well. IS measured a higher BC from filter than from cascade impactor (a factor of 0.7). • Difference between the methods in this experiment was large, but apparently of a systematic nature, because the correlations were all very good.
RAOS – Evaluation of Aethalometer with Photoacoustic Instrument. (Arnott et al., 2005a) • Period: 6/3/2002 – 6/28/2002 • Location: Reno, Nevada. • Type: Kerosene soot (largely BC), white $(NH_4)_2SO_4$ aerosols, and mixtures thereof, as well as ambient $PM_{2.5}$.	• The only commercially available multi-wavelength aethalometer, Model AE-31, operated at 370, 470, 520, 590, 660, 880, and 990 nm. • A DRI photoacoustic instrument (532 nm) and an integrating nephelometer (532 nm) used to provide reference absorption and scattering measurements. • During RAOS, the aethalometer was set up to measure light absorption by pure BC, externally mixed, and pure "white" $(NH_4)_2SO_4$ aerosols.	• The aethalometer showed non-zero responses to $(NH_4)_2SO_4$ aerosol that does not absorb. A fraction of scattering was misinterpreted as absorption. • Considerable variation of absorption measurement occurred with time as the filter darkened and multiple scattered less, even though the actual absorption coefficient was constant, as indicated by photoacoustic instrument. • A correction function was developed using multiple scattering model. The model was tested against ambient measurements and found to require coefficients that are situation specific. At least, simultaneous aerosol light-scattering measurements are required for accurate interpretation of aethalometer data for high aerosol single-scattering albedo.

Table B-1. Continued.

Study/Period/Location/Type	Sampling and Analytical Methods	Summary of Major Findings
SERDP Evaluations of Photoacoustic Instrument and Photoelectric Aerosol Sensor (PAS) (Arnott et al., 2005b) • Period: Year 1999 – 2000 • Location: Hill Air Force Base (Hill AFB), Fresno Supersite (FSF). • Type: Gasoline- and diesel-vehicle emissions, jet aircraft emission, and urban ambient air.	• DRI 1047 nm photoacoustic (PA) instrument deployed at Hill AFB and FSF. Light absorption converted to BC based on a light absorption efficiency of 5 m^2/gBC. • PAS Model 2000 (EcoChem Messtechnik GmbH) deployed at Hill AFB with 150 ºC heated inlet behind dilution tunnels. • PAS Model 2001 operated at FSF without heated inlet from December 2003-July 2004. • Solvent-extractive particulate PAH measured with PAS at Hill AFB. • Seven-wavelength aethalometer (Magee Scientific) deployed at FSF with PAS.	• Spurious negative signals were observed from PAS until the heated inlet was implemented. This may be due to charge separation occurring during evaporation of volatile aerosol from PAS filter. • Good correlations (r^2 = 0.96-0.97) were found between PAS and PA for emissions from diesel and gasoline vehicles, though the data did not cover an adequate dynamic range. • The sum of extractive PAH show only moderate correlation (r^2 = 0.67 – 0.75) with PAS measurements. • The PAS to PA ratio for ambient air in FSF is 3.7 times as large in winter (11.1fA/[μg/m^3BC]) than in summer (3.0fA/[μg/m^3BC]). • Aethalometer BC (370 nm) correlates well with PA BC at FSF with their ratio being 1.53 for winter and 1.28 for summer. • PAS appears to respond to both PAH and EC, and it can produce only a qualitative measure of either of them.
Twelve-Month Hong Kong Air Quality Study (Chow et al., 2005) • Period: every-sixth-day sampling between 11/06/2000 and 10/26/2001. • Location: Three sampling sites in Hong Kong, China: Tsuen Wan (TW), Mong Kok (MK), and Hok Tsui (HT). • Type: Roadside, urban, and rural atmospheres.	• Twenty-four hour samples acquired by a Partisol sampler (R & P, Albany NY, USA) with quartz-fiber filters at each site. • Carbon analysis were made with DRI/OGC analyzer (Desert Research Institute, Reno, NV) following the nominal IMPROVE protocol; with DRI Model 2001 Carbon Analyzer (Atmoslytic Inc., Calabasas, CA) following the STN TOT and TOR methods; and with Sunset Carbon Aerosol Analysis Laboratory Instrument (Sunset Lab Inc., Forest Grove, OR) following the HKGL TOT method. The HKGL TOT method represents a small modification from the STN/NIOSH method.	• Good agreements in TC (within ~ 10%) were achieved with all analysis methods for measured concentrations higher than 10 times the minimum detection limit (MDL). • Best agreement in EC was observed between the IMPROVE TOR and STN TOR methods. For ~ 80% of the samples the difference was less than 20%. This implies the robustness of reflectance charring correction even for different temperature protocols. • The poorest agreement in EC was found between IMPROVE TOR and HKGL TOT methods. Only 12% of the samples show a difference < 20%. TOT EC is generally 10–40% lower than the TOR EC. • The transmittance charring correction was mostly affected by heavily loaded samples, because the transmitted light was too low to be detected. • The OC/EC ratio at U.S. and Hong Kong rural areas were similar (2 – 5, based on the IMPROVE protocol), though the concentrations in Hong Kong were much higher.

Table B-1. Continued.

Study/Period/Location/Type	Sampling and Analytical Methods	Summary of Major Findings
Reference Material 8785 (Klouda et al., 2005) • Period: Reference material (RM1649a) was original collected during 1976-1977. • Location: Reference material collected at Washington, DC. • Type: Urban dust.	• RM 8785 Air Particulate Matter on filter media was produced at SRI International by resuspending SRM 1649a in air and by collecting the aerosol on 320 quartz-fiber filters. Only PM2.5 was collected by URG-2000 filter packs. • RM 8785 samples were analyzed for elemental composition by XRF and for mass by gravimetry. • RM 8785 samples were analyzed for TC, OC, and EC with the STN-NIOSH method using a Sunset Instrument and with IMPROVE methods using DRI/OGC and DRI Model 2001 Carbon Analyzers.	• The average mass and standard deviation of RM8785 on filters were 1.064 mg and 0.414 mg, respectively. • Excellent calibration curves were achieved for all methods with standard sucrose and urea solutions distributed by NIST. • TC derived from each method was highly correlated to mass with slopes ranging from 0.0227 to 0.0286. A larger intercept (12.2 $\mu g/cm^2$) was found for IMPROVE method performed with DRI/OGC analyzer. • IMPROVE EC/OC ratio reported by DRI/OGC analyzers (0.514) were much higher than STN-NIOSH EC/OC ratio (0.275 – 0.282). IMPROVE EC/OC reported by DRI/OGC analyzers was between the two extremes (0.465). • The TC reference value assignment is 0.229±0.050 g OC/g Mass. EC and OC reference values are method-dependent; they were assigned to be 0.111 gEC/gMass and 0.112 gOC/gMass for the IMPROVE method and 0.065 g EC/g Mass and 0.169 g OC/g Mass for the STN-NIOSH method.
Thermal Resistance Method to Measure BC (Nguyen et al., 2005) • Period: Not applicable (laboratory analysis) • Location: Varies. • Type: Diesel soot and sediment reference materials; wood char produced at various pyrolysis temperatures.	• Marine sediment (SRM 1944), diesel soot (SRM 1650a; SRM 2975), hexane soot, natural wood char, and 16 synthetic chars prepared for the experiment. • The chemothermal oxidization (CTO) method has three steps: (1) combustion of samples in air at 375 ºC for 24 h; (2) carbonate removal by *in-situ* acidification; and (3) quantification of remaining carbon by high-temperature combustion in an elemental analyzer. • Simultaneous thermal gravimetric (TGA) measurements conducted to study the rate of weight loss. • H/C and O/C bulk analysis provided by commercial laboratory.	• Combustion at 340 ºC in oxygen and 375 ºC in air proceeded at similar kinetic rate for both soot and char. • Combustion at 375 ºC in air removed all BC from soot or char given sufficient time (could be as long as 72 hrs). • For 19 wood chars, 24-hr carbon survival under air (340 ºC) varied between 0 and 44%, with no survival in any char formed at < 850 ºC and even in some low H/C chars formed at 1000 ºC pyrolysis. CTO was found insensitive to the detection of BC in pine chars formed at moderated temperature (e.g., < 750 ºC). • Close to 50% of diesel and hexane soot survived after 24-hr combustion in air. • Thermal resistance of BC depended not only on extent of carbonization, but also on physical attributes of particles. CTO can only be considered as a semi-quantitative measure of BC content.

Table B-1. Continued.

Study/Period/Location/Type	Sampling and Analytical Methods	Summary of Major Findings
AIDA: Soot Light Absorption Enhancement by Coating (Schnaiter et al., 2005a; 2005b) • Period: Not indicated. • Location: AIDA Facility, Forschungszentrum Karlsruhe, Germany. • Type: Diesel soot, coated with secondary organic matter (SOM).	• AIDA aerosol chamber has a volume of 84 m3 and is evaluated to pressure of ~ 0.01 mbar. • Soot aerosols were generated by a commercial diesel engine. SOM coating was produce by in-situ ozonolysis of α-pinene in the chamber. • Particle size distribution was monitored by SMPS and a DMA (TSI 3071). • Spectral aerosol extinction coefficients (200-1000 nm) were measured by a long path extinction spectrometer. Scattering was measured by a nephelometer (TSI 3563). • Aerosol light absorption was determined from the difference between extinction and scattering.	• The scattering and absorption cross sections of the coated BC particles were calculated using a Mie model for concentrically coated sphere. Refractive indexes of 1.9 +1.0i and 1.5 + 0i (550 nm) for BC and SOM produced the best agreements between the model and experiment. • In a homogeneous nucleation experiment, median mobility equivalent diameter increased to ~ 300 nm after five successive coating processes in 10 hours. • The amplification factor of internally mixed BC was estimated at 1.8 – 2.1 compared to the specific absorption cross section of externally mixed BC. • The size distribution measurements indicated that the coating of diesel soot with SOM results in a significant restructuring whereby the soot aggregates become more compact. • Mie model may produce significant errors for thinly-coated soot aggregates.
Reno Aerosol Optics Study (RAOS) (Sheridan et al., 2005) • Period: 6/3/2002 – 6/28/2002 • Location: Reno, Nevada. • Type: Kerosene soot (largely BC), white (NH4)2SO4 aerosols, and mixtures thereof, as well as ambient PM2.5.	• Cavity Ring-Down (CRD) Extinction (DRI, NASA, and Portland State University [PSU] CRD). • Classic extinction cell operated at 467, 530, and 660 nm. • Integrating nephelometers operated at 530 nm. • Photoacoustic instrument operated at 532 nm. • Aethalometer operated at 880 nm. • PSAP (Radiance) operated at 565 nm. • Multi-Angle Absorption Photometer (MAAP)	• Photoacoustic absorption and absorption by the difference of extinction and scattering agreed with each other within about 10% for aerosols with scattering albedos ranging from ~ 0.3 – 1, yielding two quasi-equivalent primary standards for aerosol light absorption. • The CRD was capable of measuring atmospheric extinction down to below 1 Mm^{-1}. • Uncorrected filter-based absorption methods, such as aethalometer and PSAP, showed substantial systematic errors. • Filter-based methods corrected for scattering interference (e.g., MAAP) generally compared well (after empirical calibration) with primary standards, such as the photoacoustic method. However, their dynamic range was limited.

Table B-1. Continued.

Study/Period/Location/Type	Sampling and Analytical Methods	Summary of Major Findings
New Approach to Measure EC in Ultrafine Particles (ten Brink et al., 2005) • Period: December 1998 – March 1999 • Location: Amsterdam, Netherlands. • Type: Suburban atmosphere.	• An ACPM (R&P 5400) was modified by replacing the particle-collection impactor in one of the sampling lines with a quartz-fiber filter. • The cut-off size of the impactor was determined to be 0.14 µm. It does not collect ultrafine particles as quartz-fiber filters do. • Carbon analyses were made alternatively at two sampling lines with a two-step method in air: 340 ºC for OC and 750 ºC for EC. Sampling duration per line was 1 h.	• The precision of EC measurements, based on blank experiments and inter-instrument comparisons, was 4%. The MDL is 0.11 µg/m^3 with impactor and 0.12 with filter. • In the field test, EC concentration averaged at 1.23 and 0.67µg/m^3 from the filter and impactor line, respectively. • A difference of 40% in EC measurement was significant, which was interpreted by the loss of EC < 0.14 µm in size through the impactor. • The same procedure was used to determine OC in ultrafine particles. However, large artifacts were observed in the filter line even with a denuder. This precluded evaluation of OC in the ultrafine particles using this method.
EPA Comparison Study of Photoelectric Aerosol Sensor (PAS) and Aethalometer (Wallace, 2005) • Period: December 1999 – May 2000 • Location: Samples acquired from an occupied house in Reston, VA. • Type: Indoor and outdoor PM samples with particular sources (automobile, wood burning, cooking, and candle burning).	• Semi-continuous measurements made by two aethalometers (Magee Scientific, Berkeley, CA), a PAS Model 1001i (Ecochem Analytic, West Hills, CA, 6.7 eV), and two PAS Model 2000 (Ecochem Analytic, 5.6 eV). • Absorption efficiency of 19 m2/g used for aethalometer. • Time resolution 1 min for PAS and 5 min for aethalometer. • Paired aethalometer and PAS 2000 placed ion the balcony and in the basement.	• Control experiments demonstrated the precision of aethalometer and PAS on the order of 4.5–5.4%. • The correlation between aethalometer and PAS was the best (R^2 = 0.84, Slope = 0.0021fA/[ng/m3BC]) for wood burning dominated period (e.g., winter nights). • Aethalometer and PAS 2000 showed R^2 = 0.72 and Slope = 0.00255fA/(ng/m3BC) for traffic-dominated period (e.g., rush hours) and R^2 = 0.77 and Slope = 0.0019fA/(ng/m^3BC) for candle burning. • PAS 2000 shows no response for cooking emissions, while BC was still detected by PAS 1001i and aethalometer. • The PAS/aethalometer ratio varies widely across studies, suggesting both instruments are site-specific. There is an unexplained difference of ~ a factor of 10 between two models of PAS.

Table B-1. Continued.

Study/Period/Location/Type	Sampling and Analytical Methods	Summary of Major Findings
Optical Extinction of Combustion-Generated Aerosol (Widmann et al., 2005) • Period: Not indicated. • Location: NIST Laboratory, Gaithersburg, MD. • Type: Combustion aerosol.	• Soot aerosol was generated in a laminar diffusion burner combusting ethene in air. • Extinction was measured in an optical cell (57.8 cm) using a solid-state laser operating at 632 nm. • Mass concentration of soot in the optical cell was determined gravimetrically by alternately collecting the soot on Teflon filters upstream and downstream of the optical cell. • Soot was collected on quartz-fiber filters for subsequent carbon analysis with a Sunset Lab Carbon Analyzer. The thermal protocol resembled the NIOSH-STN method.	• The combustion condition was described by the global equivalence ratio, ϕ, defined as the fuel-air ratio normalized by the fuel-air ratio under stoichiometric conditions. • The mass extinction efficiency of soot decreased with increasing value of ϕ, which corresponds to under-ventilated combustion (burning rich). Mass extinction efficiency ranged from 8.1 to 6.4 m^2/g. • EC/TC ratio also increased with the increasing value of ϕ. Under-ventilated combustion (burning rich) tended to produce soot with higher OC content. • The increased extinction efficiency for over-ventilated combustion (burning lean) was mostly attributed to absorption. The extinction efficiency increased from 6.4 to 8.1m^2/g when EC/TC ratio increased from 0.2 to 0.9.
Determination of EC and OC with ATOFMS (Ferge et al., 2006) • Period: Not indicated. • Location: University of Augsburg, Germany. • Type: Resuspended soot and carbon black particles.	• Eleven samples were prepared, including five from a diffusion flame soot generator (Matter Engineering, Switzerland), pure graphite, two carbon black samples, one diesel soot, one tunnel dust, and the NIST SRM1649a. • These samples were resuspended and conducted into an aerosol time-of-flight mass spectroscopy (ATOFMS), which determined the single particle size and mass spectrum simultaneously. • ATOFMS ionized aerosols using laser desorption/ionization (LDI) technique with a 266 nm Nd:YAG laser. • EC and OC in the samples were also quantified with the NIOSH5040 and German VDI2 methods.	• In most average spectra (except dust samples), the typical peak pattern of carbon clusters with an m/z progression of multiples of 12 (the mass of carbon atom). LDI theoretically ionized all carbon fractions. • The EC content was estimated by summing peaks with masses of m/z = n×12, n×12+1, n×12+2, and n×12+3. The higher mass up to three was to account for the carbon isotope and hydrogen atoms. Only positive mass spectra were taken into account. • The m/z = 39 was excluded due to the assumption that it was mainly caused by potassium. Other peaks, except those for known contaminants, were assigned to OC. • The EC/TC ratios derived from ATOFMS were generally between those derived from NIOSH5040 and VDI2 methods (within 10%). • The worst agreements occurred for dust samples. Corrections for peaks of inorganic origin are critical for the ATOMS method to quantify OC and EC.

Table B-1. Continued.

Study/Period/Location/Type	Sampling and Analytical Methods	Summary of Major Findings
Evaluation of Photoacoustic Light-Absorption with PSAP Onboard the Twin Otter Research Aircraft (Arnott et al., 2006) • Period: May and July, 2003 • Location: ARM Southern Great Plains site in Oklahoma and off the coast Monterey, California. • Type: Smoke aloft from long-range transport, and local oil and wood burning.	• A DRI photoacoustic instrument of 676 nm was deployed on board of Twin Otter unpressurized single engine light aircraft. Modifications were made to the photoacoustic instrument to overcome the fluctuation of pressure, temperature, and relative humidity aloft. • A modified three-wavelength (467 nm, 530 nm, and 660 nm) PSAP was used to measure light absorption concurrently. • An algorithm developed in Virkkula et al. (2005) that takes into account both the particle scattering coefficient and single scattering albedo was used to correct the PSAP data at 660 nm to compare with the photoacoustic data.	• The photoacoustic instrument had higher noise when the aircraft was close to the ground and was experiencing turbulent conditions, likely a result of pressure fluctuations at the inlet of the sampling tube that propagates to the photoacoustic instrument. • Even when excluding data near the surface (> 750 mb), the scatter of photoacoustic and PASP absorption is considerably greater than typical for ground-based measurements. During a Siberian fire event (very long-range transport), the PSAP is correlated to photoacoustic at $r^2 = 0.67$ and slope = 0.84. The maximum absorption in this episode is ~ 7 Mm^{-1}. • During the local oil-fire event, absorption reached as high as 250 Mm^{-1}, and the PSAP was lower than photoacoustic by 14% ($r^2 = 0.95$). The smoke is dark, so the scattering effect was small, but the loading effect might be significant for PSAP. • During the wood-burning event, the smoke was much more light-scattering. The estimated single scattering albedo is 0.943, which is used to correct PSAP measurement. The corrected PASP data agreed closely with photoacoustic at $r^2 = 0.95$ and slope = 0.999.

Table B-1. Continued.

Study/Period/Location/Type	Sampling and Analytical Methods	Summary of Major Findings
Fresno Supersite: Comparison of Continuous and Filter-Based Carbon Measurement (Park et al., 2006) • Period: December 2003 – November 2004 • Location: Fresno Supersite in central California. • Type: Urban ambient air.	• Instruments deployed at the Fresno Supersite included: 1) multi-angle absorption photometer (MAAP, λ=670 nm); 2) dual wavelength (λ=370 and 880 nm) aethalometer; 3) seven-color (λ=370, 470, 520, 590, 660, 880, and 950 nm) aethalometers; 4) the Sunset Laboratory carbon aerosol analysis field instrument; 5) photoacoustic light absorption analyzer (λ=1047 nm); and 6) the R&P 5400 ambient carbon particulate monitor. • Absorption measured by MAAP, aethalometer, and photoacoustic instrument was converted to BC concentration using manufacturer specified absorption efficiency (6.5 m^2/g for MAAP, 5 m^2/g for photo-acoustic, and 14,625/λ m^2/g for aethalometer). • Filter samples were analyzed for EC using the IMPROVE TOR protocol. • A photoelectric aerosol sensor (PAS) was used to measure particle-bound PAHs. • All analyzers were equipped with $PM_{2.5}$ cyclone or impactor inlet.	• The two-wavelength and seven-wavelength aethalometer met the equivalence criteria (the regression slope is 1±0.05, the regression intercept is 0±1 $\mu g/m^3$, $r > 0.97$, and the collocated precision is 2 $\mu g/m^3$ or 5%, whichever is larger). • IMPROVE EC is highly correlated with the photoacoustic BC ($0.97 < r < 0.99$), but the IMPROVE EC slope is 1.5 to 2 times higher. • Photoacoustic BC was much lower than either aethalometer or MAAP BC, as evidenced by the high slopes (1.3 to 2.0), but their correlations were excellent (>0.9). • When breaking up into seasons, better comparisons generally occurred in winter. Particle-bound PAH levels show higher correlations with photoacoustic BC for winter ($0.91 < r < 0.95$) than for summer ($0.70 < r < 0.78$). The R&P 5400 EC is not well-correlated with the photoacoustic BC except for December 2003 (r=0.81). Note the BC concentration in winter is ~ twice that in summer. • Compared to IMPROVE EC, mass absorption efficiencies are determined at 5.5 m^2/g for the MAAP, 10.0 m^2/g for aethalometer at 880 nm, and 2.3 m^2/g for the photoacoustic analyzer. These differ from the default values. • A lower single scattering albedo (~ 0.88) agreed in time with the rush hours. • Ratios of light absorption at 370 nm to those at 880 nm from the aethalometer were nearly twice as high in winter as in summer. This is consistent with wintertime contributions from vehicle exhaust and residential wood combustion, which is believed to absorb more shorter-wavelength light. Light absorption did not scale as λ^{-1} at Fresno.

Table B-1. Continued.

Study/Period/Location/Type	Sampling and Analytical Methods	Summary of Major Findings
Characterization of Particles from Controlled Burning of Wildland Fuels (Chen et al., 2006) • Period: 19 – 26, November 2003 • Location: U.S. Forest Service Fire Science Laboratory, Missoula, MT. • Type: Wood smoke.	• Selected wildland fuels of 250 g were burned in a fire bed and the resulting smoke was entrained into stack and sampled at a platform ~ 17 m high. • Two photoacoustic instrument (532 and 1047 nm) were deployed to measure light absorption. Light scattering and extinction were determined with nephelometer and cavity ring-down (CRD) instrument. PM mass measured with a TEOM with MDL ~ 50 $\mu g/m^3$ • Modified Mie scattering theory were developed to retrieve BC fraction in PM, based on absorption and extinction measurements. • Time-integrated samples were collected and analyzed for OC and EC using the IMPROVE and STN thermal protocol.	• Intensive flaming combustion during ponderosa pine wood (PPW) burning produces particles with a low single scattering albedo (0.32) and a mass extinction efficiency of 8.9 $m^2 g^{-1}$. • Burning white pine needles (WPN) feature a prolonged smoldering phase emitting particles that are not light-absorbing and appear much larger in size with an extinction efficiency ≈5 $m^2 g^{-1}$. • The Mie scattering model estimated black carbon fraction in the PPW and WPN smoke particles at 66% and 12%, respectively. Substantial biases may occur when retrieving BC from time-averaged optical measurements. • Linear regression of photoacoustic B_{abs} against the IMPROVE and STN EC indicated they were in good agreement. The absorption efficiencies were close to the default values for photoacoustic measurements; i.e., 5 m^2/g for 1047 nm and 10 m^2/g for 532 nm. • On average, the IMPROVE EC was ~ 15% higher than the STN EC, compared with a ±10% measurement uncertainty.
Retrieval of Black Carbon Concentration from AERONET Remote Sensing (Schuster et al., 2005) • Period: Year 1993 – 2002 • Location: 46 locations worldwide. • Type: Various environments (mostly rural).	• AERONET sun photometer provided measurements of spectral aerosol optical depth (AOD) and sky radiance at solar zenith angles of ~ 75.5°, 70.5°, and 60°, during both morning and afternoon. • The algorithm (Dubovic and King, 2000) retrieved the column-integrated bimodal particle size distribution, aerosol single scattering albedo and refractive index. • Concentric sphere, Maxwell Garnett, and external mixture models were used to calculate BC fraction in aerosol and BC absorption efficiency. A BC refractive index of 2 – 1*i* and density of 2 g/cm^3 is assumed.	• The yearly averaged black carbon column concentrations are comparable to typical measured concentrations if a 1 km boundary layer is assumed: 0.22–0.28 $\mu g\ m^{-3}$ at remote island locations, 0.96–3.47 $\mu g\ m^{-3}$ in continental regions, and 2.7–3.7 $\mu g\ m^{-3}$ in biomass burning locations. • The ocean sites have a higher specific absorption (averaging 11.3 $\mu g\ m^{-3}$) and the biomass burning sites have a lower specific absorption (8.9 $\mu g\ m^{-3}$) than the continental sites (9.9 $\mu g\ m^{-3}$). • Uncertainties resulted from: 1) the mixing rule, 2) the type of host aerosol, and 3) the refractive index and density of BC. A simple sum of all these uncertainties indicates a possible bias of -15% to +40% expected in the black carbon concentration retrieval.

Table B-1. Continued.

Study/Period/Location/Type	Sampling and Analytical Methods	Summary of Major Findings
Soot Generation from Laminar Diffusion Flames (Kim et al., 2006) • Period: Not indicated. • Location: Laboratory in Kansas State University. • Type: Flame soot.	• Laminar diffusion flames were generated using both gaseous and liquid fuels. • Static light scattering by the flame was measured to give the scattered intensity I as a function of q, the wave vector. I(q) indicates the fractal dimension of the soot in the flame. • Direct observation of the very large soot in the flame was accomplished using a 10-power photomicroscope with an object distance of 15 cm. • Samples for TEM analysis were taken by thermophoretic deposition onto TEM grids inserted quickly and briefly into the flame. • Fourier transform of the TEM images were performed to determine the fractal dimension of the soot.	• Four different and successive stages of soot growth were found in laminar diffusion flames of heavily sooting fuels. Stage 1 is the well-known, diffusion-limited cluster-aggregation (DLCA) process that leads to fractal aggregates with a fractal dimension of D ~ 1.8. Stage 3 is also a DLCA process, but one confined to two dimensions (D ~ 2.6). Stages 2 and 4 (D ~ 1.4 and 1.9) are percolation processes that occur when the DLCA clusters of Stages 1 and 3 become densely packed, in either three or two dimensions, respectively. • Each pair of stages (1-4) is separated by length scales of 1, 10, and 100 μm. • All four stages were observed in the flame of burning acetylene, toluene, naphthalene, but not in other fuels. • Soot aerosols appear to evolve from cluster dilute to cluster dense and thereby demonstrate a crossover from diffusion limited cluster aggregation kinetics to percolation. • The results and the analysis were substantiated by comparison to computer simulations of 2d DLCA process.
In-Plume PAS Method to Determine BC Emission Factors (Kurniawan and Schmidt-Ott, 2006) • Period: Not indicated. • Location: Roadside location in Netherlands. • Type: Mobile exhausts.	• The system was setup at roadside. The probed volume flows through a splitter and sampled by EC and CO_2 detectors. • The speed of most cars sampled was around 50 km/hr. There were seldom events of two or more vehicles following each other too closely to be resolved separately. • EC is quantified with a photoelectric detector (Matter Engineering, Switzerland) that has been calibrated for EC using diesel source without after-treatment. • CO_2 was quantified with a commercial NDIR sensor. • EC emission factors were determined for each individual car using the EC/CO_2 ratio.	• Sulfur compounds deposited on the particle surfaces quench photoemission, and the photoelectric signal becomes highly sensitive to temperature and vapor conditions in the car's exhaust filter system if it has one. • The measurements resulted in emission factors from $f = 6.3 \times 10^{-6}$ to 3.3×10^{-2}, ranging over more than three orders of magnitude. The average value of f was 1200×10^{-6}. • The highest-polluting 5% of all cars contribute to 43±2% of the particulate pollution of passenger cars. • The measurement under estimates diesel emissions with respect to the standards, since: (a) the standards refer to driving cycles that include acceleration. In contrast, they measured under a constant speed or even decelerating; and (b) the photoelectric detector underestimates the emissions from filter-equipped cars.

See Table 1 of Watson et al. (2005) in Section 9 for detailed thermal/optical analysis protocols.

APPENDIX C

LITERATURE REVIEW OF THERMAL DESORPTION METHODS FOR ORGANIC SPECIATION

Table C-1. Summary of organic species detected with current TD-GC/MS approaches.

Brief Method Description	Year	Citation	*n*-Alkane	PAH [1]	Hopane	Sterane	Alkyl Benzene	Furan	Phthalate	Carbonyl [2]	Nitrile	Alkanoic Acids	Esters	Others
External Thermal Desorption Unit														
TD with an Homemade Aluminum TD Block	1985	Greaves et al.	Q	Q	-	-	-	I	I	I	-	I	-	-
	1987	Greaves et al.	Q	Q	-	-	-	Q	Q	Q	-	Q	-	-
	1996	Veltkamp et al.	Q	Q	-	-	-	-	-	Q	-	-	-	Alkanols (Q)
TD with MSSV	1999	Hall et al.	I	-	I	-	I	-	-	-	-	-	-	Phenol and Phenoclic (I)
	2000	Waterman et al.	I	Q	-	-	-	-	-	-	-	-	-	-
	2001	Waterman et al.	I	Q	-	-	-	-	-	-	I	I	-	-
TD with STDS	2001	Sidhu et al.	I	I	-	-	-	I	-	I	-	I	I	
TD with Gerstel TSS2 Unit	2003	Hays et al.	-	Q	-	-	-	-	-	-	-	-	-	-
	2004	Dong et al.	-	Q	-	-	-	-	-	-	-	-	-	-
	2004	Hays et al.	-	I	-	-	I	-	-	-	-	-	-	Cycloalkanes (I)
In-Injection Port Thermal Desorption														
Modified Injector with a Bayonet Socket Cap and Backflush gas	1990	Helmig et al.	I	I	-	-	-	-	I	-	I	I	I	-
Modified Injector with Valves	1997	Blanchard and Hopper	Q	Q	-	-	-	-	-	-	-	-	-	-
	2002	Blanchard et al.	Q	Q	-	-	-	-	-	-	-	-	-	-
DSI Device as Injector	2001	Falkovich and Rudich	-	Q	-	-	Q	Q	Q	Q	-	Q	-	Furanone (Q), Phenol and phenolic (Q), Pyrroles and indoles, Cycloalkane and Cycloalkenes (Q)
	2004	Falkovich et al.	-	Q	-	-	-	-	-	-	-	-	-	-
	2004	Graham et al.	-	Q	-	-	-	-	-	-	-	-	-	-
No Modification	2004	Ho and Yu	Q	Q	-	-	-	-	-	-	-	-	-	-
	2005	Yang et al.	Q	Q	Q	Q	-	-	-	-	-	-	-	-
	2006	Ho et al.	Q	Q	Q	Q	-	-	Q	-	-	-	Q	Alkenes (Q), Cycloalkanes (Q)
Thermal Desorption GC x GC/TOFMS														
Zimmermann's Group	2003	Welthagen et al.	I	I	I	I	I	I	-	-	I	I	-	Cycloalkanes (I), Terpenes (I)
	2005	Schnelle-Kreis et al.	Q	Q	Q	-	Q		-	-	Q	-	Q	*n*-Alkanoic Acid Amides (Q), Acetic Acid Esters (Q), n-Alkanoic Acid Methylesters
Hamilton's Group	2004	Hamilton et al.	I	-	-	-	I	-	-	I	-	-	-	Alkanol (I), Furanones (I), Cycloalkanone (I), Pyranones (I), Phenol and Phenolic (I)
	2005	Hamilton et al.	-	-	-	-	-	-	-	Q	-	Q	-	Alkanol (Q), Furanones (Q)
Curie-Point Pyrolysis GC/MS														
Curie Point at 315°C	2001	Jeon et al.	I	I	I	I	-	-	I	-	-	I	-	Phenol (I), Amyrin (I)
Curie Point at 590°C	2000	Neususs et al.	Q	Q	-	-	-	-	-	-	-	Q	-	-

1 PAH includes priority PAHs, oxygenated PAHs, and substituted PAHs

2 Carbonyl includes ketone and aldehyde

"I" represents the method; includes only identification of that species

"Q" represents the method; includes quantification of that species

Table C-2. A summary of current TD-GC/MS approaches.

Author (Year)	Sample	Sample Preparation Procedures	TD Unit	Analytical Hardware and Conditions	TD Temps, Ramping Rate, Holding Time	TD Time	Desorbent Refocusing Pathway	Type of GC Column	Initial Oven Temp.	GC Oven Temperature Program	Total Analysis Time
Greaves et al. (1985[†] and 1987)	Airborne particulate matter and NIST Standard Reference Material 1649	A 1.3 cm diameter piece of quartz filter was punched and placed on the top of a 40-60 μm glass frit of a fritted glass sealing tube. The filter was firmly held on the position during sampling. The particles were collected onto the filter by passing ambient air through the glass tube which was then directly analyzed by TD.	An insulated TD apparatus was constructed in a cylindrical aluminum block containing a heating cartridge connected to a thermocouple	HP 5892A GC/MS in EI mode	Isocratic desorption temperature of 254°C.	15 min	Cold trapping onto capillary column head	Ultra Performance fused silica capillary (25m x 0.32mm i.d. x 0.52 μm film thickness)	*For ambient sample:* -60°C *For NIST standard:* 20°C	*For ambient sample:* Initially at -60°C, ramped to 0°C at 20°C/min, then to 300°C at 8°C/min; *For NIST standard:* Initially at 20°C, ramped to 180°C at 20°C/min, then to 300°C at 8°C/min	*For ambient sample:* 55.5 min *For NIST standard:* 45.5 min
Veltkamp et al. (1996)	Aerosol sample collected at Niwot Ridge, Colorado		The same as above but a new septumless injection port was designed and installed in the GC to eliminate contamination by the septum used in the Grob-type injection port	HP 5988A GC/MS in EI mode	Isocratic desorption temperature of 250°C	15 min	Cold trapping onto capillary column head	Ultra-2 (25m x 0.32mm i.d. x 0.17 μm film thickness)	-50°C	Not Listed	U*
Hall et al. (1999)[†]	NIST Standard Reference Material 1649	A pre-cleaned glass reaction tube with a capacity of 30-40 μL was filled with 5 mg NIST urban dust standard. The tube was sealed before TD.	Quantum Micro-scale sealed vessel (MSSV)-injector port.	HP 5890 GC/Fisons MD800 MS in EI mode with a scan range of *m/z* 40-500 amu	Initially at 45°C, ramped to 300°C at 15°C/min and held at 300˚C for 5 min	22 min	Cold trapping onto capillary column head	GC-5MS capillary column (25m x 0.25 mm i.d.)	45°C	Initially at 45°C for 1 min, ramped to 300°C at 6°C/min, held at 300°C for 17 min.	82.5 min
Waterman et al. (2000) [†]	NIST Standard Reference Material 1649a	NIST urban dust was weighed, transferred into a glass-lined stainless steel GC liner containing glass wool and spiked with internal standards.	Quantum Micro-scale sealed vessel (MSSV-2) thermal analysis port (GC2 Chromatography and EGO Inc.)	HP 5890 GC/Fisons MD 800 MS in EI mode with a scan range of *m/z* 40-520 amu	Initially at 175°C, increased to 300°C at 50°C/min and held at 300˚C for ~7.5 min.	10 min	Cryogenic trap. Refocused at -196°C during TD and ramped to 300°C in 20s.	Phenomenex ZB-5 (25 m x 0.25 i.d. x 25 μm)	40°C	Initially at 40°C for 13 min, increased to 300°C at 5°C/min, held at 300°C for 25 min.^	90 min
Waterman et al. (2001) [†]	NIST Standard Reference Material 1649a.	A MSSV glass tube was filled with 120 mesh glass bends and spiked with internal standard. NIST urban dust standard (1-5mg) were weighed and sealed into the tube.	Quantum Micro-scale sealed vessel (MSSV-2) thermal analysis port (GC2 Chromatography and EGO Inc.)	HP 5890 GC/Fisons MD 800 MS in EI mode with a scan range of *m/z* 40 to 520	Isocratic desorption temperature of 300˚C	2 min	Cryogenic trap. Refocused at -196°C during TD and ramped to 300°C in 20s.	Phenomenex ZB-5 (25 m x 0.25 i.d. x 25 μm)	40°C	Initially at 40°C for 3 min, increased to 300°C at 5°C/min, held at 300°C for 33 min.^	90 min
Sidhu et al. (2001)	Aerosol collected from the combustion of alternative diesel fuel.	Filter was spiked with internal standards and sealed in a TD inlet consisting of a 0.25 in o.d. stainless steel tube.	System for Thermal Diagnostic Studies (STDS)	Not Listed	Initially at 30°C, increased to 300°C at 20°C/min with no holding time.	13.5 min	Cold trapping onto capillary column head	DB-5MS column (30 m x 0.25 μm film thickness)	-60°C	Not Listed	U*

Table C-2. Continued.

Author (Year)	Sample	Sample Preparation Procedures	TD Unit	Analytical Hardware and Conditions	TD Temperatures, Ramping Rate, Holding Time	TD Time	Desorbent Refocusing Pathway	Type of GC Column	Initial Oven Temp.	GC Oven Temperature Program	Total Analysis Time
Hays et al. (2003); Dong et al. (2004); Hays et al. (2004)	Aerosol samples collected from residential wood combustion, residential oil furnace and fireplace appliance emission.	Punched filter samples were spiked with internal standards and placed into a glass desorption tubes.	TDS2 Gerstel Inc.	Agilent 6890 GC/5793 MSD in EI mode with a scan range of *m/z* 50 to 500 amu	Initially 25°C, ramped to 300°C at 12°C/min with no holding time	~23 min	Cryogenic trap. Refocused at -100°C during TD and ramped to 300°C at a rate of 720°C/min.	HP-5MS (30 m x 0.25 mm x 0.25 µm film thickness)	65°C	Initially at 65°C for 10 min, increased to 300°C at 10°C/min, held at 300°C for 41.5 min.	99 min
Helmig et al. (1990)	Aerosol samples collected on glass fiber filters in a forest in Eggegebirge.	Small piece of sample filter was placed inside a glass liner	The original GC septum cap was replaced by a bayonet socket containing cap to allow fast opening and closing of the injector. A backflush gas installed acts as an additional support at split outlet.	Carlo Erba Mega 5160 GC with a VG 250/70 SE MS in EI mode with a scan range of *m/z* 45-400 amu	Isocratic desorption temperature of 320˚C	15 min	Cold trapping onto capillary column head	Uncoated pre-column (0.3 m x 0.53 mm) followed by a SE54 (15 m x 0.23 mm).	50°C	Initially at 50˚C, increased to 175°C at 7.5˚C /min, then to 295°C at 10°C/min, held at 295°C for 5 min.	47 min
Blanchard and Hopper (1997)[#] and Blanchard et al. (2002)	Aerosol samples collected on quartz and glass fiber filters in Ontario	A one cm diameter section of sample filter was punched and transferred into a GC liner spiked with internal standards.	A GC injection port was added with three minor components, including a small T-connector, 3-way valve, and needle valve.	HP5890 GC/5972A MS in EI mode	Isocratic desorption temperature of 300˚C	15 min	Cold trapping onto capillary column head	HP-5MS (30m x 0.25 diameter x 0.25µm thickness)	30°C	Initially at 30°C for 0.75 min, increased to 175°C at 7.5˚C /min, then to 295°C at 10°C/min, held at 295°C for 5 min.	71 min
Falkovich, and Rudich (2001) [†] Falkovich et al. (2004); Graham et al. (2004)	NIST Standard Reference Material 1649a. Suspended urban air particulate matter collected with an 8 stage impactor in Tel-Aviv, Israel.	NIST standard or small piece of filter sample were loaded into a disposable microvial placed inside the GC injector. The sample vials are placed by the vial holder in the GC liner.	Direct Sample Introduction device (ChromatoProbe, Varian Co.)	Varian 3400 GC with Varian Saturn MS in EI mode	Initially at 120˚C, ramped at a rate of 200˚C/min to 350˚C with no holding time.	4.15 min	Cold trapping onto capillary column head	DB-5MS column (30 m x 0.25 mm i.d. x 0.25 µm film thickness)	40°C	Initially at 40˚C for 4 min, ramped at a rate of 5˚C /min to 300˚C, held at 300˚C for 4 min.	64.2 min
Ho and Yu (2004b)[#]; Yang et al. (2005)	Ambient aerosol samples collected on Teflon-impregnated glass fiber filters at Hong Kong and on quartz filters at Nanjing, China.	Two pieces of 1.45 cm^2 filter samples were cut and spiked with deuterated internal standards. The sample was transferred into a glass liner and held with glass wool.	Conventional GC injection port. No modification of GC injector and liner	HP 5890 GC/5791 MSD in EI mode with a scan range of *m/z* 50 to 650 amu	Initially at 100°C, and increased to 275˚C with no holding time.	7.0 min	Cold trapping onto capillary column head	HP-5MS (30 m x 0.25 mm x 0.25 µm film thickness)	30°C	Initially at 30°C for 2 min, increased to 120°C at a rate of 20°C/min, then to 300°C at 10°C/min, held at 300°C for 10 min.	41.5 min

Table C-2. Continued.

Author (Year)	Sample	Sample Preparation Procedures	TD Unit	Analytical Hardware and Conditions	TD Temperatures, Ramping Rate, Holding Time	TD Time	Desorbent Refocusing Pathway	Type of GC Column	Initial Oven Temp.	GC Oven Temperature Program	Total Analysis Time
Ho et al. (2006)	Ambient samples collected on quartz fiber filter at Malaysia	A piece of 1.45 cm^2 filter samples were cut and spiked with deuterated internal standards. The sample was transferred into a glass liner and held with glass wool.	Conventional GC injection port. No modification of GC injector and liner	Agilent 6890 GC/5793 MSD in EI mode with a scan range of *m/z* 50 to 650 amu	Initially at 50°C, increased to 275˚C with no holding time.	9.0 min	Cold trapping onto capillary column head	HP-5MS (30 m x 0.25 mm x 0.25 µm film thickness)	30°C	Initially 30°C for 2 min, increased to 120°C at 8°C/min, then to 310°C at 12°C/min, held at 310°C for 25 min.	63 min
Jeon et al. (2001)[#]	High-volume PM_{10} ambient samples collected along U.S./Mexico border	A 1.5 x 18 mm2 filter strip was cut and positioned inside a special glass reaction tube that was lined with a ferromagnetic foil characterized by the Curie point	Curie point pyrolyzer	HP 5890 GC/5792 MSD in EI mode	From ambient to 315°C with no holding time.	10 s	Cold trapping onto capillary column head	HP-5MS (30 m x 0.20 mm x 0.33 µm film thickness)	50°C	Initially at 50°C, increased to 320°C at 3-15°C/min	U[*,1]
Neususs et al. (2000)	Atmospheric aerosol particles collected during the Second Aerosol Characterization Experiment	The filter strips were wrapped in a Pyrofoil with a Curie point of 590oC and placed into the pyrolyzer.	JHP-3s Curie point pyrolyzer	Fisons Trio 1000 GC/MS system in EI mode	From ambient to 590°C with no holding time.	3.2 s	Cold trapping onto capillary column head	Chrompack CP-Sil-5 CB (30 m x 0.25 mm i.d. x 0.1 µm film thickness)	50°C	Initially at 50°C for 2 min, increased to 280°C at 10°C/min, held at 280°C for 10 mins	35 min
Welthagen et al. (2003); Schnelle-Kreis et al. (2005)	Ambient samples collected in Augsburg, Germany	The filter strip was directly inserted into the DTD liner.	ATAS-GL Injector port Optic III with autoloader.	Agilent 6890 GC/LECO Pegasus III TOFMS with a LECO Pegasus 4D GCxGC modulator	Initially at 50˚C, ramped at a rate of 60˚C/min to 350˚C with no holding time.	5 min	Cold trapping onto capillary column head	*For GC (1-D):* Deactivated fused silica (2m x 0.22 mm i.d.) followed by BPX5 (30 m x 0.22 mm i.d. x 0.25 µm film thickness) *For GCxGC (2-D):* BPX5 (50 m x 0.22 mm i.d. x 0.25 µm film thickness) followed by BPX50 (1.5 m x 0.10 mm i.d. x 0.10 µm film thickness)	*For GC (1-D):* 50°C *For GCxGC (2-D):* 60°C	*For GC (1-D):* Initially at 50°C for 22 min, increased to 150°C at 100°C/min, then to 330°C at 20°C/min, held at 330°C for 30 min. *For GCxGC (2-D):* Initially at 60°C for 10 min, increased to 300°C at 1.5°C/min. The second column was kept 5°C above the first column.	*For GC (1-D):* 69.5 min *For GCxGC (2-D):* 175 min
Hamilton et al. (2004)	$PM_{2.5}$ aerosol collected in London.	The filter strip (with 10µg loading) was inserted into the GC liner and directly introduced into the GC injector.	Conventional GC injection port.	Agilent 6890 GC/LECO Pegasus III TOFMS with a LECO Pegasus 4D GCxGC modulator with a scan range of *m/z* 20 to 350 amu	Initially at 40°C, ramped at a rate of 20˚C/min to 300˚C with no holding time.	13 min	Cold trapping onto capillary column head	HP-5 (10 m x 0.18 mm x 0.18 µm film thickness) followed by DB17 (1.66 m x 0.1 mm x 0.1 µm film thickness)	40°C	Initially 40°C for 5 min, increased to 270°C at 3.5°C/min, held at 270°C for 10 min.	93.7 min

Table C-2. Continued.

Author (Year)	Sample	Sample Preparation Procedures	TD Unit	Analytical Hardware and Conditions	TD Temperatures, Ramping Rate, Holding Time	TD Time	Desorbent Refocusing Pathway	Type of GC Column	Initial Oven Temp.	GC Oven Temperature Program	Total Analysis Time
Hamilton et al. (2005)	Secondary organic aerosol formed during the photo-oxidation of toluene with hydroxyl radicals	The filter strip was inserted into the GC liner and directly introduced into the GC injector.	Conventional GC injection port.	Agilent 6890 GC/LECO Pegasus III TOFMS with a LECO Pegasus 4D GCxGC modulator with a scan range of *m/z* 20 to 350 amu	Initially at 50°C, ramped at a rate of 20˚C/min to 300˚C with no holding time.	12.5 min	Cold trapping onto capillary column head	HP-5 (30 m x 0.32 mm x 0.10 μm film thickness) followed by BP10 (2 m x 0.1 mm x 0.1 μm film thickness)	70°C	Initially 70°C for 2 min, increased to 250°C at 2.5°C/min, held at 270°C for 16 min.	102.5 min

U* Total analysis time could not be determined as a few parameters are missing in the paper;
U*,[l] Total analysis time could not be determined since variations of oven temperature program were used in the paper;
† NIST Standard Reference Materials were used to demonstrate the TD method;
^ GC oven temperature started together with the thermal desorption process;
[#] Validation of TD method with traditional solvent extraction followed by liquid injection into GC/MS approach.

APPENDIX D

SUMMARY OF SOURCE CHARACTERIZATION TESTS CONDUCTED IN THE LABORATORY

Table D-1. Summary of Source Characterization Tests.

Run #	Teflon Filter ID	Quartz Filter ID	Date	Source	Source Condition[a]	Dilution Ratio	Start Time	End Time	Collection Time (min)	Flow Rate (L/min)	Filter Mass Loading (µg/filter)
PURE DIESEL EMISSIONS											
10	*STRST010*	*STRSQ010*	*1/7/2006*	*Diesel generator*	*Invalid - HiVol motor was not turned on*	*37.0*	*16:36:34*	*16:46:53*	*10.3*	40	*95.0*
11	STRST011	STRSQ011	1/7/2006	Diesel generator	Diesel @ 4kW, D.R. ~150; fuel batch #1; old Copper tube	149.3	17:03:58	18:03:58	60.0	40	232.0
12	STRST012	STRSQ012	1/7/2006	Diesel generator	Diesel @ 4kW, D.R. ~160; fuel batch #1; old Copper tube	162.9	18:10:15	19:11:22	61.1	40	191.3
13	STRST013	STRSQ013	1/7/2006	Diesel generator	Diesel @ 4kW, D.R.~ 165; fuel batch #1; old Copper tube	165.8	19:17:30	20:18:45	61.2	40	182.8
14	STRST014	STRSQ014	1/8/2006	Diesel generator	Diesel @ 4kW, D.R. ~40; fuel batch #1; old Copper tube	41.9	10:45:45	11:45:45	60.0	40	496.4
15	STRST015	STRSQ015	1/8/2006	Diesel generator	Diesel @ 4kW, D.R. ~40; fuel batch #1; old Copper tube	41.1	11:55:56	12:55:56	60.0	40	511.3
16	STRST016	STRSQ016	1/8/2006	Diesel generator	Diesel @ 4kW, D.R. ~40; fuel batch #1; old Copper tube	43.4	13:08:58	14:08:58	60.0	40	469.2
17	*STRST017*	*STRSQ017*	*1/8/2006*	*Diesel generator*	*Invalid - One port in sampling cone was not plugged, and hence, open to ambient air*	*43.0*	*14:23:48*	*14:43:57*	*20.2*	40	*154.0*
18	STRST018	STRSQ018	1/8/2006	Diesel generator	Diesel @ 4kW, D.R. ~40; fuel batch #1; old Copper tube	41.0	14:48:58	15:08:58	20.0	40	163.4
19	STRST019	STRSQ019	1/8/2006	Diesel generator	Diesel @ 4kW, D.R. ~40; fuel batch #1; old Copper tube	40.0	15:22:02	15:42:02	20.0	40	172.3
20	STRST020	STRSQ020	1/8/2006	Diesel generator	Diesel @ 4kW, D.R. ~40; fuel batch #1; old Copper tube	40.0	15:48:44	16:08:44	20.0	40	169.4
42	STRST042	STRSQ042	1/20/2006	Diesel generator	Diesel @ 4kW, D.R. ~80; fuel batch #2	77.6	13:14:03	14:14:03	60.0	40	587.9
43	STRST043	STRSQ043	1/20/2006	Diesel generator	Diesel @ 4kW, D.R. ~80; fuel batch #2	78.2	14:30:05	15:31:05	61.0	40	601.4
44	STRST044	STRSQ044	1/20/2006	Diesel generator	Diesel @ 4kW, D.R. ~80; fuel batch #2	78.5	15:40:06	16:40:06	60.0	40	545.7
45	STRST045	STRSQ045	1/20/2006	Diesel generator	Diesel @ 4kW, D.R. ~80; fuel batch #2	79.3	16:46:15	17:46:15	60.0	40	553.7
47	STRST047	STRSQ047	1/23/2006	Diesel generator	Diesel @ 4kW, D.R. ~80; fuel batch #2	80.6	11:44:48	12:04:48	20.0	40	197.9
48	STRST048	STRSQ048	1/23/2006	Diesel generator	Diesel @ 4kW, D.R. ~80; fuel batch #2	79.8	12:11:36	12:31:36	20.0	40	196.1
49	STRST049	STRSQ049	1/23/2006	Diesel generator	Diesel @ 4kW, D.R. ~80; fuel batch #2	79.8	12:46:15	13:06:15	20.0	40	178.9
50	STRST051	STRSQ051	1/23/2006	Diesel generator	Diesel @ 4kW, D.R. ~80; fuel batch #2	79.4	13:15:47	13:35:47	20.0	40	170.6
51	STRST052	STRSQ052	1/23/2006	Diesel generator	Diesel @ 4kW, D.R. ~80; fuel batch #2	79.8	13:42:11	14:02:11	20.0	40	169.8
52	STRST053	STRSQ053	1/23/2006	Diesel generator	Diesel @ 4kW, D.R. ~40; fuel batch #2	39.6	14:10:11	14:30:22	20.2	40	240.5
53	STRST054	STRSQ054	1/23/2006	Diesel generator	Diesel @ 4kW, D.R. ~40; fuel batch #2	41.2	14:36:23	14:56:23	20.0	40	239.2
54	STRST055	STRSQ055	1/23/2006	Diesel generator	Diesel @ 4kW, D.R. ~40; fuel batch #2	39.3	15:02:30	15:22:30	20.0	40	239.2
55	STRST056	STRSQ056	1/23/2006	Diesel generator	Diesel @ 4kW, D.R. ~40; fuel batch #2	41.7	15:27:40	15:47:40	20.0	40	254.2
56	STRST057	STRSQ057	1/23/2006	Diesel generator	Diesel @ 4kW, D.R. ~40; fuel batch #2	40.8	15:52:23	16:12:23	20.0	40	257.2
57	STRST058	STRSQ058	1/24/2006	Diesel generator	Diesel @ 4kW, D.R. ~40; fuel batch #3	38.4	11:27:44	12:27:44	60.0	40	770.3
58	*STRST059*	*STRSQ059*	*1/24/2006*	*Diesel generator*	*Invalid - torn quartz-fiber filter before sample collection*	*N/A*	*N/A*	*N/A*	*N/A*	N/A	*N/A*
59	STRST060	STRSQ060	1/24/2006	Diesel generator	Diesel @ 4kW, D.R. ~40; fuel batch #3	42.7	12:39:28	13:39:28	60.0	40	693.8
60	STRST061	STRSQ061	1/24/2006	Diesel generator	Diesel @ 4kW, D.R. ~40; fuel batch #3	43.0	13:48:00	14:48:00	60.0	40	761.1
61	STRST062	STRSQ062	1/24/2006	Diesel generator	Diesel @ 4kW, D.R. ~40; fuel batch #3	40.9	14:54:09	15:54:09	60.0	40	796.0
62	STRST063	STRSQ063	1/24/2006	Diesel generator	Diesel @ 4kW, D.R. ~40; fuel batch #3	42.0	15:59:16	16:59:16	60.0	40	702.8
77	STRTQ090	STRQQ090	2/8/2006	Diesel generator	Diesel @ 4kW D.R. ~40	39.9	12:16:42	12:36:42	20.0	40	272.5
63	STRST064	STRSQ064	1/25/2006	Diesel generator	Diesel @ 4kW, D.R. ~20; fuel batch #4	17.6	10:39:35	11:39:35	60.0	40	1022.8
64	STRST065	STRSQ065	1/25/2006	Diesel generator	Diesel @ 4kW, D.R. ~20; fuel batch #4	18.1	11:45:38	12:45:38	60.0	40	1016.4
65	STRST066	STRSQ066	1/25/2006	Diesel generator	Diesel @ 4kW, D.R. ~20; fuel batch #4	16.1	12:51:13	13:51:13	60.0	40	1013.3
66	STRST067	STRSQ067	1/25/2006	Diesel generator	Diesel @ 4kW, D.R. ~20; fuel batch #4	17.9	14:01:40	15:01:40	60.0	40	982.1
67	STRST068	STRSQ068	1/25/2006	Diesel generator	Diesel @ 4kW, D.R. ~20; fuel batch #4	17.8	15:07:00	16:07:00	60.0	40	987.1
84	STRTQ097	STRQQ097	2/9/2006	Diesel generator	Diesel @ 4kW D.R. ~20; fuel batch #6	18.3	14:34:13	15:34:13	60.0	40	884.3

Table D-1. Continued.

Run #	Teflon Filter ID	Quartz Filter ID	Date	Source	Source Condition[a]	Dilution Ratio	Start Time	End Time	Collection Time (min)	Flow Rate (L/min)	Filter Mass Loading (µg/filter)
DIESEL EMISSIONS MIXED EXTERNALLY WITH NaCl											
78	STRTQ091	STRQQ091	2/8/2006	Diesel exhaust mixed with NaCl	Diesel @ 4kW D.R. ~40 + NaCl (0.1M @ 10 psi)	37.1	14:33:00	14:53:00	20.0	40	441.1
79	STRTQ092	STRQQ092	2/8/2006	Diesel exhaust mixed with NaCl	Diesel @ 4kW D.R. ~40 + NaCl (0.1M @ 10 psi)	40.5	14:59:13	15:19:13	20.0	40	456.2
80	STRTQ093	STRQQ093	2/8/2006	Diesel exhaust mixed with NaCl	Diesel @ 4kW D.R. ~40 + NaCl (0.1M @ 10 psi)	41.8	15:24:31	15:44:31	20.0	40	458.8
81	STRTQ094	STRQQ094	2/8/2006	Diesel exhaust mixed with NaCl	Diesel @ 4kW D.R. ~40 + NaCl (0.1M @ 10 psi)	41.7	16:07:27	17:07:27	60.0	40	1265.0
82	STRTQ095	STRQQ095	2/8/2006	Diesel exhaust mixed with NaCl	Diesel @ 4kW D.R. ~40 + NaCl (0.1M @ 10 psi)	41.1	17:15:07	18:15:07	60.0	40	1429.3
83	STRTQ096	STRQQ096	2/9/2006	Diesel exhaust mixed with NaCl	Diesel @ 4kW D.R. ~40 + NaCl (0.1M batch #2 @ 10 psi); fuel batch #5	40.7	12:18:08	13:18:08	60.0	40	1258.9
85	STRTQ098	STRQQ098	2/9/2006	Diesel exhaust mixed with NaCl	Diesel @ 4kW D.R. ~20 + NaCl (0.1M batch #2 @ 10 psi); fuel batch #6	18.1	16:02:59	17:02:59	60.0	40	1351.5
86	STRTQ099	STRQQ099	2/9/2006	Diesel exhaust mixed with NaCl	Diesel @ 4kW D.R. ~20 + NaCl (0.1M batch #2 @ 10 psi); fuel batch #6	17.9	17:08:03	18:08:03	60.0	40	1382.9
87	STRTQ101	STRQQ101	2/9/2006	Diesel exhaust mixed with NaCl	Diesel @ 4kW D.R. ~20 + NaCl (0.1M batch #2 @ 10 psi); fuel batch #6	17.7	18:13:22	19:13:22	60.0	40	1390.7
PURE ACETYLENE FLAME SOOT											
88	STRTQ102	STRQQ102	2/17/2006	Acetylene flame	Acetylene Flame (2"); D.R. ~17	18.1	10:58:50	11:18:58	20.1	40	317.3
89	STRTQ103	STRQQ103	2/17/2006	Acetylene flame	Acetylene Flame (2"); D.R. ~17	16.8	11:36:51	11:56:51	20.0	40	313.8
90	STRTQ104	STRQQ104	2/17/2006	Acetylene flame	Acetylene Flame (2"); D.R. ~17	16.7	12:03:35	12:23:35	20.0	40	364.3
91	*STRTQ105*	*STRQQ105*	*2/17/2006*	*Acetylene flame*	*Invalid - incorrect filter flow setting - run aborted*	*19.6*	*12:29:45*	*12:33:00*	*3.3*	40	*N/A*
92	STRTQ106	STRQQ106	2/17/2006	Acetylene flame	Acetylene Flame (2"); D.R. ~17	16.9	12:38:45	12:58:45	20.0	40	316.2
93	STRTQ107	STRQQ107	2/17/2006	Acetylene flame	Acetylene Flame (2"); D.R. ~17	16.7	13:05:57	13:45:57	40.0	40	649.5
94	STRTQ108	STRQQ108	2/17/2006	Acetylene flame	Acetylene Flame (2"); D.R. ~17	16.8	13:57:50	14:37:50	40.0	40	633.5
95	STRTQ109	STRQQ109	2/17/2006	Acetylene flame	Acetylene Flame (2"); D.R. ~17	16.7	14:44:42	15:24:55	40.2	40	644.8
96	STRTQ110	STRQQ110	2/17/2006	Acetylene flame	Acetylene Flame (2"); D.R. ~17	16.7	15:31:27	16:41:27	70.0	40	1012.1
97	STRTQ111	STRQQ111	2/17/2006	Acetylene flame	Acetylene Flame (2"); D.R. ~17	16.5	16:57:13	18:07:13	70.0	40	958.5
98	STRTQ112	STRQQ112	2/17/2006	Acetylene flame	Acetylene Flame (2"); D.R. ~17	16.5	18:12:41	19:22:41	70.0	40	967.0
ACETYLENE FLAME SOOT MIXED EXTERNALLY WITH NaCl											
99	STRTQ113	STRQQ113	2/21/2006	Acetylene soot mixed with NaCl	Acetylene Flame (2") + NaCl (0.05M @ 10psi); D.R. ~17	16.9	12:16:58	12:36:58	20.0	40	502.3
100	STRTQ114	STRQQ114	2/21/2006	Acetylene soot mixed with NaCl	Acetylene Flame (2") + NaCl (0.05M @ 10psi); D.R. ~17	16.8	13:14:30	13:34:30	20.0	40	533.6
101	STRTQ115	STRQQ115	2/21/2006	Acetylene soot mixed with NaCl	Acetylene Flame (2") + NaCl (0.05M @ 10psi); D.R. ~17	17.0	13:40:54	14:00:54	20.0	40	463.3
102	STRTQ116	STRQQ116	2/21/2006	Acetylene soot mixed with NaCl	Acetylene Flame (2") + NaCl (0.05M @ 10psi); D.R. ~17	16.7	14:07:01	14:47:01	40.0	40	915.9
103	STRTQ117	STRQQ117	2/21/2006	Acetylene soot mixed with NaCl	Acetylene Flame (2") + NaCl (0.05M @ 10psi); D.R. ~17	16.7	14:53:16	15:33:16	40.0	40	891.2
104	STRTQ118	STRQQ118	2/21/2006	Acetylene soot mixed with NaCl	Acetylene Flame (2") + NaCl (0.05M @ 10psi); D.R. ~17	17.4	15:40:48	16:20:48	40.0	40	910.1
105	STRTQ119	STRQQ119	2/22/2006	Acetylene soot mixed with NaCl	Acetylene Flame (2") + NaCl (0.05M @ 10psi); D.R. ~17	17.0	10:42:25	11:52:25	70.0	40	1361.2
106	STRTQ120	STRQQ120	2/22/2006	Acetylene soot mixed with NaCl	Acetylene Flame (2") + NaCl (0.05M @ 10psi); D.R. ~17	16.9	11:58:45	13:08:45	70.0	40	1384.6
107	STRTQ121	STRQQ121	2/22/2006	Acetylene soot mixed with NaCl	Acetylene Flame (2") + NaCl (0.05M @ 10psi); D.R. ~17	16.8	13:22:21	14:32:21	70.0	40	1369.5

Table D-1. Continued.

Run #	Teflon Filter ID	Quartz Filter ID	Date	Source	Source Condition[a]	Dilution Ratio	Start Time	End Time	Collection Time (min)	Flow Rate (L/min)	Filter Mass Loading (µg/filter)
PURE PALAS ELECTRIC ARC SOOT											
1	STRST001	STRSQ001	1/6/2006	Electric arc soot generator	Electric Arc @ 950 a.u. current, 1.3 bar Ar, no sampling cone	6.3	15:23:30	16:08:30	45.0	10	1182.0
2	STRST002	STRSQ002	1/6/2006	Electric arc soot generator	Electric Arc @ 950 a.u. current, 1.3 bar Ar, no sampling cone	6.3	16:43:40	17:03:45	20.1	10	484.0
3	STRST003	STRSQ003	1/6/2006	Electric arc soot generator	Electric Arc @ 950 a.u. current, 1.3 bar Ar, no sampling cone	8.0	19:22:00	19:42:04	20.1	10	340.0
4	STRST004	STRSQ004	1/6/2006	Electric arc soot generator	Electric Arc @ 950 a.u. current, 1.3 bar Ar, no sampling cone	7.9	19:56:05	20:16:10	20.1	10	355.0
5	STRST005	STRSQ005	1/6/2006	Electric arc soot generator	Electric Arc @ 950 a.u. current, 1.3 bar Ar, no sampling cone	6.0	20:37:30	20:58:00	20.5	10	341.0
6	STRST006	STRSQ006	1/6/2006	Electric arc soot generator	Electric Arc @ 950 a.u. current, 1.3 bar Ar, no sampling cone	6.0	21:06:35	21:26:35	20.0	10	350.0
7	STRST007	STRSQ007	1/7/2006	Electric arc soot generator	Electric Arc @ 950 a.u. current, 1.3 bar Ar, no sampling cone	8.1	10:48:00	11:28:00	40.0	10	656.0
8	STRST008	STRSQ008	1/7/2006	Electric arc soot generator	Electric Arc @ 950 a.u. current, 1.3 bar Ar, no sampling cone	8.0	11:38:00	12:18:00	40.0	10	658.0
9	STRST009	STRSQ009	1/7/2006	Electric arc soot generator	Electric Arc @ 950 a.u. current, 1.3 bar Ar, no sampling cone	7.9	12:30:00	13:10:30	40.5	10	632.0
23	*STRST023*	*STRSQ023*	*1/17/2006*	*Electric arc soot generator*	*Invalid - incorrect filter flow setting - run aborted*	*N/A*	*10:43:15*	*10:46:00*	*2.8*	N/A	*N/A*
24	*STRST024*	*STRSQ024*	*1/17/2006*	*Electric arc soot generator*	*Invalid - incorrect filter flow setting - run aborted*	*N/A*	*10:58:50*	*11:01:00*	*2.2*	N/A	*N/A*
25	STRST025	STRSQ025	1/17/2006	Electric arc soot generator	Electric Arc @ 950 strom current; suspect: two sample ports instead of being plugged, were connected to bypass flow pumps, which were not running.	8.0	11:24:40	11:44:40	20.0	10	375.0
26	STRST026	STRSQ026	1/17/2006	Electric arc soot generator	Electric Arc @ 950 strom current; suspect: two sample ports instead of being plugged, were connected to bypass flow pumps, which were not running.	7.5	11:54:00	12:14:00	20.0	10	363.0
27	STRST027	STRSQ027	1/17/2006	Electric arc soot generator	Electric Arc @ 950 strom current; suspect: two sample ports instead of being plugged, were connected to bypass flow pumps, which were not running.	7.7	12:25:15	12:45:15	20.0	10	369.7
28	STRST028	STRSQ028	1/17/2006	Electric arc soot generator	Electric Arc @ 950 strom current; suspect: two sample ports instead of being plugged, were connected to bypass flow pumps, which were not running.	8.0	14:15:00	14:35:00	20.0	10	364.7
29	STRST029	STRSQ029	1/17/2006	Electric arc soot generator	Electric Arc @ 950 strom current	7.7	14:52:10	15:12:10	20.0	10	351.4
30	STRST030	STRSQ030	1/17/2006	Electric arc soot generator	Electric Arc @ 950 strom current	7.4	15:21:30	16:01:30	40.0	10	647.1
31	STRST031	STRSQ031	1/17/2006	Electric arc soot generator	Electric Arc @ 950 strom current	7.4	16:15:30	16:55:30	40.0	10	643.8
35	STRST035	STRSQ035	1/19/2006	Electric arc soot generator	Electric Arc @ 950 strom current	8.2	11:28:10	12:08:10	40.0	10	673.0
36	STRST036	STRSQ036	1/19/2006	Electric arc soot generator	Electric Arc @ 950 strom current	7.8	12:19:42	12:59:42	40.0	10	647.0
37	STRST037	STRSQ037	1/19/2006	Electric arc soot generator	Electric Arc @ 950 strom current	7.9	13:13:02	13:53:02	40.0	10	619.6
38	STRST038	STRSQ038	1/19/2006	Electric arc soot generator	Electric Arc @ 300 strom current;	8.3	14:04:42	15:04:42	60.0	10	320.7
39	STRST039	STRSQ039	1/19/2006	Electric arc soot generator	Electric Arc @ 300 strom current;	8.4	15:17:13	16:17:13	60.0	10	320.2
40	STRST040	STRSQ040	1/19/2006	Electric arc soot generator	Electric Arc @ 300 strom current	8.3	16:24:40	17:24:40	60.0	10	347.3
PALAS ELECTRIC ARC SOOT MIXED EXTERNALLY WITH NaCl											
68	STRTQ081	STRQQ081	2/7/2006	Electric arc soot mixed with NaCl	Electric Arc @ 300 strom current + NaCl (0.01M @ 10 psi)	8.0	12:30:25	12:50:25	20.0	10	241.6
69	STRTQ082	STRQQ082	2/7/2006	Electric arc soot mixed with NaCl	Electric Arc @ 300 strom current + NaCl (0.01M @ 10 psi)	7.4	13:19:47	13:39:47	20.0	10	209.4
70	STRTQ083	STRQQ083	2/7/2006	Electric arc soot mixed with NaCl	Electric Arc @ 300 strom current + NaCl (0.01M @ 10 psi)	7.6	13:45:00	14:05:30	20.5	10	209.3
71	STRTQ084	STRQQ084	2/7/2006	Electric arc soot mixed with NaCl	Electric Arc @ 950 strom current + NaCl (0.01M @ 10 psi)	7.0	14:19:59	14:39:59	20.0	10	350.6
72	STRTQ085	STRQQ085	2/7/2006	Electric arc soot mixed with NaCl	Electric Arc @ 950 strom current + NaCl (0.01M @ 10 psi)	6.9	14:45:51	15:05:51	20.0	10	414.6
73	STRTQ086	STRQQ086	2/7/2006	Electric arc soot mixed with NaCl	Electric Arc @ 950 strom current + NaCl (0.01M @ 10 psi)	7.1	15:12:07	15:32:07	20.0	10	402.7
74	STRTQ087	STRQQ087	2/7/2006	Electric arc soot mixed with NaCl	Electric Arc @ 950 strom current + NaCl (0.01M @ 10 psi)	7.0	15:37:20	16:17:20	40.0	10	755.3
75	STRTQ088	STRQQ088	2/7/2006	Electric arc soot mixed with NaCl	Electric Arc @ 950 strom current + NaCl (0.01M @ 10 psi)	7.0	16:31:20	17:11:20	40.0	10	731.9
76	STRTQ089	STRQQ089	2/7/2006	Electric arc soot mixed with NaCl	Electric Arc @ 950 strom current + NaCl (0.01M @ 10 psi)	7.2	17:19:11	17:59:11	40.0	10	742.5

Table D-1. Continued.

Run #	Teflon Filter ID	Quartz Filter ID	Date	Source	Source Condition[a]	Dilution Ratio	Start Time	End Time	Collection Time (min)	Flow Rate (L/min)	Filter Mass Loading (µg/filter)
PURE WOOD COMBUSTION EMISSIONS											
108	STRTQ122	STRQQ122	3/8/2006	Wood smoke	4-5 lbs wood each filter run; D.R. ~117	117.1	11:40:21	12:02:30	22.1	10.0	52.1
109	STRTQ123	STRQQ123	3/8/2006	Wood smoke	4-5 lbs wood each filter run; D.R. ~117	117.7	12:13:40	12:33:40	20.0	10.0	100.7
110	STRTQ124	STRQQ124	3/8/2006	Wood smoke	4-5 lbs wood each filter run; D.R. ~110	110.8	13:58:01	14:18:01	20.0	10.0	30.8
111	STRTQ125	STRQQ125	3/8/2006	Wood smoke	4-5 lbs wood each filter run; D.R. ~110	110.2	14:40:12	15:00:12	20.0	10.0	69.8
112	STRTQ126	STRQQ126	3/8/2006	Wood smoke	4-5 lbs wood each filter run; D.R. ~105	107.8	15:33:03	15:53:03	20.0	25.0	125.2
113	STRTQ127	STRQQ127	3/8/2006	Wood smoke	4-5 lbs wood each filter run; D.R. ~105	106.0	16:28:07	16:48:07	20.0	25.0	111.4
114	STRTQ128	STRQQ128	3/8/2006	Wood smoke	4-5 lbs wood each filter run; D.R. ~105	105.0	17:28:40	17:48:40	20.0	25.0	629.6
115	STRTQ129	STRQQ129	3/8/2006	Wood smoke	4-5 lbs wood each filter run; D.R. ~105	104.5	17:54:14	18:14:14	20.0	25.0	71.9
116	STRTQ130	STRQQ130	3/9/2006	Wood smoke	4-5 lbs wood each filter run; D.R. ~40	41.1	12:11:18	12:36:18	25.0	40.0	179.1
117	STRTQ131	STRQQ131	3/9/2006	Wood smoke	4-5 lbs wood each filter run; D.R. ~40	42.8	14:02:37	14:27:37	25.0	40.0	325.4
118	STRTQ132	STRQQ132	3/9/2006	Wood smoke	4-5 lbs wood each filter run; D.R. ~40	41.0	14:42:07	15:07:07	25.0	40.0	317.4
137	STRTQ133	STRQQ133	3/13/2006	Wood smoke	4-5 lbs wood each filter run; D.R. ~40	39.2	13:06:10	13:31:10	25.0	40	277.4
138	STRTQ134	STRQQ134	3/13/2006	Wood smoke	4-5 lbs wood each filter run; D.R. ~40	40.0	13:48:06	14:13:06	25.0	40	222.0
139	STRTQ135	STRQQ135	3/13/2006	Wood smoke	4-5 lbs wood each filter run; D.R. ~40	40.5	14:31:30	14:56:30	25.0	40	180.5
140	STRTQ136	STRQQ136	3/13/2006	Wood smoke	4-5 lbs wood each filter run; D.R. ~40	38.6	15:18:04	15:43:04	25.0	40	118.5
141	STRTQ137	STRQQ137	3/15/2006	Wood smoke	4-5 lbs wood each filter run; D.R. ~18	18.5	10:41:30	11:06:30	25.0	40	71.1
142	STRTQ138	STRQQ138	3/15/2006	Wood smoke	4-5 lbs wood each filter run; D.R. ~18	17.3	11:24:09	11:49:09	25.0	40	132.2
143	STRTQ139	STRQQ139	3/15/2006	Wood smoke	4-5 lbs wood each filter run; D.R. ~18	17.5	12:02:21	12:27:21	25.0	40	68.8
144	STRTQ140	STRQQ140	3/15/2006	Wood smoke	4-5 lbs wood each filter run; D.R. ~18	18.1	12:52:57	13:17:57	25.0	40	53.8
145	STRTQ141	STRQQ141	3/15/2006	Wood smoke	4-5 lbs wood each filter run; D.R. ~18	17.9	13:38:41	14:03:41	25.0	40	67.8
146	STRTQ142	STRQQ142	3/15/2006	Wood smoke	4-5 lbs wood each filter run; D.R. ~18	17.7	14:41:05	15:06:05	25.0	40	47.0
147	STRTQ143	STRQQ143	3/15/2006	Wood smoke	4-5 lbs wood each filter run; D.R. ~18	17.7	15:24:06	15:49:06	25.0	40	7.0
148	STRTQ144	STRQQ144	3/15/2006	Wood smoke	4-5 lbs wood each filter run; D.R. ~18	17.9	16:20:25	16:45:25	25.0	40	33.1
WOOD COMBUSTION EMISSIONS MIXED EXTERNALLY WITH NaCl											
149	*STRTQ145*	*STRQQ145*	*3/16/2006*	*Wood smoke mixed with NaCl*	*INVALID, 4-5 lbs wood each filter run; 0.05M NaCl @ 10psi, - leak in sampling line noticed on 3/23/06, potential contamination*	*N/A*	*11:11:48*	*11:36:48*	*25.0*	40	*Not analysed*
150	*STRTQ146*	*STRQQ146*	*3/16/2006*	*Wood smoke mixed with NaCl*	*INVALID, 4-5 lbs wood each filter run; 0.05M NaCl @ 10psi, - leak in sampling line noticed on 3/23/06, potential contamination*	*N/A*	*12:02:43*	*12:27:43*	*25.0*	40	*Not analysed*
151	*STRTQ147*	*STRQQ147*	*3/16/2006*	*Wood smoke mixed with NaCl*	*INVALID, 4-5 lbs wood each filter run; 0.05M NaCl @ 10psi, - leak in sampling line noticed on 3/23/06, potential contamination*	*N/A*	*12:51:56*	*13:16:56*	*25.0*	40	*Not analysed*
152	*STRTQ148*	*STRQQ148*	*3/16/2006*	*Wood smoke mixed with NaCl*	*INVALID, 4-5 lbs wood each filter run; 0.05M NaCl @ 10psi, - leak in sampling line noticed on 3/23/06, potential contamination*	*N/A*	*13:39:22*	*14:04:22*	*25.0*	40	*Not analysed*
153	*STRTQ149*	*STRQQ149*	*3/16/2006*	*Wood smoke mixed with NaCl*	*INVALID, 4-5 lbs wood each filter run; 0.05M NaCl @ 10psi, - leak in sampling line noticed on 3/23/06, potential contamination*	*N/A*	*14:22:03*	*14:47:03*	*25.0*	40	*Not analysed*
154	*STRTQ151*	*STRQQ151*	*3/16/2006*	*Wood smoke mixed with NaCl*	*INVALID, 4-5 lbs wood each filter run; 0.05M NaCl @ 10psi, - leak in sampling line noticed on 3/23/06, potential contamination*	*N/A*	*15:08:12*	*15:33:12*	*25.0*	40	*Not analysed*
155	*STRTQ152*	*STRQQ152*	*3/16/2006*	*Wood smoke mixed with NaCl*	*INVALID, 4-5 lbs wood each filter run; 0.05M NaCl @ 10psi, - leak in sampling line noticed on 3/23/06, potential contamination*	*N/A*	*15:57:02*	*16:22:02*	*25.0*	40	*Not analysed*

Table D-1. Continued.

Run #	Teflon Filter ID	Quartz Filter ID	Date	Source	Source Condition[a]	Dilution Ratio	Start Time	End Time	Collection Time (min)	Flow Rate (L/min)	Filter Mass Loading (µg/filter)
WOOD COMBUSTION EMISSIONS MIXED EXTERNALLY WITH NaCl											
156	*STRTQ153*	*STRQQ153*	*3/22/2006*	*Wood smoke mixed with NaCl*	*INVALID, 4-5 lbs wood each filter run; 0.05M NaCl @ 10psi, - leak in sampling line noticed on 3/23/06, potential contamination*	*N/A*	*10:20:28*	*10:45:28*	*25.0*	40	*Not analysed*
157	*STRTQ154*	*STRQQ154*	*3/22/2006*	*Wood smoke mixed with NaCl*	*INVALID, 4-5 lbs wood each filter run; 0.05M NaCl @ 10psi, - leak in sampling line noticed on 3/23/06, potential contamination*	*N/A*	*11:03:35*	*11:28:35*	*25.0*	40	*Not analysed*
158	*STRTQ155*	*STRQQ155*	*3/22/2006*	*Wood smoke mixed with NaCl*	*INVALID, 4-5 lbs wood each filter run; 0.05M NaCl @ 10psi, - leak in sampling line noticed on 3/23/06, potential contamination*	*N/A*	*11:47:52*	*12:12:52*	*25.0*	40	*Not analysed*
159	*STRTQ156*	*STRQQ156*	*3/22/2006*	*Wood smoke mixed with NaCl*	*INVALID, 4-5 lbs wood each filter run; 0.05M NaCl @ 10psi, - leak in sampling line noticed on 3/23/06, potential contamination*	*N/A*	*12:41:00*	*13:06:00*	*25.0*	40	*Not analysed*
160	*STRTQ157*	*STRQQ157*	*3/22/2006*	*Wood smoke mixed with NaCl*	*INVALID, 4-5 lbs wood each filter run; 0.05M NaCl @ 10psi, - leak in sampling line noticed on 3/23/06, potential contamination*	*N/A*	*13:31:26*	*13:56:26*	*25.0*	40	*Not analysed*
161	*STRTQ158*	*STRQQ158*	*3/22/2006*	*Wood smoke mixed with NaCl*	*INVALID, 4-5 lbs wood each filter run; 0.05M NaCl @ 10psi, - leak in sampling line noticed on 3/23/06, potential contamination*	*N/A*	*14:24:10*	*14:49:10*	*25.0*	40	*Not analysed*
162	*STRTQ159*	*STRQQ159*	*3/22/2006*	*Wood smoke mixed with NaCl*	*INVALID, 4-5 lbs wood each filter run; 0.05M NaCl @ 10psi, - leak in sampling line noticed on 3/23/06, potential contamination*	*N/A*	*15:13:43*	*15:38:43*	*25.0*	40	*Not analysed*
166	STRTQ160	STRQQ160	4/5/2006	Wood smoke mixed with NaCl	4-5 lbs wood each filter run; NaCl 0.05M @ 10 psi; D.R. ~40	40.5	11:38:36	12:03:36	25.0	40	176.4
167	STRTQ161	STRQQ161	4/5/2006	Wood smoke mixed with NaCl	4-5 lbs wood each filter run; NaCl 0.05M @ 10 psi; D.R. ~40	40.5	12:24:30	12:49:30	25.0	40	166.3
168	STRTQ162	STRQQ162	4/5/2006	Wood smoke mixed with NaCl	4-5 lbs wood each filter run; NaCl 0.05M @ 10 psi; D.R. ~40	41.5	13:13:13	13:38:13	25.0	40	132.6
169	STRTQ163	STRQQ163	4/5/2006	Wood smoke mixed with NaCl	4-5 lbs wood each filter run; NaCl 0.05M @ 10 psi; D.R. ~40	42.2	13:58:30	14:23:30	25.0	40	112.7
170	STRTQ164	STRQQ164	4/5/2006	Wood smoke mixed with NaCl	4-5 lbs wood each filter run; NaCl 0.05M @ 10 psi; D.R. ~40	42.4	15:01:58	15:26:58	25.0	40	108.7
171	STRTQ165	STRQQ165	4/5/2006	Wood smoke mixed with NaCl	4-5 lbs wood each filter run; NaCl 0.05M @ 10 psi; D.R. ~40	42.3	15:57:05	16:22:20	25.3	40	175.5
172	STRTQ166	STRQQ166	4/5/2006	Wood smoke mixed with NaCl	4-5 lbs wood each filter run; NaCl 0.05M @ 10 psi; D.R. ~40	42.5	16:51:27	17:16:27	25.0	40	139.6
173	STRTQ167	STRQQ167	4/6/2006	Wood smoke mixed with NaCl	4-5 lbs wood each filter run; NaCl 0.05M @ 10 psi; D.R. ~19	19.0	10:15:13	10:40:13	25.0	40	159.7
174	STRTQ168	STRQQ168	4/6/2006	Wood smoke mixed with NaCl	4-5 lbs wood each filter run; NaCl 0.05M @ 10 psi; D.R. ~19	19.1	11:05:01	11:30:01	25.0	40	160.7
175	STRTQ169	STRQQ169	4/6/2006	Wood smoke mixed with NaCl	4-5 lbs wood each filter run; NaCl 0.05M @ 10 psi; D.R. ~19	19.1	11:55:51	12:20:51	25.0	40	151.2
176	STRTQ170	STRQQ170	4/6/2006	Wood smoke mixed with NaCl	4-5 lbs wood each filter run; NaCl 0.05M @ 10 psi; D.R. ~19	19.5	12:43:51	13:08:51	25.0	40	131.0
177	STRTQ171	STRQQ171	4/6/2006	Wood smoke mixed with NaCl	4-5 lbs wood each filter run; NaCl 0.05M @ 10 psi; D.R. ~19	19.3	13:30:04	13:55:04	25.0	40	153.7
178	STRTQ172	STRQQ172	4/6/2006	Wood smoke mixed with NaCl	4-5 lbs wood each filter run; NaCl 0.05M @ 10 psi; D.R. ~19	19.4	14:15:21	14:40:21	25.0	40	138.2
179	STRTQ173	STRQQ173	4/6/2006	Wood smoke mixed with NaCl	4-5 lbs wood each filter run; NaCl 0.05M @ 10 psi; D.R. ~19	19.5	15:10:34	15:35:34	25.0	40	144.0

Table D-1. Continued.

Run #	Teflon Filter ID	Quartz Filter ID	Date	Source	Source Condition[a]	Dilution Ratio	Start Time	End Time	Collection Time (min)	Flow Rate (L/min)	Filter Mass Loading (µg/filter)
CARBON BLACK RESUSPENDED											
128	REST1751	RESQ1751	3/10/2006	Carbon Black powder	Carbon black collection using resuspension chamber	N/A	N/A	N/A	2.3	9^{I}, 10^{Q}	480.0
129	REST1752	RESQ1752	3/10/2006	Carbon Black powder	Carbon black collection using resuspension chamber	N/A	N/A	N/A	2.9	9^{T}, 10^{Q}	183.0
130	REST1753	RESQ1753	3/10/2006	Carbon Black powder	Carbon black collection using resuspension chamber	N/A	N/A	N/A	5.3	9^{I}, 10^{Q}	155.0
131	REST1755	RESQ1755	3/10/2006	Carbon Black powder	Carbon black collection using resuspension chamber	N/A	N/A	N/A	2.6	9^{I}, 10^{Q}	170.0
132	REST1756	RESQ1756	3/10/2006	Carbon Black powder	Carbon black collection using resuspension chamber	N/A	N/A	N/A	4.8	9^{I}, 10^{Q}	535.0
133	REST1757	RESQ1757	3/10/2006	Carbon Black powder	Carbon black collection using resuspension chamber	N/A	N/A	N/A	2	9^{T}, 10^{Q}	450.0
134	REST1759	RESQ1759	3/10/2006	Carbon Black powder	Carbon black collection using resuspension chamber	N/A	N/A	N/A	2.1	9^{T}, 10^{Q}	1008.0
135	REST1761	RESQ1761	3/10/2006	Carbon Black powder	Carbon black collection using resuspension chamber	N/A	N/A	N/A	2.2	9^{I}, 10^{Q}	984.0
136	REST1762	RESQ1762	3/10/2006	Carbon Black powder	Carbon black collection using resuspension chamber	N/A	N/A	N/A	4.2	9^{T}, 10^{Q}	1021.0
CARBON BLACK NEBULIZED											
163	STRST069	STRSQ069	4/4/2006	Carbon black nebulized	Carbon Black: 0.1g in 200ml (95% H2O, 5% Methanol) Sonicated 30 min. Nebulize 15min prior to sample collection	0.0	9:02:28	10:12:28	70.0	10	18.0
164	STRST070	STRSQ070	4/4/2006	Carbon black nebulized	Carbon Black: 0.1g in 200ml (95% H2O, 5% Methanol) Sonicated 12 min. Nebulize 15min prior to sample collection	0.0	12:15:35	14:15:35	120.0	10	22.9
165	STRST071	STRSQ071	4/4/2006	Carbon black nebulized	Carbon Black: 0.1g in 200ml (95% H2O, 5% Methanol) Sonicated 12 min. Nebulize 15min prior to sample collection	0.0	15:03:49	17:03:49	120.0	10	26.0
GRAPHITE POWDER RESUSPENDED											
119	REST1741	RESQ1741	3/10/2006	Graphite powder	Graphite powder collection using resuspension chamber	N/A	N/A	N/A	1.3	9^{T}, 10^{Q}	96.0
120	REST1742	RESQ1742	3/10/2006	Graphite powder	Graphite powder collection using resuspension chamber	N/A	N/A	N/A	3.7	9^{I}, 10^{Q}	154.0
121	REST1743	RESQ1743	3/10/2006	Graphite powder	Graphite powder collection using resuspension chamber	N/A	N/A	N/A	5	9^{I}, 10^{Q}	145.0
122	REST1744	RESQ1744	3/10/2006	Graphite powder	Graphite powder collection using resuspension chamber	N/A	N/A	N/A	5.6	9^{T}, 10^{Q}	408.0
123	REST1745	RESQ1745	3/10/2006	Graphite powder	Graphite powder collection using resuspension chamber	N/A	N/A	N/A	3.1	9^{T}, 10^{Q}	522.0
124	REST1746	RESQ1746	3/10/2006	Graphite powder	Graphite powder collection using resuspension chamber	N/A	N/A	N/A	3	9^{I}, 10^{Q}	517.0
125	REST1747	RESQ1747	3/10/2006	Graphite powder	Graphite powder collection using resuspension chamber	N/A	N/A	N/A	2.6	9^{T}, 10^{Q}	1162.0
126	REST1748	RESQ1748	3/10/2006	Graphite powder	Graphite powder collection using resuspension chamber	N/A	N/A	N/A	5.2	9^{T}, 10^{Q}	1547.0
127	REST1749	RESQ1749	3/10/2006	Graphite powder	Graphite powder collection using resuspension chamber	N/A	N/A	N/A	5	9^{T}, 10^{Q}	1449.0
DYNAMIC BLANKS											
21	STRST021	STRSQ021	1/12/2006	Dilution sampling system blank	Dilution sampling system blank	N/A	9:50:45	11:50:45	120.0	40	22.0
41	STRST041	STRSQ041	1/20/2006	Dilution sampling system Blank	Dilution sampling system Blank	N/A	11:13:06	12:13:06	60.0	40	14.0
46	STRST046	STRSQ046	1/23/2006	Dilution sampling system Blank	Dilution sampling system Blank	N/A	10:42:29	11:02:29	20.0	40	17.1
32	STRST032	STRSQ032	1/19/2006	Electric arc Blank	Electric arc Blank	N/A	10:03:27	10:23:27	20.0	10	0.0
33	STRST033	STRSQ033	1/19/2006	Electric arc Blank	Electric arc Blank	N/A	10:30:58	10:50:58	20.0	10	0.0
34	STRST034	STRSQ034	1/19/2006	Electric arc Blank	Electric arc Blank	N/A	10:57:27	11:17:27	20.0	10	0.0
22	STRST022	STRSQ022	1/12/2006	Nebulizer blank	Nebulizer Blank (10% MeOH, 90% H2O)	N/A	13:39:40	14:24:40	45.0	10	11.1

[a]D.R. Dilution Ratio; N/A: Not applicable or not available.

APPENDIX E
DATABASE STRUCTURE

E.1. DATABASE DESCRIPTION

This section introduces the features, the structure of the database, and contents of the data archive. The approach that was followed to obtain the final data files is illustrated in Figure E-1. Detailed data processing and data validation procedures are documented in Sections 5 and 6. These data are available in Microsoft Excel (.xls) format for convenient distribution to data users. The file extension identifies the file type according to the following definitions:

- TXT = ASCII text file
- DOC = Microsoft Word document
- XLS = Microsoft Excel spreadsheet

The data files have the following attributes:

- They contain the ambient observables needed to assess source/receptor relationships.
- They are available in a well-documented, computerized form accessible by personal computers and over the internet.
- Measurement methods, locations, and schedules are documented.
- Precision and accuracy estimates are reported for filter-pack measurements.
- Validation flags are assigned.

The assembled aerosol database for filter pack measurements taken during the study is fully described in Table E-1, which documents variable names, description, and measurement units. The continuous measurements are documented in Table E-2. Field and chemical flags for filter pack sample collection and analysis are listed in Tables E-3 and E-4, respectively.

E.1.1 Database Structure

E.1.1a Filter-pack analysis data

The raw data was processed with Microsoft FoxPro 2.6 for Windows (Microsoft Corp., 1994), a commercially available relational database management system. FoxPro can handle 256 fields of up to 4,000 characters per record and up to one billion records per file. This system can be implemented on most IBM PC-compatible desktop computers. The data base files (∗.DBF) can also be read directly into a variety of popular statistical, plotting, data base, and spreadsheet programs without having to use any specific conversion software. After processing, the data was converted from FoxPro to Microsoft Excel format for ease of reporting and general use purposes.

In FoxPro, one of five field types (character, date, numerical, logical, or memo) was assigned to each observable. Sampling sites and particle size fractions are defined as "Character" fields, sampling dates are defined as "Date" fields, and measured data are defined as "Numeric" fields. "Logical" fields are used to represent a "yes" or "no" value applied to a variable, and "Memo" fields accommodate large blocks of textual information and are used to document the data validation results.

Data contained in different database files can be linked by indexing on and relating to common attributes in each file. Sampling site, sampling hour, sampling period, particle size, and sampling substrate IDs are common fields among various data files that can be used to relate data in one file to the corresponding data in another file. To assemble the final data files, information was merged from many data files derived from field monitoring and laboratory analyses by relating information on the common fields cited above.

Each observable is identified by a field name which follows a pattern for that type of observable. For example, in the filter-based aerosol concentration file, the first two characters represent the measured species (e.g., AL for aluminum, SI for silicon, CA for calcium), the third character designates the analysis method (i.e., "G" for gravimetric weighing, "X" for XRF analysis, "I" for IC, "A" for atomic absorption spectrophotometry, "C" for automated colorimetry, "T" for thermal/optical carbon analysis), and the last character uses a "C" to identify a species concentration or a "U" to identify the uncertainty (i.e., precision) of the corresponding measurement. Each measurement method is associated with a separate validation field to document the sample validity for that method. Missing or invalidated measurements have been removed and replaced with –99. All times show the start and end of the sampling period.

E.1.1b Continuous monitoring data

Data from the continuous instruments were uploaded and stored on a server as part of a sophisticated SQL (structured query language) database system. The continuous data were validated and flagged for invalid, suspect and valid measurements (see Section 5.2.2). All processed and flagged data are exported into Microsoft Excel (.xls) format for ease of reporting and distribution. Table E-2 summarizes the parameters reported and their description, for the continuous instruments operated during the summer and winter intensive operating periods (IOPs) at the Fresno Supersite, as well as during the source characterization experiments conducted in the laboratory. The "Instrument Name" identifies the instrument from which the data was obtained. The "Variable Name" lists the column headers that identify the data reported by the respective instrument, and the "Description" explains what data each header represents.

E.1.2 Data Archive

All data files are included in the enclosed compact disc (CD). Figure E-2 displays a flow diagram of the location and organization of the data files on the CD. The number in

parentheses indicate the number of excel files in each folder. Table E-5 summarizes the data file names and their path on the CD. The data files are grouped into two main folders, separated by continuous measurements ("Continuous") and filter pack measurements ("Filter"). Within these two directories, the data files are organized by laboratory measurements ("Source Lab") and by ambient measurements during the two intensive periods at Fresno ("Summer IOP" and "Winter IOP"). The data files within the "Continuous/Source Lab" folder are organized by the different sources tested in the laboratory. Within each of those folders are the Excel data files, identified by instrument name followed by time resolution of the data. For the summer and winter IOP folders, each is grouped into the different instrument types (absorption, carbon, ions, mass, scatter and size distribution) and within each of those folders are the individual instrument data files, identified by the instrument name and time resolution of data. The filter data files contain multiple sheets of data corresponding to the following: IMPROVE_A carbon analysis, ions and elements (Sheet name: "IMP_A, others"), STN carbon analysis (Sheet name: "STN") and French carbon analysis (Sheet name: "French"). For source-sample filter database (Filter/Source Lab/), the excel file also contains two additional sheets, that include IMPROVE_A carbon analysis on the backup quartz-fiber filters behind Teflon (Sheet name: "Teflon backup") and quartz (Sheet name: "Quartz backup"). For ambient samples, the backup filter analysis is included in the "IMP_A, others" sheet. The winter IOP data from PC-BOSS sampler that was obtained from BYU is included as a separate file.

Table E-1. Variable names, descriptions, and measurement units in the assembled aerosol database for filter pack measurements

Field Code	Description	Measurement Unit
SITE	Sampling site (ambient samples only)	
DATE	Sampling date (ambient samples only)	
Source	Sampling Source Type (source samples only)	
Sampler	Type of sampler (ambient samples only)	
SIZE	Particulate matter size cut (ambient samples only)	µm
STRTHHMM	Sampling start time (ambient samples only)	
STOPHHMM	Sampling stop time (ambient samples only)	
Duration	Sampling duration (ambient samples only)	hours
Channel	Sampler channel (ambient samples only)	
Filter Stage	Front or backup filter identification (ambient samples only)	
TID	Teflon Filter ID	
QID	Quartz Filter ID	
TFFLG	Teflon filter field flag[a]	
QFFLG	Quartz filter field flag[a]	
MSGF	Gravimetry analysis flag[b]	
BBDF	b_{abs} analysis flag[b]	
ANIF	Anion analysis flag[b]	
N4CF	Ammonium analysis flag[b]	
NAAF	Soluble sodium analysis flag[b]	
KPAF	Soluble potassium analysis flag[b]	
OETF	Carbon analysis flag[b]	
ELXF	XRF analysis flag[b]	
TVOC	Teflon filter volume	m^3
TVOU	Teflon filter volume uncertainty (estimated at 5% of volume)	m^3
QVOC	Quartz filter volume	m^3
QVOU	Quartz filter volume uncertainty (estimated at 5% of volume)	m^3
MSGC	Teflon Mass concentration by gravimetry	$\mu g/m^3$
MSGU	Teflon Mass concentration uncertainty	$\mu g/m^3$
BBDC	Light Absorption by denistometry	Mm^{-1}
BBDU	Light Absorption uncertainty	Mm^{-1}
CLIC	Soluble Chloride concentration by IC	$\mu g/m^3$
CLIU	Soluble Chloride concentration uncertainty	$\mu g/m^3$
N3IC	Soluble Nitrate concentration by IC	$\mu g/m^3$
N3IU	Soluble Nitrate concentration uncertainty	$\mu g/m^3$
S4IC	Soluble Sulfate concentration by IC	$\mu g/m^3$
S4IU	Soluble Sulfate concentration uncertainty	$\mu g/m^3$
N4CC	Soluble Ammonium concentration by AC (ambient samples only)	$\mu g/m^3$
N4CU	Soluble Ammonium concentration uncertainty	$\mu g/m^3$
N4IC	Soluble Ammonium concentration by IC (source samples only)	$\mu g/m^3$
N4IU	Soluble Ammonium concentration uncertainty	$\mu g/m^3$
NAAC	Soluble Sodium concentration by AAS (ambient samples only)	$\mu g/m^3$
NAAU	Soluble Sodium concentration uncertainty	$\mu g/m^3$
NAIC	Soluble Sodium concentration by IC (source samples only)	$\mu g/m^3$

Table E-1. Continued

Field Code	Description	Measurement Unit
NAIU	Soluble Sodium concentration uncertainty	µg/m^3
KPAC	Soluble Potassium concentration by AAS (ambient samples only)	µg/m^3
KPAU	Soluble Potassium concentration uncertainty	µg/m^3
KPIC	Soluble Potassium concentration by IC (source samples only)	µg/m^3
KPIU	Soluble Potassium concentration uncertainty	µg/m^3
O1TC	Organic Carbon Fraction 1concentration (IMPROVE_A and STN only)	µg/m^3
O1TU	Organic Carbon Fraction 1 concentration uncertainty	µg/m^3
O2TC	Organic Carbon Fraction 2 concentration (IMPROVE_A and STN only)	µg/m^3
O2TU	Organic Carbon Fraction 2 concentration uncertainty	µg/m^3
O3TC	Organic Carbon Fraction 3 concentration (IMPROVE_A and STN only)	µg/m^3
O3TU	Organic Carbon Fraction 3 concentration uncertainty	µg/m^3
O4TC	Organic Carbon Fraction 4 concentration (IMPROVE_A and STN only)	µg/m^3
O4TU	Organic Carbon Fraction 4 concentration uncertainty	µg/m^3
O5TC	Organic Carbon Fraction 5 concentration (STN only)	µg/m^3
O5TU	Organic Carbon Fraction 5 concentration uncertainty (STN only)	µg/m^3
OPTTC	Pyrolyzed Organic Carbon concentration by Laser transmittance (IMPROVE_A and STN only)	µg/m^3
OPTTU	Pyrolyzed Organic Carbon by laser transmittance concentration uncertainty	µg/m^3
OPTRC	Pyrolyzed Organic Carbon concentration by Laser reflectance (IMPROVE_A and STN only)	µg/m^3
OPTRU	Pyrolyzed Organic Carbon by laser reflectance concentration uncertainty	µg/m^3
OCTTC	Organic Carbon concentration by Laser transmittance (IMPROVE_A and STN only)	µg/m^3
OCTTU	Organic Carbon by laser transmittance concentration uncertainty	µg/m^3
OCTRC	Organic Carbon concentration by Laser reflectance (IMPROVE_A and STN only)	µg/m^3
OCTRU	Organic Carbon by laser reflectance concentration uncertainty	µg/m^3
E1TC	Elemental Carbon Fraction 1 concentration (IMPROVE_A and STN only)	µg/m^3
E1TU	Elemental Carbon Fraction 1 concentration uncertainty	µg/m^3
E2TC	Elemental Carbon Fraction 2 concentration (IMPROVE_A and STN only)	µg/m^3
E2TU	Elemental Carbon Fraction 2 concentration uncertainty	µg/m^3
E3TC	Elemental Carbon Fraction 3 concentration (IMPROVE_A and STN only)	µg/m^3
E3TU	Elemental Carbon Fraction 3 concentration uncertainty	µg/m^3
E4TC	Elemental Carbon Fraction 4 concentration (STN only)	µg/m^3
E4TU	Elemental Carbon Fraction 4 concentration uncertainty	µg/m^3
E5TC	Elemental Carbon Fraction 5 concentration (STN only)	µg/m^3
E5TU	Elemental Carbon Fraction 5 concentration uncertainty	µg/m^3
ECTTC	Elemental Carbon concentration by Laser transmittance (IMPROVE_A and STN only)	µg/m^3
ECTTU	Elemental Carbon by laser transmittance concentration uncertainty	µg/m^3
ECTRC	Elemental Carbon concentration by Laser reflectance (IMPROVE_A and STN only)	µg/m^3
ECTRU	Elemental Carbon by laser reflectance concentration uncertainty	µg/m^3
ECTC	Elemental Carbon concentration (French only)	µg/m^3
ECTU	Elemental Carbon concentration uncertainty	µg/m^3

Table E-1. Continued

Field Code	Description	Measurement Unit
TCTC	Total Carbon concentration (IMPROVE_A and STN only)	µg/m^3
TCTU	Total Carbon concentration uncertainty	µg/m^3
NAXC	Sodium concentration by XRF	µg/m^3
NAXU	Sodium concentration uncertainty	µg/m^3
MGXC	Magnesium concentration by XRF	µg/m^3
MGXU	Magnesium concentration uncertainty	µg/m^3
ALXC	Aluminum concentration by XRF	µg/m^3
ALXU	Aluminum concentration uncertainty	µg/m^3
SIXC	Silicon concentration by XRF	µg/m^3
SIXU	Silicon concentration uncertainty	µg/m^3
PHXC	Phosphorous concentration by XRF	µg/m^3
PHXU	Phosphorous concentration uncertainty	µg/m^3
SUXC	Sulfur concentration by XRF	µg/m^3
SUXU	Sulfur concentration uncertainty	µg/m^3
CLXC	Chlorine concentration by XRF	µg/m^3
CLXU	Chlorine concentration uncertainty	µg/m^3
KPXC	Potassium concentration by XRF	µg/m^3
KPXU	Potassium concentration uncertainty	µg/m^3
CAXC	Calcium concentration by XRF	µg/m^3
CAXU	Calcium concentration uncertainty	µg/m^3
TIXC	Titanium concentration by XRF	µg/m^3
TIXU	Titanium concentration uncertainty	µg/m^3
VAXC	Vanadium concentration by XRF	µg/m^3
VAXU	Vanadium concentration uncertainty	µg/m^3
CRXC	Chromium concentration by XRF	µg/m^3
CRXU	Chromium concentration uncertainty	µg/m^3
MNXC	Manganese concentration by XRF	µg/m^3
MNXU	Manganese concentration uncertainty	µg/m^3
FEXC	Iron concentration by XRF	µg/m^3
FEXU	Iron concentration uncertainty	µg/m^3
COXC	Cobalt concentration by XRF	µg/m^3
COXU	Cobalt concentration uncertainty	µg/m^3
NIXC	Nickel concentration by XRF	µg/m^3
NIXU	Nickel concentration uncertainty	µg/m^3
CUXC	Copper concentration by XRF	µg/m^3
CUXU	Copper concentration uncertainty	µg/m^3
ZNXC	Zinc concentration by XRF	µg/m^3
ZNXU	Zinc concentration uncertainty	µg/m^3
GAXC	Gallium concentration by XRF	µg/m^3
GAXU	Gallium concentration uncertainty	µg/m^3
ASXC	Arsenic concentration by XRF	µg/m^3

Table E-1. Continued

Field Code	Description	Measurement Unit
ASXU	Arsenic concentration uncertainty	µg/m^3
SEXC	Selenium concentration by XRF	µg/m^3
SEXU	Selenium concentration uncertainty	µg/m^3
BRXC	Bromine concentration by XRF	µg/m^3
BRXU	Bromine concentration uncertainty	µg/m^3
RBXC	Rubidium concentration by XRF	µg/m^3
RBXU	Rubidium concentration uncertainty	µg/m^3
SRXC	Strontium concentration by XRF	µg/m^3
SRXU	Strontium concentration uncertainty	µg/m^3
YTXC	Yttrium concentration by XRF	µg/m^3
YTXU	Yttrium concentration uncertainty	µg/m^3
ZRXC	Zirconium concentration by XRF	µg/m^3
ZRXU	Zirconium concentration uncertainty	µg/m^3
MOXC	Molybdenum concentration by XRF	µg/m^3
MOXU	Molybdenum concentration uncertainty	µg/m^3
PDXC	Palladium concentration by XRF	µg/m^3
PDXU	Palladium concentration uncertainty	µg/m^3
AGXC	Silver concentration by XRF	µg/m^3
AGXU	Silver concentration uncertainty	µg/m^3
CDXC	Cadmium concentration by XRF	µg/m^3
CDXU	Cadmium concentration uncertainty	µg/m^3
INXC	Indium concentration by XRF	µg/m^3
INXU	Indium concentration uncertainty	µg/m^3
SNXC	Tin concentration by XRF	µg/m^3
SNXU	Tin concentration uncertainty	µg/m^3
SBXC	Antimony concentration by XRF	µg/m^3
SBXU	Antimony concentration uncertainty	µg/m^3
BAXC	Barium concentration by XRF	µg/m^3
BAXU	Barium concentration uncertainty	µg/m^3
LAXC	Lanthanum concentration by XRF	µg/m^3
LAXU	Lanthanum concentration uncertainty	µg/m^3
AUXC	Gold concentration by XRF	µg/m^3
AUXU	Gold concentration uncertainty	µg/m^3
HGXC	Mercury concentration by XRF	µg/m^3
HGXU	Mercury concentration uncertainty	µg/m^3
TLXC	Thallium concentration by XRF	µg/m^3
TLXU	Thallium concentration uncertainty	µg/m^3
PBXC	Lead concentration by XRF	µg/m^3
PBXU	Lead concentration uncertainty	µg/m^3
URXC	Uranium concentration by XRF	µg/m^3
URXU	Uranium concentration uncertainty	µg/m^3

Table E-1. Continued

[a] See Table E-3

[b] See Table E-4

Table E-2. Instruments, variable names, description, and measurement units in the assembled database for continuous measurements Fresno Supersite (winter and summer IOPs) as well as the source characterization laboratory

Instrument Name	Variable Name	Description	Unit
Light absorption			
Dual wavelength aethalometer	uv	Black Carbon (BC) concentration at 370 nm	$\mu g/m^3$
Dual wavelength aethalometer	bc	BC concentration at 880 nm	$\mu g/m^3$
Seven-color aethalometer	w370	BC concentration at 370 nm	$\mu g/m^3$
Seven-color aethalometer	w470	BC concentration at 470 nm	$\mu g/m^3$
Seven-color aethalometer	w520	BC concentration at 520 nm	$\mu g/m^3$
Seven-color aethalometer	w590	BC concentration at 590 nm	$\mu g/m^3$
Seven-color aethalometer	w660	BC concentration at 660 nm	$\mu g/m^3$
Seven-color aethalometer	w880	BC concentration at 880 nm	$\mu g/m^3$
Seven-color aethalometer	w950	BC concentration at 950 nm	$\mu g/m^3$
Multi-Angle Absorption Photometer	cbc	BC concentration at 670 nm	$\mu g/m^3$
Multi-Angle Absorption Photometer	cbca	BC concentration at 670 nm calculated similar to aethalometer algorithm	$\mu g/m^3$
Photoacoustic 1047nm	Babs_1/Mm	Light absorption (b_{abs}) at 1047 nm	Mm^{-1}
Photoacoustic 1047nm	NoiseEqBabs_1/Mm	Instrument measurement noise at 1047 nm	Mm^{-1}
Photoacoustic 1047nm	Temperature_C	Internal temperature	°C
Photoacoustic 1047nm	Pressure_mb	Internal pressure	mbar
Photoacoustic 532nm	Babs_1/Mm	Light absorption (b_{abs}) at 532 nm	Mm^{-1}
Photoacoustic 532nm	NoiseEqBabs_1/Mm	Instrument measurement noise at 532 nm	Mm^{-1}
Photoacoustic 532nm	Temperature_C	Internal temperature	°C
Photoacoustic 532nm	Pressure_mb	Internal pressure	mbar
Particle soot absorption photometer	psap467raw	Instrument reported b_{abs} at 467 nm	Mm^{-1}
Particle soot absorption photometer	psap530raw	Instrument reported b_{abs} at 530 nm	Mm^{-1}
Particle soot absorption photometer	psap660raw	Instrument reported b_{abs} at 660 nm	Mm^{-1}

Table E-2. continued.

Instrument Name	Variable Name	Description	Unit
Particle soot absorption photometer	psap467adj	b_{abs} at 467 nm adjusted for light scattering effects following Virkkula et al. (2005)	Mm^{-1}
Particle soot absorption photometer	psap530adj	b_{abs} at 530 nm adjusted for light scattering effects following Virkkula et al. (2005)	Mm^{-1}
Particle soot absorption photometer	psap660adj	b_{abs} at 660 nm adjusted for light scattering effects following Virkkula et al. (2005)	Mm^{-1}
Light scattering			
NGN2 nephelometer	bscat	Light scattering (b_{scat})	Mm^{-1}
Radiance 903 PM2.5 nephelometer	Rad25	$PM_{2.5}$ Light scattering (b_{scat})	Mm^{-1}
Radiance 903 PM2.5 nephelometer	Radrh	Internal relative humidity	%
Radiance 903 TSP Nephelometer	RadTSP	Light scattering (b_{scat})	Mm^{-1}
Radiance 903 TSP Nephelometer	Radrh	Internal relative humidity	%
EcoTech nephelometer TSP	Scat coeff(1/Mm)	Light scattering (b_{scat})	Mm^{-1}
TSI nephelometer PM2.5	Sblue (1/Mm)	Total scatter	Mm^{-1}
TSI nephelometer PM2.5	Sgreen (1/Mm)	Total scatter	Mm^{-1}
TSI nephelometer PM2.5	Sred (1/Mm)	Total scatter	Mm^{-1}
TSI nephelometer PM2.5	Bblue (1/Mm)	Backscatter	Mm^{-1}
TSI nephelometer PM2.5	Bgreen (1/Mm)	Backscatter	Mm^{-1}
TSI nephelometer PM2.5	Bred (1/Mm)	Backscatter	Mm^{-1}
Mass			
BAM-1020 PM 2.5	bam25	$PM_{2.5}$ mass concentration	$\mu g/m^3$
BAM-1020 PM10	bam10	PM_{10} mass concentration	$\mu g/m^3$
Kimoto BAM	PM25(mg/m3)	$PM_{2.5}$ mass concentration	mg/m^3
Kimoto BAM	PM10(mg/m3)	PM_{10} mass concentration	mg/m^3
Kimoto BAM	OBC (ug/m3)	Optical BC concentration	$\mu g/m^3$
TEOM 1400a PM10	Teom10	PM_{10} mass concentration	$\mu g/m^3$
TEOM 1400a PM25	Teom25	$PM_{2.5}$ mass concentration	$\mu g/m^3$
Differential TEOM PM2.5	diffteom25	$PM_{2.5}$ mass concentration	$\mu g/m^3$
FDMS TEOM PM2.5	fdmsteom25	$PM_{2.5}$ mass concentration	$\mu g/m^3$
30°C TEOM PM2.5	teom25	$PM_{2.5}$ mass concentration	$\mu g/m^3$
Dust Trak	Aerosol	$PM_{2.5}$ mass concentration	$\mu g/m^3$
Grimm PM2.5	grimm25	$PM_{2.5}$ mass concentration	$\mu g/m^3$
Grimm PM2.5 with heated inlet	grimm25heat	$PM_{2.5}$ mass concentration	$\mu g/m^3$
Carbon			
PAH EcoChem PAS_2000	pah	Particle-bound poly aromatic hydrocarbon concentration	femto amps

Table E-2. continued.

Instrument Name	Variable Name	Description	Unit
R&P 5400	tc	Total carbon concentration	µg/m^3
Sunset	thermal_oc	Organic carbon concentration by thernal analysis	µg/m^3
Sunset	thermal_ec	Elemental carbon concentration by thermal analysis	µg/m^3
Sunset	tc_ugc_m3	Total carbon concentration	µg/m^3
Sunset	optoc_ugc	"Optical OC" concentration, which is equal to TC minus optical EC concentration	µg/m^3
Sunset	optec_ugc	Optical EC concentration: EC concentration determined using principle of aethalometer	µg/m^3
Ions			
R&P 8400N1	NO3	Nitrate concentration	µg/m^3
R&P 8400N2	NO3	Nitrate concentration	µg/m^3
R&P 8400S	SO4	Sulfate concentration	µg/m^3
Dionex	sulfate	Sulfate concentration	µg/m^3
Dionex	nitrate	Nitrate concentration	µg/m^3
Dionex	chloride	Chloride concentration	µg/m^3
Dionex	nitrite	Nitrite concentration	µg/m^3
Dionex	ammonium	Ammonium concentration	µg/m^3
Meteorology			
Barometric Pressure	pr	Ambient atmospheric pressure	mbar
Relative Humidity	RH	Ambient relative humidity	%
Solar Radiation	SR	Solar radiance	W/m^2
Temperature	Temp	Ambient temperature	°C
Wind Direction	WDV	Uni-vector wind direction	Degrees North
Wind Direction	SGY	Standard deviation of wind direction	Degrees North
Wind Speed	WSS	Scalar wind speed	m/s
Particle sizing			
Climet Spectro.3	d1	size bin 300 to 400 nm	#/cm^3
Climet Spectro.3	d2	size bin 400 to 500 nm	#/cm^3
Climet Spectro.3	d3	size bin 500 to 630 nm	#/cm^3
Climet Spectro.3	d4	size bin 630 to 800 nm	#/cm^3
Climet Spectro.3	d5	size bin 800 to 1000 nm	#/cm^3
Climet Spectro.3	d6	size bin 1000 to 1300 nm	#/cm^3
Climet Spectro.3	d7	size bin 1300 to 1600 nm	#/cm^3
Climet Spectro.3	d8	size bin 1600 to 2000 nm	#/cm^3
Climet Spectro.3	d9	size bin 2000 to 2500 nm	#/cm^3
Climet Spectro.3	d10	size bin 2500 to 3200 nm	#/cm^3
Climet Spectro.3	d11	size bin 3200 to 4000 nm	#/cm^3

Table E-2. continued.

Instrument Name	Variable Name	Description	Unit
Climet Spectro.3	d12	size bin 4000 to 5000 nm	#/cm^3
Climet Spectro.3	d13	size bin 5000 to 6300 nm	#/cm^3
Climet Spectro.3	d14	size bin 6300 to 8000 nm	#/cm^3
Climet Spectro.3	d15	size bin 8000 to 10000 nm	#/cm^3
Climet Spectro.3	d16	size bin >10000 nm	#/cm^3
Lasair 1003	d1	size bin 100 to 200 nm	#/cm^3
Lasair 1003	d2	size bin 200 to 300 nm	#/cm^3
Lasair 1003	d3	size bin 300 to 400 nm	#/cm^3
Lasair 1003	d4	size bin 400 to 500 nm	#/cm^3
Lasair 1003	d5	size bin 500 to 700 nm	#/cm^3
Lasair 1003	d6	size bin 700 to 1000 nm	#/cm^3
Lasair 1003	d7	size bin 1000 to 2000 nm	#/cm^3
Lasair 1003	d8	size bin >2000 nm	#/cm^3
Grimm SMPS	d01	size bin < 5.76 nm	#/cm^3
Grimm SMPS	d02	size bin 5.76 to 6.29 nm	#/cm^3
Grimm SMPS	d03	size bin 6.29 to 6.86 nm	#/cm^3
Grimm SMPS	d04	size bin 6.86 to 7.49 nm	#/cm^3
Grimm SMPS	d05	size bin 7.49 to 8.18 nm	#/cm^3
Grimm SMPS	d06	size bin 8.18 to 8.93 nm	#/cm^3
Grimm SMPS	d07	size bin 8.93 to 9.74 nm	#/cm^3
Grimm SMPS	d08	size bin 9.74 to 10.64 nm	#/cm^3
Grimm SMPS	d09	size bin 10.64 to 11.62 nm	#/cm^3
Grimm SMPS	d10	size bin 11.62 to 12.69 nm	#/cm^3
Grimm SMPS	d11	size bin 12.69 to 13.87 nm	#/cm^3
Grimm SMPS	d12	size bin 13.87 to 15.15 nm	#/cm^3
Grimm SMPS	d13	size bin 15.15 to 16.55 nm	#/cm^3
Grimm SMPS	d14	size bin 16.55 to 18.09 nm	#/cm^3
Grimm SMPS	d15	size bin 18.09 to 19.78 nm	#/cm^3
Grimm SMPS	d16	size bin 19.78 to 21.63 nm	#/cm^3
Grimm SMPS	d17	size bin 21.63 to 23.66 nm	#/cm^3
Grimm SMPS	d18	size bin 23.66 to 25.89 nm	#/cm^3
Grimm SMPS	d19	size bin 25.89 to 28.33 nm	#/cm^3
Grimm SMPS	d20	size bin 28.33 to 31.02 nm	#/cm^3
Grimm SMPS	d21	size bin 31.02 to 33.98 nm	#/cm^3
Grimm SMPS	d22	size bin 33.98 to 37.23 nm	#/cm^3
Grimm SMPS	d23	size bin 37.23 to 40.81 nm	#/cm^3
Grimm SMPS	d24	size bin 40.81 to 44.77 nm	#/cm^3
Grimm SMPS	d25	size bin 44.77 to 49.14 nm	#/cm^3
Grimm SMPS	d26	size bin 49.14 to 53.96 nm	#/cm^3
Grimm SMPS	d27	size bin 53.96 to 59.31 nm	#/cm^3
Grimm SMPS	d28	size bin 59.31 to 65.24 nm	#/cm^3

Table E-2. continued.

Instrument Name	Variable Name	Description	Unit
Grimm SMPS	d29	size bin 65.24 to 71.82 nm	#/cm^3
Grimm SMPS	d30	size bin 71.82 to 79.15 nm	#/cm^3
Grimm SMPS	d31	size bin 79.15 to 87.33 nm	#/cm^3
Grimm SMPS	d32	size bin 87.33 to 96.47 nm	#/cm^3
Grimm SMPS	d33	size bin 96.47 to 106.72 nm	#/cm^3
Grimm SMPS	d34	size bin 106.72 to 118.23 nm	#/cm^3
Grimm SMPS	d35	size bin 118.23 to 131.22 nm	#/cm^3
Grimm SMPS	d36	size bin 131.22 to 145.9 nm	#/cm^3
Grimm SMPS	d37	size bin 145.9 to 162.57 nm	#/cm^3
Grimm SMPS	d38	size bin 162.57 to 181.55 nm	#/cm^3
Grimm SMPS	d39	size bin 181.55 to 203.27 nm	#/cm^3
Grimm SMPS	d40	size bin 203.27 to 228.2 nm	#/cm^3
Grimm SMPS	d41	size bin 228.2 to 256.95 nm	#/cm^3
Grimm SMPS	d42	size bin 256.95 to 290.23 nm	#/cm^3
Grimm SMPS	d43	size bin 290.23 to 328.9 nm	#/cm^3
Grimm SMPS	d44	size bin > 328.9 nm	#/cm^3
TSI SMPS_LONG	Long_d01	size bin 9.31 to 10 nm	#/cm^3
TSI SMPS_LONG	Long_d02	size bin 10 to 10.7 nm	#/cm^3
TSI SMPS_LONG	Long_d03	size bin 10.7 to 11.5 nm	#/cm^3
TSI SMPS_LONG	Long_d04	size bin 11.5 to 12.4 nm	#/cm^3
TSI SMPS_LONG	Long_d05	size bin 12.4 to 13.3 nm	#/cm^3
TSI SMPS_LONG	Long_d06	size bin 13.3 to 14.3 nm	#/cm^3
TSI SMPS_LONG	Long_d07	size bin 14.3 to 15.4 nm	#/cm^3
TSI SMPS_LONG	Long_d08	size bin 15.4 to 16.5 nm	#/cm^3
TSI SMPS_LONG	Long_d09	size bin 16.5 to 17.8 nm	#/cm^3
TSI SMPS_LONG	Long_d10	size bin 17.8 to 19.1 nm	#/cm^3
TSI SMPS_LONG	Long_d11	size bin 19.1 to 20.5 nm	#/cm^3
TSI SMPS_LONG	Long_d12	size bin 20.5 to 22.1 nm	#/cm^3
TSI SMPS_LONG	Long_d13	size bin 22.1 to 23.7 nm	#/cm^3
TSI SMPS_LONG	Long_d14	size bin 23.7 to 25.5 nm	#/cm^3
TSI SMPS_LONG	Long_d15	size bin 25.5 to 27.4 nm	#/cm^3
TSI SMPS_LONG	Long_d16	size bin 27.4 to 29.4 nm	#/cm^3
TSI SMPS_LONG	Long_d17	size bin 29.4 to 31.6 nm	#/cm^3
TSI SMPS_LONG	Long_d18	size bin 31.6 to 34 nm	#/cm^3
TSI SMPS_LONG	Long_d19	size bin 34 to 36.5 nm	#/cm^3
TSI SMPS_LONG	Long_d20	size bin 36.5 to 39.2 nm	#/cm^3
TSI SMPS_LONG	Long_d21	size bin 39.2 to 42.2 nm	#/cm^3
TSI SMPS_LONG	Long_d22	size bin 42.2 to 45.3 nm	#/cm^3
TSI SMPS_LONG	Long_d23	size bin 45.3 to 48.7 nm	#/cm^3
TSI SMPS_LONG	Long_d24	size bin 48.7 to 52.3 nm	#/cm^3
TSI SMPS_LONG	Long_d25	size bin 52.3 to 56.2 nm	#/cm^3
TSI SMPS_LONG	Long_d26	size bin 56.2 to 60.4 nm	#/cm^3

Table E-2. continued.

Instrument Name	Variable Name	Description	Unit
TSI SMPS_LONG	Long_d27	size bin 60.4 to 64.9 nm	#/cm^3
TSI SMPS_LONG	Long_d28	size bin 64.9 to 69.8 nm	#/cm^3
TSI SMPS_LONG	Long_d29	size bin 69.8 to 75 nm	#/cm^3
TSI SMPS_LONG	Long_d30	size bin 75 to 80.6 nm	#/cm^3
TSI SMPS_LONG	Long_d31	size bin 80.6 to 86.6 nm	#/cm^3
TSI SMPS_LONG	Long_d32	size bin 86.6 to 93.1 nm	#/cm^3
TSI SMPS_LONG	Long_d33	size bin 93.1 to 100 nm	#/cm^3
TSI SMPS_LONG	Long_d34	size bin 100 to 107 nm	#/cm^3
TSI SMPS_LONG	Long_d35	size bin 107 to 115 nm	#/cm^3
TSI SMPS_LONG	Long_d36	size bin 115 to 124 nm	#/cm^3
TSI SMPS_LONG	Long_d37	size bin 124 to 133 nm	#/cm^3
TSI SMPS_LONG	Long_d38	size bin 133 to 143 nm	#/cm^3
TSI SMPS_LONG	Long_d39	size bin 143 to 154 nm	#/cm^3
TSI SMPS_LONG	Long_d40	size bin 154 to 165 nm	#/cm^3
TSI SMPS_LONG	Long_d41	size bin 165 to 178 nm	#/cm^3
TSI SMPS_LONG	Long_d42	size bin 178 to 191 nm	#/cm^3
TSI SMPS_LONG	Long_d43	size bin 191 to 205 nm	#/cm^3
TSI SMPS_LONG	Long_d44	size bin 205 to 221 nm	#/cm^3
TSI SMPS_LONG	Long_d45	size bin 221 to 237 nm	#/cm^3
TSI SMPS_LONG	Long_d46	size bin 237 to 255 nm	#/cm^3
TSI SMPS_LONG	Long_d47	size bin 255 to 274 nm	#/cm^3
TSI SMPS_LONG	Long_d48	size bin 274 to 294 nm	#/cm^3
TSI SMPS_LONG	Long_d49	size bin 294 to 316 nm	#/cm^3
TSI SMPS_LONG	Long_d50	size bin 316 to 340 nm	#/cm^3
TSI SMPS_LONG	Long_d51	size bin 340 to 365 nm	#/cm^3
TSI SMPS_LONG	Long_d52	size bin 365 to 422 nm	#/cm^3
TSI SMPS_LONG	Long_d53	n/a	#/cm^3
TSI SMPS_LONG	Long_d54	n/a	#/cm^3
TSI SMPS_Nano	Nano_d01	size bin 2.94 to 3.16 nm	#/cm^3
TSI SMPS_Nano	Nano_d02	size bin 3.16 to 3.4 nm	#/cm^3
TSI SMPS_Nano	Nano_d03	size bin 3.4 to 3.65 nm	#/cm^3
TSI SMPS_Nano	Nano_d04	size bin 3.65 to 3.92 nm	#/cm^3
TSI SMPS_Nano	Nano_d05	size bin 3.92 to 4.22 nm	#/cm^3
TSI SMPS_Nano	Nano_d06	size bin 4.22 to 4.53 nm	#/cm^3
TSI SMPS_Nano	Nano_d07	size bin 4.53 to 4.87 nm	#/cm^3
TSI SMPS_Nano	Nano_d08	size bin 4.87 to 5.23 nm	#/cm^3
TSI SMPS_Nano	Nano_d09	size bin 5.23 to 5.62 nm	#/cm^3
TSI SMPS_Nano	Nano_d10	size bin 5.62 to 6.04 nm	#/cm^3
TSI SMPS_Nano	Nano_d11	size bin 6.04 to 6.49 nm	#/cm^3
TSI SMPS_Nano	Nano_d12	size bin 6.49 to 6.98 nm	#/cm^3
TSI SMPS_Nano	Nano_d13	size bin 6.98 to 7.5 nm	#/cm^3
TSI SMPS_Nano	Nano_d14	size bin 7.5 to 8.06 nm	#/cm^3

Table E-2. continued.

Instrument Name	Variable Name	Description	Unit
TSI SMPS_Nano	Nano_d15	size bin 8.06 to 8.66 nm	#/cm^3
TSI SMPS_Nano	Nano_d16	size bin 8.66 to 9.31 nm	#/cm^3
TSI SMPS_Nano	Nano_d17	size bin 9.31 to 10 nm	#/cm^3
TSI SMPS_Nano	Nano_d18	size bin 10 to 10.7 nm	#/cm^3
TSI SMPS_Nano	Nano_d19	size bin 10.7 to 11.5 nm	#/cm^3
TSI SMPS_Nano	Nano_d20	size bin 11.5 to 12.4 nm	#/cm^3
TSI SMPS_Nano	Nano_d21	size bin 12.4 to 13.3 nm	#/cm^3
TSI SMPS_Nano	Nano_d22	size bin 13.3 to 14.3 nm	#/cm^3
TSI SMPS_Nano	Nano_d23	size bin 14.3 to 15.4 nm	#/cm^3
TSI SMPS_Nano	Nano_d24	size bin 15.4 to 16.5 nm	#/cm^3
TSI SMPS_Nano	Nano_d25	size bin 16.5 to 17.8 nm	#/cm^3
TSI SMPS_Nano	Nano_d26	size bin 17.8 to 19.1 nm	#/cm^3
TSI SMPS_Nano	Nano_d27	size bin 19.1 to 20.5 nm	#/cm^3
TSI SMPS_Nano	Nano_d28	size bin 20.5 to 22.1 nm	#/cm^3
TSI SMPS_Nano	Nano_d29	size bin 22.1 to 23.7 nm	#/cm^3
TSI SMPS_Nano	Nano_d30	size bin 23.7 to 25.5 nm	#/cm^3
TSI SMPS_Nano	Nano_d31	size bin 25.5 to 27.4 nm	#/cm^3
TSI SMPS_Nano	Nano_d32	size bin 27.4 to 29.4 nm	#/cm^3
TSI SMPS_Nano	Nano_d33	size bin 29.4 to 31.6 nm	#/cm^3
TSI SMPS_Nano	Nano_d34	size bin 31.6 to 34 nm	#/cm^3
TSI SMPS_Nano	Nano_d35	size bin 34 to 36.5 nm	#/cm^3
TSI SMPS_Nano	Nano_d36	size bin 36.5 to 39.2 nm	#/cm^3
TSI SMPS_Nano	Nano_d37	size bin 39.2 to 42.2 nm	#/cm^3
TSI SMPS_Nano	Nano_d38	size bin 42.2 to 45.3 nm	#/cm^3
TSI SMPS_Nano	Nano_d39	size bin 45.3 to 48.7 nm	#/cm^3
TSI SMPS_Nano	Nano_d40	size bin 48.7 to 52.3 nm	#/cm^3
TSI SMPS_Nano	Nano_d41	size bin 52.3 to 56.2 nm	#/cm^3
TSI SMPS_Nano	Nano_d42	size bin 56.2 to 60.4 nm	#/cm^3
TSI SMPS_Nano	Nano_d43	size bin 60.4 to 64.9 nm	#/cm^3
TSI SMPS_Nano	Nano_d44	size bin 64.9 to 69.8 nm	#/cm^3
TSI SMPS_Nano	Nano_d45	size bin 69.8 to 75 nm	#/cm^3
TSI SMPS_Nano	Nano_d46	size bin 75 to 80.6 nm	#/cm^3
TSI SMPS_Nano	Nano_d47	size bin 80.6 to 86.6 nm	#/cm^3
TSI SMPS_Nano	Nano_d48	n/a	#/cm^3
TSI SMPS_Nano	Nano_d49	n/a	#/cm^3
MSP WPS	wps_d01	size bin 10.00 to 10.74 nm	#/cm^3
MSP WPS	wps_d02	size bin 10.74 to 11.53 nm	#/cm^3
MSP WPS	wps_d03	size bin 11.53 to 12.39 nm	#/cm^3
MSP WPS	wps_d04	size bin 12.39 to 13.32 nm	#/cm^3
MSP WPS	wps_d05	size bin 13.32 to 14.31 nm	#/cm^3
MSP WPS	wps_d06	size bin 14.31 to 15.38 nm	#/cm^3
MSP WPS	wps_d07	size bin 15.38 to 16.53 nm	#/cm^3

Table E-2. continued.

Instrument Name	Variable Name	Description	Unit
MSP WPS	wps_d08	size bin 16.53 to 17.77 nm	#/cm^3
MSP WPS	wps_d09	size bin 17.77 to 19.11 nm	#/cm^3
MSP WPS	wps_d10	size bin 19.11 to 20.54 nm	#/cm^3
MSP WPS	wps_d11	size bin 20.54 to 22.09 nm	#/cm^3
MSP WPS	wps_d12	size bin 22.09 to 23.77 nm	#/cm^3
MSP WPS	wps_d13	size bin 23.77 to 25.57 nm	#/cm^3
MSP WPS	wps_d14	size bin 25.57 to 27.51 nm	#/cm^3
MSP WPS	wps_d15	size bin 27.51 to 29.62 nm	#/cm^3
MSP WPS	wps_d16	size bin 29.62 to 31.88 nm	#/cm^3
MSP WPS	wps_d17	size bin 31.88 to 34.33 nm	#/cm^3
MSP WPS	wps_d18	size bin 34.33 to 36.98 nm	#/cm^3
MSP WPS	wps_d19	size bin 36.98 to 39.85 nm	#/cm^3
MSP WPS	wps_d20	size bin 39.85 to 42.95 nm	#/cm^3
MSP WPS	wps_d21	size bin 42.95 to 46.31 nm	#/cm^3
MSP WPS	wps_d22	size bin 46.31 to 49.95 nm	#/cm^3
MSP WPS	wps_d23	size bin 49.95 to 53.90 nm	#/cm^3
MSP WPS	wps_d24	size bin 53.90 to 58.18 nm	#/cm^3
MSP WPS	wps_d25	size bin 58.18 to 62.85 nm	#/cm^3
MSP WPS	wps_d26	size bin 62.85 to 67.92 nm	#/cm^3
MSP WPS	wps_d27	size bin 67.92 to 73.45 nm	#/cm^3
MSP WPS	wps_d28	size bin 73.45 to 79.46 nm	#/cm^3
MSP WPS	wps_d29	size bin 79.46 to 86.04 nm	#/cm^3
MSP WPS	wps_d30	size bin 86.04 to 93.24 nm	#/cm^3
MSP WPS	wps_d31	size bin 93.24 to 101.11 nm	#/cm^3
MSP WPS	wps_d32	size bin 101.11 to 109.76 nm	#/cm^3
MSP WPS	wps_d33	size bin 109.76 to 119.27 nm	#/cm^3
MSP WPS	wps_d34	size bin 119.27 to 129.73 nm	#/cm^3
MSP WPS	wps_d35	size bin 129.73 to 141.27 nm	#/cm^3
MSP WPS	wps_d36	size bin 141.27 to 154.04 nm	#/cm^3
MSP WPS	wps_d37	size bin 154.04 to 168.19 nm	#/cm^3
MSP WPS	wps_d38	size bin 168.19 to 183.9 nm	#/cm^3
MSP WPS	wps_d39	size bin 183.9 to 201.42 nm	#/cm^3
MSP WPS	wps_d40	size bin 201.42 to 221 nm	#/cm^3
MSP WPS	wps_d41	size bin 221 to 242.9 nm	#/cm^3
MSP WPS	wps_d42	size bin 242.9 to 267.52 nm	#/cm^3
MSP WPS	wps_d43	size bin 267.52 to 295.23 nm	#/cm^3
MSP WPS	wps_d44	size bin 295.23 to 326.53 nm	#/cm^3
MSP WPS	wps_d45	size bin 326.53 to 361.96 nm	#/cm^3
MSP WPS	wps_d46	size bin 361.96 to 402.17 nm	#/cm^3
MSP WPS	wps_d47	size bin 402.17 to 447.88 nm	#/cm^3
MSP WPS	wps_d48	size bin 447.88 to 500 nm	#/cm^3

Table E-2. continued.

Instrument Name	Variable Name	Description	Unit
MSP WPS	wps_d49	size bin 500 to 550 nm	#/cm^3
MSP WPS	wps_d50	size bin 550 to 600 nm	#/cm^3
MSP WPS	wps_d51	size bin 600 to 700 nm	#/cm^3
MSP WPS	wps_d52	size bin 700 to 800 nm	#/cm^3
MSP WPS	wps_d53	size bin 800 to 1000 nm	#/cm^3
MSP WPS	wps_d54	size bin 1000 to 1200 nm	#/cm^3
MSP WPS	wps_d55	size bin 1200 to 1400 nm	#/cm^3
MSP WPS	wps_d56	size bin 1400 to 1700 nm	#/cm^3
MSP WPS	wps_d57	size bin 1700 to 2100 nm	#/cm^3
MSP WPS	wps_d58	size bin 2100 to 2500 nm	#/cm^3
MSP WPS	wps_d59	size bin 2500 to 3000 nm	#/cm^3
MSP WPS	wps_d60	size bin 3000 to 3500 nm	#/cm^3
MSP WPS	wps_d61	size bin 3500 to 4000 nm	#/cm^3
MSP WPS	wps_d62	size bin 4000 to 5000 nm	#/cm^3
MSP WPS	wps_d63	size bin 5000 to 6000 nm	#/cm^3
MSP WPS	wps_d64	size bin 6000 to 7000 nm	#/cm^3
MSP WPS	wps_d65	size bin 7000 to 8000 nm	#/cm^3
MSP WPS	wps_d66	size bin 8000 to 9000 nm	#/cm^3
MSP WPS	wps_d67	size bin 9000 to 10000 nm	#/cm^3
TSI SMPS_Nano	tsi_d01	diameter midpoint 2.5.0 nm	#/cm^3
TSI SMPS_Nano	tsi_d02	diameter midpoint 2.59 nm	#/cm^3
TSI SMPS_Nano	tsi_d03	diameter midpoint 2.69 nm	#/cm^3
TSI SMPS_Nano	tsi_d04	diameter midpoint 2.79 nm	#/cm^3
TSI SMPS_Nano	tsi_d05	diameter midpoint 2.89 nm	#/cm^3
TSI SMPS_Nano	tsi_d06	diameter midpoint 3.00 nm	#/cm^3
TSI SMPS_Nano	tsi_d07	diameter midpoint 3.11 nm	#/cm^3
TSI SMPS_Nano	tsi_d08	diameter midpoint 3.22 nm	#/cm^3
TSI SMPS_Nano	tsi_d09	diameter midpoint 3.34 nm	#/cm^3
TSI SMPS_Nano	tsi_d10	diameter midpoint 3.46 nm	#/cm^3
TSI SMPS_Nano	tsi_d11	diameter midpoint 3.59 nm	#/cm^3
TSI SMPS_Nano	tsi_d12	diameter midpoint 3.72 nm	#/cm^3
TSI SMPS_Nano	tsi_d13	diameter midpoint 3.85 nm	#/cm^3
TSI SMPS_Nano	tsi_d14	diameter midpoint 4.00 nm	#/cm^3
TSI SMPS_Nano	tsi_d15	diameter midpoint 4.14 nm	#/cm^3
TSI SMPS_Nano	tsi_d16	diameter midpoint 4.29 nm	#/cm^3
TSI SMPS_Nano	tsi_d17	diameter midpoint 4.45 nm	#/cm^3
TSI SMPS_Nano	tsi_d18	diameter midpoint 4.61 nm	#/cm^3
TSI SMPS_Nano	tsi_d19	diameter midpoint 4.78 nm	#/cm^3
TSI SMPS_Nano	tsi_d20	diameter midpoint 4.96 nm	#/cm^3

Table E-2. continued.

Instrument Name	Variable Name	Description	Unit
TSI SMPS_Nano	tsi_d21	diameter midpoint 5.14 nm	#/cm^3
TSI SMPS_Nano	tsi_d22	diameter midpoint 5.33 nm	#/cm^3
TSI SMPS_Nano	tsi_d23	diameter midpoint 5.52 nm	#/cm^3
TSI SMPS_Nano	tsi_d24	diameter midpoint 5.73 nm	#/cm^3
TSI SMPS_Nano	tsi_d25	diameter midpoint 5.94 nm	#/cm^3
TSI SMPS_Nano	tsi_d26	diameter midpoint 6.15 nm	#/cm^3
TSI SMPS_Nano	tsi_d27	diameter midpoint 6.38 nm	#/cm^3
TSI SMPS_Nano	tsi_d28	diameter midpoint 6.61 nm	#/cm^3
TSI SMPS_Nano	tsi_d29	diameter midpoint 6.85 nm	#/cm^3
TSI SMPS_Nano	tsi_d30	diameter midpoint 7.10 nm	#/cm^3
TSI SMPS_Nano	tsi_d31	diameter midpoint 7.37 nm	#/cm^3
TSI SMPS_Nano	tsi_d32	diameter midpoint 7.64 nm	#/cm^3
TSI SMPS_Nano	tsi_d33	diameter midpoint 7.91 nm	#/cm^3
TSI SMPS_Nano	tsi_d34	diameter midpoint 8.20 nm	#/cm^3
TSI SMPS_Nano	tsi_d35	diameter midpoint 8.51 nm	#/cm^3
TSI SMPS_Nano	tsi_d36	diameter midpoint 8.82 nm	#/cm^3
TSI SMPS_Nano	tsi_d37	diameter midpoint 9.14 nm	#/cm^3
TSI SMPS_Nano	tsi_d38	diameter midpoint 9.47 nm	#/cm^3
TSI SMPS_Nano	tsi_d39	diameter midpoint 9.82 nm	#/cm^3
TSI SMPS_Nano	tsi_d40	diameter midpoint 10.2 nm	#/cm^3
TSI SMPS_Nano	tsi_d41	diameter midpoint 10.6 nm	#/cm^3
TSI SMPS_Nano	tsi_d42	diameter midpoint 10.9 nm	#/cm^3
TSI SMPS_Nano	tsi_d43	diameter midpoint 11.3 nm	#/cm^3
TSI SMPS_Nano	tsi_d44	diameter midpoint 11.8 nm	#/cm^3
TSI SMPS_Nano	tsi_d45	diameter midpoint 12.2 nm	#/cm^3
TSI SMPS_Nano	tsi_d46	diameter midpoint 12.6 nm	#/cm^3
TSI SMPS_Nano	tsi_d47	diameter midpoint 13.1 nm	#/cm^3
TSI SMPS_Nano	tsi_d48	diameter midpoint 13.6 nm	#/cm^3
TSI SMPS_Nano	tsi_d49	diameter midpoint 14.1 nm	#/cm^3
TSI SMPS_Nano	tsi_d50	diameter midpoint 14.6 nm	#/cm^3
TSI SMPS_Nano	tsi_d51	diameter midpoint 15.1 nm	#/cm^3
TSI SMPS_Nano	tsi_d52	diameter midpoint 15.7 nm	#/cm^3
TSI SMPS_Nano	tsi_d53	diameter midpoint 16.3 nm	#/cm^3
TSI SMPS_Nano	tsi_d54	diameter midpoint 16.8 nm	#/cm^3
TSI SMPS_Nano	tsi_d55	diameter midpoint 17.5 nm	#/cm^3
TSI SMPS_Nano	tsi_d56	diameter midpoint 18.1 nm	#/cm^3
TSI SMPS_Nano	tsi_d57	diameter midpoint 18.8 nm	#/cm^3
TSI SMPS_Nano	tsi_d58	diameter midpoint 19.5 nm	#/cm^3
TSI SMPS_Nano	tsi_d59	diameter midpoint 20.2 nm	#/cm^3
TSI SMPS_Nano	tsi_d60	diameter midpoint 20.9 nm	#/cm^3
TSI SMPS_Nano	tsi_d61	diameter midpoint 21.7 nm	#/cm^3
TSI SMPS_Nano	tsi_d62	diameter midpoint 22.5 nm	#/cm^3
TSI SMPS_Nano	tsi_d63	diameter midpoint 23.3 nm	#/cm^3

Table E-2. continued.

Instrument Name	Variable Name	Description	Unit
TSI SMPS_Nano	tsi_d64	diameter midpoint 24.1 nm	#/cm^3
TSI SMPS_Nano	tsi_d65	diameter midpoint 25.0 nm	#/cm^3
TSI SMPS_Nano	tsi_d66	diameter midpoint 25.9 nm	#/cm^3
TSI SMPS_Nano	tsi_d67	diameter midpoint 26.9 nm	#/cm^3
TSI SMPS_Nano	tsi_d68	diameter midpoint 27.9 nm	#/cm^3
TSI SMPS_Nano	tsi_d69	diameter midpoint 28.9 nm	#/cm^3
TSI SMPS_Nano	tsi_d70	diameter midpoint 30.0 nm	#/cm^3
TSI SMPS_Nano	tsi_d71	diameter midpoint 31.1 nm	#/cm^3
TSI SMPS_Nano	tsi_d72	diameter midpoint 32.2 nm	#/cm^3
TSI SMPS_Nano	tsi_d73	diameter midpoint 33.4 nm	#/cm^3
TSI SMPS_Nano	tsi_d74	diameter midpoint 34.6 nm	#/cm^3
TSI SMPS_Nano	tsi_d75	diameter midpoint 35.9 nm	#/cm^3
TSI SMPS_Nano	tsi_d76	diameter midpoint 37.2 nm	#/cm^3
TSI SMPS_Nano	tsi_d77	diameter midpoint 38.5 nm	#/cm^3
TSI SMPS_Nano	tsi_d78	diameter midpoint 40.0 nm	#/cm^3
TSI SMPS_Nano	tsi_d79	diameter midpoint 41.4 nm	#/cm^3
TSI SMPS_Nano	tsi_d80	diameter midpoint 42.9 nm	#/cm^3
TSI SMPS_Nano	tsi_d81	diameter midpoint 44.5 nm	#/cm^3
TSI SMPS_Nano	tsi_d82	diameter midpoint 46.1 nm	#/cm^3
TSI SMPS_Nano	tsi_d83	diameter midpoint 47.8 nm	#/cm^3
TSI SMPS_Nano	tsi_d84	diameter midpoint 49.6 nm	#/cm^3
TSI SMPS_Nano	tsi_d85	diameter midpoint 51.4 nm	#/cm^3
TSI SMPS_Nano	tsi_d86	diameter midpoint 53.3 nm	#/cm^3
TSI SMPS_Nano	tsi_d87	diameter midpoint 55.2 nm	#/cm^3
TSI SMPS_Nano	tsi_d88	diameter midpoint 57.3 nm	#/cm^3
TSI SMPS_Nano	tsi_d89	diameter midpoint 59.4 nm	#/cm^3
TSI SMPS_Nano	tsi_d90	diameter midpoint 61.5 nm	#/cm^3
TSI SMPS_Nano	tsi_d91	diameter midpoint 63.8 nm	#/cm^3
TSI SMPS_Nano	tsi_d92	diameter midpoint 66.1 nm	#/cm^3
TSI SMPS_Nano	tsi_d93	diameter midpoint 68.5 nm	#/cm^3
TSI SMPS_Nano	tsi_d94	diameter midpoint 71.0 nm	#/cm^3
TSI SMPS_Nano	tsi_d95	diameter midpoint 73.7 nm	#/cm^3
TSI SMPS_Nano	tsi_d96	diameter midpoint 76.4 nm	#/cm^3
TSI SMPS_Nano	tsi_d97	diameter midpoint 79.1 nm	#/cm^3
Gas			
LiCor	CO2(ppm)	carbon dioxide	ppm
LiCor	H2O(ppt)	water	ppt

n/a not available

Table E-3. Ambient and source field sampling data validation flags.

Validation Flag[a]	Sub Flag	Description
A		Sampler adjustment or maintenance.
	A1	Sampler audit during sample period.
	A2	Sampler cleaned prior to sample period.
	A3	Particle size cut device regreased or replaced prior to sample period.
B		Field Blank.
D		Sample dropped.
	D1	Sample dropped after sampling.
	D2	Filter dropped during unloading.
	D3	Sample dropped before sampling
F		Filter damaged or ripped.
	F1	Filter damaged in the field.
	F2	Filter damaged when removed from holder.
	F3	Filter wrinkled.
	F4	Filter torn due to over-tightened filter holder.
	F5	Teflon membrane separated from support ring.
	F6	Pinholes in filter.
G		Filter deposit damaged.
	G1	Deposit scratched or scraped, causing a thin line in the deposit.
	G2	Deposit smudged, causing a large area of deposit to be displaced.
	G3	Filter returned to lab with deposit side down in PetriSlide.
	G4	Part of deposit appears to have fallen off; particles on inside of PetriSlide.
	G5	Finger touched filter in the field (without gloves).
	G6	Finger touched filter in the lab (with gloves).
H		Filter holder assembly problem.
	H1	Filter misaligned in holder - possible air leak.
	H2	Filter holder loose in sampler - possible air leak.
	H3	Filter holder not tightened sufficiently - possible air leak.
	H4	Filter support grid upside down.
	H5	Two substrates loaded in place of one.
I		Inhomogeneous sample deposit.
	I1	Evidence of impaction - deposit heavier in center of filter.
	I2	Random areas of darker or lighter deposit on filter.
	I3	Light colored deposit with dark specks.
	I4	Non-uniform deposit near edge - possible air leak.
L		Sample loading error.
	L1	Teflon and quartz filters were loaded reversely in SFS.
	L2	$PM_{2.5}$ and PM_{10} filter pack switched.
	L3	Fine and Coarse filters were loaded reversely in dichotomous sampler.

Table E-3. continued.

Validation Flag[a]	Sub Flag	Description
	L4	Filter loaded in wrong port.
M		Sampler malfunction.
N		Foreign substance on sample.
	N1	Insects on deposit, removed before analysis.
	N2	Insects on deposit, not all removed.
	N3	Metallic particles observed on deposit.
	N4	Many particles on deposit much larger than cut point of inlet.
	N5	Fibers or fuzz on filter.
	N6	Oily-looking droplets on filter.
	N7	Shiny substance on filter.
	N8	Particles on back of filter.
	N9	Discoloration on deposit.
O		Sampler operation error.
	O1	Pump was not switched on after changing samples.
	O2	Timer set incorrectly.
	O3	Dichotomous sampler assembled with virtual impactor 180° out of phase; only PM_{10} data reported.
P		Power failure during sampling.
Q		Flow rate error.
	Q1	Initial or final flow rate differed from nominal by > ±10%.
	Q2	Initial or final flow rate differed from nominal by > ±15%.
	Q3	Final flow rate differed from initial by > ±15%.
	Q4	Initial or final flow rate not recorded, used estimated flow rate.
	Q5	Nominal flow rate assumed.
R		Replacement filter used.
	R1	Filter that failed flow rate or QC checks replaced with spare.
	R2	Filter sampling sequence changed from order designated on field data sheet.
S		Sample validity is suspect.
T		Sampling time error.
	T1	Sampling duration error of > ±10%.
	T2	Sample start time error of > ±10% of sample duration.
	T3	Elapsed time meter reading not recorded or recorded incorrectly. Sample duration estimated based on readings from previous or subsequent sample.
	T4	Nominal sample duration assumed.
	T5	Sample ran during prescribed period, plus part of next period.

Table E-3. continued.

Validation Flag[a]	Sub Flag	Description
T6		More than one sample was run to account for the prescribed period.
U		Unusual local particulate sources during sample period.
	U1	Local construction activity.
	U2	Forest fire or slash or field burning.
V		Invalid sample (Void).
W		Wet Sample.
	W1	Deposit spotted from water drops.
	W2	Filter damp when unloaded.
	W3	Filter holder contained water when unloaded.
X		No sample was taken this period, sample run was skipped.

[a] Samples are categorized as valid, suspect, or invalid. Unflagged samples, or samples with any flag except 'S' or 'V' indicate valid results. The 'S' flag indicates samples of suspect validity. The 'V' flag indicates invalid samples. Field data validation flags are all upper case.

Table E-4. Chemical Analysis Data Validation Flags.

Validation Flag[a]	Sub Flag	Description
b		Blank.
	b1	Field/dynamic blank.
	b2	Laboratory blank.
	b3	Distilled-deionized water blank.
	b4	Method blank.
	b5	Extract/solution blank.
	b6	Transport blank.
c		Analysis result reprocessed or recalculated.
	c1	XRF spectrum reprocessed using manually adjusted background.
d		Sample dropped.
f		Filter damaged or ripped.
	f1	Filter damaged, outside of analysis area.
	f2	Filter damaged, within analysis area.
	f3	Filter wrinkled.
	f4	Filter stuck to PetriSlide.
	f5	Teflon membrane separated from support ring.
	f6	Pinholes in filter.
g		Filter deposit damaged.
	g1	Deposit scratched or scraped, causing a thin line in the deposit.
	g2	Deposit smudged, causing a large area of deposit to be displaced.
	g3	Filter deposit side down in PetriSlide.
	g4	Part of deposit appears to have fallen off; particles on inside of PetriSlide.
	g5	Ungloved finger touched filter.
	g6	Gloved finger touched filter.
h		Filter holder assembly problem.
	h1	Deposit not centered.
	h2	Sampled on wrong side of filter.
	h4	Filter support grid upside down- deposit has widely spaced stripes or grid pattern.
	h5	Two filters in PetriSlide- analyzed separately.
i		Inhomogeneous sample deposit.
	i1	Evidence of impaction - deposit heavier in center of filter.
	i2	Random areas of darker or lighter deposit on filter.
	i3	Light colored deposit with dark specks.
	i4	Non-uniform deposit near edge - possible air leak.
m		Analysis results affected by matrix effect.

Table E-4. continued.

Validation Flag[a]	Sub Flag	Description
	m1	Organic/elemental carbon split undetermined due to an apparent color change of non-carbon particles during analysis; all measured carbon reported as organic.
	m2	Non-white carbon punch after carbon analysis, indicative of mineral particles in deposit.
	m3	A non-typical, but valid, laser response was observed during TOR analysis. This phenomena may result in increased uncertainty of the organic/elemental carbon split. Total carbon measurements are likely unaffected.
	m4	FID drift quality control failure
n		Foreign substance on sample.
	n1	Insects on deposit, removed before analysis.
	n2	Insects on deposit, not all removed.
	n3	Metallic particles observed on deposit.
	n4	Many particles on deposit much larger than cut point of inlet.
	n5	Fibers or fuzz on filter.
	n6	Oily-looking droplets on filter.
	n7	Shiny substance on filter.
	n8	Particles on back of filter.
	n9	Discoloration on deposit.
q		Standard.
	q1	Quality control standard.
	q2	Externally prepared quality control standard.
	q3	Second type of externally prepared quality control standard.
	q4	Calibration standard.
r		Replicate analysis.
	r1	First replicate analysis on the same analyzer.
	r2	Second replicate analysis on the same analyzer.
	r3	Third replicate analysis on the same analyzer.
	r4	Sample re-analysis.
	r5	Replicate on different analyzer.
	r6	Sample re-extraction and re-analysis.
	r7	Sample re-analyzed with same result, original value used.
s		Suspect analysis result.
v		Invalid (void) analysis result.
	v1	Quality control standard check exceeded ± 10% of specified concentration range.
	v2	Replicate analysis failed acceptable limit specified in SOP.
	v3	Potential contamination.
	v4	Concentration out of expected range.

Table E-4. continued.

Validation Flag[a]	Sub Flag	Description
w		Wet Sample.
	w1	Deposit spotted from water drops.
y		Data normalized
	y1	XRF data normalized to a sulfate/sulfur ratio of three
	y2	Each species reported as a percentage of the measured species sum

[a] Analysis results are categorized as valid, suspect, or invalid. Unflagged samples, or samples with any flag except 's' or 'v' indicate valid results. The 's' flag indicates results of suspect validity. The 'v' flag indicates invalid analysis results. Chemical analysis data validation flags are all lower case.

Table E-5. Summary of data files.

Study	Instrument	File type	Location	CD directory <path\file>
n/a	<this file>	XLS	CD	\Readme.xls
n/a	<list of instruments table>	XLS	CD	\InstrumentList.xls
Summer	Dual wavelength aethalometer	XLS	CD or CCAQS database*	\continuous\SummerIntensiveFresno\absorption\aeth2_5min.xls
Summer	Seven-color aethalometer	XLS	CD or CCAQS database*	\continuous\SummerIntensiveFresno\absorption\aeth7_5min.xls
Summer	Multi-Angle Absorption Photometer	XLS	CD or CCAQS database*	\continuous\SummerIntensiveFresno\absorption\maap_1min.xls
Summer	Photoacoustic 532nm	XLS	CD	\continuous\SummerIntensiveFresno\absorption\pa532nm_5min.xls
Summer	Photoacoustic 1047nm	XLS	CD	\continuous\SummerIntensiveFresno\absorption\pa1047nm_5min.xls
Summer	Particle soot absorption photometer	XLS	CD	\continuous\SummerIntensiveFresno\absorption\psap_5min.xls
Summer	PAH EcoChem PAS_2000	XLS	CD or CCAQS database*	\continuous\SummerIntensiveFresno\carbon\pah_5min.xls
Summer	Sunset	XLS	CD or CCAQS database*	\continuous\SummerIntensiveFresno\carbon\sunset_60min.xls
Summer	R&P 8400N1	XLS	CD or CCAQS database*	\continuous\SummerIntensiveFresno\ion\rp8400n1_10min.xls
Summer	R&P 8400N2	XLS	CD or CCAQS database*	\continuous\SummerIntensiveFresno\ion\rp8400n2_10min.xls
Summer	R&P 8400S	XLS	CD or CCAQS database*	\continuous\SummerIntensiveFresno\ion\rp8400s_10min.xls
Summer	BAM-1020 PM10	XLS	CD or CCAQS database*	\continuous\SummerIntensiveFresno\mass\bam10_60min.xls
Summer	BAM-1020 PM2.5	XLS	CD or CCAQS database*	\continuous\SummerIntensiveFresno\mass\bam25_60min.xls
Summer	Kimoto BAM	XLS	CD	\continuous\SummerIntensiveFresno\mass\kimotobam_60min.xls
Summer	TEOM 1400a PM10	XLS	CD or CCAQS database*	\continuous\SummerIntensiveFresno\mass\teom10_5min.xls
Summer	TEOM 1400a PM2.5	XLS	CD or CCAQS database*	\continuous\SummerIntensiveFresno\mass\teom25_5min.xls

Table E-5. continued.

Study	Instrument	File type	Location	CD directory <path\file>
Summer	EcoTech nephelometer TSP	XLS	CD	\continuous\SummerIntensiveFresno\scatter\ecotsp_5min.xls
Summer	NGN2 nephelometer	XLS	CD or CCAQS database*	\continuous\SummerIntensiveFresno\scatter\ngn2_1min.xls
Summer	Radiance 903 PM2.5 nephelometer	XLS	CD or CCAQS database*	\continuous\SummerIntensiveFresno\scatter\rad25_1min.xls
Summer	Radiance 903 TSP Nephelometer	XLS	CD or CCAQS database*	\continuous\SummerIntensiveFresno\scatter\radtsp_1min.xls
Summer	TSI nephelometer PM2.5	XLS	CD	\continuous\SummerIntensiveFresno\scatter\tsi25_5min.xls
Summer	Climet Spectro.3	XLS	CD or CCAQS database*	\continuous\SummerIntensiveFresno\sizedistn\climet_5min.xls
Summer	Grimm SMPS	XLS	CD	\continuous\SummerIntensiveFresno\sizedistn\grimm_3.83min.xls
Summer	Lasair 1003	XLS	CD or CCAQS database*	\continuous\SummerIntensiveFresno\sizedistn\lasair_5min.xls
Summer	TSI SMPS_LONG	XLS	CD or CCAQS database*	\continuous\SummerIntensiveFresno\sizedistn\tsilong_5min.xls
Summer	TSI SMPS_Nano	XLS	CD or CCAQS database*	\continuous\SummerIntensiveFresno\sizedistn\tsinano_5min.xls
Summer	MSP WPS	XLS	CD	\continuous\SummerIntensiveFresno\sizedistn\wps_2.65min.xls
Winter	Dual wavelength aethalometer	XLS	CD or CCAQS database*	\continuous\WinterIntensiveFresno\absorption\aeth2_5min.xls
Winter	Seven-color aethalometer	XLS	CD or CCAQS database*	\continuous\WinterIntensiveFresno\absorption\aeth7_5min.xls
Winter	Multi-Angle Absorption Photometer	XLS	CD or CCAQS database*	\continuous\WinterIntensiveFresno\absorption\maap_1min.xls
Winter	Photoacoustic 1047nm	XLS	CD or CCAQS database*	\continuous\WinterIntensiveFresno\absorption\pa1047nm_5min.xls

Table E-5. continued.

Study	Instrument	File type	Location	CD directory <path\file>
Winter	R&P 5400	XLS	CD or CCAQS database*	\continuous\WinterIntensiveFresno\carbon\rp5400_60min.xls
Winter	Sunset	XLS	CD or CCAQS database*	\continuous\WinterIntensiveFresno\carbon\sunset_60min.xls
Winter	Dionex	XLS	CD	\continuous\WinterIntensiveFresno\ion\dionex_60min.xls
Winter	R&P 8400N1	XLS	CD or CCAQS database*	\continuous\WinterIntensiveFresno\ion\rp8400n1_10min.xls
Winter	R&P 8400N2	XLS	CD or CCAQS database*	\continuous\WinterIntensiveFresno\ion\rp8400n2_10min.xls
Winter	R&P 8400S	XLS	CD or CCAQS database*	\continuous\WinterIntensiveFresno\ion\rp8400s_10min.xls
Winter	BAM-1020	XLS	CD or CCAQS database*	\continuous\WinterIntensiveFresno\mass\bam25_60min.xls
Winter	Differential TEOM PM2.5	XLS	CD	\continuous\WinterIntensiveFresno\mass\diffteom25_60min.xls
Winter	FDMS TEOM PM2.5	XLS	CD	\continuous\WinterIntensiveFresno\mass\fdmsteom25_60min.xls
Winter	Grimm PM2.5	XLS	CD	\continuous\WinterIntensiveFresno\mass\grim25_60min.xls
Winter	Grimm PM2.5 heater	XLS	CD	\continuous\WinterIntensiveFresno\mass\grimm25heat_60min.xls
Winter	TEOM 1400a PM2.5	XLS	CD	\continuous\WinterIntensiveFresno\mass\teom25_5min.xls
Winter	30°C TEOM PM2.5	XLS	CD	\continuous\WinterIntensiveFresno\mass\teom25_30c_60min.xls
Winter	NGN2 nephelometer (1min)	XLS	CD or CCAQS database*	\continuous\WinterIntensiveFresno\scatter\ngn2_1min.xls
Winter	NGN2 nephelometer (5min)	XLS	CD or CCAQS database*	\continuous\WinterIntensiveFresno\scatter\ngn2_5min.xls
Winter	Radiance 903 PM2.5 nephelometer	XLS	CD or CCAQS database*	\continuous\WinterIntensiveFresno\scatter\rad25_1min.xls
Winter	Radiance 903 TSP Nephelometer	XLS	CD or CCAQS database*	\continuous\WinterIntensiveFresno\scatter\radtsp_1min.xls

Table E-5. continued.

Study	Instrument	File type	Location	CD directory <path\file>
Winter	Climet Spectro.3	XLS	CD or CCAQS database*	\continuous\WinterIntensiveFresno\sizedistn\climet_5min.xls
Winter	Lasair 1003	XLS	CD or CCAQS database*	\continuous\WinterIntensiveFresno\sizedistn\lasair_5min.xls
Winter	TSI SMPS_LONG	XLS	CD or CCAQS database*	\continuous\WinterIntensiveFresno\sizedistn\tsilong_5min.xls
Winter	TSI SMPS_Nano	XLS	CD or CCAQS database*	\continuous\WinterIntensiveFresno\sizedistn\tsinano_5min.xls
Source-Diesel	Seven-color aethalometer	XLS	CD	\continuous\SourceCharacterizationLab\diesel\aeth7_2min.xls
Source-Diesel	DRI dilution/residence chamber datalogger	XLS	CD	\continuous\SourceCharacterizationLab\diesel\datalogger_1min.xls
Source-Diesel	Grimm SMPS	XLS	CD	\continuous\SourceCharacterizationLab\diesel\grimm_3.83min.xls
Source-Diesel	MSP WPS	XLS	CD	\continuous\SourceCharacterizationLab\diesel\msp_2.5min.xls
Source-Diesel	Photoacoustic 1047 nm	XLS	CD	\continuous\SourceCharacterizationLab\diesel\pa1047nm_1sec.xls
Source-Diesel	PAH EcoChem PAS_2000	XLS	CD	\continuous\SourceCharacterizationLab\diesel\pah_1min.xls
Source-Diesel	Dust Trak	XLS	CD	\continuous\SourceCharacterizationLab\diesel\dusttrak_1min.xls
Source-Diesel	TSI SMPS_Nano	XLS	CD	\continuous\SourceCharacterizationLab\diesel\tsinano_2.5min.xls
Source-Acetylene	Seven-color aethalometer	XLS	CD	\continuous\SourceCharacterizationLab\acetylene\aeth7_2min.xls
Source-Acetylene	DRI dilution/residence chamber datalogger	XLS	CD	\continuous\SourceCharacterizationLab\acetylene\datalogger_1min.xls
Source-Acetylene	Grimm SMPS	XLS	CD	\continuous\SourceCharacterizationLab\acetylene\grimm_3.83min.xls
Source-Acetylene	Photoacoustic 1047nm	XLS	CD	\continuous\SourceCharacterizationLab\acetylene\pa1047nm_1sec.xls
Source-Acetylene	PAH EcoChem PAS_2000	XLS	CD	\continuous\SourceCharacterizationLab\acetylene\pah_1min.xls
Source-Acetylene	Dust Trak	XLS	CD	\continuous\SourceCharacterizationLab\acetylene\dusttrak_1min.xls
Source-Acetylene	TSI SMPS_Nano	XLS	CD	\continuous\SourceCharacterizationLab\acetylene\tsinano_2.5min.xls

Table E-5. continued.

Study	Instrument	File type	Location	CD directory <path\file>
Source-Electric Arc	Seven-color aethalometer	XLS	CD	\continuous\SourceCharacterizationLab\palas\aeth7_2min.xls
Source-Electric Arc	DRI dilution/residence chamber datalogger	XLS	CD	\continuous\SourceCharacterizationLab\palas\datalogger_1min.xls
Source-Electric Arc	Grimm SMPS	XLS	CD	\continuous\SourceCharacterizationLab\palas\grimm_3.83min.xls
Source-Electric Arc	MSP WPS	XLS	CD	\continuous\SourceCharacterizationLab\palas\msp_2.5min.xls
Source-Electric Arc	Photoacoustic 1047 nm	XLS	CD	\continuous\SourceCharacterizationLab\palas\pa1047nm_1sec.xls
Source-Electric Arc	PAH EcoChem PAS_2000	XLS	CD	\continuous\SourceCharacterizationLab\palas\pah_1min.xls
Source-Electric Arc	Dust Trak	XLS	CD	\continuous\SourceCharacterizationLab\palas\dusttrak_1min.xls
Source-Electric Arc	TSI SMPS_Nano	XLS	CD	\continuous\SourceCharacterizationLab\palas\tsinano_2.5min.xls
Source-Wood Smoke	Seven-color aethalometer	XLS	CD	\continuous\SourceCharacterizationLab\woodsmoke\aeth7_2min.xls
Source-Wood Smoke	DRI dilution/residence chamber datalogger	XLS	CD	\continuous\SourceCharacterizationLab\woodsmoke\datalogger_1min.xls
Source-Wood Smoke	Grimm SMPS	XLS	CD	\continuous\SourceCharacterizationLab\woodsmoke\grimm_3.83min.xls
Source-Wood Smoke	LiCor	XLS	CD	\continuous\SourceCharacterizationLab\woodsmoke\licor_1sec.xls
Source-Wood Smoke	MSP WPS	XLS	CD	\continuous\SourceCharacterizationLab\woodsmoke\msp_2.5min.xls
Source-Wood Smoke	Photoacoustic 1047nm	XLS	CD	\continuous\SourceCharacterizationLab\woodsmoke\pa1047nm_1sec.xls
Source- Wood Smoke	PAH EcoChem PAS_2000	XLS	CD	\continuous\SourceCharacterizationLab\woodsmoke\pah_1min.xls
Source-Wood Smoke	Dust Trak	XLS	CD	\continuous\SourceCharacterizationLab\woodsmoke\dusttrak_1min.xls

Table E-5. continued.

Study	Instrument	File type	Location	CD directory <path\file>
Source-Wood Smoke	TSI SMPS_Nano	XLS	CD	\continuous\SourceCharacterizationLab\woodsmoke\tsinano_2.5min.xls
Source-Carbon Black	Seven-color aethalometer	XLS	CD	\continuous\SourceCharacterizationLab\carbonblack\aeth7_2min.xls
Source-Carbon Black	DRI dilution/residence chamber datalogger	XLS	CD	\continuous\SourceCharacterizationLab\carbonblack\datalogger_1min.xls
Source-Carbon Black	Grimm SMPS	XLS	CD	\continuous\SourceCharacterizationLab\carbonblack\grimm_3.83min.xls
Source-Carbon Black	MSP WPS	XLS	CD	\continuous\SourceCharacterizationLab\carbonblack\msp_2.5min.xls
Source-Carbon Black	Photoacoustic 1047nm	XLS	CD	\continuous\SourceCharacterizationLab\carbonblack\pa1047nm_1sec.xls
Source-Carbon Black	PAH EcoChem PAS_2000	XLS	CD	\continuous\SourceCharacterizationLab\carbonblack\pah_1min.xls
Source-Carbon Black	Dust Trak	XLS	CD	\continuous\SourceCharacterizationLab\carbonblack\dusttrak_1min.xls
Source-Carbon Black	TSI SMPS_Nano	XLS	CD	\continuous\SourceCharacterizationLab\carbonblack\tsinano_2.5min.xls
Source-Blanks	Seven-color aethalometer	XLS	CD	\continuous\SourceCharacterizationLab\blanks\aeth7_2min.xls
Source-Blanks	DRI dilution/residence chamber datalogger	XLS	CD	\continuous\SourceCharacterizationLab\blanks\datalogger_1min.xls
Source-Blanks	Grimm SMPS	XLS	CD	\continuous\SourceCharacterizationLab\blanks\grimm_3.83min.xls
Source-Blanks	MSP WPS	XLS	CD	\continuous\SourceCharacterizationLab\blanks\msp_2.5min.xls
Source-Blanks	Photoacoustic 1047nm	XLS	CD	\continuous\SourceCharacterizationLab\blanks\pa1047nm_1sec.xls
Source-Blanks	PAH EcoChem PAS_2000	XLS	CD	\continuous\SourceCharacterizationLab\blanks\pah_1min.xls
Source-Blanks	Dust Trak	XLS	CD	\continuous\SourceCharacterizationLab\blanks\dusttrak_1min.xls

Table E-5. continued.

Study	Instrument	File type	Location	CD directory <path\file>
Source-Blanks	TSI SMPS_Nano	XLS	CD	\continuous\SourceCharacterizationLab\blanks\tsinano_2.5min.xls
Summer	Teflon and quartz filter analysis	XLS	CD	\filter\SummerIntensiveFresno\Summer_IOPs.xls
Winter	PC-BOSS	XLS	CD	\filter\WinterIntensiveFresno\pcboss.xls
Winter	Teflon and quartz filter analysis	XLS	CD	\filter\WinterIntensiveFresno\Winter_IOPs.xls
Source	Teflon and quartz filter analysis	XLS	CD	\filter\SourceCharacterizationLab\SourceSamplesFilterAnalysis.xls

* CCAQS: Central California Air Quality Studies database

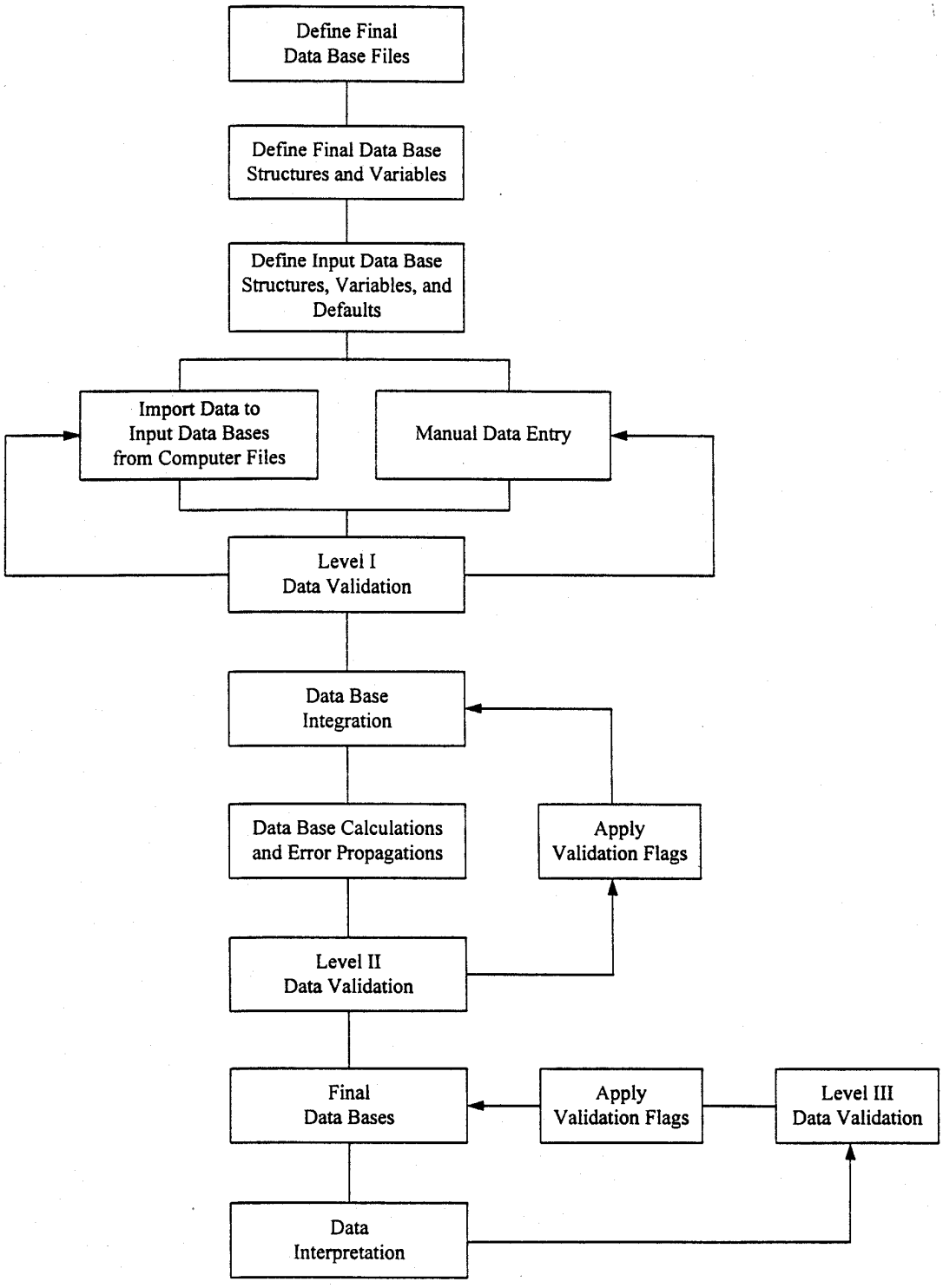

Figure E-1. Flow diagram of the database management system

Figure E-2. Flow diagram of the data files contained on the CD where the number in parenthesis is the number of Excel files.

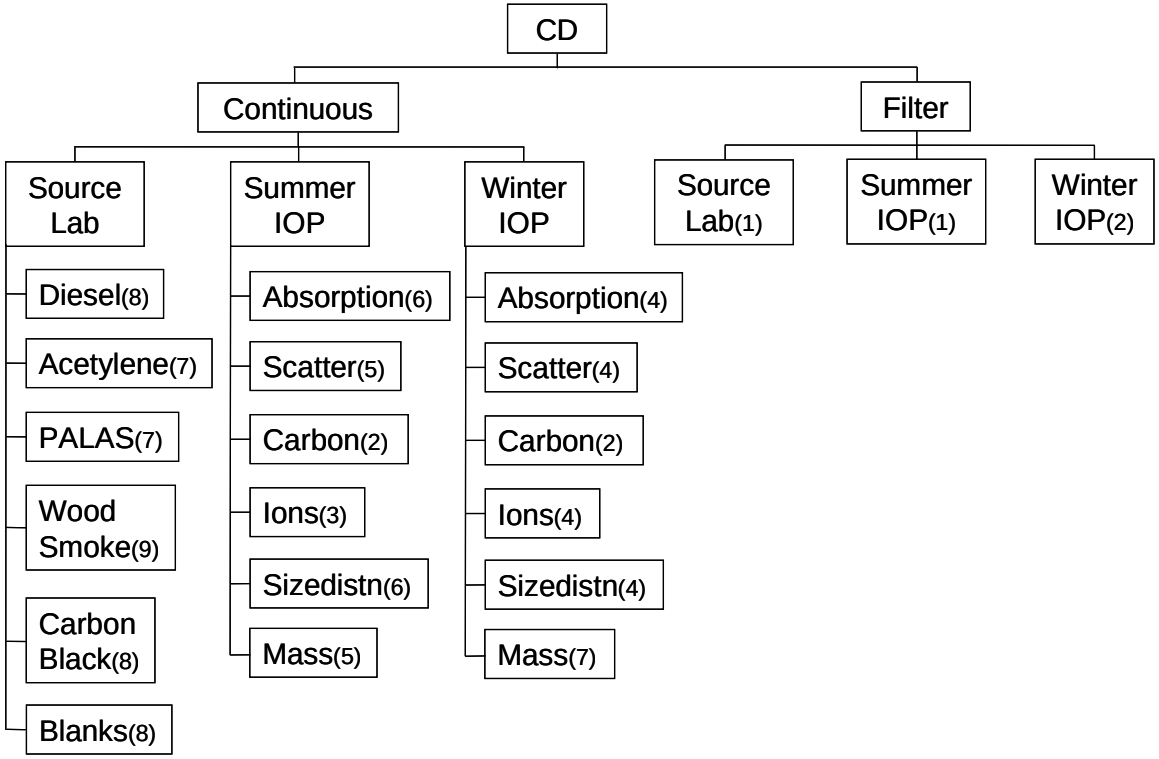

Climate Change – Characterization of Black Carbon and Organic Carbon Air Pollution Emissions and Evaluation of Measurement Methods

Phase I: Method Intercomparison
Volume II: Quality Assurance Project Plan (QAPP)

DRI Contract Number: 04-307

Submitted to:

Nehzat Motallebi, Ph.D.

California Air Resources Board
Research Division
1001 I Street
Sacramento, CA 95812

Prepared for:
The California Air Resources Board and the California Environmental Protection Agency

By:

Richard J. Tropp, Ph.D.
Judith C. Chow, Sc.D.
John G. Watson, Ph.D.
Prakash Doraiswamy, Ph.D.
David A. Sodeman, Ph.D.

Desert Research Institute
Nevada System of Higher Education
2215 Raggio Parkway
Reno, NV 89512

Kochy K. Fung, Ph.D.

Atmoslytic, Inc.
24801 Alexandra Ct.
Calabasas, CA 91302

7/11/2006

TABLE OF CONTENTS

LIST OF FIGURES

Number Page

LIST OF TABLES

1. DISTRIBUTION

A hardcopy of this QAPP has been distributed to the individuals listed in Table 1-1. The document is also available on the Desert Research Institute (DRI) LAN for other interested parties within DRI. An electronic copy will be distributed to the California Air Resources Board (ARB). The ARB Project Coordinator and the DRI Project Quality Assurance (QA) Officer are responsible for distributing any additional hardcopies of this QAPP to other individuals within ARB, local programs, or other contractors.

Table 1-1. Distribution List for DRI Team.

Name	Position	Location	E-Mail
Judith Chow	Principal Investigator (PI) and Director of the Environmental Analysis Facility (EAF)	Northern Nevada Science Center (NNSC) – Reno	judy.chow@dri.edu
John Watson	Co-PI and Director of Source Characterization Lab	NNSC – Reno	john.watson@dri.edu
Richard Tropp	QA Manager	NNSC – Reno	ricky.tropp@dri.edu
Prakash Doraiswamy	Source Testing Coordinator	NNSC – Reno	prakash.doraiswamy@dri.edu
Steven Ho	Carbon Laboratory Testing Coordinator	NNSC – Reno	steven.ho@dri.edu
Antony Chen	Data Analyst	NNSC – Reno	lung-wen.chen@dri.edu
David Sodeman	Source Testing Specialist	NNSC – Reno	david.sodeman@dri.edu

2. PROJECT/TASK ORGANIZATION

2.1 Organizational Responsibilities

The project organization is shown in Figure 2-1, which illustrates the overall organizational structure for the DRI team for this project. Division of responsibilities among the participating organizations or units is as follows:

2.1.1 California Air Resources Board

- Provides technical guidance, overall management, and funding.
- Reviews and approves deliverables.
- Provides oversight of project QA activities.
- Provides technical oversight of work of contractor DRI.
- Interacts with DRI personnel to resolve questions or problems.
- Processes invoices and pays for services rendered in a timely fashion.

2.1.2 Contractor - DRI

- Provides overall management of contractor work.
- Prepares and provides deliverables such as the QAPP, periodic progress reports, data reports, project reports, periodic invoices, QA reports, etc.
- Submits deliverables to the ARB for review and approval.
- Provides source sampling and characterization, field sampling and monitoring, and laboratory analysis services for project.
- Provides data entry, processing, management, and storage of filter and sampler data.
- Provides the results of literature reviews and data assessments to ARB.
- Develops database to process, validate, and store project data.
- Purchases, tests, and maintains laboratory analytical equipment for the analysis of samples collected for the project.
- Performs scheduled QA/QC checks on sampling, monitoring, and analytical equipment.
- Maintains documentation for laboratory and project activities.
- Participates in audits or reviews conducted by an independent laboratory or by the sponsor

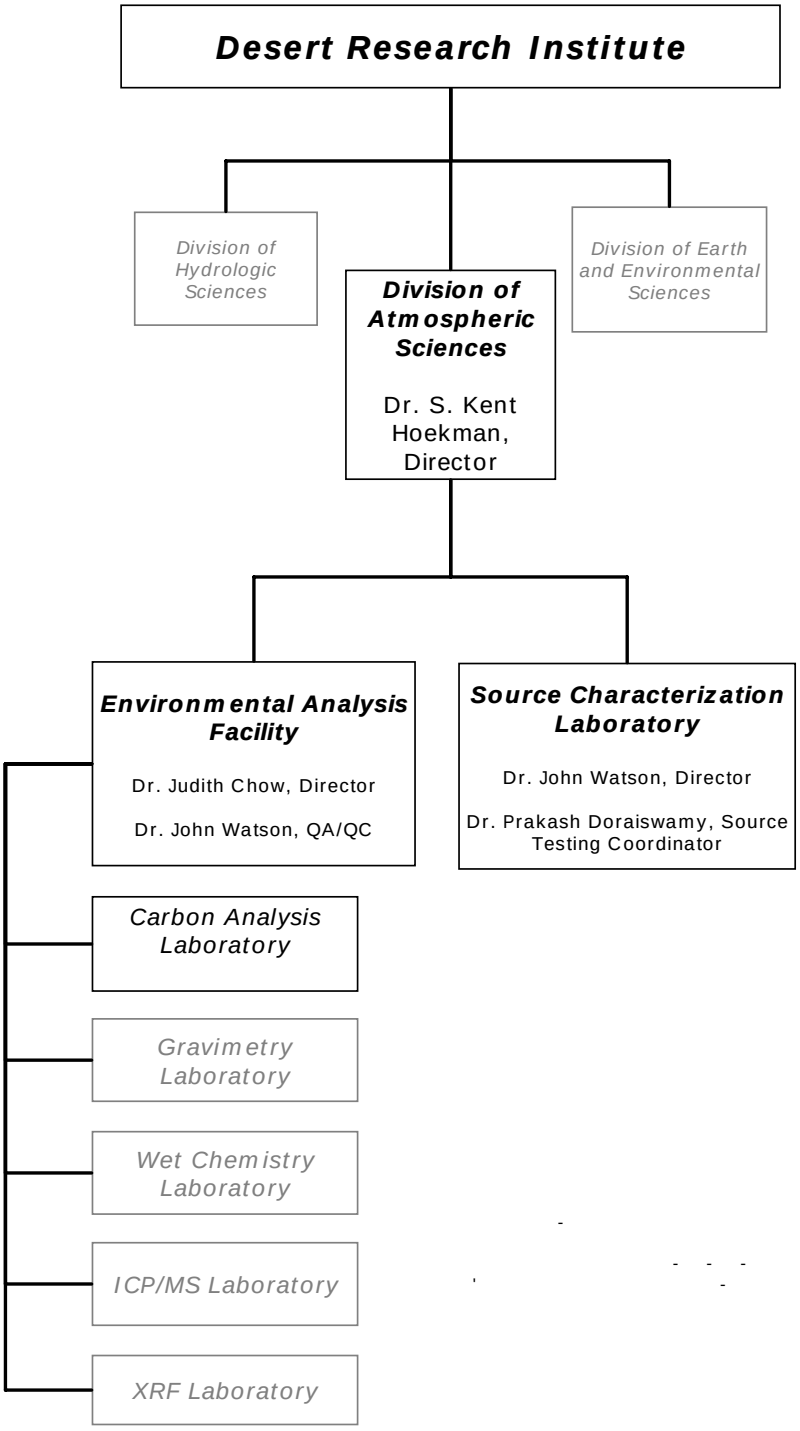

Figure 2-1. Overview of DRI Project Organization.

2.2 Individual Roles and Responsibilities

Key persons and their project responsibilities are given in Table 2-1. Table 2-2 gives the qualifications and experience of key DRI personnel.

2.2.1 Key ARB Personnel

2.2.1.a ARB Project Manager

Dr. Nehzat Motallebi

The responsibilities of the ARB Project Coordinator are to:

- Provide technical guidance, overall management, and funding.
- Review and approves deliverables such as the QA Project Plan, progress reports, project reports, and QA reports.
- Provide oversight of work of contractor, DRI.
- Interact with the DRI Principal Investigator to ensure successful completion of project through conference calls and e-mail communications.

2.3 Key DRI Project Personnel

2.3.1.a Dr. Judith Chow

DRI PI and EAF Director

2.3.1.b Dr. John Watson

DRI Co-PI and Source Characterization Laboratory Director

Dr. Chow and Dr. Watson's responsibilities are to:

- Provide overall oversight of DRI project work and ensures that sufficient DRI resources are available to guarantee project success
- Provide ongoing oversight of laboratory operations, logistical support, documentation, and reporting
- Provide logistical and communications support between the CARB project coordinator and DRI personnel
- Provide ongoing review, assessment, and distribution of project data and reports
- Review and approves project deliverables such as the QAPP and reports

- Review all field and laboratory data for correctness and assesses whether QA objectives are being met
- Ensure that any necessary corrective actions are implemented
- Review all reports, data analyses, and other deliverables for correctness and format
- Direct and provide oversight of the EAF and Source Characterization Laboratory, respectively

2.3.1.c Dr. Richard Tropp

DRI QA Manager

Dr. Tropp's responsibilities are to:

- Provide institutional oversight of the quality of EAF and Source Characterization Lab and project data
- Review and approves quality-related documents such as the QAPP and the Standard Operating Procedures (SOPs)
- Provide senior technical review and advice on project data, operations, and deliverables

2.3.1.d Dr. Kochy Fung

External QA Auditor

Dr. Fung's responsibilities are to:

- Provide periodic technical assessments, performance evaluations, and troubleshooting of field and laboratory instrumentation and measurements
- Provide review of quality-related documents such as the QAPP and SOPs and deliverables

2.3.1.e Dr. Prakash Doraiswamy

DRI Source Testing Coordinator

Dr. Doraiswamy's responsibilities are to:

- Provide day-to-day oversight of project source-testing operations and coordination
- Ensure that project source-testing data reviews and data validation are performed on time
- Assist in preparing the QAPP, progress reports, data reports, and project reports

2.3.1.f Dr. Steven Ho

DRI Carbon Laboratory Testing Coordinator

Dr. Ho's responsibilities are to:

- Provide day-to-day oversight of project carbon analysis laboratory testing operations and coordination
- Ensure that project laboratory data reviews and Level II data validation are performed on time
- Assist in preparing the QAPP, progress reports, data reports, and project reports
- Oversee the procurement of laboratory supplies

Table 2-1. Key DRI Project Personnel.

Position	Name/Title/Unit	Address	Phone/Fax/E-mail
Principal Investigator (PI) and EAF Director	Judith Chow	Desert Research Institute - DAS 2215 Raggio Parkway Reno, NV 89512	775-674-7050 775-674-7009 judy.chow@dri.edu
Co-PI and Source Characterization Lab Director	John Watson	Desert Research Institute - DAS 2215 Raggio Parkway Reno, NV 89512	775-674-7046 775-674-7009 john.watson@dri.edu
DRI QA Manager	Richard Tropp	Desert Research Institute - DAS 2215 Raggio Parkway Reno, NV 89512	775-674-7094 775-674-7009 ricky.tropp@dri.edu
Source Testing Coordinator	Prakash Doraiswamy	Desert Research Institute - DAS 2215 Raggio Parkway Reno, NV 89512	775-674-7097 775-674-7009 prakash.doraiswamy@dri.edu
Carbon Laboratory Testing Coordinator	Steven Ho	Desert Research Institute - DAS 2215 Raggio Parkway Reno, NV 89512	775-674-7172 775-674-7009 steven.ho@dri.edu
Source Testing Specialist	David Sodeman	Desert Research Institute - DAS 2215 Raggio Parkway Reno, NV 89512	775-674-7078 775-674-7009 david.sodeman@dri.edu
Data Analyst	Antony Chen	Desert Research Institute - DAS 2215 Raggio Parkway Reno, NV 89512	775-674-7028 775-674-7009 lung-wen.chen@dri.edu
External QA Auditor	Kochy Fung	Atmoslytic, Inc. 24801 Alexandra Ct. Calabasas, CA 91302	818-591-8168 818-222-9533 kochy@sbcglobal.net

Table 2-2. Qualifications and Experience of Key DRI Project Personnel.

Name and Title	Project Role	Highest Degree	Years of Experience	Relevant Experience/Projects
Judith C. Chow Research Professor and Director of DRI's Environmental Analysis Facility	Principal Investigator	Sc.D., Environmental Sciences. Harvard University, 1985	28	Expert in aerosol measurements, data validation, and data analysis. Director of DRI's Environmental Analysis Facility since 1985. National Research Council (NRC) Review Committee for $PM_{2.5}$; NRC Board on Environmental Sciences and Toxicology; co-author of U.S. EPA Guidance Documents for Chemical Speciation and Continuous Monitoring; and PI or co-PI for over 100 $PM_{2.5}$ and PM_{10} sampling and analysis studies.
John G. Watson Research Professor and Director of DRI's Source Characterization Laboratory	Co-Principal Investigator	Ph.D., Environmental Sciences. Oregon Graduate Institute, 1979	32	Expert in designing and conducting integrated aerosol studies. Author of the Air and Waste Management Association's Critical Review on "Visibility: Science and Regulation," Chemical Mass Balance software, and validation protocols. PI or Co-PI for over 100 ambient and source characterization studies.
Richard J. Tropp Associate Research Professor	Quality Assurance Manager	Ph.D., Physics. University of Texas at Austin, 1979	27	Expert on $PM_{2.5}$ regulation and measurements. PI for $PM_{2.5}$ FRM and chemical speciation for TX, carbon analysis support for EPA $PM_{2.5}$ chemical speciation program, and QA manager for eastern fine particle and visibility monitoring network.
Prakash Doraiswamy Post-Doctoral Research Associate	Source Testing Coordinator	Ph.D., Civil Engineering. University of Tennessee, Knoxville, 2004	5.5	Expert in dispersion modeling and emission inventory development and processing. Responsible for carbon source characterization lab that generates combustion aerosol for carbon speciation. Performs carbon data validation and participates in several relevant carbon projects.
Steven Ho Post-Doctoral Research Associate	Carbon Laboratory Testing Coordinator	Ph.D., Chemistry. Hong Kong UST, 2004	8	Expert in thermal desorption organic speciation. Maintains ten DRI Model 2001 and five DRI/OGC carbon analyzers. Performs carbon calibrations and provides training on the operation of carbon analyzers.
David Sodeman Post-Doctoral Research Associate	Source Testing Specialist	Ph.D., Chemistry. University of California at San Diego, 2004	6	Expert in dilution source testing, combustion processes, aerosol generation, nano- and ultrafine particle measurements, and single particle time-of-flight mass spectrometry. Performs carbon data validation and participates in several source characterization studies.
L.-W. Antony Chen Assistant Research Professor	Optical Modeling Specialist	Ph.D., Chemical Physics. University of Maryland, College Park, 2002	6	Expert in various carbon evolution measurements. Worked on experimental and theoretical analyses of pyrolyzed carbon. Investigated effects of different detectors on carbon measurements.
Kochy K. Fung Director, Atmoslytic Inc., Calabasas, CA	External AQ Auditor	Ph.D., Pharmaceutical Chemistry. University of Southern California, 1978	35	Expert in carbon measurement and method development. Developed the thermal manganese oxidation (TMO) method for speciation of OC and EC. Familiar with IMPROVE, STN, and other thermal evolution protocols. Has participated in over 100 aerosol studies.

3. PROBLEM DEFINITION/BACKGROUND

With the signing of AB 1493 in July 2002, California became the first state in the nation to begin a process of reducing greenhouse gas emissions to ameliorate climate change. AB 1493 requires the California Air Resources Board (ARB) to develop carbon pollution (i.e., greenhouse gas) standards for on-road vehicle exhaust for model year 2009 and beyond. California's specific interests in global warming include potential effects on agricultural productivity, wildfire frequency and intensity, coastal flooding, energy consumption, and water stored in the Sierra Nevada snow pack. The State's general interests include the desire of its citizens to protect and enhance the global environment while maintaining a high quality of life.

Particulate matter (PM) emissions, which often accompany emissions of greenhouse gases (GHG) such as carbon dioxide (CO_2), affect the Earth's climate, human health, visibility, surface soiling, and crop productivity. Direct and indirect radiation forcing by atmospheric PM poses the largest uncertainty in current predictions of climate change (Twomey, 1977, Twomey et al., 1984, Charlson et al., 1992, Penner et al., 1994, Chuang et al., 1997, IPCC, 2001). The global direct radiative effect of light-scattering aerosols containing sulfates and nitrates is on the order of -1 W/m^2 (IPCC, 2001), resulting in global cooling. However, light-absorbing aerosols, mainly black carbon, or "soot," from fossil fuel and biomass combustion, produce a warm forcing of +0.2 to +1 W/m^2 (Lloyd and Cackette, 2001, IPCC, 2001).

Black carbon (BC) aerosols contribute to warm forcing mainly by heating the air around them as they re-radiate energy from the absorbed light. BC also enhances evaporation of tropical cumulus (Ackerman et al., 2000, Jacobson, 2002). Deposited BC may change the planetary albedo (reflectivity) by darkening snow and ice surfaces (Warren, 1984; (Warren and Clarke, 1990). Hansen and Nazarenko (2004) concluded that albedo effects of BC in snow and ice could account for 25% of observed global warming between 1880 and 2000.

Global BC emission inventories are based on international fuel-consumption estimates. Global inventories used for climate studies include: 1) Cooke and Wilson (1996) for anthropogenic fossil fuel (8 Tg BC/yr) and biomass (6 Tg BC/yr) combustion; 2) Cooke et al. (1999) for fossil fuel combustion (5.1 Tg BC/yr); 3) Global Emissions Inventory Activity (GEIA, Molina, 1992, Penner et al., 1993) which includes a BC inventory based on fuel consumption (12.6 Tg BC/yr) and another based on sulfur dioxide (SO_2) emissions (24 Tg BC/yr), relying on observed region-specific correlations between BC and SO_2; and 4) Liousse et al. (1993) for fossil fuel and biomass combustion (12.3 Tg BC/yr).

Regional BC inventories have also been created. Bond et al. (2002) estimated that North American sources contribute 6% of global emissions (6.63 Tg BC/yr). Battye et al. (2002) ranked the major contributors to U.S. BC emissions as: 1) non-road diesel exhaust (21%); 2) on-road diesel exhaust (15%); 3) prescribed forest fires (7.9%); 4) open burning (7.7%); and 5)

residential wood combustion (4.8%). Natural wildfires were not considered as manmade sources in Battye's analysis, although 100 years of fire suppression have caused them to be large emitters in recent years. Gasoline engine cold-starts and high emitters, which have been shown to contain substantial BC fractions (Zielinska et al., 1998), were not considered in this analysis.

These inventories rely on different assumptions and on data related to emission activities, PM emission factors, and source profiles; all of which apportion PM mass to BC and other chemical constituents. These differences may be a major cause of discrepancies and uncertainties in model predictions. Bond et al. (1998) identifies PM mass emission factors and the BC fraction (fBC) of emitted PM (i.e., "source profiles") as the most variable. Cooke and Wilson (1996) based fBC for heavy-duty diesel vehicles on source profiles from Cass et al. (1982), Lowenthal et al. (1994), and others. Streets et al. (2001) based fBC for diesel vehicles in China on profiles from Gillies and Gertler (2000) and others. Currie et al. (2002) show more than a factor of seven in the range of BC concentrations for different measurement methods commonly used throughout the world.

Since radiative forcing calculations are based on aerosol optical properties, not BC mass concentration, Bond et al. (1998) recommends measuring emission absorption coefficients directly and reporting "absorption cross section" emission factors (i.e., m^2/sec, m^2/unit of activity, m^2/unit CO_2, or m^2/unit fuel burned). In addition to characterizing $PM_{2.5}$ emissions in terms of organic carbon (OC), elemental carbon (EC), or BC, light absorption (b_{abs}) should be quantified with emission rates and source profiles.

Elemental carbon (EC) and BC are defined operationally by the measurement method applied, although the terms EC and BC are often used interchangeably. In its purest forms, EC occurs either as the mineral graphite or as diamond, but these structures are not found in ambient PM. Even soot freshly emitted from incomplete combustion contains non-carbon components and has a non-crystalline structure (Akhter et al., 1984, 1985). It has a large surface-to-volume ratio and reactive surfaces, so it attracts condensable materials (e.g., polycyclic aromatic hydrocarbon [PAH] gases) soon after cooling.

Of the major components of $PM_{2.5}$ and PM_{10}, organic carbon (OC) and EC are the most uncertain with respect to sampling and analysis (Turpin et al., 1994, Huebert and Charlson, 2000, Jacobson, 2000). Most EC and BC characterization involves collecting PM on filters and measuring either the carbon content on the filter or the attenuation of light reflected from or transmitted through the filter. Filter-based optical techniques include the British Smoke Shade method (Hill, 1936), the coefficient of haze (COH, Hemeon et al., 1953), the "integrating plate" method (IPM, Lin et al., 1973), the aethalometer (Hansen et al., 1984), and the particle soot absorption photometer (PSAP, Bond et al., 1999). The scattering and absorption properties of particles distributed on top of and throughout a filter are not the same as they are in the atmosphere, however, and babs determined from these methods is often biased (Horvath, 1993).

Thermal evolution methods quantify the amount of carbon that leaves the filter at different temperatures (Schmid et al., 2001, Currie et al., 2002). These use different combinations of temperature and analysis atmospheres to evaporate, pyrolyze, and combust the carbon-containing compounds in a filter sample with subsequent detection of the evolved carbon gases. The separation of OC from EC is ambiguous because some of the EC combusts in an oxidizing atmosphere, and some of the OC chars (turns to EC) in an oxygen-free atmosphere. Light reflected from the filter (Johnson, 1981, Huntzicker et al., 1982, Chow et al., 1993) or transmitted through the filter during the analysis (Turpin et al., 1990, Birch and Cary, 1996a, 1996b, Chow et al., 2001) is used to monitor and correct for this charring. Interlaboratory and intermethod comparisons (i.e., Countess, 1990, Chow et al., 2001, Schmid et al., 2001, Currie et al., 2002) show EC differences of a factor of two or more among different thermal methods, depending on the protocol and type of sample. Different analysis methods alone can account for the large differences in BC emission rates among inventories.

A fundamental measurement of in situ aerosol b_{abs} can be achieved by the photoacoustic instrument (Moosmüller et al., 1997, Arnott et al., 1999, 2003), which quantifies minute changes in the speed of sound in response to heating and cooling of PM by a modulated laser beam. Photoacoustic measurements collocated with filter samples offer the best method of relating EC/BC measurements to their absorption properties, thereby fulfilling the recommendation of Bond et al. (1998).

The goal of this project is to improve BC emissions inventories applicable to global climate change by understanding what is currently available, by better characterizing measurement methods, and by measuring emission rates and chemical profiles from BC-emitting sources. Uncertainties and differences are assessed among inventories with respect to activity levels, emission factors, and BC content. Commonly available BC measurements are related to their radiative transfer properties. Specific project objectives are: 1) identify, compile, evaluate, and summarize existing information on BC inventories, combustion processes, emission factors, source profiles, and source/ambient measurement methods; 2) develop and apply BC analysis methods to determine causes of differences among concentrations in source emissions and in ambient monitoring networks; 3) develop relationships among different BC measurement methods and light-absorbing properties of emitted particles; 4) measure OC and BC emission factors for selected combustion processes; 5) compile and compare OC and BC emission factors relevant to California, the U.S., and global inventories; and 6) evaluate and quantify emissions inventory uncertainties and describe how the results of this study might reduce them.

Phase I consists of gaining a better understanding of OC and BC measurement methods. This is accomplished by generating test aerosols from carbon powders and combustion sources in a test chamber where they can be sampled simultaneously by a photoacoustic particle absorption instrument, as well as onto filters suitable for other thermal and optical analyses. Several thermal evolution methods typical of those used in California source and ambient samples and in international inventories will be applied. A fundamental measure of BC absorption, the

photoacoustic instrument, is used as a benchmark and primary calibration standard. This QAPP covers those environmental data collection activities associated with Phase I of the project.

Phase II evaluates existing inventories, determining their similarities and differences, and enhancing understanding about why those differences exist. It compiles and compares available particulate matter (PM) and BC emission factors relevant to California combustion sources and determines how these relate to national and global inventories.

4. PROJECT/TASK DESCRIPTION

In order to meet the goal of improving BC emissions inventories it is necessary to understand what is currently available, to better characterize EC and BC measurement methods, and to measure emission rates and profiles from BC-emitting sources. These inventories should be applicable to California, the U.S., and global-climate concerns. Uncertainties and differences among inventories with respect to activity levels, emission factors, and BC content should be assessed. Commonly available EC and BC measurements should be related to their radiative transfer properties.

Specific objectives for the project (Phases I and II) are to:

- Identify, compile, evaluate, and summarize existing information on BC inventories, combustion processes, emission factors, source profiles, and source/ambient measurement methods.
- Develop and apply analysis methods to determine causes of differences among EC/BC measurements in source emissions and in ambient monitoring networks.
- Develop relationships between different EC/BC measurement methods and light absorbing properties of emitted particles.
- Measure OC and BC emission factors for selected combustion processes.
- Compile and compare OC and BC emission factors that are relevant to California, U.S., and global inventories.
- Evaluate and quantify emissions inventory uncertainties and describe how the results of this study might reduce them.

4.1 Description of Work to be Performed for Phase I

Phase I intends a better understanding of OC and EC/BC measurement methods. This is accomplished by generating test aerosols from carbon powders and combustion sources into a test chamber, where they can be sampled simultaneously by the photoacoustic b_{abs} instrument and onto filters suitable for other thermal and optical analyses. Several thermal-evolution methods typical of those used in California source and ambient samples and in international inventories are applied. Absorption efficiencies (m^2/g) are derived for each sample and analysis method by dividing the photoacoustic b_{abs} by the measured EC and BC concentrations. Replicate samples determine the derived uncertainties.

Phase I also includes a field evaluation of in-situ and integrated measurements at the Fresno Supersite (Watson et al., 2000) during summer and winter, when different source influences

prevail. The field test generalizes the results of the laboratory tests and provides empirical formulae applicable to other California monitors that do not have collocated measurements. Radiative transfer models (Chen et al., 2004) are adapted to modeling particle deposits on the surface of and within filters to better understand why particulate optical properties in free air differ from their properties on top of and within a filter.

Phase II evaluates existing inventories, determining their similarities and differences, and understanding why those differences exist. It compiles and compares available PM and BC emission factors relevant to California combustion sources and determines how these relate to national and global inventories. Since source testing is expensive and project resources are limited, several leveraging opportunities for source testing are identified. A photoacoustic instrument and additional filters could be added to these tests to meet the needs of this project while enhancing the data obtained by the primary sponsor.

The following sections describe the tasks and measurements required for the routine field and laboratory activities for Phase I of the project. Phase I provides a basis for refining the Phase II source-test matrix, sampling approach, laboratory analysis, and data interpretation. There are five main tasks for Phase I:

- Critically review literature on carbon analysis methods and comparisons.
- Develop carbon analysis QA/QC methods and plans.
- Conduct a laboratory comparison of particle absorption (b_{abs}) BC, EC, and OC measurement methods.
- Perform field comparisons at the Fresno Supersite.
- Prepare an interim report.

4.1.1 Task 1a – Critically Review Literature on Carbon Analysis Methods and Comparisons

Under this task, DRI will:

- Assemble, catalog, key-word, read, annotate, summarize, and critique published articles and reports on carbon measurement methods, standards, intercomparison studies, and source tests.
- Create tabular summaries of published thermal and optical carbon analysis methods that state their operating principles, protocols (e.g., temperatures, analysis atmospheres, optical monitoring), standardization, lower quantifiable limits, precision, and types of samples analyzed.
- Discuss similarities and differences among hardware and protocols that might result in differences in OC and EC by different methods.

- Create tabular summaries of published carbon comparison studies that state the methods, samples compared, and results of the comparisons.

- Evaluate how operating parameters of different analysis protocols (e.g., thermal programs, gas mixtures) contribute to variability in measured OC and EC, evolved carbon fractions, and pyrolyzed carbon.

- Discuss how variations in sampling parameters (e.g., flow rate, face velocity, filter loading) combine with variations in analysis protocols to produce variation in measured OC and EC.

- Assess the variability in the relationship between b_{abs} and EC derived from various methods, especially the link between actual (in-situ) aerosol light absorption and filter EC using reflectance or transmission as optical pyrolysis correction.

4.1.2 Task 2a – Develop Carbon Analysis QA/QC Methods and Plans

Under this task, DRI will create and test methods to standardize and audit thermal and optical measurement methods. These include:

- Neutral density filters for optical reflectance and transmission.

- Temperature-sensitive dyes to evaluate differences between sample temperatures and measured temperatures in thermal evolution devices.

- Detection of trace amounts of oxygen (O_2) in non-oxidizing combustion atmospheres.

- Traceable standards to calibrate carbon detection and verify efficiencies of oxidizing and reducing ovens.

As part of this task, DRI will also prepare a Quality Assurance Project Plan.

4.1.3 Task 3a – Conduct a Laboratory Comparison of b_{abs}, BC, EC, and OC Measurement Methods

Under this task, DRI will generate carbon aerosols into a dilution and sampling chamber from the following sources: acetylene or hexane flame, electric arc, wood combustion and diesel engine.

DRI will perform two different tests with each source, one containing pure combustion aerosol and a second containing combustion plus an interferent to evaluate multiple scattering artifacts and potential for mineral oxidation. These will supplement similar measurements of powdered graphite and carbon black to be generated and sampled under another DRI project (U.S. EPA Science to Achieve Results [STAR] Grant No. R831086). DRI will sample the suspended aerosol through a $PM_{2.5}$ inlet onto filters; simultaneously measure b_{abs} in-situ with the photoacoustic (PA) instrument at a wavelength of 1047 nm; and measure filter-based b_{abs} with a

seven-wavelength aethalometer and by densitometry on samples collected on Teflon filters. DRI will produce test filters on at least five parallel channels that include: 1) one Teflon-membrane and one pre-baked quartz-fiber filter at the same flow rate, and 2) three pre-baked quartz-fiber filters sampled at different flow rates to obtain different particle loadings. Each test will be performed in replicate. The measurement approaches to determine b_{abs}, EC, and OC for each test aerosol are summarized in Table 4-1.

DRI will submit one Teflon-membrane filter and the four differently loaded quartz-fiber filters to optical transmittance analysis before and after sampling using an integrating plate densitometer to determine b_{abs}. DRI will also submit portions of the quartz-fiber filters to thermal/optical analysis using three commonly used thermal evolution protocols (e.g., Cachier et al., 1989a, 1989b, Chow et al., 1993, Patashnick et al., 2001, Peterson and Richards, 2002). Table 4-1 identifies the IMPROVE_TOR, STN_TOT, and the French two-step thermal methods. These protocols represent a wide range of variability in thermal and optical parameters including temperature plateaus, analysis times, combustion atmospheres, heating rates, and optical pyrolysis monitoring by reflectance (TOR) and transmittance (TOT) that will be used to assess the impact of these variables on the determination of OC and EC. In addition, DRI will quantify mass on the Teflon-membrane filter by gravimetry and metals by x-ray fluorescence (XRF).

DRI will calculate the following performance statistics (Mathai et al., 1990) for b_{abs} from each transmission measurement (aethalometer and densitometer) versus the photoacoustic and b_{abs}:

- Effective variance weighted linear regression slope and intercept
- Average ratio and standard deviation
- Ratio of averages and standard deviation
- Distribution of differences
- Collocated precision
- Propagated precision

DRI will define criteria for equivalence (values are the same within measurement precision), comparability (values are the same within a stated uncertainty), or predictability (values are systematically different, but can be estimated from one another by a derived relationship). For thermal EC measurements, DRI will calculate absorption efficiency (m^2/g) as the ratio of photoacoustic b_{abs} (Mm^{-1}) to EC ($\mu g/m^3$), calculate performance statistics, and apply equivalence/comparability/predictability criteria.

Table 4-1. In-Situ and Filter-Based Methods for b_{abs}, BC, EC, and OC.

Method	Principle	Detection limit
Time Integrated Filter-Based Thermal Evolution Methods for Elemental (EC) and Organic Carbon (OC)		
IMPROVE Thermal/Optical Reflectance and Transmittance (TOR/TOT) (DRI Model 2001)	Carbonaceous aerosol deposited on quartz-fiber filters is analyzed through thermal evolution. The sample is heated to 120ºC, 250ºC, 450ºC, and 550ºC in He and 550ºC, 700ºC, and 800ºC in 2%O2/98%He environment. EC is defined as the non-volatile carbon evolved in the oxidative atmosphere. Filter reflectance and transmittance are both monitored for adjusting the charred organic carbon during thermal analysis.	0.5 μgC/cm^2 filter
STN Thermal/Optical Transmittance and Reflectance (TOT/TOR) (DRI Model 2001)	Carbonaceous aerosol deposited on quartz-fiber filters is analyzed by thermal evolution. The sample is heated to 310ºC, 480ºC, 615ºC and 900ºC in He and 600ºC, 675ºC, 750ºC, 825ºC and 920ºC in 2%O2/98%He environment. EC is defined as the non-volatile carbon evolved in the oxidative atmosphere. Filter reflectance and transmittance are both monitored for adjusting the charred organic carbon during thermal analysis.	0.5 μgC/cm^2 filter
Two-Step Pure Oxygen Thermal Method (DRI Model 2001)	Carbonaceous aerosol deposited on quartz-fiber filters is analyzed by thermal evolution. A sample punch is heated to 340ºC in pure O2 for 2 hrs and the residue carbon is measured as EC. Total carbon is determined using another sample punch without oxygen exposure.	0.5 μgC/cm^2 filter
Filter Transmittance Methods for Black carbon (BC) and B_{abs}		
Seven-Wavelength Aethalometer (Magee Scientific)	Air is drawn continuously through a quartz-fiber filter tape for particle collection. Particles deposited on the filter cause attenuation of a light beam. The net attenuation signal is converted into black carbon concentration by assuming a mass attenuation efficiency of black carbon. b_{abs} is converted to BC by using 14625/λ..	0.06 μgC/m^3 for a 5-min average
Transmission Densitometer (Tobias Associates, Inc., Ivyland, PA)	Light transmission is measured through Teflon membrane filters with an integrating plate using white light before and after aerosol sampling. The optical density of the particle deposit is determined from the logarithm of the ratio of transmitted intensities with and without the deposit, and converted to b_{abs}.	Lower limit: an optical density of ~0.05 Upper limit: 50% attenuation of the incident light.
In-Situ (Continuous) Methods for Light Absorption, Scattering, and Extinction		
Photoacoustic Photometer (PA) (DRI, Reno, NV)	Absorption of a laser beam by particles in the air causes heating of the surrounding air. The expansion of the heated air produces a sound wave at the same frequency as the laser modulation. This acoustic signal is detected by a microphone to determine the amount of absorption (b_{abs}).	0.4 Mm^{-1} for a 10-min average

4.1.4 Task 4a – Perform a Field Comparison at the Fresno Supersite

Assemble and analyze measurements from previous field evaluations that included a photoacoustic instrument with other BC measurements. These include: 1) Fresno Supersite; 2) the Reno Carbon Intercomparison; 3) Big Bend Regional Aerosol and Visibility Study (BRAVO) anchor site; 4) Northern Front Range Air Quality Study (NFRAQS); 5) Southern Nevada Air Quality Study (SNAQS); 6) Gas/Diesel Split source sampling; and 7) Missoula Forest Fire Characterization Study. Special emphasis will be placed on Fresno Supersite special studies, which include: 1) an aethalometer intercomparison; 2) a December 2003 wintertime carbon method intercomparison; and 3) long-term sampling with several continuous and carbon-based filter measurement systems. Ongoing Fresno Supersite measurements are detailed in Table 4-2.

Conduct a one-month study in summer or fall during the forest fire and agricultural burning season at the Fresno Supersite to complement the winter 2003 study. Table 4-3 lists the supplemental measurements for the December 2003 winter study while Table 4-4 lists the supplemental measurements for the summer/fall study during August and September of 2005.

Collocate the DRI photoacoustic instrument with the following continuous measurement systems 1) a Sunset Laboratory Carbon Aerosol Analysis Field Instrument; 2) a dual-wavelength aethalometer; 3) a seven-wavelength aethalometer; 4) the multi-angle absorption photometer (MAAP) system; 5) a photoelectric aerosol sensor (PAS) ionization polycyclic aromatic hydrocarbon (PAH) detector; and 6) a multi-wavelength sun photometer (optical depth). Complementary measurements at the Fresno Supersite include: 1) continuous particle size distribution measurements with TSI nano- and standard-scanning mobility particle sizers (SMPSs) and Lasair optical particle counters (OPCs); 2) continuous criteria gas measurements (NO_x, NO, NO_2, O_3, CO); and 3) continuous $PM_{2.5}$ and PM_{10} mass concentrations by Met-One Beta Attenuation Monitors (BAM) and R&P tapered element oscillating microbalances (TEOMs). Filter samples include: 1) $PM_{2.5}$ carbon denuder/backup samples with an Andersen Reference Ambient Air Sampler (RAAS); 2) $PM_{2.5}$ high-volume quartz-fiber filters (suitable for many replicate analyses); and 3) the Speciation Trends Network (STN) Met-One monitor, which obtains chemical analyses from Research Triangle Institute (Research Triangle Park, NC). While the R&P 5400 ambient carbon particulate monitor was proposed to be included as part of the summer intensive, frequent instrument malfunctions and problems caused the instrument to be placed offline.

The RAAS sampler enables an evaluation of carbon sampling artifacts: positive (absorption of volatile organics by the quartz filter), and negative (volatilization of organic material from particles on the quartz filter). RAAS channels 1 and 2 are undenuded. Channel 1 samples carbon on a quartz backup to a Teflon filter. Channel 2 samples particles on a quartz filter and volatilized carbon on a quartz backup filter. Channel 3 is preceded by a Brigham Young University carbon denuder and contains a quartz-quartz filter pair. The difference between the total carbon (EC + OC) from Channels 2 and 3 should provide an estimate of the positive artifact. The difference between the backup filters in Channels 1 and 2 should provide a limit on

the negative artifact. Analyze up to 15 of the high-volume filters by the three thermal methods selected for Task 3a described in Table 4-1. Analyze up to 15 of the Andersen RAAS denuded and non-denuded

Table 4-2. Summary of Air Quality and Meteorological Measurements at the Fresno Supersite.

Observable and Method	Size Range	Avg Time	Frequency	Period
Gases				
Nitrogen oxides (NO/NO_x) (TEI 42 chemiluminescence with internal converter)[a]	Gas	1-hr	daily	1990 onward [b]
NO_2/PAN (UC Riverside Luminol)	Gas	5-min	daily	12/1/00 to 4/25/03
Ozone (API 400 UV absorption) [a]	Gas	1-hr	daily	1990 onward [b]
Carbon monoxide (Dasibi 3008 infrared gas filter correlation)	Gas	1-hr	daily	1990 onward [b]
Non-methane hydrocarbons (TEI 55C flame ionization)	Gas	1-hr	daily	1998 onward [b]
Reactive nitrogen (NOy) (TEI 42C chemiluminescence with external converter) [a]	Gas	1-min	daily	12/15/99 onward
Nitric acid (HNO_3) (TEI 42C chemiluminescence with external converters and denuders) c	Gas	1-min	daily	12/1/00 onward
Filter Mass and Chemistry				
TSP mass (Thermo Electron HiVol w/ quartz filters) and lead	TSP	24-hr	12th day	1990 to 2001 [b]
$PM_{2.5}$ mass and carbon (Thermo Electron HiVol w/ quartz filters)	<2.5 µm	24-hr	Every 3rd to 6th day	8/24/02 onward
PM_{10} mass, sulfate, nitrate, chloride, and ammonium (Thermo Electron HiVol SSI w/ quartz filters)	<10 µm	24-hr	6th day	1990 onward [b]
$PM_{2.5}$ and coarse mass, elements, endotoxins[e], spores[e], molds[e], and fungi[e] (dichotomous samplers with Teflon filters)	<2.5 µm <10 µm	24-hr	6th day	1990 to 2000 [b]
$PM_{2.5}$ and coarse mass, elements, endotoxins[e], spores[e], molds[e], and fungi[e] (two R&P 2025 sequential FRMs w/ Teflon filters)	<2.5 µm <10 µm	24-hr	daily for primary 6th day collocated	3/1/99 to 2007 [b]

Table 4-2. Continued.

Observable and Method	Size Range	Avg Time	Frequency	Period
Filter Mass and Chemistry (continued)				
$PM_{2.5}$ mass, light absorption, elements, ions, and carbon (two Thermo Electron single-channel RAAS 100 FRMs w/ Teflon and quartz filters)	<2.5 µm	24-hr	6th day	7/5/99 onward
$PM_{2.5}$ mass, elements, ions, and carbon (six-channel Thermo Electron RAAS 400 speciation sampler w/ denuders and backup filters)	<2.5 µm	24-hr	6th day	7/5/99 onward
$PM_{2.5}$ mass, ions, and carbon (PC-BOSS [Particle concentration-Brigham Young University organic sampling system] w/ denuders and backup filters)	<2.5 µm	3-hr	daily on 4 episode days	12/15, 12/17, 12/18, 12/22/03
Particle morphology (Airmetrics MiniVol w/ polycarbonate filter for scanning electron microscopy)	< ~30 µm	24-hr	6th day	7/5/99 to 6/29/00 (method evaluation)
$PM_{2.5}$ mass, elements, ions, and carbon (three-channel Met One speciation sampler [SASS])	<2.5 µm	24-hr	3rd day	2001 onward [b]
$PM_{2.5}$ mass, elements, ions, carbon, and ammonia (two-channel DRI sequential filter sampler w/ nitric acid denuders and backup filters; mass on all, chemistry on 100 samples)[a]	<2.5 µm	24-hr	daily	12/1/99 to 2/3/01[d]
$PM_{2.5}$ mass, elements, ions, and carbon (two-channel sequential filter sampler w/ denuders and backup filters) [a]	<2.5 µm	3-, 5-, and 8-hr (5 samples per day)	daily on episode days	15 episode days 12/1/00 to 2/3/01[d]
Toxic species (metals, chromium VI, aldehydes) (Xontec 920)	<~30 µm	24-hr	12th day	1996 onward [b]
R&P 2300 Speciation Sampler	<2.5 µm	24-hr	6th day	7/02 to 1/03
Burkard Pollen and Spore Counter[e]	TSP	168-hr	weekly	8/01 onward

Table 4-2. Continued.

Observable and Method	Size Range	Avg Time	Frequency	Period
Continuous Particle Mass and Chemistry				
$PM_{2.5}$ mass (50 °C R&P 1400a TEOM)	<2.5 µm	5-min	daily	7/10/99 onward
PM_{10} mass (50 °C R&P 1400a TEOM)	<10 µm	5-min	daily	7/10/99 onward
$PM_{2.5}$ mass (ambient temperature Met One 1020 BAM) [e]	<2.5 µm	1-hr	daily	12/16/99 to 1/2/04
PM_{10} mass (ambient temperature Met One 1020 BAM) [e]	<10 µm	1-hr	daily	12/4/99 onward
PM_{10} mass (ambient temperature Met One 1020 BAM) #2 [e]	<10 µm	1-hr	daily	1/2/04 onward
$PM_{2.5}$ (fine) and PM_{10} (coarse) mass SPM-613 (Kimoto Electric, Tokyo, Japan)	<2.5 µm <10 µm	1-hr	daily	11/30/03 onward (sporadic operation due to frequent instrument problems)
$PM_{2.5}$ mass (30 °C R&P 1400a TEOM)	<2.5 µm	1-hr	daily	12/1/03-12/22/03
$PM_{2.5}$ mass (30 °C R&P Differential TEOM)	<2.5 µm	1-hr	daily	12/1/03-12/22/03
$PM_{2.5}$ mass (30 °C R&P FDMS TEOM)	<2.5 µm	1-hr	daily	12/1/03-12/22/03
$PM_{2.5}$ nitrate Unit 1 (R&P/ADI flash volatilization with NOx detector) [c, e]	<2.5 µm	10-min	daily	08/23/00 onward
$PM_{2.5}$ nitrate Unit 2 (R&P/ADI flash volatilization with NOx detector) [c, e]	<2.5 µm	10-min	daily	10/12/00 onward
$PM_{2.5}$ sulfate (R&P/ADI flash volatilization with SO_2 detector) [e]	<2.5 µm	10-min	daily	1/29/02 onward
$PM_{2.5}$ organic and elemental carbon (R&P Series 5400 thermal evolution, OC at 340 °C, EC at 700 °C) [e]	<2.5 µm	1-hr	daily	1/13/00 to 03/07/05
$PM_{2.5}$ organic and elemental carbon (Sunset Laboratory carbon aerosol analysis field instrument, NDIR detection of carbon) [e]	<2.5 µm	1-hr	daily	7/23/03 onward

Table 4-2. Continued.

Observable and Method	Size Range	Avg Time	Frequency	Period
Continuous Particle Mass and Chemistry (continued)				
Particle-bound polycyclic aromatic hydrocarbons (PAH) (EcoChem Analytics PAS2000 w/ UV radiation and photoelectric aerosol sensors) [e] [PAS-PAH]	<1 µm	5-min	daily	9/30/99 onward
Individual particle size and chemistry (UC Riverside time-of-flight spectrometer)	<10 µm	5-min	daily on episode days	12/1/00 to 2/3/01 [d]
Time Integrated Organic Gases and Particles				
Toxic hydrocarbons (C2 to C12) (Xontec 910 canister sampler)	gas	24-hr	12th day	1995 onward
Carbonyls (Xontec 925 2,4-dinitrophenylhydrazine [DNPH] cartridge sampler) [a]	gas	24-hr summer (4 samples per day)	12th day 3rd day	1995 to 2003 [b]
Carbonyls (Xontec 910/912 canister PAMS sampler) [a]	gas	24-hr summer (4 samples per day)	12th day 3rd day	1995 to 2003 [b]
Carbonyls (DRI sequential sampler with DNPH cartridge) [a]	gas	5- to 8-hr, (4 samples per day)	daily for episodes	15 episode days 12/1/00 to 2/3/01 [d]
Light hydrocarbons (C_2 to C_{12}) (canister sampler) [a]	gas	5- to 8-hr, (4 samples per day)	daily for episodes	15 episode days 12/1/00 to 2/3/01 [d]
Heavy hydrocarbons (C_{10} to C_{20}) (TENAX sampler) [a]	gas	5- to 8-hr, (4 samples per day)	daily for episodes	15 episode days 12/1/00 to 2/3/01 [d]
$PM_{2.5}$ organic compounds (DRI sequential sampler with Teflon-coated glass-fiber/PUF/XAD filters) [a]	<2.5 µm	5- to 8-hr, (4 samples per day)	daily for episodes	15 episode days 12/1/00 to 2/3/01 [d]
		24-hr	6th day	6/1/00-9/30/00 [d]
$PM_{2.5}$ organic compounds (Airmetrics Minivol w/ Teflon-coated glass-fiber filters) (aggregate 60 samples for organic compound analysis) [a]	<2.5 µm	24-hr	6th day	2/1/00 to 2/3/01 [d]

Table 4-2. Continued.

Observable and Method	Size Range	Avg Time	Frequency	Period
Continuous Light Scattering				
Ambient particle light scattering (Optec NGN2 ambient-temperature nephelometer at 550 nm)	<~30 µm	5-min	daily	2/1/00 to 12/21/03
Ambient particle light scattering (Optec NGN2 ambient-temperature nephelometer at 550 nm)	<~30 µm	1-min	daily	12/22/03 onward
Total particle light scattering (Radiance M903 nephelometer with smart heater at 530 nm) [a, e]	<~30 µm	5-min	daily	1/21/00 to 8/5/03
Total particle light scattering (Radiance M903 nephelometer with smart heater at 530 nm) [a, e]	<~30 µm	1-min	daily	8/5/03 onward
$PM_{2.5}$ particle light scattering (Radiance M903 nephelometer with smart heater at 530 nm) [e]	<2.5 µm	5-min	daily	9/8/00 to 8/1/03
$PM_{2.5}$ particle light scattering (Radiance M903 nephelometer with smart heater at 530 nm) [e]	<2.5 µm	1-min	daily	8/1/03 onward
Total particle light scattering (GreenTek GT640A photometer at 780 nm)	<~30 µm	5-min	daily	2/8/00 to 1/22/03
Total particle light scattering (EcoTech M9003 nephelometer at 525 nm)	<~30 µm	5-min	daily	7/31/05 to 9/26/05
$PM_{2.5}$ particle light scattering (TSI 3563 three wavelength nephelometer: 450, 550, 700 nm) [e]	<2.5 µm	5-min	daily	7/30/05 to 9/19/05
Total particle light scattering (TSI DustTrak 8520 photometer at 780 nm)	<2.5 µm	5-min	daily	5/15/99 to 6/28/03
Continuous Light Absorption				
Coefficient of haze (RAC 205019-1 paper tape sampler)	<~30 µm	2-hr	daily	1990 – 2002 [b]
Single-wavelength light absorption (1-AE, Magee AE-16 aethalometer at 880 nm)	<2.5 µm	5-min	daily	12/17/99 to 9/27/02

Table 4-2. Continued.

Observable and Method	Size Range	Avg Time	Frequency	Period
Continuous Light Absorption (continued)				
Dual-wavelength light absorption (2-AE Magee AE-21 aethalometer at 370 and 880 nm) [e]	<2.5 µm	5-min	daily	2/25/03 onward
Seven-wavelength light absorption (7-AE, Magee AE-30 multi-color [370, 470, 520, 590, 660, 880, and 950 nm] aethalometer) [e]	<2.5 µm	5-min	daily	5/12/99 onward
PSAP (Radiance Research light absorption monitor at 467, 530 and 660-nm)	<2.5 µm	3-sec	daily	8/1/05 to 9/17/05
MAAP (Thermo-Electron Black Carbon Monitor at 670 nm)	<2.5 µm	1-min	daily	11/30/03 onward
DRI PA (532 nm)	<2.5 µm	4-sec	daily	8/1/05 to 9/17/05
DRI PA (1047 nm)	<2.5 µm	5-min	daily	12/8/03 to 8/31/04
		3-sec	daily	8/1/05 to 9/17/05
Black carbon SPM-613 (Kimoto Electric, Tokyo, Japan)	<2.5 µm	1-hr	daily	2/9/04 onward (sporadic operation due to frequent instrument problems)
Black Carbon by Sunset Optical	< 2.5 µm	1-hr	daily	7/23/03 onward
Sun Photometer (CIMEL)–operated by JPL	NA	NA	Satellite Uplink	2001 onward
Particle Sizing				
Ultrafine particle number by size (TSI 3936N25A nano-SMPS) [a, e]	3 to 80 nm	5-min	daily	8/25/02 onward
Fine particle number by size (TSI 3936L10 SMPS) [a, e]	10 to 407 nm	5-min	daily	3/17/00 onward
Grimm SMPS	5 to 350 nm	3.5-min	daily	8/18/05 to 9/19/05
WPS (MSP 1000XP)	10 to 10,000 nm	5-min	daily	8/18/05 to 9/18/05

Table 4-2. Continued.

Observable and Method	Size Range	Avg Time	Frequency	Period
Particle Sizing (continued)				
Coarse particle size distribution in 16 size fractions (Climet Spectro .3 optical particle counter) [a]	0.3 to 10 µm (<0.3, <0.4, <0.5, <0.63, <0.8, <1.0, <1.3, <1.6, <2.0, <2.5, <3.2, <4.0, <5.0, <6.3, <8.0, and <10 µm)	5-min	daily	1/6/00 onward
Lasair (Particle Measuring Systems)	0.1 to 2.0 µm	5-min	daily	1/6/00 onward
Mass and ion size distribution in 9 size fractions (MOUDI with Teflon filters for mass and ions)	0.054 to 10 µm (<0.054, <0.105, <0.180, <0.37, <0.54, <1.0, <2.5, <5.6, and <10 µm)	5- to 8-hr	daily for episodes	15 episode days 12/1/00-2/3/01 [d]
Carbon size distribution in 9 size fractions (MOUDI with aluminum filters for organic and elemental carbon)	0.054 to 10 µm (<0.054, <0.105, <0.180, <0.37, <0.54, <1.0, <2.5, <5.6, and <10 µm)	5- to 8-hr	daily for episodes	15 episode days 12/1/00-2/3/01 [d]
Meteorology				
Wind speed/direction (Met One 05305L high-sensitivity wind vane and anemometer) [a]	NA [f]	5-min	daily	7/10/99 onward
Ambient Temperature (Met One CS500L platinum resistance sensor) [a]	NA	5-min	daily	7/10/99 onward
Relative humidity (RH) (Met One CS500L capacitance sensor) [a]	NA	5-min	daily	7/10/99 onward
Solar radiation (Li-Cor LI200X-L pyranometer) [a]	NA	5-min	daily	9/30/99 onward
Atmospheric pressure (Met One piezofilm sensor) [a]	NA	5-min	daily	5/24/00 onward

Table 4-2. Continued.

Observable and Method	Size Range	Avg Time	Frequency	Period
Data Acquisition System				
Campbell Scientific 24-input analog data logger with modem dialup	NA	All times	daily	5/15/99 onward
PC-LABVIEW serial data logger with modem dialup [a]	NA	All times	daily	12/1/99 onward

[a] These ground-level measurements were also taken at the non-urban Angiola site established by the California Regional Particulate Air Quality Study (CRPAQS) from 2/1/00 through 2/3/01 and during pollution episodes. This site is located 100 km south of Fresno in a flat area of the San Joaquin Valley surrounded by agricultural fields dominated by cotton and alfalfa. CRPAQS episodic measurements at Angiola were taken at the same time as those acquired at Fresno.

[b] Part of the California Air Resources Board's (ARB) compliance monitoring network.

[c] Measurements at Angiola are available from 12/1/00 through 2/3/01.

[d] Measurements from CRPAQS. Three to five wintertime episodes of four- to eight-day duration were monitored for a total of 15 days between 12/1/00 and 2/3/01 based on a forecast of high $PM_{2.5}$ concentrations under clear sky stagnation and stagnation with fog conditions.

[e] Part of the Fresno Asthmatic Children's Environment Study (FACES) sponsored by ARB.

[f] Not applicable.

Table 4-3. December 2003 Wintertime Carbon Method Study.

Observable and Method	Size Range	Avg. Time	Sampling Period	Determination of Mass and Semivolatile Organic Carbon
BYU Trailer Instruments				
Differential TEOM	<2.5 µm	5 minutes	12/1/03 12/31/03	– Two flow channels and two TEOM sensors. – A Nafion diffusion dryer removes moisture in the air stream. – An electrostatic precipitator removes particulates from one of the two channels. – Total mass of non-volatile and semi-volatile PM is the difference between mass measured by the two TEOMs.
Filter Dynamics Measurement System (FDMS) TEOM	<2.5 µm	5 minutes	12/1/03 12/31/03	– Two flow channels and one TEOM sensor. – An integrated Sampling Equilibrium System (SES) dryer removes moisture. – One channel collects particles at 4°C, followed by purging after sampling period. – The mass of volatile PM is compensated by the measurement of mass in the purged air stream.
50°C TEOM	<2.5 µm	5 minutes	12/1/03 12/31/03	– Heat up the sampling inlet to 50°C to remove moisture prior to mass being measured by the TEOM.

Table 4-3. Continued

Observable and Method	Size Range	Avg. Time	Sampling Period	Determination of Mass and Semivolatile Organic Carbon
Particle Concentrator-Brigham Young University Organic Sample System (PC-BOSS)	<2.5 μm	1 hour	12/1/03 12/31/03	– A virtual impactor is used to increase particle concentration (0.1-2.5 μm) to reduce loss of volatile species. – The sample flow passes through multi-channel denuder to remove gaseous species for adsorption. – Two filter channels are sampled in parallel. – The Teflon filter channel is followed by a Nylon filter to determine filter retained nonvolatile $PM_{2.5}$ mass, sulfate and nitrate. – The quartz filter channel is followed by a CIF filter to determine fine particulate carbonaceous material and semi-volatile species lost from particles during sampling.
Aethalometer (visible and UV channels)	Carbon	5 minutes	12/1/03 12/31/03	– Light absorbing particles (assuming only BC) deposited on a quartz filter results in attenuation of a light beam. – A constant between the net attenuation and BC is used to convert the changes in attenuation signal to the amount of BC. – The attenuation signal detected with UV wavelength is used to qualitatively monitor change of volatile carbonaceous compounds.
Automated acid gases and soluble anions Dionex Sampler	Ion	15 minutes	12/1/03 12/31/03	– Two independent parallel flow channels. – One channel collects soluble acid gases with wet denuder. – Another channel removes particles with cyclones and acid gases with wet denuder; particles are collected on one of the two alternative glass fiber filter samples followed by wet extraction for IC analysis. – Analytes collected in each channel are quantified by ion chromatography (IC).

Table 4-3. Continued

Observable and Method	Size Range	Avg. Time	Sampling Period	Determination of Mass and Semivolatile Organic Carbon
Other Instruments Added to the Fresno Supersite during this Study				
Photo-acoustic monitor (1047 nm)	Black Carbon	5 minutes	12/8/03 – 08/31/04	– Sample air is drawn through an acoustical resonator where a laser beam passes through. – Light absorption by gases and particles results in heat transfer to surrounding air. – The heated surrounding air expands and this expansion induces a detectable acoustic sound which is used to quantify the amount of BC.

Table 4-4. Measurements for 2005 Summer Intensive Study.

	Instruments[a]	Observable (unit)	Measurement Principle[b]	Wavelength (nm)	Particle Size	Collection Medium	Flow Rate (L/min)	Averaging Time
Continuous Particle Light Absorption	2-AE	b_{abs} (Mm^{-1}) BC ($\mu g/m^3$)	Attenuation of light transmitted through the filter tape is measured and converted to a BC mass concentration using σ_{abs} of 14625/λ (m^2/g).	370, 880	$PM_{2.5}$	Quartz-fiber filter tape	6.6	5 min
	7-AE	b_{abs} (Mm^{-1}) BC ($\mu g/m^3$)		370, 470, 520, 590, 660, 880, 950	$PM_{2.5}$	Quartz-fiber filter tape	6.7	5 min
	MAAP	b_{abs} (Mm^{-1}) BC ($\mu g/m^3$)	Light transmittance at 0° and reflectance from the filter at 130° and 165° from the illumination direction are used in a radiative transfer model to estimate b_{abs} and is converted to BC using σ_{abs} of 6.6 m^2/g.	670	$PM_{2.5}$	Glass-fiber filter tape	16.7	1 min
		b_{abs} (Mm^{-1})	Attenuation of light transmitted through the filter tape is measured.	467, 530, 660	$PM_{2.5}$	Quartz-fiber filter punch	0.5	3 sec
PSAP	PA (532 nm)	b_{abs} (Mm^{-1}) BC ($\mu g/m^3$)	Light absorption by particles in air results in a heating of the surrounding air. The expansion of the heated air produces an acoustic (sound wave) signal which is detected by a microphone to determine b_{abs}, which is confined to BC using σ_{abs}=5 m^2/g for the 1047 nm instrument and σ_{abs}=10 m^2/g for the 532 nm instrument.	532	$PM_{2.5}$	Acoustic resonator	1	4 sec
	PA (1047 nm)			1047				3 sec
	Sunset Optical	BC ($\mu g/m^3$)	Light transmitted through the filter is monitored during the collection phase to quantify BC.	660	$PM_{2.5}$	Quartz-fiber filter tape	8.5	1 hr

Table 4.4. Continued.

	Instruments[a]	Observable (unit)	Measurement Principle[b]	Wavelength (nm)	Particle Size	Collection Medium	Flow Rate (L/min)	Averaging time
Continuous Particle Light Scattering	NGN2	b_{scat} (Mm^{-1})	Measures light scattering coefficient at ambient conditions. The air sample is illuminated and a photodiode detector produces a signal in proportion to the chopped light signal. Zero air calibration is done every 6 to 24 hrs.	550	TSP	none	2	1 min
		b_{scat} (Mm^{-1})	The air sample is illuminated and a photodiode detector produces a signal in	530	$PM_{2.5}$		6.9	1 min
				530	TSP	none	6.9	1 min
Rad903	Ecotech Neph	b_{scat} (Mm^{-1})	A light source illuminates the sample air, and the light scattered at angles between 10^{o} and 70^{o} is detected. The signal is proportional to the concentration of the particles giving an estimate of the particle light scattering coefficient. Zero air calibrations are performed using particle-free air. It is equipped with a heater that turns on when the RH is > 70%.	525	none TSP[d]	none	5	5 min
	TSI 3-color Neph	b_{scat} (m^{-1})	A light source illuminates the sample air and the light scattered at angles between 7^{o} and 170^{o} is detected. The signal is proportional to the concentration of the particles giving an estimate of the particle light scattering coefficient. Zero air calibrations are performed using particle-free air every hour.	450, 550, 700	$PM_{2.5}$ none		20	5 min
Continuous Particle Chemistry	R&P 8400N	Nitrate ($\mu g/m^3$)	Air sample is humidified and impacted on the strip. Flash volatization is followed by transport to a NO_x chemiluminescence sensor.	NA[e]	$PM_{2.5}$	nichrome strip	1.2	10 min
	R&P 8400S	Sulfate ($\mu g/m^3$)	Air sample is humidified and impacted on the strip. Flash volatization is followed by transport to a SO_2 fluorescence sensor.	NA	$PM_{2.5}$	platinum strip	1.2	10 min

Table 4.4. Continued.

	Instruments[a]	Observable (unit)	Measurement Principle[b]	Wavelength (nm)	Particle Size	Collection Medium	Flow Rate (L/min)	Averaging time
Continuous Particle Chemistry (Continued)	Sunset	OC, EC ($\mu g/m^3$)	Particles collected on a quartz-fiber filter are subject to different temperature ramps following the NIOSH 5040_TOT protocol and the resulting CO_2 is analyzed by nondispersive infrared (NDIR). Pyrolysis correction is by laser transmittance.	660	$PM_{2.5}$	Quartz-fiber filter tape	8.5	1 hr
	PAS-PAH	Particle-bound PAH (fA)	The air stream is exposed to UV radiation, which ionizes the particle-bound PAH molecules. The charged particles are collected on a filter element and the piezoelectric current is proportional to the particle-bound PAH.	225	$PM_{2.5}$	Filter element mounted in a Faraday cage	2	5 min
Particle Sizes	TSI nano SMPS	Number ($\#/cm^3$)	The air sample is bipolarly charged to a known distribution. The particles are classified according to their ability to traverse an electric field. The classified particles are coated with alcohol from a heated alcohol bath and grow to a size where they can be counted optically.	NA	3 - 80 nm	none	0.95	5 min
	TSI standard SMPS	Number ($\#/cm^3$)		NA	10 - 407 nm	none	0.95	5 min
	GRIMM SMPS	Number ($\#/cm^3$)		NA	5 - 350 nm	none	0.3	3.5 min
	Climet OPC	Number ($\#/cm^3$)	The air sample is illuminated and the scattered light is focused onto a photodetector. The amount of light scattered is proportional to the particle size.	NA	300 - 10000nm	none	0.95	5 min
	Lasair OPC	Number ($\#/cm^3$)		NA	100 nm - 2000 nm	none	0.03	5 min
	MSP WPS	Number ($\#/cm^3$)	The air sample is split into two flows. The first flow is bipolarly charged to a known distribution; classified according to the charged particle's ability to traverse an electric field; coated with alcohol and counted optically. The second flow is illuminated and the amount of photodetected scattered light is proportional to particle size.	NA	10 - 10000 nm	none	1	5 min
Continuous Mass	MetOne BAM	Mass ($\mu g/m^3$)	Beta rays (electrons) are passed through a filter on which particles are collected. The loss of electrons (beta attenuation) caused by the particle loading on the filter is converted to mass concentration, after subtraction of blank filter attenuation.	NA	PM_{10}	Quartz-fiber filter tape	16.7	1 hr
				NA	$PM_{2.5}$	Quartz-fiber filter tape	16.7	1 hr

Table 4.4. Continued.

	Instruments[a]	Observable (unit)	Measurement Principle[b]	Wavelength (nm)	Particle Size	Collection Medium	Flow Rate (L/min)	Averaging time
Continuous Mass (Continued)	Kimoto BAM	Mass (µg/m^3)	Beta rays (electrons) are passed through a filter on which particles are collected. The loss of electrons (beta attenuation) caused by the particle loading on the filter is converted to mass concentration, after subtraction of blank filter attenuation.	NA	PM_{10}	Teflon-membrane filter tape	15.4	1 hr
				NA	$PM_{2.5}$	Teflon-membrane filter tape	1.3	1 hr
	TEOM	Mass (µg/m^3)	Air is drawn through a size selective inlet onto the filter mounted on an oscillating hollow tube. The oscillation frequency changes with mass loading on the filter, which is used to calculate mass concentration by comparing measured frequency to standards.	NA	$PM_{2.5}$	Teflon coated borosilicate glass-fiber filter	16.7	5 min
				NA	PM_{10}		16.7	5 min
Integrated Measurements	FRM filter samples analyzed by IMPROVE_A_TOR/TOT	OC, EC, and TC (µg/m^3)	Particles collected on a quartz-fiber filter are subject to different temperature ramps following the IMPROVE_A protocol. The resulting CO_2 is converted to CH_4 and analyzed using FID. Pyrolysis correction is using laser reflectance (TOR) and transmittance (TOT).	632.8	$PM_{2.5}$	Quartz-fiber filter	16.7	24 hr, every 2 days
	RAAS filter samples analyzed by IMPROVE_A_TOR/TOT and STN_TOT	OC, EC, and TC (µg/m^3)	Particles collected on a quartz-fiber filter are subject to thermal carbon analysis following the IMPROVE_A and STN TOT protocols. Pyrolysis correction made by TOR/TOT in IMPROVE_A and laser transmittance in STN_TOT. STN_TOT analysis conducted on selected filters only.	632.8	$PM_{2.5}$	Quartz-fiber filter	16.7 (Channel 1); 7.3 (Channels 2 & 4)	24 hr, every 2 days
	Hi-Vol filter[c] samples analyzed by IMPROVE_A_TOR/TOT, STN_TOT, French 2-step	OC, EC, and TC (µg/m^3)	Particles collected on a quartz-fiber filter are subject to thermal carbon analysis following the IMPROVE_A, STN_TOT and French 2-step protocols. Pyrolysis correction made by TOR/TOT in IMPROVE_A, by TOT in STN_TOT and none in French 2-step protocol. STN and French analysis conducted on selected filters only.	632.8	$PM_{2.5}$	Quartz-fiber filter	1130	24 hr, every 2 days

Table 4.4. Continued.

	Instruments[a]	Observable (unit)	Measurement Principle[b]	Wavelength (nm)	Particle Size	Collection Medium	Flow Rate (L/min)	Averaging time
Continuous Gaseous Measurements	TEI 42	Nitrogen Oxides (NO/NOx)	The sample gas is exposed to O_3 initiating a chemical reaction between NO and O_3 that gives off light (chemiluminescence). A catalytic converter converts any NO_2 in the sample gas to NO, which is then reported as NO_x. NO_2 is calculated as a difference between NO_x and NO.	NA	gas	none	0.6	1 hr
	TEI 42CY	Reactive Nitrogen (NOy) and Nitric Acid (HNO_3)	The air sample is pulled through an external molybdenum converter, reacts with O_3 and the chemiluminescence is measured.	NA	gas	none	1	5 min
	TEI 55C	Non-Methane hydrocarbons (NMHC)	CH_4 is separated using a separation column and detected by FID. NMHC is then flushed out of the column by reversing the carrier gas flow, which is then detected by the FID.	NA	gas	none	0.5	1 hr
	Dasibi 3008	Carbon Monoxide (CO)	Infrared light is absorbed by CO in the air sample. The quantity of light absorbed is proportional to the concentration of CO in the air sample.	NA	gas	none	NA	1 hr
	API 400	Ozone (O_3)	254nm light is absorbed by O_3 in the air sample. The ratio of the scrubbed (O_3 free) air light intensity to that of the sample air is used to calculate the O_3 concentration as per Beer-Lambert law.	NA	gas	none	NA	1 hr
Meteorology	Met One 05305L	Wind Speed/Direction	High-sensitivity wind vane and anemometer.	NA	NA	none	NA	5 min
	Met One CS500L	Temperature	Temperature is measured by the resistance change of a platinum resistance sensor thermistor.	NA	NA	none	NA	5 min
	Met One CS500L	Relative Humidity (RH)	Relative Humidity is measured based upon the capacitance change of a polymer thin film capacitor.	NA	NA	none	NA	5 min

Table 4.4. Continued.

	Instruments[a]	Observable (unit)	Measurement Principle[b]	Wavelength (nm)	Particle Size	Collection Medium	Flow Rate (L/min)	Averaging time
Meteorology (Continued)	Met One	Atmospheric Pressure	Atmospheric pressure is measured by a solid state pressure transducer (Piezofilm sensor) whose voltage response is linear and proportional of pressure.	NA	NA	none	NA	5 min

[a] 2-AE—dual wavelength aethalometer (Magee Scientific, Inc., Berkeley, CA)
7-AE—seven-color aethalometer (Magee Scientific, Inc., Berkeley, CA)
MAAP—Multi-angle absorption photometer (Thermo Electron, Franklin, MA)
PSAP—particle soot absorption photometer (Radiance Research, Seattle, WA)
PA—DRI photoacoustic analyzer (Reno, NV)
Sunset—Semi-continuous Sunset Laboratory aerosol analyzer field instrument carbon analyzer, following the NIOSH thermal/optical transmittance (TOT) protocol (Sunset Laboratory, Inc., Tigard, OR)
NGN2: Optec—NGN2 Open air integrating nephelometer (Optec, Inc.)
Rad903—Radiance Research M903 integrating nephelometer (Radiance Research, Seattle, WA)
EcoTech Neph—EcoTech M9003 integrating nephelometer (EcoTech, East Providence, RI)
TSI 3-color Neph—TSI 3-color nephelometer (TSI, Shoreview, MN)
R&P 8400N—R&P ambient particulate nitrate monitor (Thermo Electron, Franklin, MA)
R&P 8400S—R&P ambient particulate sulfate monitor (Thermo Electron, Franklin, MA)
PAS-PAH—EcoChem PAS2000 PAH monitor (EcoChem Analytics, Inc., League City, TX)
TSI SMPS—TSI Inc. (Shoreview, MN) scanning mobility particle sizer
GRIMM SMPS: Grimm Aerosol Technik (Germany) SMPS
Climet OPC—Climet instruments (Redlands, CA) Spectro 0.3 optical particle counter
Lasair OPC—Lasair Particle Measuring Systems (PMS, Boulder, CO) optical particle counter
MSP WPS—MSP Corp. (Minneapolis, MN) wide range particle spectrometer
MetOne BAM—MetOne Beta-attenuation monitor (MetOne Instruments, Grants Pass, OR)
Kimoto BAM—Tisch Environmental Kimoto beta-attenuation monitor (Cleves, OH)
TEOM—Tapered element oscillating microbalance series 1400a ambient particulate monitor (Thermo Electron, Franklin, MA)
FRM—Thermo Electron single-channel Federal Reference Monitor (Thermo Electron, Franklin, MA)
RAAS—Thermo Electron reference ambient air speciation sampler (Thermo Electron, Franklin, MA)
Hi-Vol—high volume sampler (collocated Thermo Electron and EcoTech samplers)
TEI 42—Thermo Electron model 42 NO-NO2-NOx analyzer (Thermo Electron, Franklin, MA)
TEI 42CY—Thermo Electron model 42CY NOy analyzer (Thermo Electron, Franklin, MA)
TEI 55C—Thermo Electron direct methane, non-methane analyzer (Thermo Electron, Franklin, MA)
Dasibi 3008—Dasibi model 3008 carbon monoxide analyzer (Dasibi Environmental Corp, Glendale, CA)
API 400—Advanced Pollution Instrumentation, Inc. ozone analyzer (API, San Diego, CA)
All meteorological instruments are from MetOne (MetOne Instruments, Grants Pass, OR)

Table 4-4. Continued.

[b] BC—Black carbon
CO_2—Carbon dioxide
CH_4—Methane
FID—Flame Ionization Detector
IMPROVE_A—Interagency Monitoring of Protected Visual Environments carbon analysis protocol
NDIR—Non-dispersive Infrared
NIOSH_TOT—National Institute for Occupational Safety and Health Thermal/Optical Transmittance
NMHC—Non-methane hydrocarbons
NO—Nitric oxide
NO_2—Nitrogen dioxide
NO_x—Oxides of nitrogen
O_3—Ozone
PAH—Polycyclic-aromatic hydrocarbon
RH—Relative humidity
SO_2—Sulfur dioxide
STN_TOT—Speciation Trends Network thermal/optical transmittance (TOT) protocol
UV—Ultraviolet

[c] Collocated Thermo Electron and EcoTech as High Volume Samplers

[d] TSP—Total suspended particulate matter

[e] NA: Not available, Not applicable

samples and backup filters by the IMPROVE, STN, and two-step methods. All of the methods for measuring b_{abs} and EC and OC under laboratory conditions will also be applied in the field study. Apply the data analysis methods described in Task 3a to paired measurements from these experiments, using the photoacoustic b_{abs} as a benchmark. From these comparisons, determine the extent to which conclusions from the laboratory studies hold true for ambient samples with a broad and varying mixture of diesel exhaust, gasoline exhaust, residential wood combustion, cooking, and agricultural/forest fire contributions.

4.1.5 Task 5a – Prepare Interim Report

Under this task, DRI will prepare an interim report containing:

- Text and tables describing OC, EC, and BC measurement methods and previous comparison studies.
- Procedures for generating test aerosols.
- Calibration and audit procedures and results.
- Methods for generating and sampling test aerosols.
- Descriptions of field comparison databases.
- Results of laboratory and field comparison and evaluation studies.
- Conclusions about different OC, EC, BC, and babs measurement methods and their relevance to climate-relevant emissions inventories.

Appendices will include descriptions of the databases compiled in this project, which will also be made available in electronic format. Several bound paper copies and a PDF electronic copy will be delivered.

4.2 Field Activities

Field activities will be conducted at the Fresno Supersite location. Sampling, monitoring, and maintenance activities will be performed by ARB and DRI personnel. Table 4-2 lists the general measurements at the Fresno supersite and their schedule. Table 4-3 lists the supplemental measurement at the site for the December 2003 carbon method study and Table 4-4 lists the supplemental measurements for the 2005 summer intensive study.

4.3 Laboratory Activities

DRI laboratory support activities for the Phase I project tasks include the following:

Create and evaluate methods to standardize and audit thermal and optical measurement

methods, including:

I. Neutral density filters for optical reflectance and transmittance

II. Temperature sensitive dyes to evaluate differences between sample temperatures and measured temperatures in thermal evolution devices

III. Detection of trace amounts of oxygen (O2) in non-oxidizing combustion atmospheres

IV. Traceable standards to calibrate carbon detection and verify efficiencies of oxidizing and reducing ovens

Produce a Quality Assurance Project Plan (QAPP) in accordance. Interact with ARB, EPA, or other auditors for $PM_{2.5}$ FRM and chemical speciation programs (such as EPA Region 6 and the National Air and Radiation Environmental Laboratory [NAREL]). Analyze performance evaluation samples and participate in inter-laboratory comparisons as needed.

4.4 Laboratory Support Project Assessment Techniques

Table 4-5 lists types of laboratory support assessments that will be performed for this project and their frequency.

Table 4-5. Assessment Techniques and Schedule.

Assessment Type	Assessment Group	Frequency
DRI External QA Audit	Kochy Fung, Atmoslytic	~2 per year
DRI Internal Systems Audit	DRI QA Officer or designee	~2 per year
Data Quality Assessment	DRI QA Officer or designee	~2 per year
Technical Systems Audit	EPA NAREL*	~1 per year
Speciation Performance Evaluation	EPA NAREL*	~1 per year
Inter-laboratory Comparison	EPA NAREL*	~1 per year
Inter-laboratory Comparison	Other speciation and carbon analysis laboratories	TBD

* as part of arrangement for existing Texas $PM_{2.5}$ chemical speciation laboratory support program

4.5 Schedule of Project Activities

Figure 4-1 lists major milestones for Phase I of the project .

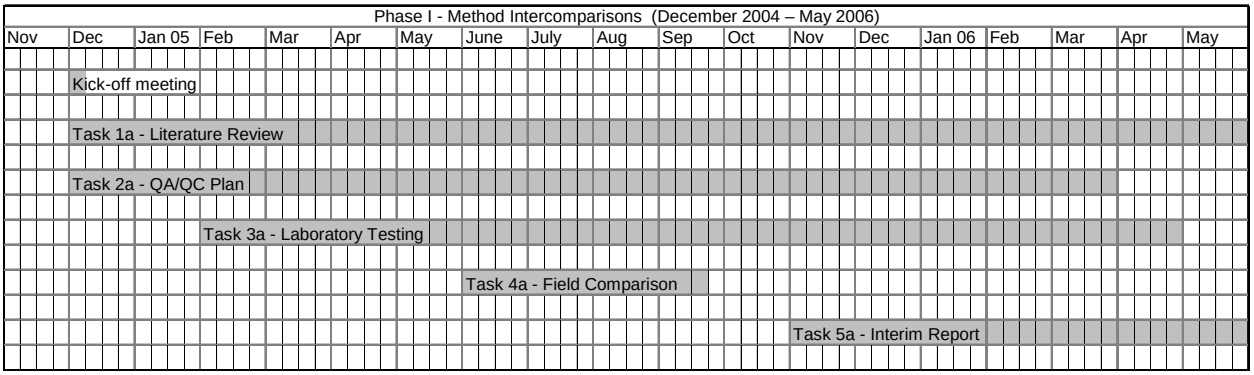

Figure 4-1. Project Schedule and Deliverables.

4.6 Project Records

Section 7 of this plan discusses project documentation and records.

5. QUALITY OBJECTIVES AND CRITERIA FOR MEASUREMENT DATA

DRI is fully committed to developing an effective Quality Assurance/Quality Control (QA/QC) Program and to delivering a quality product. For much of DRI's work, that product includes data gathered from field measurements, sampling and analysis activities, engineering assessments and the analysis of data for planning purposes. The QA Program works to provide complete, precise, accurate and representative data in a timely manner for each project, considering both the project's needs and budget constraints. DRI's QA Program conforms to EPA recommendations contained in EPA's Quality Assurance Handbook for Air Pollution Monitoring Systems (EPA 600/R-94-038).

DRI is responsible for implementing procedures that make sure precision, accuracy and completeness of the study data are known, documented and of acceptable quality. Since this is not a standard-setting or compliance-related environmental data collection effort, data quality objectives (DQOs) have not been established for this effort. In addition, this is primarily a research study on carbon sources for which measurement standards are not currently available. Rather, the results from this project will be used to establish measurement quality objectives (MQOs) for various phases of the environmental data collection process.

5.1 Data Quality Objective Process

The DQO process is a strategic planning approach used to ensure that an environmental data collection effort will obtain data of sufficient quality to meet the needs of decision makers. The formal DQO process consists of seven steps to ensure that the experimental design will meet specific decision criteria specified by decision makers and other stakeholders.

- State the problem
- Identify the decision
- Identify the inputs to the decision
- Define the study
- Develop a decision rule
- Specify tolerable limits on decision errors

The process is described in the EPA document, Guidance for the Data Quality Objectives Process (EPA QA/G-4), EPA/600/R-96/055 (August 2000).

5.2 Criteria for Measurement Data

Whether or not a DQO is established, the quality of the data must be assessed and controlled to ensure that it meets the established acceptance criteria. MQOs are designed to assess various phases of the measurement process to ensure that total measurement uncertainty is within the acceptable range established by the DQOs or to establish the quality of the data collected. MQOs may be defined in terms of the following data quality indicators:

- **Precision**: Precision is the degree of mutual agreement among individual measurements under prescribed conditions. Measurements will be made of analytical precision and overall precision. Analytical precision will be determined as the Relative Percent Difference (RPD) of replicate measurements made on the same and different instruments (if more than one is available). Overall precision will be determined as the RPD of separate measurements taken by different sampling instruments and includes both sampling and analytical instrument precision.

- **Bias**: Bias is the systematic or persistent distortion of a measurement process that causes error in one direction. There is no program established yet for establishing bias for carbon measurements. As part of this study, potential biases among carbon analysis methods will be assessed.

- **Accuracy**: Accuracy is the correctness of data and refers to the degree of difference between observed and known, or true values. For particulate measurements in general and carbon measurements in particular, there are no known true values. Sampler accuracy will be measured by performance (flow) checks and audits between the samplers and a certified flow meter. The goal is ±5% RPD of the audit standard and within ±5% of the design flow rate. Where transfer standards for calibration and auditing are available, the general goal for accuracy is to be within one standard deviation of the precision for each measurement.

- **Representativeness**: Representativeness is a measure of the extent to which data accurately and precisely represents a characteristic of a population, parameter variations at a sampling location, or an environmental condition. It is usually determined by assessing whether a monitoring location meets certain specified criteria. It may also be determined by assessing whether the quantities measured or determined constitute those most commonly used or reported.

- **Detectability**: Detectability is the low range critical value that a method-specific procedure can reliably discern. Table 4-1 gives the detection limits for the in-situ and filter-based methods focused in this project for b_{abs}, BC, EC, and OC.

- **Completeness**: Completeness is the percentage of valid data compared to the total expected data. Completeness will be measured as a percentage of valid data for a given study period. For the field studies, the project goal for completeness is that at least 75% of the scheduled

measurement intervals have valid data for all the instruments to be compared directly. A secondary goal is to have the completeness for each instrument be at least 90% for the period

- **Comparability**: Comparability is a measure of the confidence with which one set of data may be compared with another. Comparability is enhanced when the results are obtained using a consistent methodology and reported in standard units. This study will use the following definitions to evaluate equivalence, comparability, and predictability (or lack thereof) among different carbon measurements:

    I. *Equivalent*. For $PM_{2.5}$ mass concentration, U.S. EPA (1997) requires Federal Equivalency Methods (FEM) to meet the following requirements when collocated with a Federal Reference Method (FRM): 1) collocated precision of 2 $\mu g/m^3$ or 5% (whichever is larger); 2) linear regression slope of 1 ± 0.05; 3) linear regression intercept of 0 ± 1 $\mu g/m^3$; and 4) linear regression correlation coefficient (r) of ≥0.97 (U.S.EPA, 1997). Although these criteria are specific to $PM_{2.5}$ mass equivalence, they are also used for carbon equivalence to maintain consistency.

    II. *Comparable*. A comparable monitor should provide readings in units of EC or BC mass concentration, be equipped with a standardized size selective inlet, and yield measurements that are the same as collocated sampler measurements. Within stated precision intervals, the criteria for comparability are met when: 1) the slope (by either ordinary least squares [OLS] or effective variance [EF] weighting) equals unity within three standard errors, or average ratios (y/x) equal unity within one standard deviation; 2) the intercept does not significantly differ from zero within three standard errors; and 3) the correlation coefficient (r) exceeds 0.9 (Berkson, 1950, Kendall, 1951, Madansky, 1959). This is a less demanding definition than equivalence because it considers the reported precisions of the two measurements being compared; these may be larger than that required for an FEM used to determine compliance, but still sufficient to discern concentration differences in space and time.

    III. *Predictable*. Some measures, such as PAH and b_{abs}, may be correlated with EC or BC mass concentrations even though they measure different observables in other units. The criterion for predictability between two measurements is met when the correlation coefficient exceeds 0.9, although the slope may substantially deviate from unity and the intercept from zero. Predictability may be qualified, especially when there is high correlation for all but a few outlier measurements. The regression equation is used to estimate carbon concentrations from the measured observable.

IV. *Non-related*. Measurements are deemed to be poor or non-related when the correlation coefficient is less than 0.9 and there is no consistent or linear relationship between them.

The comparison procedure developed by Watson and Chow (2002) will be adapted. They employed several performance statistics that have been used inconsistently by other comparison studies. Regression slopes and intercepts with ordinary least squares (Bevington, 1969) and effective variance weighting (Watson et al., 1984), with their standard errors, provide one measure. Ordinary least squares does not weight measurements when computing linear regression statistics, whereas effective variance weighting accounts for measurement uncertainties in both independent (x) and dependent (y) variables to make the dataset less likely to be biased by extreme values.

Other useful statistics are averages of y/x, standard deviations of the average ratios, and the distribution of the data pairs whose difference (y minus x) is less than 1σ, between 1 and 2σ, between 2 and 3σ, and greater than 3σ (σ is the measurement uncertainty of y–x, which is the square root of the sum of the squared uncertainties $[\sigma^2_x+\sigma^2_y]$, where σ_x and σ_y are the one standard deviation precisions for the x and y observables, respectively). Measurement precisions are estimated from replicate analyses of samples collected by that sampler. Other performance statistics include: 1) the average of the paired differences (y–x); 2) the collocated precision, which is the standard deviation of the paired differences; and 3) the root mean squared (RMS) precision (the square root of the mean squared precisions), which is essentially the average measurement uncertainty of "y–x." The average differences and collocated precisions can be used to test the statistical hypothesis that the difference between samplers x and y is zero. A parametric test (Student's t-test) is performed for each pair of samplers.

6. SPECIAL TRAINING REQUIREMENTS/CERTIFICATION

Personnel assigned to the project activities will meet the educational, work experience, responsibility, personal attributes, and training requirements for their positions. All personnel involved in project activities will have at least two years experience in performing the same or very similar activities or be under the direct supervision of someone who has. Any new personnel that may be necessary will be trained in each of the activities they are to perform and will have their work checked by an experienced staff member. Personnel receiving project-related training or laboratory-specific training will have the successful completion of such training documented and retained by the laboratory coordinator.

7. DOCUMENTATION AND RECORDS

DRI will keep the following project-related records for at least three years after project completion:

- Management and Organization:
    - Personnel qualifications, training, and certifications
    - Purchase orders, invoices, and project correspondence
- Environmental Data Operations:
    - Quality Assurance Project Plan
    - Standard Operating Procedures
    - Laboratory notebooks, logbooks, and log sheets
    - Sample handling and custody records
    - Inspection and maintenance records
- Raw Data:
    - Original data (routine and QC) from laboratory information systems
    - Original data downloaded from samplers
    - Field data sheets
    - Other data entry sheets and forms
- Data Reporting:
    - Data/summary reports
    - Articles, papers, or presentations
- Data Management:
    - Data algorithms
    - Database design

    - Hardware/software test results
    - Data management plans, flow charts, and SOPs
- Quality Assurance:
    - Control charts
    - Data quality assessments
    - QA reports
    - System audits and reviews
    - Inter-laboratory comparisons

Wherever possible, automated systems will be used to record the information found in logs and data entry forms. Instructions for maintaining specific logs are given in specific SOPs.

The storage location of project-related records depends on the type of record or document and whether it is in hardcopy and/or electronic format. Personnel qualifications, training, and certifications are kept by DRI's Human Resources Office. Similarly, purchase orders and invoices are kept by DRI's Purchasing and Contracts Offices. Quality assurance documents such as the QAPP and SOPs are kept in hardcopy form by the EAF Administrative Assistant and in electronic form on the LAN and archive tapes. Laboratory notebooks, logbooks, and log sheets, along with sample handling and custody record, inspection and maintenance records, field data sheets, and other data entry sheets and forms are kept in the shipping and receiving room or the weighing room. Original data (routine and QC) from laboratory information systems and data downloaded from the samplers is kept on the LAN, backed up to a separate computer, and archived to tape. Data summary reports, formatted data submittals (to be specified by ARB), and QA reports are also kept on the LAN and stored on CD-ROM in addition to the other archive mechanisms. Other project-related documents such as project correspondence, articles, papers, presentations, or reports are maintained in hardcopy form by the EAF Administrative Assistant and on the LAN if available in electronic form.

DRI will archive all project samples in walk-in refrigerators for at least three years after project completion. The walk-in refrigerators are equipped with alarms and kept locked.

At ARB's request, DRI will furnish them with all electronic records by electronic transfer to a secure site. DRI will retain project data on its LAN. New or modified LAN files are backed up hourly to a separate backup computer. Each day, incremental backups are made to tape. The

incremental backup tapes are recycled after a month. Each month, complete backups are made to tape and stored indefinitely.

At the completion of the project, DRI will post project data to a secure website to which the ARB can have access or e-mail the data to select project personnel.

8. SAMPLING DESIGN

The sampling design for Phase I of this project can be divided into two parts: 1) sampling that will take place in the laboratory setting to produce source-related samples that can subsequently be analyzed by different analytical instruments or protocols; and 2) sampling that will take place at the Fresno Supersite to provide evaluation of different sampling/monitoring instruments under varying field conditions and to generate integrated filter samples that can subsequently be used to evaluate different analytical instruments and protocols for carbon analysis.

8.1 Laboratory Sampling Design

Figure 8-1 shows a schematic diagram of the dilution sampler to be used for Phase I of this project. Figure 8-2 shows the sampling train configuration. Table 8-1 lists the parameters to be measured and the sampling matrix for source samples generated in the laboratory setting. This matrix is based on preliminary testing conducted to date and may be modified as source testing continues.

Test aerosols from controlled combustion processes that are known to generate BC provide new knowledge about how thermal and optical methods respond to pure emissions and emissions combined with a known interferent (e.g., iron pentacarbonyl, a smoke suppressant added to fuels; ferric oxide, a potential oxidizer; or sodium chloride [NaCl], a potential catalyst). Methods for powders and combustion exhaust are being developed under U.S. EPA STAR Grant No. R831086 using the resuspension method of Chow et al. (1994). The number of tests on graphite and carbon black powders will be expanded in the STAR Grant Program to match the number of samples proposed here for more realistic soot and soot mixed with contaminants. Soot of increasing chemical complexity will be produced by standardized electric arc, acetylene or hexane flame, a small diesel generator, and burning a small honeycombed wooden block.

This will be sampled through a dilution source sampling system similar to that of Hildemann et al. (1989), characterized by Chang et al. (2004), according to the procedures of McDonald et al. (2000, 2003). The photoacoustic instrument will be operated during each of these experiments to provide a b_{abs} benchmark against which the thermal and optical EC and BC values can be compared. The quartz-fiber filters with different loadings, determined by a range of flow rates from 10 to 40 l/m, will allow the effect of light and heavy particle deposits on measurement results to be determined.

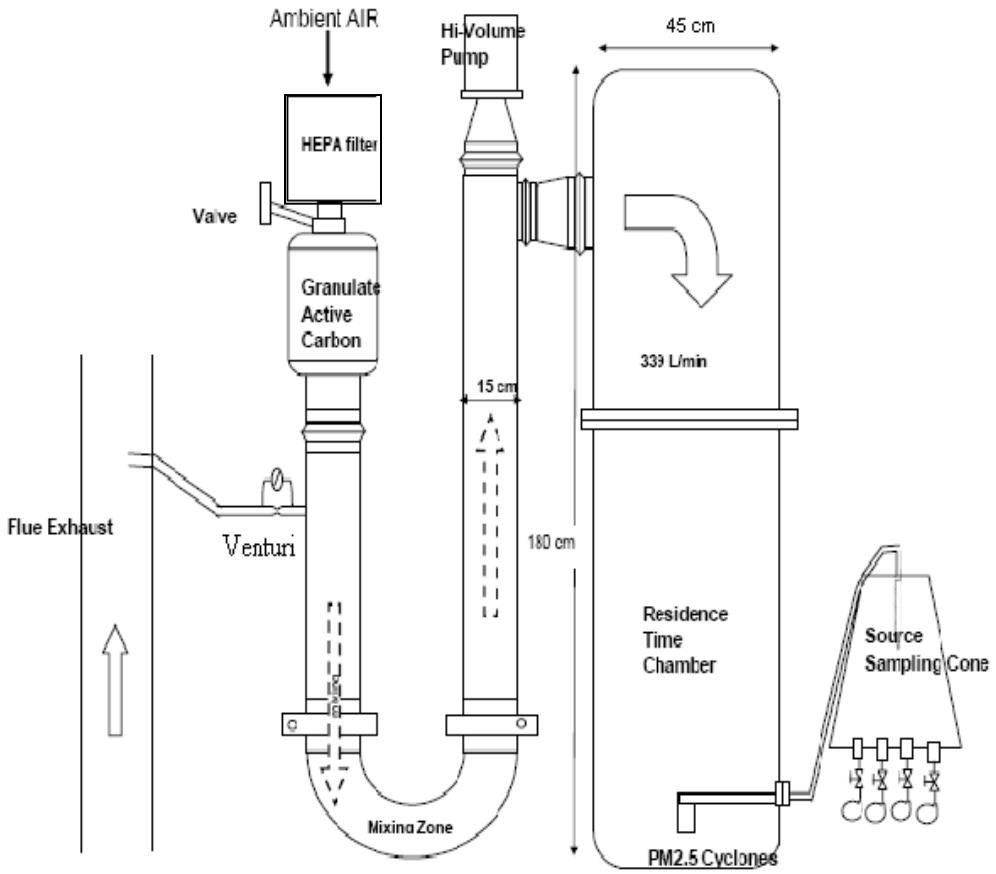

Figure 8-1. Schematic Diagram of Dilution Sampler.

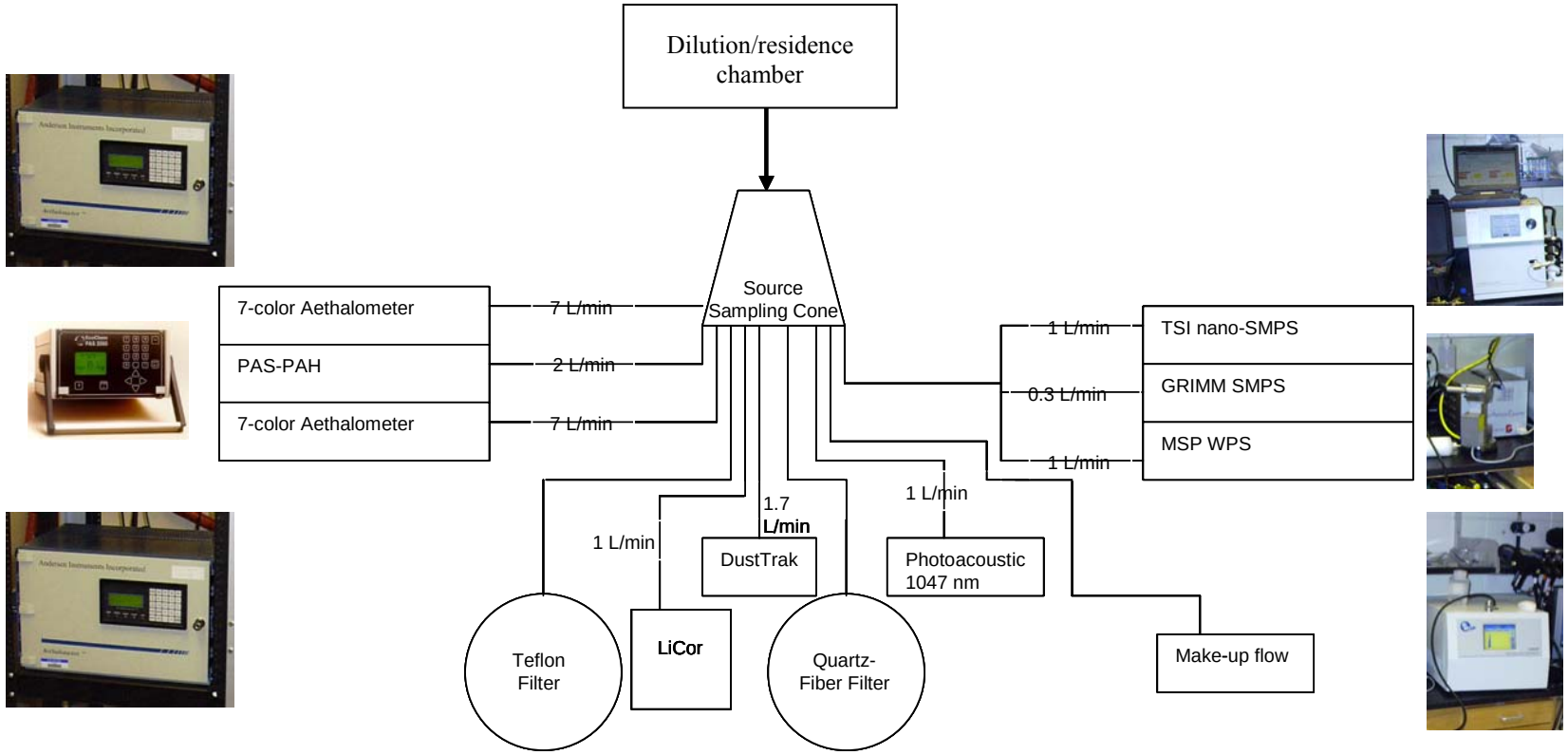

Figure 8-2. Sampling System Configuration.

Table 8-1. Sampling matrix for source samples generated in the laboratory setting

	Diesel particles*	PALAS Electric arc particles*	Wood smoke particles*	Acetylene soot particles*	Carbon powders
Estimated sampling time per one run	30 min (pre-run) 30 - 60 min (sampling) Total = 60 - 90 min	Total = 30 - 60 min	Total = 25 min	Total = 20 - 70 min	Total = 1 -2 hour
Conditions	4kW (32% engine load)	High and low current (arc rate) with medium Argon flow rate	4-5 lbs per load	2 inch flame	Nebulized @ 10psi
Estimated particle size	20-200 nm	20–100 nm	50-250 nm	50-250 nm	100-500 nm
Instruments to be used	Photoacoustic Aethalometer PAS WPS Nano SMPS GRIMM SMPS Dusttrak	Photoacoustic Aethalometer PAS WPS Nano SMPS GRIMM SMPS Dusttrak	Photoacoustic Aethalometer PAS WPS Nano SMPS GRIMM SMPS Dusttrak	Photoacoustic Aethalometer PAS WPS Nano SMPS GRIMM SMPS Dusttrak	Photoacoustic Aethalometer PAS WPS Nano SMPS GRIMM SMPS Dusttrak
Filter configuration	1 Q-Q for EC/OC 1 T-Q for Mass & b_{abs} Each in triplicate	1 Q-Q for EC/OC 1 T-Q for Mass & b_{abs} Each in triplicate	1 Q-Q for EC/OC 1 T-Q for Mass & b_{abs} Each in triplicate	1 Q-Q for EC/OC 1 T-Q for Mass & b_{abs} Each in triplicate	1 Q-Q for EC/OC 1 T-Q for Mass & b_{abs} Each in triplicate

* Each combustion source will be run with pure combustion aerosol and combustion aerosol mixed with an interferent.

8.2 Field Sampling Design

The sampling period and locations for the field studies are given in Sections 4.1 of this plan.

The Fresno Supersite provides a good infrastructure for field comparisons because it has instrument bays, power, security, and trained technicians and support staff that can be leveraged to benefit this project. Previous source apportionment studies (Chow et al., 1992, Schauer and Cass, 2000, Poore, 2000, Chow and Watson, 2002, Poore, 2002) show that $PM_{2.5}$ carbon at Fresno includes contributions from vegetative burning, cooking, diesel exhaust, gasoline exhaust, geological material, and secondary organic aerosol that vary throughout the year. Many of the sampling systems needed are already at the site (Tables 4-2 through 4-4). A mass and carbon comparison which was conducted during winter 2003 will be supplemented with a summer experiment to obtain a different source mixture. Of special use to this project will be the acquisition of large, pre-baked 406 cm^2 quartz-fiber filter samples on a high-volume (1130 L min-1) sampler with a $PM_{2.5}$ size-selective inlet (Andersen Instruments, Smyrna, GA). These allow for numerous punches that can be used for many different analysis protocols, in contrast to the smaller 47-mm diameter samples from the speciation samplers that permit a limited number of analyses.

9. SAMPLING METHODS REQUIREMENTS

In the field, operators will follow the Fresno Supersite field SOPs for operating instruments and handling samples. Table 12-1 summarizes laboratory, ambient monitoring, and source monitoring standard operating procedures applicable to this project. Installation and operation of the samplers and sites is the responsibility of CARB, field support contractors, and DRI. However, the following procedures will be used to prevent sample contamination or degradation.

- Sample Contamination Prevention:
  - Powder-free gloves will be worn when handling filters or filter holders
  - Filters will only be handled using plastic-coated tweezers
  - Filter holders will not be disassembled except at DRI's laboratory in accordance with SOPs to prevent contamination
  - Filters will be stored in static resistant Petri slides in the laboratory except when conditioned, pre-treated, weighed, or being loaded into holders
  - Filters/cassettes will be stored in static resistant containers and zip lock bags before shipping
- Temperature Preservation:
  - After sampling, filters will be kept cool (< 4 C°) during storage at a field location and during transport
  - Packages containing sampled filters will be loaded into coolers with frozen blue ice packs
  - Coolers will be shipped from the field location to DRI using overnight express service

10. SAMPLE HANDLING AND CUSTODY

Filter samples will be stored cold at the Fresno Supersite location and shipped or transported cold to DRI at the end of an intensive period. Filters will have a barcode or other unique identifiers that are entered on the field data sheet/chain of custody form (FDS). The filters are loaded into protective containers accompanied by their FDSs and shipped cold in coolers with blue ice. Samples at the laboratory are stored at 4 ºC until and following analysis; quartz-fiber filters are archived at -15 ºC for at least three years after project end.

Filters used in the source characterization laboratory will be transported by hand to the EAF in protective containers and are then handled similarly to field samples. Relevant SOPs are given in Table 12-1.

11. ANALYTICAL METHODS REQUIREMENTS

11.1 Overview

Figure 11-1 provides a general overview of the speciation filter processing and analysis activities.

Teflon-membrane filters received from the manufacturer are acceptance tested, which includes checking the filters for visual defects and analyzing a subset (typically 2%) for background levels of elements by XRF. Quartz fiber filters are also checked for visual defects and analyzed for background levels of anions by IC, ammonium by AC and soluble sodium and potassium by AA. Batches of filters that pass these acceptance tests are then cleared for use in field sampling.

Teflon-membrane filters are pre-conditioned for at least six weeks to allow for any out-gassing of material from the filter membrane, support ring and adhesive. This ensures stable and reproducible initial weights are obtained. Prior to initial weighing filters are equilibrated for at least 24 hours in the gravimetric laboratory at a temperature of 21.5 ± 2 °C and relative humidity of 35 ± 5 %RH. All initial weights are verified by a second analyst.

Quartz-fiber filters are pre-fired at 900 °C for at lease four hours to remove any residual carbon impurities. Two out of every 100 filters are analyzed for background levels of anions by IC, ammonium by AC, soluble sodium and potassium by AA and organic and elemental carbon by thermal methods. If any filter contains species above the levels specified in DRI analysis SOPs, then that batch of filters is not used for field sampling. Filter batches that pass acceptance testing are refrigerated (at < 4 °C) until needed.

Filters are loaded into filter cassettes in laminar flow hoods and then shipped to the field in coolers packed with blue ice.

After field sampling and transport back to the laboratory, filter holders are disassembled, filters conditioned for at least 24 hours at the same conditions used for pre-weighing, and then post-weighed (including 30% replicate weights). Sampler data are entered into the laboratory information system from the field data sheets. Mass concentrations in µg/m3 at ambient conditions are determined from the mass difference between the pre- and post-weights divided by the total volume of air sampled.

After post-weight gravimetric analysis is complete, the filters are returned to their Petri slides and stored under refrigeration until XRF analysis is started. After XRF analysis is completed the filters the filters are return to their Petri slides and stored under refrigeration until Level I data validation has been completed.

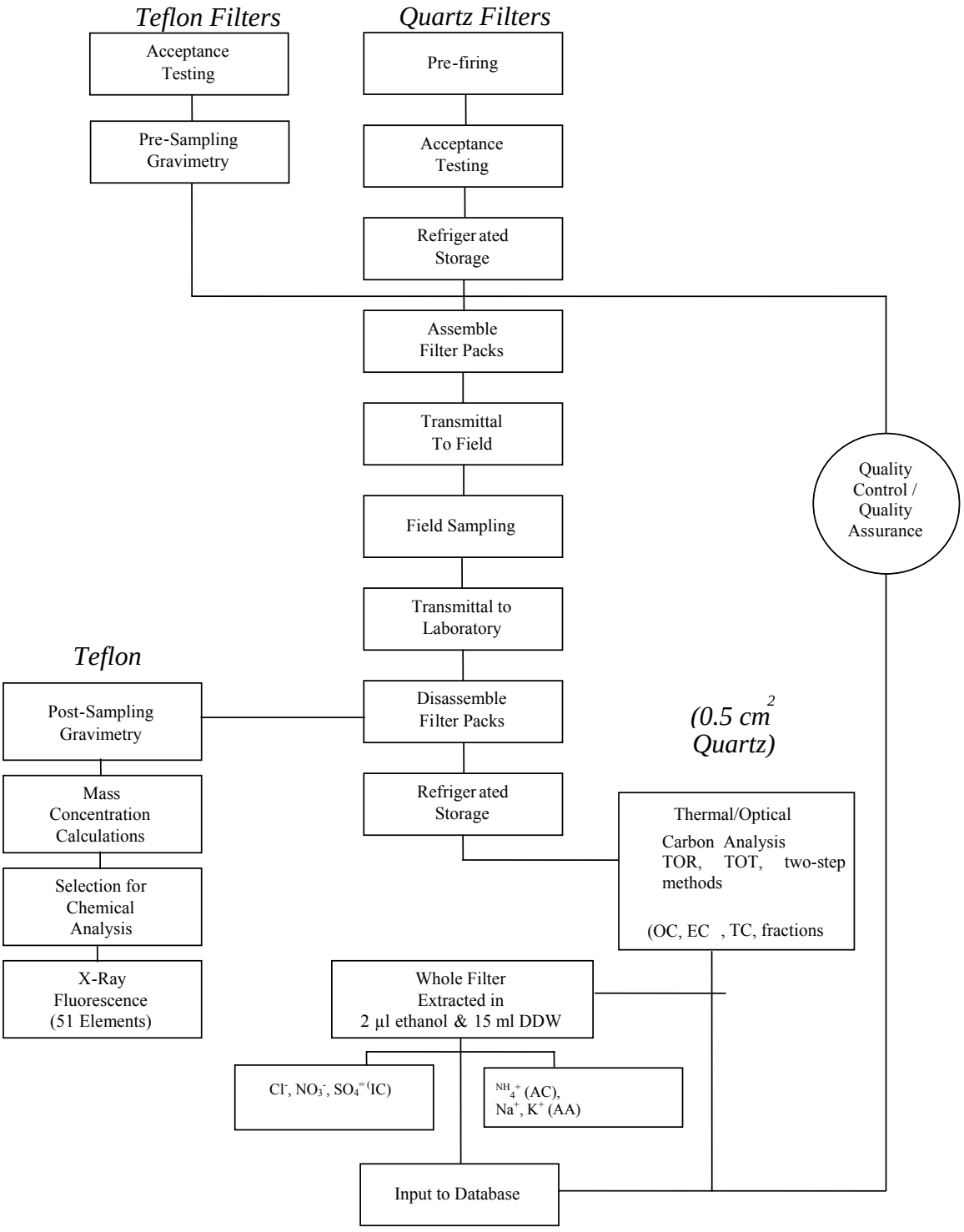

Figure 11-1. Overview of Speciation Filter Processing and Analysis Activities.

Data is entered into the laboratory information management system from the field data sheets. If available data downloaded from the samplers or monitors is transmitted to DRI and loaded into the project database. Mass concentrations in $\mu g/m^3$ at ambient conditions are determined from the mass difference between the pre- and post-weights divided by the total volume of air sampled. Elemental concentrations are determined from the XRF results in $\mu g/cm^2$, multiplied by the deposit area and divided by the sampled volume to get the concentration in µg/m3. Similarly, carbon species and fractions are determined from the carbon analysis instrument results in $\mu g/cm^2$, multiplied by the deposit area and divided by the sampled volume to get the concentration in $\mu g/m^3$. Ionic species are reported by the IC, AC and AA in µg/ml, then converted to µg/filter by multiplying by the extraction volume. Field blanks are treated and analyzed the same as samples.

11.2 Substrate Preparation

11.2.1 Speciation Teflon-membrane Filter Preparation

Teflon-membrane filters are removed from vendor boxes, identified by manufacturing batch number, given a DRI lot number, and kept in the weighing room environment for about a month. During this time, each filter is examined over a light table for pinholes, tears, visible contamination, and inhomogeneities. Filters with pinholes, discoloration, tears, or non-uniform texture are discarded or returned to the manufacturer for credit or replacement. After inspection, filters are placed in large glass Petri dishes that are labeled with the DRI lot number. DRI also performs chemical blank acceptance tests on about 4% of all these filters – approximately 2% undergo acceptance texts by XRF and another 2% undergo extraction and analysis by IC for potential contamination (if ion analysis is to be performed on the Teflon filter). Filters passing all tests are placed in equilibration trays. Batches of filters that fail to pass acceptable background concentration limits of 1 µg per 47 mm filter are removed from the queue.

Filters are then equilibrated in the weighing environment (i.e., mean temperature of 20 to 23 °C and standard deviation of < 2 °C; mean relative humidity [RH] of 30% to 40% and standard deviation of < 5% RH) in equilibration trays for at least three weeks. This procedure reduces the potential variability of blank concentrations to acceptable levels (within ±15 µg/filter for re-weights of 46.2 mm ringed Teflon-membrane filters).

When it is time to weigh the filters, they are placed into 47 mm plastic Petri slides and labeled with gummed, bar-coded, alphanumeric filter identification numbers. An alphanumeric ID is assigned to each filter. Each filter ID is scanned into a database and associated with its filter batch number and any acceptance test data. Filters are usually organized into batches of 40 to 50 Petri slides in ascending order by ID code. Approximately 2% of all filters are retained in the laboratory as laboratory blanks.

11.2.2 Speciation Quartz-fiber Filter Preparation

DRI will assign lot numbers and pre-treat the filters to reduce residual carbon content. Pre-treatment includes pre-firing the filters at 900 °C for three hours and allowing the filters to cool.

The filters are visually inspected over a light table for defects and discolorations. Approximately 2% of the filters then undergo carbon analysis blank acceptance tests. If any filter analyzed gives a measured blank value that exceeds 1.5 μg/cm^2 for OC, 0.5 μg/cm^2 for EC, or 2.0 μg/cm^2 for total carbon (TC), the filters from that batch will be either re-treated or rejected. Filter batches that pass the acceptance tests are placed in refrigerated storage (at < 4 °C) until the filters are ready to be loaded into filter holders prior to transport to the field.

Upon return to the DRI laboratory, the quartz filters will be removed from the holders, then placed in barcode-labeled Petri slides, and stored under refrigeration until they are analyzed. Each filter is removed from a cooler just before analysis. One or more punches are taken from the filter for analysis and the remainder of the filter is placed in the Petri slide and returned to the cooler. At least one second punch is taken from 10% of the filter samples for replicate analysis. At the end of the analysis day, all filters are removed from the cooler and placed in a refrigerator. After analysis results have been reviewed and the results approved, the Petri slides are placed into long-term archive storage under refrigeration. Quartz-fiber filters will be archived for at least three years after contract completion.

Further information on filter preparation may be found in the SOPs listed in Table 12-1.

11.3 Gravimetric Analysis

Petri slides containing filters are opened and equilibrated for at least 24-hours in a temperature- and relative humidity-controlled environment. To minimize particle volatilization and aerosol liquid water bias, $PM_{2.5}$ reference methods require that filters be equilibrated for 24 hours at a constant (within ±5%) relative humidity between 30% and 40% and at a constant (within ±2 °C) temperature between 20 °C and 23 °C. Nominal values of 35% RH and 21.5 °C best conserve the particle deposits during sample weighing, and these are maintained in the weighing room.

The weighing room is kept under positive pressure with HEPA filtered air. The microbalance is maintained in a laminar flow hood within which Petri dishes are opened to prevent contamination by human breath. The microbalance is placed on a marble stone to isolate it from building vibrations and to minimize biases during weighing. Filters are handled by experienced personnel wearing powderless gloves and weighed in batches of 40-50 on a Mettler Toledo MT5 microbalance with a sensitivity of ±0.001 mg (±1 μg). The balance is calibrated with Class 1.1 weights prior to every weighing session, and the calibration is verified after every 10 filters. The balance is re-calibrated if these performance tests show differences exceeding ±5 μg and the preceding set of 10 filters is re-weighed. The bar-code ID is scanned into the data acquisition system, and the filter is placed over a low-level radioactive source (500 picocuries of polonium210) prior to and during sample weighing. When the balance reading stabilizes, the mass is recorded by the data acquisition system and the filter is removed for placement in its open Petri slide. After the weighing, 100% of the filters are re-weighed in batches of 10 by another technician. If any of these re-weights deviate from the initial pre-weight by more than

±10 μg, then the balance is checked with a standard weight and the entire batch is re-weighed. The re-weighing of unexposed filters exceeds the requirements in the current EPA Section 2.12 guidance, but is necessary (based on DRI's experience in microgravimetric analysis) to ensure the accuracy and precision of the weights, since it is not possible to get a second pre-weight after a filter sample returns from the field and has a questionable post-weight.

For post-weighing, at least 30% of the weights are checked by an independent technician and samples are re-weighed if these check-weights do not agree with the original weights within ±0.015 mg. Pre- and post-weights, check weights, and re-weights (if required) are recorded on data sheets as well as being directly entered into a database via an RS232 connection. The estimated detection limit for $PM_{2.5}$ mass is about 0.2 $\mu g/m^3$ or 1.3% of the annual $PM_{2.5}$ NAAQS.

Table 11-1 gives the MDLs (determined from laboratory blanks) and LQLs (determined from field blanks for all species analyzed by gravimetry, ion chromatography and STN thermo-optical transmittance using 47 mm diameter filters and a sample volume of 24 m^3.

Table 11-1. Detection Limits for Mass, Ions, and Carbon Species.

Species	Symbol	Analysis Method	DRI ID	MDL[a] (µg/m^3)	LQL[b] (µg/m^3)
Mass	$PM_{2.5}$	Gravimetry	MSGC	0.2	0.3
Ions		IC			
Sulfate	$SO_4^=$		S4IC	0.0315	0.0028
Nitrate	NO_3^-		N3IC	0.0071	0.1796
Ammonium	NH_4^+	AC	N4IC	0.0011	0.0016
Sodium	Na^+	AA	NAIC	0.0007	0.0143
Potassium	K^+	AA	KPIC	0.0004	0.0397
Carbon		TOT			
Organic Carbon STN	OC		OCTC	0.5034	0.8310
Organic Carbon (TOR)	OCR	TOR	OCRC	0.5023	TBD
OC-Peak 1	Pk1_OC		O1TC	0.1199[c]	TBD
OC-Peak 2	Pk2_OC		O2TC	0.1489[c]	TBD
OC-Peak 3	Pk3_OC		O3TC	0.0668[c]	TBD
OC-Peak 4	Pk4_OC		O4TC	0.0185[c]	TBD
Pyrolized Carbon STN	PyrolC		OPTC	0.0045	TBD
Pyrolized Carbon (TOR)	OPR	TOR	OPRC	0.0000	TBD
Elemental Carbon	EC		ECTC	0.0308	0.1211
Elemental Carbon	ECR	TOR	ECRC	0.0326	TBD
EC-Peak 1	Pk1_EC		E1TC	0.0015[c]	TBD
EC-Peak 2	Pk2_EC		E2TC	0.0036[c]	TBD
EC-Peak 3	Pk3_EC		E3TC	0.0015[c]	TBD
EC-Peak 4	Pk4_EC		E4TC	0.0000[c]	TBD
EC-Peak 5	Pk5_EC		E5TC	0.0316[c]	TBD
Total Carbon	TC		TCTC	0.5029	0.5938

[a] The MDL is three times the standard deviation of mean concentrations of laboratory blanks, assuming a deposit area of 11.78 cm^2 and a sample volume of 24 m^3.

[b] The LQL is three times the standard deviation of mean concentrations of field blanks, assuming a deposit area of 11.78 cm^2 and a sample volume of 24 m^3.

[c] MDLs for carbon fractions are method dependent. It is not clear what they may truly represent. DRI will reassess these MDLs once sufficient data is obtained from field blanks to determine LQLs.

11.4 XRF Analysis for Elements

Energy dispersive X-ray Fluorescence (EDXRF) analysis will be performed on Teflon-membrane filters for at least the following 51 elements: sodium (Na), magnesium (Mg), aluminum (Al), silicon (Si), phosphorus (P), sulfur (S), chlorine (Cl), potassium (K), calcium (Ca), scandium (Sc), titanium (Ti), vanadium (V), chromium (Cr), manganese (Mn), iron (Fe), cobalt (Co), nickel (Ni), copper (Cu), zinc (Zn), gallium (Ga), arsenic (As), selenium (Se), bromine (Br), rubidium (Rb), strontium (Sr), yttrium (Y), zirconium (Zr), niobium (Nb), molybdenum (Mo), palladium (Pd), silver (Ag), cadmium (Cd), indium (In), tin (Sn), antimony

(Sb), cesium (Cs), barium (Ba), lanthanum (La), cerium (Ce), samarium (Sm), europium (Eu), terbium (Tb), hafnium (Hf), tantalum (Ta), tungsten or wolfram (W), iridium (Ir), gold (Au), mercury (Hg), thallium (Tl),lead (Pb) and Uranium (U). XRF analysis is performed on a PANalytical Epsilon 5 XRF analyzer. Currently, 10 separate XRF analyses are conducted by the PANalytical instrument on each sample to optimize the detection limits for the specified elements. Table 11-2 shows the detection limits for the elements in ng/cm2 and in µg/m3, based on an assumed filter deposit area of 11.78 cm^2 and a flow rate of 16.67 L/min for 24 hours (24 m^3 sampled air volume).

Two types of XRF standards are used for calibration, performance testing, and auditing: 1) vacuum-deposited thin-film elements and compounds from Micromatter Co. (Deer Harbor, WA); and 2) polymer films. The vacuum deposit standards cover all elements except for Ir, Ta, Zr, and Hf (which may be determined by interpolation) and are used as calibration standards. The polymer film and National Institute of Standards and Technology (NIST) standards are used as QC standards. During EDXRF analysis, filters are removed from their Petri slides, and loaded into the carousel for entry into the x-ray analysis chamber. The vacuum in the x-ray chamber and the heat induced by the absorption of x-rays may evaporate some materials, such as ammonium nitrate. A QC standard and a replicate from a previous analysis will be analyzed with each set of 10 filters. When a QC value differs from specifications by ±10% or more, or when a replicate value differs from the original value (where values exceed 10 times the detection limits) by ±10% or more, the previous 10 filters are reanalyzed. If further tests of standards show that the system calibration has changed by more than ±5%, the instrument is recalibrated. After XRF analysis, the Teflon-membrane filters are returned to their Petri slides and stored under refrigeration until the XRF data validation is completed and indicates that the runs were acceptable.

Table 11-2. Analytical Detection Limits for XRF Elements.

Element	Symbol	Atomic No.	DRI ID	Condition No.	MDL[a] (ng/cm^2)	MDL[a] ($\mu g/m^3$)[b]
Sodium	Na	11	NAXC	1	193	0.0946
Magnesium	Mg	12	MGXC	1	84	0.0411
Aluminum	Al	13	ALXC	1	34	0.0167
Silicon	Si	14	SIXC	1	25	0.0122
Phosphorous	P	15	PHXC	1	9	0.0045
Sulfur	S	16	SUXC	1	6	0.0029
Chlorine	Cl	17	CLXC	1	12	0.0058
Potassium	K	19	KPXC	1	5	0.0025
Calcium	Ca	20	CAXC	2	6	0.0027
Scandium	Sc	21	SCXC	2	5	0.0025
Titanium	Ti	22	TIXC	3	7	0.0036
Vanadium	V	23	VAXC	3	29	0.0140
Chromium	Cr	24	CRXC	3	33	0.0160
Manganese	Mn	25	MNXC	4	3	0.0017
Iron	Fe	26	FEXC	4	6	0.0029
Cobalt	Co	27	COXC	4	5	0.0023
Nickel	Ni	28	NIXC	4	4	0.0020
Copper	Cu	29	CUXC	4	13	0.0064
Zinc	Zn	30	ZNXC	4	4	0.0019
Gallium	Ga	31	GAXC	5	3	0.0013
Arsenic	As	33	ASXC	5	8	0.0039
Selenium	Se	34	SEXC	5	4	0.0021
Bromine	Br	35	BRXC	5	15	0.0073
Rubidium	Ru	37	RBXC	5	7	0.0035
Strontium	Sr	38	SRXC	6	14	0.0069
Yttrium	Y	39	YTXC	6	15	0.0076
Zirconium	Zr	40	ZRXC	7	14	0.0067
Niobium	Nb	41	NBXC	7	20	0.0100
Molybdenum	Mo	42	MOXC	7	13	0.0066
Palladium	Pd	46	PDXC	8	14	0.0071
Silver	Ag	47	AGXC	8	19	0.0094
Cadmium	Cd	48	CDXC	8	19	0.0093
Indium	In	49	INXC	8	55	0.0270
Tin	Sn	50	SNXC	9	74	0.0362
Antimony	Sb	51	SBXC	9	115	0.0564
Cesium	Cs	55	CSXC	10	107	0.0527
Barium	Ba	56	BAXC	10	120	0.0588
Lanthanum	La	57	LAXC	10	171	0.0842
Cerium	Ce	58	CEXC	10	193	0.0948
Samarium	Sm	62	SMXC	10	50	0.0247
Europium	Eu	63	EUXC	10	39	0.0190
Terbium	Tb	65	TBXC	10	71	0.0350
Hafnium	Hf	72	HFXC	5	19	0.0092
Tantalum	Ta	73	TAXC	5	24	0.0120
Wolfram	W	74	WOXC	5	3	0.0015
Iridium	Ir	77	IRXC	5	13	0.0062
Gold	Au	79	AUXC	5	15	0.0074
Mercury	Hg	80	HGXC	5	22	0.0106
Thallium	Tl	81	TLXC	5	21	0.0105
Lead	Pb	82	PBXC	5	8	0.0040
Uranium	U	92	URXC	6	4	0.0018

[a] The MDL is three times the standard deviation of mean concentrations of laboratory blanks

[b] Assumes a deposit area of 11.78 cm^2 and a sample volume of 24 m^3.

Detailed information on the XRF analysis of Teflon-membrane filters is given in SOP #2-209.1, X-Ray Fluorescence (XRF) Analysis of Aerosol Filter Samples (PANalytical Epsilon 5) listed in Table 12-1.

11.5 Extraction and Analysis of Anions and Cations

Water soluble ions (e.g., NO_3^-, $SO_4^=$, Na^+, NH_4^+, and K^+) are obtained by extracting one half of the quartz fiber filter in 15 ml of deionized distilled water (DDW). The filter half is placed in a polystyrene extraction vial and each vial is labeled with a barcode sticker containing the filter ID. Extraction tubes are placed in tube racks, and the extraction solutions are added. Extraction vials are capped and sonicated for 60 minutes, shaken for 60 minutes, and then aged overnight under refrigeration to ensure the complete extraction of deposited material in the solvent. The temperature of the ultrasonic bath is monitored to prevent temperature increases due to the dissipation of ultrasonic energy in the water. These extracts are stored under refrigeration prior to and after analysis.

Anion analyses are performed using a Dionex 500 IC system. The chemical compounds are identified by matching each peak with the retention times in the chromatograms of the standards. A DDW blank is analyzed after every 20 samples and a calibration standard is analyzed after every 10 samples in order to verify the baseline and calibration, respectively. Environmental Research Associates standards, traceable to NIST simulated rainwater standards, are used daily as an independent QC check. If values obtained for these QC standards do not coincide within a pre-specified uncertainty level (typically three standard deviations of the baseline level or ±5% of the average concentrations), the samples analyzed between that QC standard and the previous calibration standards are reanalyzed.

After analysis, the printout for each sample in the batch is reviewed for the following: 1) proper operational settings, 2) correct peak shapes and integration windows, 3) peak overlaps, 4) correct background subtraction, and 5) QC sample comparisons. When values for replicates (~10% replicate analyses) differ by more than ±10% or values for standards differ by more than ±5%, samples before and after these QC checks are designated for reanalysis in a subsequent batch. Individual samples with unusual peak shapes, overlapping peaks, background subtractions, or deviations from standard operating parameters are also designated for reanalysis.

Ammonium analysis is performed using an Astoria Pacific Automated Colorimetry system based on the Berthelot reaction (Berthelot, 1855). Indophenol blue, a blue dye, is formed when phenol and hypochlorite react with ammonium in an alkaline solution. Sodium nitroferricyanide is added to intensify the color.

The sample is drawn into the reaction coils by a peristaltic pump, mixed with alkaline phenol, sodium nitroferricyanide, sodium hypochlorite, and the disodium salt of ethylenediaminetetraacetic acid (EDTA), passed through a heated zone (37 °C for two minutes), and passed through a photocell detector. The absorbance at 660 nm is measured and converted

to µg/ml. Brij-35 is added as a surfactant to the EDTA solution to aid in bubble formation. Bubbles are introduced into the sample tubing to aid in mixing the reagents and to serve as delimiters between samples.

Soluble sodium and potassium analysis is performed using a Varian 880 atomic absorption spectrophotometer. A light beam from a hollow cathode lamp is directed through the flame, into a monochromator, and onto a photoelectric detector that measures the amount of light absorbed by the atomized element in the flame. The cathode of a hollow cathode lamp contains the pure metal which results in a line source emission spectrum. Since each element has its own characteristic absorption wavelength, the source lamp composed of that element is used. The amount of energy of the characteristic wavelength absorbed in the flame is proportional to the concentration of the element in the sample.

Further details on the extraction of ionic species from filter samples may be found in the SOPs listed in Table 12-1.

11.6 Carbon Analyses

A punch (~0.5 cm^2) from the quartz-fiber filter will be analyzed for OC, EC, TC, and carbon fractions by one of the three time-integrated thermal evolution methods described in Table 4-1 using the DRI Model 2001 thermal/optical carbon analyzer. Figure 11-2 shows the experimental configuration for carbon analyses using the DRI Model 2001 analyzer. Quartz-fiber filters used for the dilution sampler and the usual $PM_{2.5}$ speciation sampler are 47 mm in diameter and may yield up to 12 punches per filter. However, special high volume samplers were used for the summer and winter intensives at the Fresno supersite. These samplers used 8"x10" quartz-fiber filters which can yield up to 800 punches per filter for greater flexibility in method assessments.

The temperature sensors used to establish the temperature profiles are calibrated semiannually using a set of six Tempilaq° G (Tempil Inc., South Plainfield, NJ) quick-drying temperature indicating liquids of different melting points spanning the temperature range of 121 to 816 °C. Each indicator is certified accurate to ±1% of its designated temperature. The analyzer system is calibrated by analyzing samples of known amounts of methane, carbon dioxide, sucrose, and potassium hydrogen phthalate (KHP). The flame ionization detector (FID) response is the reference level of methane injected at the end of each sample analysis. Performance tests of each instrument are conducted with calibration with methane at the beginning and end of each day's operation. Intervening samples are re-analyzed when calibration changes of more than ±5% are observed. Twenty-two different standards are used for calibration of the carbon analyzer semi-annually. Widely accepted primary standards and/or reference materials for OC and/or EC are still lacking. Approximately 10% replicate punches are analyzed on an instrument chosen at random to determine precision.

The remaining quartz-fiber filters will be archived in Petri slides and stored at less than −15 °C for at least three years after contract completion.

Further information on the carbon analysis of quartz-fiber filters may be found in Table 12.1 of the SOPs.

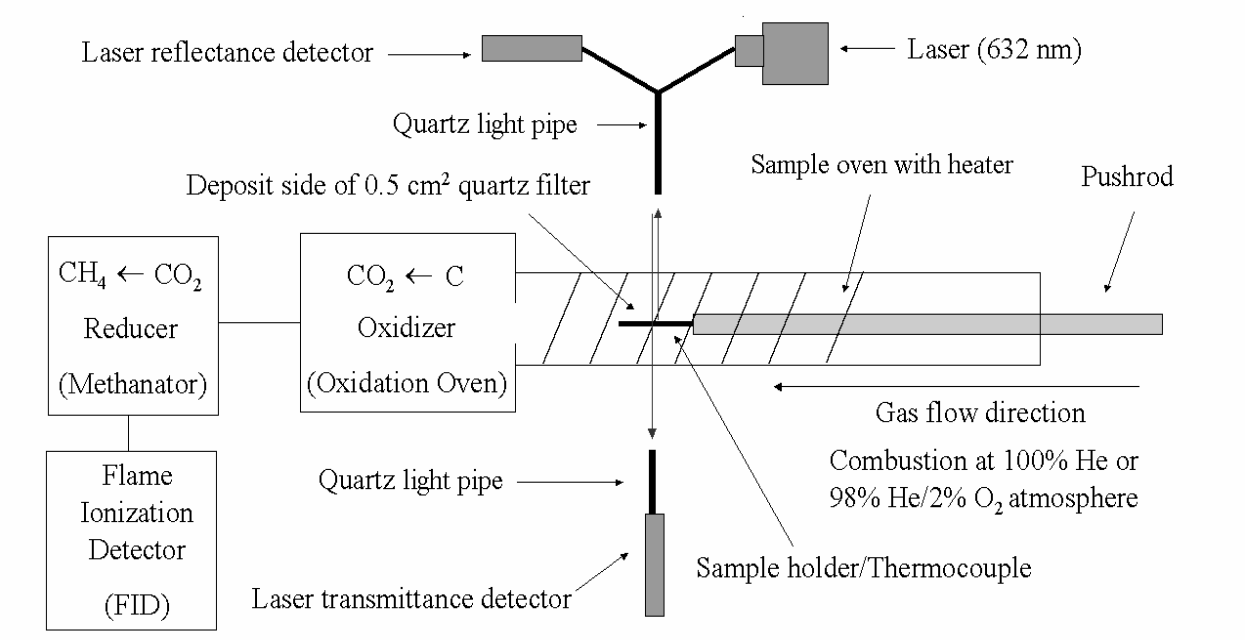

Figure 11-2. Experimental Configuration for Carbon Analysis Using DRI 2001 Thermal/Optical Carbon Analyzer.

12. QUALITY CONTROL REQUIREMENTS

Field sampling and monitoring and laboratory activities and analyses are described in detailed SOPs. Table 12-1 summarizes the SOPs applicable to this project.

12.1 Sampling

Table 12-2 summarizes some of the QC measures used for the sampling system in the source characterization laboratory. Flow rates are checked before and after each run using rotameters. Flow rates through the sample filters are checked every five minutes using TSI digital flow meters. The rotameters and digital flow meters are calibrated annually against a NIST-traceable Roots meter by the QA laboratory supervisor.

In addition, several QC blanks and filters are taken to assess system performance. A minimum of three dynamic blanks are taken for each source in which only the carbon sample is not generated. For each quartz-fiber filter collected in each run, two filter punches are taken – one at the center of the deposit area and the second at the outer edge of the deposit area – to assess potential filter inhomogeneity. Backup quartz-fiber filters are used during each run to assess potential adsorption of gaseous organic compounds.

Other QC measures are routinely taken to ensure proper system performance and valid measurement results. For example, all tubing form the sample plenum to measurement filters or instruments is made of conductive black tubing to minimize particle loss due to triboelectric and electrostatic effects. At the start of each day of sampling, the timing of all real-time instruments is synchronized to within 3 seconds and all size-selective impactors are cleaned. Prior to each run, all filters are visually inspected for physical integrity and flaws (such as pin holes, discoloration, tears, and noticeable inhomogeneities). At the end of each sampling day, all electronic data from real-time measurement devices are downloaded to a laptop and then uploaded to the DRI server.

Table 12-3 summarizes the QC measures for the continuous measurement instruments used for the source characterization laboratory sampling efforts. In general, each of these instruments has a set of internal checks which are performed daily before laboratory runs. Each instrument is returned to the manufacturer yearly for recalibration and factory maintenance.

12.2 QC for Laboratory Analyses

Laboratory QC measures are summarized in Tables 12-4 through 12-7 for $PM_{2.5}$ mass, ions, elements, and carbon, respectively. Further QC information may also be found in the laboratory SOPs in Table 12-1.

12.3 QC for Gravimetric Analyses

Table 12-4 summarizes the gravimetric analysis QC measures for $PM_{2.5}$ mass.

For pre-weighing, the balance is calibrated with Class 1.1 weights prior to every weighing session, and the calibration is verified after every 10 filters. The balance is re-calibrated if these performance tests show differences exceeding ±5 μg and the preceding set of 10 filters is re-weighed. The bar-code ID is scanned into the data acquisition system, and the filter is placed over a low-level radioactive source (500 picocuries of polonium210) prior to and during sample weighing. When the balance reading stabilizes, the mass is recorded by the data acquisition system and the filter is removed for placement in its open Petri container. After weighing, 100% of the filters are re-weighed in batches of 10 by another technician. If any of these replicate weights deviate from the initial pre-weight by more than ±10 μg, then the balance is checked with a standard weight and the filters which failed the replicate criteria are re-weighed.

Post-weight filters are weighed and 30% of the filters in each batch of 10 are selected by another technician and used for replicate weighing. If any of these re-weighing deviate from the initial post-weight by more than ±15 μg, the entire batch of filters is reweighed.

Microbalances are calibrated annually or more frequently as needed by a certified technician. The primary and working mass standards are recertified annually against NIST-traceable mass standards by a measures laboratory having a NIST certificate of traceability. The accuracy of the weighing room temperature and relative humidity (RH) sensors readings are checked annually using NIST-traceable standards by staff of the DRI QA laboratory.

Control charts of the temperature and humidity in the weighing room are printed each morning and examined to make sure that both are within limits before proceeding with weighing.

Additional information on gravimetric analysis QC measures may be found in the SOPs in Table 12-1.

Table 12-1. Summary of Standard Operating Procedures Applicable to this Project.

DRI SOP#	DRI SOP Title
Environmental Analysis Facility	
2-102.5	Gravimetric Analysis Procedure
2-104.3	Impregnating, Drying, and Acceptance Testing of Filters for Sampling Gases in Air
2-106.5	Pre-firing and Acceptance Testing of Quartz-Fiber Filters for Aerosol and Carbonaceous Material Sampling
2-107.2	Light Transmission Analysis Procedure
2-108.3	Sectioning of Teflon and Quartz Filter Samples
2-109.5	Extraction of Ionic Species from Filter Samples
2-110.4	Filter Pack Assembling, Disassembling, and Cleaning Procedure
2-111.5	Sample Shipping, Receiving, and Chain-of-Custody
2-112.2	$PM_{2.5}$ FRM Filter Pack Assembly, Disassembly, and Cleaning
2-113.2	$PM_{2.5}$ FRM Sample Shipping, Receiving, and Chain-of-Custody
2-114.2	$PM_{2.5}$ FRM Gravimetric Analysis
2-203.6	Anion Analysis of Filter Extracts and Precipitation Samples by Ion Chromatography
2-208.1	Cation Analysis of Filter Extracts and Precipitation Samples by Ion Chromatography
2-206.3	Analysis of Filter Extracts and Precipitation Samples by Atomic Absorption Spectroscopy
2-207.5	Analysis of Filter Extracts and Precipitation Samples for Ammonium by Automated Colorimetric Analysis
2-209.1	X-Ray Fluorescence Analysis of Aerosol Filter Samples (Panalytical Epsilon 5)
2-204.6	Thermal/Optical Reflectance Carbon Analysis of Aerosol Filter Samples – IMPROVE Protocol
2-216.4	DRI Model 2001 Thermal/Optical Carbon Analysis (TOR/TOT) of Aerosol Filter Samples – IMPROVE_A Protocol
2-201.2	DRI Model 2001 Thermal/Optical Carbon Analysis (TOR/TOT) of Aerosol Filter Samples – STN Protocol
2-218.1	DRI Model 2001 Thermal/Optical Carbon Analysis of Aerosol Filter Samples – French Two-Step Protocol
2-217.1	In-injection Port Thermal Desorption and Subsequent GC/MS Analysis of Non-Polar Organic Species in Aerosol Filter Samples
Field Instruments	
1-201.1	High Volume (Hi-Vol) Samplers: Operation, Maintenance, and Field Calibration
1-223.1	EcoTech High Volume Sampler (HiVol): Operation and Maintenance
1-226.1	Anderson Single Channel FRM Sampler (FRM): Operation and Maintenance
1-233.1	Andersen Reference Ambient Air Sampler (RAAS) 2.5-400 Chemical Speciation Monitor: Operation and Maintenance
1-221.1	MetOne Beta Attenuation Monitor: Operation and Maintenance
1-215.1	Kimoto SPM-613D Beta Gauge Monitor (BAM): Operation and Maintenance
1-236.1	Rupprecht and Patashnick (R&P) Series 1400a Tapered Element Oscillating Microbalance (TEOM): Operation and Maintenance
1-234.1	Rupprecht and Patashnick 8400N Ambient Particulate Nitrate Monitor: Operation and Maintenance
1-235.1	Rupprecht and Patashnick 8400S Ambient Particulate Sulfate Monitor: Operation and Maintenance
1-224.1	Sunset Laboratory Semi-Continuous OCEC Carbon Aerosol Analyzer: Operation and Maintenance
1-218.1	EchoChem Analytics Realtime Polycyclic Aromatic Hydrocarbon (PAH) Monitor PAS 2000: Operation and Maintenance
1-214.1	TSI DustTrak Photometer: Operation and Maintenance
1-416.1	Optec NGN2 Open-Air Integrating Nephelometer: Operation and Maintenance
1-415.1	Radiance Research Model 903 Nephelometer: Operation and Maintenance
1-413.1	EcoTech Nephelometer: Operation and Maintenance
1-414.1	TSI 3 wavelength Nephelometer: Operation and Maintenance
1-406.1	Magee Aethalometer: Operation and Maintenance
1-417.1	Radiance Research Particle Soot Absorption Photometer (PSAP): Operation and Maintenance
1-225.1	Multi-Angle Absorption Photometer (MAAP): Operation and Maintenance
1-407.1	DRI Photoacoustic Spectrometer (PA): Operation and Maintenance
1-211.1	TSI Scanning Mobility Particle Sizing Instrument (SMPS): Operation and Maintenance
1-212.1	GRIMM Scanning Mobility Particle Sizing + Counter Instrument (SMPS + C): Operation and Maintenance
1-213.1	MSP Wide-Range Particle Spectrometer (WPS): Operation and Maintenance
1-219.1	Climet Instruments SPECTRO 0.3: Operation and Maintenance
1-220.1	Particle Measuring Systems Lasair 1003: Operation and Maintenance
1-250.1	Resuspension of Bulk Samples onto Teflon and Quartz Filters
1-412.1	DRI Dilution Sampling System: Operation and Maintenance
1-216.1	DRI Monomodal Aerosol Generator: Operation and Maintenance

Table 12-2. QC Measures for Laboratory Sampling.

Requirement	Frequency	Calibration Standard	Performed By	Acceptance Criteria	Corrective Action
Flowmeter Calibrations					
Rotameters	1/year	NIST traceable Roots meter	QA laboratory supervisor	± 3%	Recalibrate
Digital flowmeters	1/year	NIST traceable Roots meter	QA laboratory supervisor	± 3%	Recalibrate
FlowChecks					
Initial and final flows	Before and after each laboratory run	Rotameters	System operator	± 10% of previous limits	Troubleshhoot system and check components and setting
Flowrates during run	Every 5 minutes during laboratory run	TSI digital flowmeter	System operator	± 10% of previous limits	Troubleshhoot system and check components and setting
QC Samples					
Dynamic blanks	>3 per sampling configuration	N/A	System operator	Within 3 σ of MDLs	Check system and filter lots
Inhomogeneity checks	Each run	N/A	System operator	± 10%	Repeat run
Backup filters	Each run	N/A	System operator	N/A	Quantify adsorption of gaseous organic compounds by quartz filters
Other QC Measures					
Visual inspection of filters	Each run	N/A	System operator	Filter integrity, no foreign objects, no discoloration, no pin holes, no inhomogeneities	Replace filter
Synchronize timing of real-time instruments	Daily	N/A	System operator	± 3 seconds	Redo synchronization
Clean sizing instrument impactors	Daily or hourly (depending on loading)	N/A	System operator	No noticeable deposits	Redo cleaning
Download data from all real-time instruments to server	Daily	N/A	System operator	Successful transfer of data	Redo transfer
Use conductive tubing for all sample lines from sampling cone to sample filters and real-time instruments	All times	N/A	System operator	Presence of black conductive tubing	Replace tubing

Table 12-3. Summary of QC Measures for Continuous Sampling Instruments.

Requirement	Frequency	Calibration Standard	Performed By	Acceptance Criteria	Corrective Action
Aethalometer Self Test	Daily	N/A	System operator	OK	Troubleshoot instrument per instruction manual
PAS Instrument Checks					
Light intensity	Daily	N/A	System operator	100 ±10%	Troubleshoot instrument per instruction manual
Pump	Daily	N/A	System operator	40 – 55%	Check pump
Flow rate	Daily	N/A	System operator	2.0 ±0.1 lpm	Troubleshoot instrument per instruction manual
Factory calibration	1/year	N/A	Manufacturer	N/A	N/A
Dusttrak					
Zero Calibration	Daily	Zero filter	System operator	± 0.001 mg/m^3	Calibrate zero
Factory calibration	1/year	N/A	Manufacturer	N/A	N/A
Grimm SMPS					
Internal Checks	Before each run	N/A	System operator	OK	Troubleshoot instrument per instruction manual
Factory calibration	1/year	N/A	Manufacturer	N/A	N/A
TSI Nano-SMPS					
Internal Checks	Daily	N/A	System operator	OK	Troubleshoot instrument per instruction manual
Factory calibration	1/year	N/A	Manufacturer	N/A	N/A
MSP WPS					
Internal Checks	Daily	N/A	System operator	OK	Troubleshoot instrument per instruction manual
Factory calibration	1/year	N/A	Manufacturer	N/A	N/A
Photoacoustic Instrument					
Internal Checks	Daily	N/A	System operator	OK	Troubleshoot instrument per instruction manual
Factory calibration	1/year	N/A	Manufacturer	N/A	N/A

Table 12-4. DRI Gravimetric Laboratory QC Measures.

Requirement	Frequency	Calibration Standard	Performed By	Acceptance Criteria
Lab Blanks	2/lot of 100	N/A	Analyst	±10 µg difference
Calibration/Verification				
Balance Calibration	1/year	NIST Class 1	Contractor	Manufacturer's specs.
Temp. Calibration	1/year	NIST-traceable	QA lab	±2 ºC
RH Calibration	1/year	NIST-traceable	QA lab	±2% RH
Accuracy				
Balance Check (200 mg Working Std.)	Start, 1/10 samples, end	NIST Class 1.1	Analyst	±5 µg
Calibration Standards				
Working Mass Stds. (NIST Class 1.1).	1/year	NIST Class 1	Contractor	60 µg
Primary Mass Stds. (NIST Class 1.1).	1/year	NIST Class 1	Contractor	25 µg
Precision				
Replicate Pre-Weight	Every sample	N/A	Independent Tech.	±10 µg
Replicate Post-Weight	30% of sample	N/A	Independent Tech.	±15 µg

12.4 QC for Ion (Anion and Cation) Analyses

Ion analyses are performed using a Dionex 500 IC system (anions), Astoria Pacific Automated Colorimeter (ammonium) and Varian 880 Atomic Absorption spectrophotometer (soluble sodium and potassium). For each type of analysis (i.e., anions and cations), standards used in generating the calibration curves are checked and remade, if necessary. A DDW blank is analyzed after every 20 samples and a calibration standard is analyzed after every 10 samples in order to verify the baseline and calibration, respectively. Environmental Research Associates standards, or other standards traceable to NIST simulated rainwater standards, are used daily as an independent QC check. If values obtained for these QC standards do not coincide within a pre-specified uncertainty level (typically three standard deviations of the baseline level or ±5% of the average concentrations), the samples analyzed between that QC standard and the previous calibration standards are reanalyzed.

After analysis, the instrument data for each sample in the batch is reviewed for the following: 1) proper operational settings; 2) correct peak shapes and integration windows; 3) peak overlaps; 4) correct background subtraction; and 5) QC sample comparisons. When values for replicates (~10% replicate analyses) differ by more than ±10% or values for standards differ by more than ±5%, samples before and after these QC checks are designated for reanalysis in a subsequent

batch. Individual samples with unusual peak shapes, overlapping peaks, background subtractions, or deviations from standard operating parameters are also designated for reanalysis.

More detailed information on the QC measures for ion analyses may be found in the SOPs in Table 12-1.

12.5 QC for XRF Elemental Analyses

Two types of XRF standards are used for calibration, performance testing, and auditing: 1) vacuum-deposited thin-film elements and compounds from Micromatter Co. (Deer Harbor, WA); and 2) polymer films. The vacuum deposit standards cover all elements except for Ir, Ta, Zr, and Hf (which may be determined by interpolation) and are used as calibration standards. The polymer film and NIST standards are used as QC standards. During EDXRF analysis, filters are removed from their Petri slides, and loaded into the sample chamber for entry into the x-ray analysis chamber.

The vacuum in the x-ray chamber and the heat induced by the absorption of x-rays may evaporate some materials, such as ammonium nitrate. A QC standard and a replicate from a previous analysis will be analyzed with each set of 10 filters. When a QC value differs from specifications by ±10% or more, or when a replicate value differs from the original value (where values exceed 10 times the detection limits) by ±10% or more, the previous 10 filters are reanalyzed. If further tests of standards show that the system calibration has changed by more than ±5%, the instrument is recalibrated.

12.6 QC for Carbon Analyses

The system is calibrated by analyzing samples of known amounts of methane, carbon dioxide, sucrose, and potassium hydrogen phthalate (KHP). The FID response is the reference level of methane injected at the end of each sample analysis. Performance tests of an instrument's calibration are conducted at the beginning and end of each day's operation. Intervening samples are re-analyzed when calibration changes of more than ±5% are observed. Known amounts of ACS-certified reagent grade crystal sucrose and KHP are analyzed by TOR to verify the organic carbon fractions. Fifteen different standards are used for each calibration. Widely accepted primary standards for OC and/or EC are still lacking. Approximately 10% replicate punches are analyzed on an instrument determined at random to determine precision.

Table 12-5. DRI Ion (Anion and Cation) Analysis QC Measures.

Requirement	Frequency	Calibration Standard	Performed By	Acceptance Criteria	Corrective Action
Multipoint Calibrations	Column change or retention time shift	Lab prepared or derived from ERA standards	Analyst	R2 > 0.997	Identify and correct problem before analyzing samples
Minimum Detection Limit (MDL)	Quarterly or after major instrument change	Lab blanks	Analyst, Project Manager	Within ±10% of previous limits	Troubleshoot IC instrument and check filter lots
Lower Quantifiable Limit (LQL)	Quarterly	Field blanks	Analyst, Project Manager	Within ±10% of previous limits	Troubleshoot IC instrument and check filters
QC Samples					
Reagent (DDW) blank	Daily, before analysis of samples, and 1/20 samples	DDW	Analyst	Within 3 σ of baseline	Samples before QC standard and previous standards reanalyzed
QC standard	1/10 samples	NIST traceable standard solutions	Analyst	±10%	Samples before QC standard and previous standards reanalyzed
NIST-traceable commercial standard solution	Daily, before analysis of samples	ERA mineral or nutrient standards	Analyst	±10%	Samples before QC standard and previous standards reanalyzed
Replicates	1/10 samples	Sample extract	Analyst	±10%	Reanalysis of sample
Chromatogram Review	Every sample	N/A	Analyst	No unusual peak shape, overlapping peaks, or background subtractions	Reanalysis of problem sample

Table 12-6. DRI Elemental Analysis by XRF QC Measures.

Requirement	Frequency	Calibration Standard	Performed By	Acceptance Criteria	Corrective Action
Multipoint Calibrations	1/6 months	QC standards	XRF lab supervisor	±5%	Recalibrate
Minimum Detection Limit (MDL)	Initially, then quarterly or after major instrument change	Lab blanks	XRF lab supervisor, Project Manager	Within ±10% of previous limits	Troubleshoot instrument and check filter lots
Lower Quantifiable Limit (LQL)	Quarterly	Field blanks	XRF lab supervisor, Project Manager	Within ±10% of previous limits	Troubleshoot instrument and check filters
QC Samples					
Lab blanks	1/20 samples	N/A	Analyst	Within 3 σ of MDLs	Check instrument and filter lots
QC standards	Daily	Micromatter thin films	Analyst	±10%	Samples before QC standard and previous standards reanalyzed
NIST-traceable standards	Weekly	Micromatter thin films	Analyst	±10%	Samples before QC standard and previous standards reanalyzed
Replicates	1/10 samples	N/A	Analyst	±10% when value >10*MDL	Reanalysis of previous samples
Level 1 Review	Every sample	N/A	XRF lab supervisor	Per SOP	Reanalysis of problem samples or flagging per SOP

Table 12-7. DRI Carbon Analysis QC Measures.

Requirement	Calibration Standard	Calibration Range	Calibration Frequency	Performed By	Acceptance Criteria	Corrective Action
System Blank Check	N/A	N/A	Beginning of analysis day	Carbon Analyst	≤ 0.2 µg C/cm^2	Check instrument and filter lots
Leak Check	N/A	N/A	Beginning of analysis day	Carbon Analyst	Oven pressure drops less than 0.01 per second	Locate leaks and fix
Laser Performance Check	N/A	N/A	Beginning of analysis day	Carbon Analyst	Transmittance >700 mv; Reflectance >1500 mv	Check laser and filter holder position
Calibration Peak Area Check	NIST 5% CH_4/Helium gas standard	20 µg C (Carle valve injection loop, 1000 µl)	Every analysis	Carbon Analyst	Counts >20,000 and 95-105% of average calibration peak area of the day	Discard analysis result and repeat analysis with second filter punch
Auto-Calibration Check	NIST 5% CH_4/Helium gas standard	20 µg C (Carle valve injection loop, 1000 µl)	Beginning of analysis day	Carbon Analyst	95-105% recovery and calibration peak area 90-110% of weekly average	Troubleshoot and correct system before analyzing samples
Manual Injection Calibration	NIST 5% CH_4/Helium or NIST 5% CO_2/Helium gas standards	20 µg C (Certified gas-tight syringe, 1000 µl)	End of analysis day	Carbon Analyst	95-105% recovery and calibration peak area 90-110% of weekly average	Troubleshoot and correct system before analyzing samples
Multiple Point Calibrations	1800 ppm Potassium hydrogen phthalate (KHP) and sucrose; NIST 5% CH_4/Helium and NIST 5% CO_2/Helium gas standards	9-36 µg C for KHP and sucrose; 2-30 µg C for CH_4 and CO_2	Six months	Carbon Analyst	All slopes ±5% of average	Troubleshoot instrument and repeat calibration until results are satisfactory
Sample Replicates	N/A	N/A	Every 10 analyses	Carbon Analyst on same or different analyzer	±10% when OC, EC, TC ≥ 10 µg C/cm^2 or < ±1 µg/cm^2 when OC, EC, TC < 10 µg C/cm^2	Investigate instrument and sample anomalies and rerun replicate if reason for poor result not found
Temperature Calibrations	Tempilaq^o G (Tempil, Inc., South Plainfield, NJ, USA)	Three replicates each of 121, 184, 253, 510, 704, 816 ºC	Six months, or whenever thermocouple is replaced	Carbon Analyst	Reflectance-based method gives a lower liquefying temperature than the transmittance-based method within ±2 °C	Troubleshoot instrument and repeat calibration until results are satisfactory
Oxygen Level in Helium Atmosphere	Certified gas-tight syringe	0-100 ppbv	Quarterly or whenever leak is detected	Carbon Analyst using a GC/MS system	Less than the certified amount of helium cylinder	Replace the helium cylinder and/or O_2 scrubber

12.7 Uncertainty Calculations

Uncertainty values include components of both the analytical and volumetric uncertainty. The analytical uncertainty reflects both the MDLs for the analysis and replicate precision. The reported uncertainties are estimated 1-sigma standard deviation values.

Other factors will also be considered when determining uncertainties. For example, the potential effect of the inhomogeneity of the filter deposit on carbon analysis results will be assessed by taking punches at both the center and edge of filters.

Section 5 of the most of the analytical SOPs given in Table 12-1 gives the formulas used to estimate uncertainty as does Section 5 of the data processing SOP.

12.8 Minimum Detection Limit

Minimum detection limits (MDLs) are determined as three times the standard deviation of the average concentration of more than seven blanks. The blanks are DDW samples for the ion analyses and laboratory blank filters for the other analyses. Tables 11-1 and 11-2 give the MDLs for the various species that were determined using the instruments and filters to be routinely used for the project.

12.9 Lower Quantifiable Limit

Lower quantifiable limits (LQLs) are determined as three times the standard deviation of the average concentration of more than seven field blanks. For ions, Table 11-1 gives the expected LQLs based on an analysis of 20 field blanks from the FRM program.

13. INSTRUMENT TESTING, INSPECTION, AND MAINTENANCE REQUIREMENTS

13.1 Sampling

Instrument testing, inspection, and maintenance for sampling are described in Section 2 of the SOPs listed in Table 12-1.

13.2 Laboratory Analysis and Support

Information on instrumentation, inspection, and maintenance requirements is given in Section 2 of the SOPs listed in Table12-1.

14. INSTRUMENT CALIBRATION AND FREQUENCY

The following subsections reference the instrument calibration procedures and frequency used by the DRI laboratory.

14.1 Sampling

Sampling instrument calibration and frequency is given in Sections 3.0 and 5.0 of the SOPs listed in Table 12-1.

14.2 DRI Laboratory

Information on instrument calibrations and frequency is given in Tables 12-4 through 12-7 of Section 12 of this QAPP and also in Sections 3.0 and 5.0 of the SOPs listed in Table 12-1.

15. INSPECTION/ACCEPTANCE REQUIREMENTS FOR SUPPLIES AND CONSUMABLES

Detailed information on inspection/acceptance requirements for supplies and consumables is generally given in Section 2.0 of the SOPs given in Table 12-1.

16. DATA ACQUSITION REQUIREMENTS (NON-DIRECT MEASUREMENTS)

Non-direct measurements may be used routinely for this project. Most indirect measurement data will be provided to DRI as a result of literature reviews and archived data in databases. DRI will review such data for reasonableness and consistency before they are used.

17. DATA MANAGEMENT

This section describes DRI's data management system for this project. It also discusses how the system enhances overall QA/QC program activities.

17.1 Overview

Data management encompasses four general tasks: 1) data processing; 2) data validation; 3) database development and maintenance; and 4) reporting. Additional aspects of reporting are discussed in Section 19 of this QAPP while additional aspects of data validation are discussed in Section 20.

This section provides a brief overview of the DRI data management system for the project. Inputs to the system include continuous instrument data (downloaded from the instruments and uploaded into a database), field data sheet (FDS) information entered manually usually with the aid of computerized data entry forms, scanned barcode identifiers for filters and other items, the analysis results from individual computers linked to analytical systems, and manually entered support information such as site information. Information from analytical and other laboratory computers are automatically transferred to intermediate databases or transferred by the analyst once a set of analysis runs are completed. In addition, the files on these computers are incrementally backed up nightly to special sections of the local area network (LAN). Information in intermediate databases are reviewed by the laboratory supervisor, laboratory coordinator, QA officer, and/or other personnel and transferred periodically to the main project database using a combination of automatic and manual file transfers. A series of built in check routines and report forms help to ensure that data are complete, consistent, and reasonable.

17.2 Data Processing

Data processing includes: 1) creating data sheets, forms, and logs on which project information are recorded; 2) recording information onto forms or into computer files; 3) entering recorded information into computer files; 4) downloading data files from instruments; 5) retrieving data from various files and instruments pertaining to a given sample or sampling event and relating them to one another; 6) combining data items in mathematical expressions to yield a desired result (e.g., species concentrations); 7) verifying data against earlier or redundant information, calibration records, or each other; and arranging data into desired formats for delivery to the client.

DRI uses a sophisticated SQL database system utilizing an MS Access front end for data entry and reporting that links laboratory instruments and data sets. The system encompasses a series of networked, stand-alone, and redundant computers. Individual computers in the weighing

room record scanned filter IDs and the results of gravimetric analyses, while another computer records environmental conditions. Other computers in the shipping and receiving area are used to keep track of shipments, filters received, and samples scheduled for analysis and to generate forms and barcode labels. Other laboratory computers may be used to enter FDS information using an MS Access database form that provides automatic screening and check features. Within each chemical speciation laboratory (e.g., x-ray fluorescence [XRF] lab, wet chemistry lab, carbon analysis lab) are one or more stand-alone computers that acquire and process the analytical data. Their data is incrementally backed up nightly to a special LAN area. When a batch of analyses is completed, the analyst transfers the data to the laboratory projects database for additional review by the laboratory coordinator and other researchers.

Several databases will be created as a part of Phase I (and also Phase II) that will be tailored for data analysis and uncertainty estimation. These include: 1) chemical concentrations from filters measured in laboratory tests and field comparisons (Phase I), 2) continuous measurements from laboratory tests and field tests (Phase I), 3) chemical concentrations from filters measured in source tests (Phase II), 4) continuous measurements from source tests (Phase II); 5) fuel-based $PM_{2.5}$ emission factors from this and other projects (Phase II);and 6) source profiles from this and other studies (Phase II). Each database will consist of a set of inter-related files with referential integrity in Microsoft Access tables. The following types of tables will be included in the project database:

Measurement locations: Each measurement location is identified with a unique alphanumeric site ID accompanied by its name and address, coordinates, elevation, and its primary operator, and a summary of measurements taken at the site for different monitoring periods. Coordinates are determined by global positioning system (GPS) using map basis NAD-83 (Federal Aviation Administration convention). The GPS time stamp is recorded to correct coordinate deviations. This is especially important for source tests that may be at various locations.

Variable definitions: Each variable is assigned a unique code that is accompanied by its definition, units, averaging time, measurement method, applicable temperature and pressure adjustments, and data reporting format.

Data validation flags: Flags specific to each measurement are translated into a common set of validation flags that are carried with each data point.

Data tables: Basic data tables are constructed in normalized formats that have the same structure for different types of data. Each record contains the site code, sample date (MM/DD/YYYY), sample time (HH:MM:SS PST), variable code, measurement value, measurement precision, validity code, and validation level. These files will be transparent to

most users and can be easily manipulated into convenient data analysis forms. Missing or invalid measurements contain a "NULL" value. Separate tables are produced for different averaging times and for non-uniform data sets.

Validation tables: Detailed information on specific samples indicating the nature of the data qualification. These tables also contain the validation level assigned to each data item.

Source description tables: Entries describe each of the source tests terms of the combustion source type, combustor, fuels, and test cycles. These are related to the continuous and integrated data sets.

17.3 Data Validation

Data validation is the most important function of data processing because it identifies deviations from measurement assumptions and procedures. Data validity levels are designated in the validation tables for different stages of data acquisition and interpretation. Level 0 designates data sets downloaded from a field instrument that have not been examined. These measurements are used to evaluate instrument performance and to forecast conditions for special experiments. Level 0 data are not used for interpretive purposes.

Level I data has been evaluated by the measurement investigator prior to submission to the database. Values are removed for instrument downtime and performance tests, adjustments for calibration deviations are applied, extreme values are investigated, internal comparisons are made, blanks are subtracted, precisions are estimated and propagated, and appropriate data qualification flags are assigned.

Level II data have completed intercomparison tests between datasets. These tests often result in the investigation of several samples that do not follow the same pattern as other measurements. These samples are investigated, sometimes re-analyzed, and re-designated as valid, invalid, or suspect as a result of the investigation.

Level III data validation occurs after measurements are used in data analysis and values that are found to be contradictory to other values have been investigated. The quality of these measurements is especially important because they often indicate large deviations from conventional wisdom that should not be confused with measurement error. The first assumption upon finding a measurement inconsistent with physical expectations is that the unusual value is due to a measurement error. If, upon tracing the path of the measurement, nothing unusual is found, the value can be assumed to be a valid result of an environmental cause. Unusual values are identified during the data interpretation process as the following: 1) extreme values; 2)

values that would normally track the values of other variables in a time series; and 3) values for observables that would normally follow a qualitatively predictable spatial or temporal pattern.

17.4 Database Development and Maintenance

Database development tasks include designing enhancements to the existing databases to add new elements, merge and calculate additional information, and develop new forms and routines for database entry, retrievals, and reports, as needed. Database maintenance procedures include archiving old files, providing for increased storage as needed, recovering from extended power outages, trouble shooting problems as they may arise, providing secure access to certain sites for data uploads while protecting DRI networks behind a firewall, and providing backups and redundancies in data storage.

DRI's EAF computers, laboratory information management systems, and databases are all based on PCs and networked into a number of LANs. Uninterruptible power supplies (UPSs) and backup generators are provided for analytical instrumentation and their associated computers and network server PCs. DRI includes redundant platforms for storing the database information. All final sampler and laboratory data will be stored in a database residing on the DRI EAF LAN server. The LAN server files are incrementally backed up every two hours to a second hard drive and are mirrored nightly to a second backup computer. In addition, incremental backups are made to tape daily. A complete backup to tape is performed weekly and archived indefinitely (at least five years) to the database. Access to the LAN is password protected. Raw data is handwritten on data sheets, transferred using an electronic form, and stored on a laboratory computer which writes the data to two disks. The data are then written to an SQL database and ASCII files. The SQL database is replicated on a backup computer nightly. DRI writes the database to DVD weekly. The DVDs are stored in a special fireproof and waterproof storage area. Monthly DVDs are stored off site.

17.5 Reporting

For Phase I of this project, DRI will provide reports of validated continuous data and integrated chemical data of samples from field and lab measurements, and QA/QC metadata.

18. ASSESSMENTS AND RESPONSE ACTIONS

The following general assessments will be performed:

- surveillance
- peer review
- systems audits
- performance audits
- audits of data quality
- data quality assessments

Table 4-5 in Section 4.4 of this plan provides further information about the performance assessments to be performed for this project.

As part of routine surveillance of project work, the DRI PI will routinely check the status of analyses, shipments, data reports, and invoicing. The DRI PI will also review project data after they have undergone routine review by the laboratory coordinator and support staff. Data will be checked for traceability and data quality by the QA Officer and all data reports and the final report will be peer reviewed by the parties involved.

DRI will respond to any findings of any of the assessments made and take and document any necessary corrective actions. The DRI PI and QA officer will approve a formal response that commits DRI to implement specified corrective actions.

19. REPORTS TO MANAGEMENT

For Phase I of this project, DRI will prepare the following reports and revise them as needed during the project period:

- Quality Assurance Project Plan

- Standard Operating Procedures

In addition, DRI will provide progress report(s) and invoices to ARB:

The final report for Phase I (which will constitute the interim report of this project) will include:

- text and tables describing OC, EC, and BC measurement methods and previous comparison studies;

- procedures for generating test aerosols;

- calibration and audit procedures and results;

- methods for generating and sampling test aerosols;

- descriptions of field comparison data bases;

- results of laboratory and field comparison and evaluation studies; and

- conclusions about different OC, EC, BC, and b_{abs} measurement methods

Appendices will include descriptions of the data bases compiled in this project, which will also be made available in electronic format. Several bound paper copies and a PDF electronic copy of the report will be delivered.

20. DATA REVIEW, VALIDATION, AND VERIFICATION REQUIREMENTS

Detailed information on data processing and data validation are given in Sections 6.4 and 6.5 of the instrumental analysis SOPs listed in Table 12-1 and SOP #3-003.4, Dry Deposition Field, Mass, and Chemical Data Processing and Data Validation.

Section 17.3 of this QAPP also discusses aspects of data review and validation.

21. VALIDATION AND VERIFICATION METHODS

Data processing and validation are discussed in Section 17. Section 20 provides additional information on data review, validation, and verification requirements.

22. RECONCILIATION WITH DATA QUALITY OBJECTIVES

Data validation is described in Sections 17 of this QAPP. Substantial comparisons among measurements will be made to determine their equivalence, comparability, and predictability. Although the different observables measured are diverse, it is possible that they may be highly correlated. The DRI, PI, data analysts, and QA officer will review the data for corrections, completeness, traceability, and conformance with data quality and MQOs. In addition, ARB will conduct its review of reports and databases as part of the project management. Scientific papers will be submitted to external peer review, and the resulting comments will be addressed in finally published papers.

Confidence in study conclusions will be evaluated according to the following criteria: 1) high confidence: low uncertainty in the data or data analysis approach, or more than one independent analysis approach, each of which has moderate uncertainties; 2) medium confidence: moderate uncertainty in the data or data analysis approach and independent analysis approaches were not applied; and 3) low confidence: large uncertainty in the data or data analysis approach and independent analysis approaches were not applied or were contradictory.

Success of the project will be evaluated in terms of: 1) accuracy, precision, validity, and completeness of acquired data; 2) extent to which data can be used to achieve project objectives; 3) confidence in study conclusions; 4) consistency of comparisons and emission factors from this project with those from other studies; 5) integration with other research studies and databases; 6) leveraging of this project with resources available from other projects; and 7) relevance of study results to global warming studies.

The final report will discuss accomplishments with respect to each of these areas. The first topic will be assessed by the data qualification statement described above. The second topic will be assessed by the data analysts as they use the acquired measurements to test the hypotheses. The databases will allow analysts to quickly integrate measurements that are most convenient for their tasks. Consistency with other studies will result from comparing field test (Phase I) and source emission factors (Phase II) and profiles (Phase II) with those of other studies. This will be facilitated by use of the relational database that will contain these values.

23. REFERENCES

Ackerman, A.S.; Toon, O.B.; Stevens, D.E.; Heymsfield, A.J.; Ramanathan, V.; and Welton, E.J. (2000). Reduction of tropical cloudiness by soot. *Science*, **288**(5468):1042-1047.

Akhter, M.S.; Chughtai, A.R.; and Smith, D.M. (1984). Reactions of hexane soot with NO_2/N_2O_4. *Journal of Physical Chemistry*, **88**:5334-5342.

Akhter, M.S.; Chughtai, A.R.; and Smith, D.M. (1985). The structure of hexane soot I. Spectroscopic studies. *Applied Spectroscopy*, **39**(1):143-153.

Arnott, W.P.; Moosmüller, H.; Rogers, C.F.; Jin, T.; and Bruch, R. (1999). Photoacoustic spectrometer for measuring light absorption by aerosol: Instrument description. *Atmos. Environ.*, **33**(17):2845-2852.

Arnott, W.P.; Moosmüller, H.; Sheridan, P.J.; Ogren, J.A.; Raspet, R.; Slaton, W.V.; Hand, J.L.; Kreidenweis, S.M.; and Collett, J.L., Jr. (2003). Photoacoustic and filter-based ambient aerosol light absorption measurements: Instrument comparison and the role of relative humidity. *J. Geophys. Res.*, **108**(D1):AAC 15-1-AAC 15-11.

Battye, W.; and Boyer, K. (2002). Catalog of global emissions inventories and emissions inventory tools for black carbon, Draft report. Report No. EPA Contract No. 68-D-98-046. Prepared for U.S. Environ. Protection Agency, Research Triangle Park, NC, by EC/R Incorporated, Chapel Hill, NC.

Berkson, J. (1950). Are there two regressions? *J. Am. Stat. Assoc.*, **45**:164-180.

Bevington, P.R. (1969). *Data Reduction and Error Analysis for the Physical Sciences*. McGraw Hill, New York, NY.

Birch, M.E.; and Cary, R.A. (1996a). Elemental carbon-based method for monitoring occupational exposures to particulate diesel exhaust. *Aerosol Sci. Technol.*, **25**(3):221-241.

Birch, M.E.; and Cary, R.A. (1996b). Elemental carbon-based method for occupational monitoring of particulate diesel exhaust: Methodology and exposure issues. *Analyst*, **121**:1183-1190.

Bond, T.C.; Anderson, T.L.; and Campbell, D.E. (1999). Calibration and intercomparison of filter-based measurements of visible light absorption by aerosols. *Aerosol Sci. Technol.*, **30**(6):582-600.

Bond, T.C.; Charlson, R.J.; and Heintzenberg, J. (1998). Quantifying the emission of light-absorbing particles: Measurements tailored to climate studies. *Geophys. Res. Lett.*, **25**(3):337-340.

Bond, T.C.; Streets, D.G.; Fernandes, S.; Nelson, S.M.; Yarber, K.F.; Woo, J.H.; and Klimont, Z. (2002). Black carbon inventories. Presentation at the "Air Pollution as a Climate Forcing" workshop in Honolulu, HI, Apr. 29, 2002.

Cachier, H.; Bremond, M.P.; and Buat-Ménard, P. (1989a). Determination of atmospheric soot carbon with a simple thermal method. *Tellus*, **41B**(3):379-390.

Cachier, H.; Bremond, M.P.; and Buat-Ménard, P. (1989b). Thermal separation of soot carbon. *Aerosol Sci. Technol.*, **10**(2):358-364.

Cass, G.R.; Boone, P.M.; and Macias, E.S. (1982). Emissions and air quality relationships for atmospheric carbon particles in Los Angeles. In *Particulate Carbon: Atmospheric Life Cycle*, G.T. Wolff and R.L. Klimisch, Eds. Plenum Press, New York, NY, pp. 207-243.

Chang, M.C.; Chow, J.C.; and Watson, J.G. (2004). Characterization of particulate emissions from casting processes using a dilution sampling system. A preliminary study to optimize the dilution sampling system in a foundry process, draft report. Prepared for Technikon LLC, McClellan, CA, by Desert Research Institute, Reno, NV.

Charlson, R.J.; Schwartz, S.E.; Hales, J.M.; Cess, R.D.; Coakley, J.A., Jr.; Hansen, J.E.; and Hofmann, D.J. (1992). Climate forcing by anthropogenic aerosols. *Science*, **255**:423-430.

Chen, L.-W.A.; Chow, J.C.; Watson, J.G.; Moosmüller, H.; and Arnott, W.P. (2004). Modeling reflectance and transmittance of quartz-fiber filter samples containing elemental carbon particles: Implications for thermal/optical analysis. *J. Aerosol Sci.*, **35**(6):765-780.

Chow, J.C.; and Watson, J.G. (2002). Review of $PM_{2.5}$ and PM_{10} apportionment for fossil fuel combustion and other sources by the chemical mass balance receptor model. *Energy & Fuels*, **16**(2):222-260. http://pubs3.acs.org/acs/journals/doilookup?in_doi=10.1021/ef0101715.

Chow, J.C.; Watson, J.G.; Crow, D.; Lowenthal, D.H.; and Merrifield, T.M. (2001). Comparison of IMPROVE and NIOSH carbon measurements. *Aerosol Sci. Technol.*, **34**(1):23-34.

Chow, J.C.; Watson, J.G.; Houck, J.E.; Pritchett, L.C.; Rogers, C.F.; Frazier, C.A.; Egami, R.T.; and Ball, B.M. (1994). A laboratory resuspension chamber to measure fugitive dust size distributions and chemical compositions. *Atmos. Environ.*, **28**(21):3463-3481.

Chow, J.C.; Watson, J.G.; Lowenthal, D.H.; Solomon, P.A.; Magliano, K.L.; Ziman, S.D.; and Richards, L.W. (1992). PM_{10} source apportionment in California's San Joaquin Valley. *Atmos. Environ.*, **26A**(18):3335-3354.

Chow, J.C.; Watson, J.G.; Pritchett, L.C.; Pierson, W.R.; Frazier, C.A.; and Purcell, R.G. (1993). The DRI Thermal/Optical Reflectance carbon analysis system: Description, evaluation and applications in U.S. air quality studies. *Atmos. Environ.*, **27A**(8):1185-1201.

Chuang, C.C.; Penner, J.E.; Taylor, K.E.; Grossman, A.S.; and Walton, J.J. (1997). An assessment of the radiative effects of anthropogenic sulfate. *J. Geophys. Res.*, **102**(D3):3761-3778.

Cooke, W.F.; Liousse, C.; Cachier, H.; and Feichter, J. (1999). Construction of a 1 degrees x 1 degrees fossil fuel emission data set for carbonaceous aerosol and implementation and radiative impact in the ECHAM4 model. *J. Geophys. Res.*, **104**(D18):22137-22162.

Cooke, W.F.; and Wilson, J.J.N. (1996). A global black carbon aerosol model. *J. Geophys. Res.*, **101**:19395-19409.

Countess, R.J. (1990). Interlaboratory analyses of carbonaceous aerosol samples. *Aerosol Sci. Technol.*, **12**:114-121.

Currie, L.A.; Benner, B.A., Jr.; Cachier, H.; Cary, R.; Chow, J.C.; Druffel, E.R.M.; Eglinton, T.I.; Gustafsson, Ö.; Hartmann, P.C.; Hedges, J.I.; Kessler, J.D.; Kirchstetter, T.W.; Klinedinst, D.B.; Klouda, G.A.; Marolf, J.V.; Masiello, C.A.; Novakov, T.; Pearson, A.; Prentice, K.M.; Puxbaum, H.; Quinn, J.G.; Reddy, C.M.; Schmid, H.; Slater, J.F.; Watson, J.G.; and Wise, S.A. (2002). A critical evaluation of interlaboratory data on total, elemental, and isotopic carbon in the carbonaceous particle reference material, NIST SRM 1649a. *J. Res. National Bureau Standards*, **107**(3):279-298.

Gillies, J.A.; and Gertler, A.W. (2000). Comparison and evaluation of chemically speciated mobile source $PM_{2.5}$ profiles. *J. Air Waste Manage. Assoc.*, **50**(8):1459-1480.

Hansen, A.D.A.; Rosen, H.; and Novakov, T. (1984). The aethalometer - An instrument for the real-time measurement of optical absorption by aerosol particles. *Sci. Total Environ.*, **36**:191-196.

Hansen, J.; and Nazarenko, L. (2004). Soot climate forcing via snow and ice albedos. *Proc. Natl. Acad. Sci. U. S. A*, **101**(2):423-428. www.pnas.org/cgi/doi/10.1073/pnas.2237157100.

Hemeon, W.C.; Haines, G.F., Jr.; and Ide, H.M. (1953). Determination of haze and smoke concentrations by filter paper samples. *Air Repair*, **3**:22-28.

Hildemann, L.M.; Cass, G.R.; and Markowski, G.R. (1989). A dilution stack sampler for collection of organic aerosol emissions: Design, characterization and field tests. *Aerosol Sci. Technol.*, **10**(10-11):193-204.

Hill, A.S.G. (1936). Measurement of the optical densities of smokestains of filter papers. *Trans. Faraday Soc.*, **32**:1125-1131.

Horvath, H. (1993). Atmospheric light absorption - A review. *Atmos. Environ.*, **27A**(3):293-317.

Huebert, B.J.; and Charlson, R.J. (2000). Uncertainties in data on organic aerosols. *Tellus*, **52B**(5):1249-1255.

Huntzicker, J.J.; Johnson, R.L.; Shah, J.J.; and Cary, R.A. (1982). Analysis of organic and elemental carbon in ambient aerosols by a thermal-optical method. In *Particulate Carbon: Atmospheric Life Cycle*, G.T. Wolff and R.L. Klimisch, Eds. Plenum Press, New York, NY, pp. 79-88.

IPCC (2001). *Climate Change 2001: The Scientific Basis,* J.T. Houghton, Ed. Cambridge University Press, Cambridge.

Jacobson, M.Z. (2000). A physically-based treatment of elemental carbon optics: Implications for global direct forcing of aerosols. *Geophys. Res. Lett.*, **27**:217-220.

Jacobson, M.Z. (2002). Control of fossil-fuel particulate black carbon plus organic matter, possibly the most effective method of slowing global warming. *J. Geophys. Res.*, **107**(D19):ACH 16-1-ACH 16-22.

Johnson, R.L. (1981). Development and evaluation of a thermal/optical method for the analysis of carbonaceous aerosol. M.S. Thesis, Oregon Graduate Center, Beaverton, OR.

Kendall, M.G. (1951). Regressions, structure and functional relationship, Part I. *Biometrika*, **39**:96-108.

Lin, C.I.; Baker, M.B.; and Charlson, R.J. (1973). Absorption coefficient of atmospheric aerosol: A method for measurement. *Appl. Opt.*, **12**(6):1356-1363.

Liousse, C.; Cachier, H.; and Jennings, S.G. (1993). Optical and thermal measurements of black carbon aerosol content in different environments: Variation of the specific attenuation cross-section, sigma (σ). *Atmos. Environ.*, **27A**(8):1203-1211.

Lloyd, A.C.; and Cackette, T.A. (2001). 2001 Critical review - Diesel engines: Environmental impact and control. *J. Air Waste Manage. Assoc.*, **51**(6):809-847.

Lowenthal, D.H.; Zielinska, B.; Chow, J.C.; Watson, J.G.; Gautam, M.; Ferguson, D.H.; Neuroth, G.R.; and Stevens, K.D. (1994). Characterization of heavy-duty diesel vehicle emissions. *Atmos. Environ.*, **28**(4):731-743.

Madansky, A. (1959). The fitting of straight lines when both variables are subject to error. *J. Am. Stat. Assoc.*, **54**:173-205.

Mathai, C.V.; Watson, J.G.; Rogers, C.F.; Chow, J.C.; Tombach, I.H.; Zwicker, J.O.; Cahill, T.A.; Feeney, P.J.; Eldred, R.A.; Pitchford, M.L.; and Mueller, P.K. (1990). Intercomparison of ambient aerosol samplers used in western visibility and air quality studies. *Enivron. Sci. Technol.*, **24**(7):1090-1099.

McDonald, J.D.; Zielinska, B.; Fujita, E.M.; Sagebiel, J.C.; Chow, J.C.; and Watson, J.G. (2000). Fine particle and gaseous emission rates from residential wood combustion. *Environ. Sci. Technol.*, **34**(11):2080-2091.

McDonald, J.D.; Zielinska, B.; Sagebiel, J.C.; and McDaniel, M.R. (2003). Characterization of fine particle material in ambient air and personal samples from an underground mine. *Aerosol Sci. Technol.*, **36**:1033-1044.

Molina, L.T. (1992). Global emission inventory activity (GEIA). Prepared by International Global Atmospheric Chemistry Core Project Office, Cambridge, MA.

Moosmüller, H.; Arnott, W.P.; and Rogers, C.F. (1997). Methods for real-time, *in situ* measurement of aerosol light absorption. *J. Air Waste Manage. Assoc.*, **47**(2):157-166.

Patashnick, H.; Rupprecht, G.; Ambs, J.L.; and Meyer, M.B. (2001). Development of a reference standard for particulate matter mass in ambient air. *Aerosol Sci. Technol.*, **34**(1):42-45.

Penner, J.E.; Charlson, R.J.; Hales, J.M.; Laulainen, N.S.; Leifer, R.; Novakov, T.; Ogren, J.; Radke, L.F.; Schwartz, S.E.; and Travis, L. (1994). Quantifying and minimizing uncertainty of climate forcing by anthropogenic aerosols. *Bull. Am. Meteor. Soc.*, **75**:375-400.

Penner, J.E.; Eddleman, H.; and Novakov, T. (1993). Towards the development of a global inventory for black carbon emissions. *Atmos. Environ.*, **27A**(8):1277-1295.

Peterson, M.R.; and Richards, M.H. (2002). Thermal-optical-transmittance analysis for organic, elemental, carbonate, total carbon, and OCX2 in $PM_{2.5}$ by the EPA/NIOSH method. In *Proceedings, Symposium on Air Quality Measurement Methods and Technology-2002*, E.D. Winegar and R.J. Tropp, Eds. Air & Waste Management Association, Pittsburgh, PA, pp. 83-1-83-19.

Poore, M.W. (2000). Oxalic acid in $PM_{2.5}$ in California. *J. Air Waste Manage. Assoc.*, **50**(11):1874-1875.

Poore, M.W. (2002). Levoglucosan in $PM_{2.5}$ at the Fresno supersite. *J. Air Waste Manage. Assoc.*, **52**(1):3-4.

Schauer, J.J.; and Cass, G.R. (2000). Source apportionment of wintertime gas-phase and particle-phase air pollutants using organic compounds as tracers. *Environ. Sci. Technol.*, **34**(9):1821-1832.

Schmid, H.P.; Laskus, L.; Abraham, H.J.; Baltensperger, U.; Lavanchy, V.M.H.; Bizjak, M.; Burba, P.; Cachier, H.; Crow, D.; Chow, J.C.; Gnauk, T.; Even, A.; ten Brink, H.M.; Giesen, K.P.; Hitzenberger, R.; Hueglin, C.; Maenhaut, W.; Pio, C.A.; Puttock, J.; Putaud, J.P.; Toom-Sauntry, D.; and Puxbaum, H. (2001). Results of the "Carbon Conference" international aerosol carbon round robin test: Stage 1. *Atmos. Environ.*, **35**(12):2111-2121.

Streets, D.G.; Gupta, S.; Waldhoff, S.T.; Wang, M.Q.; Bond, T.C.; and Bo, Y. (2001). Black carbon emissions in China. *Atmos. Environ.*, **35**(25):4281-4296.

Turpin, B.J.; Huntzicker, J.J.; and Adams, K.M. (1990). Intercomparison of photoacoustic and thermal-optical methods for the measurement of atmospheric elemental carbon. *Atmos. Environ.*, **24A**(7):1831-1835.

Turpin, B.J.; Huntzicker, J.J.; and Hering, S.V. (1994). Investigation of organic aerosol sampling artifacts in the Los Angeles Basin. *Atmos. Environ.*, **28**(19):3061-3071.

Twomey, S. (1977). *Atmospheric Aerosols*. Elsevier Scientific Publishing Co., New York, NY.

Twomey, S.; Piepgrass, M.; and Wolfe, T.L. (1984). An assessment of the impact of pollution on global cloud albedo. *Tellus*, **36B**:356-366.

U.S.EPA (1997). Revised requirements for designation of reference and equivalent methods for $PM_{2.5}$ and ambient air surveillence for particulate matter - final rule. *Federal Register*, **62**(138):38763-38854. http://www.epa.gov/ttn/amtic/files/cfr/recent/pm-mon.pdf.

Warren, S.G.; and Clarke, A.D. (1990). Soot in the atmosphere and snow surface of Antarctica. *J. Geophys. Res.*, **95**:1811-1816.

Watson, J.G.; and Chow, J.C. (2002). Comparison and evaluation of in-situ and filter carbon measurements at the Fresno Supersite. *J. Geophys. Res.*, **107**(D21):ICC 3-1-ICC 3-15.

Watson, J.G.; Chow, J.C.; Bowen, J.L.; Lowenthal, D.H.; Hering, S.; Ouchida, P.; and Oslund, W. (2000). Air quality measurements from the Fresno Supersite. *J. Air Waste Manage. Assoc.*, **50**(8):1321-1334. ISI:000089085700005.

Watson, J.G.; Cooper, J.A.; and Huntzicker, J.J. (1984). The effective variance weighting for least squares calculations applied to the mass balance receptor model. *Atmos. Environ.*, **18**(7):1347-1355.

Zielinska, B.; McDonald, J.D.; Hayes, T.; Chow, J.C.; Fujita, E.M.; and Watson, J.G. (1998). Northern Front Range Air Quality Study, Volume B: Source measurements. Prepared for Colorado State University, Fort Collins, CO, by Desert Research Institute, Reno, NV. http://charon.cira.colostate.edu/DRIFinal/ZipFiles/.